NUREG/CP-0041
Vol. 2

Proceedings of the U.S. Nuclear Regulatory Commission

Tenth Water Reactor Safety Research Information Meeting

Volume 2
- Analysis of Transients in Light Water Reactors
- Fuel Behavior and Fission Product Release
- Severe Accident Assessment
- Severe Accident Sequence Analysis

Held at
National Bureau of Standards
Gaithersburg, Maryland
October 12-15, 1982

U.S. Nuclear Regulatory Commission

Office of Nuclear Regulatory Research

Available from

GPO Sales Program
Division of Technical Information and Document Control
U.S. Nuclear Regulatory Commission
Washington, DC 20555

Printed copy price: $11.00

and

National Technical Information Service
Springfield, VA 22161

NUREG/CP-0041
Vol. 2
R1, R3 and R4

Proceedings of the U.S. Nuclear Regulatory Commission

Tenth Water Reactor Safety Research Information Meeting

Volume 2
- Analysis of Transients in Light Water Reactors
- Fuel Behavior and Fission Product Release
- Severe Accident Assessment
- Severe Accident Sequence Analysis

Held at
National Bureau of Standards
Gaithersburg, Maryland
October 12-15, 1982

Date Published: January 1983

Compiled by: Stanley A. Szawlewicz, Consultant

Office of Nuclear Regulatory Research
U.S. Nuclear Regulatory Commission
Washington, D.C. 20555

ABSTRACT

This report is a compilation of papers which were presented at the Tenth Water Reactor Safety Research Information Meeting held at the National Bureau of Standards, Gaithersburg, Maryland, October 12-15, 1982. It consists of six volumes. The papers describe recent results and planning of safety research work sponsored by the Office of Nuclear Regulatory Research, NRC. It also includes a number of invited papers on water reactor safety research prepared by the Electric Power Research Institute and various government and industry organizations from Europe and Japan.

PROCEEDINGS OF THE
TENTH WATER REACTOR SAFETY RESEARCH
INFORMATION MEETING

October 12-15, 1982

PUBLISHED IN SIX VOLUMES

GENERAL INDEX

PROCEEDINGS OF THE
TENTH WATER REACTOR SAFETY RESEARCH
INFORMATION MEETING

held at the

NATIONAL BUREAU OF STANDARDS
GAITHERSBURG, MARYLAND

October 12-15, 1982

TABLE OF CONTENTS - VOLUME 2

FUEL BEHAVIOR AND FISSION PRODUCT RELEASE
Chairman: M. Silberberg, NRC

SEVERE ACCIDENT ASSESSMENT
Co-Chairmen: T. J. Walker and J. T. Larkins, NRC

SEVERE ACCIDENT ASSESSMENT (Cont'd)

SEVERE ACCIDENT SEQUENCE ANALYSIS
Chairman: R. T. Curtis, NRC

SEVERE ACCIDENT SEQUENCE ANALYSIS (Cont'd)

PREFACE

This report, published in six volumes, includes 160 papers which were presented at the Tenth Water Reactor Safety Research Information Meeting. The papers are printed in the order of their presentation in each session. The titles of the papers and the names of the authors have been updated and may differ from those which appeared in the Final Agenda for this meeting.

Five papers, which were submitted for presentation at the meeting but could not be scheduled, are also included in this report. They are the following:

Calculations of Pressurized Thermal Shock Problems with the SOLA-PTS Method, B. J. Daly, B. A. Kashiwa, and M. D. Torrey, LANL, (Pages 113-130, Volume 2)

Hydrogen Migration Modeling for the EPRI/HEDL Standard Problems, J. R. Travis, LANL, (Pages 131-144, Volume 2)

Independent Code Assessment at BNL in FY 1982, P. Saha, U. S. Rohatgi, J. H. Jo, L. Neymotin, G. Slivik, and C. Yuelys-Miksis, BNL, (Pages 145-168, Volume 2)

Experimental Evidence for the Depencence of Fuel Relocation upon the Maximum Local Power Attained, D. D. Lanning, PNL, (Pages 285-296, Volume 2)

PRA Has Many Faces - Can the Safety Goal Be Well-Posed? H. Bargmann, Swiss Federal Institute for Reactor Research, (Pages 105-114, Volume 6).

BNL PLANT ANALYZER DEVELOPMENT

H. S. Cheng, K. Fujiki, S. V. Lekach,
A. N. Mallen and W. Wulff, BNL

1. PROGRAM OBJECTIVES

The LWR Plant Analyzer Program is being conducted at Brookhaven National Laboratory to develop an engineering plant analyzer capable of performing, in a dedicated facility, accurate real-time and faster than real-time simulations of plant transients and small-break loss of coolant accidents in LWR power plants. The program is designed to reduce sharply the time and cost of input preparation, code execution and evaluation of results by combining existing modern, interactive, high-speed, special-purpose minicomputer technology with existing advanced modeling techniques for neutron kinetics, thermohydraulics and plant controls.

The technology developed in this program is required to obtain timely and cost-effective answers to a wide variety of safety questions related to the nuclear steam supply system, the balance of the plant and its control systems, particularly where a large number of simulations is required for parametric investigations, for human factors studies (error rate measurements) and for risk assessments. The technology is also needed for monitoring continuously the operation of a particular power plant, for the detection of instrument, component or system failures, and for anticipating the consequences from mitigating operator actions following an accident.

The emphasis of this program lies in the development of a decentralized facility which is small and dedicated to a specific office or utility or to a specific power plant.

2. PREVIOUS PROGRAM ACHIEVEMENTS

The program was initiated in October 1980 with the review and assessment of capabilities and limitations in current commercial training simulators for nuclear power plant operators [1-3] and with the selection and acquisition of a special-purpose peripheral processor, specifically designed for high-speed interactive system simulations. The AD10 of Applied Dynamics International was selected. A system of two units became operational at BNL on March 15, 1982.

The special-purpose peripheral processor AD10 is specifically designed for fast, efficient integration of ordinary differential equations and is, therefore, particularly suited for system simulations. The AD10 is programmed through a PDP-11/34 host computer, by using either basic machine language or the high-level modular, state equation oriented, simulation language MPS-10 which was developed by ADI for the AD10 processor, and which has the features of known simulation languages, such as DARE (Korn and Wait 1978). The AD10 processor interacts directly with other digital computers (array processors or general purpose computers), with instrumentation, recorders or oscilloscopes, or with a second AD10 processor. The AD10 provides for on-line interaction between itself and four users and it features simultaneous, on-line display of up to 128 computed parameters.

The AD10 processor consists of six special-purpose microprocessors, each equipped with its own instruction memory:

Control Processor	(COP)	for control and timing of all processors
Decision Processor	(DEP)	for logic and binary search needed for function generation,
Arithmetic Processor	(ARP)	for addition, multiplication and interpolation (function generation),
Numerical Integration Processor	(NIP)	for numerical integration of ordinary differential equations,
Memory Address Procesor	(MAP)	for addressing data memory,
Input/Output Channel Processor	(IOCC)	for I/O control.

The six microprocessors execute in parallel and communicate with each other, with the data memory and with the Host Interface Controller via a Multibus. The Multibus broadcast data simultaneously to all processors (prepared for data reception at a given time) at the rate of 20 MHz. All microprocessors are synchronized and execute at the frequency of 10 MHz. Pipe-lining in the ARP and NIP processors affords composite operations (i.e. $(\overline{A+B}) * \overline{C+D}$ in the ARP) to be executed at the rate of ten million composite operations per second. Interleaving of memory allows data transfer between processors at the rate of twenty million 16-bit words per second.

The AD10 processor has the data memory capacity of up to one million 16-bit words. The AD10 can integrate up to 195 ordinary differential equations with a fourth-order (Runge-Kutta) integration algorithm, or up to 975 equations with a first-order (Euler) algorithm. The processor allows for any combination of up to ten integration algorithms, which are built into the NIP processor and may be selected and changed during the program execution. The AD10 numerical processor combines 16-bit fixed-point function generation (ARP) with 48-bit integration (NIP).

The computing speed in the AD10 processor results firstly from its architecture, namely the parallel processing by six microprocessors, pipe-line executions (seven stages in ARP), interleaving of data memory, synchronous broadcasting of data, hard-wired arithmetic and the combination of fixed-point 16-bit arithmetic with 48-bit pseudo floating point arithmetic, and secondly from special programming, namely the function generation instead of the extended arithmetic (multiple evaluation of polynomials) in general purpose computers, and the efficient, high-order integration algorithms. For more details about the AD10 system see ADI 1981.

Prior to the arrival of the AD10 and its host computer, a lumped-parameter conduction model was developed specifically for high-speed simulation of plant transients and small-loss-of-coolant accidents [4].

3. CURRENT FEASIBILITY DEMONSTRATION

3.1 Purpose

The current program phase serves to demonstrate the feasibility of performing realistic, accurate thermohydraulics simulations interactively at

much faster computing speed and with comparable accuracy as those of the large main-frame computer CDC-7600.

3.2 Selected LWR System and Thermohydraulics Model

A four-equation slip flow model for nonhomogeneous, nonequilibrium two-phase flow in a BWR system was selected for implementation on the AD10 because its FORTRAN version had been extensively executed on the CDC-7600 and was available for obtaining reference data to assess the AD10 performance. The thermohydraulics model has been scaled for the fixed-point arithmetic of the AD10 and programmed in the high-level simulation language MPS10 of the AD10. The resulting High-Speed Interactive Plant Analyzer program is called HIPA. Since it is specifically programmed for the Peach Bottom II BWR power plant, this program version is called HIPA-PB2.

The four field equations of the thermohydraulics model are the vapor mass balance and the balance equations for mixture mass, momentum and energy. The constitutive relations for wall shear are taken from Blasius for single-phase flow and augmented for two-phase flow with the multiplier by Becker, Hernborn and Bode [5]. Standard Dittus-Doelter and Jens-Lottes correlations are used for heat transfer in single and two-phase flows, respectively. The slip correlation used is that by Bankoff and Jones modified by Lelluche [6]. The vapor generation rate is a proprietary correlation and accounts for both surface boiling and bulk flashing or condensation.

The nuclear steam supply system is subdivided into 55 nodes as shown in Figure 1. Notice the differences of nodalization in the HIPA-PB2 and the reference calculation shown in Table 1. These differences are caused by the limitations of the reference code: for one-dimensional neutron kinetics the FORTRAN code can accommodate only one core channel and one bypass channel. The HIPA-PB2 has also a hot channel. Care was taken to make sure that the AD10 program had more, rather than less, computational effort than the CDC-7600.

3.3 Selected Transient

The Design Basis Transient, induced by a turbine trip at full power and under the conditions of disabled bypass and disabled recirculation pump trips, was selected for assessing the AD10 processor performance. The steam line dynamics introduce flow and pressure oscillations with characteristic times of approximately 80 ms. Figures 2 through 5 show the histories of normalized power, of volumetric steam flow rate, of volumetric feedwater flow rate and of a typical wall heating rate (at the midplane of the core). These figures characterize the selected transient, particularly with respect to the integration time step limitation imposed by the characteristic frequencies of the transient.

3.4 Results

The completed feasibility demonstration consists of:

(i) assessing the computing accuracy and the adequacy of 15-bit precision,

(ii) assessing the computing speed and

(iii) assessing the computing capacity

of the AD10 processor.

3.4.1 Computing Accuracy

The computing accuracy of the AD10 has been assessed by comparing its computed results with the results from the CDC-7600 main frame computer executing the same basic equations (reference calculations). Figures 6 through 12 show these comparisons. The error is less than 5% for almost all parameters at any time.

An issue has often been raised with the claim that the 15-bit precision of the 16-bit word in the arithmetic processor ARP is not adequate. The performance of the ARP processor affects the calculation of all the right-hand sides of the state equations (ordinary differential equations). Following the suggestion by Professor Walter Karplus of UCLA, we computed the transient with 13 and 14-bit precision. We replaced the last two bits by zeros in 111 out of 116 integrator inputs. The result was equal to that with the full 15-bit precision. One can conclude that 15-bit precision is adequate. However, we have taken great care in scaling to avoid leading zeros in the decimal fractions of all intermediate and final output parameters.

Finally, we have computed a steady-state as a transient with fixed initial conditions. We observed no numerical drift during ten minutes of real-time calculation.

3.4.2 Computing Speed

The computing speed of the AD10 has been assessed by comparing it against the clock and against the speed with which the mainframe CDC-7600 computer executed the integration of the same equation sets as the AD10, but with slightly fewer nodes than the AD10 as shown above in Table 1.

The result is that the AD10:

(i) computes 10 times faster than real-time calculations when using two time steps for the momentum balance, while advancing overall by one time step.

(ii) computes 8.5 times faster than real time with a single time step.

(iii) computes 110 times faster than the CDC computer.

(iv) needs 78 microseconds per time step and computational cell, compared to the 2000 microseconds needed by the CDC-7600.

It must be emphasized that the AD10 is not interrupted for I/O data processing. Up to 128 output parameters can be displayed simultaneously. The AD10 is only interrupted through the host computer for the purpose of changing parameters, running speed, integration mechanisms, etc.

3.4.3 Computing Capacity

The thermohydraulics, exclusive of steam line and recirculation loop dynamics, requires 3,800 out of 7,600 available words of instructional memory. Precomputed tables for function generation require 150,000 words (16-bit each) of data memory. We have used half of the available ARP memory and half of the available data areas but only a small fraction of our available data memory.

4. IMPLICIT INTEGRATION WITH THE AD10

The integrators in NIP processor employ only explicit integration algorithms. In order to accommodate the extremely small time constant of the prompt neutron kinetics equation, an implicit integration scheme by H. S. Cheng [7] has been implemented and successfully executed. All other kinetics equations are being integrated by the NIP processor.

5. FUTURE ACTIVITIES

It is planned to replace the limited slip model used for the comparison of the AD10 with an existing FORTRAN program result by the more advanced drift flux model. The drift flux model affords flow reversal and level tracking.

It is also planned to implement the previously developed conduction model and to interface the existing neutron kinetics model. Following this activity, NSSS-related control systems will be implemented.

Existing multi-color CRT display systems will be added later to complete the plant analyzer.

REFERENCES

1. Wulff, W., "PWR Training Simulator, An Evaluation of the Thermohydraulic Models for its Main Steam Supply System," Informal Report, BNL-NUREG-28955, 1980.

2. Wulff, W., "BWR Training Simulator, An Evaluation of the Thermohydraulic Models for its Main Steam Supply System," Informal Report, BNL-NUREG-29815, 1981.

3. Cheng, H. S. and W. Wulff, "A PWR Training Simulator Comparison with RETRAN for a Reactor Trip from Full Power," Informal Report, BNL-NUREG-30602, 1981.

4. Wulff, W., "Plant Analyzer Development Program," Quarterly Report, Chapter 6; A. J. Romano, Editor, BNL-NUREG-51454, Vol. 1, No. 4.

5. Becker, K. Hernborg and M. Bode, "An Experimental Study of Pressure Gradients for Flow of Boiling Water in a Vertical Round Duct," Parts 1, 2 and 3, AE-69, 70 and 85, AB Atomenergi, Studsvik (1962).

6. Jones, A. B. and D. G. Dight, "Hydrodynamics Stability of a Boiling Channel," KAPL-2208, Knoll Atomic Power Laboratory (1962).

7. Cheng, H. S., Internal Memo, Brookhaven National Laboratory (1976).

TABLE 1

DIFFERENCES BETWEEN CDC AND AD10 NODALIZATION

AD10 SIMULATION	CDC-7600 SIMULATION
55 Nodes	43 Nodes
3 Channels	2 Channels
ΔP_{jp} Imposed	1 Recirc. Loop (Incompressible)

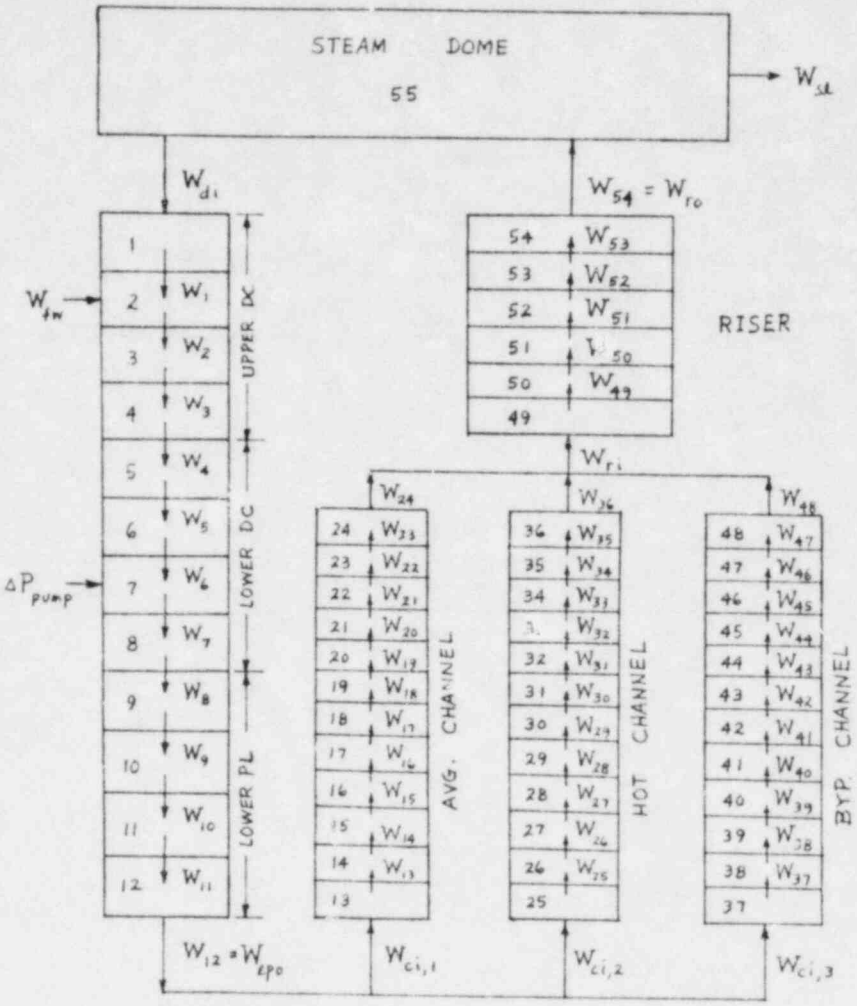

FIGURE 1 - HIPA-PB NODALIZATION SCHEME

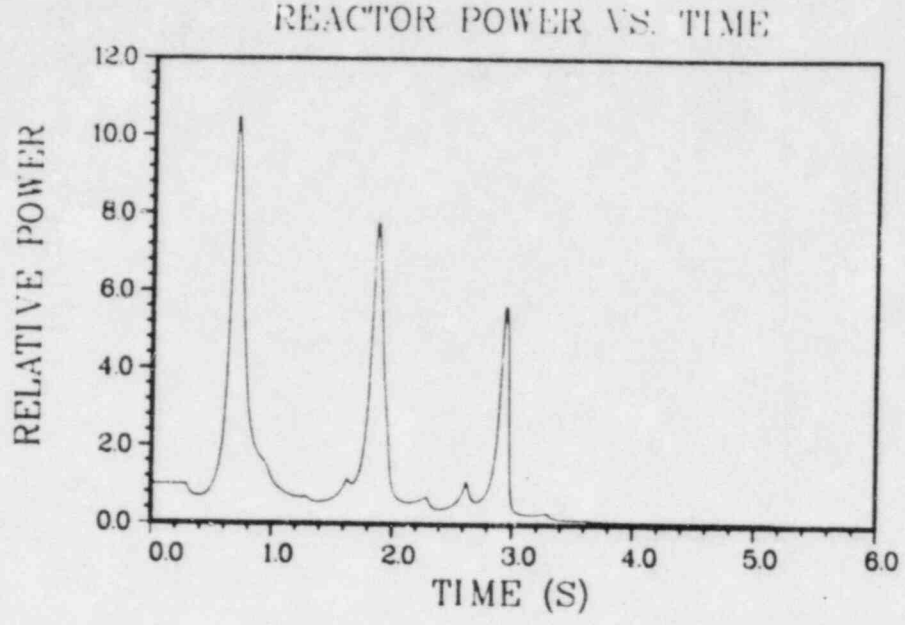

FIGURE 2 - Reactor Power Vs. Time

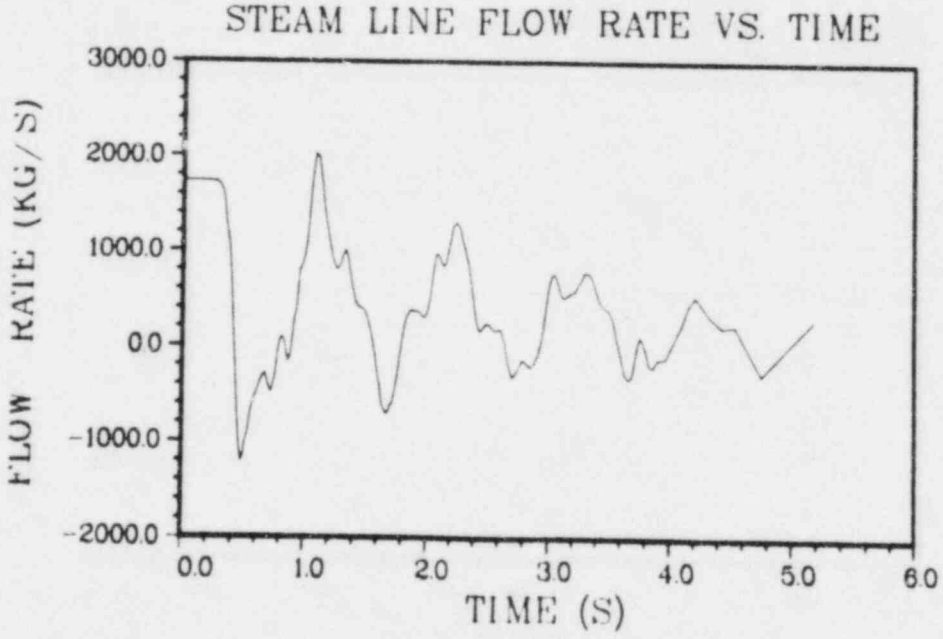

FIGURE 3 - Steam Line Flow Rate Vs. Time

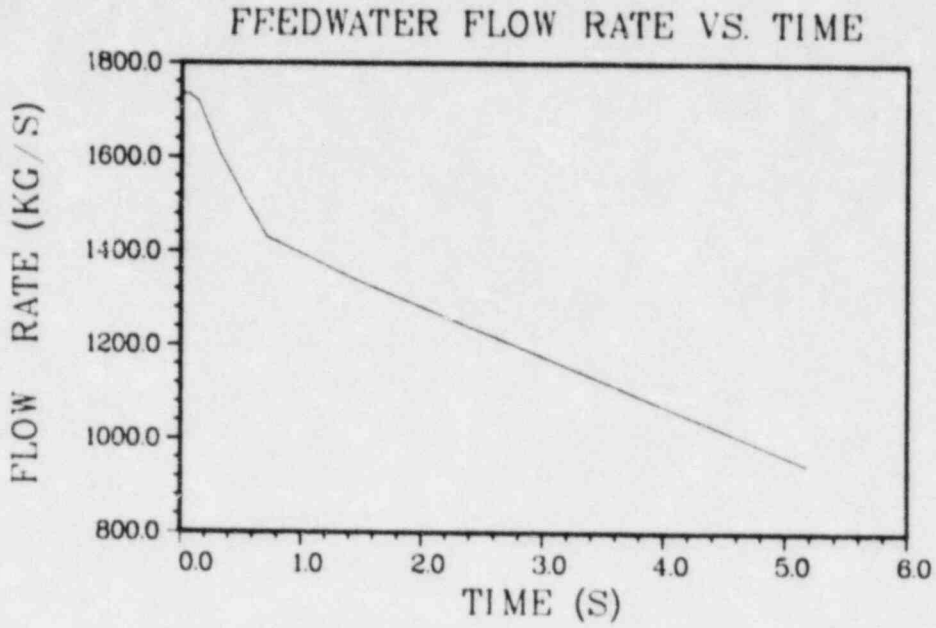

FIGURE 4 - Feedwater Flow Rate Vs. Time

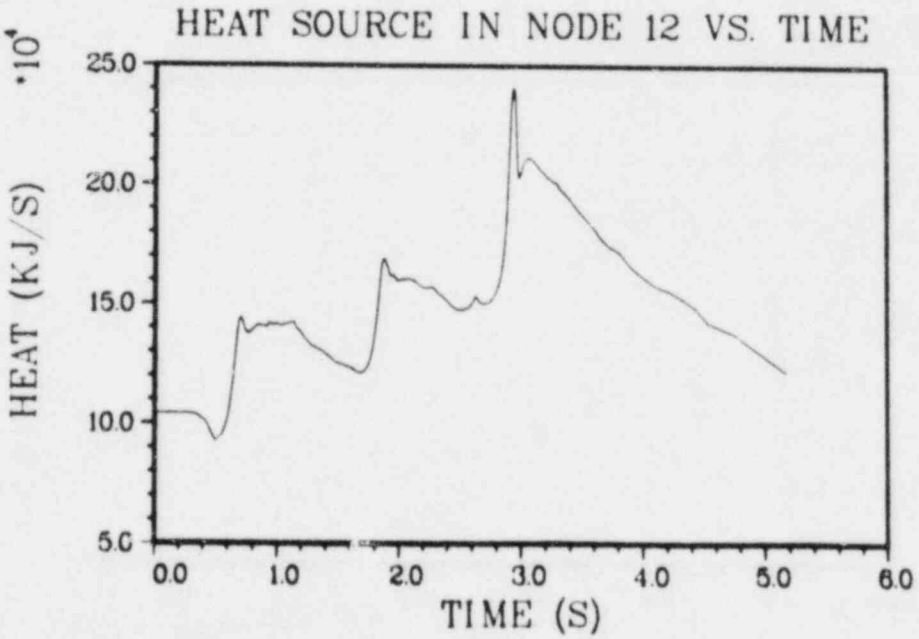

FIGURE 5 - Heat Source in Node 12 Vs. Time

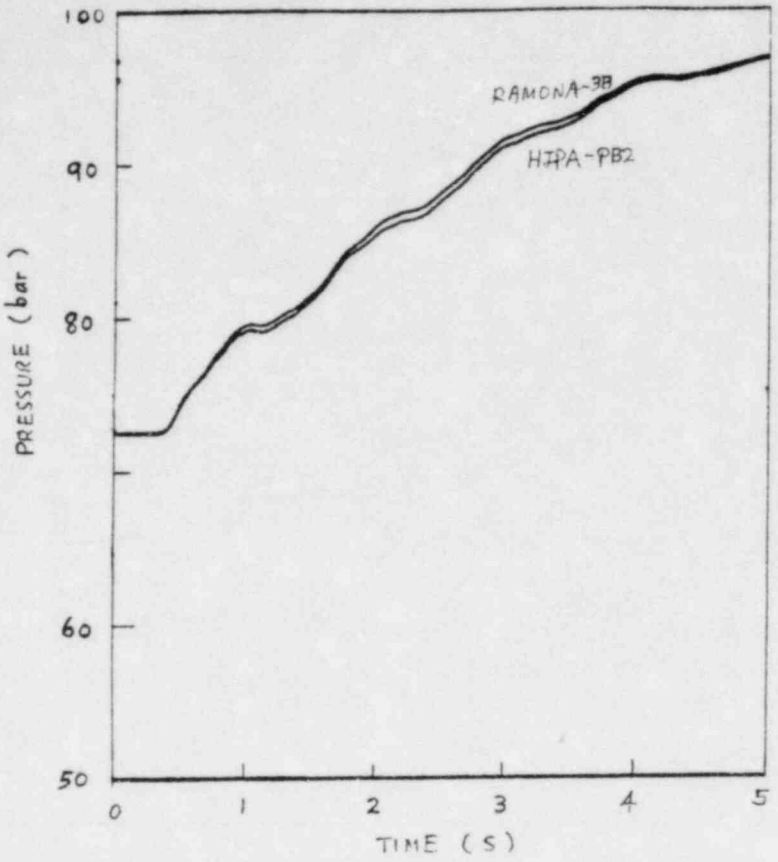

FIGURE 6 - System Pressure Response

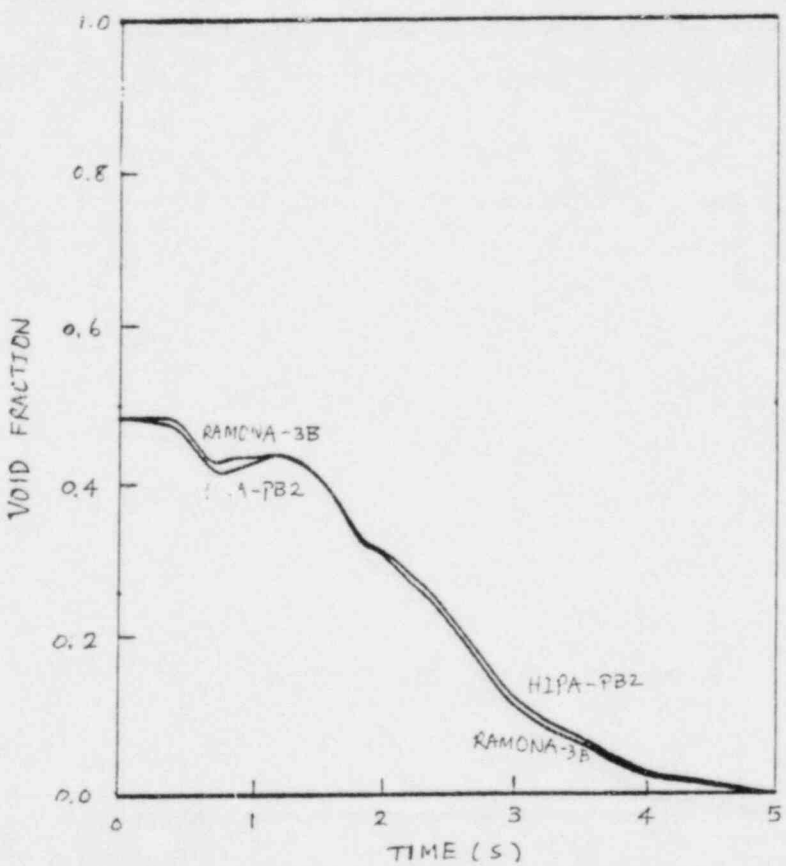

FIGURE 7 - Void Fraction at Mid-Core

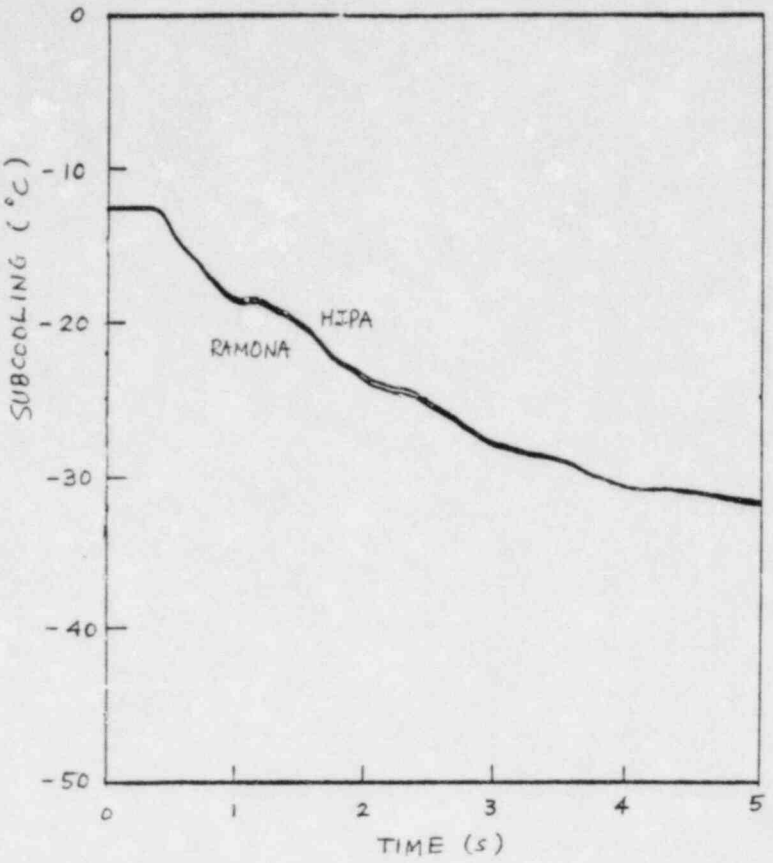

FIGURE 8 - Core Inlet Subcooling

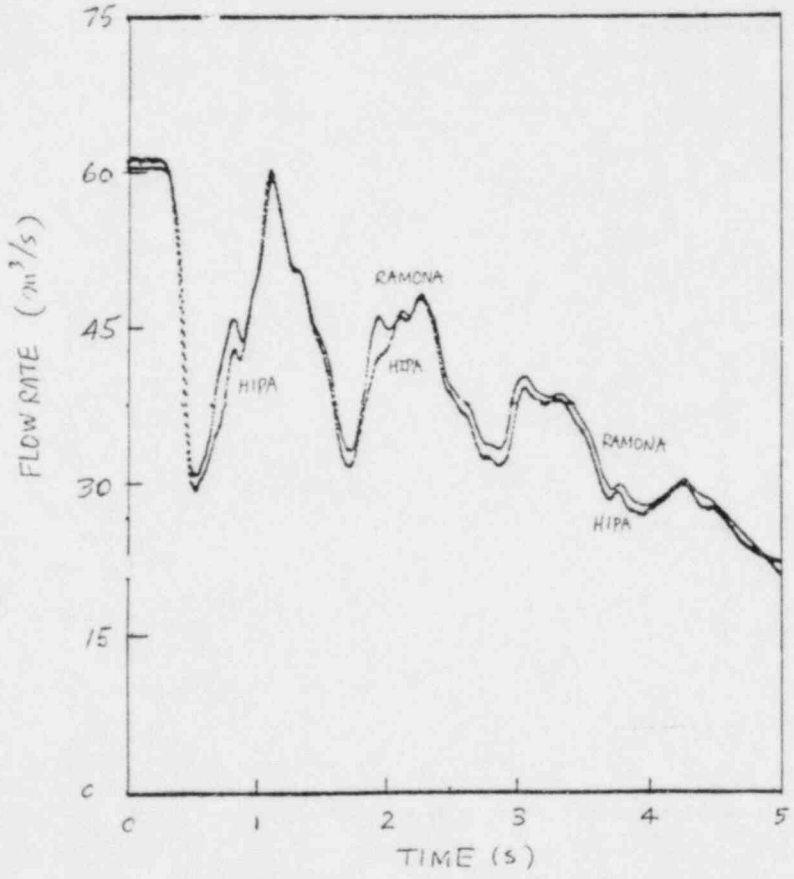

FIGURE 9 - Mixture Volumetric Flow Rate at Riser Exit

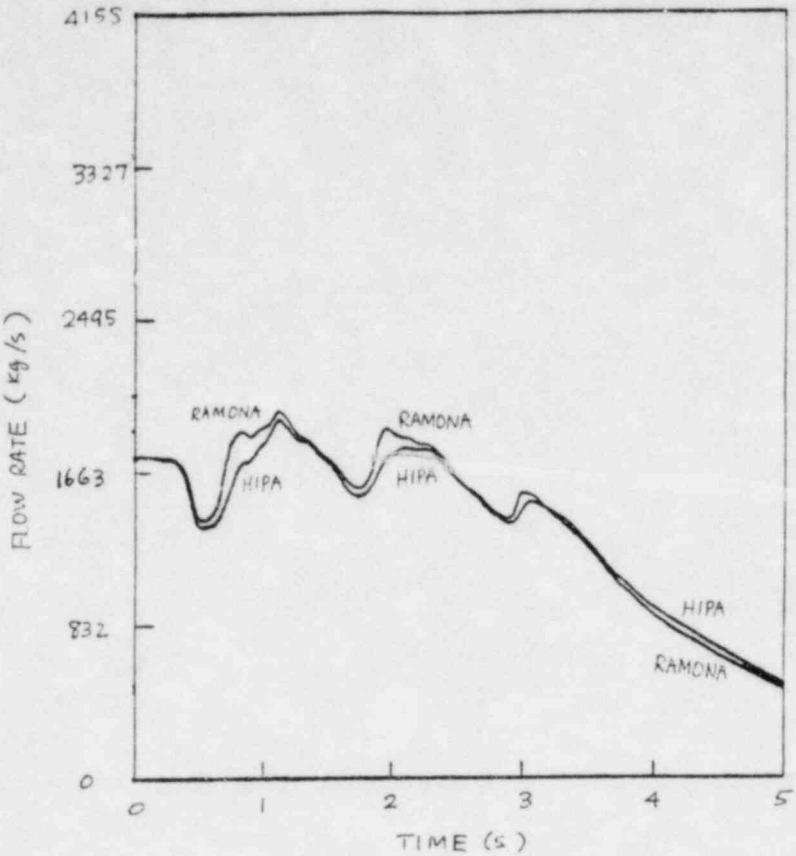

FIGURE 10 - Vapor Mass Flow Rate at Core Exit

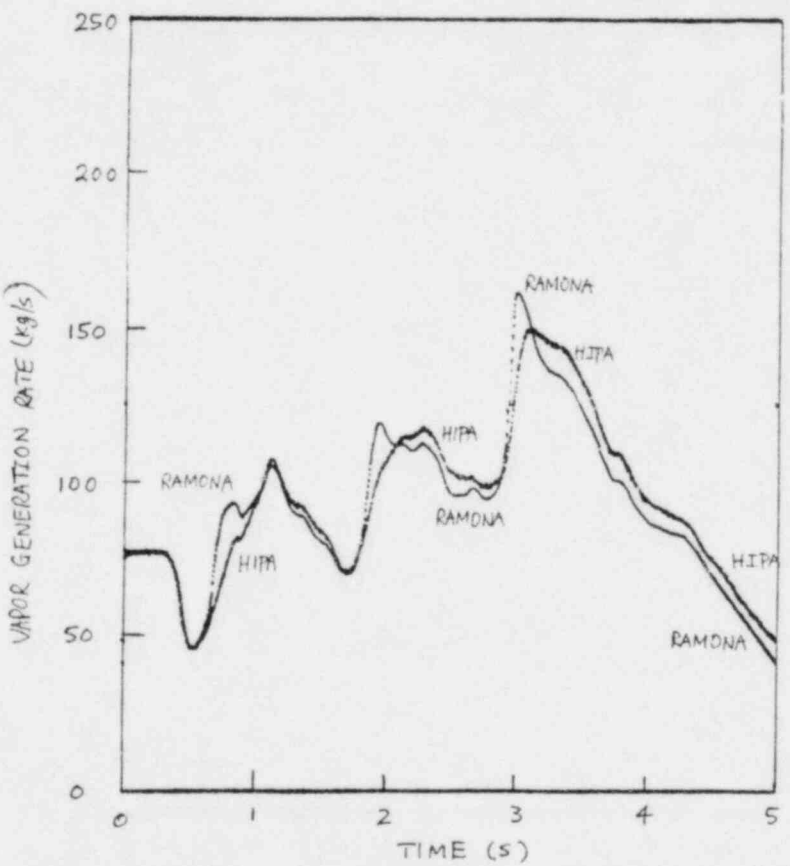

FIGURE 11 - Vapor Generation Rate At Core Exit

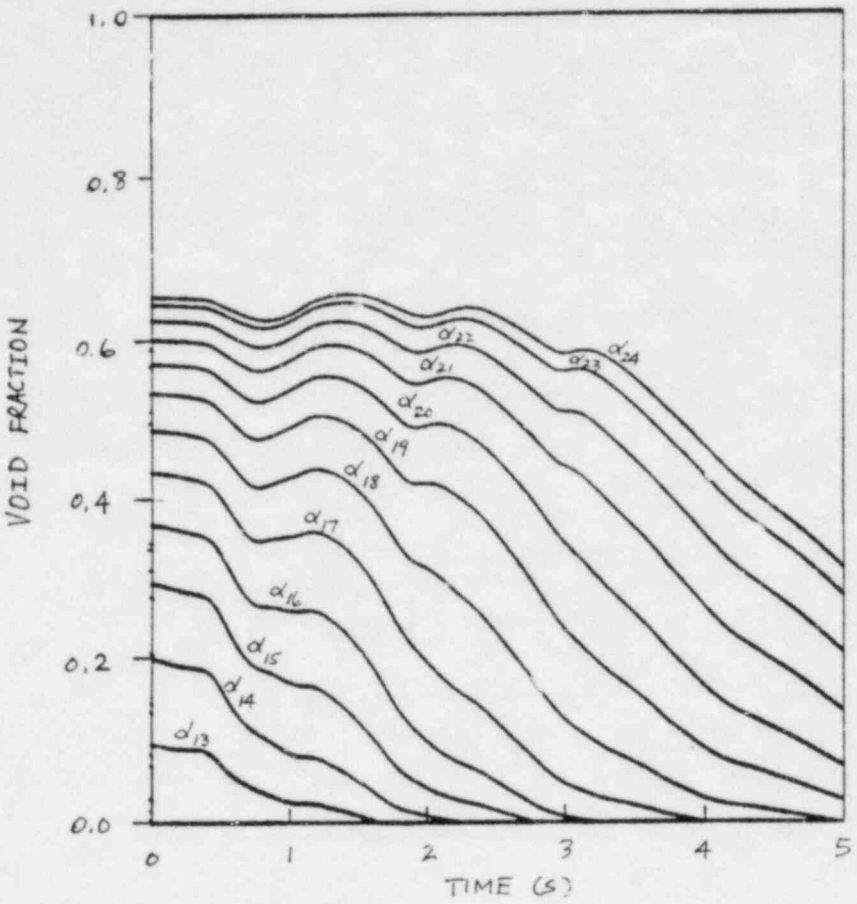

FIGURE 12 - Void Fractions in the Core

NRC NUCLEAR PLANT ANALYZER CONCEPT AND STATUS AT INEL[a]

by

F. Aguilar
R. J. Wagner
EG&G Idaho, Inc.

The Office of Research of the U.S. Nuclear Regulatory Commission (NRC) has proposed development of a software-hardware system called the Nuclear Plant Analyzer (NPA). The nuclear plant analyzer project, which will be undertaken jointly by the Idaho National Engineering Laboratory (INEL) and the Los Alamos National Laboratory, is in the embryonic stage of growth--the detailed technical specifications for the NPA are not formulated as yet. This paper describes how we of the INEL envision the nuclear plant analyzer. The paper also describes a pilot RELAP5 plant analyzer project completed during the past year and current work. A great deal of analysis is underway at the direction of the NRC to determine nuclear steam system response. This research will almost certainly continue well into the next decade. These analyses are being done with the advanced "best estimate" system codes developed by NRC: RELAP5,[1] TRAC-BD1,[2] and TRAC-PF1.[3] The development and assessment of these advanced codes are continuing, the emphasis generally being on obtaining an accurate solution to the system analysis problem. However, the need is greater than just obtaining an accurate solution, as formidable as that task is. System transient analysis being so complex, there is the need to present analytical results in a way that interconnections among phenomena and all the nuances of the transient are apparent. There is the need for the analyst to dynamically control system calculations to simulate plant operation in order to perform "what if" studies as well as the need to

---

a. Work supported by the U.S. Nuclear Regulatory Commission, Office of Nuclear Regulatory Research under DOE Contract No. DE-AC07-76ID01570.

perform system analysis within hours of a plant emergency to diagnose the state of the stricken plant and formulate recovery actions. The NRC-proposed nuclear plant analyzer can meet these needs.

INEL Concept of the Nuclear Plant Analyzer

We at the INEL view the nuclear plant analyzer as an engineering simulator, the technical base of which is inherent in existent software and multi-purpose computing facilities to which NRC has access. The primary mission of the NPA is safety analysis of nuclear steam systems as done now--but faster, at less cost, and with higher quality results. Testing and evaluation of proposed operator guidelines for abnormal transients is a new variation of safety analysis that would be made possible by the NPA. An extremely important aspect of the NPA's prime mission is to enable safety analysis of any stricken plant within hours of an accident to help diagnose the state of the plant and formulate recovery actions. Another mission for the NPA is to aid human factors researchers, for example, to drive proposed plant data displays. Still another mission is to complement the training of plant operators, operator examiners, emergency center personnel, and safety analysts. However, the nuclear plant analyzer is not an operator training simulator with the requirement of duplicating control room environment. It is not an on-line, plant accident recovery device with the requirement that it have a data link to operating plants.

The general requirements for the NPA are: it must have an accurate prediction capability--accuracy cannot be compromised; it must be fast running, permit dynamic control of the calculation, and enable easy and thorough comprehension of analytical results; it should provide a ready capability to analyze abnormal transients in any plant; it must give the analyst access to the nuclear plant data bank (NPDB) for reference data and for modifying or building plant analytical models; it must be user oriented in order to reduce analysis labor and time requirements and assure quality.

Our concept of the nuclear plant analyzer is a software and hardware configuration, the heart of which is a library of advanced system analysis codes featuring RELAP5, TRAC-BD1, and TRAC-PF1. RELAP5 provides an

accurate, fast running, and full modeling capability: two-fluid thermal-hydraulics accounting for nonhomogeneous and nonequilibrium effects, comprehensive system representation including plant control systems, and an interactive feature enabling dynamic, on-line control of the simulation and display of calculated quantities. A plant input deck library is also a major software component. This library has optimal models for each plant according to class of transient, desired accuracy, and run time. Another major software component is advanced graphics software that allows plant simulation data to be dynamically displayed at a console in the manner the analyst chooses. The final major software component would be "user friendly" access software through which the analyst selects, modifies, or builds plant input decks, controls the simulation, and chooses graphical displays. This software teaches the analyst how to use the NPA and provides access to the system codes, input deck library, nuclear plant data bank, and even documentation such as analysis reports, user guidelines, etc.

The NPA hardware consists of a console of one or more high performance color cathode ray tube (CRT) monitors with a telephone tie to a mainframe computer, for example, INEL's twin CDC 176 system. The monitors provide a wide menu of interesting data displays ranging from simultaneous, differing views of the same data to a simple plant control panel mockup. The master terminal provides "plant controls" and communicates with the mainframe computer. The NPA console includes a mini-computer and disk memory system to reduce the volume of data transmitted from the mainframe computer. This improves the speed at which an analysis can be run interactively, increases the variety and quality of graphics displays, and reduces mainframe computer use fees. This also allows storing previous analyses locally at the NPA for play back without using the mainframe computers.

Pilot RELAP5 Nuclear Plant Analyzer

A pilot RELAP5 nuclear plant analyzer was demonstrated to NRC personnel, contractors, and the public during the RELAP5 Users Meeting held in Bethesda, Md. on March 8, 1982 and also to a meeting of Advisory Committee on Reactor Safeguards in Albuquerque, NM on March 24, 1982. In each demonstration, a loss-of-feedwater accident in a pressurized water

reactor was modeled. The calculation was done with RELAP5 in the interactive mode and on-line to the INEL mainframe computers. The "operator" took control of the "plant" and attempted recovery. The audience was consulted for operations advice, and various pumps were tripped and started, valves opened and closed, etc. Figure 1 shows the plant schematic (mimic) that was displayed at the "operator's" CRT during the transient. The actual display was in color and the digital information was updated every 5 s. RELAP5 actually executed the transient at an average rate of twice faster than real (transient) time, and the data updating was slowed to real time.

The mimic was prepared by MAPPER,[4] a general purpose graphics tool, and was generated outside the RELAP5 code. The mimic file was stored on a floppy disk attached to the CRT. Once the mimic is displayed, any number of RELAP5 simulations may be made. The modification to the basic interactive RELAP5 (interactive control is a standard feature of RELAP5/MOD1.5 and subsequent versions) was minimal, primarily providing screen coordinates for the digital output. Program changes are now required to accommodate new displays since no communication between RELAP5 and MAPPER has been provided as yet.

The pilot demonstration sparked interest among NRC/NRR personnel who forsee the potential value of the RELAP5 plant analyzer to assist in operator guideline evaluation. A project is underway to develop new mimics for the RELAP5 plant analyzer using the Babcock and Wilcox (B&W) abnormal transient operation guidelines (ATOG) as the vehicle for the study. The mimic shown in Figure 2 is a B&W plant schematic in which color is used dynamically to indicate system voiding, pump and valve trips, core heatup, and liquid levels in the pressurizer, accumulator, and steam generator. Arrows indicate flow direction. Other mimics will simulate B&W's ATOG display device and the set of instruments that an operator will most likely consult when using the ATOG guidelines.

This project will provide NRC/NRR with an interim nuclear plant analyzer until the NRC plant analyzer is ready for production use. Not only will this project provide NRC/NRR with a tool for operator guideline

evaluation, but it will contribute significantly to formulating the detailed technical specifications for the production version of the nuclear plant analyzer.

REFERENCES

1. V. H. Ranson et al., RELAP5/MOD1 Code Manual Volumes 1, 2, NUREG/CR-1826, EGG-2070, March 1982.

2. J. W. Spore et al., TRAC-BD1: An Advanced Best Estimate Computer Program for Boiling Water Reactor Loss-of-Coolant Accident Analysis, NUREG/CR-2178, EGG-2109, October 1981.

3. "TRAC-PF1 7.0/EXTUPD7.6--Input Specifications," Los Alamos National Laboratory, LA-TIA-TN-82-1, June 1982.

4. H. R. Bruestle etal., Idaho National Engineering Laboratory Data Management System, Release 1.2, EGG-15-5528, 15 DMS 1.2.

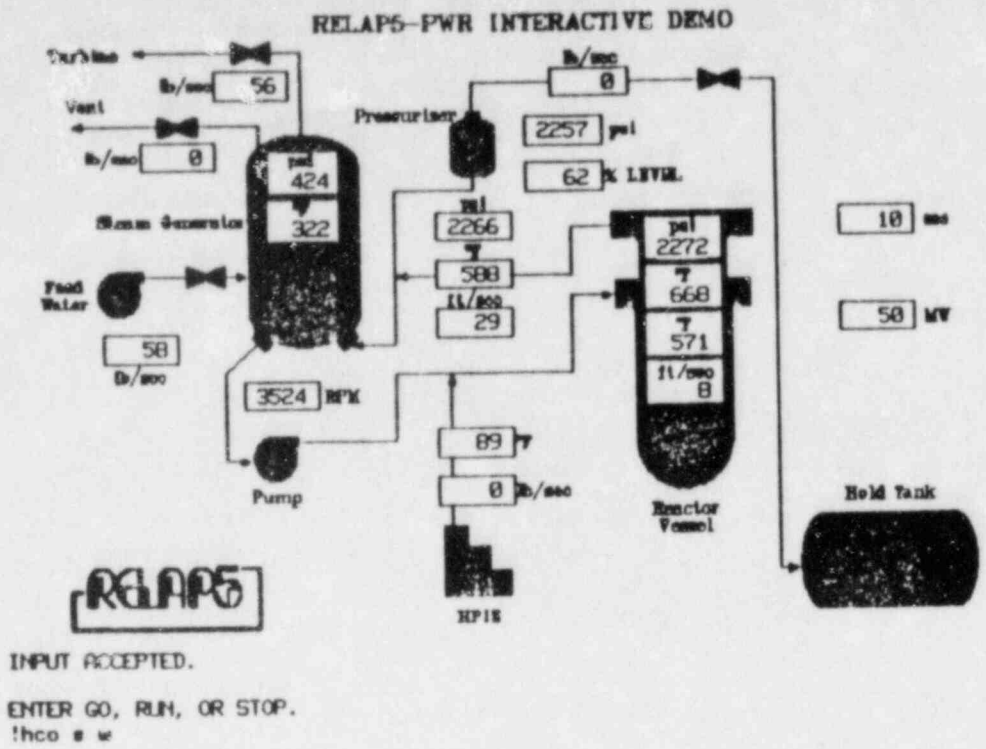

Figure 1. CRT Display for Pilot RELAP5 Nuclear Plant Analyzer (Actual Display in Color).

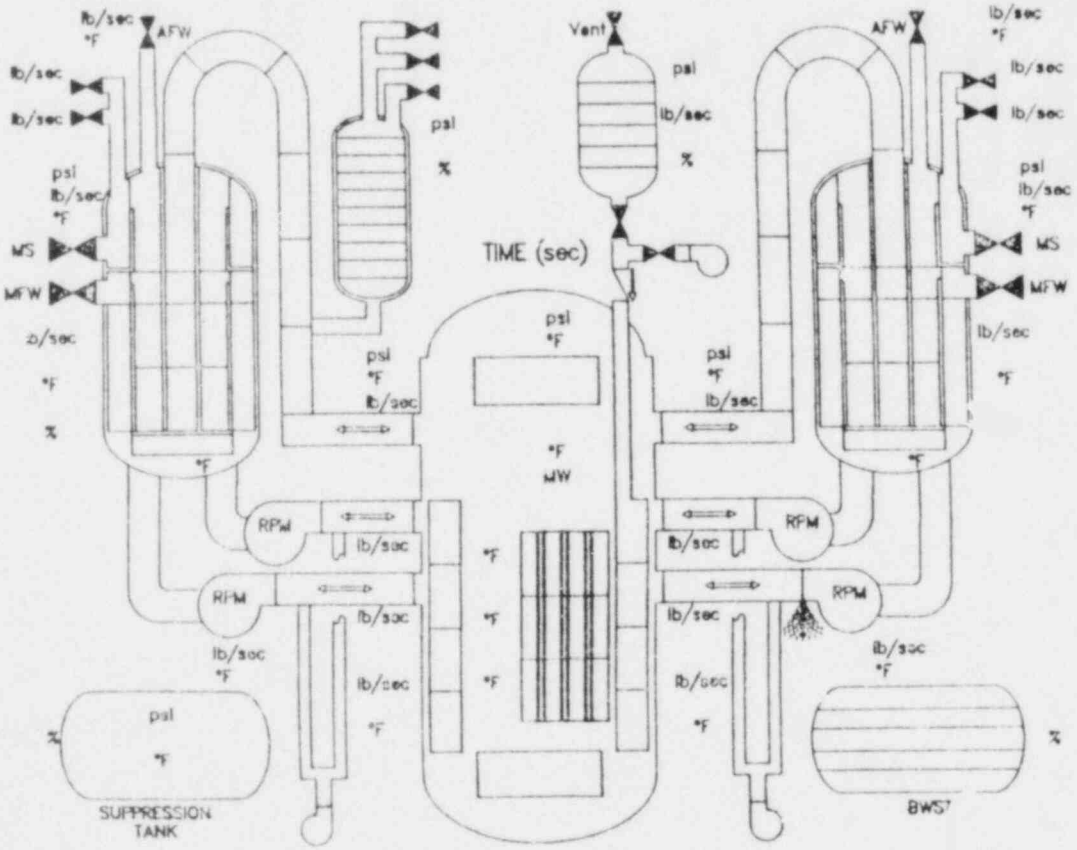

Figure 2. CRT Display for B&W ATOG Evaluation (Actual Display in Color).

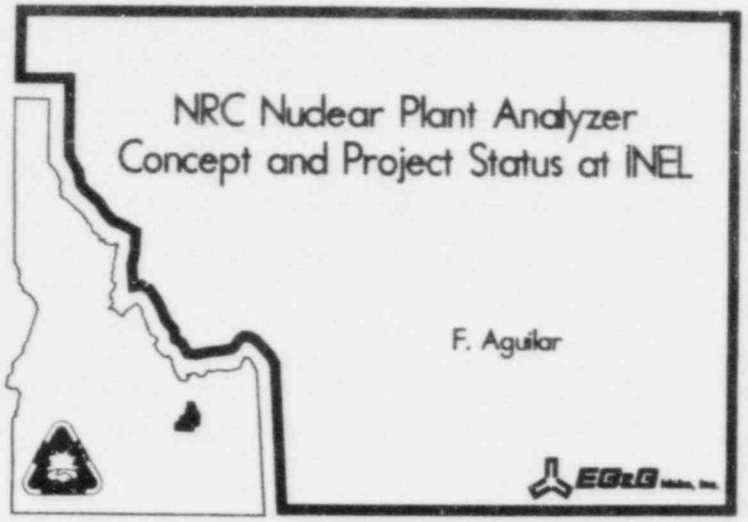

What is a Nuclear Plant Analyzer? - An Engineering Simulator

- Accurate and fast predictive capability
- Dynamic control of calculation
- Easy, thorough comprehension of analysis
- Ready capability for every plant
- Modest analytical skills required of user

C2 0662

Why a Nuclear Plant Analyzer?

- Safety analysis
  - Evaluation of operator guidelines
  - Enhance comprehension of licensing calculations
  - Enhance quality assurance of codes and analyses
  - Reduce analysis time and cost

C2 0663

Why a Nuclear Plant Analyzer? (cont'd)

- Aid management of plant abnormal events
- Complement training of operators, examiners, and safety analysts
- Aid human factors research

C2 0664

Movie

Demonstration

of

RELAP5 Nuclear Plant Analyzer

INEL Plant Analyzer Concept
Software and Hardware Components

- RELAP5 best-estimate system analysis code
  - Accurate predictive capability
  - Fast running
  - Interactive feature
  - Plant controls modeling package
- Plant input deck library

INEL Plant Analyzer Concept
Software and Hardware Components (cont'd)

- Mainframe computers with telephone tie
- Advanced graphics display software and hardware
- "User friendly" software providing access to :
  - System codes
  - Graphics displays
  - Input deck library
  - Nuclear plant data bank
  - User guidelines

INEL Plant Analyzer Status

- Pilot RELAP5 plant analyzer demonstration
  - Remote execution on INEL computers from Washington, D. C., and Albuquerque, N. M.
  - Dynamic control of plant simulation from terminal
  - Plant data display on color terminal
  - Fast running of system transients

INEL Plant Analyzer Status (cont'd)

- Evaluation of abnormal transient guidelines with RELAP5 pilot analyzer underway for NRC/NRR
- Coordinated development of NRC nuclear plant analyzer and nuclear plant data bank started among INEL, LANL, and TDC

C2 0698

LA-UR-88-822

NUCLEAR PLANT ANALYZER DEVELOPMENT AT LOS ALAMOS*

by

Dennis Liles

LANL

I. INTRODUCTION

The accident at Three Mile Island (TMI) changed the primary emphasis in nuclear reactor safety research from large-break LOCAs to the entire spectrum of reactor accidents including small-break LOCAs, ATWS, operational transients, and other transients or accidents that eventually might cause an inability to cool the core.

Since that accident, much progress has been made on advanced best-estimate computer codes to analyze system transients. Consequently, a code such as TRAC-PF1 can run reliably a wide variety of both slowly and rapidly developing accidents including those involving core uncovery and reflood. TRAC was the first computer code capable of running in one continuous calculation an entire large-break LOCA sequence including blowdown, refill, and reflood. Numerous analysts both at Los Alamos and at other facilities have assessed the TRAC models and their calculational results generally compare well with the experimental data. Early TRAC versions often required large amounts of computer time. However, TRAC-PF1 (the current, released version) can run many slow transients much faster than real time on a CDC 7600 or a similar large computer because it uses an innovative one-dimensional numerical procedure, a stability-enhancing two-step (SETS) technique. This also has opened up the possibility of running the code in real time on slower, cheaper computers.

---

*Work performed under the auspices of the US Nuclear Regulatory Commission.

TRAC and comparable codes were designed originally to run basically in a batch mode on large computers. Interactive features (Sec. II.D) are now available that allow the analyst to simulate reactor operator intervention and enable the programs to replicate an accident scenario that an operator might see during a transient.

Interactive color graphics are being investigated as a next step in developing an analyst-oriented package for use in accident management studies of severe accident sequences. The use of color for both input and output displays considerably enhances the analyst's ability to note trends and to initiate input deck changes, and adds only incrementally to the total cost. As a logical extension of these recent developments, an interactive, integrated, and very fast NPA using well-assessed physical models is now possible. Thus, primary and secondary loops, control and trip systems, and many of the auxiliary hydrodynamic systems (water makeup and letdown, for example) can be analyzed quickly and accurately for a wide variety of nuclear plants and over a wide range of accidents, including severe accident sequences extending into core uncovery and early core degradation (for example, hydrogen generation and transport). The output from our proposed NPA will include most of the variables in the control room and other computed variables that will be inaccessible to the reactor operator. The NPA will allow various operator actions so that their consequences can be studied quickly and efficiently. Personnel who are not extremely knowledgeable about either computer hardware or software could run the entire package through the extensive use of easily accessed menus, tables, and a touch panel. Color cathode ray tubes will display the output as a transient progresses.

An effective NPA will use a combination of computer software and hardware that can analyze a large variety of accidents of interest. For NRC use, the hardware could be based either on a Los Alamos computer (for example, a CDC 7600) with a dedicated link to one or more NRC locations, or on a dedicated, packaged system at an NRC site. In either case, we propose to supply the NRC with a well-tested user-oriented interactive output console using one or more color graphics terminals with hard-copy units. In the latter case, our proposed hardware configuration includes a small host computer driving an array processor. Disk drives will augment the memory and store most

of the I/O files. The core of the proposed software is a special version of TRAC-PF1/MOD1. If the NPA were constructed from scratch or from less proven algorithms and models, then verifying the effectiveness of the methods and models will require much development time and cost. Consequently, by building the NPA around TRAC, model development and assessment can be achieved faster and more efficiently at modest cost.

In addition to TRAC and the interactive graphics software, we will supply input decks for a wide variety of generic and specific operating reactors that can be modified by the user, an input preprocessor that will perform the modifications, and an online graphics processor that will contain the algorithms to drive the color graphics. If the NRC chooses the integral, packaged computing system, the array processor primarily will run TRAC whereas the host computer will perform the I/O functions.

We propose a staged, three-year development to produce a complete NPA. However, we wish to stress that a useful tool can be available almost immediately so that the NRC or other outside laboratories will benefit from the software even before the end of the first year. In the remainder of this proposal, we discuss the development of an NPA operating on a dedicated NRC computer, but we will note the differences between this proposal and the development schedule, capital equipment requirements, and operating costs for an NPA run on a Los Alamos computer.

A. Proposed First-Year Products

Throughout the first year, the NRC users can run problems using TRAC-PF1 and existing input decks by accessing a 9600-baud tie line to an open CDC 7600 computer at Los Alamos. Graphics and hard copy will be transferred over a dedicated telephone connection to existing or new NRC graphics terminals. Initially, because the main computer in Los Alamos will contain all of the graphics software, the transfer of information will be slow. The code will run faster than real time (depending on the number of users who are active and their assigned priority) but the final information will not be displayed as fast as possible.

By the end of the first year, a minicomputer (approximate cost $25 thousand) can be provided to the selected NRC site. This will allow graphics to be generated locally and effect an overall better than real-time

capability. Other outside users also could use this NPA version by purchasing color graphics terminals and touch panels and by running the graphics algorithms on local computers.

B. Proposed Second-Year Products

By the end of the second year, the NRC could have a system consisting of an NPA console using graphics terminals, including interactive operation through touch panels, and, if desired, the main host computer. Although the basic computation still would be performed on a Los Alamos CDC 7600 computer, the response will be faster because the NRC users will perform locally all of the output processing and much of the input manipulation.

A large variety of graphical displays for PWRs will be provided. A sample display is shown in Fig. 1. These displays, coupled with catalogs of input decks and output displays, should increase greatly the efficiency of the user. Touch panels will almost eliminate the requirement that information be typed into the terminals.

Also, by the end of this year, in collaboration with personnel from the TRAC-BWR program at the Idaho National Engineering Laboratory (INEL), we will add BWR models to TRAC-PF1 if this capability is desired by the NRC.

C. Proposed Third-Year Products

If the NRC desires a complete, packaged system running faster than real time, an array processor can be attached to the host computer. Los Alamos will modify the TRAC code to run efficiently on this computer combination. The BWR models will be tested and the final BWR and PWR input decks and output displays will be completed. Under this proposed program, we will supply the minimum number of input decks needed to perform generic analyses (for example, 3-loop Westinghouse, 4-loop Westinghouse). Separate input decks for specific operating plants developed in other programs can be adapted for use in the NPA. Thus, the complete NPA will be provided as a final product by the end of the third year, except for a reduced level of maintenance.

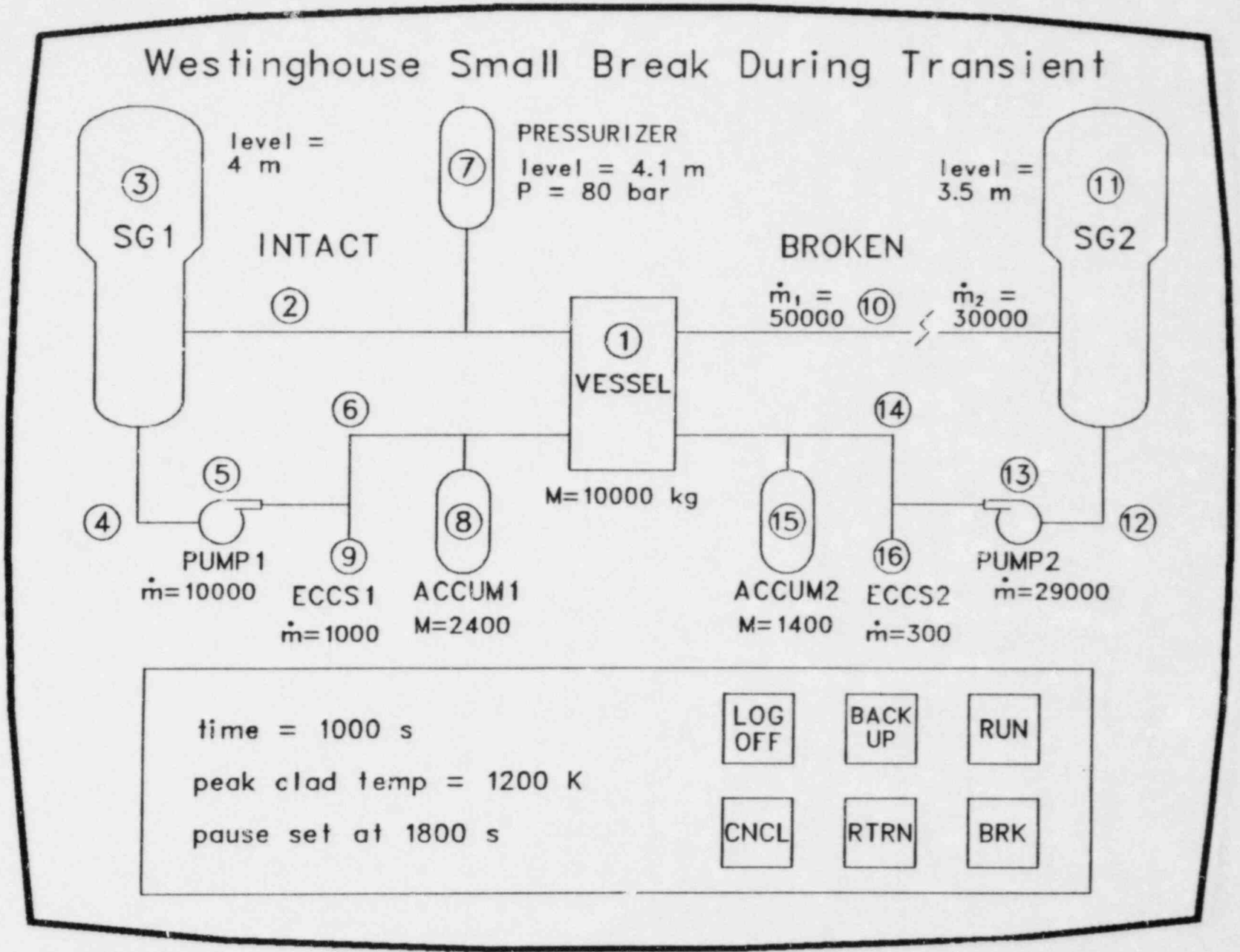

Fig. 1. Small-break transient display.

NUCLEAR PLANT DATA BANK
AND
INPUT DECK PREPARATION

Work Performed by

TECHNOLOGY DEVELOPMENT OF CALIFORNIA, INC.
3990 FREEDOM CIRCLE
SANTA CLARA, CALIFORNIA 95054

SCOPE

The Nuclear Plant Data Bank is a computer-based system that organizes a nuclear power plant's technical data, providing mechanisms for data storage, retrieval and computer-aided engineering analysis. It has the specific objective to describe thermohydraulic and containment systems in order to support:

- Rapid information retrieval and display
- Thermohydraulic analysis modelling

The current application is supports thermohydraulic analysis of reactor safety systems, including all fluid passages and containment structures.

KEY FEATURES

The system operates so that NO computer programming knowledge or skill is required by the user. Therefore, users of the system can focus on their data handling and analysis problems (Figure 1). A user only needs to know what data-oriented results he wants to accomplish, and the Nuclear Plant Data Bank system walks him through the steps to reach his goal.

The Nuclear Plant Data Bank system fully automates the storage and retrieval of a large amount of technical data, as well as automates technical analysis based on this data. This system combines the benefits of a structured data base system and computer-aided modelling with links to large-scale computer codes for engineering analysis, as well as graphical display applications (Figure 2).

Specific features are:

- Organization and storage of thermohydraulic data
- Ease in locating specific data items
- Graphical and tabular display capabilities
- Interactive model construction capability
- Organization and display of model input parameters
- Input deck construction and execution of analysis programs

OVERALL DESIGN

The Nuclear Plant Data Bank system consists of the following five major subsystems:

- Structured data base
- Data display system
- Model input preparation system
- Data input system
- Analysis program interfaces

The relationship of these five subsystems is illustrated by Figure 3 and described in the following sections.

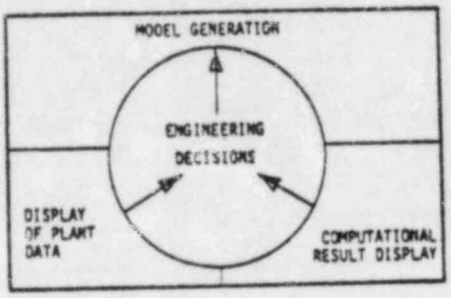

FIGURE 1. USERS PERCEPTION OF THE NUCLEAR PLANT DATA BANK

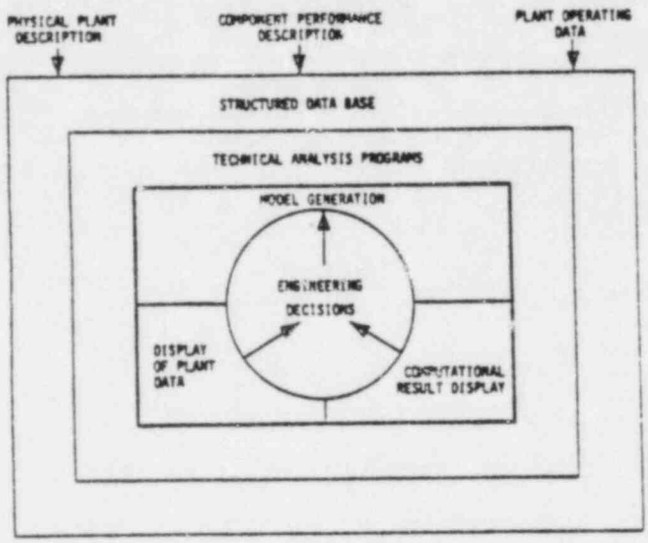

FIGURE 2. OVERALL NUCLEAR PLANT DATA BANK SYSTEM

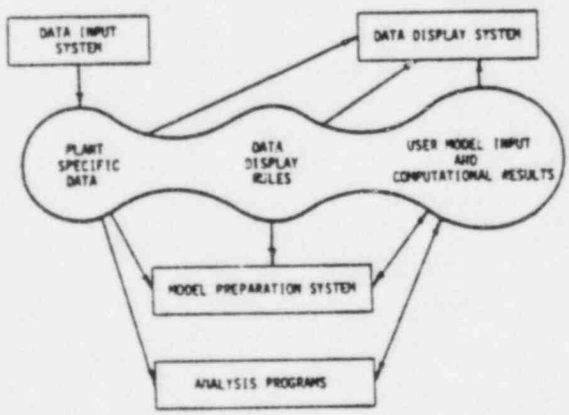

FIGURE 3. NUCLEAR PLANT DATA BANK ARCHITECTURE

STRUCTURED DATA BASE

The structured data base subsystem uses a hierarchic index. The uppermost level of the index is the name of the nuclear reactor power plant; and the level immediately under that consists of summary information for the previous level, categories for the major plant subsystems and categories for model input to specific analysis programs (Figure 4). Within each of the major categories, data is stored for the physical plant descriptions, plant system performance and plant operating parameters. This data is stored in sufficient detail to perform state-of-the-art reactor safety analysis.

Data is organized by "engineering" systems so that engineers can rapidly locate and use the data in ways already familiar to them. An important element of user convenience is that screen displays can be obtained simply by positioning a horizontal cross-hair over the hierarchical name of the item to be displayed and hitting the "SPACE" key followed by the "RETURN" key. This cross-hair approach allows one to proceed further from the top of the hierarchy to retrieve greater detail about the nuclear reactor power plant. It also allows one to return to the top levels of the hierarchy as desired. For example, by placing the cross-hair through the name element "RXCOOL" illustrated in Figure 4, one obtains a display of the data structure for the reactor cooling system (Figure 5). The reactor cooling system index indicates that the following types of data are available:

INFO	Summary data
SKETCH	System process flow diagram
OPER-TH	Operating plant parameters (temperature, pressure, etc.)
components	Detailed technical data about individual components
MODEL	Capability to interactively generate an analysis model

Greater detail can be obtained by using the cross-hair to select a specific component. Figure 6 illustrates the hierarchic index that results when detail is required regarding the reactor vessel (selection of VESSEL by the cross-hair). Selection of the D.ZION-1.RXCOOL.VESSEL hierarchic index displays sublevel selections which will result in the display of technical information. The number of levels varies from index branch to index branch, depending upon the intrinsic complexity of the engineering system being described. Note that summary information, a process flow diagram, component technical data, and modelling capability are available just as they were at the preceeding index level. Because the same scheme is used throughout the data structure, engineering users are expected to have little difficulty in locating the information they desire.

```
D.ZION-1.INFO
        .RXCOOL
        .SECOND
        .ESAFETY
        .CONTAIN
        .AUXPOWER
        .TRAC-PD2
        .RELAP5
```

FIGURE 4. TOP OF THE HIERARCHIC INDEX FOR ZION-1

HIERARCHIC STRUCTURE FOR THE
REACTOR COOLING SYSTEM

```
D.ZION-1.RXCOOL.INFO
                .SKETCH
                .MODEL
                .OPER-TH
                .PUMP
                .VESSEL
                .CORE
                .STMGEN
                .PIPESYS
                .PRESSURE
                .VALVE
```

FIGURE 5. REACTOR COOLING SYSTEM HIERARCHIC INDEX

```
D.ZION-1.RXCOOL.VESSEL.SKETCH
                      .MODEL
                      .INFO     .ELEV
                                .DIM
                                .VOLUMES
                                .DESIGN
                      .CR-DRIVE.INFO
                      .US-PLATE.DRAWING
                                .INFO
                      .UC-PLATE.DRAWING
                                .INFO
                      .T-SHIELD.INFO
                      .BARREL   .INFO
                      .FORMER   .INFO
                      .BAFFLE   .INFO
                      .LC-PLATE.DRAWING
                                .INFO
                      .D-PLATE  .DRAWING
                                .INFO
                      .SUP-CAST.DRAWING
                                .INFO
                      .OUT-NOZZ.INFO
                      .IN-NOZZ  .INFO
                      .SLICE.   .DRAWING
                      .OPER-TH  .START-3
                                .START-85
                                .RATED
```

FIGURE 6. REACTOR VESSEL HIERARCHIC INDEX

DATA DISPLAY SYSTEM

Data is maintained in the Data Bank according to the hierarchic index previously described. This data may be operated upon by the data display system to generate video screen displays. In some cases, the same data can be operated upon by more than one display program. For example, a tabular presentation and a graphical representation of the same data are given by Figures 7 and 8. It is important to understand that data, not displays of data, are maintained in the data structure and that displays are generated from these data. The following types of displays are currently generated:

Data Tables	Screen displays of data (e.g., Figure 7)
Sketches	Displays of qualitative data (e.g., Figure 8)
Plots	Graphic interpretation of tabular data (linear, logarithmic, contour, perspective - Figures 9, 10 and 11)
Piping Isometrics	Scaled isometric drawings at user-selected rotation angles (e.g., Figure 12)
Planar Geometry	Slices through three-dimensional geometry (e.g., Figure 13)

MODEL INPUT PREPARATION SYSTEM

The display subsystem, in conjunction with the structured data base subsystem, provides the capability to generate analysis models in a very short time span and with very little labor. This represents a major step in improving one's ability to respond to an incident. Not only can models be created from scratch with this system, but the model decisions are stored in such a manner that an engineer other than the original modeller can modify the input in a safe manner in a very short time. Graphic displays are used extensively for this purpose. The two major modelling capabilities are:

- Vessel modelling suitable for TRAC or RELAP
- Piping fluid dynamics modelling for TRAC or RELAP

The data needed to generate models is maintained in the data structure, and programs operate upon this data to generate the models. The engineer must still exercise judgement regarding engineering model decisions. Figures 14 and 15 illustrate the type of screen displays currently used for the vessel and piping models, respectively. Note that the piping model display provides scaled lengths and elevations and is also useful for obtaining an understanding of pipe systems.

Much of the TRAC capability for generic modelling is in the final development phase. Current plans anticipate initial RELAP5 capability in the spring of 1983.

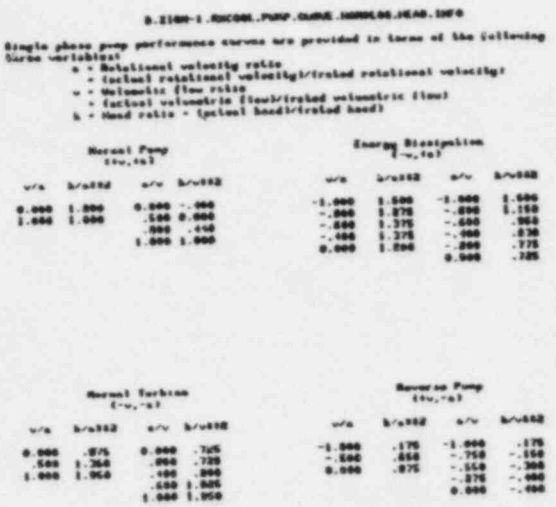

FIGURE 7. TABULAR DATA DISPLAY FOR MAIN COOLANT PUMP

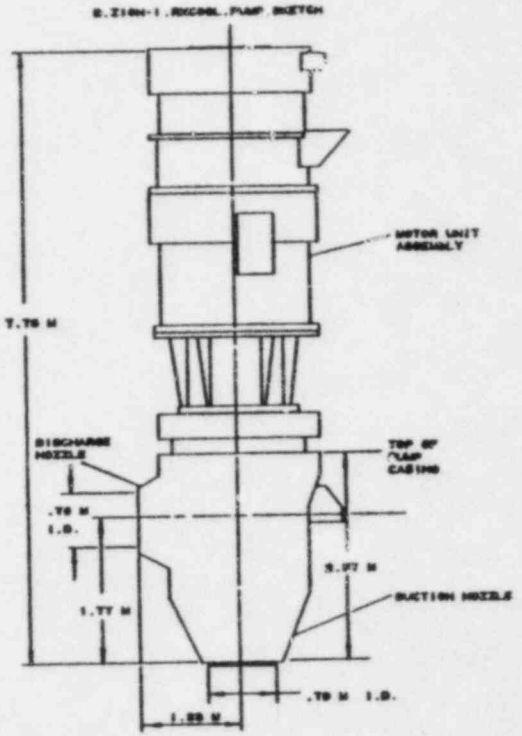

PRIMARY COOLANT PUMP

FIGURE 8. SKETCH OF MAIN COOLANT PUMP

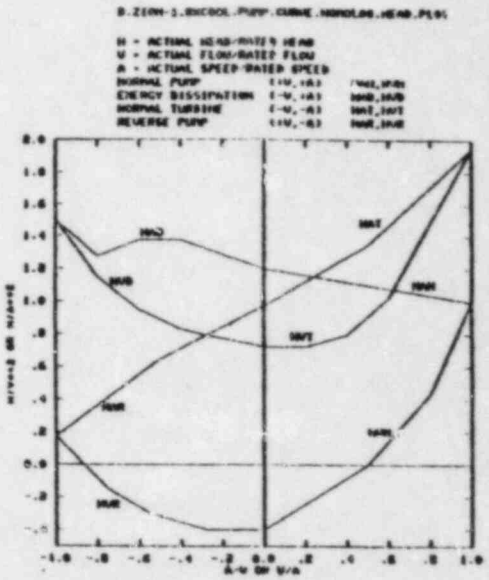

SINGLE PHASE HEAD CURVE

FIGURE 9. PLOT OF DATA SHOWN IN FIGURE 7

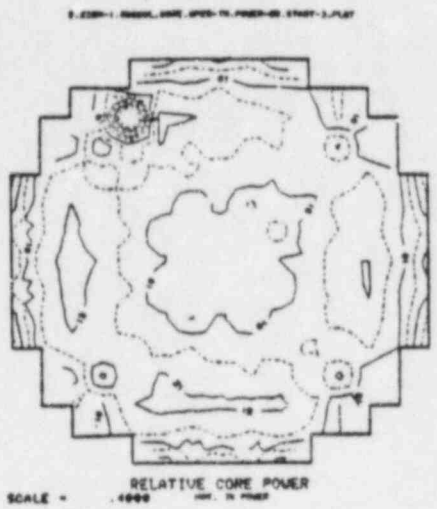

FIGURE 10. CONTOUR PLOT -- POWER DISTRIBUTION

FIGURE 11. PERSPECTIVE PLOT -- POWER DISTRIBUTION

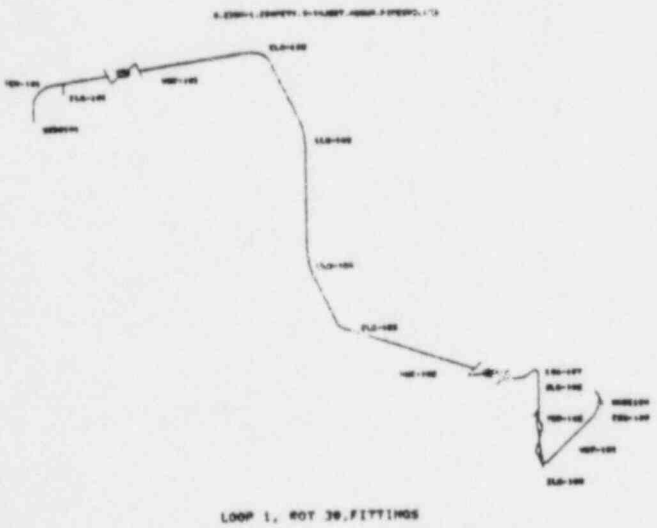

FIGURE 12. ACCUMULATOR PIPING ISOMETRIC

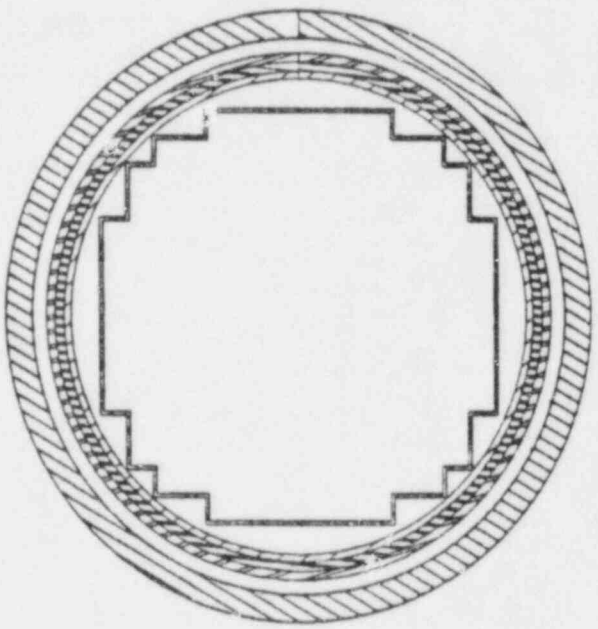

FIGURE 13. VESSEL SLICE AT CORE MIDPLANE

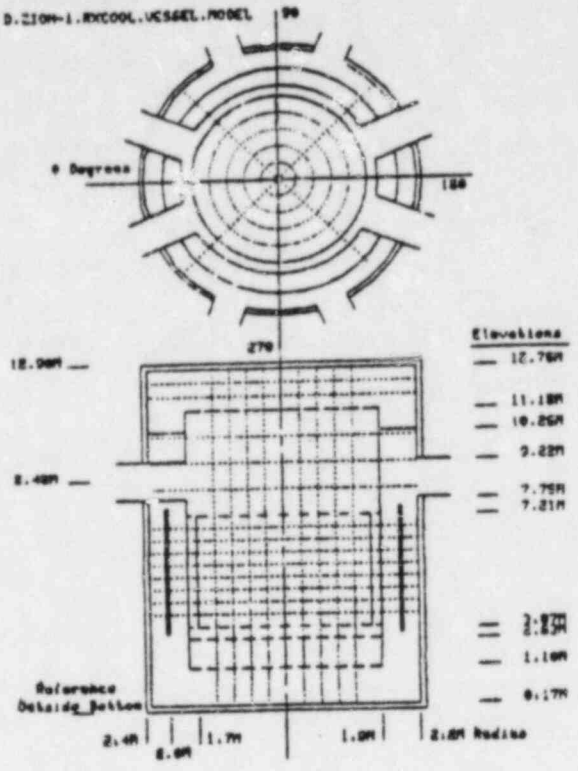

FIGURE 14. VESSEL MODEL INTERACTIVE DISPLAY

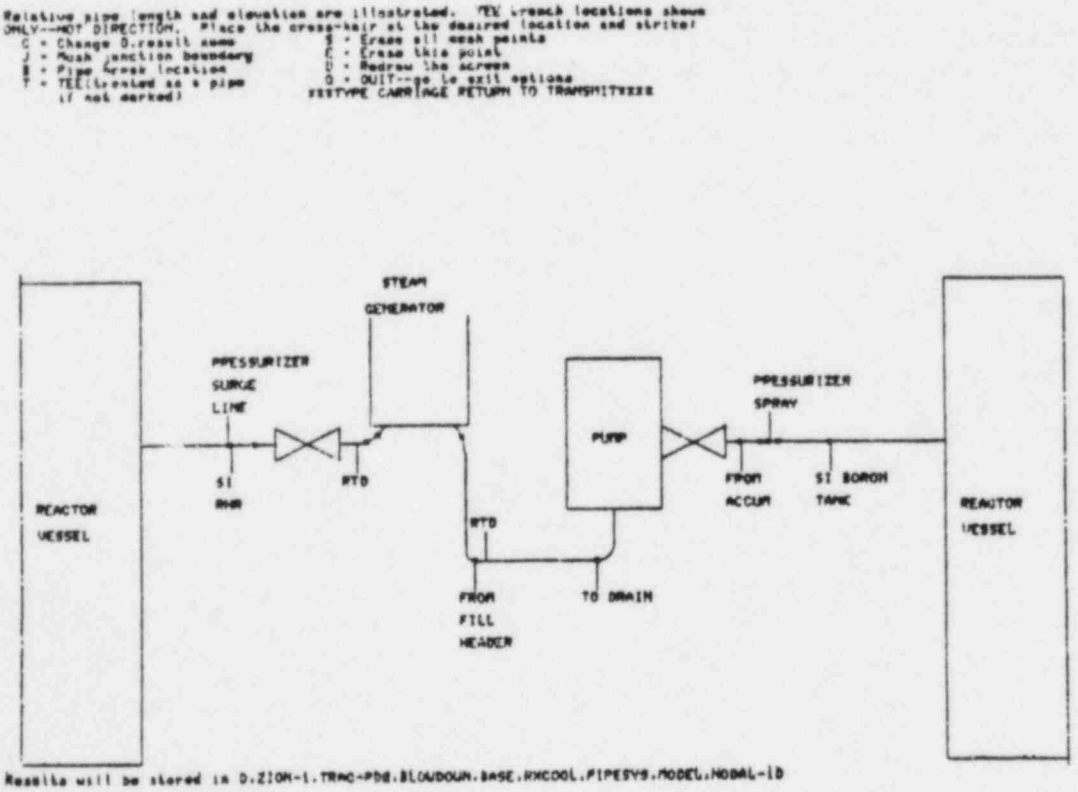

FIGURE 15. PIPING MODEL INTERACTIVE DISPLAY

DATA ENTRY SUBSYSTEM

Four major categories of data have been entered into the Nuclear Plant Data Bank, to date. These categories are:

Tabular Data	Entered from "blank" forms
Sketches	Entered via digitizing tablet
Geometry Data	Entered by a draftsman
Piping Data	Entered by a draftsman

Experience has been obtained through the entry of data for the ZION-1 power plant. TDC acknowledges the cooperation of Commonwealth Edison Company, especially Dr. W. Naughten, in providing assistance in obtaining the desired information.

ANALYSIS PROGRAMS

A number of analysis programs were reviewed to insure that the Nuclear Plant Data Bank contained sufficient information to support their requirements for best-estimate calculations. These programs were:

TRAC	RELAP	RAMONA
RETRAN	IRT	COBRA
BEACON	CONTEMPT	

The development of the interface program to TRAC is nearing a major milestone, and use is anticipated in the near future. A very complete and specific interface to RELAP5 is proposed as the next major activity, with first applications planned for the spring of 1983.

The Nuclear Plant Data Bank design is open-ended and can readily be extended to accommodate the data required for other analysis programs. The focus of the current development has been for thermohydraulics in order to provide a limited scope of high priority.

FUTURE PLANS

Planning for the next fiscal year is focused on an operational RELAP5 interface, along with the entry of plant-specific data currently available to the USNRC. This program is intended to supply the basic plant descriptions needed to support the plant analyzer project.

CALCULATIONS OF PRESSURIZED THERMAL SHOCK TRANSIENTS IN B&W PLANTS

B. Bassett
N. S. DeMuth
J. L. Elliott

Los Alamos National Laboratory
Los Alamos, New Mexico

Analysis to help determine the risk of pressurized thermal shock (PTS) to the reactor vessel is in progress for the Oconee-1 B&W power plant, using the Transient Reactor Analysis Code (TRAC)[1]. Extensive effort has been put into developing a TRAC model, and production runs are now beginning.

The concern over PTS arises because the material properties of the vessel wall change after several years of irradiation[2]. The vessel wall becomes embrittled and its nil-ductility temperature (NDT) increases. If during an accident, cold liquid from the high-pressure injection system cools the vessel wall below the NDT and the system subsequently repressurizes, the possibility exists that defects could be initiated or propagated in the vessel wall.

Because the risk of initiating or propagating flaws in the vessel wall depends on the coupling of the thermal stresses produced by overcooling with the mechanical stresses from repressurization, detailed thermal-hydraulic calculations are required. Modeling both the primary and secondary systems of the the Oconee-1 plant is necessary to properly analyze the PTS issue. The steam generator secondary-side inlet conditions directly affect primary temperature, pressure, and the emergency core coolant injection. Secondary-side inlet conditions are highly dependent on pump operation and the termination of the extracted steam supply to the feedwater heaters.

The primary-side model of the Oconee-1 plant includes a three-dimensional representation of the reactor pressure vessel. The six azimuthal segments allow a vessel connection for each of the hot legs and cold legs. The vessel model has eight axial levels, with one for the lower plenum, four for the core, two to represent the upper plenum, and one to model the upper head. The vessel is divided at the inner downcomer wall into two radial rings.

The B&W plant and the TRAC model have two loops, with one hot leg, one steam generator and two cold legs per loop. A detailed model of the steam generators includes the aspirated feedwater flow, steam exit annulus, and an elevated port for injection of emergency feedwater. The emergency core cooling flow is dependent on primary pressure with slightly different flowrates for each loop as in the actual plant. Accumulator flow is regulated by a static check valve.

On the secondary side, the main steam lines from each steam generator to the turbine stop valves are modeled. The turbine bypass lines lead to the condenser, which is input as a pipe with a constant temperature heat sink. The condensate collects in the hotwell.

The hotwell and condensate-booster pumps deliver the condensate to the feedwater heaters. These heaters are modeled as one-cell pipes with three heat-conduction nodes in the pipe wall. The first node is to model the metal walls of the heat exchange tubes, and the outer two nodes model the volume of saturated water on the shell side of the heaters. A volumetric heat source is included in the third node to account for the extracted steam supply until the turbine is tripped. The liquid entering the main feedwater flow from the shell side of the heater is taken into account in the model.

A model of the B&W Integrated Control System (ICS) used at the Oconee-1 plant is included in the TRAC model. The ICS monitors the primary flows and temperatures to determine the feedwater demand. The ICS regulates the main and startup flow control valves, the main feedwater pumps, and the turbine bypass valves.

Several overcooling transients have been identified, and additional transients will be specified after initial results are evaluated. The initial transients include a main steam line break with a delay in isolating the affected steam generator, a small-break LOCA (full-open failure of pressurizer relief valve) with failure of the ICS to throttle main feedwater flow, and a turbine trip transient with steam generator overfeed.

REFERENCES

1. Safety Code Development Group, "TRAC-PF1: An Advanced Best-estimate Computer Program for Pressurized Water Reactor Analysis," Los Alamos National Laboratory draft report.

2. R. C. Kryter, et al, "Evaluation of Pressurized Thermal Shock," NUREG/CR-2083, ORNL TM-8072, Oak Ridge National Laboratory (October 1981).

REACTOR SAFETY ANALYSIS GROUP
ENERGY DIVISION
LOS ALAMOS NATIONAL LABORATORY

CALCULATIONS OF PRESSURIZED THERMAL SHOCK TRANSIENTS IN B & W PLANTS

TENTH WATER REACTOR SAFETY
RESEARCH INFORMATION MEETING
NUCLEAR REGULATORY COMMISSION
WASHINGTON, D.C.

OCTOBER 14, 1982

OVERCOOLING TRANSIENTS AS PRECURSORS TO PRESSURIZED THERMAL SHOCK

SEVERE OVERCOOLING -

- MAIN STEAM LINE BREAK
- TURBINE BYPASS VALVE FAILURE
- TURBINE TRIP WITH RUNAWAY FEEDWATER
- SMALL-BREAK LOCA IN HOT LEG

REPRESSURIZATION -

- HIGH PRESSURE INJECTION

LOS ALAMOS

THERMAL-HYDRAULIC ASPECTS OF PRESSURIZED THERMAL SHOCK

VESSEL THERMAL RESPONSE -

- PRIMARY AND SECONDARY ENERGY LOSSES
- FORCED OR NATURAL CONVECTION (LOOP) FLOWS
- INJECTION OF EMERGENCY CORE COOLING WATER
- VENT VALVE BEHAVIOR
- HEAT TRANSFER FROM DOWNCOMER WALLS
- THERMAL MIXING IN COLD LEGS AND DOWNCOMER

PRIMARY REPRESSURIZATION -

- CONDENSATION IN PRESSURIZER, HOT-LEG CANDY CANES, AND VESSEL HEAD
- HIGH PRESSURE INJECTION FLOW CAPACITY

LOS ALAMOS

NUMERICAL SIMULATIONS WITH TRAC ACCOUNT FOR IMPORTANT THERMAL-HYDRAULIC CHARACTERISTICS

TRAC-PF1 CODE

- TWO-FLUID WITH NON EQUILIBRIUM CONSTITUTIVE RELATIONS
- THREE-DIMENSIONAL VESSEL MODEL
- WALL HEAT TRANSFER
- IMPROVED BREAK FLOW MODEL
- CONTROL SYSTEM
- IMPROVED CONDENSATION MODELS

PLANT MODEL

- 3-D VESSEL WITH INTERNAL VENT VALVES AND SPLIT COLD LEGS
- STEAM GENERATOR WITH ASPIRATED FEEDWATER FLOW
- COMPLETE SECONDARY LOOP
- MODEL OF INTEGRATED CONTROL SYSTEM

LOS ALAMOS

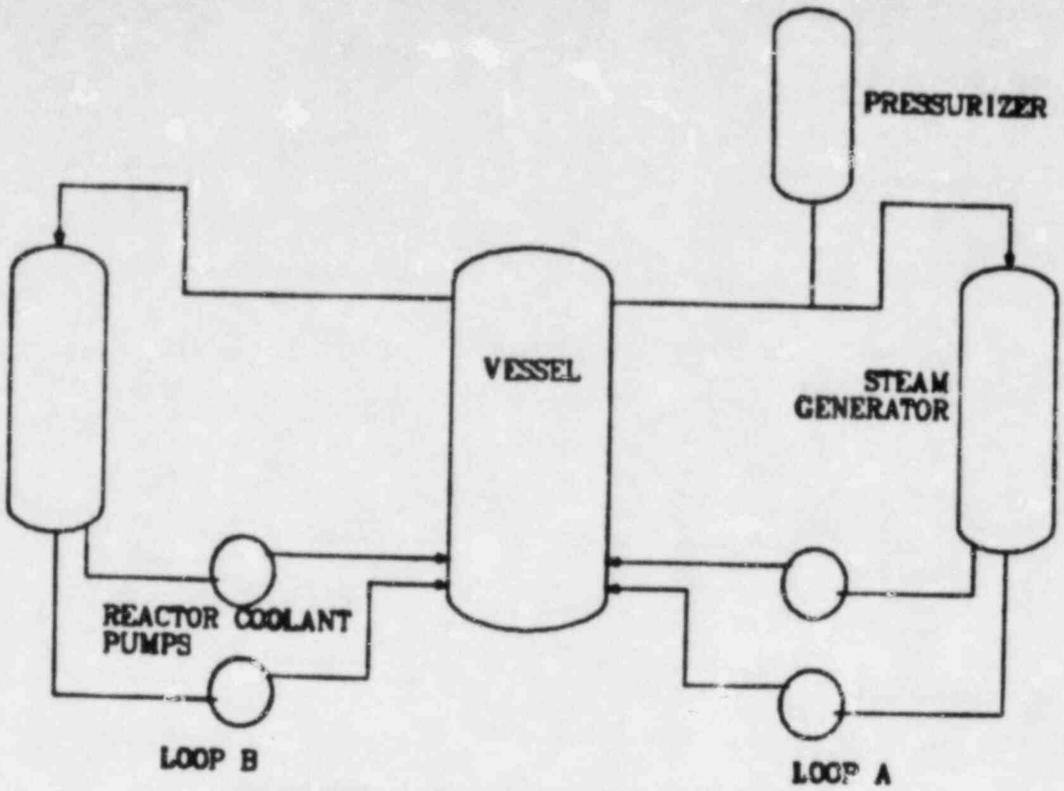

OCONEE-1 PRIMARY SCHEMATIC

Los Alamos

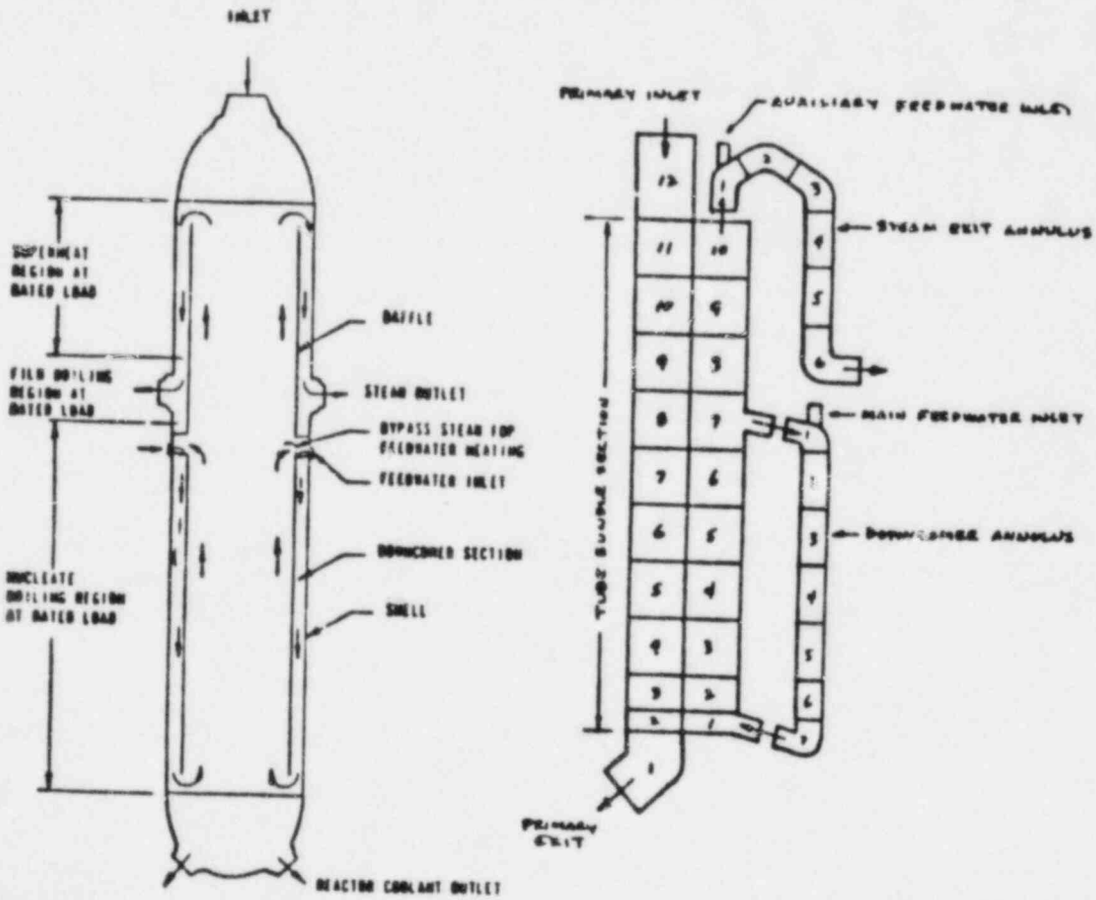

ONCE-THROUGH STEAM GENERATOR MODEL

Los Alamos

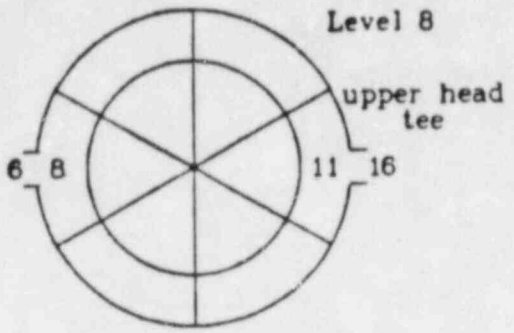

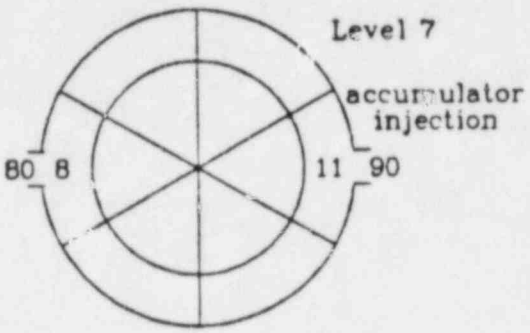

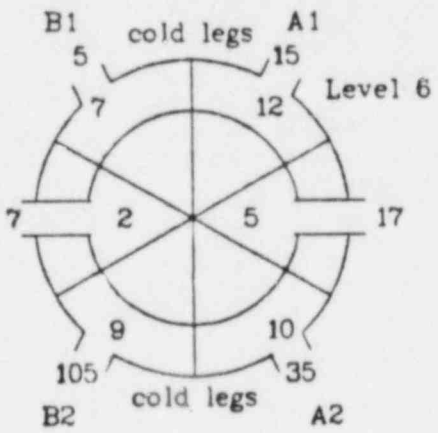

OCONEE – 1 REACTOR VESSEL

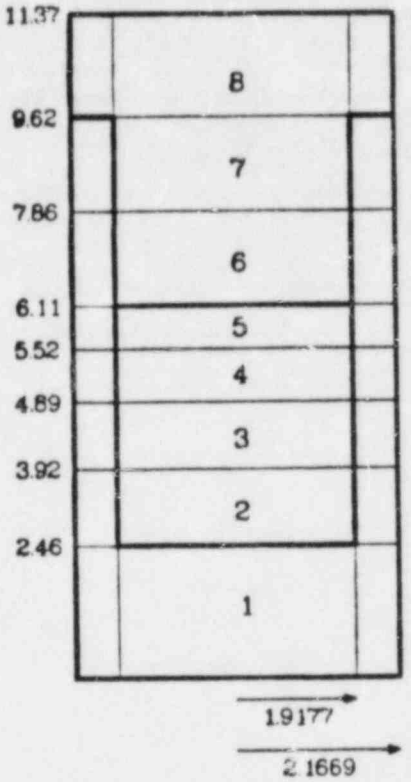

Los Alamos

TRAC SYSTEM SCHEMATIC
FOR B&W PRESSURIZED WATER REACTOR

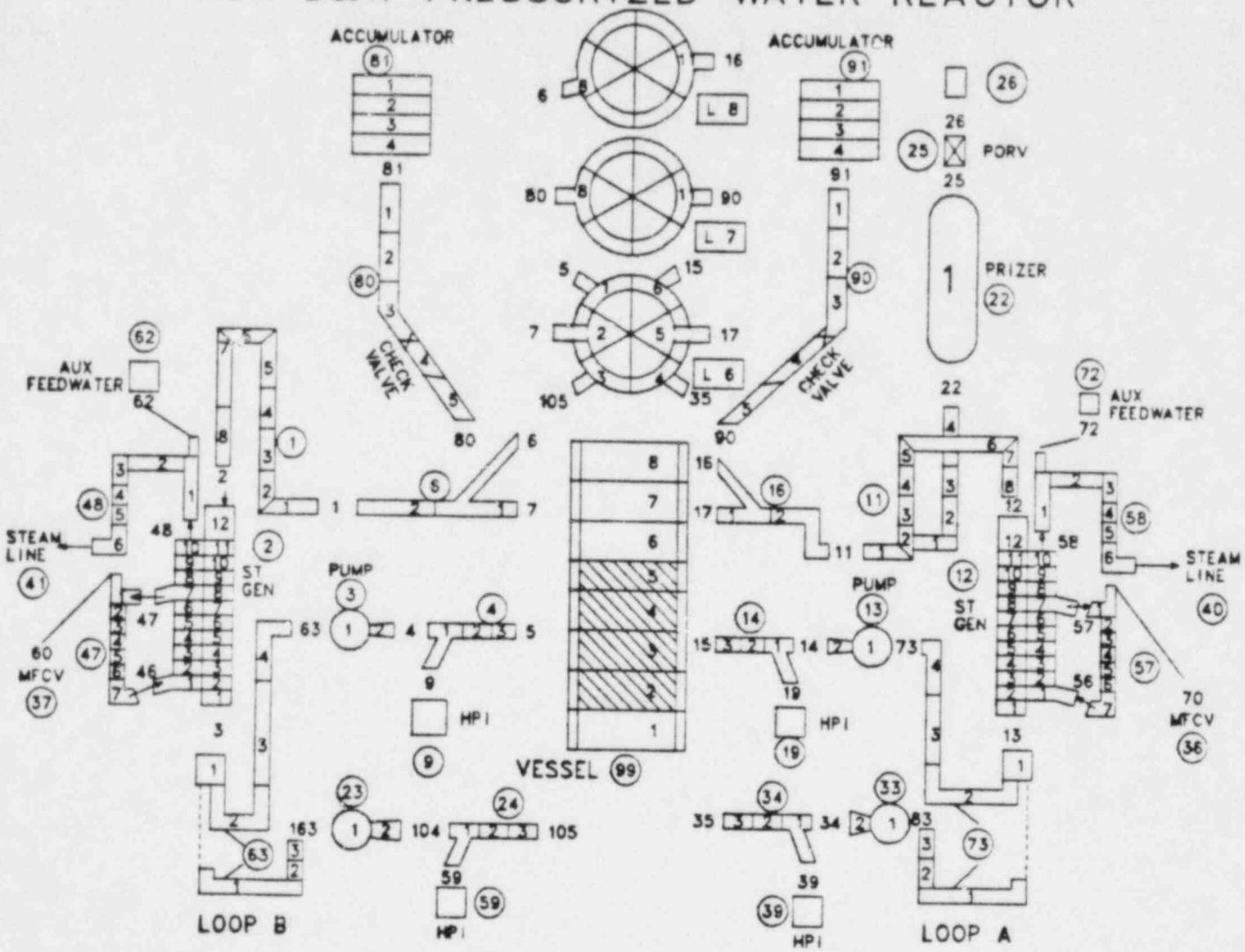

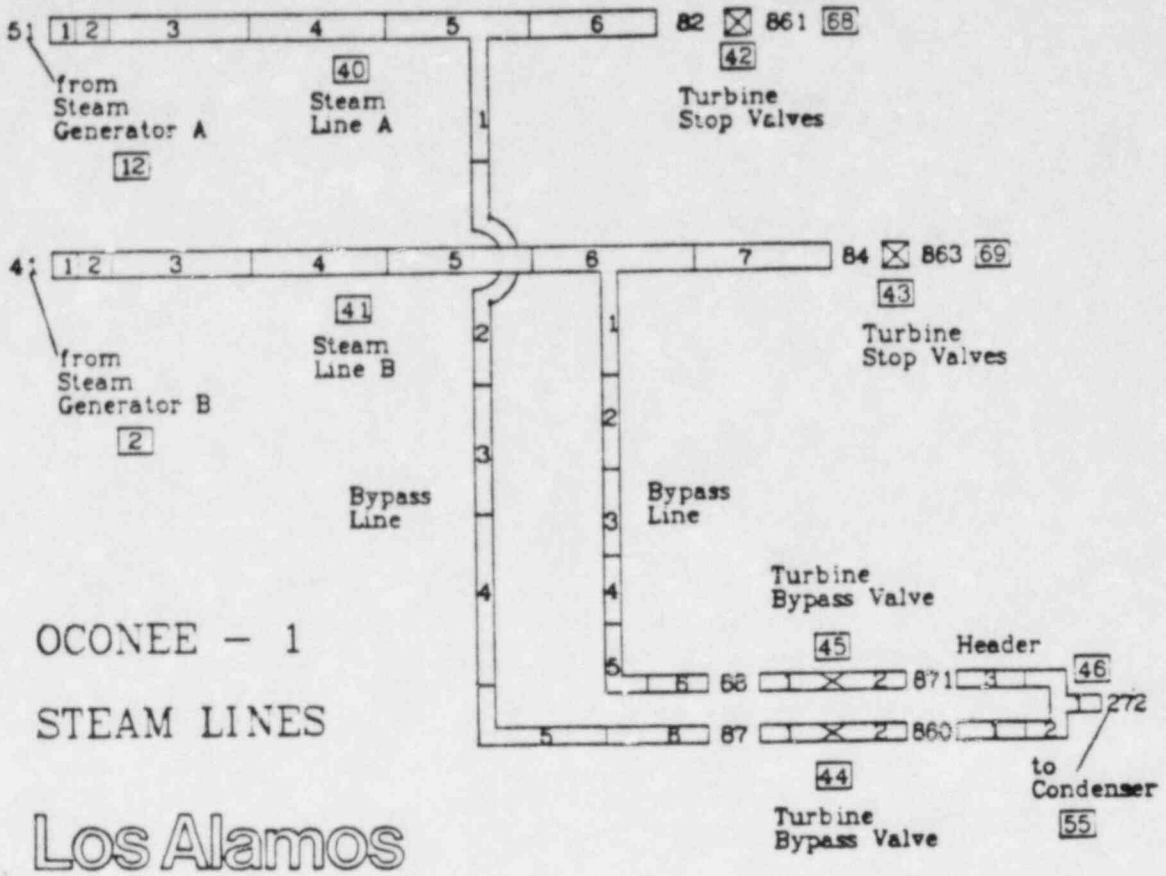

OCONEE – 1

STEAM LINES

Los Alamos

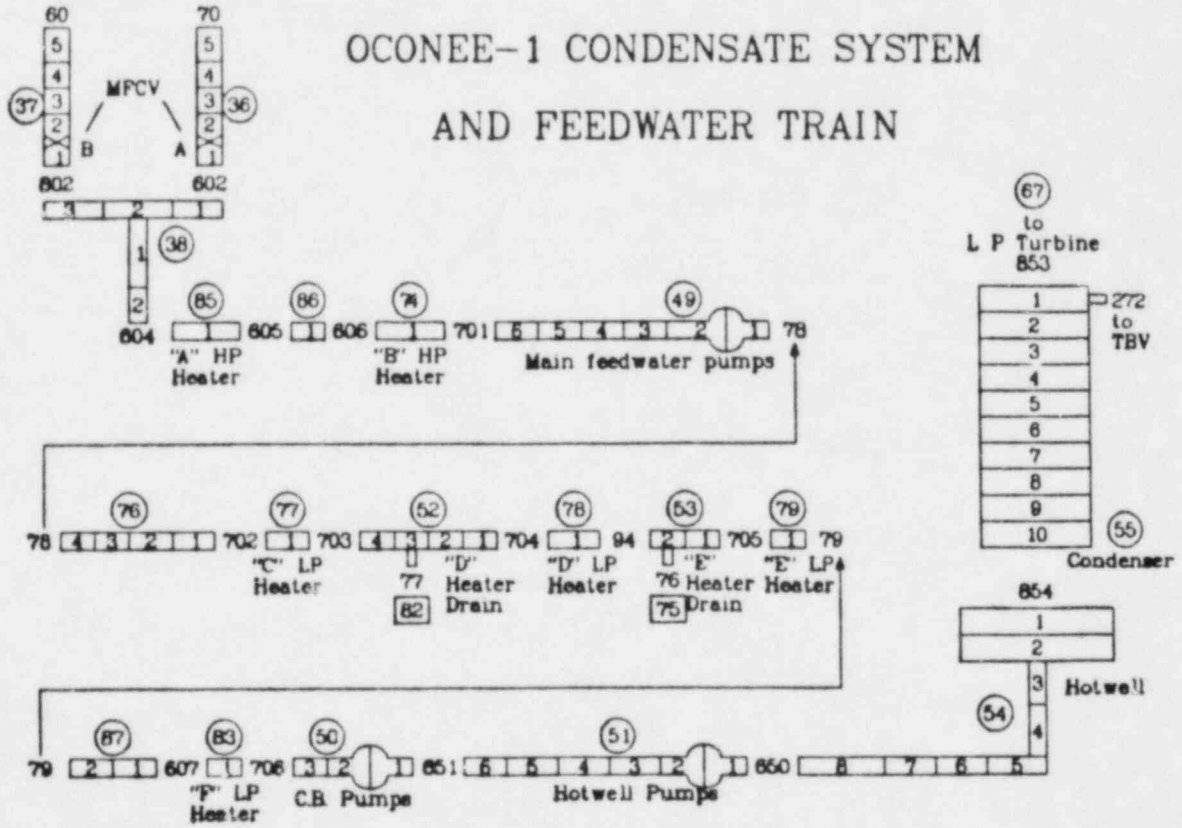

OCONEE–1 CONDENSATE SYSTEM

AND FEEDWATER TRAIN

INTEGRATED CONTROL SYSTEM

IN THE ICS, THE REACTOR, STEAM GENERATORS, AND TURBINE-GENERATOR ARE COUPLED USING FEED FORWARD CONTROL SIGNALS TO ACHIEVE FAST LOAD CHANGE CAPABILITY WHILE MAINTAINING TIGHT CONTROL OVER STEAM PRESSURE AND OTHER IMPORTANT NSSS PARAMETERS.

LOS ALAMOS

OCONEE-1 MODEL

RESPONDS TO EARLY CRITICISMS OF PLANT AND TRANSIENT MODELING

INCORPORATES MODELS FOR :

(1) THREE-DIMENSIONAL VESSEL WITH INTERNAL VENT VALVES

(2) ASPIRATED-FLOW STEAM GENERATOR

(3) COMPLETE SECONDARY LOOP

(4) INTEGRATED CONTROL SYSTEM

USES FAST-RUNNING, TWO-FLUID TRAC-PF1 WITH IMPROVED CONDENSATION AND BREAK FLOW MODELS

LOS ALAMOS

RELAP5 CALCULATIONS FOR A BABCOCK AND WILCOX PLANT OF PRESSURIZED THERMAL SHOCK TRANSIENTS[a]

A. C. Peterson

EG&G Idaho, Inc.

The possibility of reactor vessel failure due to a severe pressurized overcooling event has been identified as an unresolved safety issue (USI) by the Nuclear Regulatory Commission (NRC). This USI has been identified by the NRC as Task A-49 "Pressurized Thermal Shock." In support of the resolution of the pressurized thermal shock USI, calculations of the thermal-hydraulic conditions during selected overcooling transients for the Oconee 1 pressurized water reactor (PWR) were performed using the RELAP5 computer code. The Oconee 1 PWR is a Babcock and Wilcox designed nuclear steam supply system.

The RELAP5 model of the Oconee PWR consisted of detailed modeling of the primary system, the secondary system including the feed train from the condenser hot well to the steam generator inlet, and the integrated control system (ICS). The total thermal-hydraulic model of the primary and secondary system contained 220 volumes and 208 heat structures. The unit load demand, integrated master, feedwater control, and reactor control components of the ICS were modeled by 220 control variables.

The MOD1.5 version of the RELAP5 computer code was used for the calculations. The RELAP5/MOD1.5 computer code is an interim version of the RELAP5/MOD2 computer code and was developed for use by the NRC and NRC contractors.

---

a. Work supported by the U.S. Nuclear Regulatory Commission, Office of Nuclear Regulatory Research under DOE Contract No. DE-AC07-76ID01570.

The detailed scenarios that were calculated were developed by the Oak Ridge National Laboratory (ORNL) as part of their responsibility in the pressurized thermal shock integration study. The transients that were calculated were a main steam line break, a steam generator overfeed, and a small hot leg loss-of-coolant accident (LOCA). Four additional transients will be calculated when they are identified by ORNL.

Main Steam Line Break

The main steam line break was initiated from normal 100% power operating conditions by a 34 in. main steam line break coincident with a reactor trip. The ICS and plant protection systems on the hot well, the condensate booster, main feedwater, and emergency feedwater pumps (EFW) functioned as designed. The operator actions during the transient were to trip the reactor coolant pumps 30 s after high pressure injection initiation (HPI), isolate the feedwater to the affected steam generator 10 min after the main steam line break, and restart one reactor coolant pump in each loop 10 min after attaining 50°F subcooling in the hot legs.

The calculations showed that following the main steam line break, the primary system depressurized due to the increased density of the primary system. This increase results from the reactor trip and increased cooling of the primary by the affected steam generator. HPI was initiated at 23 s and the reactor coolant pumps were tripped at 53 s. The pressurizer was water solid at 836 s and the power operated relief valve (PORV) began to cycle to relieve pressure. One reactor coolant pump was restarted in each loop at 963 s. The lowest fluid temperature in the downcomer was 405°F and occurred at 963 s when one reactor coolant pump in each loop was restarted. The fluid temperature immediately increased to 453°F following the initial drop when the pump was started. The calculation was stopped at 1434 s with the downcomer fluid temperatures increasing and the primary system pressure near the PORV setpoint of 2465 psia.

Steam Overfeed

The steam generator overfeed transient was initiated from normal 100% power operating conditions by a reactor and turbine trip. The turbine stop valves closed and the turbine bypass valves opened. In this scenario, the ICS failed to run back the main feedwater flow, therefore, full main feedwater flow was continued. The plant protection system on the hot well, the condensate booster, the main feedwater, and the emergency feedwater pumps functioned as designed. The steam generator high-level trip fails in this scenario.

The calculations showed that the main feedwater pumps tripped at 4 s due to low suction pressure. At 18 s, the turbine and motor driven EFW system was initiated due to low pressure at the main feedwater pump discharges. After an initial decrease in the secondary level, the levels begin to increase at 250 s due to flow from the EFW system. The steam generators were full at 1270 s. The primary system pressure increases to the PORV setpoint at 1740 s. The lowest fluid temperature in the downcomer was 450°F and occurred at 2800 s.

Small Hot Leg LOCA

The small hot leg LOCA was initiated from normal 100% power operating conditions by a 1.0 in. break at the top of the pressurizer. In this scenario, the ICS fails to run back the main feedwater pumps.

The calculations showed that the reactor tripped at 108 s due to low primary system pressure. The system voided with the minimum mass in the system at 372 s, however, the core was covered. The system refilled by HPI coolant and the pressurizer was water solid at 680 s. The highest pressure in the primary system was 1730 psia. The calculation was terminated at 1200 s with the system pressure stable at 1710 psia and the downcomer fluid temperature decreasing slowly. The downcomer fluid temperature 7200 s after the initiation of the break was estimated to be 520°F and the lowest temperature attained.

In conclusion, for the scenarios selected and calculated with the RELAP5 computer code, the lowest downcomer fluid temperature was 405°F. Preliminary analysis indicates that the transients calculated would not cause severe thermal shock to the reactor vessel.

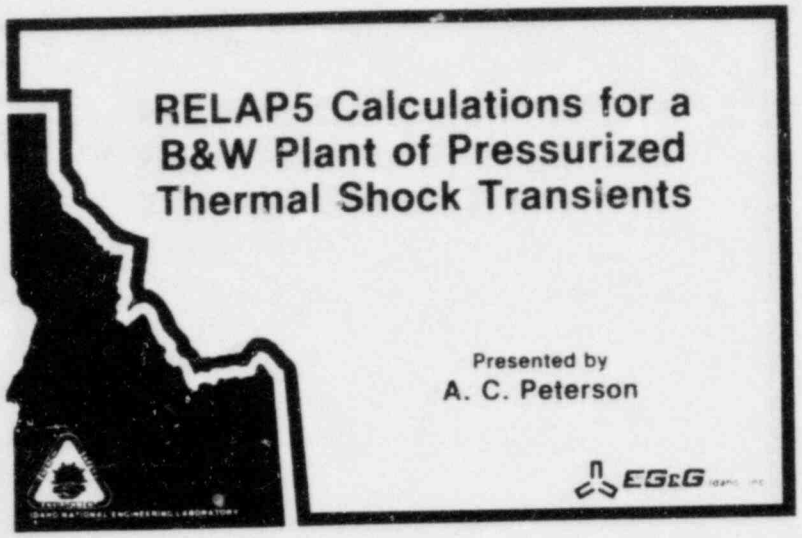

Outline

- Objective of calculations
- RELAP5 model
- Calculation matrix
- Preliminary results
- Preliminary conclusions

S2 10 592

Objectives of Calculations

- Support resolution of unresolved safety issue
  - Pressurized thermal shock (A-49)
    - Provide thermal hydraulic results of selected overcooling transients in Oconee-1 Pressurized Water Reactor

S2 10 593

RELAP5 Model

- Reactor vessel
- Loops
- Feedtrain
- Integrated control system

S2 10 590

Reactor Vessel

- Downcomer
- Core
- Core-by-pass
- Inlet annulus to upper plenum leakage
- Vent value
- Heat structure

S2 10 591

Reactor Vessel Model

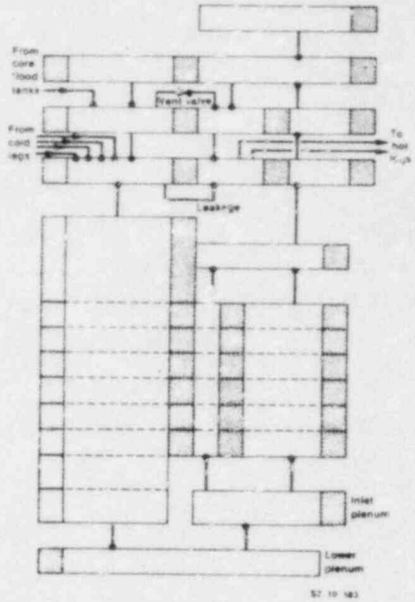

S2 10 583

Loops

- Hot leg piping with "candy cane"
- Two pumps and piping in cold leg
- Pressurizer
- Once-through steam generator
  - — Main feedwater
  - — Auxillary feedwater
  - — Aspirator flow
- Heat slabs on all components

S2 10 584

Loop Model

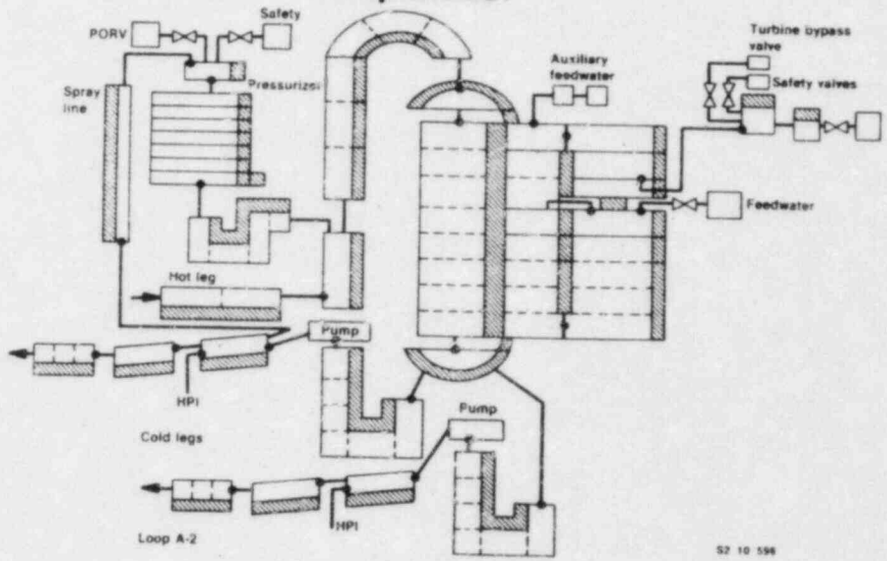

S2 10 598

Feed Train

- Pumps
  - Hotwell
  - Condensate booster
  - Two main feedwater pumps
- Heaters
  - Low pressure
  - High pressure
- Heater drains
- Start up and main feedwater control valves
- Heat structure
  - Heaters
  - Piping

S2 10 587

Feedtrain Model

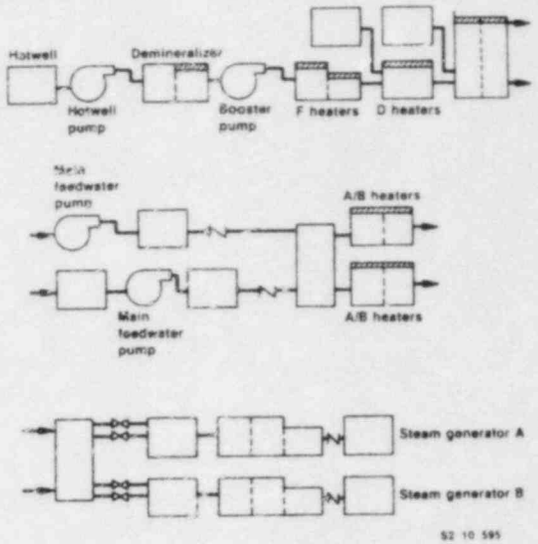

S2 10 595

Calculation Matrix

- Main steamline break
- Steam generator overfeed
- Small hot leg break LOCA
- 4 additional transients to be specified

S2 10 589

Integrated Control System

- Components
  - Unit load demand
  - Integrated master
  - Feedwater control
  - Reactor control
- RELAP5 model
  - 220 control variables

S2 10 588

Preliminary Results

Main steam line break

- Normal operating conditions
- Reactor trip coincident with 34 inch steam line break
- Operator actions
  - — Trip reactor coolant pumps 30s after HPI initiation
  - — Isolate feedwater to affected steam generator 10 minutes after break
  - — Start one reactor coolant pump in each loop 10 minutes after attaining 50 °F subcooling in hot legs

S2 10 598

Results from Main Steam Line Break

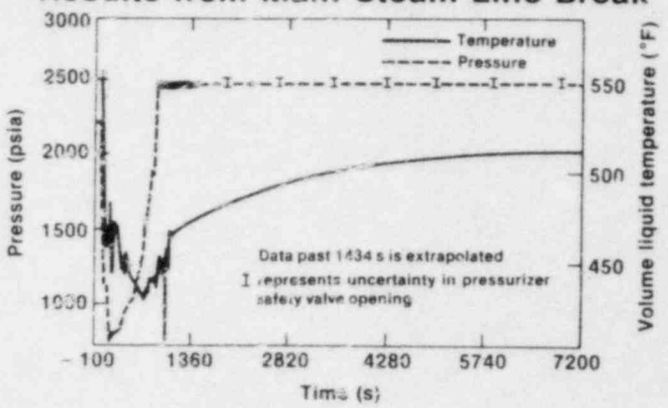

S2 10 599

Preliminary Results (continued)

Steam generator overfeed

- Normal operating conditions
- Reactor trip and turbine trip
- Full main feedwater flow continues
- Plant protection system functions as designed
- Reactor coolant pumps not tripped

92 10 586

Results from Steam Generator Overfeed Transient

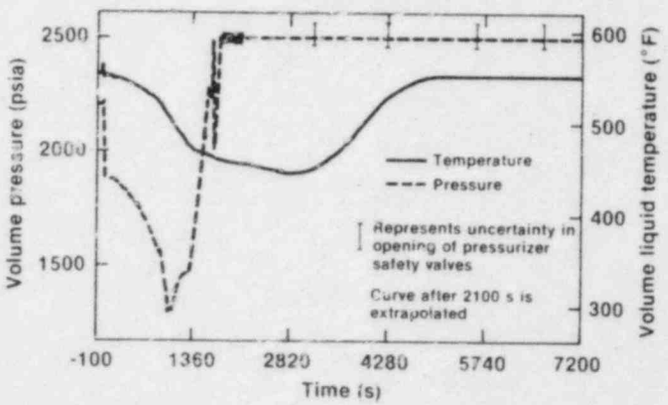

S2 3874

Preliminary Results
(continued)

Small hot leg break LOCA

- Normal operating conditions
- 1 inch break in top of pressurizer
- ICS fails to run back main feedwater
- EFW system functions as designed

S2 10 585

Results from Small Hotleg Break

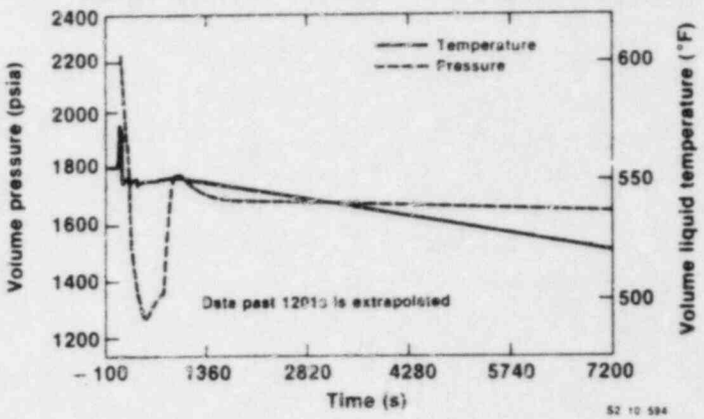

S2 10 594

Preliminary Conclusions

- Best estimate calculations of downcomer fluid temperatures for scenarios selected did not cause severe thermal shock to the reactor vessel

S2 10 597

COBRA/TRAC LARGE BREAK LOCA CALCULATIONS IN A UHI EQUIPPED PWR

T.E. GUIDOTTI

Battelle

Pacific Northwest Laboratory

INTRODUCTION

The COBRA/TRAC computer program has been developed to predict the thermal-hydraulic response of nuclear reactor primary coolant systems to small and large break loss-of-coolant accidents and other anticipated transients. It was derived from the merging of COBRA-TF and TRAC-PD2 [1].

The COBRA-TF computer code provides a two-fluid, three-field representation of two-phase flow. Continuous vapor, continuous liquid, and entrained liquid drops are the three fields. The conservation equations for each of the fields and for heat transfer from and within the solid structures in contact with the fluid are solved using a semi-implict finite-difference numerical technique on an Eulerian mesh. COBRA-TF features extremely flexible noding for both the hydrodynamic mesh and the heat transfer solution. This flexibility provides the capability to model the wide variety of geometries encountered in vertical components of nuclear reactor primary systems.

TRAC-PD2 is a systems code designed to model the behavior of the entire reactor primary system. It features special models for each component in the system. These include accumulators, pumps, valves, pipes, pressurizers, steam generators and the reactor vessel. With the exception of the reactor vessel, the thermal-hydraulic response of these components to transients is treated with a five-equation drift flux representation of two-phase flow. The vessel component of TRAC-PD2 is somewhat restricted in the geometries that can be modeled and cannot treat the entrainment of liquid drops from the continuous liquid phase directly.

The TRAC-PD2 vessel module has been removed and COBRA-TF has been implemented as the new vessel component. The resulting code is COBRA/TRAC. The vessel component in COBRA/TRAC has the extended capabilities provided by the three-field representation of two-phase flow and the flexible noding. The code has been assessed against a variety of two-phase flow data from experiments that were conducted to simulate important phenomena anticipated during postulated accidents and transients.

Concurrent with the COBRA/TRAC program are two other code development programs that use COBRA-TF as a foundation. A hot bundle code is being developed for detailed analysis of the core. It includes 1) rod deformation feedback via an active link with appropriate models in FRAP-T6 [2], 2) thermal radiation and 3) a non-condensible gas field. In addition, a best-estimate containment analysis capability is being developed. This code, known as "COBRA-NC," includes 1) the droplet field from COBRA-TF, 2) multiple non-condensible gas fields and 3) flexible nodalization. Because the results of these programs have been presented recently at other meetings [3,4], they will not be discussed in this report.

ASSESSMENT

The COBRA/TRAC code has been compared with experimental data for the following phenomena:

- counter-current flow limiting
  - tube
  - orifice
  - downcomer
- transient downcomer behavior

- condensation
- subcooled boiling
- nucleate boiling
  - axial void profile
  - two-phase pressure drop
- natural circulation
- upper head drain behavior
- reflood
  - bottom reflood
  - system effect gravity reflood
  - top reflood
- CHF film dryout
- phase separation
- uncovery/recovery

Examples of data comparisons that assess most of these phenomena are shown in Figures 1 through 11 of the presentation. They are representative data comparisons and are intended to give an indication of the breadth of the assessment. Also listed in each figure are the physical models in COBRA-TF that the particular test verified. In general, comparisons with all of the data are very good.

LARGE BREAK LOCA CALCULATIONS

COBRA/TRAC has been applied to a 200% cold leg break LOCA in a pressurized water reactor (PWR) equipped with upper head injection (UHI). Three versions of the accident were simulated. The first, referred to as the "October 1981" calculation [5] was a preliminary calculation performed before the initial assessment of COBRA/TRAC was completed.

Weaknesses in that calculation led to modifications which were incorporated into a final best-estimate calculation. Then, a third simulation was performed with new power levels in the core. These power levels were chosen according to evaluation model criterion used for licensing analysis.

OCTOBER 1981 CALCULATION

The peak clad temperature for the October 1981 calculation was 1675 F as shown in Figure 12. The core remained dry until bottom reflood. Because this calculation was preliminary, no further discussion will be given here, except to consider the subsequent modifications to the code.

Primarily, there were two problems with the calculation. The initial stored energy of the rods was too high for a best-estimate calculation and the UHI heat transfer (during top reflood) was too low.

Low values of gap conductance caused the stored energy in the rods to be over-predicted. Comparisons were made using FRAPCON-2 [6], a best-estimate, steady state fuel pin code. They showed that COBRA/TRAC was substantially over-predicting the fuel surface temperatures as shown in Figure 13. Modifications were made. Dynamic gap conductance was used and a fuel relocation model was added. These changes greatly improved the comparison with the FRAPCON-2 calculation (see Figure 13).

In addition, the October 1981 calculation under-predicted the falling film heat transfer rates. This was determined from the Westinghouse G-2 tests (because G-2 data is proprietary, it is not shown in the figures). Two modifications were made to the code. First, the falling film heat flux was modified by an exponential decay as a function of distance from the quench front [7]. Figure 14 shows a plot of the CHF heat flux modifier. The dashed line is used in the BE and EM-power calculations. This change increased the heat transfer ahead of the quench front. The second modification was to raise the upper limit on the minimum film boiling temperature from 1100 F to 1200 F. It applies at pressures greater than about 150 psia as shown by the curve in Figure 15. This change was developed from the G-2 data and later verified by GE data [8] and LOFT L2-3 data [9].

Figure 17 shows the comparison of the October 1981 calculation (dashed line) with the G-2 data, and the improvement when the above modifications were incorporated.

Other modifications to the October 1981 calculation included:

1) Use of ANS 5.1 (1979) decay heat curve instead of ANS + 20%.
2) Use of best-estimate peaking factors which were lower than values in the October 1981 calculation.
3) Use of a pump model based on recent Westinghouse pump data.
4) Replacing TRAC-P1A with TRAC-PD2 for the loop components.
5) Addition of the Cathcart [10] metal-water reaction heat source.
6) Minor noding improvements in the lower and upper plenums.

BEST-ESTIMATE AND EM-POWER CALCULATIONS

The evaluation model (EM) power calculation used the same input and code version as the best-estimate (BE) simulation. Only the power levels were different. The EM-power calculation used 1) 102% total power, 2) 120% of ANS 5.1 decay heat [11], 3) a 17% higher total peaking factor, and 4) the Baker-Just metal water reaction heat source [12]. This gave the EM-power calculation a 43% larger peak heat flux during bottom reflood.

There is a dramatic difference in the temperature response of the two calculations. The best-estimate calculation exhibited an early quench of the entire core at 14 s when water from the upper head was forced into the core. Whereas, the hottest bundles in the EM calculation remained above the minimum film boiling temperature (1200 F at high pressure) during UHI delivery and did not quench until bottom reflood. The peak clad surface temperatures for the hot rods are plotted in Figure 20. Curve 1 shows the best-estimate temperature and curve 2 shows the EM-power temperature. Although the center region of the EM-powered core remained dry, the rest of the core quenched during UHI water delivery as plotted on curve 3 in Figure 21. This curve shows the peak clad temperature in an outside channel (one of eight outside channels). Curve 1 of the figure shows the peak clad temperature of the hot rod in the center channel of the core.

The hydrodynamic behavior in the EM-power calculation was similar to the BE calculation. Figure 22 is a plot of the collapsed liquid level for both calculations. It shows liquid being delivered to the core on four occasions. The best-estimate calculation (curve 1) allowed slightly more liquid in the core and allowed it to enter the core at earlier times than the EM-power calculation. The difference occurred because the lower power levels and, hence, lower vapor generation rates allowed less counter-current flo limiting in the BE calculation.

The liquid came from two sources during the first core delivery. Beginning at 3 s flashing in the lower plenum forced liquid into the core and caused the liquid inventory to peak at 5 s. Then around 6 s additional liquid was provided as flashing in the upper head forced liquid down the support columns and into the core.

During this time, the upper head was filling with cold water from the UHI accumulator (since 2.4 s). Eventually, the cold water mixed with the hot water in the upper head interrupting the flashing and leading to condensation of steam (at 14 s). The condensation lowered the upper head pressure and caused the flow in the support columns to reverse. By 17 s the upper head had refilled with water.

Because the flow in the support columns was upward, liquid delivery to the core was interrupted allowing the core to dry out by 18 s. This prevented further cooling of the hot spot in the EM-power calculation. The hot spot may have quenched early with the rest of the core if the condensation period had been delayed.

Once the upper head was refilled, continued accumulator injection forced liquid down the support columns and into the core once again. This second forced UHI water delivery ended when the accumulator reached the low level setpoint and was shut off at 23.2 s (BE calc.).

Without forced injection, the pressure in the upper head fell below the upper plenum pressure because of condensation. This diminished the support column downflow until the gravity head was enough to overcome the decreasing pressure drop. This marked the beginning of upper head drain which provided liquid to the core for the third time.

During upper head drain, large vapor generation rates in the core led to large downward vapor velocities which prevented bottom reflood. However, once the upper head emptied, the core began to dry out. This lowered the vapor generation rate and allowed the liquid accumulated in the downcomer to collapse into the lower plenum and core inlet. Bottom reflood began at 73 s in the BE calculation and 75 s in the EM-power calculation.

The peak clad temperatures were 1150 F at 8 s for the BE calculation and 1513 F at 96.1 s for the EM-power calculation. The entire core quenched at 14 s in the BE calculation. All but the center had quenched by then in the EM-power calculation and the center quenched at 266 s.

CONCLUSION

The occurence of an early quench is quite sensitve to the value of the minimum film boiling temperature. In this calculation a best-estimate value of 1200 F was used based on the G-2 data and confirmed by data from GE and LOFT. However, the amount of quenching data at these pressures and with initial wall temperatures greater than 1200 F is limited. Further study may be warranted.

Early quench is also sensitive to upper head condensation. Earlier condensation may not allow the UHI water enough time to quench the core. Later condensation may provide additional time for the high pressure top quench. Therefore, system parameters that effect the time upper head condensation occurs may have a strong influence on the core cooling behavior.

The purpose of these simulations was to determine the effectiveness of the UHI emergency core cooling system in maintaining the temperature of the fuel cladding within acceptably safe

limits during the 200% cold leg break. Results of these simulations indicate that the UHI system will be very effective in the event of such an accident.

REFERENCES

1. "TRAC-PD2: An Advanced Best-Estimate Computer Program for Pressurized Water Reactor Loss-of-Coolant Accident Analysis," April 1981. NUREG/CR-2054, LA-8709-MS.

2. Siefken, L.J., et.al. May 1981. "FRAP-T6: A Computer Code for the Transient Analysis of Oxide Fuel Rods," NUREG/CR-2148.

3. Kelly, J.M., Kohrt, R.J., and Thurgood, M.J. September 22-24 1982. "Assessment of the COBRA-TF Subchannel Code," ANS Topical Meeting: Advances in Reactor Physics and Thermal Hydraulics, Kiamesha Lake.

4. Thurgood, M.J. October 4-7 1982. "Aplication of COBRA-NC to Hydrogen Distribution," Second International Workshop on Hydrogen in Reactor Safety, Sandia National Laboratory, Alberquerque, NM.

5. Edler, S.K., ed. March 1982. "Reactor Safety Research Programs Quarterly Report," October-December 1981, NUREG/CR-2127, vol. 4, PNL-3810-4, Pacific Northwest Laboratory, Richland, Washington.

6. "FRAPCON-2: A Computer Code for the Calculation of Steady State Thermal-Mechanical Behavior of Oxide Fuel Rods," January 1981. NUREG/CR-1845.

7. Edler, S.K., ed. July 1982. "Reactor Safety Research Programs Quarterly Report," January-March 1982, NUREG/CR-2716, vol. 1, PNL-4275-1, Pacific Northwest Laboratory, Richland, Washington.

8. Janssen, E., and Kervinen, J.A. August 1975. "Film Boiling and Rewetting," NEDO-20975, Class I, 75NED50.

9. Reeder, D.L. August 1979. "Quick-Look Report on LOFT Nuclear Experiment L2-3, Supplement 1, Supplement 1 to QLR L2-3, USNRC P 394.

10. Cathcart, V.J. August 1976. "Quarterly Progress Report on the Zirconium Metal-Water Oxidation Kinetics Program. ORNL/NUREG/TM-41.

11. ANS/ANSI 5.1, 1979. American Nuclear Society/American National Standands Institute Standard 5.1, "Decay Heat Power in Light Water Reactors", ANS, 555 N. Kensington Ave., LaGrange Park, IL 60525.

12. Baker, L., and Just, L.C. May 1962. "Studies of Metal Water Reactions at High Temperatures, III, Experimental and Theoretical Studies of the Zirconium-Water Reaction," ANL-6548.

CONTENTS

- INTRODUCTION
- COBRA/TRAC ASSESSMENT
- OCTOBER 1981 PWR/UHI CALCULATION
- BEST-ESTIMATE PWR/UHI CALCULATION
- EVALUATION MODEL POWER, PWR/UHI CALCULATION
- PARTICLE TRACKER MOVIE OF B.E. CALC.

PROGRAM AND STAFF

M.J. THURGOOD

COBRA-TF

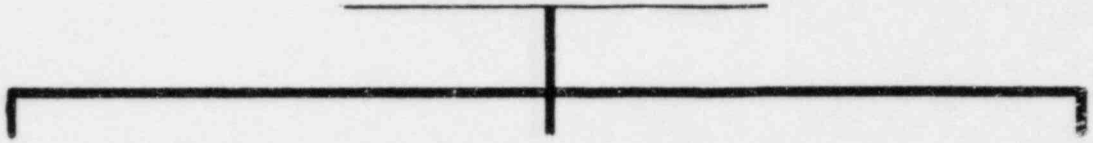

COBRA/TRAC

- SYSTEMS CODE
- UHI APPLICATION

HOT BUNDLE

- DETAILED ANAL.
- THERMAL RAD.
- NON-CONDENSIBLE GAS

CONTAINMENT

- DROPLET FIELD
- NON-CONDENSIBLE GAS
- FLEXIBLE NODALIZATION

S.H. BIAN
J.M. CUTA
D.E. DEBELLIS
T.E. GUIDOTTI

J.M. KELLY
R.J. KOHRT
G.A. SLY
C.A. WILKINS

DARTMOUTH COLLEGE

- TUBE CCFL
- FILM FLOW REGIME
  - INTERFACIAL SHEAR
  - ENTRAINMENT RATE
  - DROP DEPOSITION

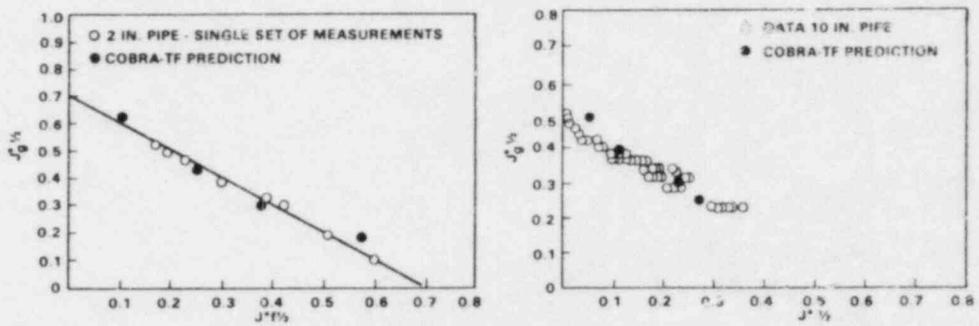

Figure 1

NORTHWESTERN UNIVERSITY

- ORIFICE PLATE CCFL
- MODELING OF UPPER CORE PLATE

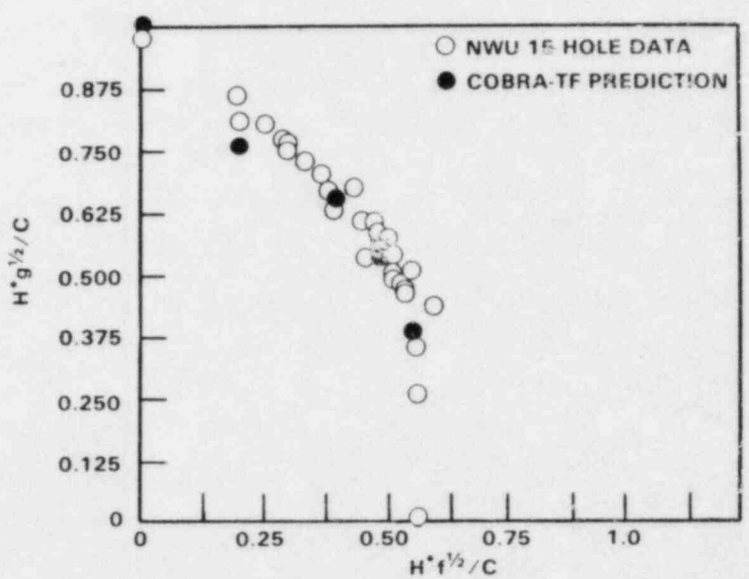

Figure 2

CREARE

- STEADY STATE DOWNCOMER CCFL (1/15th SCALE)
- ECC BYPASS

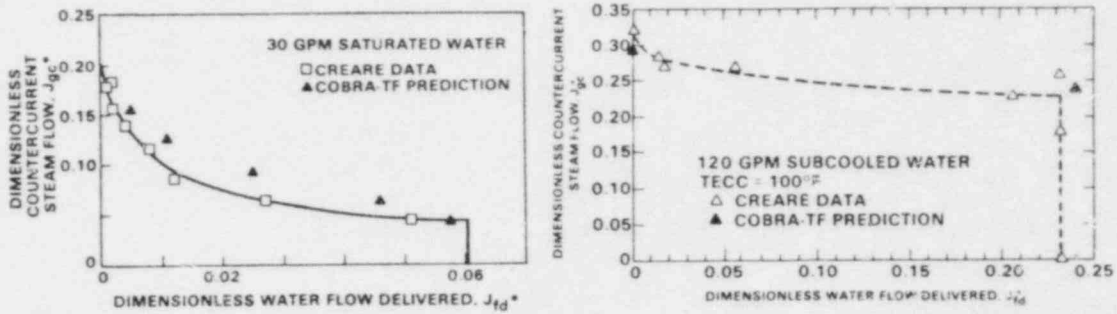

Figure 3

BATTELLE COLUMBUS

- TRANSIENT DOWNCOMER CCFL (2/15th SCALE)
- TRANSIENT ECC BYPASS WITH:
  - HOT WALLS
  - SUBCOOLED LIQUID

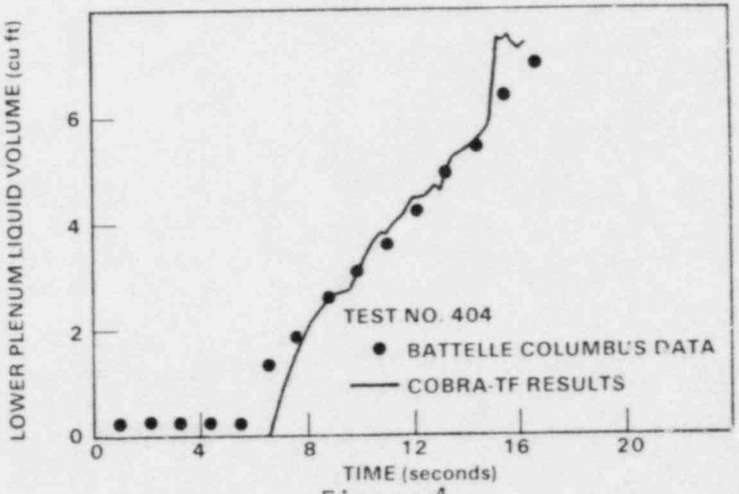

Figure 4

NORTHWESTERN UNIVERSITY

- COUNTERCURRENT FILM CONDENSATON
- FILM FLOW REGIME
  - CONDENSATION H.T.

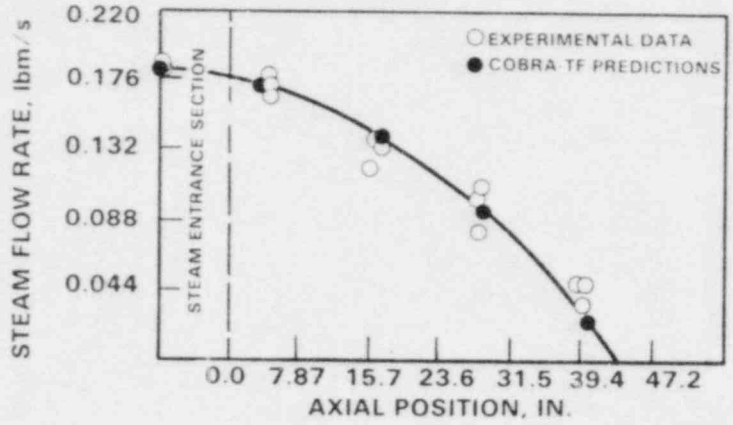

Figure 5

FRIGG

- NATURAL CIRCULATION TESTS
- ALL FLOW REGIMES
  - TWO PHASE ΔP
  - INTERFACIAL SHEAR

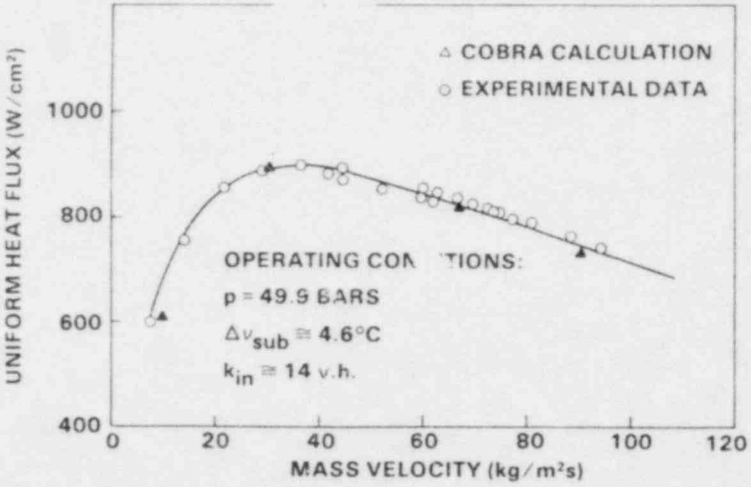

Figure 7

FRIGG

- FORCED CIRCULATION TESTS
- ALL FLOW REGIMES
  - SUBCOOLED BOILING H.T.
  - INTERFACIAL SHEAR

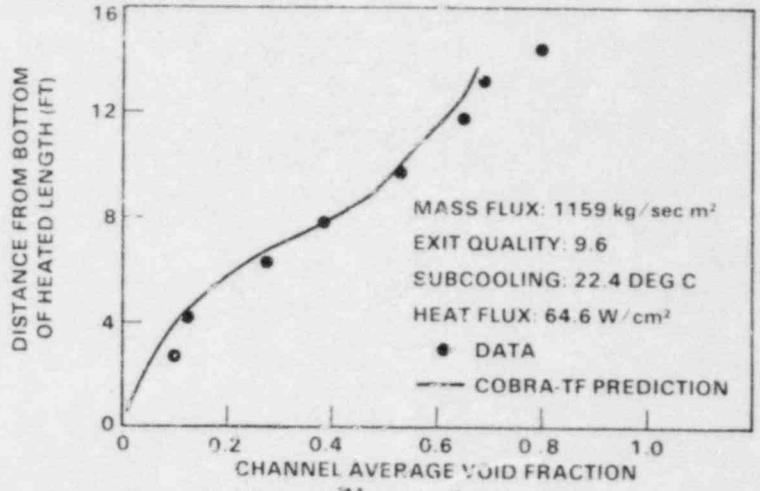

Figure 6

WESTINGHOUSE

- UPPER HEAD DRAIN TEST
  - FULL SCALE GUIDE TUBE
- MODELING
  - UPPER HEAD
  - SUPPORT COLUMN
  - GUIDE TUBES

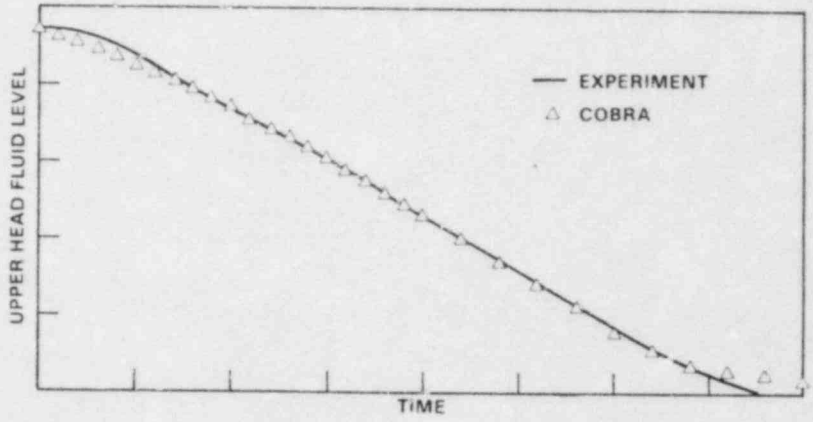

Figure 8

NRU

- BOTTOM REFLOOD; NUCLEAR FUEL
- ASSESSED
  - BOILING CURVE H.T.C.'s
  - GAP CONDUCTANCE
  - REFLOOD FLOW REGIMES
  - ENTRAINMENT

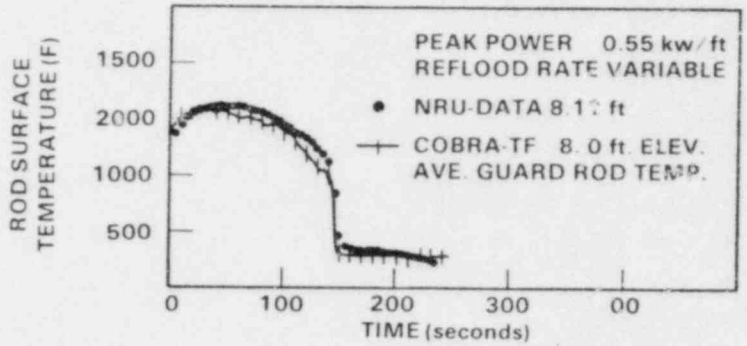

Figure 9

PKL

- SYSTEM EFFECT GRAVITY REFLOOD
- ASSESSED
  - LIQUID CARRYOVER
  - UPPER PLENUM DEENTRAINMENT
  - STEAM BINDING

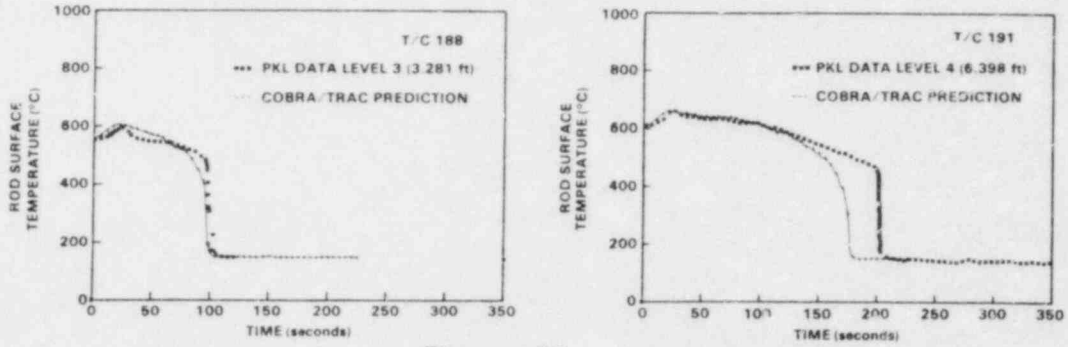

Figure 10

BENNETT

- TUBE CHF TESTS
- ASSESSED
  - FILM DRYOUT CHF
  - ENTRAINMENT AND DEPOSITION
  - SUPERHEATED VAPOR TO DROP H.T.

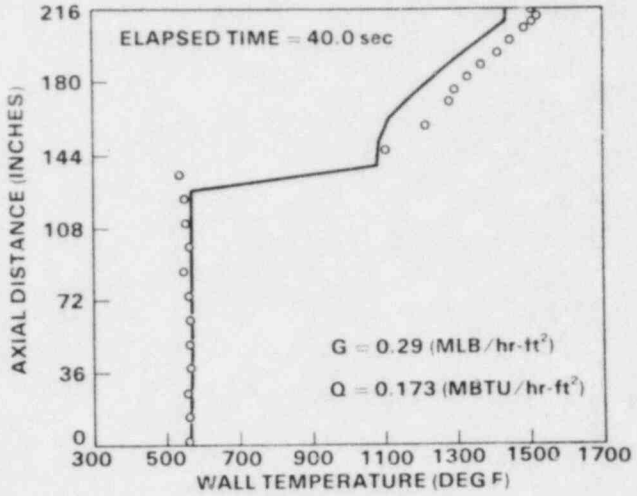

Figure 11

OCTOBER 1981 PWR/UHI CALCULATION

PERFORMED BEFORE ASSESSMENT OF COBRA/TRAC WAS COMPLETED

PROBLEM AREAS:

- INITIAL STORED ENERGY TOO HIGH
- UHI HEAT TRANSFER TOO LOW

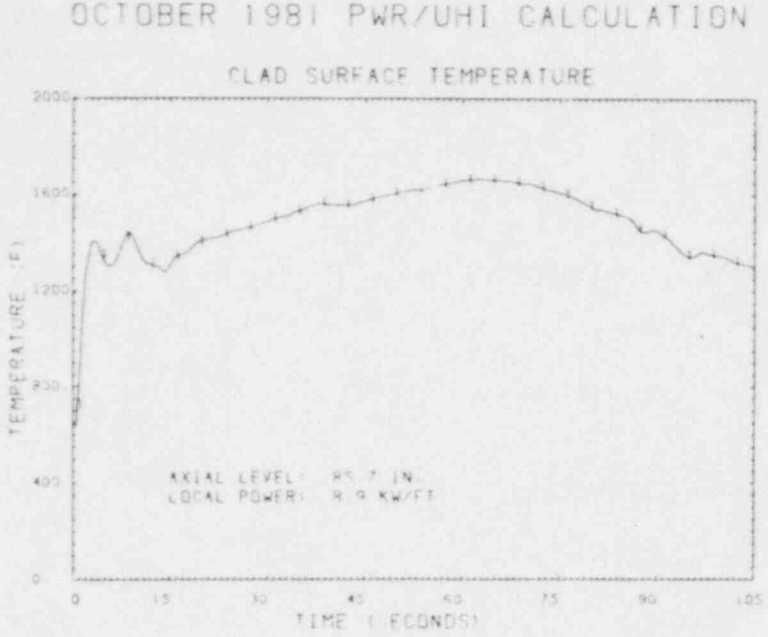

Figure 12

GAP CONDUCTANCE-ASSESSMENT

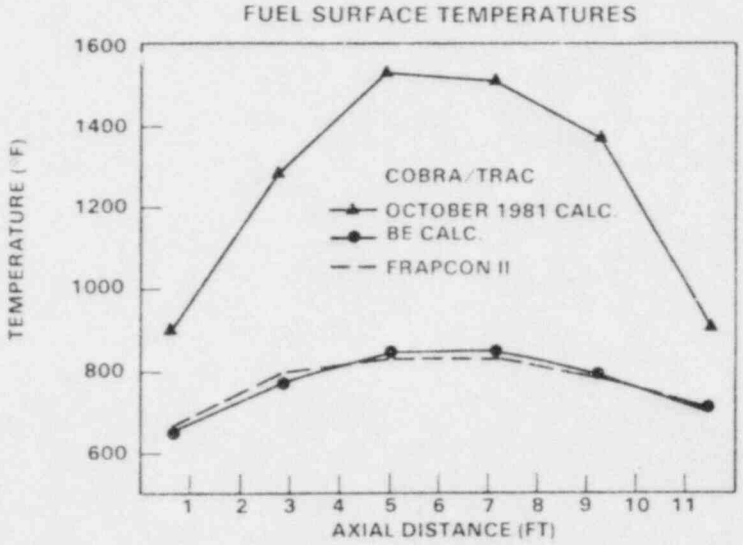

Figure 13

GAP CONDUCTANCE

- TOO LOW
  - -AS ASSESSED BY FRAPCON II
  - -USED VALUES TYPICAL OF EM NUMBERS
- MODIFICATIONS
  - -USED DYNAMIC GAP CONDUCTANCE
  - -ADDED RELOCATION MODEL

FALLING FILM H.T.

- TOO LOW
  - -AS ASSESSED BY G2 DATA
- MODIFICATIONS
  - -TRANSITION BOILING
    MODIFIED FALLING FILM HEAT FLUX BY AN EXPONENTIAL DECAY AS A FUNCTION OF DISTANCE FROM THE QUENCH FRONT
  - -MINIMUM FILM BOILING TEMPERATURE
    RAISED UPPER LIMIT ON T_{min} FROM 1100°F TO 1200°F

FALLING FILM H.T. - TRANSITION BOILING

- PREVIOUS MODEL

$$q''_{TB} = (1-\alpha)\cdot\delta\cdot q''_{CHF} + q''_{DFFB} \quad (\Delta Z > \tfrac{1}{2}\text{ in})$$

$$q''_{TB} = 1 \cdot\delta\cdot q''_{CHF} + q''_{DFFB} \quad (\Delta z < \tfrac{1}{2}\text{ in})$$

- PRESENT MODEL

$$q''_{TB} = \zeta \cdot\delta\cdot q''_{CHF} + q''_{DFFB}$$

$$\zeta = \text{EXP}\,[-0.229\,(\Delta Z - 1.2)],$$
$$1-\alpha < \zeta < 1$$

ΔZ = DISTANCE BELOW TOP O.F.

FALLING FILM H.T. - TRANSITION BOILING

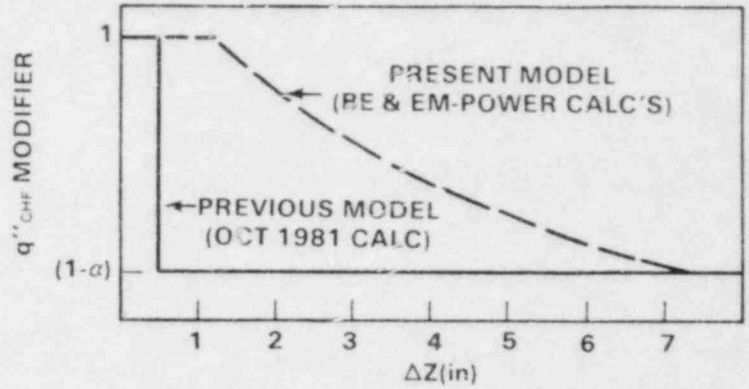

Figure 14

FALLING FILM H.T. - T_{min}

$T_{min} \leq 1200°F$

- DEVELOPED FROM WESTINGHOUSE G2 DATA
  - -UHI H.T. FACILITY
  - -PRESSURE RANGE 20-800 PSIA
  - -PROPRIETARY DATA
- CONSISTENT WITH GE AND LOFT DATA
- KEY VARIABLE - PRESSURE

FALLING FILM H.T. - T_{min}

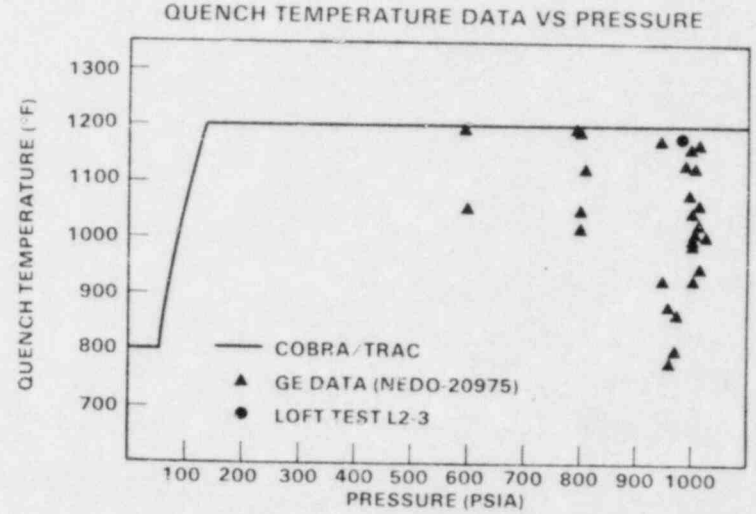

Figure 15

FALLING FILM H.T.-T_{min}

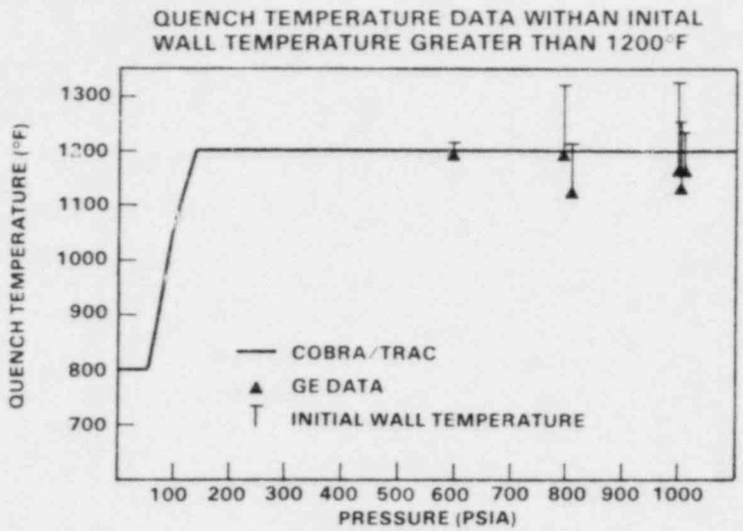

Figure 16

FALLING FILM H.T.-ASSESSMENT

G2 QUENCH ENVELOP DATA

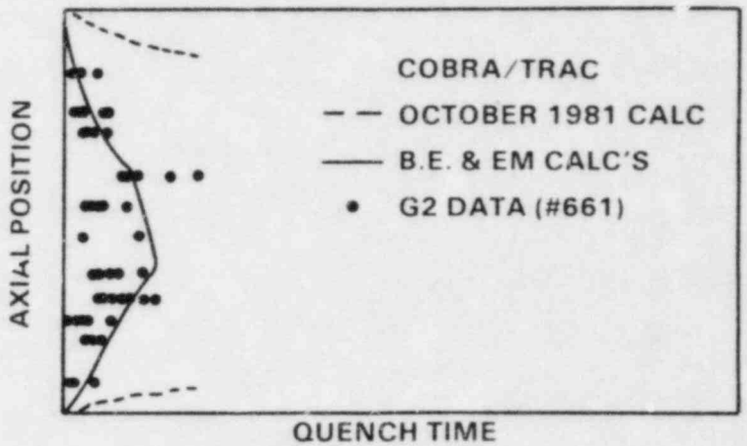

Figure 17

FALLING FILM H.T.-ASSESSMENT

G2 CLAD TEMPERATURE IN THE UPPER REGION OF THE BUNDLE

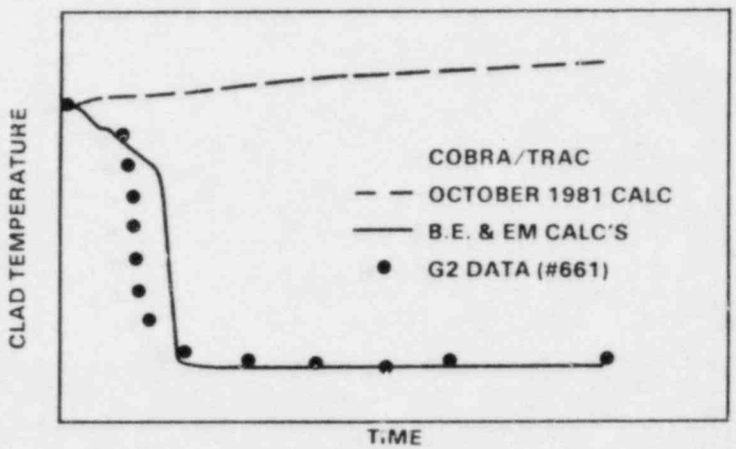

Figure 18

BEST ESTIMATE CALCULATION

OTHER MODIFICATIONS FOR B.E. CALCULATION

- BE DECAY HEAT ANS 5.1 + 0%
- BE PEAKING FACTORS (11.0 VS 13.2 kW/ft)
- PUMP MODEL → NEW WESTINGHOUSE DATA
- TRAC-PD2 LOOP VS TRAC-P1A
- CATHCART METAL-WATER REACTION
- MINOR NODING IMPROVEMENTS

BEST ESTIMATE PWR/UHI CALCULATION

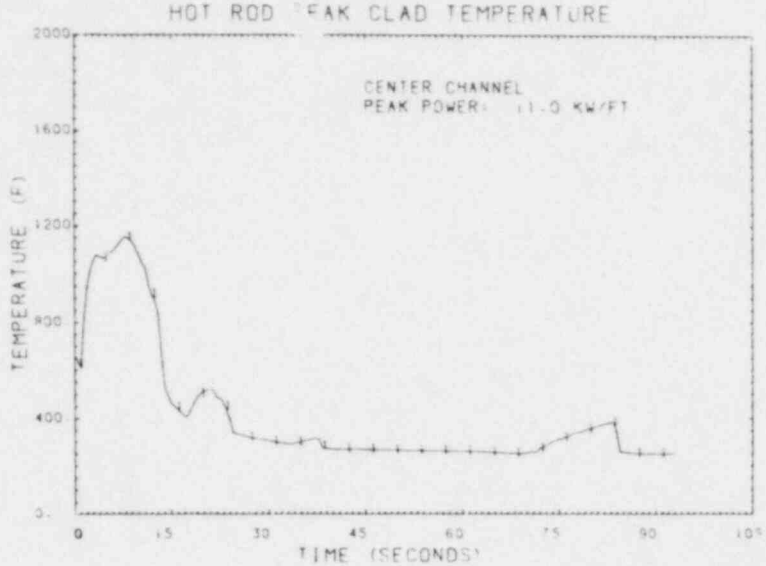

Figure 19

BE/EM-POWER -- HEAT TRANSFER

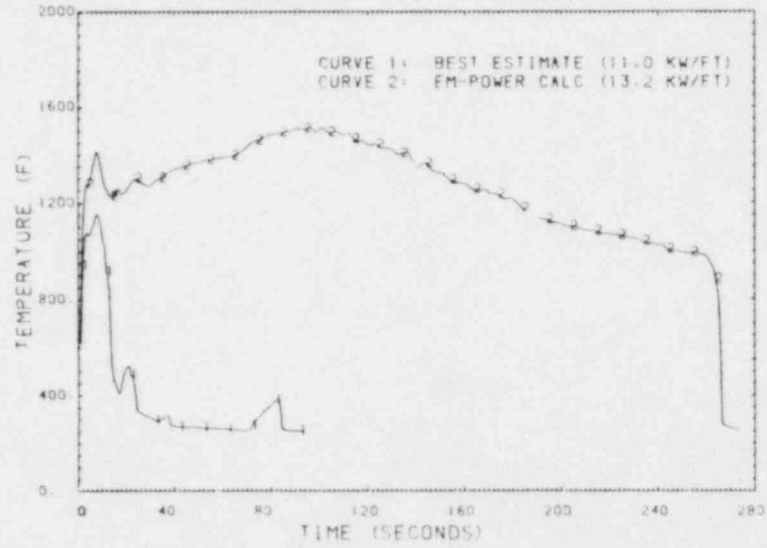

Figure 20

EVALUATION MODEL POWER ASSUMPTIONS

102%	TOTAL POWER
120%	ANS 5.1 DECAY HEAT
117%	TOTAL PEAKING FACTOR
	BAKER-JUST M-W REACTION
43%	HIGHER PEAK HEAT FLUX DURING REFLOOD

COMPARISON BE/EM-POWER CALCULATIONS

- HEAT TRANSFER

  B.E. - CORE QUENCHED BY 14 SEC.
  T_{PEAK} = 1150°F AT 8 SEC

  E.M. - MOST OF CORE QUENCHED BY 14 SEC
  -CENTER NOT QUENCHED UNTIL 266 SEC
  T_{PEAK} = 1513°F AT 96.1 SEC

EM-POWER PWR/UHI CALCULATION

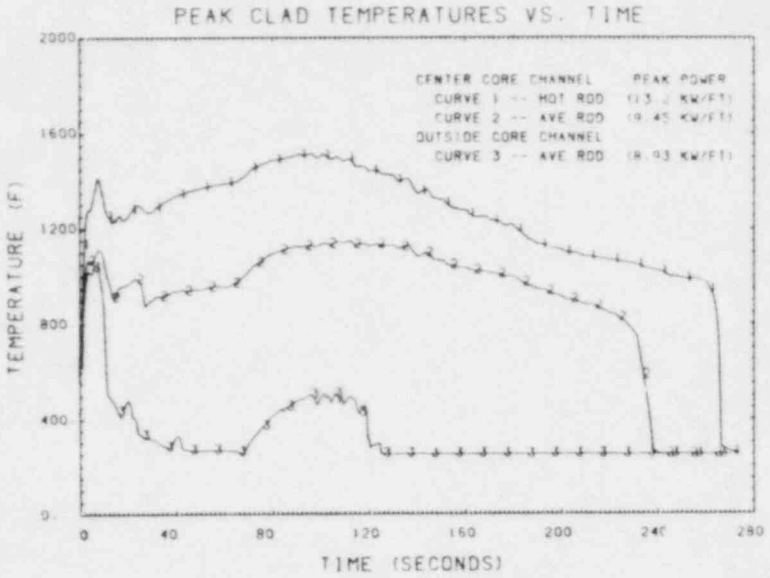

Figure 21

BE/EM-POWER -- HYDRODYNAMICS

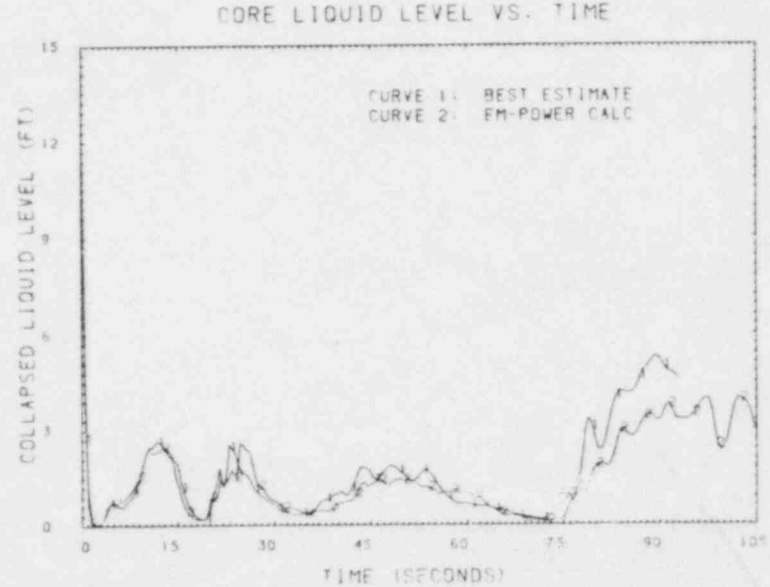

Figure 22

COMPARISON BE/EM-POWER

WHY DIDN'T THE EM-POWER CALC. QUENCH DURING UHI?

- FIRST UHI-WATER DELIVERY TO THE CORE
  - -SIGNIFICANT COOLING
  - -HOT ROD WAS STILL ABOVE 1200°F (T_{min}) WHEN UPPER HEAD CONDENSATION ALLOWED THE CORE TO EMPTY
- SECOND UHI-WATER DELIVERY
  - -TEMPERATURE DECREASES AGAIN
  - -STILL ABOVE 1200°F WHEN FORCED UHI ENDS
- UHI DRAIN PERIOD
  - -TEMPERATURE CONTINUES TO RISE
    VAPOR STAGNATION POINT IN CORE
    MOST LIQUID FLOWING AROUND HOT SPOT DOWN OUTER, QUENCHED REGIONS

SUMMARY

- COBRA/TRAC HAS BEEN ASSESSED AGAINST A WIDE VARIETY OF DATA
  - -NEED MORE ASSESSMENT OF SYSTEM TESTS
- BEST-ESTIMATE PWR/UHI CALCULATION
  - -QUENCH DURING UHI
  - -T_{PEAK} = 1150°F
- EVALUATION MODEL POWER PWR/UHI CALCULATION
  - -OUTSIDE QUENCHED DURING UHI
  - -CENTER QUENCH DURING BOTTOM REFLOOD
  - -T_{PEAK} = 1513°F
- NEED MORE DATA
  - -QUENCH TEMPERATURE
  - -TRANSITION BOILING

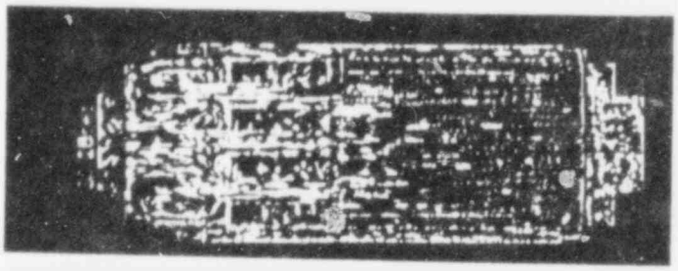
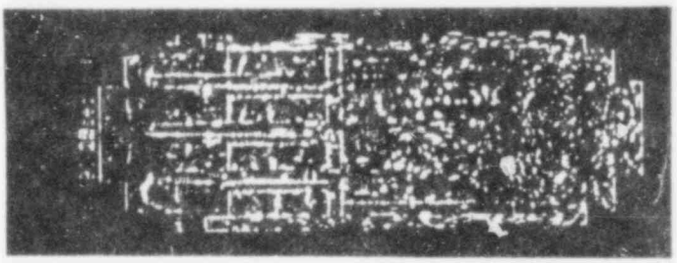
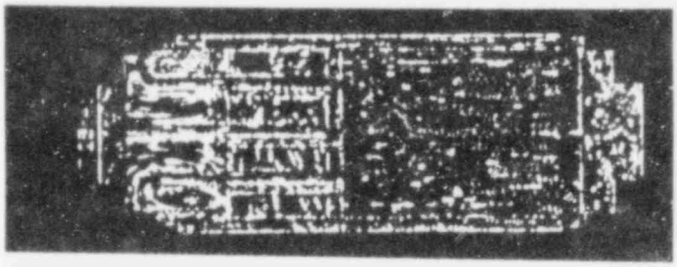
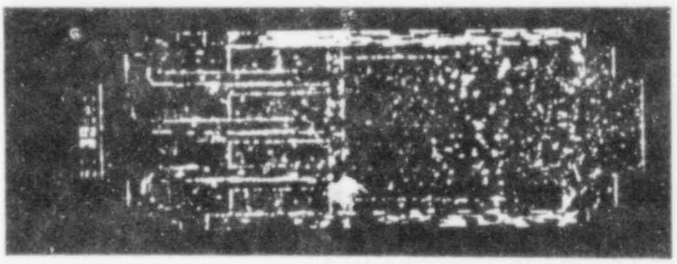
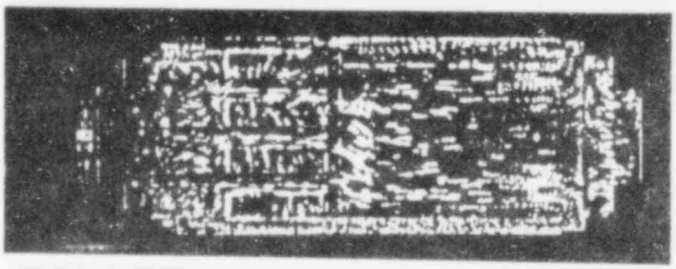
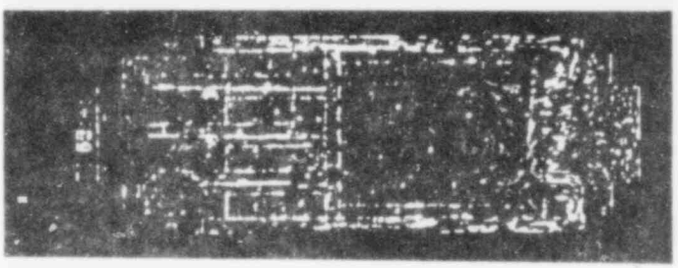
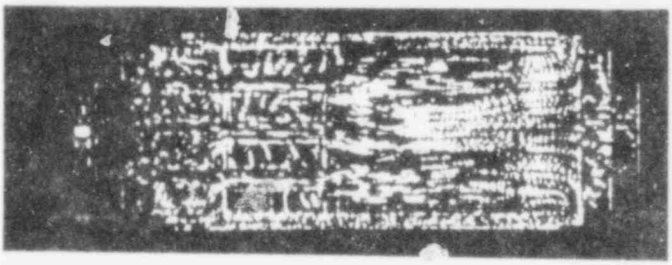
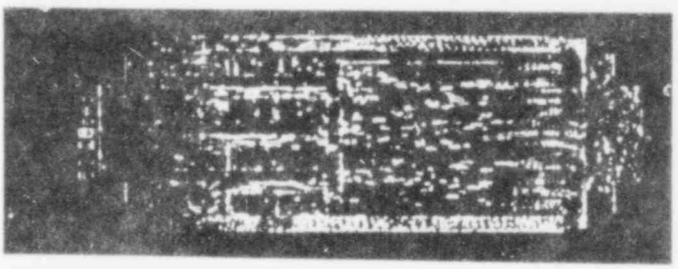
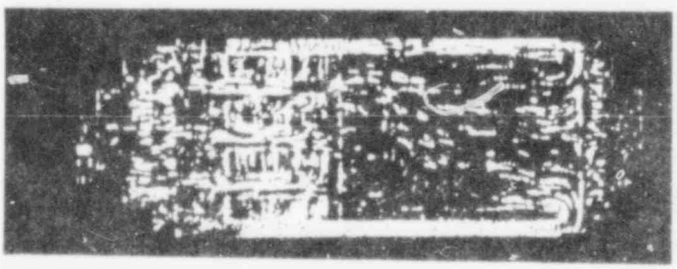
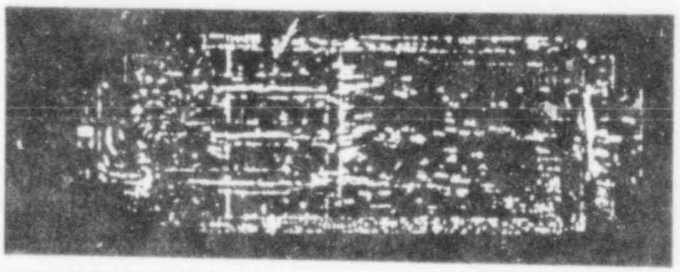
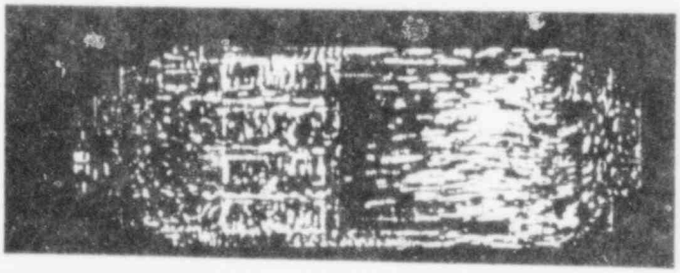
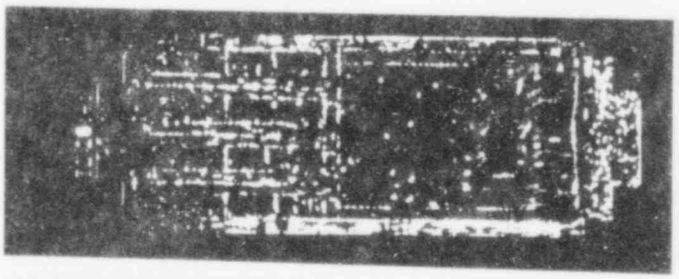

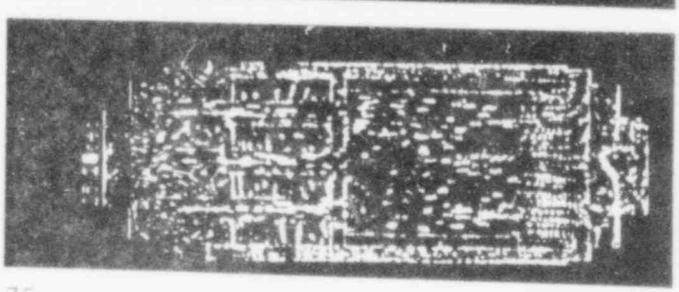

Results of Independent Assessment

F. Odar
Division of Accident Evaluation
Office of Nuclear Regulatory Research, NRC

1.0 Introduction

The independent assessment of NRC sponsored advanced best-estimate codes is being undertaken in four national laboratories. They are Los Alamos National Laboratory (LANL), Idaho National Engineering Laboratory (INEL), Brookhaven National Laboratory (BNL), and Sandia National Laboratory (SNL). The assessment is performed in three ways. The first is a quantitative assessment where the uncertainties in calculating selected key parameters are determined. The second is an assessment through separate effects and basic tests where the capabilities of the code to predict basic two phase flow phenomena are addressed. The third is a qualitative assessment where overall predictive capability of the code is assessed.

1.1 Overall Status

a. TRAC-PD2 Assessment

TRAC-PD2 is a large break LOCA code for PWR's. It has the capability to analyze multi-dimensional thermal hydraulics. Its independent assessment is completed and reported in Reference 1. The assessment work indicates that the TRAC-PD2 code can predict peak clad temperatures in a large break LOCA within accuracy limits of $\pm$ 80K (2 standard deviations). User guidelines will be provided in FY 83.

b. TRAC-PF1 Assessment

TRAC-PF1 is basically a small break LOCA code for PWR's although it may also perform large break LOCA analysis. It has the capability to analyze multi-dimensional thermal hydraulics. Its independent assessment is in progress. The status will be reported here.

c. RELAP5/MOD1 Assessment

RELAP5/MOD1 is basically a small break LOCA code for PWR's. It has the capability to analyze one-dimensional thermal hydraulics. Its independent assessment is in progress. The status will be reported here.

d. TRAC-BD1 Assessment

TRAC-BD1 is a large and small break LOCA code for BWR's. It has the capability to analyze multi-dimensional thermal hydraulics. Its independent assessment is in progress. The status will be reported here.

2.0 Key Parameters for Small Break LOCA

In assessing the safety of nuclear reactors, the concept of multiple-barriers is used. In this concept the first barrier for the fission product release is the cladding of the fuel. The second barrier is the primary system walls, i.e., reactor vessel, loop piping, valves and steam generator tubes, which keeps fission products inside the primary system if the cladding fails. The third barrier is the containment which will keep fission products inside the containment if the other two barriers fail. In a Loss of Coolant Accident (LOCA) scenario it is assumed that the second barrier has failed. Hence, we will concentrate on the first barrier and select key parameters accordingly. The key parameters selected for analysis of small break LOCA are listed in Table 2.1.

The first key parameter is the peak clad temperature which is also the key parameter used in licensing. It address s the temperature of the first barrier. The next two parameters help the understanding of physical phenomena which are important in calculating peak clad temperatures. The next four parameters provide information on core inventory. If the core is uncovered, the temperature of the rods will increase. These four parameters measure important quantities which affect the peak clad temperature. The other parameters involve inventory distribution in the loop and primary-to-secondary (or reverse) heat transfer processes in the steam generator. They also indicate how well the primary pressure variation is predicted. All of these parameters affect the most important key parameter, the peak clad temperature.

3.0 Status of TRAC-PF1 Independent Assessment

TRAC-PF1 is being independently assessed at LANL, INEL and BNL. In general, LANL and INEL assess the code using integral system tests while BNL performs assessment using separate effects and basic tests.

3.1 TRAC-PF1 Quantitative Assessment

This assessment is primarily being performed by LANL. There is also a small effort at INEL. Tables 3.1, 3.2, 3.3, and 3.4 summarize the results of this assessment performed by LANL so far. This assessment will continue in FY 83. As can be judged from these results, the experimental data predictions are reasonably accurate. Uncertainty in predictions of peak clad temperature (the most important key parameter) seems to be comparable to that in TRAC-PD2.

3.2 TRAC-PF1 Assessment Through Separate Effects and Basic Tests

This assessment is performed to understand the basic capability of the code to predict physical phenomena occurring during a small break LOCA and to explain the reasons for some of the differences in key parameters calculated in quantitative assessment. It has been performed by BNL and presented in Reference 2 which is published in these proceedings. The following phenomena occurring in a small break LOCA and associated tests are considered in this assessment.

1. Critical Flow: Marviken Tests, Moby Dick Air-Water Tests, BNL Flashing Tests.

   Primary Conclusion: TRAC-PF1 underpredicts critical flow during subcooled blowdown. The code predicts saturated blowdown accurately. The capability of the code to predict critical flow is almost the same as TRAC-PD2, Reference 1.

2. CCFL - Entrainment: University of Houston, Dartmouth Single Tube.

   Primary Conclusion: The code predicts excessive entrainment similar to TRAC-PD2, Reference 1.

3. Level Swell: GE Large Break Vessel Blowdown Tests.

   Primary Conclusion: The code accurately predicts the pressure transient. In the beginning, the level is overpredicted because TRAC-PF1 does not have a delayed nucleation model. After a short time the experimental and calculated levels agree well with each other. Later in the transient, the level is again overpredicted. Calculations show more vapor fraction in the two-phase region than measured.

4. Steam Generator Heat Transfer: Flecht-Seaset and B&W IEOSG and OTSG Tests.

   Primary Conclusions: In Flecht-Seaset tests where the primary side contains two-phase flow and the heat transfer is from the secondary to the primary, the heat transfer is overpredicted as the two-phase mixture advances inside of the primary tube initially filled with steam. The code predicts lower steam temperature in film boiling regime. Excessive interfacial heat transfer between the phases evaporates most of the liquid.

The code predicted all thermal hydraulic parameters in 15-20% load following tests performed by B&W using the Integral Economizer Once Through Steam Generator Component. However, in tests performed using the Once Through Steam Generator Component with aspirator flow, the code predicted too little condensation at the bottom of the downcomer. A sensitivity study using a high condensation rate produced reasonable agreement with data.

More details on this assessment work can be found in Reference 2.

4.0 Status of RELAP5/MOD1 Independent Assessment

RELAP5/MOD1 is being independently assessed at SNL and BNL. SNL performs the assessment using integral system tests, while BNL performs the assessment using separate effects and basic tests. The assessment will continue in FY 83 in these laboratories. Some contribution will also be made by INEL in FY 83 by evaluating analyses previously performed by experimental programs at INEL.

4.1 RELAP5/MOD1 Quantitative Assessment

Quantitative assessment of RELAP5/MOD1 is still in progress. It is being performed at SNL. It will be completed in FY 83. Table 4.1 presents a sample of comparisons for peak clad temperatures. This limited comparison promises accurate predictive capability.

4.2 RELAP5/MOD1 Assessment Through Separate Effects and Basic Tests

As in the case of TRAC-PF1, this assessment has been performed by BNL and presented in Reference 2 which is published in these proceedings. The same phenomena examined in the TRAC-PF1 assessment are also examined in the RELAP5/MOD1 assessment.

1. Critical Flow: Marviken 24 Test, Moby Dick Air-Water Tests.

   Primary Conclusion: Critical flow rate predictions depend on nodalization of the break. If zero volume nozzle (Marviken) is used, break flow prediction including subcooled blowdown region is accurate. However, pressure is underpredicted. This assessment will continue in FY 83 to include more tests.

2. CCFL-Entrainment: University of Houston, Dartmouth Single Tube.

   Primary Conclusion: Predictions of CCFL and entrainment are inadequate, the flow regime map at high void fractions does not contain liquid film on the walls. It contains only droplets. The interfacial shear carries practically all droplets away.

3. Level Swell: GE Large Break Vessel Blowdown.

   Primary Conclusion: Quality of predictions is poor. Level swell and pressure are underpredicted. Code predicts irregular void fraction profiles within the two-phase region. This type of prediction may cause numerical oscillations in some transients.

4. Steam Generator Heat Transfer: Flecht-Seaset and B&W IEOSG and OTSG Tests.

   Primary Conclusions: In Flecht-Seaset where the primary side contains two-phase flow and the heat transfer is from the secondary to the primary, the heat transfer is overpredicted as the two-phase mixture advances inside the primary tube initially filled with steam. The code predicts saturated conditions in the primary until all liquid is evaporated. This does not allow the presence of superheated steam with liquid and leads to a large temperature differential between the secondary and primary. The code predicts oscillatory behavior in secondary side steam temperatures. Time steps must be reduced to eliminate the oscillations.

   In both B&W IEOSG and OTSG tests oscillatory behaviors were calculated. Time steps must be reduced to eliminate oscillations.

More details on this assessment work can be found in Reference 2.

4.3 Preliminary Conclusions from Integral Tests

Assessment of the RELAP5/MOD1 code through integral system tests is being performed by SNL. This assessment will continue in FY 83. Hence, the conclusions reached so far are preliminary. Following is the list of the conclusions and their discussions.

1. Peak Clad Temperatures are accurately predicted.

   This conclusion has been reached only from LOBI tests. There is a need to expand the data basis. LOFT and Semiscale tests will be considered for comparison in FY 83.

2. Natural circulation is qualitatively predicted well (about 40% error).

   This conclusion has been reached from PKL and Semiscale natural circulation tests, Figures 4.1 through 4.5. Comparison between calculated and measured values indicates that the code predicts natural circulation reasonably well. At certain inventories the code predicts also oscillations. The amplitudes of these oscillations calculated at different inventories are indicated by vertical bars in Figures 4.1, 4.2, 4.4. and 4.5. Figure 4.3 illustrates the details of oscillations at 80% inventory in test SSNC-2 for 30KW. These oscillations are obtained after making extensive time step reduction studies. They are independent of the time step used. Examination of data shows that the data also indicate oscillations in these tests at these particular inventories. However, the resolution of the data in the tape is poor and does not allow comparison of frequencies and amplitudes. It should be noted that the fact that the code calculates oscillations at certain inventories as data indicate, is encouraging.

3. It is difficult to obtain nominal steady-state conditions for primary and secondary matching simultaneously.

   This problem was encountered in all integral system tests such as LOFT, Semiscale MOD3 and LOBI. The assessment program will provide some user guidelines.

4. Hot leg superheat not predicted.

   This is observed in LOBI and Semiscale MOD3 calculations.

5. Calculated time steps are large. This causes excessive oscillations.

   Excessive oscillations are observed in LOBI, PKL and Semiscale Natural Circulation tests. These oscillations occur, in general, in the secondary side, particularly in steam temperatures. The user needs to choose a smaller time step. This increases running time drastically. Similar problems are also observed at BNL in separate effects tests. The code needs better numerics eliminating these oscillations.

6. There are mass and energy conservation errors in stagnant nodes.

   This is observed in calculations of LOFT L6-7/L9-2 and L9-1 tests. Another mass conservation error is also observed in PKL calculations. Figures 4.6 illustrates the nodalization used by SNL for L6-7/L9-2. Figure 4.7 illustrates the temperatures in the volumes of the stagnant loop. In these tests the broken loop was flanged off and this provided stagnant volumes. Notice that the temperature of Volume 407 increases due to the energy conservation error. This error disappears when the loop containing stagnant volumes is removed. Similarly in calculations of L9-1 a mass conservation error is observed. Figure 4.8 illustrates the variation of the total primary inventory with time. This is a loss of feedwater transient and until the pressurizer relief valve opens the inventory in the primary system should have remained constant. However, with the stagnant loop connected to the system, there is a mass conservation error. When the stagnant loop is removed the error disappears and the inventory changes as the PORV opens.

   These mass and energy conservation errors originate from the oscillatory behavior calculated in the primary system several volumes away. In these particular instances the oscillatory behavior was traced to modeling of leakage paths. If leakage paths are modeled using real geometrical areas (specifically if the leakage area used is 1% or less than the adjacent volume areas), the code calculates oscillatory behavior. If the leakage paths are modeled by sacrificing modeling of the geometry (specifically if the leakage path is modelled artificially using a large K factor between two volumes having areas of the same order of magnitude), the oscillatory behavior disappears and the code does not produce mass and energy errors.

This is certainly an important user guideline and should be applied by the users. However, evaluation also shows that these oscillations propogate throughout the system and cause mass and energy conservation errors far away from the leakage paths. The basic numerics see only oscillations and does not recognize how these oscillations originate. Fortunately no mass or energy conservation was observed in Semiscale Natural Circulation tests where some oscillations have been calculated. However, it is an uneasy feeling for a user if he calculates oscillations for a transient where natural circulation stops and most of the volumes become stagnant. Although at this juncture this problem does not appear to be very serious and perhaps the user can identify the problem if it occurs and make necessary changes in his input deck to circumvent it, it is highly recommended that improvements in numerics should be made to alleviate this problem. It is doubtful that very comprehensive user guidelines identifying all possible future problems can be provided.

5.0 Status of TRAC-BD1 Independent Assessment

The version of the code released to the National Energy Software Center (NESC) is version 8. However, the independent assessment was performed on improved versions, Versions 11 and 12. These new versions contain the Anderson & Ishii interfacial shear and entrainment models. In BWR's it is very important to accurately calculate the vapor fraction profile since the vapor fraction is one of the dominant factors in calculations of reactivity feedback in transients. The interfacial shear model is an important contributor in calculation of vapor fractions.

TRAC-BD1 is the first best-estimate "state-of-the-art" code for BWR's. It is the first time that the code was exercised by people who did not develop it. Assessment started using Version 11. Many mistakes and programming errors were found. These were communicated to the code developers and it was necessary to create another version of the code (Version 12). Assessment continued and still continues on this version. Basically, assessment indicates the need for improvement in major areas.

5.1 Key Parameters for LOCA Calculations

Table 5.1 presents the key parameters to be used in a BWR LOCA (large or small break) analysis. The first key parameter is the important peak clad temperature. As stated earlier, this parameter is involved with the state of cladding which is the first barrier against the fission product release. The other parameters involve describing phenomena which are important to determine the state of cladding.

Particularly important are the parameters involving inventory distribution such as time for jet pump uncovery, recirculation line uncovery, and ECC activations which are based on various levels in the downcomer. Times for PCT and initial rod dryout involve important phenomena determining peak clad temperatures. Time for core quench is an important parameter for the core recovery.

In addition to the parameters listed in Table 5.1, it is planned to add the value of minimum downcomer DP or minimum lower plenum inventory as a key parameter.

5.2 TRAC-BD1 Quantitative Assessment

This assessment is primarily being performed by INEL. Table 5.2 summarizes some of the results obtained so far. It is apparent that the predictions are not accurate. One prediction is off by 316K. This was obtained using Version 11. It is expected that a more accurate prediction would be obtained if the calculation is repeated using Version 12. However, observing the overall results of ROSA-III, Reference 3, it can still be concluded that the code needs improvement in calculation of inventory distribution. Hence, the assessment will continue on TRAC-BD1/MOD1 after major improvements in the code are made.

5.3 TRAC-BD1 Assessment Through Separate Effects and Basic Tests

This assessment has been performed by INEL and partly by BNL, Reference 2, and Toshiba Corp., Reference 4. The following phenomena occurring in large and small break LOCA's in BWR's and associated tests are considered in this assessment:

1. Critical Flow: Marviken 15, 24.

   Primary Conclusion: The critical flow model from RELAP5/MOD1 was implemented wrong. The error has been corrected in Version 13 (which is not assessed here) and the results are similar to those obtained by TRAC-PF1; i.e., the subcooled blowdown is under-predicted and predictions for saturated blowdown seem accurate.

2. CCFL - Entrainment: University of Houston, Dartmouth Single Tube, 18° Sector Test Apparatus (ESTA) Tests by Toshiba Corp.

   Primary Conclusions: The code calculated CCFL very well in the University of Houston tests (see Reference 2).

Since the University of Houston tests were performed using air and water, it can be concluded that the Anderson & Ishii interfacial shear package performed very well in this region. This is a distinct improvement over TRAC-PF1 and RELAP5/MOD1 codes. Toshiba analysis of ESTA tests also shows that the code (although Version 8 was used) predicts CCFL reasonably well for saturated conditions, (Reference 4).

3. CCFL - Breakdown: ESTA tests from Toshiba Corp.

   Primary Conclusions: The code can predict subcooled CCFL breakdown only qualitatively (see also Reference 4). Predictions depend on interfacial heat transfer, upper plenum nodalization and jet momentum. Assessment and code improvement in these areas will continue in FY 83.

4. Multi-D Calculations: ESTA tests from Toshiba Corp.

   Primary Conclusions: As stated in Items 2 and 3 above, saturated CCFL is predicted well in the multi-D upper plenum. The code also predicts multi-D behavior in subcooled conditions (CCFL breakdown in peripheral bundles) qualitatively. More assessment will be performed using 30° SSTF data to assess this capability and to provide necessary feedback to code developers for further improvement.

5. Reflood Calculations: Gota 42.

   Primary Conclusion: Reflood calculations are not accurate. Moving fine mesh quench front nodalization (similar to the one in TRAC-PD2 or TRAC-PF1) is needed.

6. Radiation Heat Transfer: Gota 11.

   Primary Conclusion: When rod groupings of 5 based on the location are used, the clad temperatures in the bundle are calculated accurately. The average difference between the calculated and experimental values is about 10K while the standard deviation is about 25K. User guidance for selection of groupings will be provided.

7. Inventory Distribution: TLTA tests, ISP 12.

Primary Comments: In general, code needs to be improved to calculate inventory distribution more accurately. The inventory in the lower plenum is consistently predicted lower than the tests indicate. Inventories in the upper plenum, core and downcomer are not accurately predicted in a consistent manner. Possible reasons for discrepancies are:

a. Experimental uncertainties are not well understood.

b. Modeling improvements are needed in calculating

   i. Break flow rate
   ii. Level tracking (jet pump uncovering at the inlet and exit)
   iii. CCFL breakdown in subcooled region
   iv. Interfacial heat transfer and perhaps to a lesser extent interfacial shear package.

The assessment will continue using the improved version of the code (TRAC-BD1/MOD1).

6.0 Code Execution Statistics

In this section, statistics on execution of TRAC-PF1, RELAP5/MOD1 and TRAC-BD1 will be presented and compared. The goals of accurate predictions and fast calculations usually have opposite requirements. Accurate predictions usually require an increase in the number of thermal & hydraulic nodes (cells). On the other hand, performing fast calculations requires as few nodes as possible. The same argument also applies to the selection of the time steps (when the user has the option to select the time step size) or to the selection of heat slabs and heat transfer surfaces and number of nodes in conduction calculations. The accuracy of calculations will also depend on the nodalization technique used by the engineer to predict some specific phenomena. Hence, engineering judgment plays an important role in accuracy and speed of calculations. An important part of the assessment process is to provide user guidelines for the use of codes. These guidelines will be provided by the completion of the assessment.

The statistics are derived from the noding models developed at BNL, LANL, SNL, and INEL. They are applicable to the models as developed by these laboratories. No optimization between accuracy and speed of calculations has been made. In the future, part of the code assessment and application work will be devoted to the optimization studies to provide guidance to the users.

6.1 Separate Effects Tests

Tables 6.1 through 6.5 present the code execution statistics for TRAC-PF1, RELAP5/MOD1 and TRAC-BD1 codes. Tables 6.1 and 6.2 present the statistics for TRAC-PF1 and RELAP5/MOD1 for the same separate effects tests. These analyses have been performed by BNL using the same number of nodes. This removes an important user effect. In order to have the same basis for comparison, TRAC-PF1 calculations were performed using the 1-D option. The comparison shows that:

1. The running times of both codes, i.e., CPU/RT, are comparable. In some runs TRAC-PF1 runs faster while in the others RELAP5/MOD1 runs faster.

2. The ratio of CPU/(#C X #DT), the basic grind time, which is the CPU time that the code spends per each node per each time step, is 2.5≈3 times larger for TRAC-PF1. The basic grind time depends on the efficiency of the code structure, programming, iterations, data management, table look-up technique, etc. Hence, its value for a code should remain almost the same or should change only slightly when similar transients or phenomena are considered. Some changes would occur if transients are drastically different using time consuming calculational routines. However, within a certain class of transients large variations should not occur from transient to transient. This ratio is useful in estimating the required CPU time for any problem given the nodalization and approximate time step.

   Judging from the values of this ratio, it appears that RELAP5/MOD1 is more efficiently structured than TRAC-PF1. This is also consistent with findings in Reference 5. TRAC-PF1 has superior numerics in two-step method permitting it to take larger time steps than the RELAP5/MOD1 for each test case. For the case where numbers of time steps are almost comparable (FLECHT-SEASET 21806), RELAP5/MOD1 ran faster than TRAC-PF1 by almost a factor of two. However, the predictions were poorer. Note, that the time steps were selected by the code logic rather than by the user in all calculations.

6.2 Integral System Tests

Tables 6.3 and 6.4 present the execution statistics for TRAC-PF1 and RELAP5/MOD1 for integral tests. Analyses in Table 6.3 were performed by LANL while those in Table 6.4 were performed by SNL. The tests are different; however, Semiscale and LOBI are somewhat comparable in scale and there are LOFT tests in both sets of analyses. The comparison shows that:

1. TRAC-PF1 using 1-D option for Semiscale tests runs faster than RELAP5/MOD1 does for LOBI tests. Numbers of nodes are almost the same for both facilities. The basic grind times, CPU/(#C X #DT), for both codes are consistent with those calculated in Tables 6.1 and 6.2. However, in the case of RELAP5/MOD1, the user had to select a smaller time step than the code logic dictated, in order to supress instabilities. The selected time steps by the code logic would be smaller than those selected by TRAC-PF1 due to two-step numerics in TRAC-PF1. The selection of still smaller time steps made the RELAP5/MOD1 code a very slow running code. There is a definite need to improve the numerics in RELAP5/MOD1 to eliminate instabilities. Perhaps some of these instabilities can be avoided by defining user guidelines. However, these guidelines may not cover all possible unstable situations.

2. The TRAC-PF1 code using the 3-D option for LOFT tests (with approximately 30% of the nodes being vessel nodes where 3-D calculations are performed) calculates transients about 4≈5 times slower than the 1-D option would calculate (comparing with Semiscale runs). The basic grind time is also about 50% larger than that in the 1-D calculations. This time does not vary too much for the three 3-D calculations in the table. Apparently, efficiency of the code remains the same for both blowdown and reflood stages. Although the basic grind time does not change much for the reflood stage, more time steps are required to perform the calculations. Approximately 4000 time steps were used for 20 seconds of reflood, while about 8000 time steps were required to perform calculations for 300 seconds of transient before the reflood. Hence, more CPU time is required to perform reflood calculations. Using the basic grind time and estimating the time steps required, the user can estimate the length of CPU time for his reflood calculations for his specific nodalization.

3. In the case of LOFT calculations, RELAP5/MOD1 runs relatively slow for L3-6 while it runs relatively fast for L9-1 in comparison to TRAC-PF1. Since the average ratio of CPU/RT for TRAC-PF1 for LOFT calculations which include 3-D calculations for 30% of the nodes, is about 20, the ratio of 28.4 for L3-6 for RELAP5/MOD1 is high. A ratio lower than 20, perhaps on the order of 8-10, similar to that in L9-1, is expected. The calculations for L3-6 required a large number of time steps with RELAP5/MOD1. In these calculations the time step was chosen by the code logic and not by the user. This result is surprising and the reasons for slow calculations will be further investigated.

Table 6.5 presents the code execution statistics for TRAC-BD1. These calculations were performed at INEL. It is quite obvious that TRAC-BD1 runs slower than TRAC-PF1 or RELAP5/MOD1. The basic grind time (except for the last case) is slightly better than TRAC-PF1. This is probably due to small time steps taken by TRAC-BD1 which probably demands less iterations. The number of time steps required for each transient is large and this causes large CPU/RT ratios. Inclusion of two-step numerics in this code should substantially improve the speed of calculations.

The last case, BWR-3 calculations, runs extremely slow and requires twice the grind time required by the BWR-6 calculations. The grind time is independent of nodalization and time steps. Hence, one would expect similar grind times for both cases. One difference between these two cases is in the number of heat transfer surfaces. Since a substantial amount of time is spent in heat transfer routines, the number of heat transfer surfaces would be a major contributor to the grind time. Hence, the user should carefully evaluate the need for each heat transfer surface. Another difference could be in the nodalization scheme. At this time a detailed comparison between these two cases has not yet been made. After making these comparisons and further evaluations, user guidelines will be provided to reduce grind time and to speed up calculations.

6.3 Conclusions

1. Based on separate effects tests performed by BNL, the running times of TRAC-PF1 and RELAP5/MOD1 are comparable. In some runs TRAC-PF1 runs faster and in the others RELAP5 runs faster.

2. It appears that RELAP5/MOD1 has more efficient code structure, data management and perhaps better table look-up technique. However, TRAC-PF1 has superior numerics in two-step method. This is apparently why two codes run at comparable speeds.

3. Based on integral tests performed at LANL and Sandia, the 1-D option of TRAC-PF1 runs faster than RELAP5/MOD1. This is due to the two-step numerics in TRAC-PF1 which permits the code to use large time steps. In the case of RELAP5/MOD1 the code logic selects small time steps. Even smaller time steps were used by the user to avoid oscillations.

4. If the 3-D option of TRAC-PF1 is used (about 30% of the total number of nodes selected to perform 3-D calculations), the code will run about 5 times slower than the 1-D option.

5. RELAP5/MOD1 needs improvement in numerics. It takes small time steps and sometimes the user may make them even smaller in order to eliminate or minimize oscillations. Mass and energy conservation problems in stagnant volumes should be corrected.

6. TRAC-BD1 is a slow running code compared to TRAC-PF1. With about the same ratio of 3-D nodes used in TRAC-PF1 calculations, the code runs about 2.5-3 times slower than 3-D TRAC-PF1. Inclusion of two-step numerics in TRAC-BD1 should speed up the calculations.

7. Use of excessive number of heat transfer surfaces in TRAC-BD1 drastically slows the calculations. The user should carefully evaluate the need for each heat transfer surface.

TABLE 2.1

KEY PARAMETERS FOR A SMALL BREAK LOCA

- GLOBAL PEAK CLAD TEMPERATURE
- TIME FOR PEAK CLAD TEMPERATURE
- TIME FOR CHF
- MIN CORE LEVEL
- TIME FOR MIN CORE LEVEL
- LENGTH OF TIME 2-Ø LEVEL STAYS BELOW TOP OF CORE
- TIME FOR INITIATION OF CORE UNCOVERING
- TIME FOR HPI INITIATION
- TIME FOR ACCUMULATOR INJECTION
- STEAM GENERATOR PEAK PRESSURE
- TIME FOR STEAM GENERATOR PEAK PRESSURE
- TIME FOR PRIMARY-SECONDARY PRESSURE EQUALIZATION
- TIME FOR LOOP SEAL CLEARANCE

TABLE 3.1

TRAC-PF1
COMPARISON OF CALCULATED AND MEASURED
PEAK CLAD TEMPERATURES (K)

TEST ID	CALC.	MEAS.	CALC-MEAS DIFF.
S-UT-2 (10% BR W. UHI)	596	620	-24
S-UT-6 (5% BR W/O UHI)	702	651	+51
S-UT-7 (5% BR W UHI)	571	569	+ 2
L5-1 (INT. BR.)	699	715	-16
L8-2 (INT. BR. DEGRADED ECCS)	875	978	-103

TABLE 3.2

TRAC-PF1

COMPARISON OF CALCULATED AND MEASURED TIME FOR CHF

TEST ID.	CALC.	MEAS.	CALC-MEAS DIFF.
S-UT-2 (10% BR W. UHI)	49	56	-7
S-UT-6 (5% BR W/O UHI)	499	600	-101
S-UT-7 (5% BR W. UHI)	692	777	-85
L5-1 (INT. BR.)	118	121	-3
L8-2 (INT. BR. DEGRADED ECCS)	161	115	46

TABLE 3.3

TRAC-PF1

COMPARISON OF CALCULATED AND MEASURED

TIMES FOR ACCUMULATOR INJECTION

TEST ID.	CALC.	MEAS.	CALC-MEAS. DIFF.
S-UT-2 (10% BR W. UHI)	344	345	-1
S-UT-6 (5% BR W/O UHI)	667	740	-73
S-UT-7 (5% BR W. UHI)	745	738	7
L5-1 (INT. BR.)	166	184	-18
L8-2 (INT. BR. DEGRADED ECCS)	294	294	0

TABLE 3.4

TRAC-PF1

COMPARISON OF CALCULATED AND MEASURED

TIMES FOR HPI INJECTION

TEST ID.	CALC.	MEAS.	DIFF.
S-UT-2 (10% BR W. UHI)	2.5	2.5	0
S-UT-6 (5% BR W/O UHI)	33	35.2	-2.2
S-UT-7 (5% BR W. UHI)	33	34	-1
L5-1 (INT. BR.)	3.8	2.9	.9
L8-2 (INT. BR. DEGRADED ECCS)	3.4	3.0	.4

TABLE 4.1

RELAP5/MOD1

COMPARISON OF CALCULATED AND MEASURED
PEAK CLAD TEMPERATURES (K)

TEST ID.	CALC.	MEAS.	CALC-MEAS. DIFF.
LOBI A1-03	829	828	1
LOBI A1-04R	842	823	19
LOBI A1-04	727	698	29

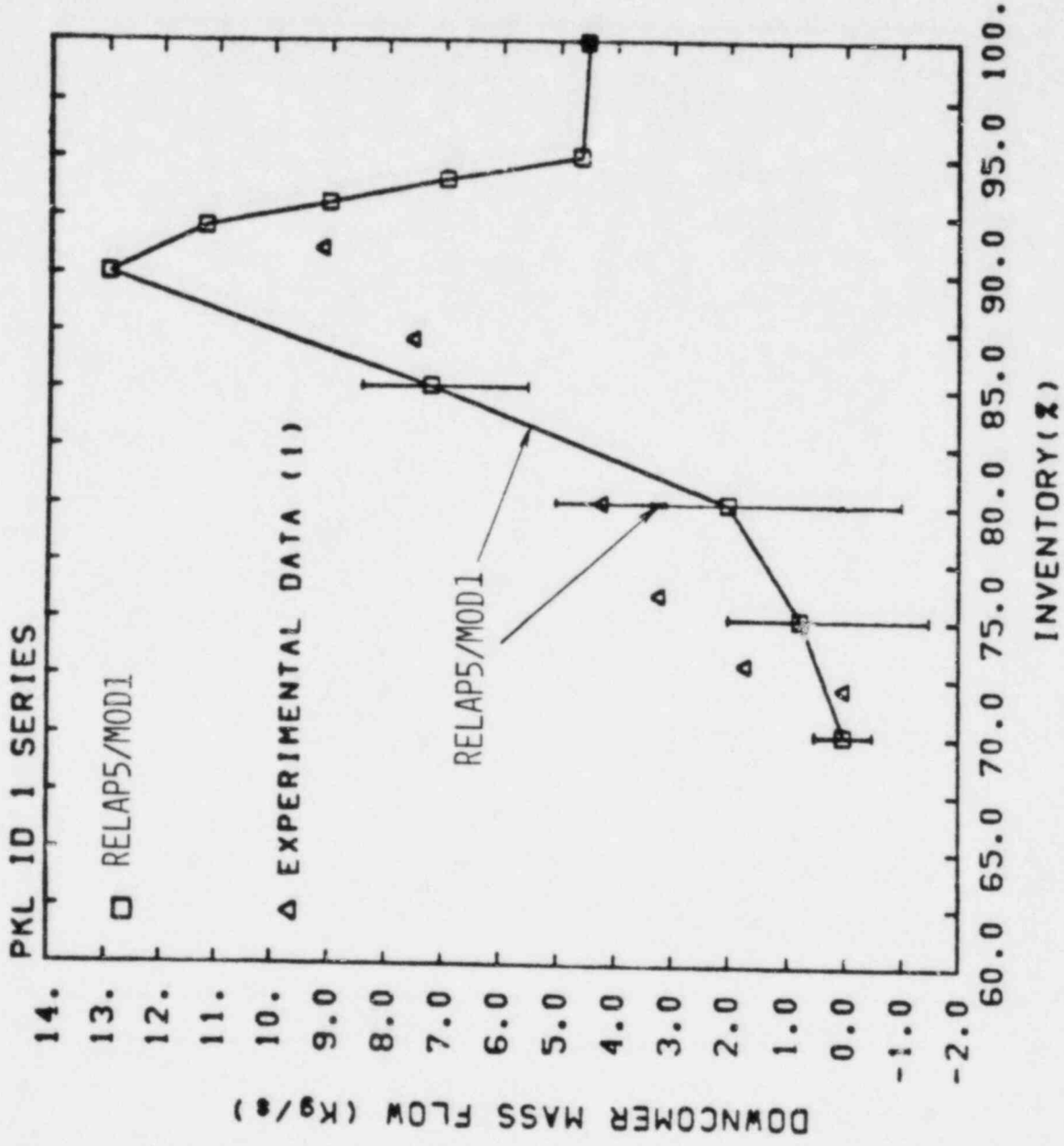

COMPARISON OF RELAP5/MOD1 CALCULATIONS WITH PKL TEST DATA

FIGURE 4.1

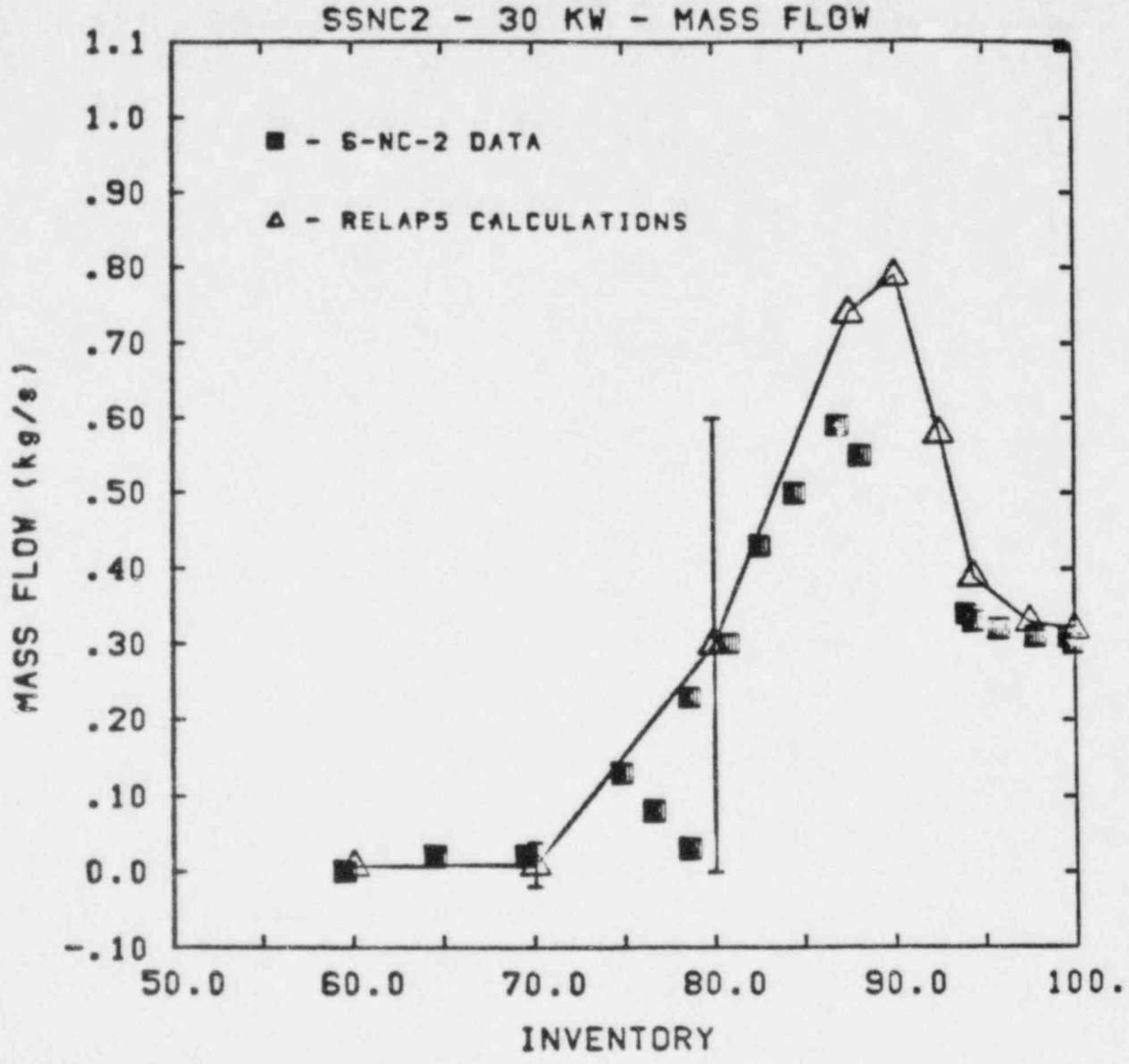

COMPARISON OF RELAP5/MOD1 CALCULATIONS WITH SEMISCALE (SSNC2) NATURAL CIRCULATION DATA

FIGURE 4.2

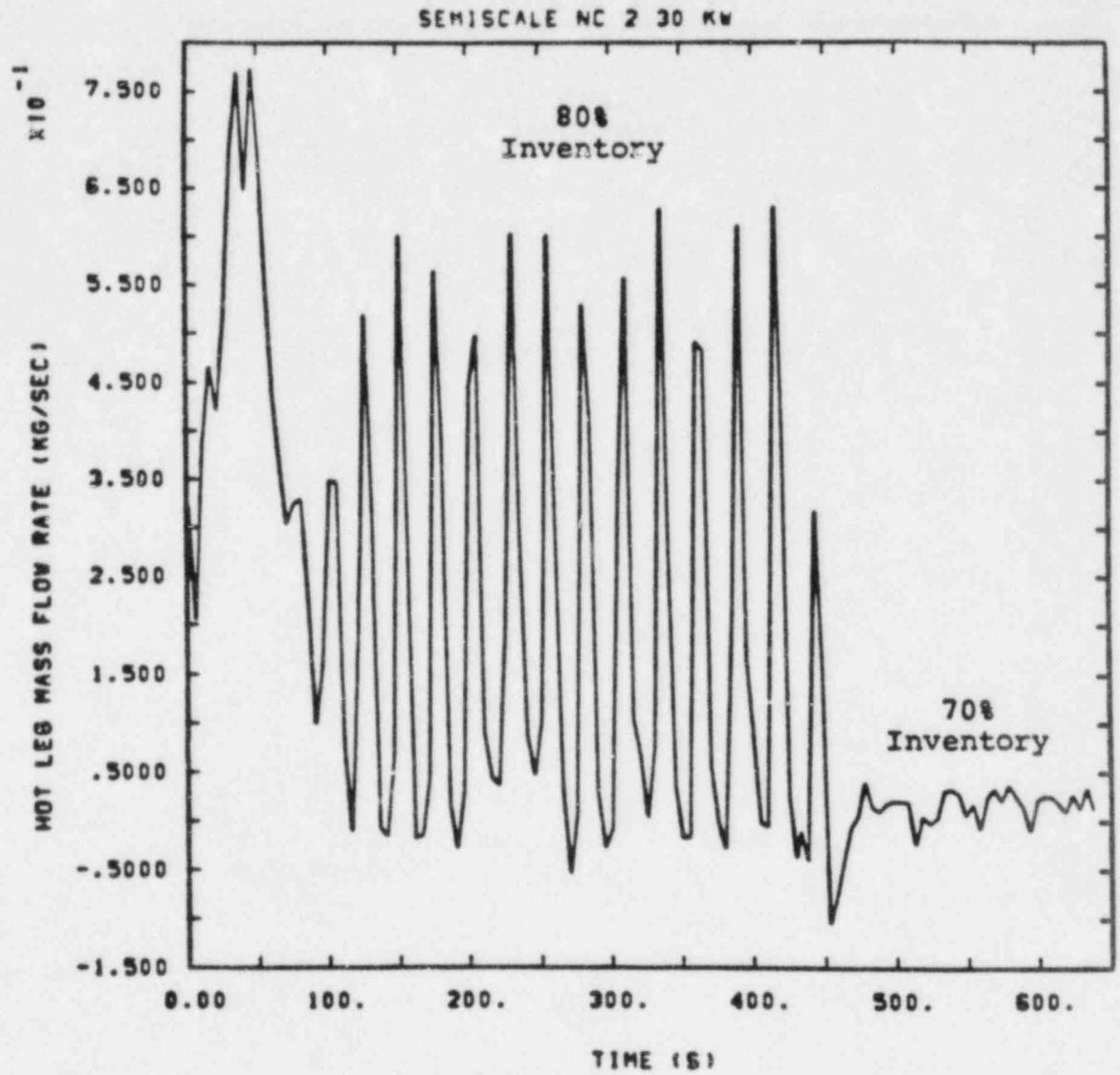

RELAP5/MOD1 CALCULATIONS FOR DIFFERENT INVENTORIES

FIGURE 4.3

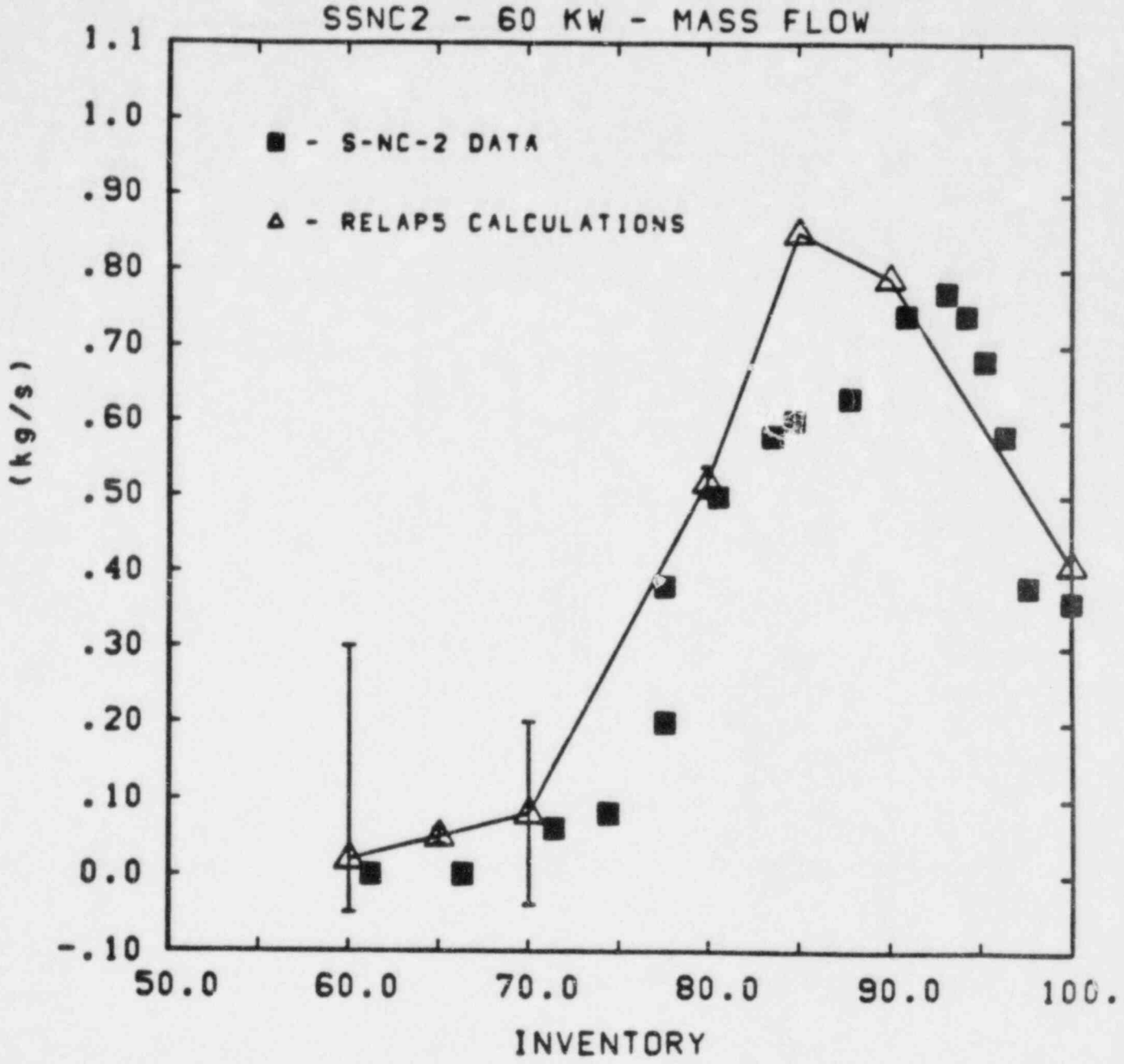

COMPARISON OF RELAP5/MOD1 CALCULATIONS WITH SEMISCALE (SSNC2) NATURAL CIRCULATION DATA

FIGURE 4 4

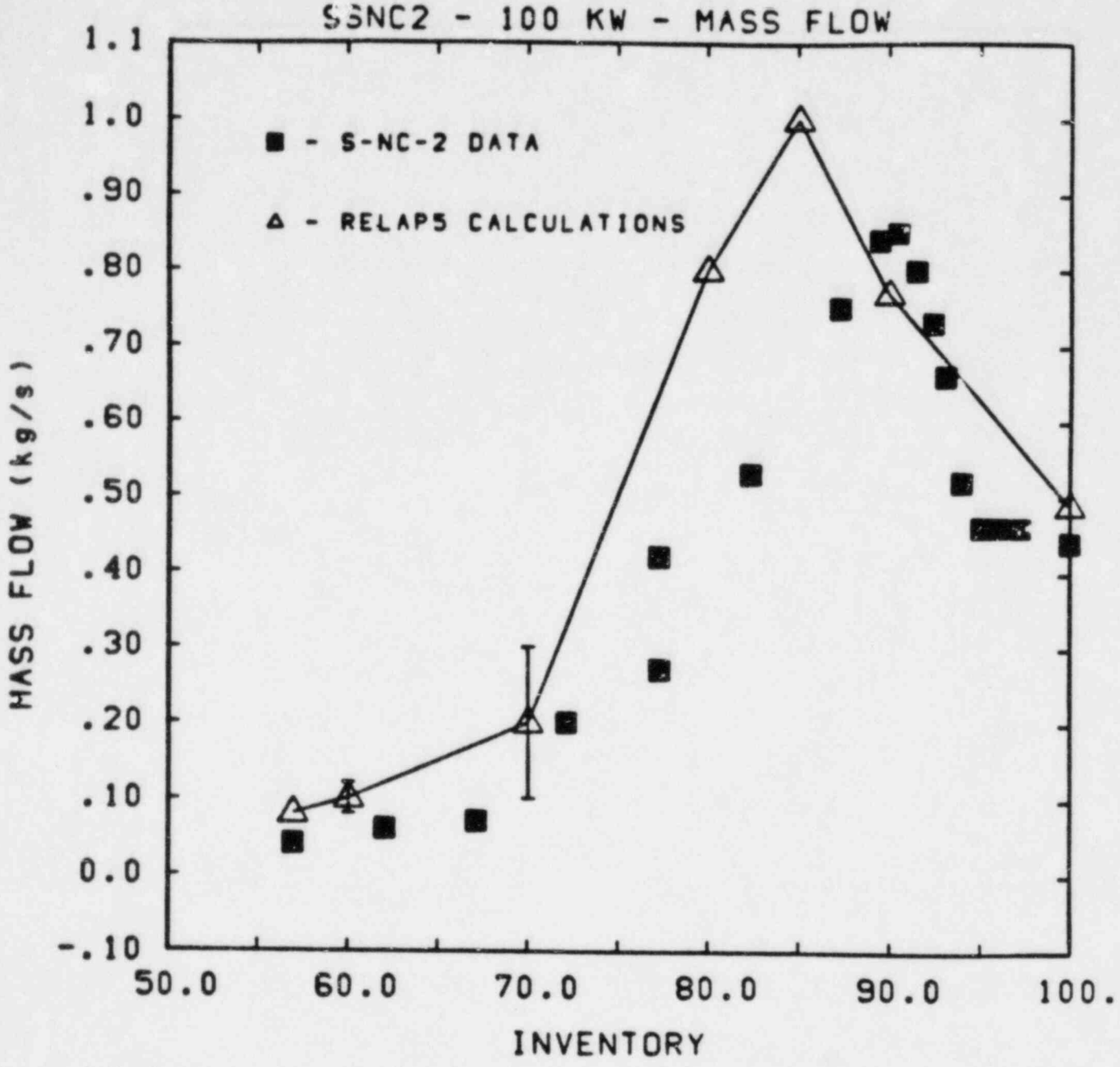

COMPARISON OF RELAP5/MOD1 CALCULATIONS WITH SEMISCALE (SSNC2) NATURAL CIRCULATION DATA

FIGURE 4.5

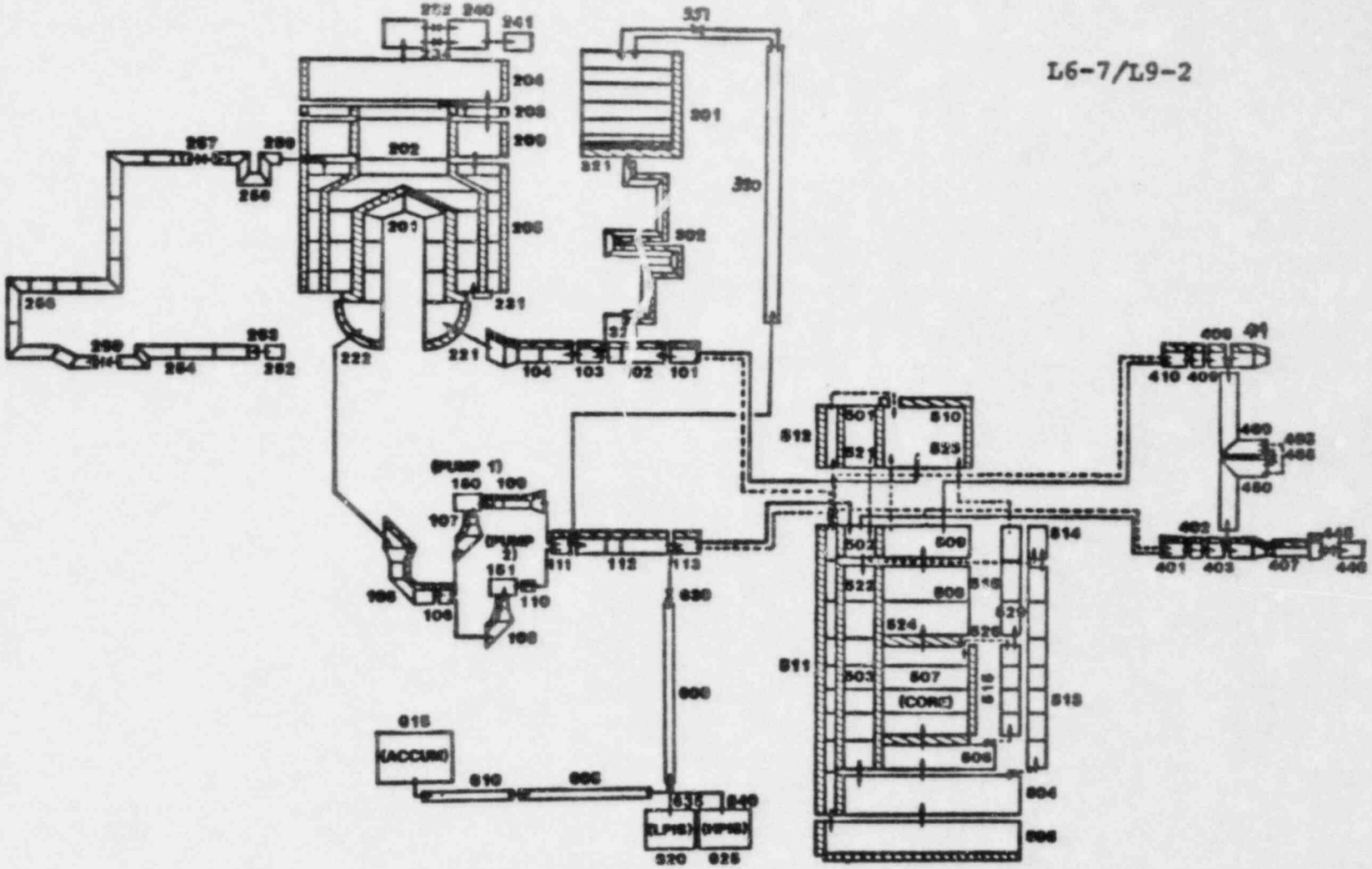

RELAP5/MOD1 NODING FOR L6-7/L9-2

FIGURE 4.6

L6-7/L9-2

TURBINE TRIP/PRIMARY PUMP TRIP

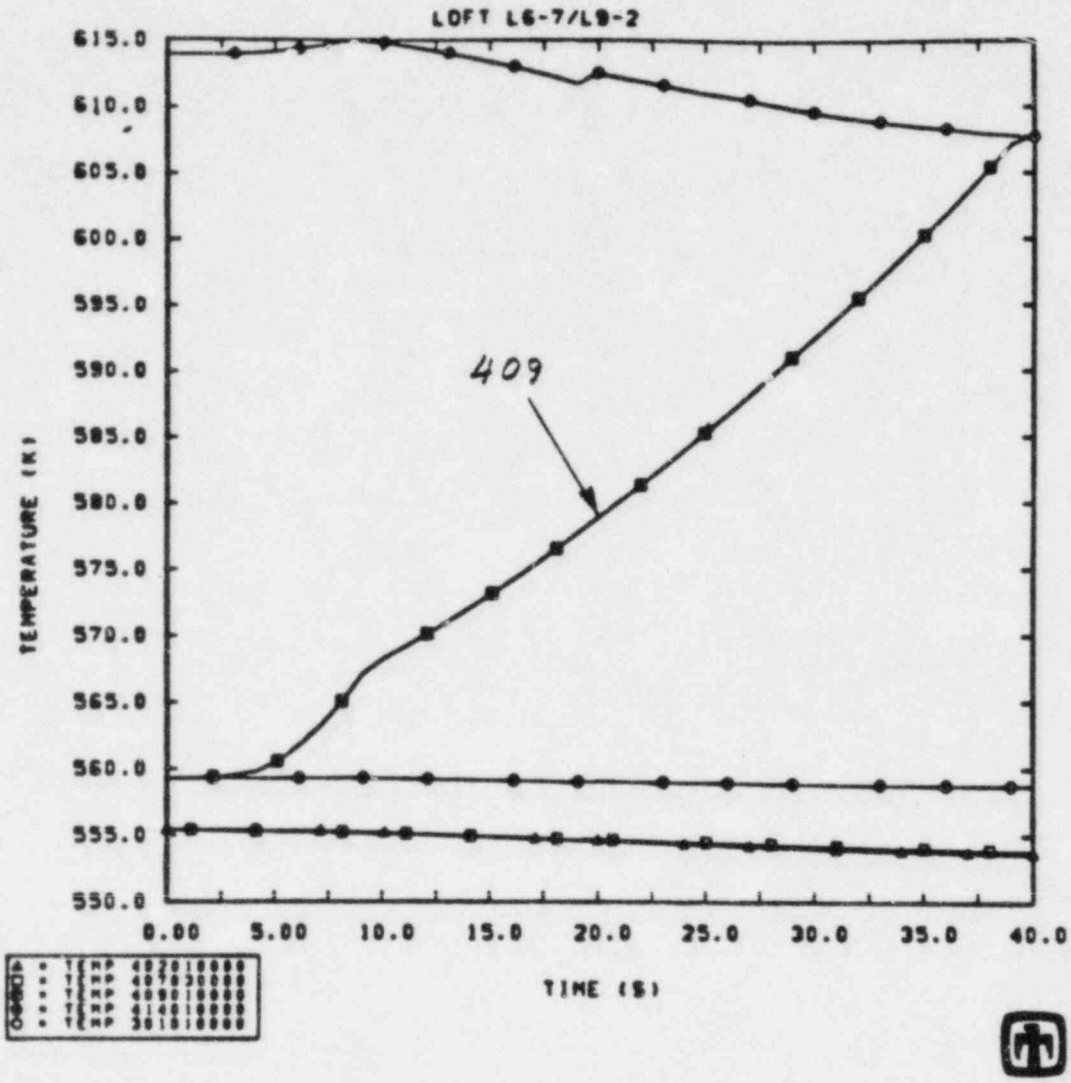

ERROR IN ENERGY CONSERVATION

IN RELAP5/MOD1

FIGURE 4.7

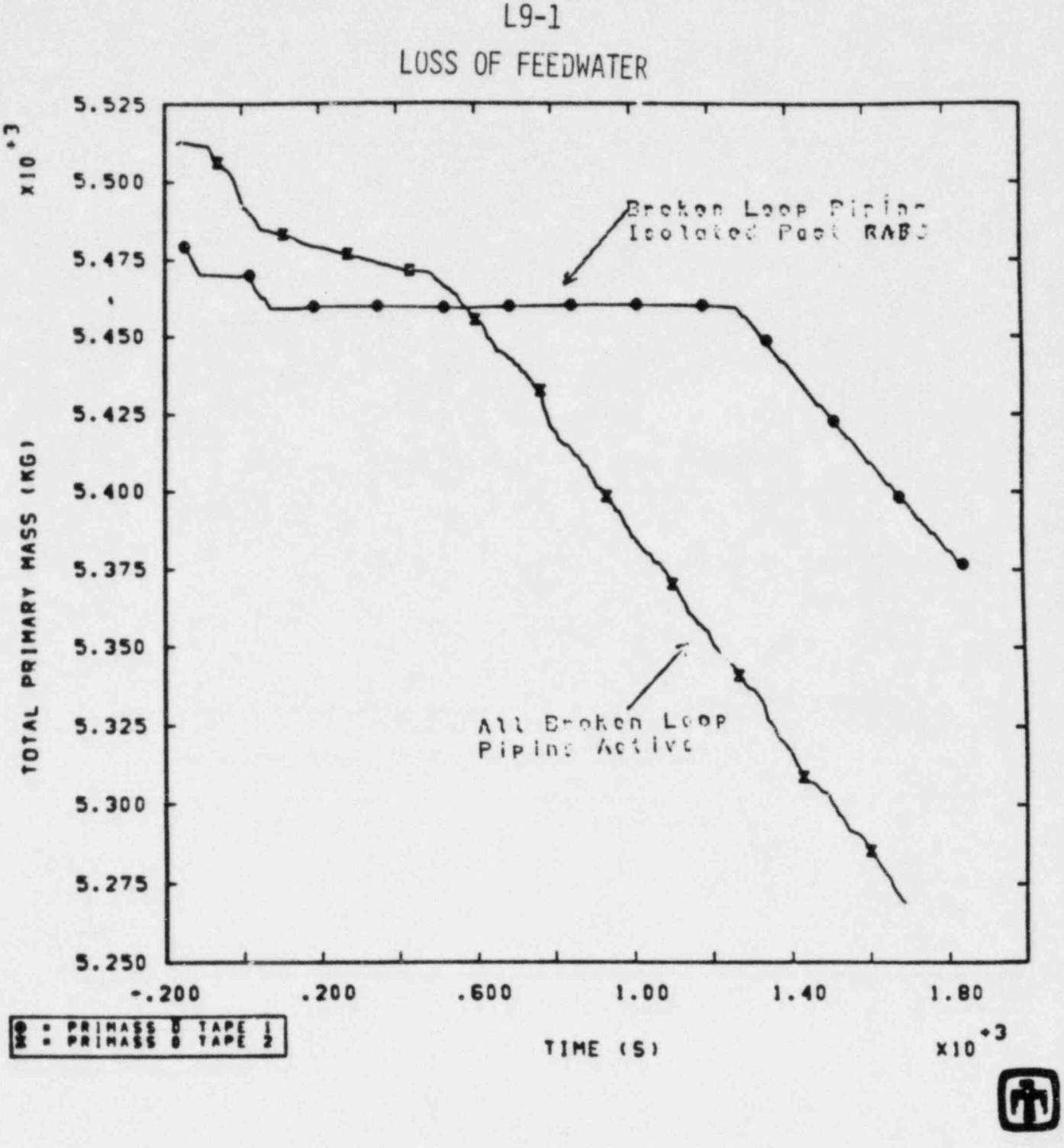

ERROR IN MASS CONSERVATION IN RELAP5/MOD1

FIGURE 4.8

TABLE 5.1

QUANTITATIVE KEY PARAMETERS

FOR BWR LOCA

PEAK CLAD TEMPERATURE (PCT)

TIME TO:

- PCT
- INITIAL ROD DRY OUT
- CORE QUENCH
- JET PUMP UNCOVERY
- RECIRCULATION LINE UNCOVERY
- ECC ACTIVATION

TIME TO MINIMUM DOWNCOMER DP

TABLE 5.2

TRAC - BD1

PEAK CLAD TEMPERATURE (K)

EXPERIMENT	TEST	CODE VERSION	CALC.	MEAS.	CALC-MEAS. DIFFERENCE
TLTA ECC/NO ECC	6425	11	612	518	94
	6426		946	1026	-80
TLTA DBA	6423	11	950	634	316
	6424		875	755	120
ROSA-III	912	11/12	665	664	1
TLTA SM. BK.	6431	12	580	580	0
	6432		580	580	0
GOTA	42	12	925	1020	-95

TABLE 6.1

TRAC-PF1 EXECUTION
(SEPARATE EFFECTS TESTS)

TEST ID	GE LARGE VES.	B&W (IEOSG)	FLECHT SEASET 21806	FLECHT SEASET 22020
REAL TIME (S) (RT)	20	50	1300	1300
# CELLS (#C)	17	26	46	46
# VES. CELLS	0	0	0	0
# HEAT SURF.	0	10	24	24
# DT STEPS (# DT)	236	255	31,022	7,048
CPU (S)	21	21	4,419	1,115
$\frac{CPU}{RT}$	1	0.42	3.4	0.86
$\frac{CPU \times 10^2}{RT \times \#C}$	6.2	1.6	7.39	1.87
$\frac{CPU \times 10^6}{RT \times \#C \times \#DT}$	260	63	2.38	2.65
$\frac{CPU \times 10^3}{\#C \times \#DT}$	5.2	3.2	3.1	3.4

COMPUTER: CDC 7600

TABLE 6.2

RELAP5/MOD1 EXECUTION
(SEPARATE EFFECTS TESTS)

TEST ID	GE LARGE VES.	B&W (IEOSG)	FLECHT 21806	SEASET 22010
REAL TIME (S) (RT)	20	50	1300	1300
# CELLS (#C)	14	26	46	46
# VES. CELLS	0	0	0	0
# HEAT SURF.	0	10	24	24
# DT STEPS (#DT)	28,814	400	42,327	167,370
CPU (S)	400	12	2,568	9,271
$\frac{CPU}{RT}$	20	0.24	1.98	7.13
$\frac{CPU}{RT \times \#C}$	1.5	0.01	0.0429	0.155
$\frac{CPU\ 10^6}{RT \times \#C \times DT}$	50	23	1.014	0.93
$\frac{CPU \times 10^3}{\#C \times \#\ DT}$	1.0	1.2	1.3	1.2

COMPUTER: CDC 7600

TABLE 6.3

TRAC-PF1 EXECUTION
(INTEGRAL TESTS)

TEST ID	SEMISCALE			LOFT		
	UT-2	UT-6	UT-7	L5-1	L8-2 BEF. REFL.	L8-2 TOTAL
REAL TIME (S) (RT)	1494.7	1500.1	1000.0	225.6	300.0	319.5
# CELLS (#C)	198	198	198	116	128	128
# VES. CELLS	0	0	0	36	36	36
# HEAT SURF.	105	105	105	94	94	94
# DT STEPS (# DT)	12,793	8,618	5,117	8,609	8,550	12,463
CPU (S)	8,243.4	5,791.7	3,460.2	4,640.9	5,201.2	7,461.6
$\frac{CPU}{RT}$	5.52	3.86	3.46	20.57	17.34	23.25
$\frac{CPU \times 10^2}{RT \times \#C}$	2.79	1.95	1.75	17.7	13.5	18.2
$\frac{CPU \times 10^6}{RT \times \#C \times \#DT}$	2.18	2.26	3.42	20.6	15.8	14.6
$\frac{CPU \times 10^3}{\#C \times \#DT}$	3.25	3.39	3.42	4.65	4.75	4.68

COMPUTER: CDC 7600

TABLE 6.4

RELAP5/MOD1 EXECUTION

(INTEGRAL TESTS)

TEST ID	LOBI A1-03 (BLD-REFL)	LOBI A1-04R (BLD-REFL)	LOBI A1-04 (BLD)	LOFT L3-6 (SB LOCA)	LOFT L9-1 LOSS FW
REAL TIME (S) (RT)	10 + 63	10 + 80	10 + 80	100 + 1844	150 + 3270
# CELLS (#C)	198	186	186	204	201
# VES. CELLS	0	0	0	0	0
# HEAT SURF.	255	255	255	150	147
# DT STEPS (# DT)	54,326	34,563	33,628	185,560	112,943
CPU (S)	14,350	11,000	10,500	55,273	28,685
$\frac{CPU}{RT}$	196	122	117	28.4	8.4
$\frac{CPU \times 10}{RT \times \#C}$	0.99	0.66	0.63	0.14	0.042
$\frac{CPU \times 10^6}{RT \times \#C \times \#DT}$	18	19	19	.75	.37
$\frac{CPU \times 10^3}{\#C \times \#DT}$	1.33	1.71	1.71	1.44	1.29

COMPUTER: CYBER 76

ESTIMATED SLOWDOWN DUE TO RESEGMENTATION: 10~15%

TABLE 6.5

TRAC-BD1
(INTEGRAL TESTS)

TEST ID	GOTA 42	ROSA III ISP 12 SBLOCA	TLTA 6423 DBA	TLTA 6432 SB LOCA	BWR 6 L3 LOCA	BWR 3 LB LOCA
REAL TIME (S) (RT)	176	600	230	1500	155	190
# CELLS (#C)	47	142	94	121	112	160
# VES. CELLS	26	36	26	32	32	52
# HEAT SURF.	60	131	110	150	176	266
# DT STEPS (# DT)	41,178	84,116	67,568	86,276	21,586	27,150
CPU (S)	8,273	32,500	18,951	30,847	8,264	32,300
$\frac{CPU}{RT}$	67	65	82	46	53.3	170
$\frac{CPU}{RT \times \#C}$	1.	0.46	0.88	0.38	.476	1.06
$\frac{CPU \times 10^6}{RT \times \#C \times \#DT}$	24.3	5.44	13.0	4.45	22	39.1
$\frac{CPU \times 10^3}{\#C \times \#DT}$	- 4.27	2.72	2.98	2.96	3.42	7.44

References

1. "Independent Assessment of the TRAC-PD2 Code," F. Odar, Proceedings of Topical Meeting on Advances in Reactor Physics and Core Thermal Hydraulics, NUREG/CR-0034, pp 960-981, September 1982, or "Status of Code Assessment," F. Odar, Proceedings of Ninth Water Reactor Safety Information Meeting, March 1982.

2. "Independent Code Assessment at BNL in FY 1982," P. Saha, et al., Department of Nuclear Energy, BNL, Proceedings of Tenth Water Reactor Safety Research Information Meeting, to be published.

3. "TRAC-BD1 Calculations and Data Compaison of International Standard Problem 12," R. Dallman, EGG-CAAD-5860, May 1982.

4. "TRAC-BD1 Calculation of ESTA Test," N. Abe, et. al., Toshiba Corp., Proceedings for Tenth Water Reactor Safety Research Information Meeting, to be published.

5. "Descriptive Evaluation of RELAP5," J. Trapp, EPRI-NP-2366, April 1982.

LA-UR-82-2805

CALCULATIONS OF PRESSURIZED THERMAL SHOCK PROBLEMS WITH THE SOLA-PTS METHOD *

Bart J. Daly, Bryan A. Kashiwa, and Martin D. Torrey
Theoretical Division, Group T-3
University of California
Los Alamos National Laboratory
Los Alamos, NM 87545

ABSTRACT

A numerical procedure has been developed for multidimensional studies of detailed fluid-thermal mixing and wall heat transfer in the cold leg and downcomer of pressurized water reactors for application to the study of pressurized thermal shock. This method is briefly described and examples of its application to various test problems are presented to demonstrate its accuracy. An application of the method to the pressurized thermal shock problem is described for the case of a main steam line break.

I. INTRODUCTION

This report describes the SOLA-PTS computational method for fluid mixing and wall heat transfer that has been developed for application to the study of pressurized thermal shock (PTS). The conditions for PTS are a high system pressure coincident with rapid cooling of a section of vessel wall, particularly in the vicinity of neutron flux-weakened welds. The fluid dynamics problem is to predict the temperature of the vessel wall for a variety of different accident scenarios.

These accident sequences can be subdivided into two main classes: those with and those without loop flow. When loop flow is maintained, the transient solution is obtained by a systems code analysis. While these codes may be able to predict the system response to a particular accident scenario quite accurately, they cannot provide detailed information about the thermal distribution along

*This paper was prepared for the report on the proceedings of the Tenth Water Reactor Safety Research Information Meeting and was not listed in the agenda for this meeting.

the vessel wall. It is the purpose of the numerical method described here to provide that detailed information for those accident scenarios where it is suspected that there is incomplete mixing in the downcomer, and for isolated times during a transient. This is accomplished by taking the systems code data at a particular location in the cold leg as input boundary conditions for the detailed calculations. Holding these boundary conditions fixed in time, a three-dimensional steady state solution is computed showing the flow field and thermal distribution in the cold leg and downcomer. The walls are generally treated adiabatically in order to hasten the approach to steady state. The steady state fluid temperature distribution adjacent to the vessel wall can then be used to conservatively estimate the temperature distribution in the metal. The use of the adiabatic wall treatment in this case is justified because the effect of wall heat transfer should be small compared to the heat exchange that results from the mixing of the emergency core coolant (ECC) water with the loop flow. If the adiabatic treatment indicates that conditions for crack initiation are present, then the inclusion of wall heat flux to avoid crack initiation cannot be conservatively justified since the fracture mechanics aspects of the problem are not well enough known.

The results of these three-dimensional calculations do not influence the system code solution, because the details of the downcomer flow have little effect on the loop flow calculation. Regardless of what fluid motions develop in the downcomer, the fluid should be throughly mixed in the lower plenum region.

The second main class of problems, those without loop flow, do not require a system code solution. The requirement in this case is to calculate the transient

mixing of ECC water with the stagnant (or rapidly decelerating) hot water in the cold leg, downcomer and lower plenum. In this case wall heat transfer is included in the calculations, since for this problem it is the rate at which the wall temperature cools that will determine the probability for crack initiation.

Section II of this paper provides a description of the numerical method. Some calculational examples that were used to test the code are described in this section. Section III provides the results of an application to a PTS problems, and concluding remarks are made in Sec. IV.

II. THE COMPUTATIONAL MODEL

The SOLA-PTS code had its origen in the SOLA[1] and SOLA-VOF[2] codes developed at Los Alamos. It is a computational model for the solution of transient, incompressible, single-phase flow problems, together with wall heat transfer and thermal transport. The code exists in both two- and three-dimensional forms. The two-dimensional code is used for testing models and for scoping studies, while the three-dimensional code is applied to the solution of detailed PTS problems.

Using the original solution algorithm incorporated in the SOLA codes, the following equations are solved in SOLA-PTS*

$$\frac{\partial u_i}{\partial x_i} = 0 \tag{1}$$

$$\frac{\partial u_i}{\partial t} + u_j \frac{\partial u_i}{\partial x_j} = -\frac{1}{\rho}\frac{\partial p}{\partial x_i} + \frac{\partial \tau_{ij}}{\partial x_j} + [1 - \beta(T - T_o)]g_i \tag{2}$$

$$\frac{\partial T}{\partial t} + u_i \frac{\partial T}{\partial x_i} = \frac{\partial}{\partial x_i}\left(\sigma_f \frac{\partial T}{\partial x_i}\right) \tag{3}$$

*The definition of the variables is provided in the nomenclature.

$$\frac{\partial T}{\partial t} = \frac{\partial}{\partial x_i}\left(\sigma_m \frac{\partial T}{\partial x_i}\right) \tag{4}$$

Equations (1) - (3) are solved in the fluid, and Eq. (4) is solved in the metal. Note that Eqs. (2) and (3) are in non-conservative form. This form is used instead of the conservative form because of a zero-order truncation error that results with the use of the latter in conjunction with a variable computational mesh. In order to optimize computing efficiency, it is essential to utilize a scheme that maintains good accuracy with a variable grid. Hence conservative schemes are unacceptable for these PTS studies.

To ensure a stable, accurate solution to the above equations we make use of the Tensor Viscosity method[3] for the calculation of spatial derivatives, together with the Filtering Remedy and Methodology (FRAM) method[4] for the suppression of dispersion errors. The Tensor Viscosity method is the multidimensional analog of one-dimensional, interpolated donor cell. It is a second-order-accurate difference scheme that is formulated by evaluating the convective terms using forward-time, space-centered derivatives, and then modifying the equations by the addition of a term,

$$-\frac{1}{2}\,\delta t\,\frac{\partial}{\partial x_i}\left(u_i u_j \frac{\partial \phi}{\partial x_j}\right) ,$$

to the right side of the equation. Here ϕ represents the temperature or a velocity component.

As with any second order method, the Tensor Viscosity method can suffer from dispersion errors when used without some type of filtering procedure, such as FRAM. In the FRAM method, a provisional estimate for the value of a variable at

an advanced time level is made using any given high-order differencing technique. The provisional value is compared to the maximum and minimum of the advanced time values obtained by neglecting convection at the computational cell in question and its four adjacent neighbors. If the provisional, high-order value falls between the maximum and minimum, it is considered to be the advanced time solution; if not, it is replaced by a solution based on a low-order, diffusive differencing technique. In all of the studies that follow, full upwind differencing is used as the low-order technique. An alternative procedure would be to replace the provisional solution by the maximum or minimum value, whichever is exceeded. However, this procedure has not yet been tested.

Dukowicz and Ramshaw[3] tested the accuracy of the Tensor Viscosity method by examining the diffusion of a step function transported with a constant velocity. In this test the scalar transport equation

$$\frac{\partial \phi}{\partial t} + u \frac{\partial \phi}{\partial x} + v \frac{\partial \phi}{\partial y} = 0 \qquad (5)$$

is solved in a square computational space with $\delta x = \delta y = 1.0$, $u = v = 1.0$ and $\delta t = 0.2$. The initial value of ϕ in the space is 1.0, and a value 2.0 is specified at the bottom and left inflow boundaries. The right and top boundaries had a continuative outflow specification. We have repeated this test for the Tensor Viscosity method and for two other second-order methods, Leith's method[5] and Crowley's method,[6] all in conjunction with FRAM. Results of these calculations, showing the appearance of the step function at times of 0.4 and 0.8, are presented in Fig. 1. The Tensor Viscosity method shows the least effects of numerical diffusion. As a measure of the differences, one can compare the increase in

the distance from the high contour line to the low contour line between the two times plotted in Fig. 1. For the Leith method this increase is 26%; for the Crowley method the increase is 23%; for the Tensor Viscosity method the increase is 17%.

The SOLA-PTS code was also tested by computing the development of the laminar thermal boundary layer in the presence of the developing hydrodynamic boundary layer between parallel planes. The solution to this problem for non-buoyant flows is available and has been verified by experiment.[7]

Figures 2 through 6 illustrate the results of the SOLA-PTS calculation of the parallel plane thermal-hydrodynamic entry length problem with a constant heat flux at one plane and zero heat flux at the other. In this study Pr = 0.7 and Re = 40. Figures 4 through 6 show comparison of SOLA-PTS results (solid line) to the analytic solution of Heaton et al.[7] (marked by A's). These figures show excellent comparison despite having only ten computing zones across the channel in the SOLA-PTS calculation. As expected, the only significant deviation from the analytic solution occurs very near the entrance where there is a significant v component to the velocity.

The two-equation k-ε turbulence model of Launder and Spalding[8] has been included in the SOLA-PTS code. The only modification to the equations presented in Ref. 8 has been the addition of a set of terms reflecting the alteration in turbulence energy and decay rate due to buoyancy. The equations as they are currently employed in this eddy diffusivity method are

turbulence viscosity:

$$\nu_t = \frac{C_\mu k^2}{\varepsilon} \quad , \tag{6}$$

turbulence energy:

$$\frac{Dk}{Dt} = \frac{\partial}{\partial x_j}\left[\left(\frac{\nu_t}{\sigma_k} + \nu_o\right)\frac{\partial k}{\partial x_j}\right] + \nu_t\left[\frac{\partial u_i}{\partial x_j}\left(\frac{\partial u_i}{\partial x_j} + \frac{\partial u_j}{\partial x_i}\right) + \beta g_i \frac{\partial T}{\partial x_i}\right] - \varepsilon \quad , \tag{7}$$

turbulence decay rate:

$$\frac{D\varepsilon}{Dt} = \frac{\partial}{\partial x_j}\left[\left(\frac{\nu_t}{\sigma_\varepsilon} + \nu_o\right)\frac{\partial \varepsilon}{\partial x_j}\right] + C_1 \frac{\varepsilon}{k} \nu_t \left[\frac{\partial u_i}{\partial x_j}\left(\frac{\partial u_i}{\partial x_j} + \frac{\partial u_j}{\partial x_i}\right) + \beta g_i \frac{\partial T}{\partial x_i}\right] - C_2 \frac{\varepsilon^2}{k} \quad , \tag{8}$$

turbulence decay rate near the wall:

$$\int_o^{y_p} \varepsilon \, dy = \frac{C_\mu}{\kappa} k_p^{3/2} \, \ell n\left[\frac{E \, y_p (C_\mu^{\frac{1}{2}} k_p)^{\frac{1}{2}}}{\nu_o}\right] \quad , \tag{9}$$

wall shear stress:

$$\frac{u_p (C_\mu^{\frac{1}{2}} k_p)^{\frac{1}{2}}}{(\tau/\rho)_w} = \frac{1}{\kappa} \ell n\left[\frac{E \, y_p (C_\mu^{\frac{1}{2}} k_p)^{\frac{1}{2}}}{\nu_o}\right] \quad . \tag{10}$$

wall heat flux:

$$\frac{(T_p - T_w) c_p \rho (C_\mu^{\frac{1}{2}} k_p)^{\frac{1}{2}}}{\dot{q}_w''} = \frac{\sigma_h}{\kappa} \ell n\left[\frac{E \, y_p (C_\mu^{\frac{1}{2}} k_p)^{\frac{1}{2}}}{\nu_o}\right]$$

$$+ \sigma_h \frac{\pi/4}{\sin(\pi/4)} \left(\frac{A}{\kappa}\right)^{\frac{1}{2}} \left(\frac{Pr}{\sigma_h} - 1\right)\left(\frac{\sigma_h}{Pr}\right)^{1/4} \tag{11}$$

The equation for wall shear stress Eq. (10) is used to account for the effect of wall drag in the PTS calculations. The wall shear stress is also used to esti-

mate the velocity gradient outside the laminar sublayer for the calculation of the shear creation terms in Eqs. (7) and (8).

The turbulence model embodied in Eqs. (6) through (11) has been extensively studied for a wide range of experimental data.[8] We have applied the model as it is included in the SOLA-PTS code to the study of turbulent flow between parallel planes. A comparison of these calculated results with Laufer's[9] experimental data for fully developed flow between parallel planes is given in Fig. 7. In this study the velocity and turbulence energy profiles are plotted versus position in the channel of half-spacing d. The computed values, given by the symbols in Fig. 7, were obtained from a one-dimensional channel flow calculation with Re = 61,600 and ν_o = 0.002 cm^2/s using a specified pressure gradient. In this way, u is a function of y alone. Three calculations were performed to test the sensitivity of results to the finite difference resolution. It is clear from Fig. 7 that the results are not sensitive to mesh size and that good agreement is achieved even when there are only five computational zones across the channel width.

III. PTS CALCULATION

As an example of a PTS application we present results obtained in SOLA-PTS calculations of a main steam line break (MSLB) transient, using data from a TRAC system code calculation as our input conditions. We chose to perform the calculation at a time of 160 s into the transient, when the pressure is at 50 bars, the pumps have coasted down, and there is no vent value flow into the downcomer. At this time the thermal-hydraulics are characterized by a high temperature (> 500 K), low velocity flow in the intact loops, and a low temperature (< 420 K), high velocity flow in the broken loop. The high velocity flow on the

broken loop side is driven by natural convection as a result of the large temperature difference between the upper plenum and the steam generator on that loop. The input conditions for these calculations are shown in Table I.

Figures 8-11 show results obtained in the broken loop calculation. Figures 8-9 are velocity vector plots in the horizontal plane at the elevation of the ECC injection and in the vertical plane through the centerline of the cold leg, respectively. In this calculation the loop flow is injected into the cold leg at a position 8.4 m upstream from the entrance to the downcomer and the coolant enters the cold leg 5.6 m upstream. Both plots show that as the fluid enters the downcomer it splashes against the core barrel wall, while the flow region adjacent to the vessel wall is relatively stagnant. The non-fluid region in the bottom left corner of Fig. 8 is the hot leg obstruction. Note the variable mesh in this calculation, with fine noding in the region of the ECC injection.

The velocity plot in Fig. 10 shows the flow development in the plane adjacent to the vessel wall. These fluid motions result primarily from recirculation of the main flow, which lies adjacent to the core barrel. The expanding flow in the top center of the plot is the cold leg inflow. The hot leg is at the upper left.

The temperature distribution adjacent to the vessel wall is shown in the contour plot of Fig. 11. The minimum temperature is at the cold leg inlet, where the fluid is approximately 10°C cooler than the average fluid temperature in this plane. However, even this coldest fluid has a temperature of 407 K, indicating that there has been thorough mixing of the 303.3 K ECC water (see Table I) with the loop flow in the cold leg. Thus, at this time in the transient there appears to be no threat of crack initiation in the vessel wall on the broken loop side.

Figures 12-15 show results obtained in the intact loop calculation. The velocity vectors in the horizontal and vertical planes corresponding to those of Figs. 8 and 9 are not shown. They appear very similar to Figs. 8 and 9 except that, because of the reduced loop flow in the present calculation, the ECC injection exerts a greater influence on the cold leg flow. Figures 12 and 13 show velocity vector plots in the planes adjacent to the core barrel and vessel walls. These plots demonstrate the coherent flow pattern adjacent to the core barrel (Fig. 12), resulting from the impact of cold leg flow, and the lack of coherent flow adjacent to the vessel wall, corresponding to relatively stagnant flow conditions. These stagnant conditions adjacent to the vessel wall are also evident in the temperature contour plot in that plane, shown in Fig. 14. With the exception of a relatively cold region near the cold leg inlet, the temperatures are practically uniform throughout this plane. The minimum temperature here is 514 K, which indicates no threat to the integrity of the vessel wall at this time in the transient.

Figure 15 shows the temperature contour plot in a vertical plane containing the cold leg centerline. The effect of the ECC injection at the cold leg boundary is evident in this centerline plot, but the temperature variation from upstream values is minor. Note that a stratified flow condition persists to the downcomer.

IV. SUMMARY

A brief description has been presented of the SOLA-PTS computational method for multidimensional calculation of fluid-thermal mixing and wall heat transfer, with particular application to the study of pressurized thermal shock. Several computational examples have been presented to demonstrate the accuracy of the computational algorithm and the turbulence model employed.

This method will be applied to two classes of computational problems that arise in the pressurized thermal shock study. The first of these is the problem of calculating the mixing of ECC water with loop flow, with or without vent valve flow, in the cold leg and downcomer in order to determine the fluid temperature distribution along the vessel wall. These problems are calculated as steady-state solutions, using systems code information to provide the inlet boundary conditions, in order to provide, "snapshots" of the thermal distributions at isolated times during a transient. An example of results obtained in a main steam line break transient have been presented as illustration of this procedure.

The second application of the SOLA-PTS method has been to the transient calculation of fluid-thermal mixing and wall heat transfer in the cold leg and downcomer when there is no loop flow in the system. In this case the temperature throughout the downcomer will eventually reach the ECC temperature. The objective is to calculate the rate of cooling of the metal in the vessel wall. Calculations of this type are being persued at the present time.

REFERENCES

1. C. W. Hirt, B. D. Nichols, and N. C. Romero, "SOLA - A Numerical Solution Algorithm for Transient Fluid Flows," Los Alamos Scientific Laboratory report LA-5852, April 1975.

2. B. D. Nichols, C. W. Hirt, and R. S. Hotchkiss, "SOLA-VOF: A Solution Algorithm for Transient Fluid Flow with Multiple Free Boundaries," Los Alamos Scientific Laboratory report LA-8355, August 1980.

3. J. K. Dukowicz and J. D. Ramshaw, "Tensor Viscosity Method for Convection in Numerical Fluid Dynamics," J. Comput. Phys. 32, 71-79 (July 1979).

4. M. Chapman, "FRAM: Nonlinear Damping Algorithms for the Continuity Equation," J. Comput. Phys. 44, 84-103 (1981).

5. P. J. Roache, Computational Fluid Dynamics, Hermosa Publishers, Albuquerque, NM (1972).

6. W. P. Crowley, "Second-Order Numerical Advection," J. Comput. Phys. 1, 471-484 (1967).

7. H. S. Heaton, W. C. Reynolds, and W. M. Kays, "Heat Transfer in Annular Passages. Simultaneous Development of Velocity and Temperature Fields in Laminar Flow," Int. J. Heat Mass Transfer 7, 763-781 (1964).

8. B. E. Launder and D. B. Spalding, "The Numerical Computation of Turbulent Flows," Comput. Meth. in App. Mech. and Eng. 3, 269-289 (1974).

9. J. Laufer, "Investigation of Turbulent Flow in a Two-Dimensional Channel," NACA Report 1053 (1951).

TABLE I

INPUT CONDITIONS, MAIN STEAM LINE BREAK

	Velocity (cm/s)	Temperature (K)	Area (cm^2)	Flow Rate (cm^3/s)
Broken Loop				
ECC	175.85	303.3	77.4	1.361×10^4
Loop	149.64	418.0	3969.0	5.939×10^5
Intact Loop				
ECC	125.6	303.3	108.4	1.361×10^4
Loop	40.1	527.9	3969.0	1.592×10^5

Nomenclature

Symbols

c_p	Specific heat
D_h	Hydraulic diameter
H	Plate spacing
k	Turbulence energy
p	Pressure
Pr	Prandtl number
$\dot{q}''_w$	Heat flux
Re	Reynolds number
t	Time
T	Temperature
u_i	Velocity component in i direction
x_i	Spatial coordinate i
y	Distance

Greek Symbols

β	Fluid volume coefficient of expansion
δt	Time increment
ε	Turbulence energy decay rate
ν	Kinematic viscosity
ρ	Fluid density
σ	Thermal diffusivity
τ	Shear stress
ϕ	Velocity component or scalar

Subscripts

e	Entrance
f	Fluid
i	Insulated
m	Metal
o	Reference or molecular value
p	Value at center of fluid cell adjacent to wall
t	Turbulent
w	Wall

Constants

A	Van Driest's constant (26.0)
C_1	1.44
C_2	1.92
C_μ	0.09
E	9.0
g_i	Gravitational acceleration in i direction
κ	0.4
σ_h	Turbulent Prandtl number (assumed 1.0)
σ_k	1.0
σ_ε	1.3

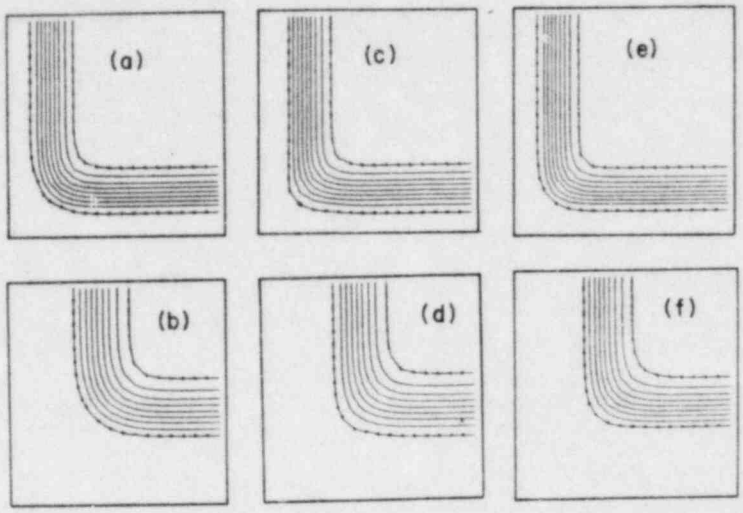

Fig. 1. Contours of ϕ for Leith's method at t = 0.4 (a) and t = 0.8 (b), Crowley's method at t = 0.4 (c) and t = 0.8 (d), and the Tensor Viscosity method at t = 0.4 (e) and t = 0.8 (f). The three methods are used in conjunction with the FRAM procedure (see text).

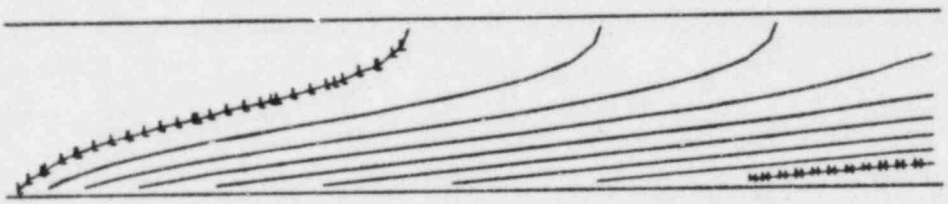

Fig. 2. Temperature contours for the laminar thermal-hydraulic entry length for parallel planes, one plane with constant heat flux and the other plane insulated. The incoming temperature is 400 K, $\dot{q}''_w/\rho c_p$ = 31.49 cm K/s, the plate spacing H is 10.0 cm, the Reynolds number Re based on mean velocity and hydraulic diameter D_h is 40, and the Prandtl number Pr is 0.7. The high contour (H) is 898.2 K and the low contour (L) is 455.4 K.

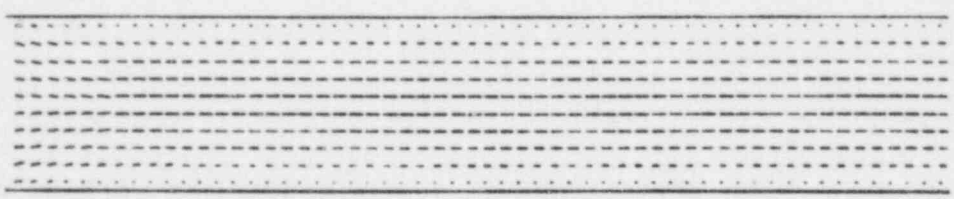

Fig. 3. Velocity vectors for the laminar thermal-hydrodynamic entry length problem, showing the developing velocity profile.

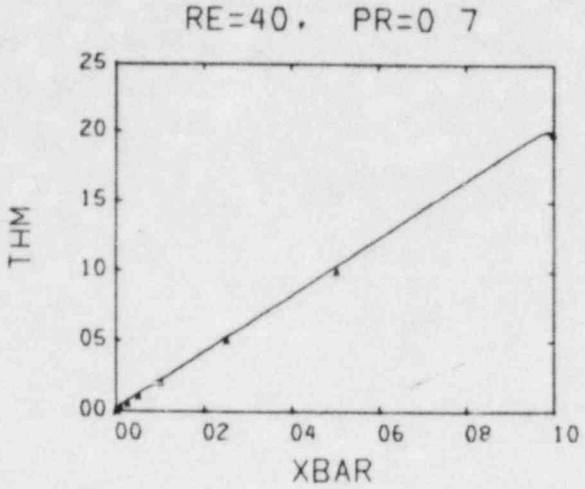

Fig. 4. Non-dimensional mean temperature THM vs non-dimensional distance XBAR for the laminar thermal-hydrodynamic entry length problem. XBAR $\equiv x/(D_h RePr)$,

$$THM \equiv (\overline{T} - T_e)\frac{\sigma_f \rho c_p}{\dot{q}''_w D_h},$$

where $\overline{T} \equiv \int_0^H uT\,dy / \int_0^H u\,dy$.

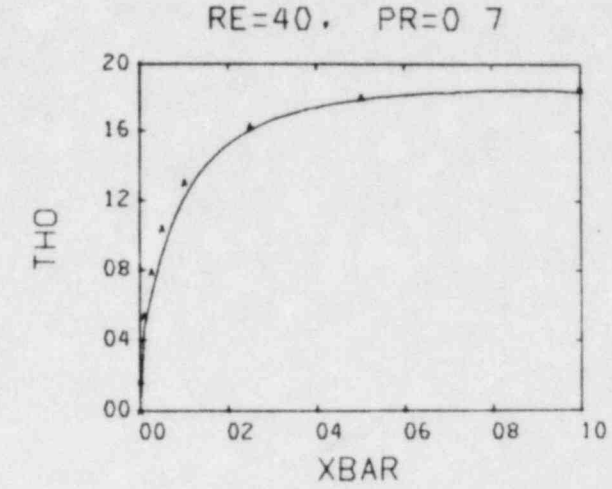

Fig. 5. Non-dimensional heated wall temperature THO vs non-dimensional distance for the laminar thermal-hydrodynamic entry length problem.

$$THO = (T_w - \overline{T})\frac{\sigma_f \rho c_p}{\dot{q}''_w D_h}.$$

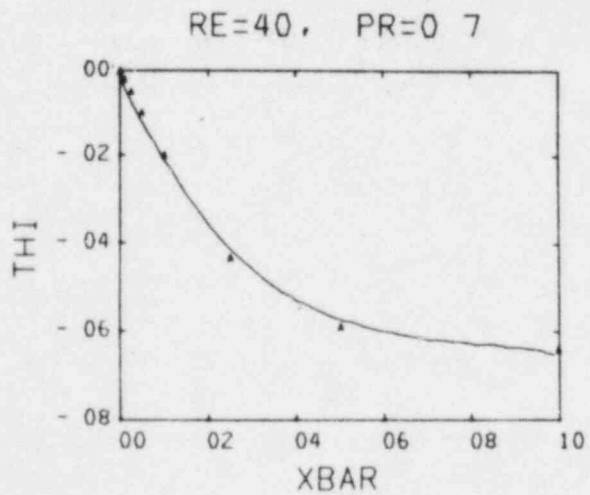

Fig. 6. Non-dimensional insulated wall temperature THI vs non-dimensional distance for the laminar thermal-hydrodynamic entry length problem.

$$THI \equiv (T_i - \overline{T})\frac{\sigma_f \rho c_p}{\dot{q}''_w D_h}.$$

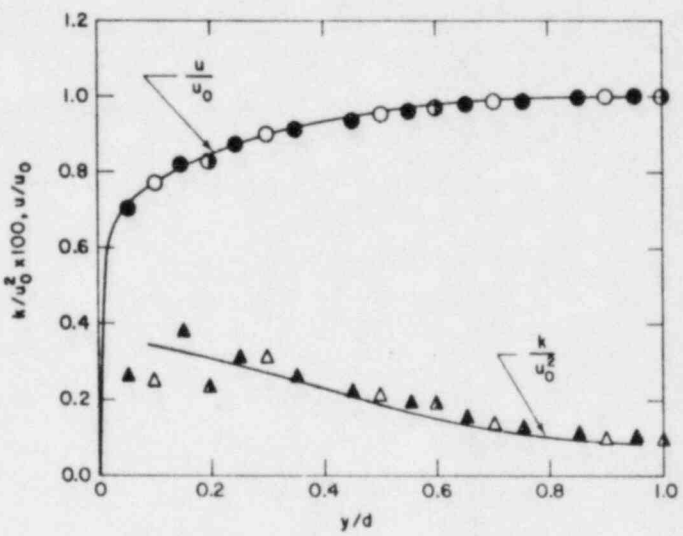

Fig. 7. Turbulence velocity and turbulence energy profiles for flow between parallel planes at Re = 61,600. The solid line is from the experimental data of Laufer (Ref. 9), the solid symbols are from a one dimensional SOLA-PTS calculation with 20 cells across the channel, the open symbols are from a calculation with 10 cells across the channel, and the half-opened symbols are from a calculation with 5 cells across the channel.

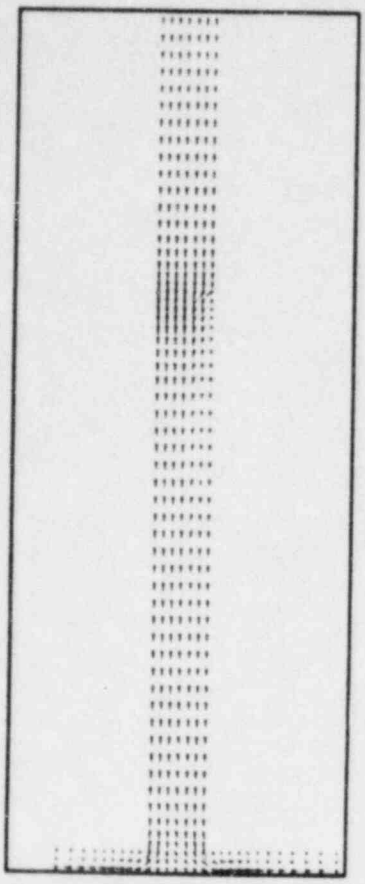

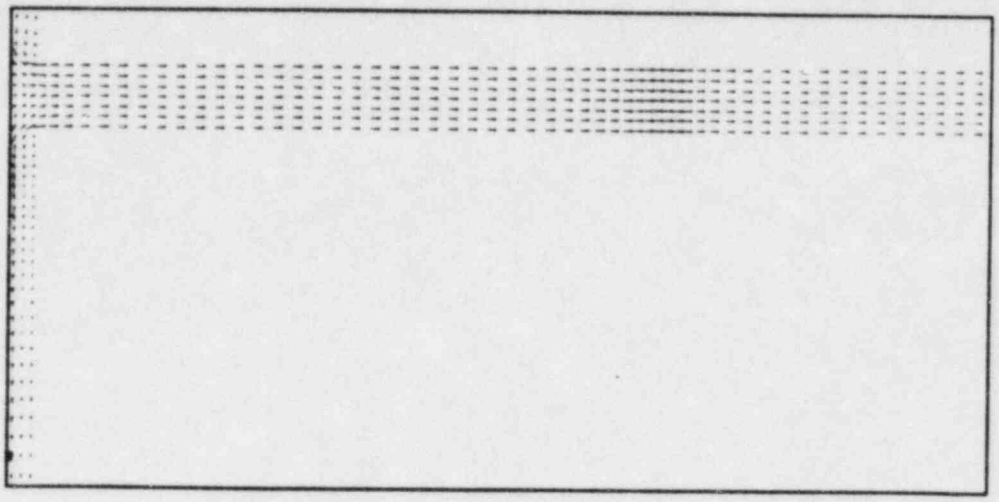

Fig. 9. Velocity vector plots in the vertical plane through the cold leg centerline for the broken loop calculation at 160 s into the MSLB transient. The cold leg flow impacts the core barrel wall at the left.

Fig. 8. (see left) Velocity vector plots in the horizontal plane at the elevation of the ECC injection for the broken loop calculation at 160 s into the MSLB transient. The cross-flow vectors in the cold leg show the ECC injection. The downcomer is located at the bottom of the plot and the hot leg obstruction is in the bottom left corner.

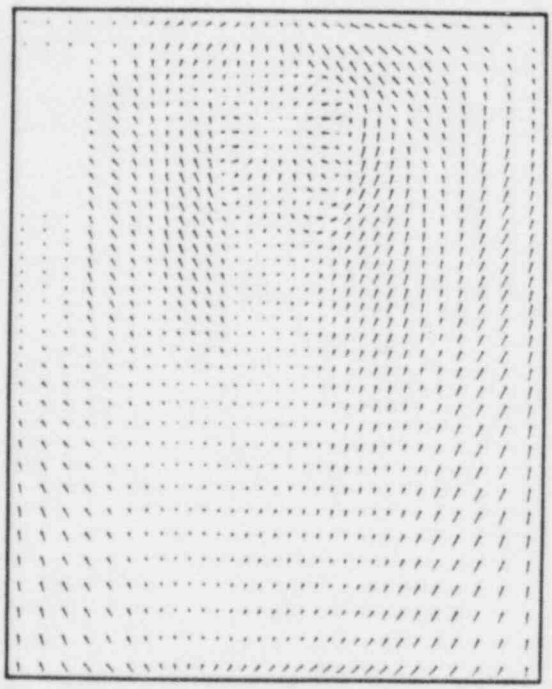

Fig. 10. Velocity vector plot in the plane adjacent to the vessel wall for the broken loop calculation at 160 s into the MSLB transient. The expanding flow in the upper center of the plot is the cold leg inflow. The hot leg obstruction is at the upper left.

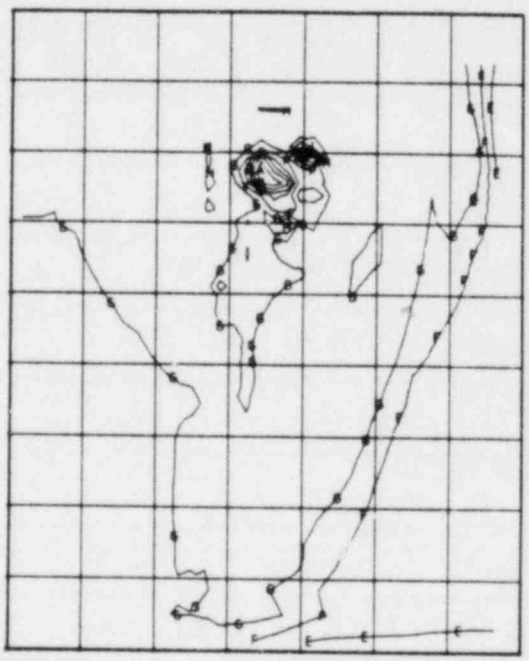

Fig. 11. Temperature contour plot in the plane adjacent to the vessel wall for the broken loop calculation at 160 s into the MSLB transient. The minimum contour (A) has the value 407.1 K and the contour interval is 1.57 K.

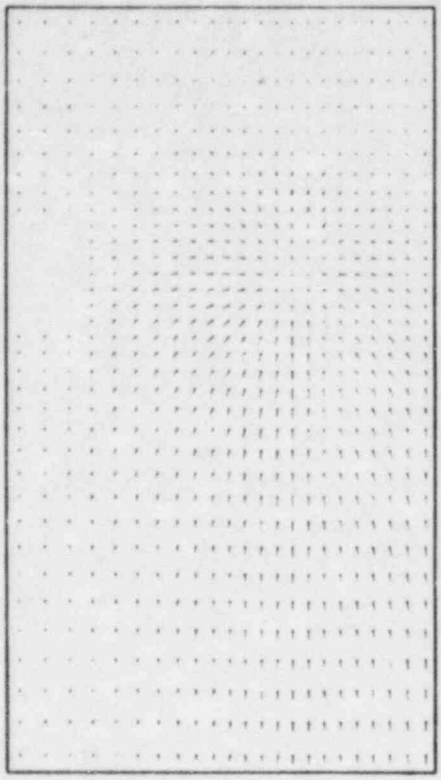

Fig. 12. Velocity vector plot in the plane adjacent to the core barrel wall for the intact loop calculation at 160 s into the MSLB transient. A greater part of the upper downcomer region is included here than in the broken loop calculation.

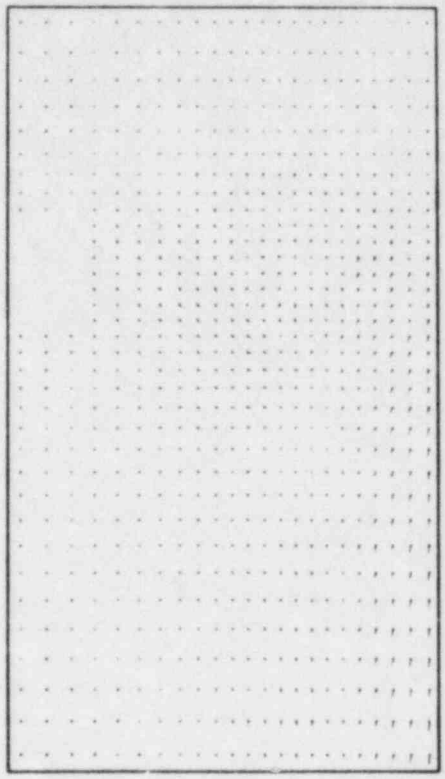

Fig. 13. Velocity vector plot in the plane adjacent to the vessel wall for the intact loop calculation at 160 s into the MSLB transient.

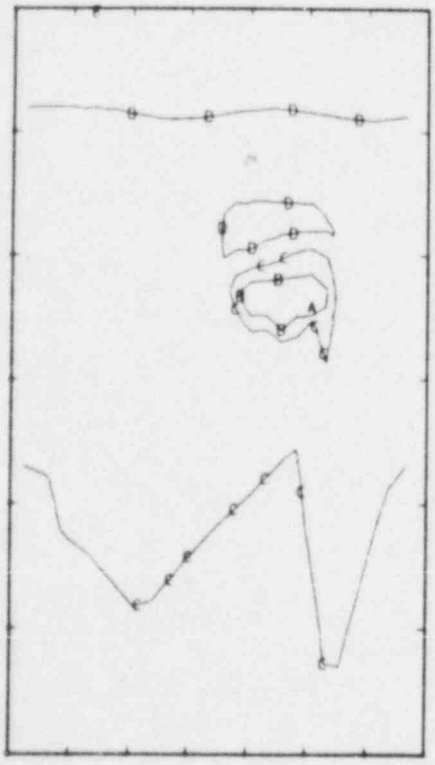

Fig. 14. (see left) Temperature contour plot in the plane adjacent to the vessel wall for the intact loop calculation at 160 s into the MSLB transient. The minimum contour (A) is 514.2 K and the contour interval is 3.41 K.

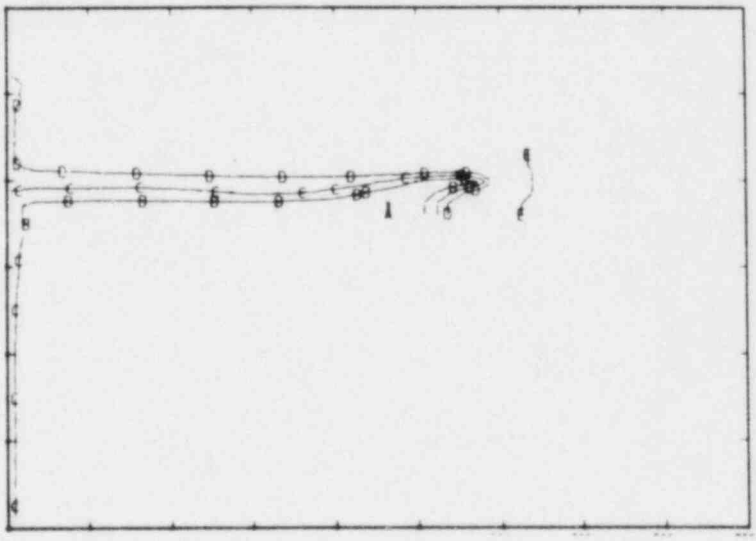

Fig. 15. Temperature contour plot in a vertical plane through the cold leg centerline for the intact loop calculation at 160 s into the MSLB transient. The minimum contour (A) is 510.9 K and the contour interval is 4.25 K.

LA-UR-82-2806

HYDROGEN MIGRATION MODELING FOR THE EPRI/HEDL STANDARD PROBLEMS *

J. R. Travis
Theoretical Division, Group T-3
University of California
Los Alamos National Laboratory
Los Alamos, NM 87545

ABSTRACT

A numerical technique has been developed for calculating the full three-dimensional time-dependent Navier-Stokes equations with multiple species transport. The method is a modified form of the Implicit Continuous-fluid Eulerian (ICE) technique to solve the governing equations for low Mach number flows where pressure waves and local variations in compression and expansion are not significant. Large density variations, due to thermal and species concentration gradients, are accounted for without the restrictions of the classical Boussinesq approximation. Calculations of the EPRI/HEDL standard problems verify the feasibility of using this finite-difference technique for analyzing hydrogen dispersion within LWR containments.

I. INTRODUCTION

During and after a loss-of-coolant accident in a light-water reactor, water may be decomposed by chemical reactions and radiolysis to release gaseous hydrogen. Should hydrogen be released, two deleterious effects could occur. The noncondensable gas can increase the containment pressure. In sufficient amounts, the hydrogen could burn in the presence of air, causing considerable loads on the containment walls or harm to crucial control devices. Each effect represents an additional safety risk. To better assess the problem, we have developed a multidimensional fluid dynamics finite-difference code (HMS: Hydrogen Migration Studies) to calculate the details of hydrogen transport through containment structures.

This detailed model of the full three-dimensional time-dependent Navier-Stokes equations with species transport is solved by a variant of the Implicit Continuous-fluid Eulerian (ICE)[1] technique. We make use of the idea that for low-speed flows pressure wave propagation need not be resolved in detail and therefore the local fluid density is a function of the average fluid pressure, local temperature, and relative concentrations of available species. This further allows accurate representation of flows driven by large density variations for which the Boussinesq approximation may not provide sufficient accuracy.[2]

Ultimately this detailed model, together with relevant experimental data, will help to benchmark existing hydrogen migration systems codes that are necessarily based on simpler models. This paper presents the governing equations, describes the solution procedure, and presents numerical results for comparison of experimental results in the three-dimensional geometry of the EPRI/HEDL standard problems.[3]

This paper could not be scheduled for presentation at the meeting and was submitted for publication in the proceedings report.

II. MATHEMATICAL DESCRIPTION

The partial-differential equations that govern the fluid dynamics and species transport are presented in this section.

A. The Mixture Equations

The mixture mass conservation equation is

$$\frac{\partial \rho}{\partial t} + \nabla \cdot (\rho \bar{u}) = \sum_{\alpha=1}^{3} S_\alpha \quad , \tag{1}$$

where

$\rho = \sum_{\alpha=1}^{3} \rho'_\alpha$; ρ'_α = macroscopic density of the individual species (air, steam, or hydrogen),

$\bar{u}$ = mass-average velocity vector, and

S_α = mass source (+) and/or sink (-) of species α per unit volume and time.

The mixture momentum conservation equations are given by

$$\frac{\partial (\rho \bar{u})}{\partial t} + \nabla \cdot (\rho \bar{\bar{u}} \bar{\bar{u}}) = - \nabla p + \nabla \cdot \bar{\bar{\sigma}} + \hat{\rho} \bar{g} + \bar{M} \quad , \tag{2}$$

where

p = pressure,

$\bar{\bar{\sigma}}$ = Newtonian viscous stress tensor,

$\hat{\rho}$ = local density relative to the average density, and

$\bar{M}$ = momentum source vector per unit volume and time.

The mixture internal energy equation is

$$\frac{\partial}{\partial t}(\rho I) + \nabla\cdot(\rho I\bar{u}) = \nabla\cdot(K\nabla T) + Q \quad , \tag{3}$$

where

I = mixture specific internal energy,

K = thermal conductivity,

T = mixture temperature, and

Q = energy source and/or sink per unit volume and time.

We assume viscous dissipation is negligible for the low-speed flows of interest.

The equation-of-state for the average fluid pressure P_o is given by the ideal gas mixture equation

$$P_o = T \sum_{\alpha=1}^{3} (\gamma_\alpha - 1)(C_v)_\alpha \rho'_\alpha \quad , \tag{4}$$

where γ_α is the ratio of specific heats for species α and $(C_v)_\alpha$ is the specific heat at constant volume for species α.

B. The Species Transport Equations

The dynamics of the individual species are determined by

$$\frac{\partial \rho'_\alpha}{\partial t} + \nabla\cdot(\rho'_\alpha \bar{u}) = S_\alpha \quad . \tag{5}$$

Summing Eq. (5) over all species results in the mixture mass Eq. (1).

III. SOLUTION PROCEUDRE

Equations (1) - (3) and (5) are written in finite difference form for their numerical solution. The nonlinear finite-difference equations are then solved iteratively using a point relaxation model. Since we are interested in low-speed

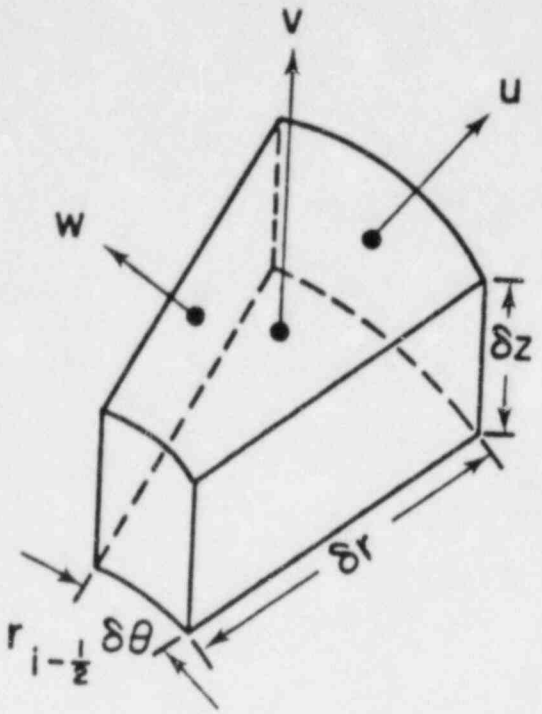

Fig. 1
Locations of velocity components for a typical cell in cylindrical geometry.

flows where the propagation of pressure waves need not be resolved, we are therefore utilizing a modified ICE[1] solution technique where the species densities are functions of the global or compartment pressure, and not of the local pressure. Time-dependent solutions can be obtained in one, two, and three space dimensions in plane and in cylindrical geometries. The geometric region of interest is divided into many finite-size, space-fixed zones called computational cells that collectively form the computing mesh. Figure 1 shows a typical computational cell with the velocities centered on the cell boundaries. All other quantities, such as I, p and (ρ'_α)'s, are positioned at the cell-center designated (i,j,k). The finite-difference equations for the quantities at time $t = (n+1)\delta t$ form a system of coupled, non-linear algebraic equations.

For the problems of interest (See Sec. IV), the source/sink terms in the species transport equations are:

(1) Air (a); $S_a = 0$;

(2) Hydrogen or helium (h); S_h = hydrogen or helium mass per unit volume and time in the jet; and

(3) Steam(s), $S_s - C_s$ = (steam mass per unit volume and time in the jet) - (condensation mass per unit volume and time).

The sources of hydrogen or helium and steam are specified by the experiment; however, the condensation rate must be modeled. We propose the simple but effective relationship, based on the assumption of local equilibrium,

$$C_s = R[\rho'_s(\text{local steam density}) - \rho'_{sat}(T)]$$

where

$\rho'_{sat}(T)$ = saturation steam density at temperature T,

$R = 10^{10}$ /s for ρ'_s(local steam density) > $\rho'_{sat}(T)$, or

$R = 0$, otherwise.

The HMS solution method starts with the explicit calculation of the source terms in the species transport equations (5), and the convection, viscous, gravity, and source terms in the mixture momentum equations (2). The solution method then proceeds with the iteration phase:

(1) The $(\rho'_\alpha)^{n+1}$'s are found from the species transport equations using the latest iterates for $(\rho')_\alpha^{n+1}$ and $\bar{u}^{n+1}$.

(2) The global or average fluid pressure, P_o^{n+1} is determined by integrating the equation-of-state (4) over the computational volume.

(3) The equation-of-state is modified slightly to find the mixture density using the $(\rho'_\alpha)^{n+1}$'s and P_o^{n+1} from steps (1) and (2)

$$\rho^{n+1}_{i,j,k} = \frac{P_o^{n+1} \sum_{\alpha=1}^{3} (\rho'_\alpha)^{n+1}_{i,j,k}}{T^n_{i,j,k} \sum_{\alpha=1}^{3} (\gamma_\alpha - 1)(C_v)_\alpha (\rho'_\alpha)^{n+1}_{i,j,k}} \quad .$$

(4) With $\rho^{n+1}_{i,j,k}$ [from step (3)] and the latest iterates for $\bar{u}^{n+1}$ the residual, $D_{i,j,k}$, in the mixture mass equation is calculated. If the convergence criterion is met, for example $|D_{i,j,k}| < \varepsilon$ where $\varepsilon = 10^{-4} \times \rho^n_{i,j,k}$, then no adjustment is made to the local pressure, $p^{n+1}_{i,j,k}$, and the velocities $\bar{u}^{n+1}_{i,j,k}$ for cell (i,j,k). When the convergence criterion is met for all cells in the computatonal mesh, the iteration phase of the cycle is complete.

(5) For any cell that the criterion is not met, the local pressure is changed by an amount

$$\delta p_{i,j,k} = - \frac{\Omega D_{i,j,k}}{\left(\frac{\partial D}{\partial p}\right)_{i,j,k}} \quad ,$$

where

$$\left(\frac{\partial D}{\partial \rho}\right)_{i,j,k} = \frac{2\delta t^2}{\delta r^2 + (r_i \delta\theta)^2 + \delta z^2} \quad ,$$

and Ω is a constant over-relaxation factor selected $1.0 \leq \Omega < 2.0$, and the momenta are changed due to the new pressure gradient. The velocities are found by simply dividing the momenta by the updated densities.

Steps (1) - (5) are repeated until the convergence criterion as presented in step (4) is satisfied on the entire computational mesh. After the iteration phase is complete, the specific internal-energy Eq. (3) is evaluated and the computational time step is finished with the advancement of the time step.

More details of the HMS solution methodology, code description, and a listing of the code are given in Ref. (4).

IV. NUMERICAL RESULTS

This computer code was developed to analyze the EPRI/HEDL standard problems "A" and "B".[3] The standard problems A and B, tests HM-5 and HM-6 in reference 5 respectively, were proposed as a bases for comparing blind predictions of detailed hydrogen distribution in reactor-like containment compartments. In both experiments a high velocity steam-hydrogen or steam-helium jet is released into the compartment. The reader is referred to Ref. 5, for a detailed discussion of the experimental facility.

Figure 2 presents the discretization of the containment compartment. We have modeled the blower which provides recirculation from the upper to lower compartments as four time-dependent prescribed inflow boundary cells. These are shown on the outer circumference (R = 3.81 m) at the axial position 2.36 m $\leq$ Z $\leq$ 3.15 m and in the azimuthal positions $20° \leq \theta \leq 40°$, $80° \leq \theta \leq 100°$, $200° \leq \theta \leq 220°$, and $260° \leq \theta \leq 280°$. Flow is allowed to exit the computational mesh by the eight continuative outflow boundary cells shown on the outer circumference (R = 3.81 m) at the axial position 3.93 m $\leq$ Z $\leq$ 4.72 m and in the azimuthal positions $0° \leq \theta \leq 20°$, $40° \leq \theta \leq 60°$, $80° \leq \theta \leq 100°$, $120° \leq \theta \leq 140°$, $160° \leq \theta \leq 180°$, $200° \leq \theta \leq 220°$, $240° \leq \theta \leq 260°$, and $280° \leq \theta \leq 300°$. Both tests started with the compartment at 65°C and 10^5 Pa (1 bar), with test A containing nitrogen and test B containing air. Table I lists the timing of events for each test.

Compartment wall temperatures were assumed constant at 65°C through both tests, while time-dependent prescribed inflow data consistent with the events of Table I are tabulated in Table II.

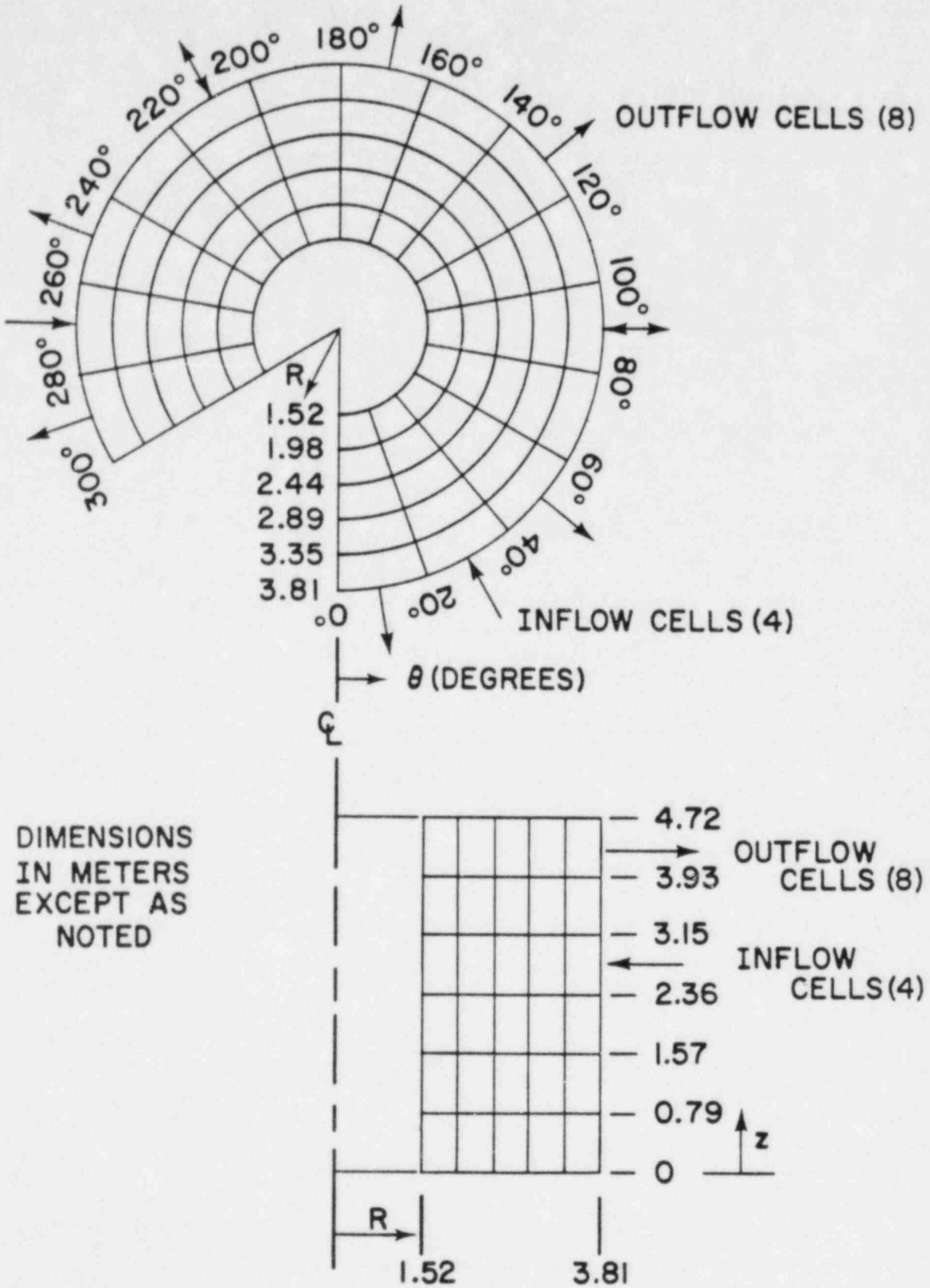

Fig. 2. HMS computing mesh for EPRI/HEDL Standard Problems A and B.

TABLE I. Timing of Events

Test A		Test B	
Time (minutes)	Event	Time (minutes)	Event
11.50	Recirculator blower on	4.00 (4.50)*	Recirculator blower on
11.75	Steam source on	4.75	Steam source on
12.50	Hydrogen source on	6.25	Helium source on
12.75	Nitrogen becomes saturated in recirculators	6.50	Air becomes saturated in recirculators
13.5	Hydrogen begins entering compartment through recirculators	7.00	Helium begins entering compartment through recirculators
23.75	Sources shut off	17.00	Sources shut off

*Blind calculation started at 4.00 minutes and the posttest calculation started at 4.50 minutes.

TABLE II. Time-Dependent Prescribed Inflow Data†

Test A		Test B	
Time (minutes)	Inlet Temperature (°C)	Time (minutes)	Inlet Temperature (°C)
0.0	35.0	0.0	35.0
8.0	35.0	4.0	35.0
10.0	35.5	7.0	42.0
13.0	40.0	10.0	43.0
18.0	53.0	11.0	46.5
21.0	57.0	16.0	52.0
23.0	58.25	17.0	52.5
24.0	58.5	20.0	49.5
32.0	53.5	29.0	46.5
35.0	52.5	31.5	46.5
46.0	51.0	32.5	48.0
60.0	50.0	70.0	47.5

Time (minutes)	Hydrogen Concentration (%)*	Time (minutes)	Helium Concentration (%)*
0.0	0.0	0.0	0.0
13.5	0.0	7.0	0.0
15.0	0.6	17.0	3.45
24.0	5.4	19.0	3.55
25.0	5.5	24.0	3.45
32.0	5.1	65.0	3.2
47.0	4.9		
70.0	4.8		

†The inlet velocity is held constant at 0.434 m/s throughout both tests.

*Hydrogen and Helium concentrations are given in volume % on a dry basis; i.e., the steam has been removed.

Experiment A had a horizontal steam-hydrogen jet that was centered in the annulus at 275° at a height of 1.52 m from the floor. The average jet velocity was assumed to be 150 m/s, and it was directed inward at 60° to a radial ray. Experiment B had a vertical steam-helium jet that was located at 180°, 1.2 m from the floor, and 2.31 m from the compartment axis. The average jet velocity was assumed to be 80 m/s.

The energy source due to the jet is calculated $S_h I_h + S_s I_s$, where $I_h = (C_v)_h T$ and $I_s = (C_v)_s T$, and T is the time-dependent jet temperature listed in Table IV. For tests A and B the mass and energy sources are associated with cells ($2.44\ m \leq R \leq 2.89\ m$, $0.79\ m \leq Z \leq 57\ m$, $260° \leq \theta \leq 280°$), and ($1.98 \leq R \leq 2.44\ m$, $0.79\ m \leq Z \leq 1.57\ m$, $160° \leq \theta \leq 180°$), respectively.

Intermediate values of the parameters in Tables II - IV may be found by linear interpolation.

TABLE III. Time-Dependent Mass Source

Test A

Time (minutes)	Steam Mass Flow Rate (kg/min)	Time (minutes)	Hydrogen Mass Flow Rate (kg/min)
0.0	0.0	0.0	0.0
11.75	0.0	12.5	0.0
12.50	21.0	13.0	0.31
14.0	24.0	23.0	0.31
23.0	24.0	23.75	0.0
23.75	0.0	60.0	0.0
60.0	0.0		

Test B

Time (minutes)	Steam Mass Flow Rate (kg/min)	Time (minutes)	Helium Mass Flow Rate (kg/min)
0.0	0.0	0.0	0.0
4.75	0.0	6.25	0.0
5.50	14.5	7.0	0.405
16.0	14.5	15.25	0.405
17.0	0.0	16.0	0.94
60.0	0.0	17.0	0.0
		60.0	0.0

TABLE IV. Time-Dependent Jet Temperature

Test A		Test B	
Time (minutes)	Temperature (°C)	Time (minutes)	Temperature (°C)
10.0	108.0	2.0	110.0
16.5	101.0	7.0	96.0
18.0	103.0	12.5	96.0
18.5	124.0	17.0	124.0
19.0	130.0	18.0	113.0
20.0	133.0	19.0	109.0
21.0	136.0	21.0	107.0
23.0	140.0	60.0	94.0
24.0	140.0		
26.0	128.0		
28.0	125.0		
60.0	109.0		

In Figs. 3 and 4, we present the test data and the blind (i.e., pretest) concentration predictions for tests A and B, respectively. The curve designated "E" represents the experimental data while the curve designated "C" represents the calculation. For test A, the horizontal jet, there is total mixing throughout the compartment as evidenced by the similarity of the concentration curves and maximum concentrations at various locations in the compartment. All concentrations in this paper are reported in volume percent on a dry basis; i.e., the steam was condensed and the gas sample passed through a drying bed in the tests. Concentrations for test B, the vertical jet, are presented for the same locations as test A. Here we see a definite concentration gradient of roughly 2 to 3 concentration percent during the gas injection phase with maximum values at the compartment top and minimum values at the bottom. This gradient quickly decays to about 1% after the jet to shut off. Our blind calculations of the concentrations are seen to predict the test data very well. The blind temperature predictions were not very good as depicted in Fig. 5. We recognized this at the time,[6] but nevertheless judged our concentrations to be substantially correct. The reason that concentration is not sensitive to temperature in these tests is because the steam is mostly superheated vapor throughout the compartment.

During the posttest analysis, an error was found in the solution of the energy equation. Recalculations showed negligible change in the concentrations and good agreement with the temperatures, as shown in Fig. 6. The corrected energy equation also includes the Uchida[7] correlation for wall-heat transfer and the assumption that $K = 0$.

For roughly 15 minutes of physical time, these problems required between 5 and 6 hours of CDC 7600 CPU times, or about 2.5 hours of Cray CPU time.

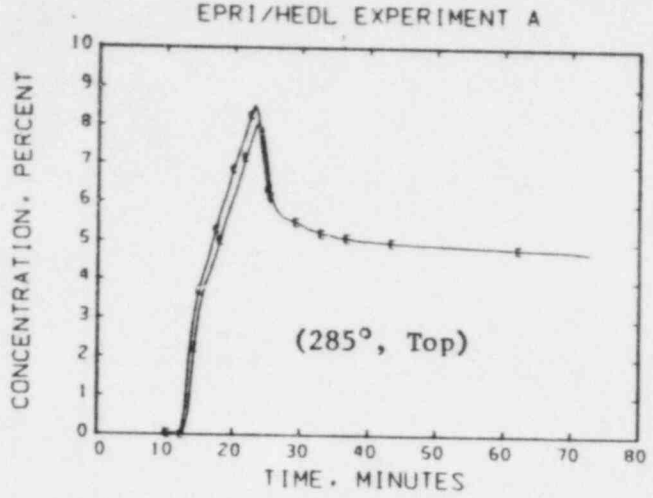

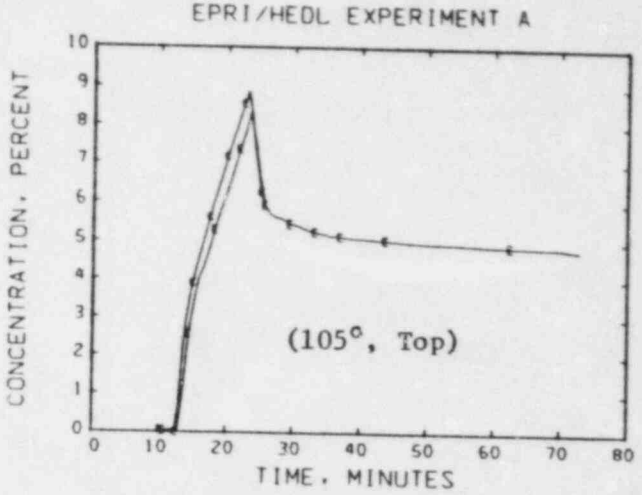

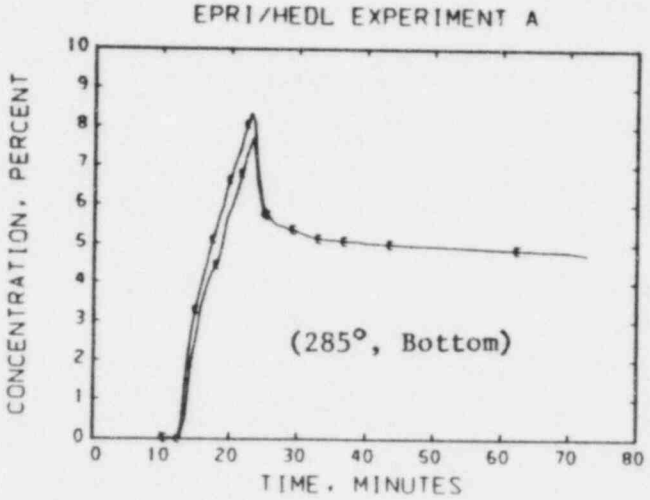

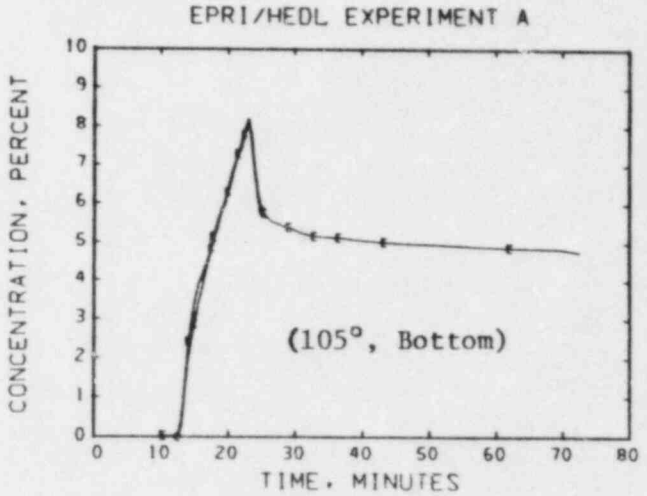

Fig. 3. Hydrogen concentrations for Test A on a dry basis for the indicated locations. The Top and Bottom designations are 0.23 m below the ceiling and 0.3 m above the lower deck, respectively. The curves labeled "E" depict experimental data and those labeled "C" represent the blind calculated results.

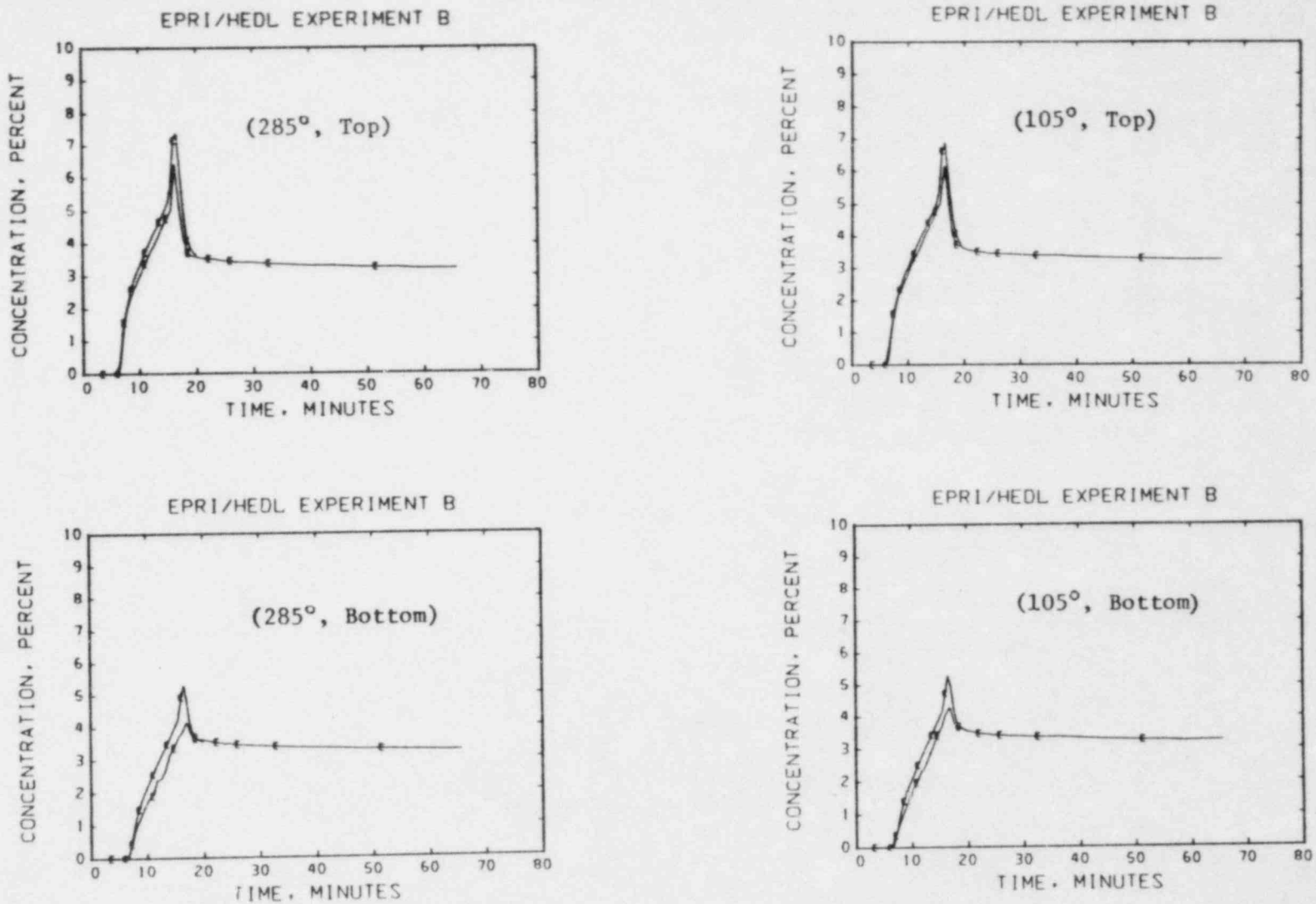

Fig. 4. Helium Concentrations for Test B on a dry basis for the indicated locations. The Top and Bottom designations are 0.23 m below the ceiling and 0.3 m above the lower deck, respectively. The curves labeled "E" depict experimental data and those labeled "C" represent the blind calculated results.

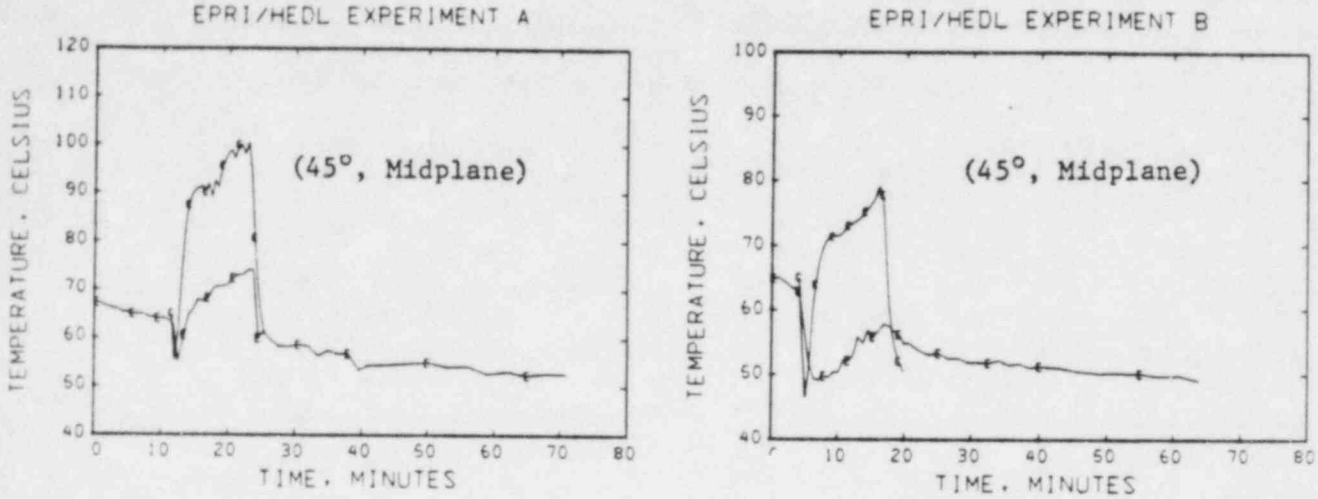

Fig. 5. Compartment temperatures for tests A and B for the indicated locations. The Midplane designation is 2.36 m above the lower deck. The curves labeled "E" depict experimental data and those labeled "C" represent the blind calculated results.

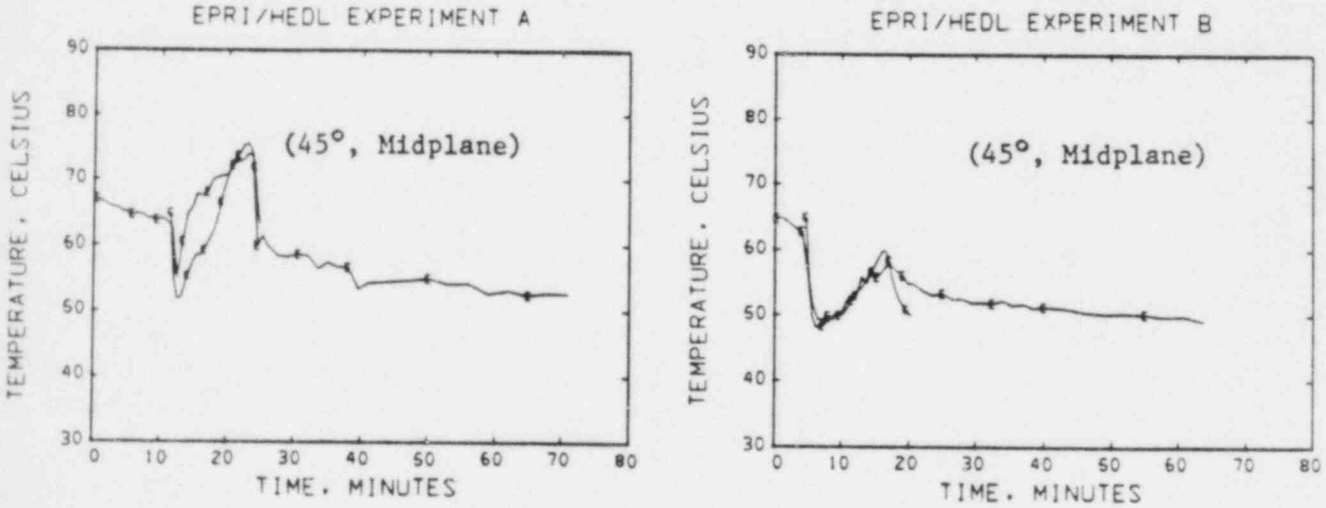

Fig. 6. Compartment temperatures for tests A and B for the indicated locations. The Midplane designation is 2.36 m above the lower deck. The curves labeled "E" depict experimental data and those labeled "C" represent the posttest calculated results.

V. CONCLUSIONS

The mathematical model and solution technique outlined above has proved to be an accurate method for calculating low speed flows with large density variations such as those found in hydrogen mixing within LWR containments. For the time-dependent, fully three-dimensional EPRI/HEDL standard problems, the calculated results compare very closely with the test data even with a fairly coarse computing mesh.

ACKNOWLEDGMENTS

It is a pleasure to express appreciation to F. H. Harlow for his helpful and guiding discussions throughout the course of this work. Additional appreciation is expressed to L. R. Stein and M. D. Torrey for their help in writing the computer programs and to N. C. Romero for his help in producing the graphics. This work was performed under the auspices of the United States Nuclear Regulatory Commission.

References

1. F. H. Harlow and A. A. Amsden, "Numerical Fluid Dynamics Calculation Method for All Flow Speeds," J. Comput. Phys. 8, 197 (1971).
2. C. K. Forester and A. F. Emergy, "A Computational Method for Low Mach Number Unsteady Compressible Free Convective Flows," J. Comput. Phys. 10, 487 (1972).
3. G. R. Bloom and S. W. Claybrook, "Standard Problems on Hydrogen Mixing and Distribution," Westinghouse Hanford Company, Richland, Washington, March 26, 1982.
4. J. R. Travis (in preparation), "A Finite-Difference Method for Time-Dependent, Three-Dimensional Low-Speed Gas Flows with Large Density Variations," Los Alamos National Laboratory report.
5. G. R. Bloom, L. D. Muhlestein, and A. K. Postma, "Hydrogren Distribution in a Compartment with a High Velocity Hydrogen-Steam Source," Second International Workshop on the Impact of Hydrogren on Water Reactor Safety, Albuquerque, NM, October 1982.
6. J. R. Travis, Letter to G. R. Bloom and S. W. Claybrook submitting standard problem results, April 27, 1982.
7. H. Uchida, A. Ogama, and Y. Togo, "Evaluation of Postincident Cooling Systems of Light-Water Power Reactors," Proc. of the Third Inter. Conf. on the Peaceful Uses of Atomic Energy, Geneva, Switzerland (August 31 - Sept. 9, 1964); Vol. 13, 93-104, United Nations, A/CONF.28, p. 436 (1965).

INDEPENDENT CODE ASSESSMENT AT BNL IN FY 1982 *

by

P. Saha, U. S. Rohatgi, J. H. Jo, L. Neymotin

G. Slovik and C. Yuelys-Miksis

Department of Nuclear Energy
Brookhaven National Laboratory
Upton, New York 11973

* Work performed under the auspices of the U. S. Nuclear Regulatory Commission. This paper could not be scheduled for presentation at the meeting and was submitted for publication in the proceedings report.

1. INTRODUCTION

Independent assessment of the advanced codes such as TRAC [1,2] and RELAP5 [3] has continued at BNL through the Fiscal Year 1982. The specific codes assessed and the tests simulated during FY 1982 are shown in Table 1. The tests can be grouped into the following five categories:

1. Critical Flow
2. Counter-Current Flow Limiting (CCFL) or "Flooding"
3. Level Swell
4. Steam Generator Thermal Performance
5. Natural Circulation

Notice that the TRAC-PF1 (Version 7.0) and RELAP5/MOD1 (Cycle 14) codes were assessed by simulating all of the above experiments, whereas the TRAC-BD1 (Version 12.0) code was applied only to the CCFL tests. The results and conclusions of the BNL code assessment activity of FY 1982 are summarized below.

2. RESULTS

2.1 Critical Flow

2.1.1 Moby-Dick Nitrogen-Water Tests [4]

Two tests (Run Nos. 3087 and 3141) with very different flow qualities (5.91×10^{-4} and 51.3×10^{-4}, respectively) were simulated with the TRAC-PF1 (Version 7.0) code. The predicted water flow rates are compared with the experimental values in Table 2. It can be seen that TRAC-PF1 with the annular flow friction factor option underpredicts the mass flow rate whereas the same with the homogeneous flow friction factor option overpredicts the water flow rate. This is in agreement with the TRAC-P1A results reported earlier [15], and was of no surprise because of the large differences in the wall friction factors for these options. The predicted axial pressure distributions, however, were in good agreement with the data for both runs and both options since the pressure boundary conditions were used for the simulation.

It should be noted that the earlier versions of TRAC, i.e., TRAC-P1A and TRAC-PD2, used a drift-flux formulation for the PIPE component and were unable to reach a steady-state for the high void fraction case, i.e., Run No. 3141. TRAC-PF1, on the other hand, uses a two-fluid model and produced stable solutions for both the low and high void fraction cases.

Simulation of the same two tests was also attempted with the RELAP5/MOD1 (Cycle 14) code. However, the code was unable to produce a stable solution for either case. No attempt was made to manually control the time steps. The RELAP5 input deck has been sent to the code developers at INEL for their review.

2.1.2 BNL Flashing Flow Tests [5]

Four tests with different operating conditions were selected for simulation with both TRAC-PF1 (Version 7.0) and RELAP5/MOD1 (Cycle 14) codes. The pressure boundary conditions at both ends were imposed, and the code predicted

Table 1. BNL Independent Code Assessment Matrix of FY 1982

EXPERIMENT \ CODE	TRAC-PF1 (Version 7.0)	RELAP5/MOD1 (Cycle 14)	TRAC-BD1 (Version 12.0)
1. Critical Flow			
a) Moby-Dick Nitrogen Water Tests [4] Run Nos. 3087, 3141	X	0	
b) BNL Nozzle Tests [5] Runs Nos. (291-295), (309-311), (318-321) (339-342)	0	0	
c) Marviken Critical Flow [6] Run No. 24	X	X	
2. CCFL or Flooding			
a) University of Houston Tests [7]	X	X	X
b) Dartmouth College Single Tube Tests [8]	0	0	0
c) Dartmouth College Parallel Tube Tests [9]	0		0
3. Level Swell			
a) GE Large Vessel Test [10] Run No. 5801-15	X	X	
4. Steam Generator Thermal Performance			
a) B&W Tests [11,12] Series (68-69-70) Series (28-29)	X	0	
b) FLECHT-SEASET Tests [13] Run Nos. 21806,22010	X	X	
5. Natural Circulation			
a) FRIGG-Loop Tests [14] Run Nos. (301017-022), (301001-009, 301012 - 016, 301044-047), (301023-030)	X	X	

NOTE: X - COMPLETE

0 - IN PROGRESS

the water flow rate through the converging-diverging test section. The predicted water flow rates are compared with the data in Table 3. The results of TRAC-PD2 are also shown for comparison purposes. In can be seen that the TRAC-PF1 and TRAC-PD2 results are comparable even though a two-fluid model is being used in TRAC-PF1 as opposed to a drift-flux model used in TRAC-PD2.

The RELAP5 flow predictions are also much lower than the data and are comparable with the TRAC predictions. Analyses of these tests are still in progress.

2.1.3 Marviken Critical Flow Test [6]

The Marviken Test 24 was simulated with both the TRAC-PF1 (Version 7.0) and RELAP5/MOD1 (Cycle 14) codes. This test is probably the most challenging of all the Marviken tests since it employed a very short nozzle with the length-to-diameter ratio of 0.33.

Figures 1 and 2 show the comparison between the measured and calculated break flow rate and vessel top pressure, respectively. The nodalization for the vessel and the discharge pipe was the same for all calculations. However, the nozzle was modeled differently in various calculations, and that led to some differences in the results.

Two calculations were performed using the TRAC-PF1 code. In one case, the nozzle was represented by 40 cells and no choking option was used. In the other case, the nozzle was divided into two volumes and the TRAC-PF1 choking option (modified Burnell model) was used. As shown in Figure 1, the TRAC-PF1 break flow rate prediction with the self or no choking option yielded slightly better results than that with the choking option. However, both calculations significantly underpredicted the break flow rate during the subcooled blowdown period, i.e., $t < 20$ seconds. The vessel top pressure, as shown in Figure 2, was also underpredicted at the early part of the transient ($t < 15$ seconds) and was overpredicted thereafter.

For the RELAP5 calculation, the nozzle was modeled with one volume and the RELAP5 choking option was used. The predicted break flow rate (see Figure 1) was in better agreement with the data than the TRAC predictions, although the vessel top pressure (see Figure 2) was not predicted that well. The same calculation was repeated with a zero-volume nozzle as suggested by the RELAP5 code developers. In this case, the predicted break flow rate was in very good agreement with the data, but the pressure prediction did not improve.

In short, the RELAP5/MOD1 code yielded slightly better results for the break flow rate, particularly during the subcooled blowdown period, than the TRAC-PF1 code. However, neither code was able to predict both the break flow rate and the vessel pressure accurately. Moreover, the results seem to depend on nodalization which should be studied further.

Table 2. Summary of Moby-Dick N_2/Water Results

Run Number	Flow Quality	Water Mass Flow Rate (kg/s)				
		Experiment	TRAC-PF1 Calculation		TRAC-PF1 Calculation	
			Annular Friction Factor Option	Error (%)	Homogeneous Friction Factor Option	Error (%)
3087	5.91×10^{-4}	1.915	1.786	-6.7	2.205	+15.1
3141	51.3×10^{-4}	1.222	1.074	-12.1	1.4978	+22.5

Table 3. Summary of BNL Flashing Flow Test Results

Run Nos.	Inlet Pressure (kPa)	Inlet Temperature (°C)	Exit Pressure (kPa)	Experiment Mass Flow Rate (kg/s)	TRAC-PF1		TRAC-PD2		RELAP5/MOD1	
					Mass Flow Rate (kg/s)	% Error	Mass Flow Rate (kg/s)	% Error	Mass Flow Rate (kg/s)	% Error
291-295	502	148.9	471	6.43	4.74	-26.2	5.08	-21.0	4.92*	-23.5
309-311	556	149.1	397	8.79	7.10	-19.2	7.28	-17.2	7.12	-19.0
318-321	32[illegible]	121.1	167	8.98	7.74	-13.8	7.79	-13.2	7.85	-12.6
339-342	320	121.3	252	8.97	7.63	-14.9	7.69	-14.3	7.62	-15.1

*Prediction using the RELAP5 choking option; the calculation without the choking option failed.

2.2 CCFL or "Flooding"

2.2.1 University of Houston Tests [7]

Two test series with two different water feed rates of 100 lb/hr and 1000 lb/hr were simulated with the TRAC-PF1 (Version 7.0), TRAC-BD1 (Version 12.0) and RELAP5/ MOD1 (Cycle 14) codes. The tests were conducted in a 2-inch inside diameter vertical pipe where air and water were injected at the bottom and middle of the test section, respectively. The predicted and measured water downflow rates vs. the injected air flow rate for both test series are shown in Figures 3 and 4.

It can be seen that TRAC-PF1 underpredicts the air flow rates necessary at the inception and completion of flooding. There is also a slight difference between the TRAC-PF1 and TRAC-PD2 results (see Figure 3). This is due to the use of Dukler's interfacial shear correlation [16] in TRAC-PF1 instead of Wallis' interfacial shear correlation [17] for the annular flow regime. Moreover, the high entrainment rate in both TRAC-PF1 and TRAC-PD2 contributed significantly to the underprediction of the air flow rate for flooding.

The TRAC-BD1 results, on the other hand, are in much better agreement with the University of Houston data. TRAC-BD1 (Version 12.0) employs the Wallis correlation for the interfacial shear, the Ishii-Grolmes [18] correlation for the onset of entrainment, and the Ishii-Mishima correlation [19] for the entrainment rate. The combined effect of these correlations produced good agreement between the data and the TRAC-BD1 predictions as shown in Figures 3 and 4.

The RELAP5 predictions for these tests are very poor. Very little air flow rate is required to cause upflow of all the injected water in the RELAP5 calculation (see Figure 3 and 4). This is caused by the inadequacy of the RELAP5 flow regime map at high void fractions ($\alpha > 0.95$). At these void fractions, the code assumes all the liquid to be in the droplet form which was not the case in the Houston test. Clearly an improved flow regime map is needed in RELAP5 for high void fractions.

2.2.2 Dartmouth College Single Tube Tests [8]

Two series of tests with two different tube diameters (1-inch and 6-inch) were selected for simulation with the TRAC-PF1, TRAC-BD1 and RELAP5/MOD1 codes. The preliminary results for the small diameter (1-inch) tube showed some anomalous behavior and the analyses are still in progress.

The results for the 6-inch diameter tube test are shown in Figures 5 and 6. The TRAC-PF1 calculations, as shown in Figure 5, are in good agreement with the data except for the nondimensional air flow rate of approximately 0.4. Here the code calculated an unreasonably low value of the liquid downflow rate. The problem has been traced back to the sharp discontinuity in the Dukler interfacial shear correlation at lower void fractions or thicker films.

Figure 6 shows the results of the TRAC-BD1 calculation for the 6-inch tube test. The code without the CCFL option overpredicted the average water downflow rate for a given air flow rate. However, as expected, the prediction with the CCFL option was slightly closer to the data.

RELAP5 predicted very little water downflow even for a low value of the air flow rate. This is consistent with the RELAP5 predictions of the University of Houston tests discussed earlier.

2.2.3 Dartmouth College Parallel Tube Tests [9]

A Dartmouth College test series conducted with three parallel tubes each of 1-inch in inside diameter has been selected for simulation with both TRAC-PF1 and TRAC-BD1. Preliminary calculations with the TRAC-BD1 code agree with some features of the experiment. However, the calculations are still in progress and it is premature to make any conclusion at this time.

2.3 Level Swell

2.3.1 GE Large Vessel Test [10]

The GE large vessel level swell test No. 5801-15 has been simulated with both the TRAC-PF1 and RELAP5/MOD1 codes. The resultant vessel pressures are shown in Figure 7, whereas the axial void distributions at various times are presented in Figure 8. The TRAC-PF1 pressure prediction is in good agreement with the data except for the very early part when a pressure dip was observed in the experiment. This discrepancy is due to the lack of a flashing delay model in TRAC-PF1. RELAP5, on the other hand, significantly underpredicts the vessel pressure throughout the transient.

Figure 8 reveals that, in general, TRAC-PF1 overpredicts the void fraction and the rate of level swell. This is in agreement with the TRAC-PD2 results for the Battelle-Frankfurt level swell test reported earlier [20]. Both of these trends could be due to the higher interfacial shear in TRAC for the bubbly and bubbly-slug regimes.

The RELAP5 results for the axial void distribution show irregularities which may be due to some errors in the interfacial shear package. A nodalization study with finer mesh did not resolve this irregular behavior.

2.4 Steam Generator Thermal Performance

2.4.1 B&W Steam Generator Tests [11, 12]

Two test series, one with the 19-tube Integral Economizer Once-Through Steam Generator (IEOTSG) and the other with the 19-tube Once-Through Steam Generator (OTSG), have been simulated with both the TRAC-PF1 and RELAP5/MOD1 codes. The IEOTSG test series 68-69-70 simulated a load change transient from 15% to 25% of the full power, whereas the OTSG test series 28-29 simulated the loss-of-feedwater transient.

Figure 9 shows the TRAC-PF1 and RELAP5 results for the IEOTSG test along with the experimental data. The vertical scales are withheld because the data are B&W proprietary. The TRAC-PF1 results are in reasonably good agreement

with the data whereas the RELAP5 results show some numerical oscillations. Further analysis with RELAP5 is in progress where the maximum time step will be controlled manually.

Figure 10 shows the TRAC-PF1 results for the OTSG test along with the data. Again, the vertical scales are withheld because the data are B&W proprietary. The original TRAC-PF1 (Version 7.0) results did not agree well with the experimental data. One of the major deficiencies in the TRAC calculation was very little condensation of the bled steam coming through the aspirator into the downcomer. This resulted in a lower liquid inventory in the downcomer and a two-phase mixture at the bottom of the tube bundle during the steady-state. Therefore, when the feedwater was lost, TRAC-PF1 considerably underpredicted the exit steam flow rate. A sensitivity study showed that if the steam-water condensation rate were increased such that the bled steam would condense completely, TRAC-PF1 would predict the steam flow rate very well. However, there was still a problem with the exit steam temperature. This was caused by the slightly lower primary-to-secondary heat transfer rate at the steady-state.

2.4.2 FLECHT-SEASET Steam Generator Tests [13]

Two tests, namely ID=21806 and ID=22010, have been simulated with both the TRAC-PF1 and RELAP/MOD1 codes. In these tests, the secondary side of the model U-tube steam generator was filled with stagnant water at high pressure ($\sim$57 bar), and a high void ($\alpha > 0.99$) steam-water mixture at low pressure ($\sim$3 bar) flowed through the primary tube. The direction of heat transfer was predominantly from the secondary to the primary.

Figures 11 through 13 show some of the TRAC-PF1 and RELAP5 results for Test ID=21806 along with the data. It can be seen that both TRAC and RELAP5 underpredicted the secondary side pressure which was the result of overprediction of the secondary-to-primary heat transfer rate. Figures 12 and 13 support this notion. It can be seen from Figure 12 that TRAC and RELAP5 did not predict any liquid carryover until the second half of the transient, although there was always some carryover during the experiment. Figure 13 depicts the primary side steam and secondary side fluid temperatures at t = 338 seconds. Notice that both codes underpredict the secondary side fluid temperature which is the direct proof of overprediction of the secondary-to-primary heat transfer rate. However, the TRAC-PF1 results are more reasonable than the RELAP5/MOD1 results. The experimental primary steam temperature shows a sharp increase between 3 and 4 m elevation at t = 338 seconds which was not predicted by either code. This sharp increase in the steam temperature represents a highly nonequilibrium situation where droplets coexist with the superheated vapor. In TRAC-PF1, the steam was superheated although the degree of superheat was not as high as in the experiment. This led to the larger temperature differential between the secondary and the primary and hence, the greater heat transfer rate. RELAP5, on the other hand, could not predict any steam superheat until all the droplets were evaporated. Thus, the temperature differential and the secondary-to-primary heat transfer rate was even greater in RELAP5/MOD1.

Similar results were obtained for test ID=22010 and they will not be repeated here because of space limitation.

2.5 Natural Circulation

2.5.1 FRIGG-Loop Natural Circulation Tests [14]

Three test series with different entrance loss coefficients (K_{ent} = 4.5, 14.0 and 19.0) have been simulated with both the TRAC-PF1 and RELAP5/MOD1 codes. Since the results of these test series were very similar, only the series with K_{ent} = 14.0 will be discussed here.

Figure 14 shows the predicted and measured flow rates as a function of bundle power. TRAC-PF1 with the annular flow friction factor produced the correct trend, although the predicted flow rates were somewhat higher than the experimental values. Since the homogeneous flow friction factor yields lower wall friction than the annular flow friction factor, the TRAC-PF1 flow rates with the former option were considerably larger than the data. The RELAP5 predictions for flow rates were also larger than the data, particularly at high bundle powers.

Figure 15 compares the bundle wall heat flux with the various CHF correlations as a function of power. The CHF was experienced during the experiment at approximately 6.2 MW. However, neither TRAC-PF1 nor RELAP5/MOD1 was able to predict this accurately. The TRAC-PF1 code which uses the Biasi correlation would highly overestimate the power needed for the CHF condition, whereas the RELAP5/MOD1 code which uses the W-3 correlation would miss the CHF completely. However, it has been found that the RELAP4/MOD7 CHF correlation [21] would predict the CHF point quite accurately for this particular FRIGG test.

3. CONCLUSIONS

3.1 Critical Flow

Both TRAC-PF1 (Version 7.0) and RELAP5/MOD1 (Cycle 14) underpredicted the steady-state subcooled critical flow rate through a converging-diverging nozzle, i.e., the BNL test section. For the Marviken Test 24, the RELAP5 critical flow rate was in better agreement with the data. However, neither code could predict both the break flow rate and the vessel inside pressure well. Further work on the subcooled critical flow rate is needed for both codes.

3.2 CCFL or Flooding

TRAC-BD1 (Version 12.0) yielded the best prediction for the University of Houston tests conducted in a 2-inch diameter pipe. However, for the Dartmouth College tests conducted in a 6-inch diameter pipe, TRAC-BD1 tends to overpredict the liquid downflow rate. TRAC-PF1 yielded better results for the same test series with the exception of one data point. Discontinuity in the Dukler interfacial shear correlation incorporated in TRAC-PF1 seems to be the reason for this discrepancy.

The RELAP5/MOD1 predictions of the University of Houston tests were very poor. The code should employ an annular-mist flow regime at high void fractions instead of only a mist or droplet regime.

Analyses of the Dartmouth single and multiple tube tests using 1-inch diameter pipe(s) are still in progress.

3.3 Level Swell

TRAC-PF1 tends to overpredict the level swell rate and the void fraction below the mixture level, although it predicts the depressurization rate quite well. Higher interfacial shear in the bubbly and bubbly-slug regimes seems to be the reason.

RELAP5/MOD1, however, tends to underpredict the level swell rate and exhibits some irregularities in the axial void fraction profile. Some errors or lack of smoothing in the interfacial shear package could be the reason.

3.4 Steam Generator Thermal Performance

For the B&W IEOTSG test, both TRAC-PF1 and RELAP5/MOD1 yielded reasonable average results, although the latter showed some numerical instabilities. Manual control of maximum time step is probably necessary to avoid these instabilities.

For the B&W OTSG test, TRAC-PF1 underpredicted the exit steam flow rate during a loss-of-feedwater transient. This was caused by the lower initial (steady-state) water inventory due to the lower rate of aspirator steam condensation. An increase in the condensation rate improved the TRAC-PF1 results. Simulation of the same experiment with the RELAP5/MOD1 code is still in progress.

For the FLECHT-SEASET U-tube steam generator tests, both TRAC-PF1 and RELAP5/MOD1 codes overpredicted the secondary-to-primary heat transfer rate. One of the main reasons for this discrepancy seems to be the higher interfacial heat transfer rate in the droplet flow regime in both codes, particularly in RELAP5 which did not produce any steam superheat until all the droplets were evaporated. There were also some numerical instabilities in RELAP5 which disappeared when the calculations were repeated with manually controlled time step.

3.5 Natural Circulation

Both TRAC-PF1 and RELAP5/MOD1 overpredicted the flow rates for the FRIGG-Loop natural circulation tests. However, slightly increased values of wall friction factors and/or form losses would yield reasonable agreement with the data.

The CHF correlations used in both codes, i.e., the Biasi and the W-3 correlations, were unable to predict the CHF condition in the FRIGG test. However, the RELAP4/MOD7 CHF correlation predicted the same condition quite well.

3.6 Computer Run Time

The BNL code assessment activity did not reveal any clear computer run time advantage for either TRAC-PF1 or RELAP5/MOD1. The run time statistics for most of the transient tests simulated at BNL are presented in Table 4. The time steps for all the calculations were selected by the time step control

of the codes and no manual intervention was made. It can be seen that although RELAP5/MOD1 has a factor of three advantage in the grind time, i.e., the CPU time per cell per time step, the advantage is lost because it takes smaller time steps. Furthermore, for some calculations such as steam generator tests where wall heat transfer is involved, the user may have to restrict the maximum time step to avoid numerical instability. In these cases, TRAC-PF1 will run significantly faster than RELAP5/MOD1.

4. FUTURE WORK

BNL will continue the independent code assessment activity in FY 1983. The codes to be assessed are: TRAC-PF1/MOD1, TRAC-BD1/MOD1 and RELAP5/MOD2. The assessment matrix will contain some of the tests simulated earlier. However, some new types of tests such as NRU reflood and ORNL post-CHF tests will be added.

Table 4. Comparison of Computer (BNL CDC-7600) Run Times for TRAC-PF1 and RELAP5/MOD1

Experiment Simulated	Code	Real Time (s)	No. of Cells	No. of Time Steps	CPU Time (s)	$\frac{\text{CPU}}{\text{Real}}$	$\frac{\text{CPU(s)}}{(\text{cell-time step})}$
Marviken Test 24	TRAC-PF1	55	42	1202	127	2.31	2.5×10^{-3}
	RELAP5/MOD1	60	41	6034	193	3.22	0.8×10^{-3}
GE Large Vessel Test (No. 5801-15)	TRAC-PF1	20	17	236	21	1.05	5.2×10^{-3}
	RELAP5/MOD1	20	14	28814	400	20	1×10^{-3}
B&W IEOTSG Test (No. 68-69-70)	TRAC-PF1	50	26	255	21	0.42	3.2×10^{-3}
	RELAP5/MOD1	50	26	400	12	0.24	1.2×10^{-3}
FLECHT-SEASET Steam Generator Test ID=21806	TRAC-PF1	1300	46	31022	4419	3.40	3.1×10^{-3}
	RELAP5/MOD1	1300	46	42322	2568	1.98	1.3×10^{-3}
FLECHT-SEASET Steam Generator Test ID=22010	TRAC-PF1	1300	46	7048	1115	0.86	3.4×10^{-3}
	RELAP5/MOD1	1300	46	167370	9271	7.13	1.2×10^{-3}

REFERENCES

1. Safety Code Development Group, "TRAC-PF1: An Advanced Best Estimate Computer Program for Pressurized Water Reactor Analysis," Los Alamos National Laboratory Report, Draft, November 1981.

2. Jay W. Spore, et al., "TRAC-BD1: An Advanced Best Estimate Computer Program for Boiling Water Reactor Loss-of-Coolant Accident Analysis," NUREG/CR-2178, EGG-2109, October 1981.

3. V. H. Ransom, et al., "RELAP5/MOD1 Code Manual," NUREG/CR-1826, EGG-2070, March 1982.

4. C. Jeandey and G. Barriere, "Part I, Etude Experimentale d'Ecoulements Eau-Air a Grande Vitesse," DTCE/STT/SETRE Note T.T. No. 599, Janvier 1979.

5. N. Abuaf, et al., "A Study of Nonequilibrium Flashing of Water in a Converging-Diverging Nozzle," NUREG/CR-1864, BNL-NUREG-51317, June 1981.

6. L. Ericson, et al., "Marviken Critical Flow Tests," Joint Reactor Safety Experiments in Marviken Power Stations, MXC-224, September 1979.

7. A. E. Dukler, and L. Smith, "Two-Phase Interactions in Counter-Current Flow: Studies of the Flooding Mechanism," NUREG/CR-0617, January 1979.

8. D. Bharathan, "Air-Water Countercurrent Annular Flow," EPRI Report NP-1165, September 1979.

9. C. R. Clark, et al., "Flooding in Multi-Path Vertical Counter-current Air-Water Flow," Dartmouth College Report, NRC0193-5, September 1978.

10. J. A. Findlay, "BWR Refill-Reflood Program Task 4.8 - Model Qualification Task Plan," NUREG/CR-1899, EPRI NP-1527, GEAP-24898, August 1981.

11. G. W. Loudin and W. J. Oberjohn, "Transient Performance of a Nuclear Integral Economizer Once-Through Steam Generator," B&W Alliance Research Center Report 4679, B&W Proprietary, January 1976.

12. H. R. Carter and D. D. Schleappi," Nuclear Once-Through Steam Generator (OTSG and IEOTSG) Loss of Feedwater (LOFW) Test," B&W Alliance Research Center Report 4707, B&W Proprietary, March 1978

13. R. C. Howard, et al., "PWR FLECHT-SEASET Steam Generator Separate Effects Task Data Report," NUREG/CR-1366, January 1980.

14. O. Nylund, et al., "Hydrodynamic and Heat Transfer Measurements on a Full-Scale Simulated 36-Rod Marviken Element with Uniform Heat Flux Distribution," FRIGG-2, R4-447/RTL-1007, 1968.

15. P. Saha, "Moby-Dick Nitrogen-Water Experiments," in the BNL Quarterly Progress Report for January 1 - March 31, 1980, NUREG/CR-1506, BNL-NUREG-51218, pp. 28-33, June 1980.

16. A. E. Dukler, "Two-Phase Interactions in Countercurrent Flow," Univ. of Houston, Department of Chemical Engineering, Annual Report for Nov. 1978 - Oct. 1979, January 1980.

17. G. B. Wallis, "Annular Two-Phase Flow, Part 1, A. Simple Theory," Journal of Basic Engineering, ASME, Vol. 92, pp. 59-72, March 1979.

18. M. Ishii and M. A. Grolmes, "Inception Criteria for Droplet Entrainment in Two-Phase Concurrent Film Flow," AIChE Journal, Vol. 21, pp. 308-318, 1975.

19. M. Ishii and K. Mishima, "Correlation for Liquid Entrainment in Annular Two-Phase Flow of Low Viscous Fluid," ANL/RAS/LWR 81-2, March 1981.

20. L. Neymotin, "Battelle Institute (Frankfurt-Main) Vessel Top Blowdown Test," in BNL Quarterly Progress Report for January 1 - March 31, 1981, NUREG/CR-2160, BNL-NUREG-51401, pp. 37-41, May 1981.

21. K. G. Condie and S. G. Bengston, "Development of the MOD7 Correlation," EG&G Report, Attachment PN-181-78, 1978.

RECENT BNL PUBLICATIONS ON CODE ASSESSMENT

1. P. Saha, et al., "LWR Code Assessment and Application," in Safety Research Programs Sponsored by Office of Nuclear Regulatory Research, BNL Quarterly Progress Reports for Oct. 1 - Dec. 31, 1981, Jan. 1 - March 31, 1982, April 1 - June 30, 1982, and July 1 - Sept. 30, 1982, NUREG/CR-2331, BNL-NUREG-51454, Vol. 1, No. 4, Vol. 2., No. 1, 2, 3.

2. L. Neymotin, "TRAC-PD2 Prediction of a FLECHT-SEASET Bottom Reflood Experiment, " ANS Transactions, Vol. 39, pp. 563 - 564, December 1981.

3. J. H. Jo, U. S. Rohatgi, and P. Saha, "Simulation of an Overcooling Transient at Rancho Seco with TRAC-PD2," ANS Transactions, Vol. 39, pp. 625 - 627, December 1981.

4. L. Neymotin, "TRAC-PD2 and RELAP5/MOD1 Predictions of Heated Rod Bundle Experiments," ANS Transactions, Vol. 39, pp. 1018 - 1019, December 1981.

5. U. S. Rohatgi, "Assessment of TRAC-PD2 with University of Houston Countercurrent Flow Tests," ANS Transactions, Vol. 39, pp. 1038-1039, December 1981.

6. P. Saha, "A Simple Subcooled Boiling Model," ANS Transactions, Vol. 39, pp. 1058-1060, December 1981.

7. G. Slovik and P. Saha, "Analysis of the BCL Transient ECC Bypass Test with the TRAC-PD2/MOD1 Code," ANS Transactions, Vol. 41, pp. 386 - 387, June 1982.

8. P. Saha, "Use of Separate Effects Experiments in Verification of System Thermal Hydraulics," ANS Transactions, Vol. 41, pp. 673 - 674, June 1982.

9. U. S. Rohatgi, J. H. Jo, and L. Neymotin, "Constitutive Relations in TRAC-PD2,"NUREG/CR Report in press.

10. P. Saha, et al., "Independent Assessment of TRAC-PD2 and RELAP5/MOD1 Codes at BNL in FY 1981," NUREG/CR Report to be published soon.

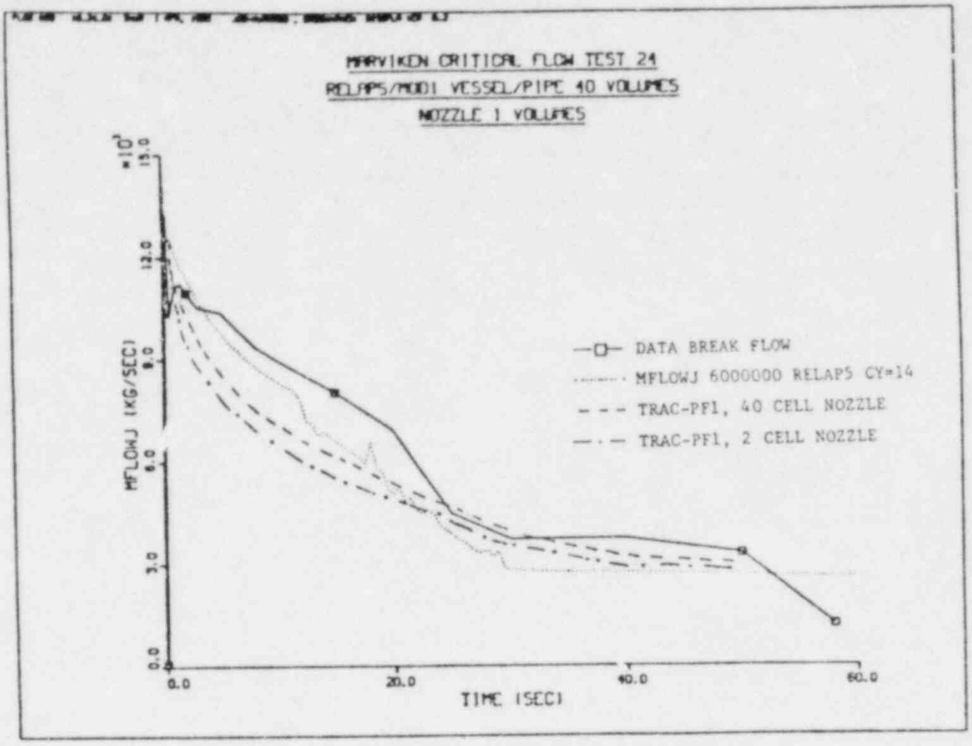

Figure 1 Comparison Between the Measured and Predicted Break Mass Flow Rate for Maryiken Test 24

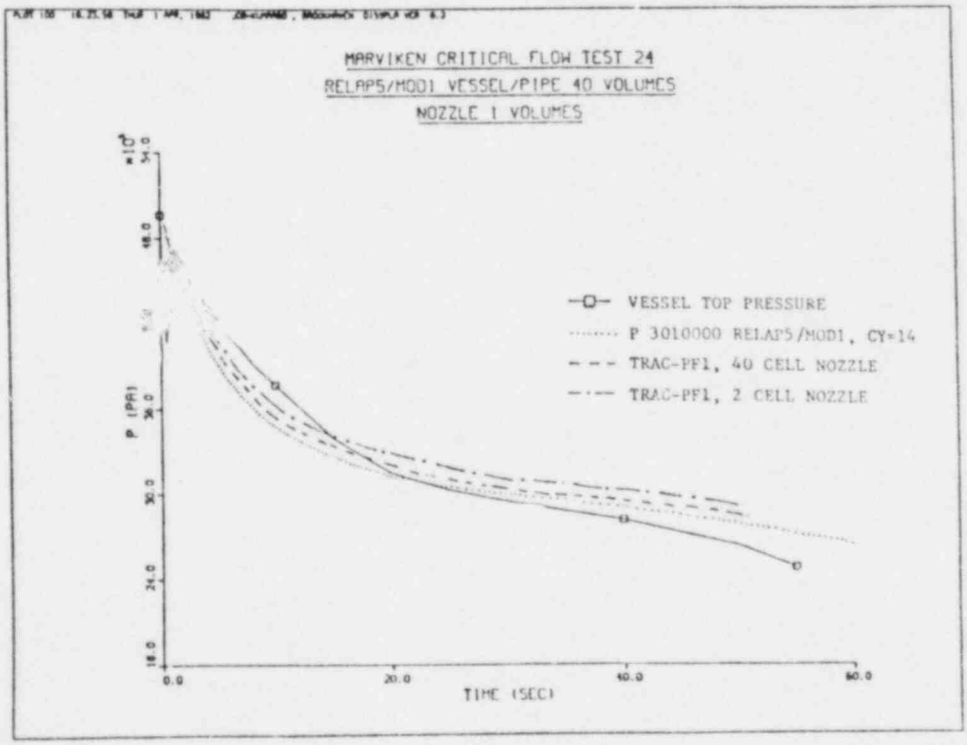

Figure 2 Comparison Between the Measured and Predicted Vessel Top Pressure for Marviken Test 24

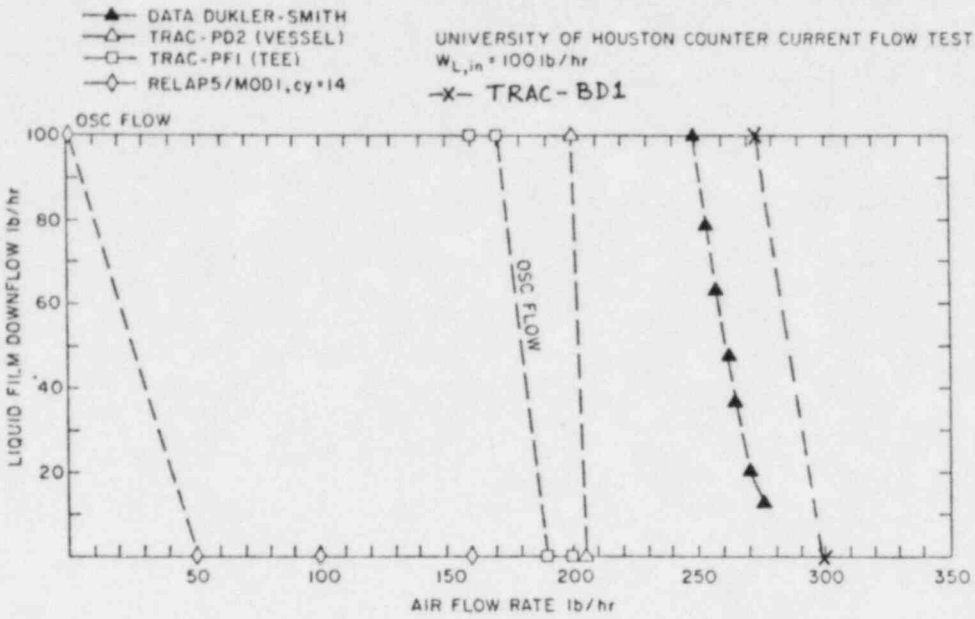

Figure 3 Comparison Between the Measured and Predicted Water Downflow Rate vs. Air Flow Rate for Water Feed Rate of 100 lb/hr

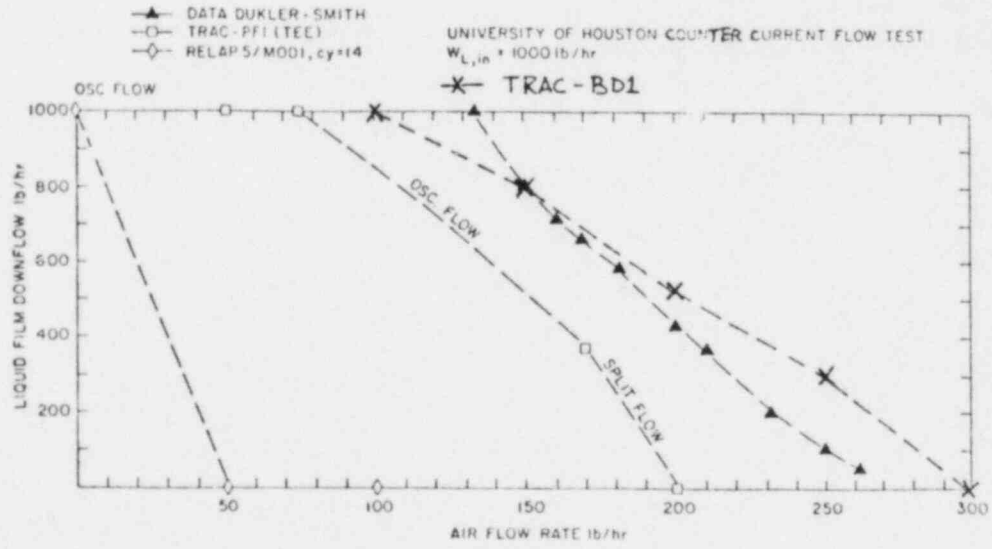

Figure 4 Comparison Between the Measured and Predicted Water Downflow Rate vs. Air Flow Rate for Water Feed Rate of 1000 lb/hr

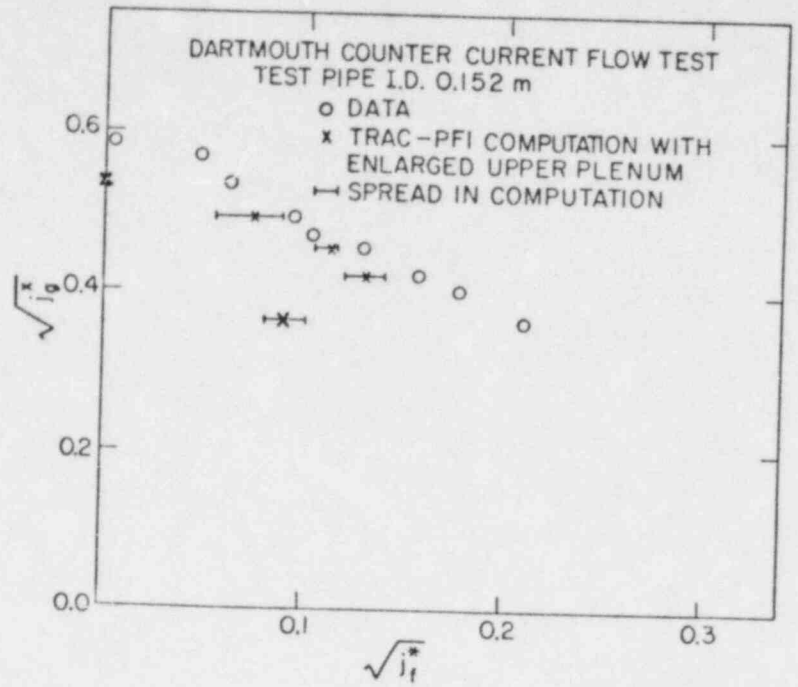

Figure 5 Comparison Between the Measured and Predicted Non-Dimensional Filling Rate for the Dartmouth Large Diameter Pipe Test

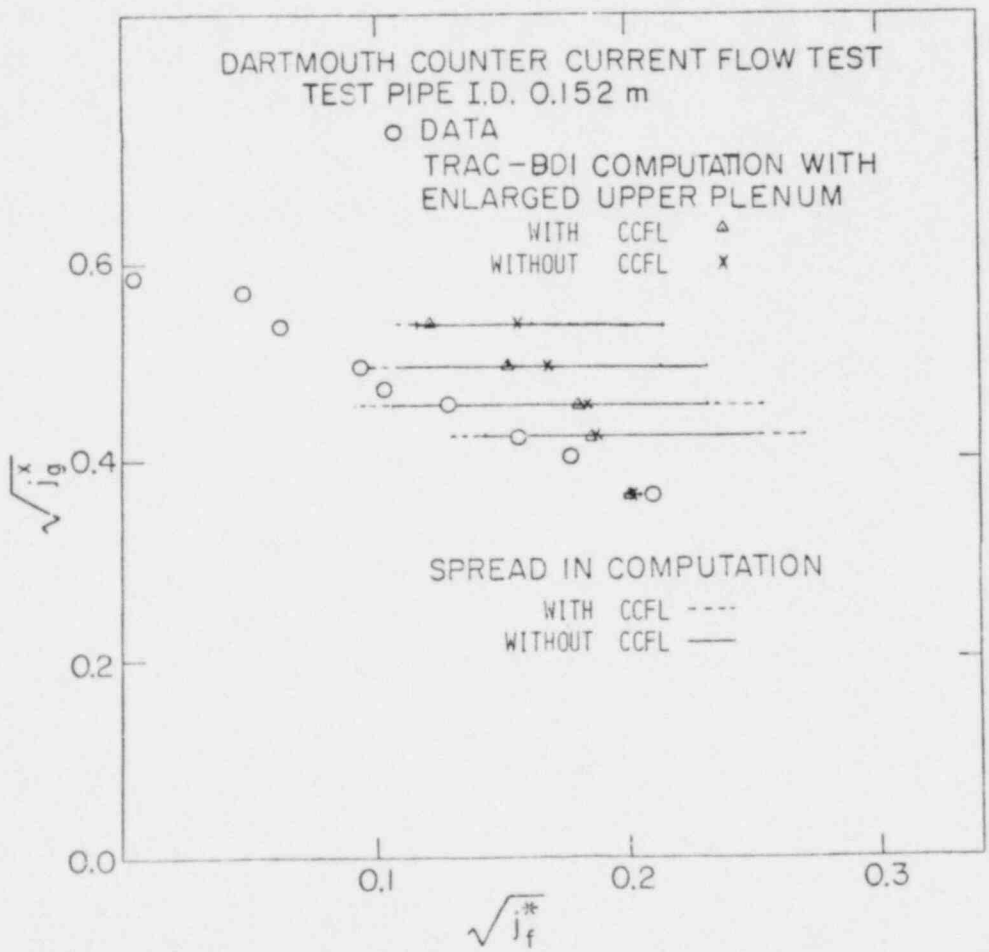

Figure 6 Comparison Between the Measurements and TRAC-BD1 Predictions for the Dartmouth Large Diameter Pipe Test

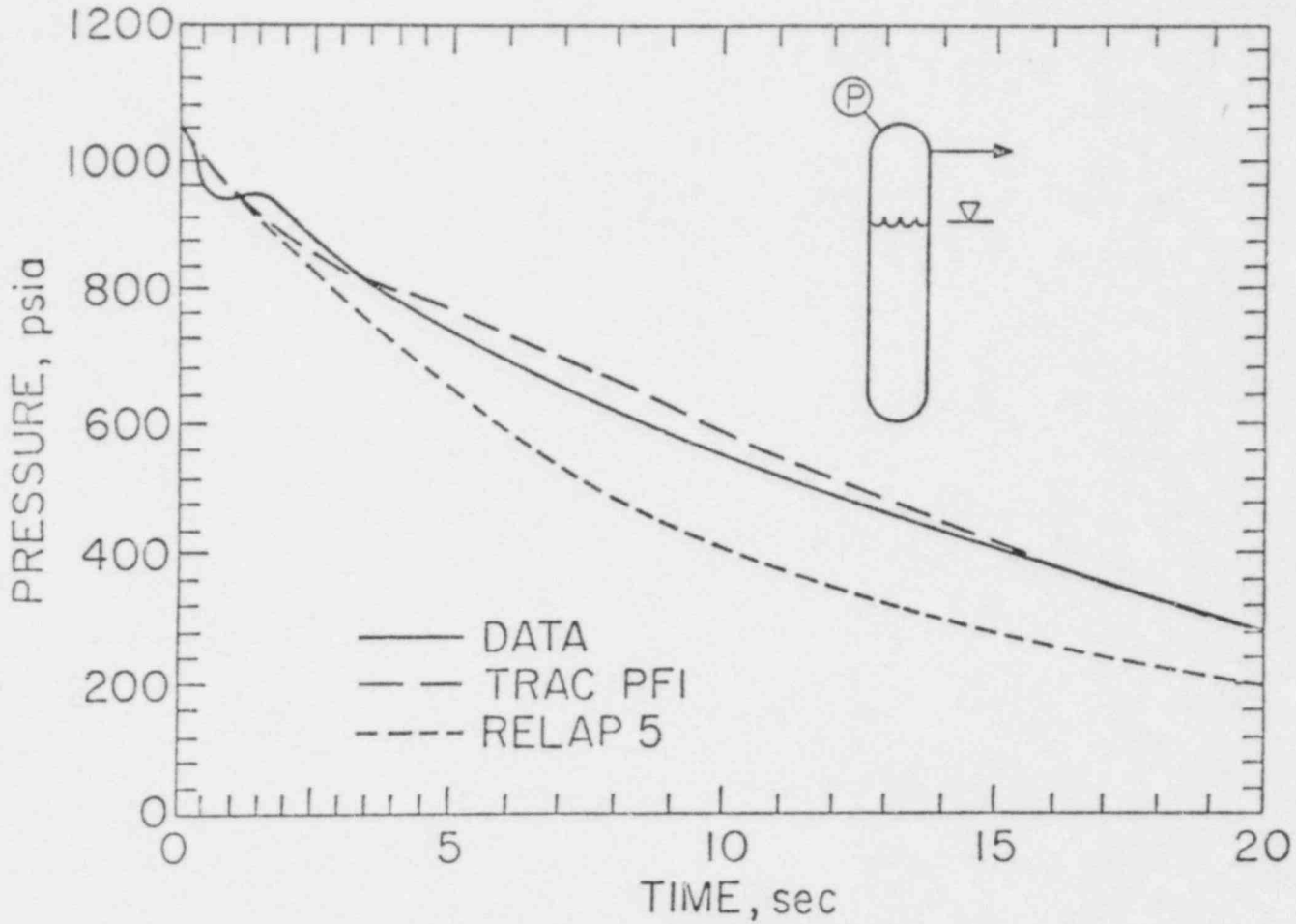

Figure 7 Comparison Between the Measured and Predicted Vessel Pressures in the GE Large Vessel Level Swell Test

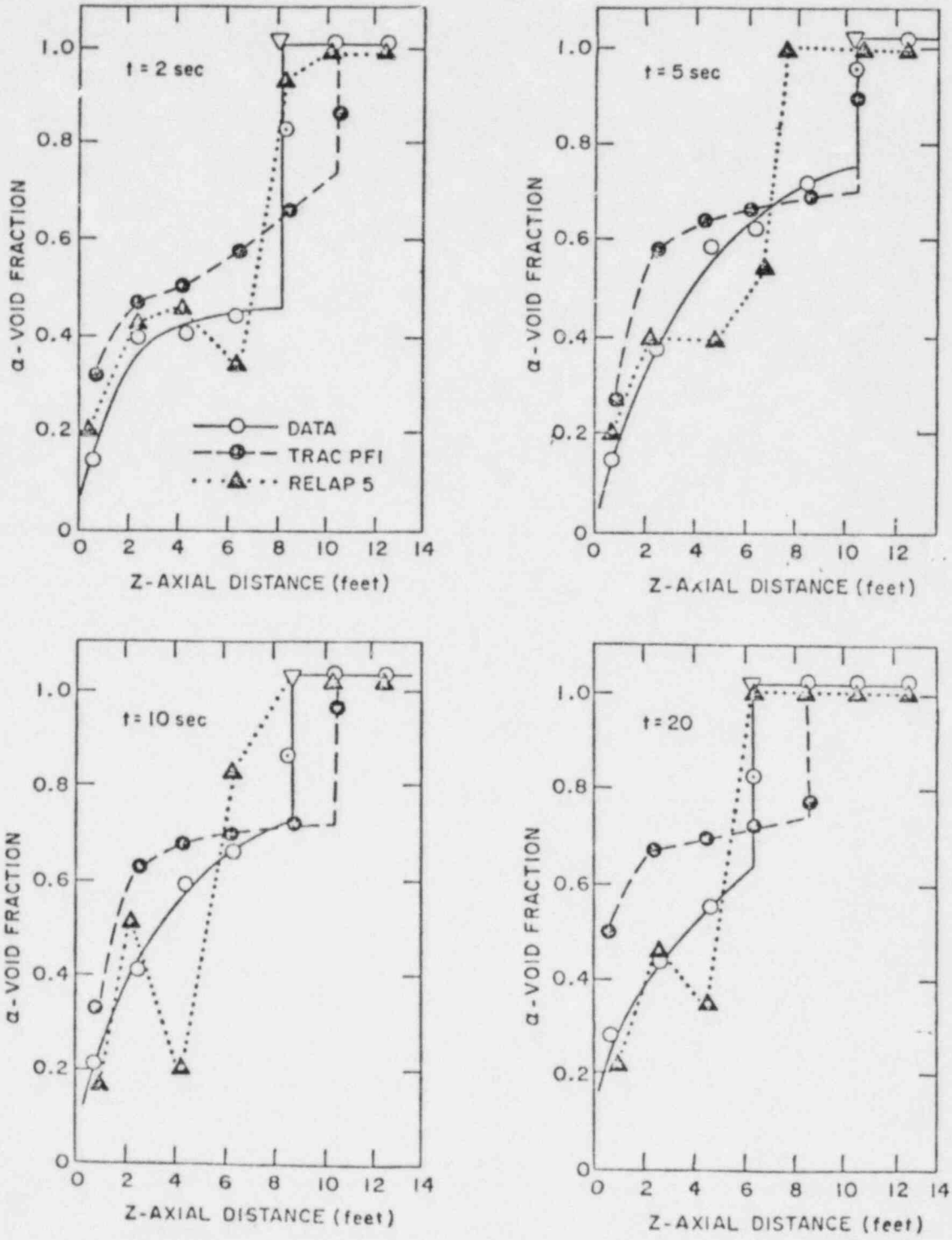

Figure 8 Comparison Between the Measured and Predicted Axial Void Distributions in the GE Level Swell Test

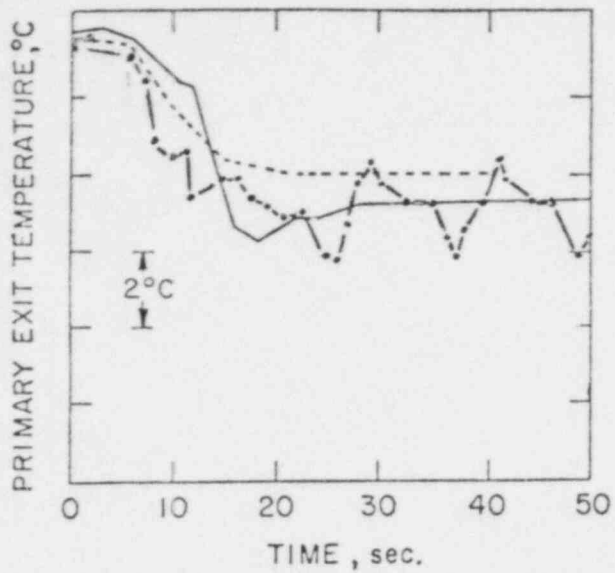

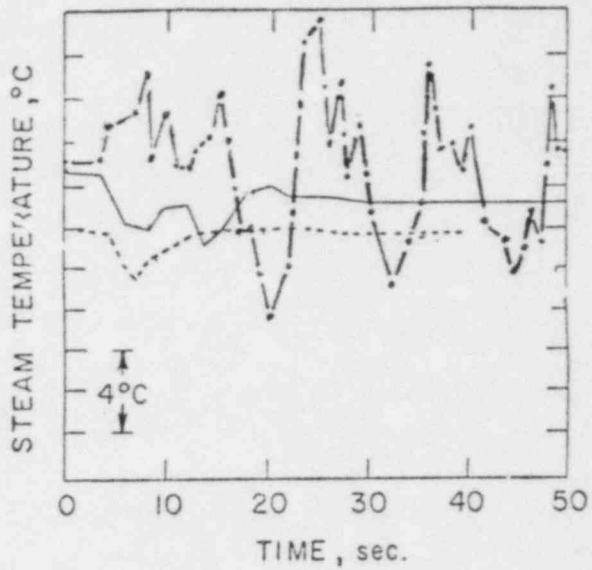

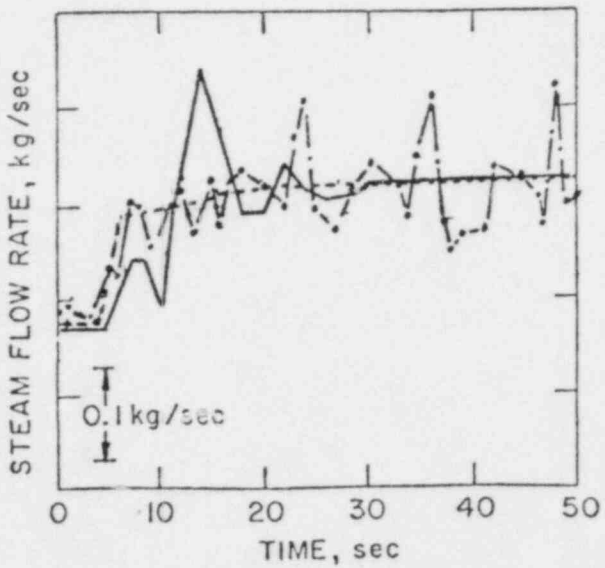

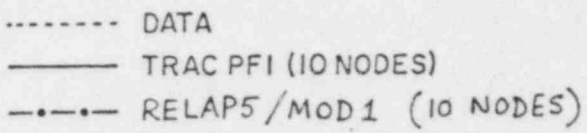

Figure 9 Comparison Between the Measurements and the Predictions of the B&W IEOTSG Test

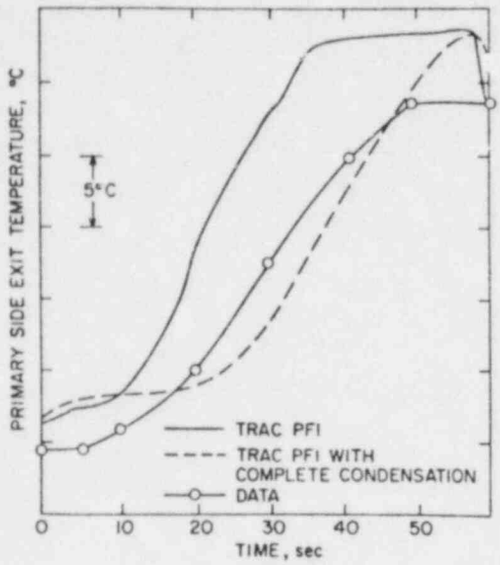

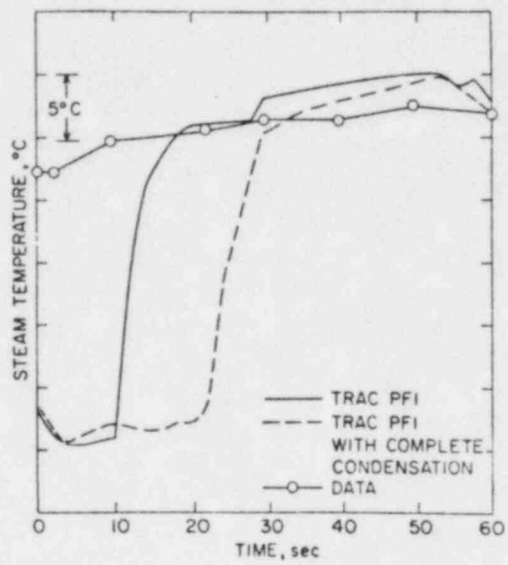

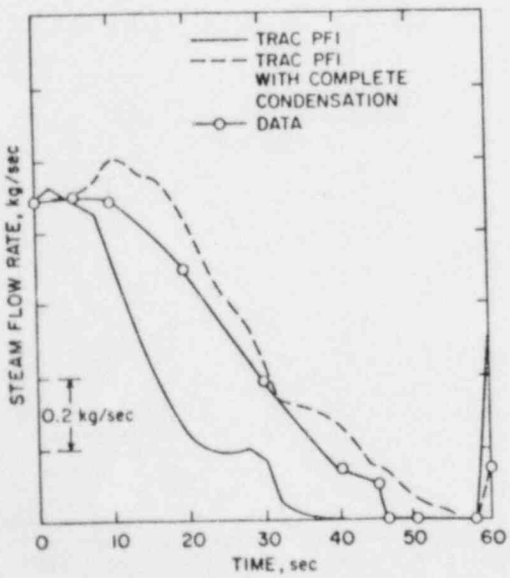

Figure 10 Comparison Between the Measurements and the TRAC-PF1 Results for the B&W OTSG Test

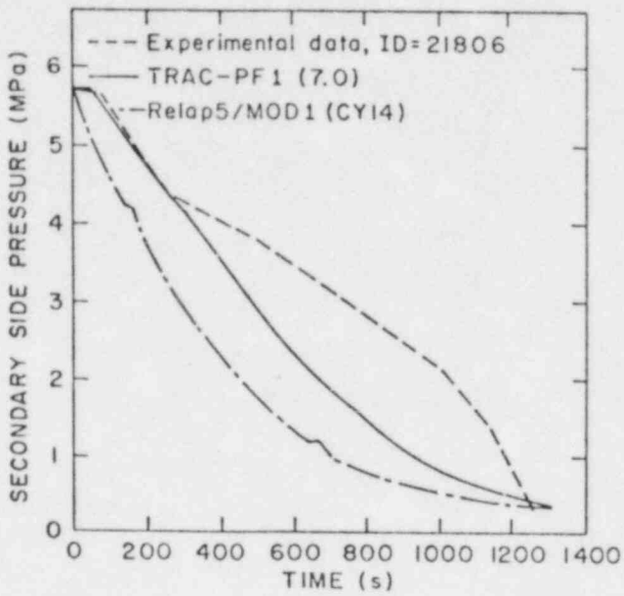

Figure 11 Comparison Between the Measured and Predicted Secondary Side Pressure for ID=21806

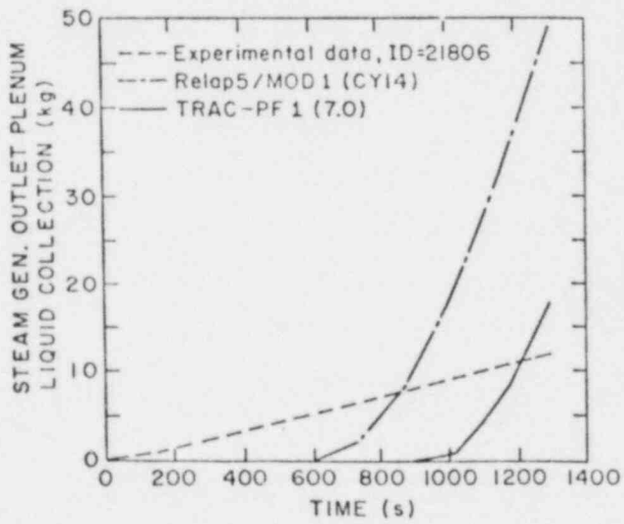

Figure 12 Comparison Between the Measured and Predicted Liquid Mass at the Primary Side Outlet Plenum for ID=21806

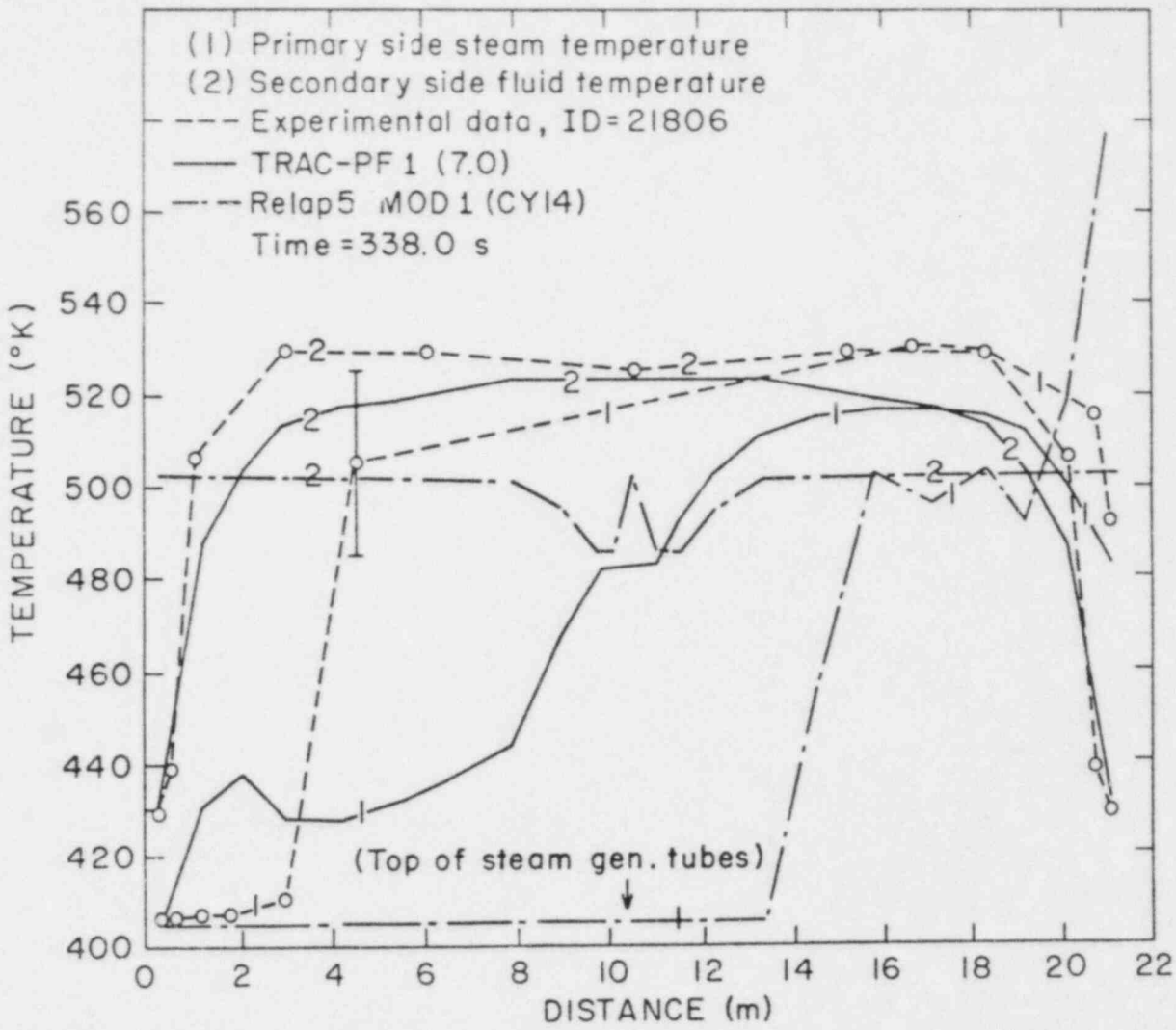

Figure 13 Comparison Between the Measured and Predicted Primary Side Steam and Secondary Side Fluid Temperatures for Test ID = 21806 at 338 s.

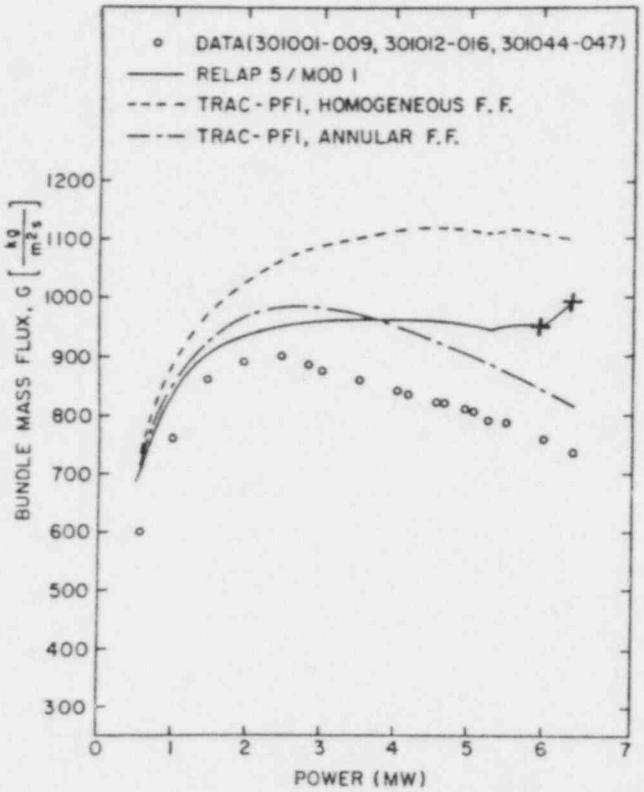

Figure 14 Comparison Between the Measured and Predicted Bundle Mass Fluxes for K_{ent}=14.0

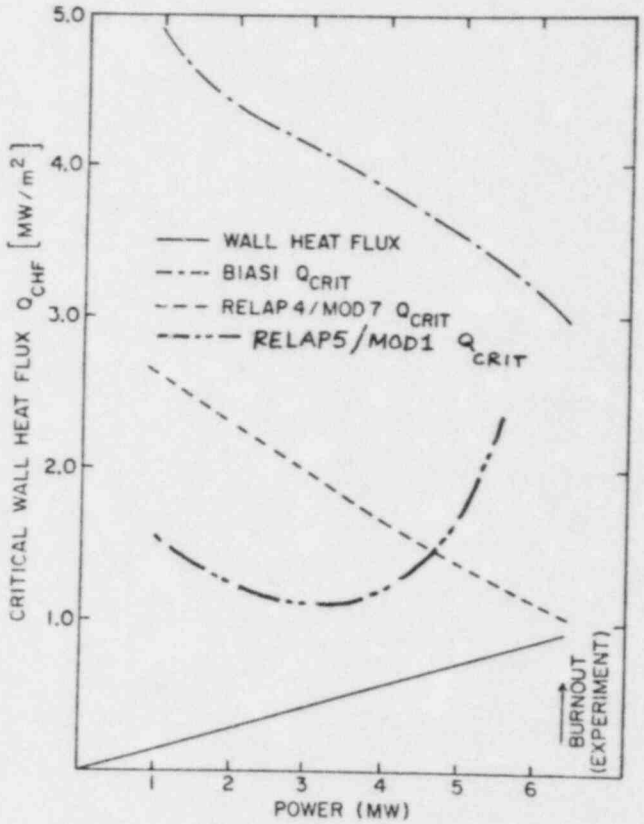

Figure 15 Comparison Between the Measured and Predicted Power for CHF or Burnout

FISSION PRODUCT RELEASE FROM IRRADIATED LWR FUEL

M. F. Osborne
R. A. Lorenz
R. P. Wichner

Chemical Technology Division
Oak Ridge National Laboratory
Oak Ridge, Tennessee 37830

SUMMARY

An experimental investigation of fission product release from commercial LWR fuel under accident conditions is being conducted at Oak Ridge National Laboratory (ORNL). This work, which is sponsored by the U. S. Nuclear Regulatory Commission (NRC), is an extension of earlier experiments up to 1600°C[1-3] and is designed to obtain the experimental data needed to reliably assess the consequences of accidents for fuel temperatures up to melting. The objectives of this program are (1) to determine fission product release rates from fully-irradiated commercial LWR fuel in high-temperature steam, (2) to collect and characterize the aerosol released, (3) to identify the chemical forms of the released material, (4) to correlate the results with related experimental data and develop a consistent source term model, and (5) to aid in the interpretation of tests using simulated LWR fuel.

In order to provide a more uniform specimen temperature and more realistic materials in the test chamber, experience in related studies[4,5] was utilized to develop a new induction furnace for heating the specimens. The principal features of this furnace are illustrated in Fig. 1. A dense ZrO_2 furnace tube isolates the steam-argon mixture flowing over the 20-cm-long fuel specimen from a tubular tungsten induction susceptor, which

is the heat source. The tungsten is protected from rapid oxidation by an inert gas purge. Fibrous ceramic insulation is used to reduce heat losses, and a fused silica vessel provides containment. Specimen temperature is measured and controlled by thermocouples and a two-color optical pyrometer. Material released from the furnace is collected on the surface of a platinum/gold thermal gradient tube (~1000 to 150°C), in a series of glass fiber filters, or on heated charcoal. Only the inert gases (Ar, Kr, and Xe) pass through the steam condenser to a cooled charcoal trap. The furnace and collection apparatus are mounted in a steel containment vessel inside a hot cell, as shown in Fig. 2. Radiation detectors monitor the accumulation of radio-active material at various collection points during the test. In addition to the primary tests with irradiated commercial fuel, control tests using unirradiated specimens with fission product and cladding tracers have been conducted at 1700°C, and tests using simulated high-burnup fuel of the type used by Albrecht et al.[5,6] will be conducted at the higher test temperatures (>2000°C).

Two tests of 30,000-MWd/MT burnup fuel (H. B. Robinson 2) have been conducted. The history of a 20 min test at 1700°C is shown in Fig. 3. The peak in total outlet flow (about 13 min to 30 min) indicates the period of hydrogen formation as a result of cladding oxidation. The on-line counting data for ^{85}Kr collected on the cooled charcoal illustrate the release behavior during the test; ^{137}Cs release was delayed slightly but showed similar release rates, compared to the ^{85}Kr.

Posttest examination and analysis of apparatus components revealed the fractional release and distribution for several fission products, as summarized for both tests in Table 1. The nuclides ^{85}Kr, ^{137}Cs, ^{125}Sb, and

^{110m}Ag were measured directly by gamma-ray spectrometry, but activation analysis of basic leach solutions was required for measurement of ^{129}I release. As shown in Table 1, the total release fractions for Kr, I, and Cs were ~2% for the test at 1400°C and ~50% for the subsequent test at 1700°C. These results agree reasonably well with predictions based on previous work[7] and with a recent review,[8] as shown in Fig. 4. In both tests, most (>99%) of the iodine that was released was collected on the thermal gradient tube and the filters, thus indicating that very small fractions of highly volatile iodine species such as I_2 or CH_3I were formed. No rapid release of cesium at ~1400°C was observed; as shown in Fig. 5, a large fraction of the released cesium had combined with the ZrO_2 ceramics in the furnace at high temperature in each test, forming a thermally and chemically stable species. The cesium and iodine distribution in the furnace and collection system is shown in Fig. 6. Most of the released antimony was tightly adhered to or alloyed with the platinum/gold thermal gradient tubes in the higher-temperature region (>500°C), as seen in Fig. 6. (Whereas leaching with either basic or acid solutions removed large fractions of the Cs, the Sb was relatively unaffected.) Other fission product elements detected in very small quantities by gamma spectrometry included Se, Ru, Ce, and Eu.

Spark source mass spectrometry (SSMS) was utilized to obtain data from a few samples. In addition to the above, the fission product elements Br, Rb, Sr, Te, Ba, and La were detected. Data obtained by the latter technique, which were evaluated relative to ^{137}Cs, confirmed that the distributions of such chemical analogs as Cs/Rb and I/Br were similar. Fission product data for three areas of the thermal gradient tube and the filters in test HI-1 are summarized in Table 2. Several structural and impurity

elements were identified also, and Sn was indicated to be alloyed with the platinum thermal gradient tube.

Radial cross sections of each fuel specimen were examined metallographically and compared with an untested control specimen. In the 1400°C test, the cladding was heavily oxidized, as indicated by flow data (hydrogen production) and the severe embrittlement apparent in handling. Microstructural changes were much more pronounced in the 1700°C test, the cladding was completely oxidized to ZrO_2 (see Fig. 7), precipitates of metallic Sn were observed in the ZrO_2, and small areas of fuel/cladding interaction were apparent (Fig. 8). More detailed examination and analysis of the specimen microstructures is being conducted at Argonne National Laboratory.

About five additional tests of irradiated fuel will be conducted at 1700 to 2000°C in the existing apparatus. Following completion of this test series, several apparatus modifications will be considered. Planned higher-temperature (up to 2400°C) tests will require ThO_2 ceramics to replace the ZrO_2 furnace components. A parallel effort to develop laser-Raman or laser-induced-fluorescence spectrometry for fission product species identification in the gas phase has indicated that such techniques may be applicable. A spectrum from one test, CsI heated to 1100 K in a fused silica cell, is shown in Fig. 9. The high sensitivity for CsI as illustrated in this case is encouraging. If further development efforts show that such species as I_2, CsI, and CsOH can be identified in the effluent from our tests, equipment to utilize this analytical technique will be included as soon as possible.

REFERENCES

1. R. A. Lorenz, J. L. Collins, A. P. Malinauskas, O. L. Kirkland, and R. L. Towns, *Fission Product Release from Highly Irradiated LWR Fuel*, NUREG/CR-0722 (ORNL/NUREG/TM-287/R2) (February 1980).
2. R. A. Lorenz, J. L. Collins, A. P. Malinauskas, M. F. Obsorne, and R. L. Towns, *Fission Product Release from Highly Irradiated LWR Fuel Heated to 1300-1600°C in Steam*, NUREG/CR-1386 (ORNL/NUREG/TM-346) (November 1980).
3. R. A. Lorenz, J. L. Collins, M. F. Osborne, R. L. Towns, and A. P. Malinauskas, *Fission Product Release from BWR Fuel Under LOCA Conditions*, NUREG/CR-1773 (ORNL/NUREG/TM-388) (July 1981).
4. M. F. Osborne and G. W. Parker, *The Effect of Irradiation on the Failure of Zircaloy-Clad Fuel Rods*, ORNL-TM-3626 (January 1972).
5. H. Albrecht, M. F. Osborne, and H. Wild, "Experimental Determination of Fission and Activation Product Release During Core Meltdown," *Proceedings of Thermal Reactor Safety Meeting*, Sun Valley, Idaho, Aug. 1-4, 1977.
6. H. Albrecht and H. Wild, "Investigation of Fission Product Release by Annealing and Melting of LWR Fuel Pins in Air and Steam," *Proceedings of the Topical Meeting on Reactor Safety Aspects of Fuel Behavior*, August 2-6, 1981, Sun Valley, Idaho.
7. R. A. Lorenz, J. L. Collins, and A. P. Malinauskas, *Fission Product Source Terms for the LWR Loss-of-Coolant Accident*, NUREG/CR-1288 (ORNL/NUREG/TM-321) (July 1980).
8. *Technical Bases for Estimating Fission Product Behavior During LWR Accidents*, NUREG-0772, U.S. Nuclear Regulatory Commission (June 1981).

Table 1. Distribution of fission products released from two tests of H. B. Robinson fuel

Test component or collector	Temperature or range (°C)	Fraction of fuel inventory found (%)				
		^{85}Kr	^{137}Cs	^{129}I	^{125}Sb	^{110m}Ag
Test HI-1 (30 min at 1400°C in steam)						
Furnace[a]	1400-900	0	0.79	0.016	0.0011	0
Thermal gradient tube	300-130	0	0.58	0.83	~0.017[b]	0
Filters	~130	0	0.38	1.18	0[c]	0
Hot charcoal	~130	0	0	0.010	0	0
Cold charcoal	-78	2.83	0	0	0	0
Totals		2.83	1.75	2.04	>0.017	0
Test HI-2 (20 min at 1700°C in steam)						
Furnace[a]	1700-1000	0	9.6	~0.14	0.68	0
Thermal gradient tube	1000-150	0	14	16.8	~0.85	1.86
Filters	~150	0	25	35.9	>0.005	0.26
Hot charcoal	~150	0	0	0.137	0	0
Cold charcoal	-78	50	0	0	0	0
Totals		50	49	53.0	>1.53	2.12

[a] In addition, particles of fuel and/or cladding recovered from the furnace contained significant amounts of ^{137}Cs, ^{125}Cs, ^{106}Ru, and ^{60}Co.

[b] Measured only after >90% of the Cs activity had been removed by leaching; the amount of Sb removed by leaching was not determined, but was indicated to be small.

[c] Not detected because of high Cs activity, possibly as high as 0.08%.

Table 2. Fission products found by spark source mass spectrometric (SSMS) analysis[a] (based on ^{137}Cs gamma spectrometric data) of test HI-1

Element	Amount on thermal gradient tube segments (μg)			Filter pack (μg)	Total in thermal gradient tube and filter[b] (μg)
	1, 2, 3	5, 6	8, 9		
Temperature (°C)	760-625	500-270	220-150	120	
Cs	600	425	64	1010	2460
I	80	240	110	210	850
Rb	80	19	5.6	88	220
Br	<8	75	5.6	88	210
Te	26	9	≤9	≤44	75 ± 30
Ag	18	<2	<0.3	≤9	29 ± 7
La	<3	<0.4	<0.3	26	28 ± 2
Ba	<5	≤0.9	≤0.8	9	13 ± 4
Sr	<0.8	<0.09	<0.14	<0.2	<1.6

[a]Amounts accurate only within a factor of 2.

[b]Includes estimated amounts in thermal gradient tube segments 4, 7, and 10.

ORNL-DWG 81-15401R

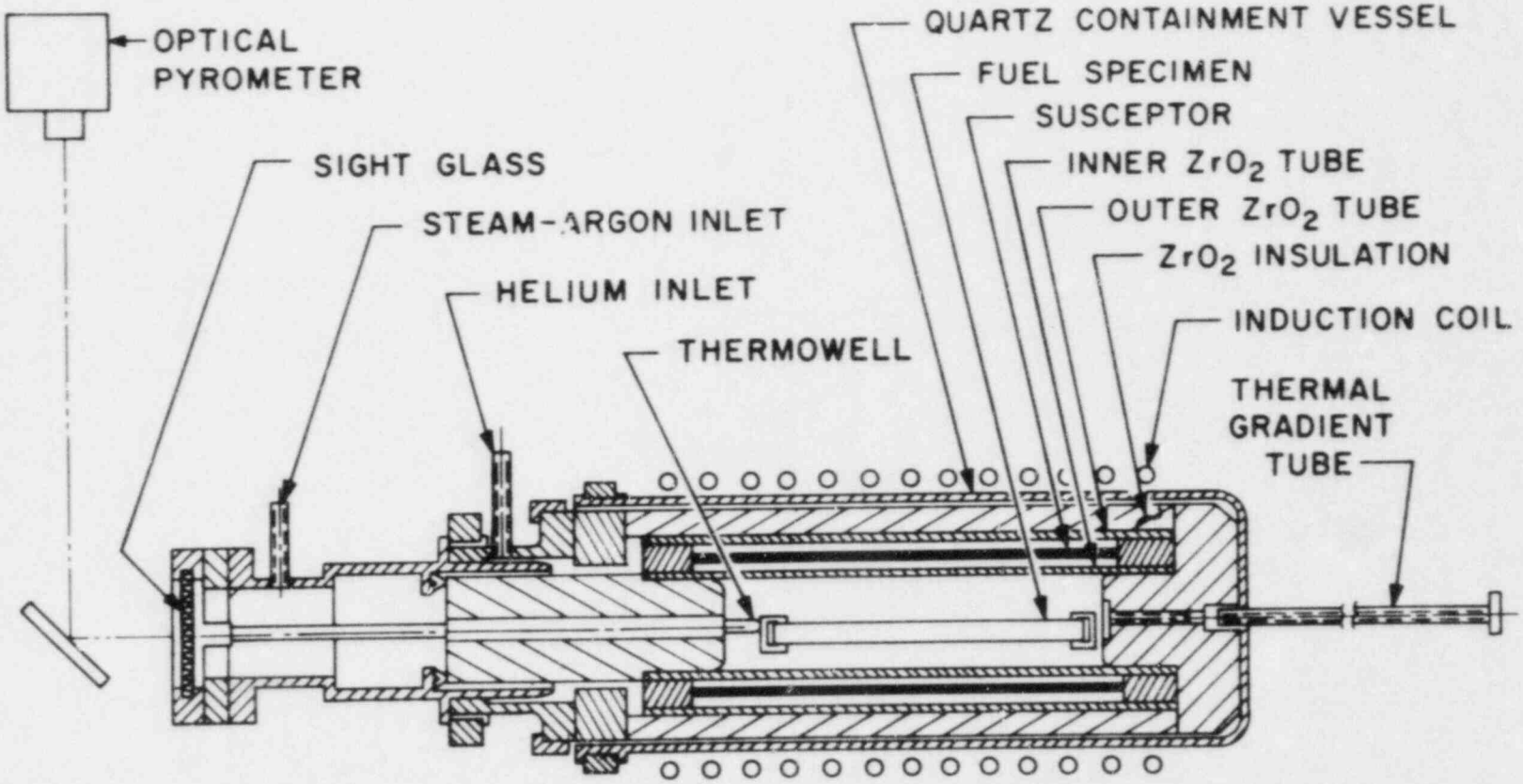

Fig. 1. Induction furnace for heating fuel specimens.

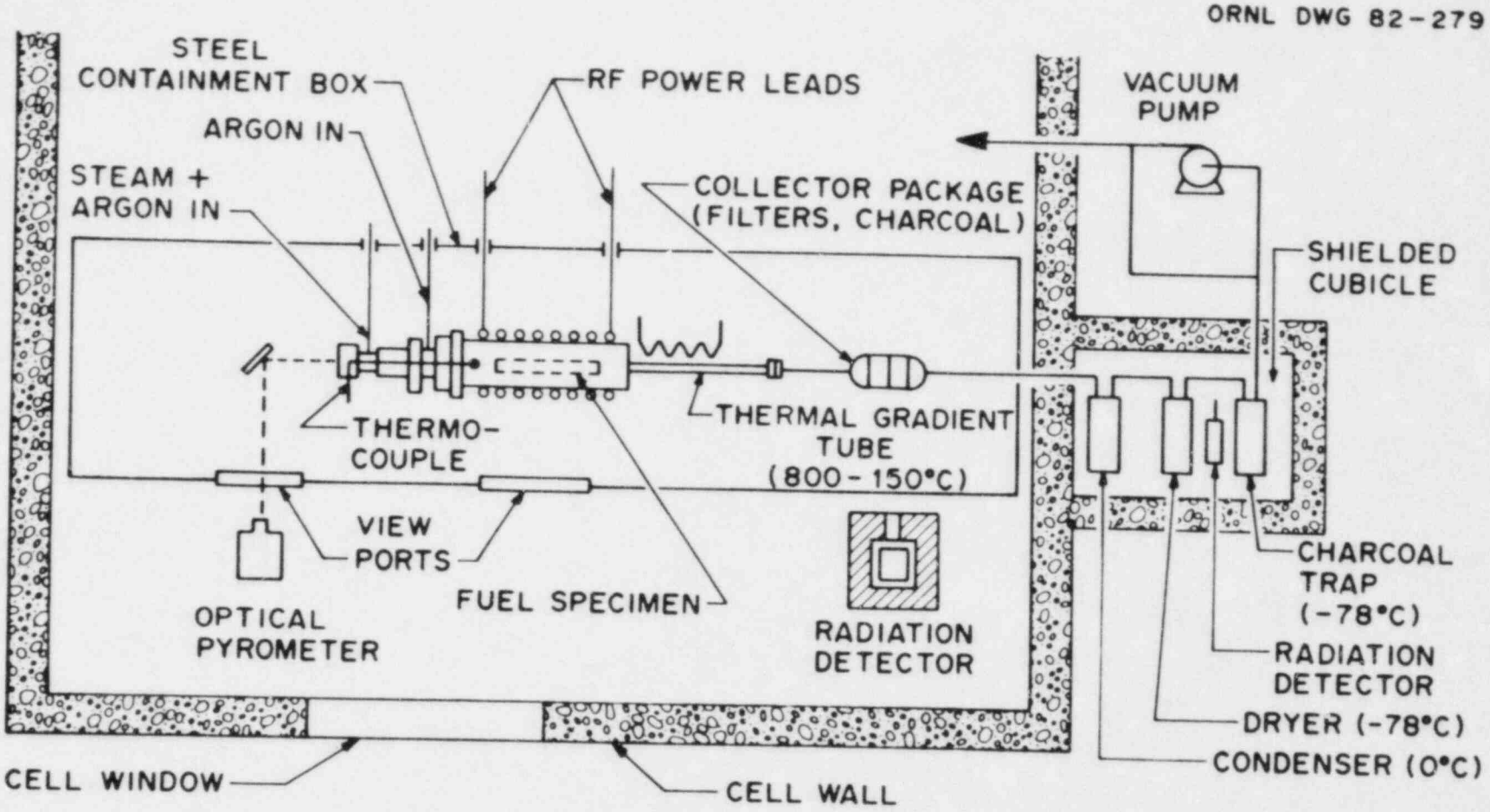

Fig. 2. Fission product release and collection system.

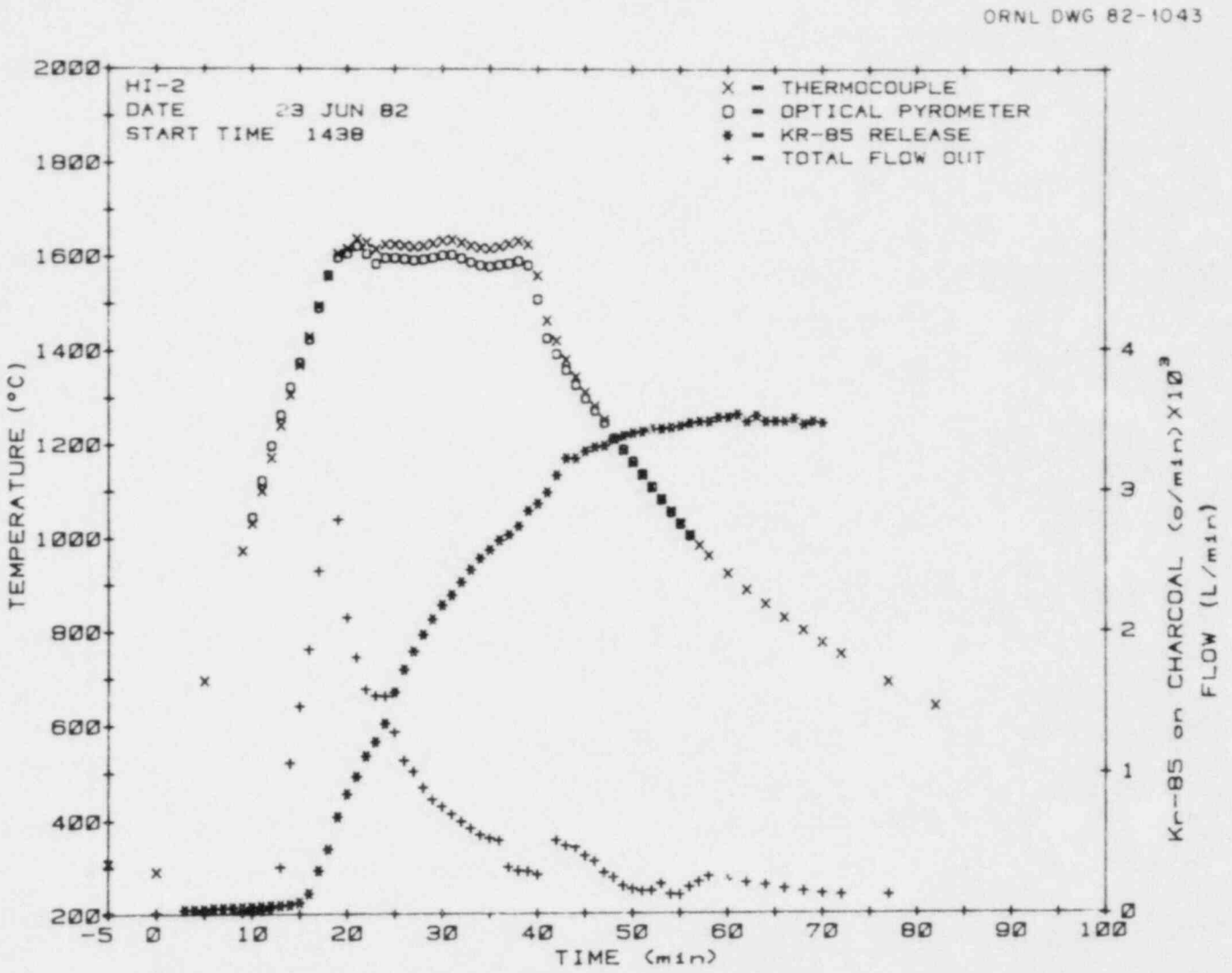

Fig. 3. Temperature, flow, and ^{85}Kr release history of test HI-2.

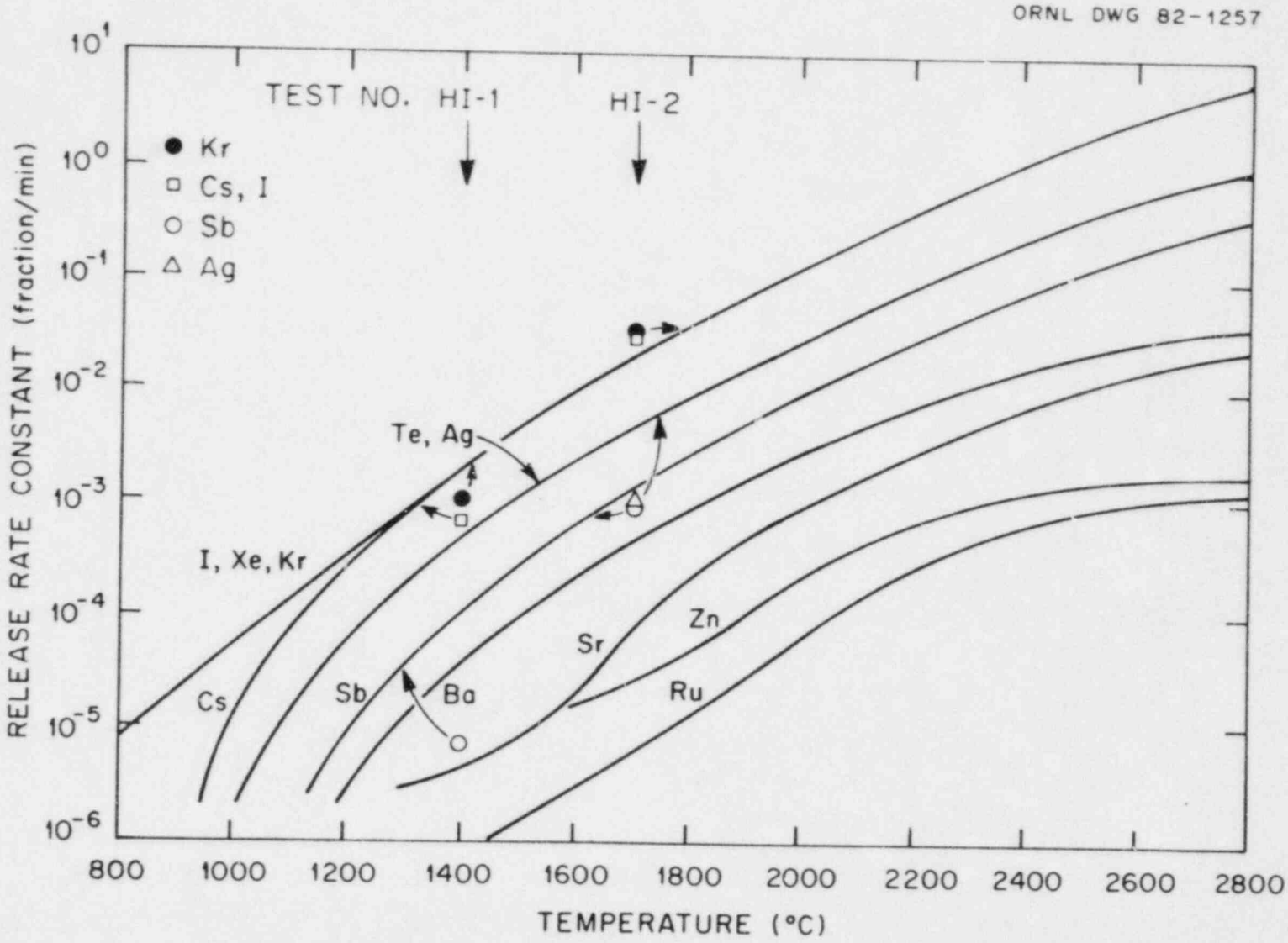

Fig. 4. Comparison of data from tests HI-1 and HI-2 with release rate curves based on previous work [from NUREG-0772 (ref. 8)].

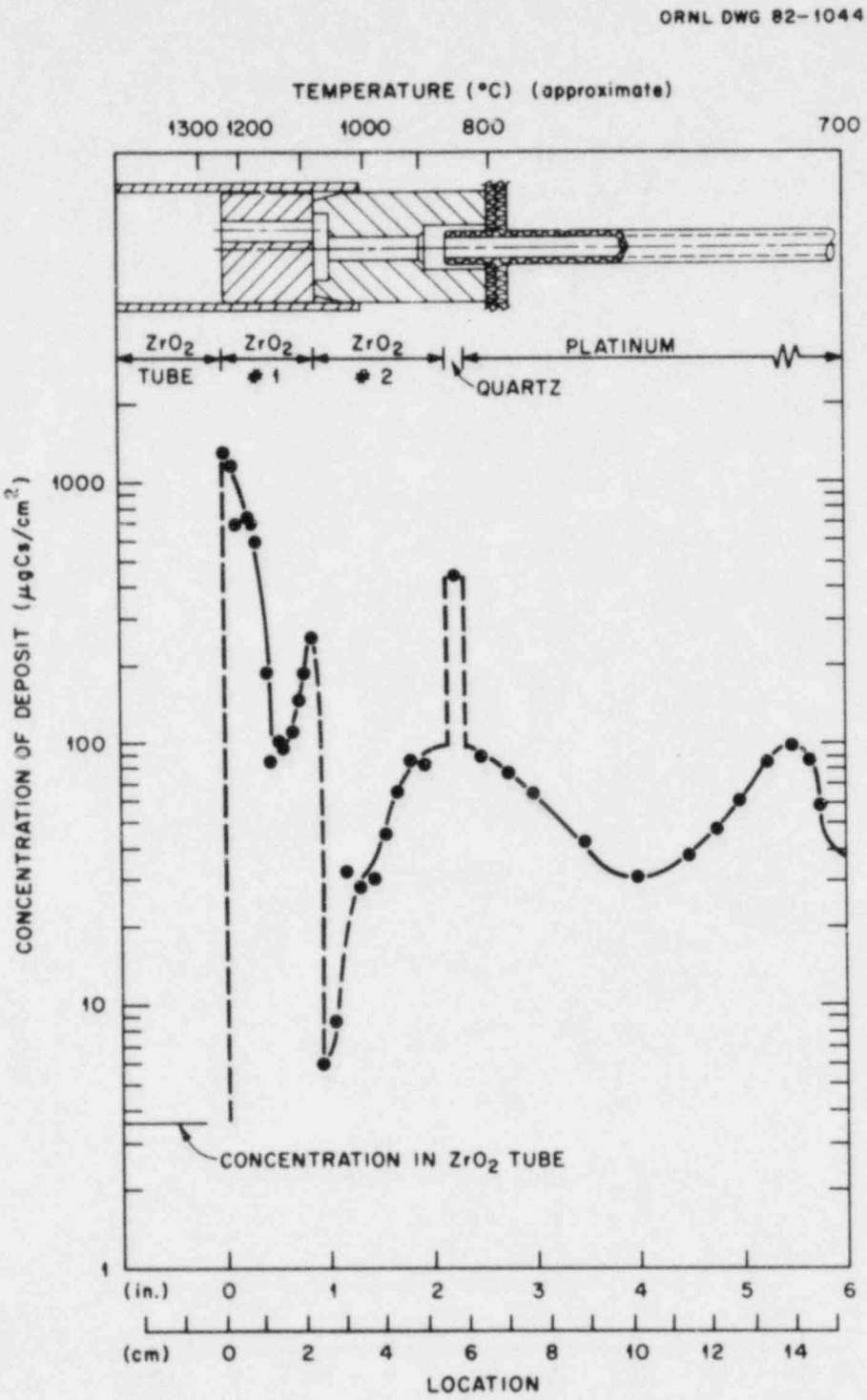

Fig. 5. Concentration of deposited cesium in test HI-1.

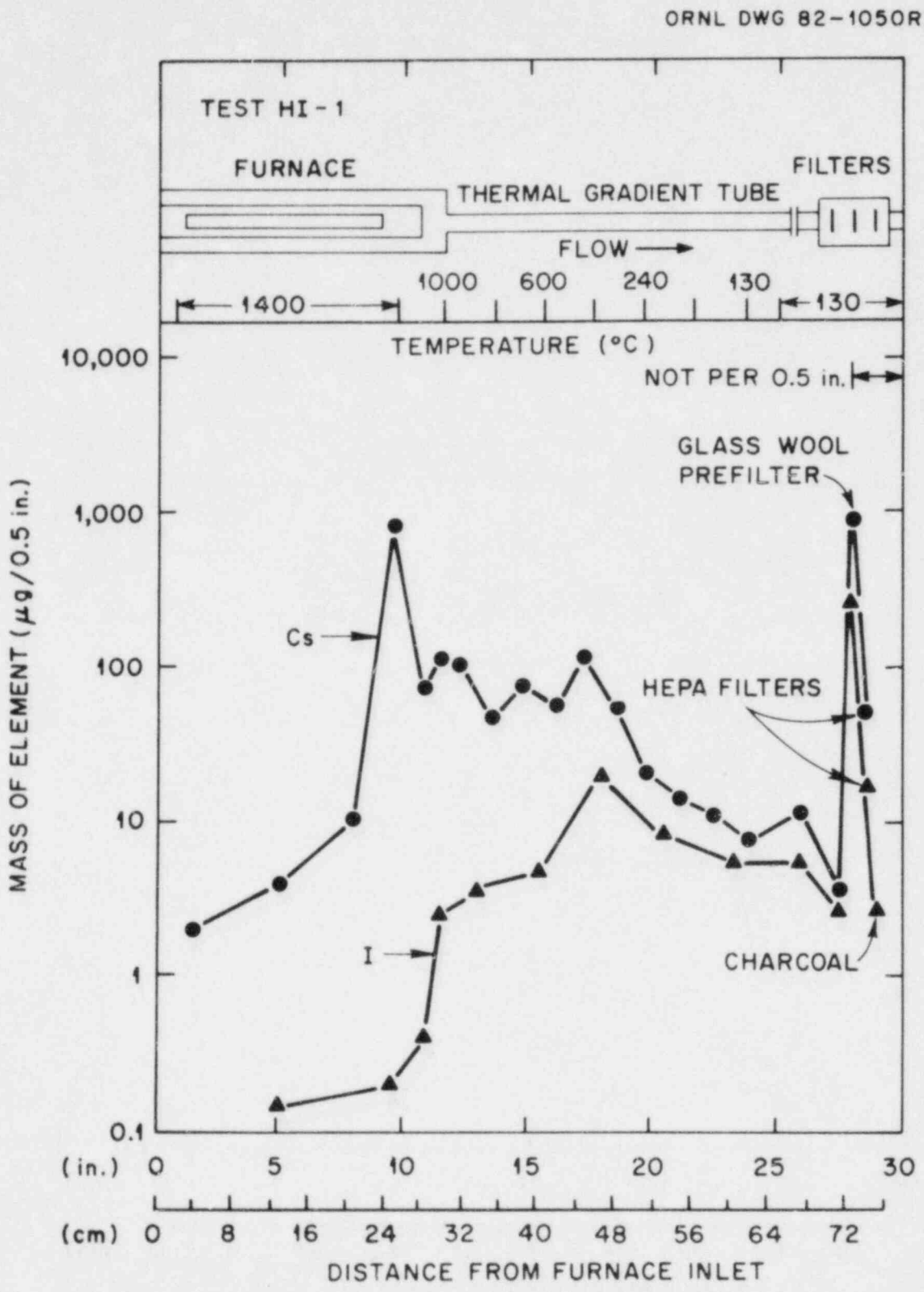

Fig. 6. Distribution of cesium and iodine in test apparatus.

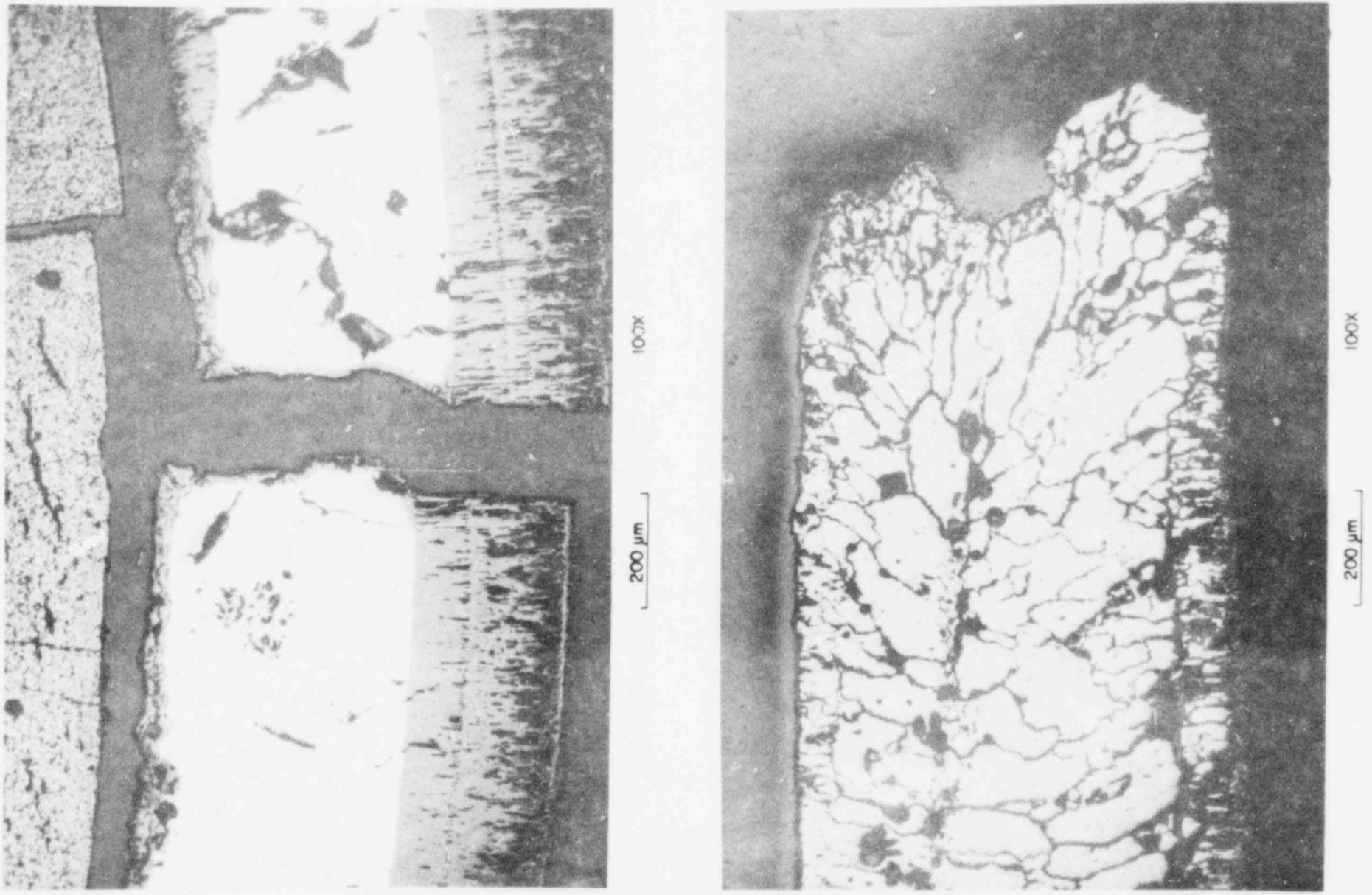

Fig. 7. Comparison of the extent of cladding oxidation during (a) test HI-1 and (b) test HI-2.

ORNL PHOTO 4044-82

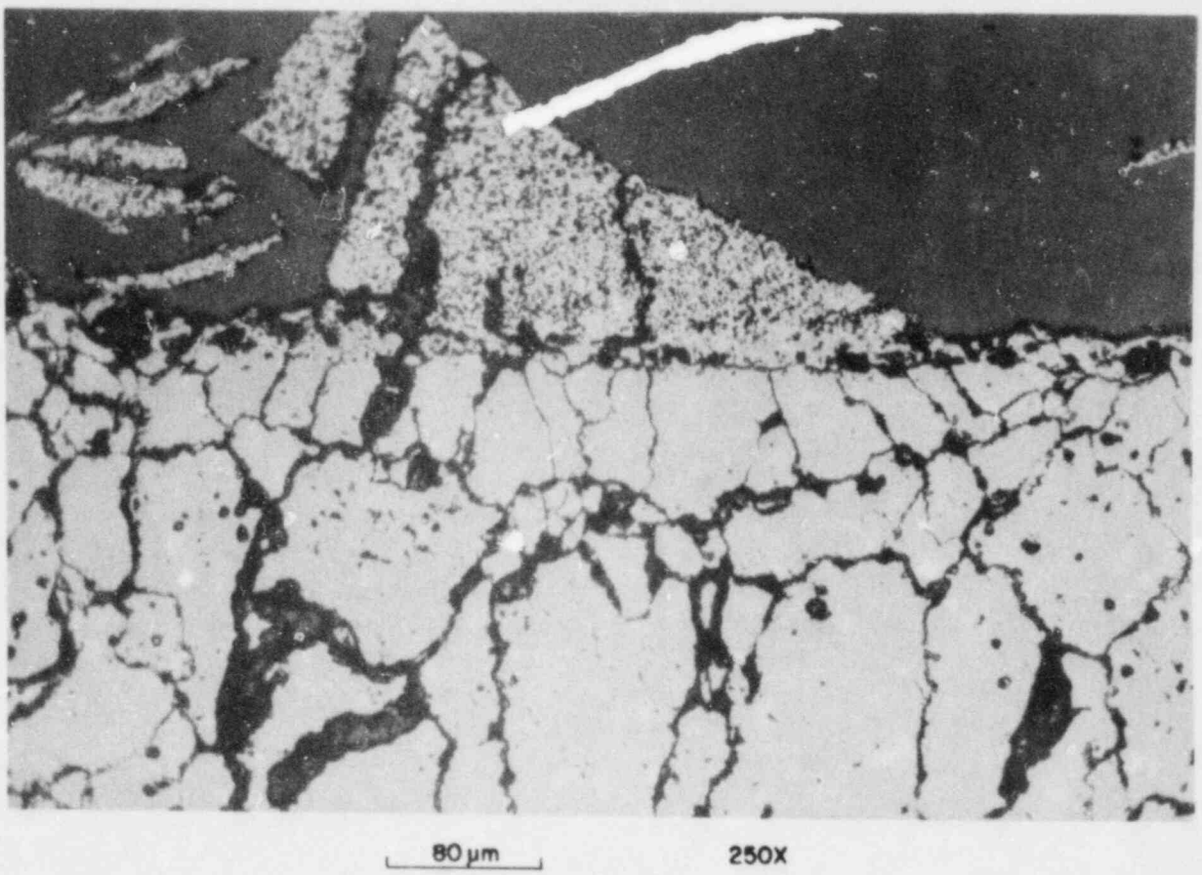

Fig. 8. Area of apparent fuel-cladding interaction in test HI-2. Note chip of UO_2 adhering to oxidized Zircaloy cladding.

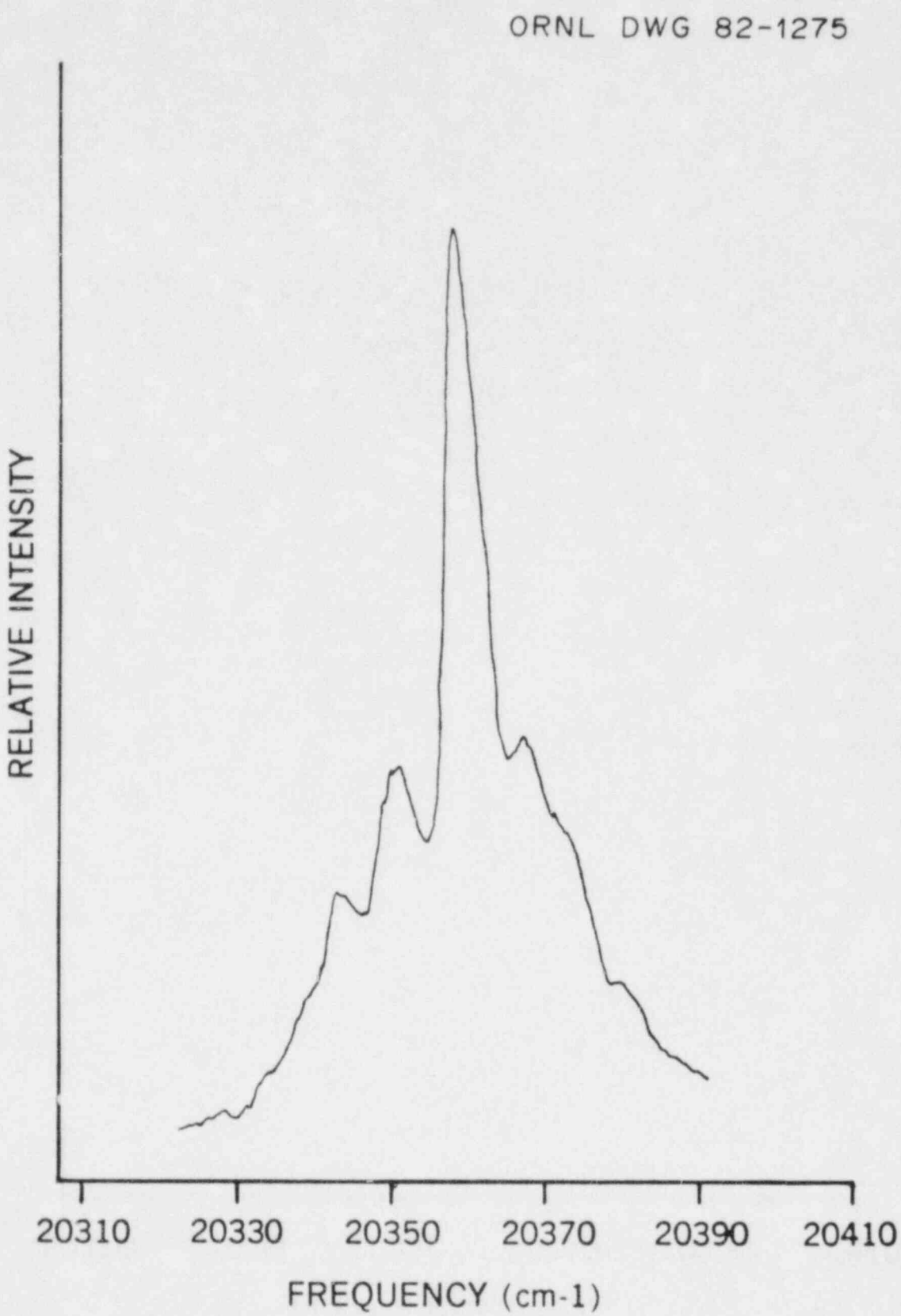

Fig. 9. Laser-induced fluorescence spectrum of CsI at 1000 K in fused-silica cell.

EXPERIMENTAL PROGRAM IN CORE MELT AEROSOL RELEASE AND TRANSPORT

G. W. Parker

Chemical Technology Division
Oak Ridge National Laboratory
Oak Ridge, Tennessee 37830

INTRODUCTION

Aerosol behavior may be expected to assume an increasing importance in Light Water Reactor (LWR) Class IX accident assessment just as it has dominated the Liquid Metal Fast Breeder Reactor (LMFBR) safety analysis. Fission products, core components, and structural materials may be vaporized in large quantities from a core melt, giving rise to high aerosol concentrations in the containment or drywell. At such high concentrations, these aerosols may initiate a scavenging process, followed by rapid settling, and thereby relieve a potentially harmful threat to the environment. Volatile fission products, including halogens in any oxidation state, may be adsorbed on the surface of the chemically active aerosols and are expected to be attenuated at the same rate as the particulate solids.

A survey of the requirements for an experimental demonstration of core-melt aerosol release has indicated that the most practical technique is that referred to as "skull melting" by rf induction. The implied "skull" would be a preformed ZrO_2 or ThO_2 shell composed of presintered powdered oxide. The advantages of this method include freedom from foreign container materials, a cold wall environment that ensures furnace integrity, and an almost unrestricted use of steam or other atmosphere as the cover gas. Scale-up is also reasonably simple and practical with this method. Mixed core-simulating charges, including clad fuel, structural and control rod

metals, and fission-product tracers, may be incorporated and melted in any combination. Melting rates and maximum temperatures may be variables, although pseudoeutectic melting at 2300-2400°C is considered most important.

Aerosols generated by this method may be readily introduced into the present CRI-II containment for further examination where well-characterized aerosol instrumentation is already available.

The major emphases of the project will be first to investigate chemical states and adsorption processes for simulant fission products, particularly iodine and cesium, and second, to measure the coagglomeration and total attenuation rate of all vaporized species with the structural material aerosols.

PROGRESS TO DATE

The initial part of the effort has been dedicated to the development of a demonstration scale (1.0-kg), water-cooled, skull container with segmented copper components. This concept permits induction melting with kilocycle frequency rf power by direct coupling to the mixed-fuel charge. A complete aerosol generation system has also been constructed on a demonstration scale using a 50-kW-rf power supply which was accessible.

A second part of the effort has been concerned with the design of a full 10- to 20-kg scale furnace and the selection of a 250-kW-rf power unit to match the furnace. At this scale, aerosol releases of 100 g or more could be expected. This would afford a special opportunity to characterize simultaneously both the mixed core-melt aerosols and the corresponding vaporization rates.

RESULTS FROM THE INITIAL 1-KG EXPERIMENTS

The initial experiments designed to match the PWR AD sequence were marked by the appearance of several unexpected effects related primarily to the interaction of the control rod silver alloy (at 1400°C) and the stainless steel molten-core support structure (at about 1500°C) with the Zircaloy fuel cladding.

Aerosols produced during the meltdown process in a hydrogen-rich environment are observed to be essentially pure metallic forms, rich in cadmium, silver, indium, and manganese and containing no fuel UO_2, or cladding Zr or ZrO_2. Limited steam flow, as measured by incomplete zirconium oxidation, gives a strongly reducing hydrogen-blanketed environment which, when combined with unoxidized zirconium, increases fission product release by enhancing the volatility of the alkaline earth metals. From the structural steel, manganese is the most volatile component, followed by iron and chromium; however, the total amount vaporized is unexpectedly low.

Most of the metallic fission products (Ru, Mo, Te) are observed in our tests to be scavenged by molten steel or by the zirconium–silver alloy and retained in the melt. Our experiments indicate, however, that strontium and barium additives are initially reduced by the zirconium to the free metals, which vaporize extensively and which react with even traces of steam and air to produce aerosols of their corresponding oxides. Other aerosols (Sn, Mn, Cd, Ag) may remain in the reduced form. The most volatile fission products, iodine and cesium, are quantitatively released.

Upon reaching the reactor containment, the remaining airborne fraction of the combined mass of mixed aerosol solids is expected to form large chain agglomerates that should be quickly dissipated by natural settling, aided by condensing steam.

THE SCOPE OF THE CORE MELT TASK ENCOMPASSES:

1. EXPERIMENTS ON A 1-10 KG SCALE USING STEEL-Zry AND FP SIMULANT FUEL MIXES AND COMPARISON OF RELATIVE RELEASE FRACTIONS WITH OTHER DATA

2. TEMPERATURES UP THROUGH MELTING (2500°) BY RF COUPLING WITH FUEL MIX IN KH RANGE

3. USE OF STABLE CHEMICAL FORMS OF FP'S OR TRACE IRRADIATION OF FISSION PRODUCTS SIMULANTS

4. EXAMINATION OF CHEMISTRY OF RELEASE RATES, AND ASSOCIATION OF FISSION PRODUCTS WITH AEROSOLS

5. RATES OF SOLUTION OF ALKALINE EARTH AND RARE EARTHS IN OXIDE PHASE AND NOBLE METALS IN METALLIC PHASE

6. AEROSOL CHARACTERIZATION: ATTENUATION RATES AND SIZE VERSUS MASS CONCENTRATION

7. TRANSPORT IN PRIMARY SYSTEM?

8. COORDINATION WITH HOT-CELL RELEASE EXPERIMENTS, AND NSPP AEROSOL BEHAVIOR IN CONTAINMENT EXPERIMENTS

THE OBJECTIVES OF THE CORE-MELT TASK ARE TO DETERMINE FOR SEVERE ACCIDENT CONDITIONS:

1. RATES OF FUEL AND STRUCTURAL AEROSOL RELEASE
   (VAPORIZATION RATES)
2. RATES OF FISSION PRODUCT RELEASE (I, Cs, Te, Sr, Ru, etc.)
3. PHYSICAL AND CHEMICAL CHARACTERISTICS OF RELEASE SPECIES
4. BEHAVIOR OF THE MIXED AEROSOLS
   IN CONTAINMENT
   IN PRIMARY SYSTEM (?)
5. CHARACTERIZATION OF MELTDOWN PHASES: ALLOYS, EUTECTICS, METALLICS, ETC. AND FISSION PRODUCT PARTITIONING
6. SCALING RULES BETWEEN SMALL AND LARGE CORE MELTS
7. EFFECTS OF H_2 IGNITION ON FISSION PRODUCT/AEROSOL TRANSPORT BEHAVIOR AND/OR PHYSICAL AND CHEMICAL CHARACTERISTICS

TECHNICAL APPROACH PLAN FOR DIFFERENTIAL CORE MELT RELEASE EXPERIMENTS

1. INITIAL EXPERIMENTS WITH SILVER ALLOY (2%) AT LIMITED TEMPERATURES (BELOW 1800°C), PWR CORE.
   (REVEALS Ag, Cd, In, SS, ZIRCALOY INTERACTION AND AND INITIAL Cd, Ag VOLATILITY)

2. SECONDARY EXPERIMENTS WITHOUT SILVER ALLOY AND WITHOUT SS, TO MELTING TEMPERATURES 1850°-2400 C.
   (MEASURES Sn RELEASE FROM ZIRCALOY)

3. TERTIARY EXPERIMENTS WITHOUT SILVER ALLOY AND WITHOUT TIN (USES ZIRCONIUM CLADDING INSTEAD OF ZIRCALOY) TO 2400°C EUTECTIC MELTING, BWR CORE.
   (MEASURES SS COMPONENT VAPORIZATION)

4. INITIAL FISSION PRODUCT SIMULANT EXPERIMENTS TO BE WITHOUT CONTROL ROD ALLOYS, BUT WITH SS. WILL INCLUDE SEPARATE TESTS FOR OXIDE GROUP (Ba, Sr, RE'S); METALLIC GROUP (Ru, Te, Mo); AND VOLATILE GROUP (Cs,I).

   (MEASURES RELEASE FROM OXIDE PHASE AND FROM METALLIC PHASE)

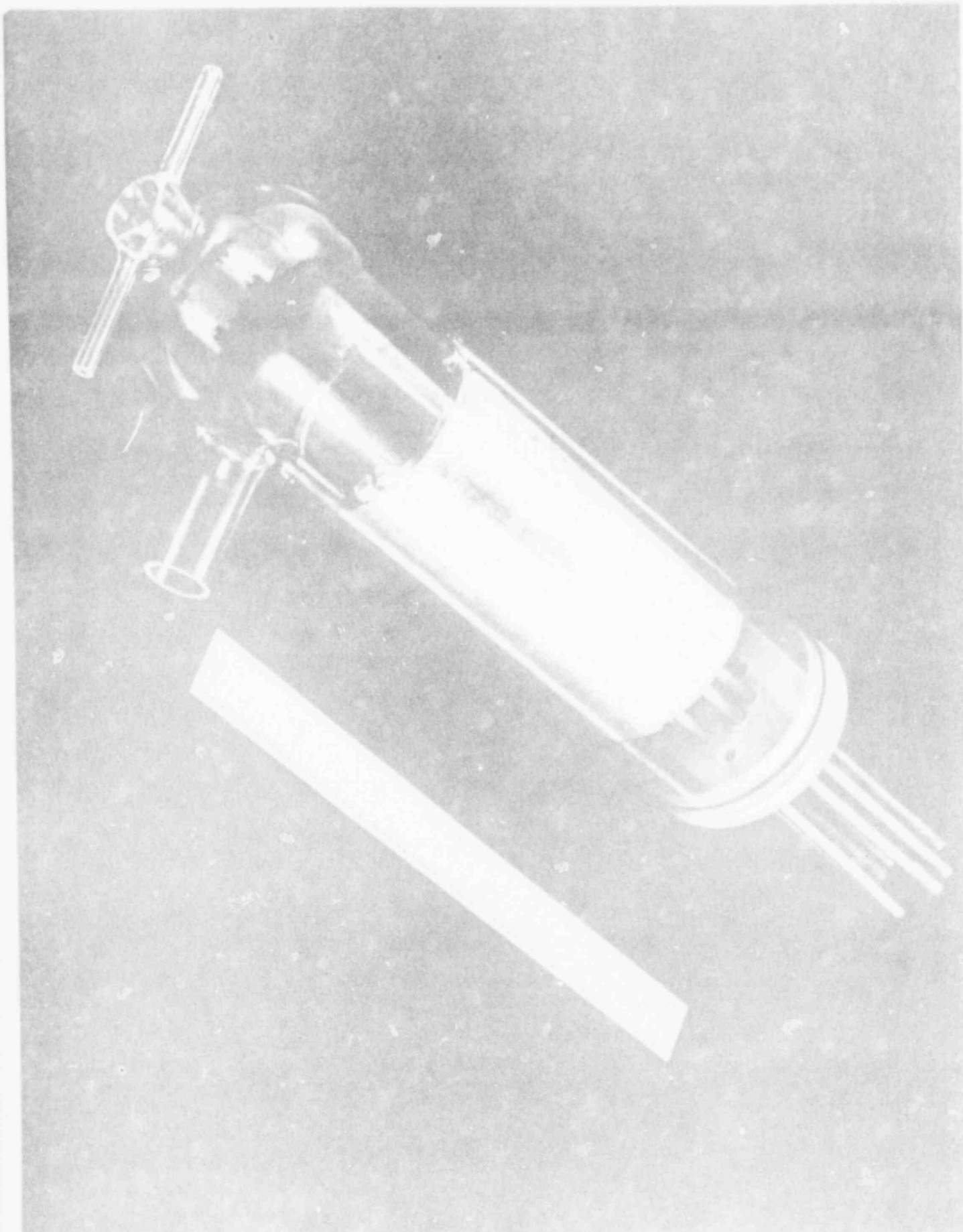

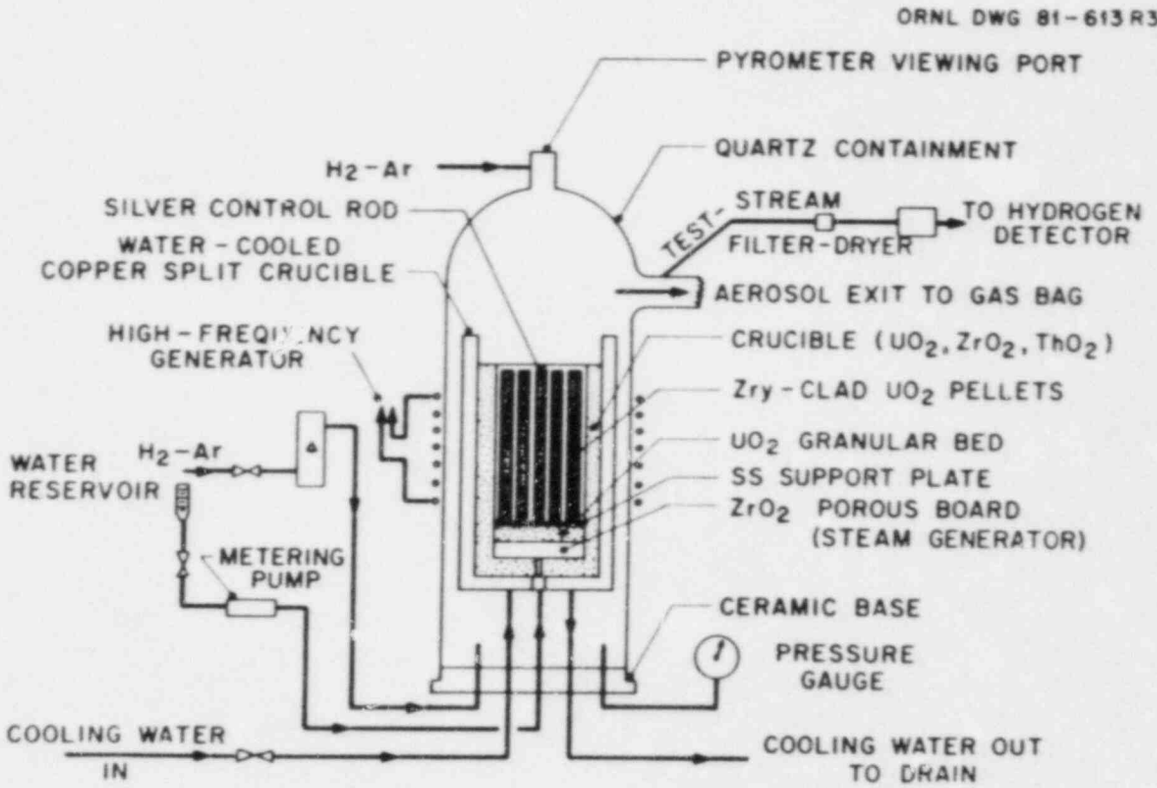

ONE-KILOGRAM CORE-MELT
INDUCTION-HEATED AEROSOL GENERATOR

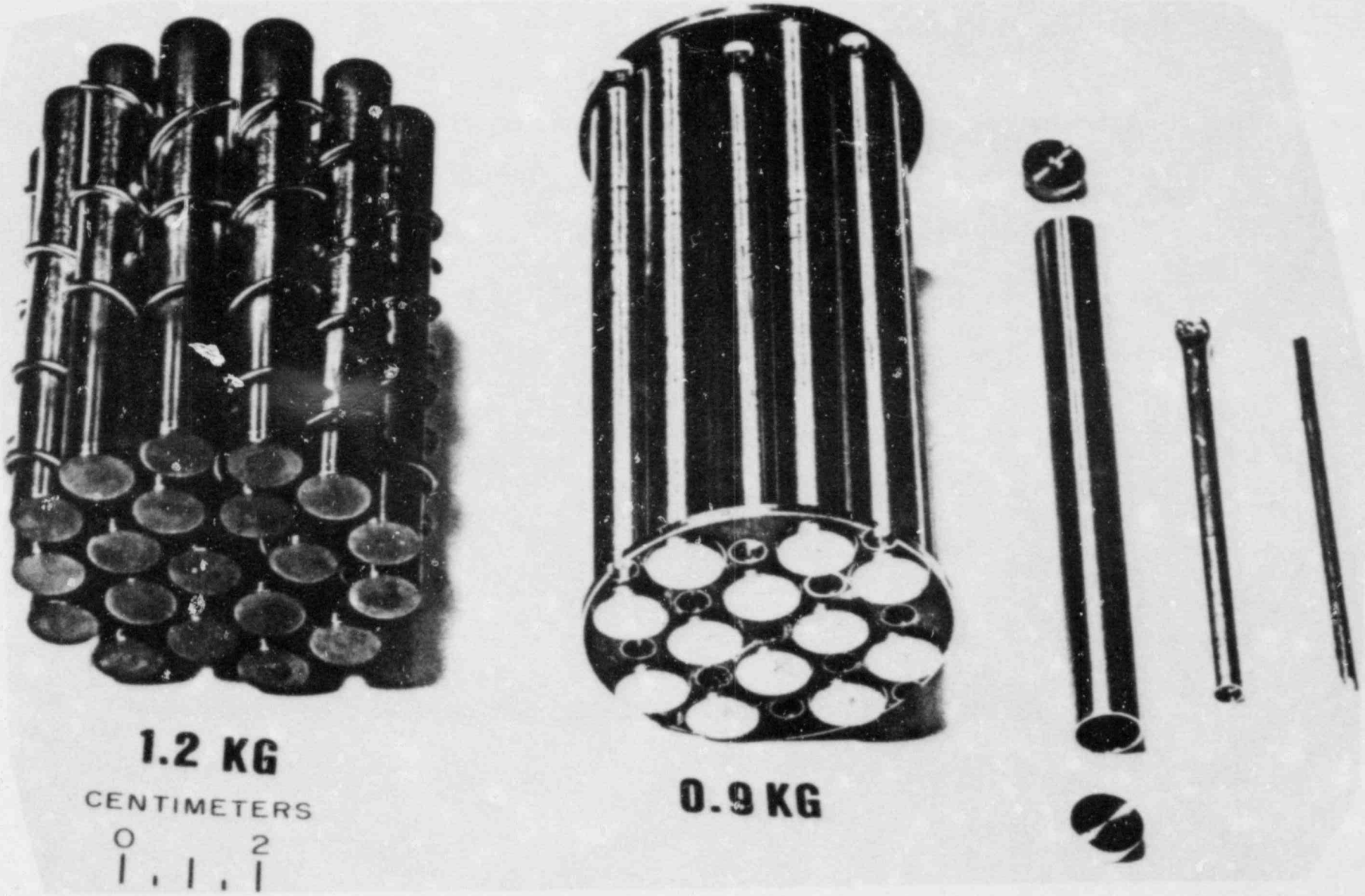

Fig. 3. Typical duel assemblies and control rod simulant used in the core melt demonstrations

ORNL DWG 81-888

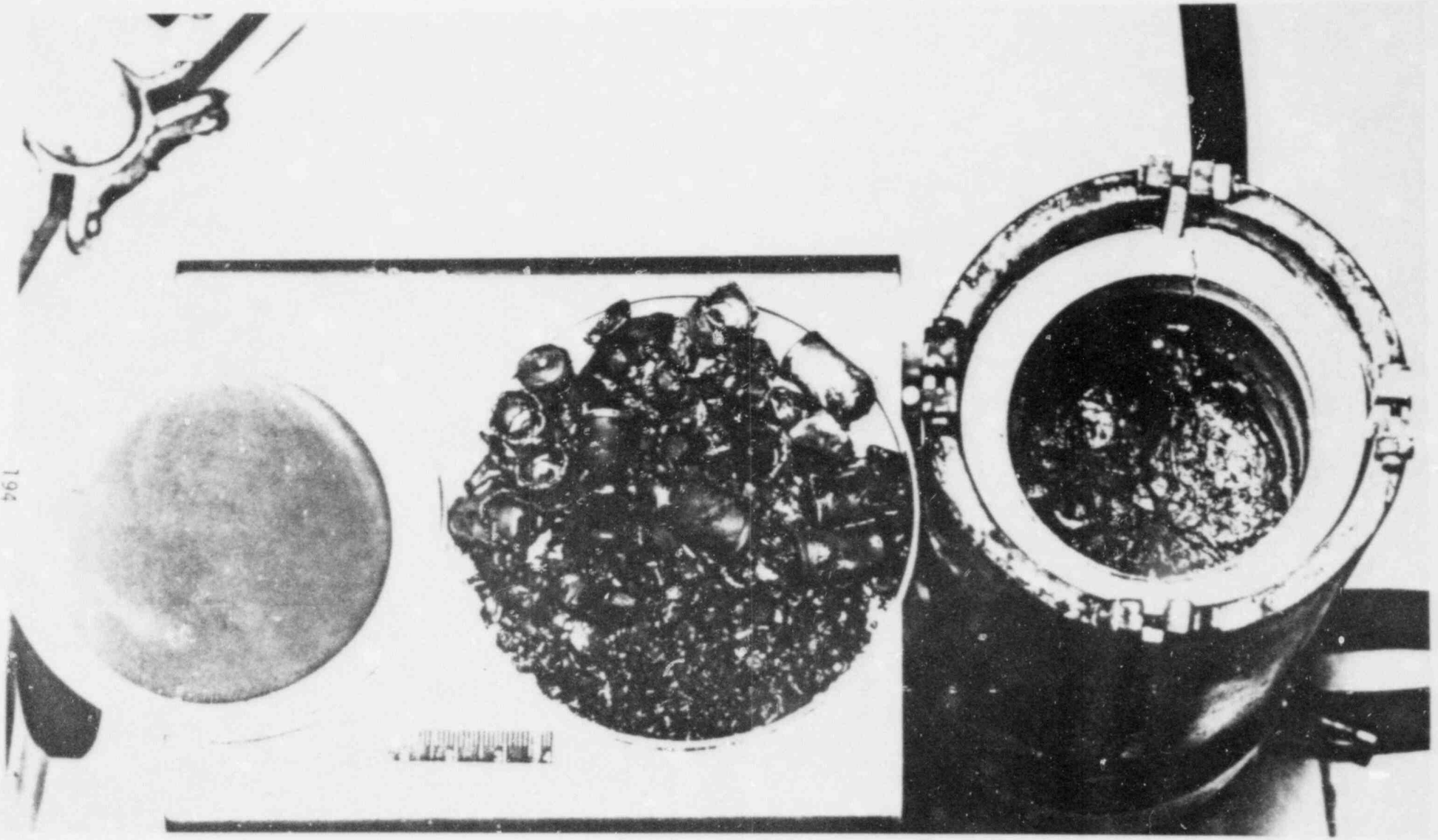

OFF-GAS AEROSOL FILTER OVERHEAD RUBBLE SEGMENTED INDUCTION CRUCIBLE

SAMPLE RESULTS OF TEST CORE-MELT EXPERIMENT

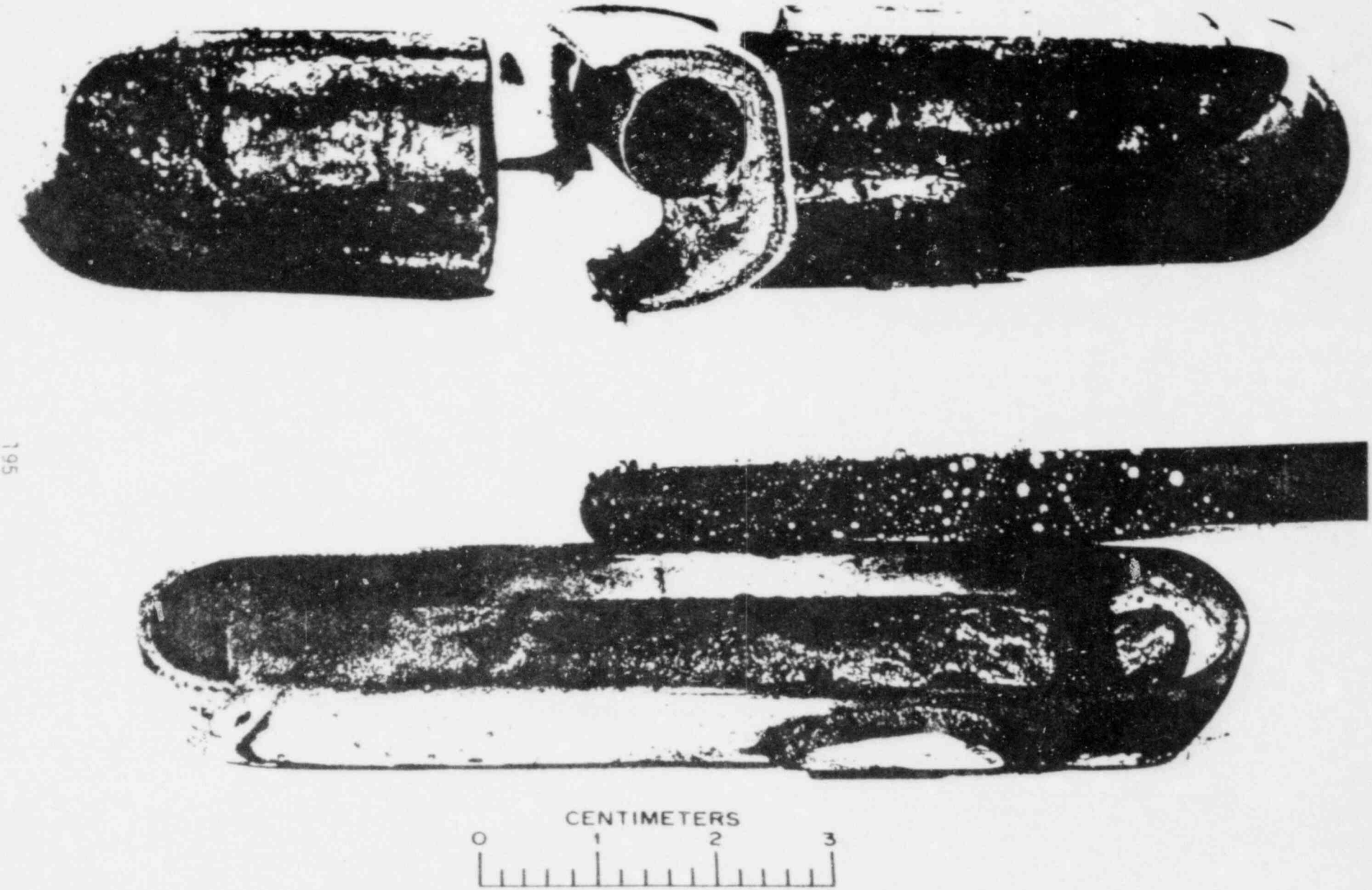

Fig. 5. Examples of silver alloy sheath rupture (below) and interaction of the silver and stainless steel with Zircaloy (above) at 1400-1450°C.

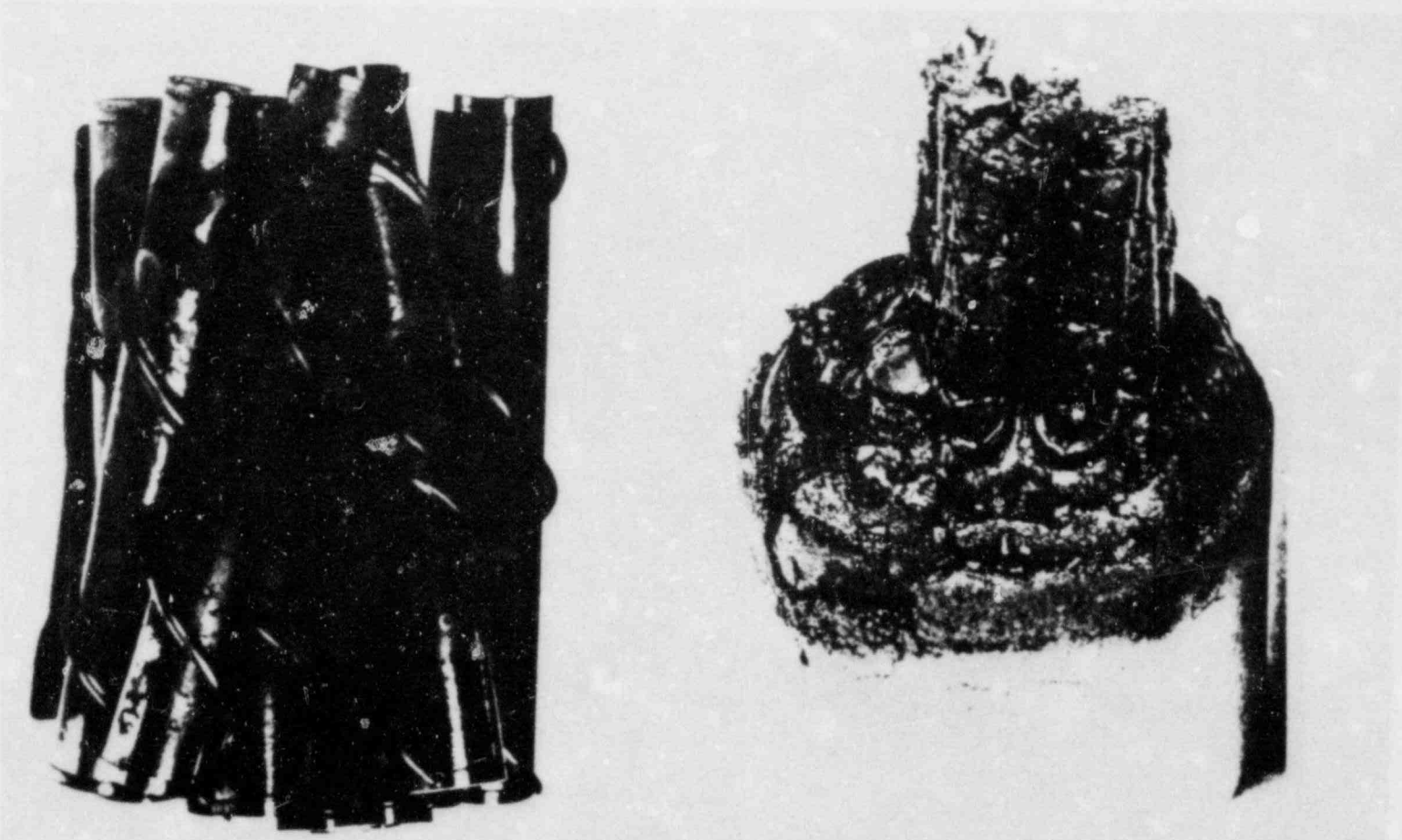

(a) (b)

Fig. 6. Examples of extensive wetting of Zircaloy by the vaporized silver-cadmium metals (a) at 1400°C and of extensive candling (b) at 1800°C.

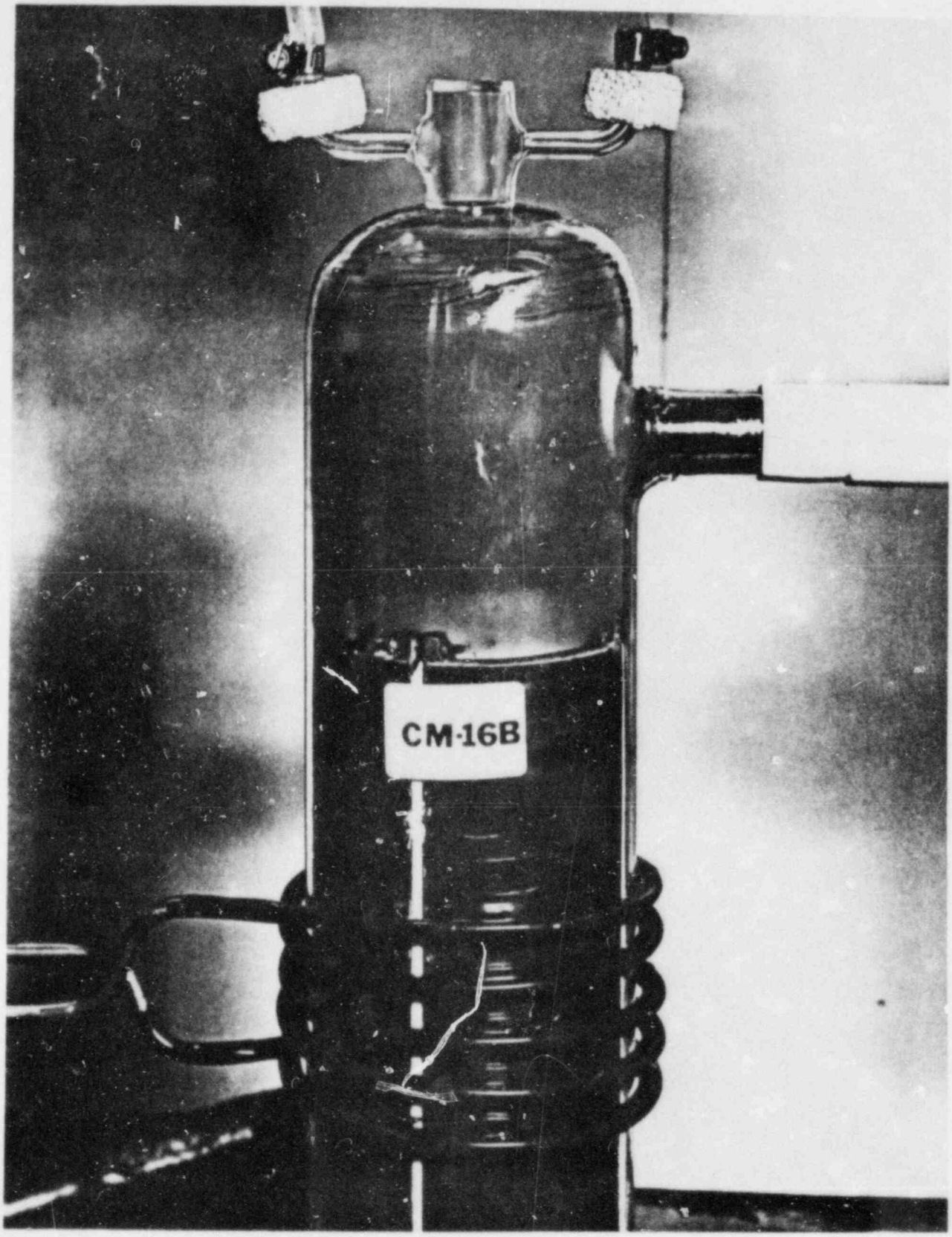

Fig. 7. Appearance of quartz furnace shroud after initial release of cadmium aerosol from control rod alloy.

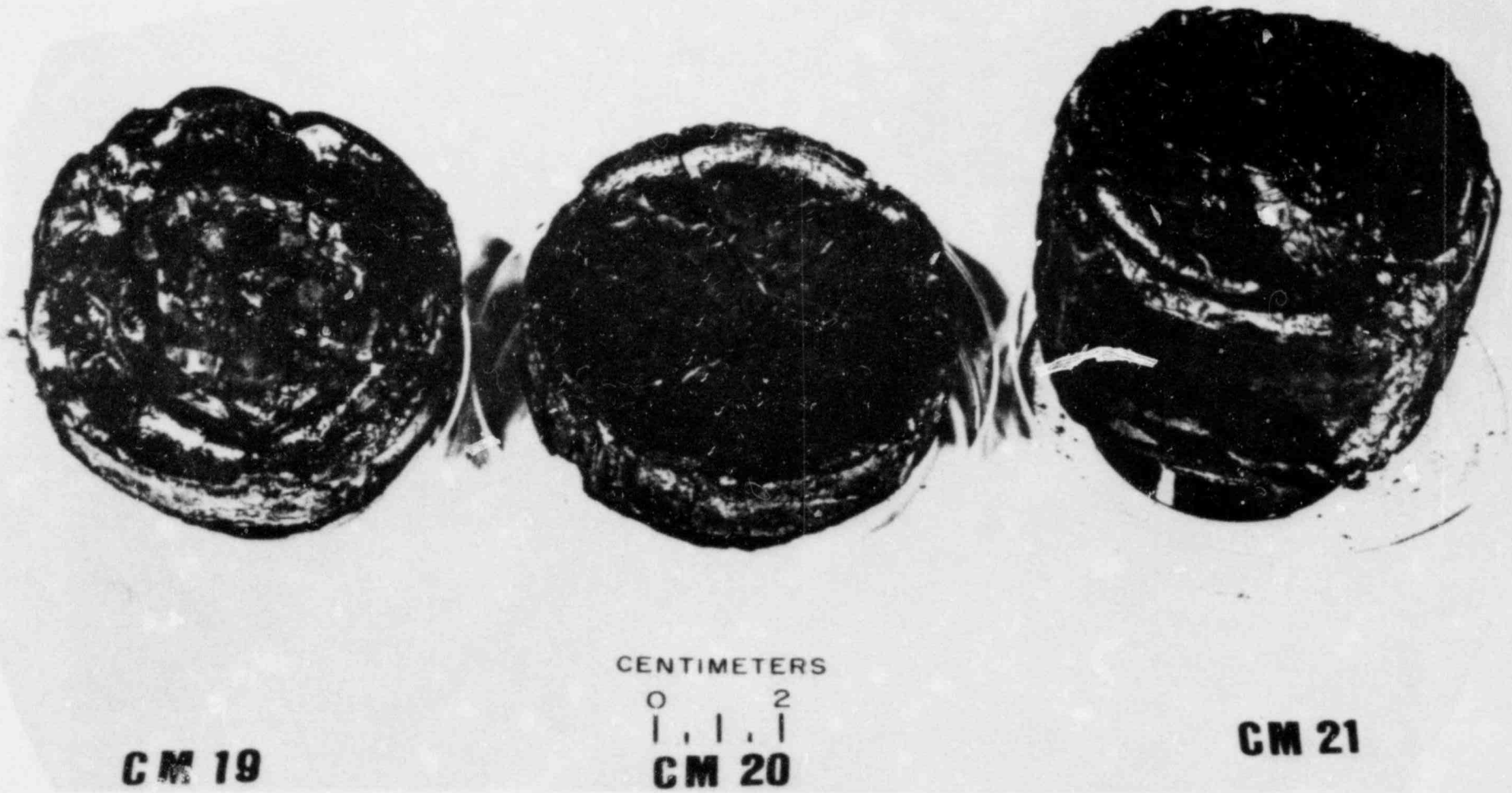

Fig. 8. Samples of the oxide phase melt residue from experiments 19, 20, and 21.

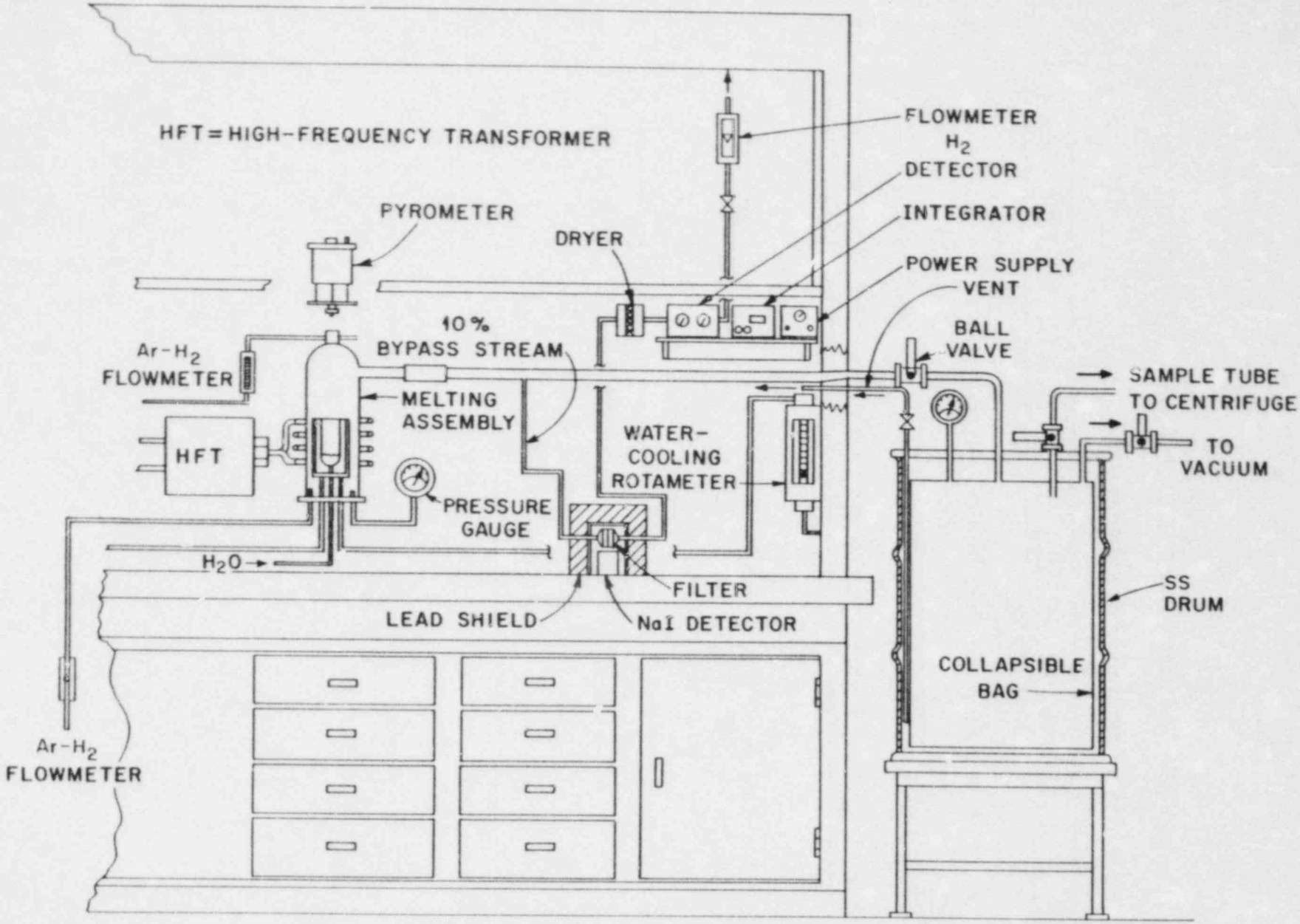

Fig. 9. Schematic of the 1-Kg core melt facility connected to air aerosol chamber.

ORNL DWG 82-1324

VAPORIZATION OF CONTROL-ROD SILVER ALLOY

CM-16 FILTER PAPER ANALYSES

SAMPLE NO.	MAXIMUM TEMPERATURE (°C)	RELEASE (mg)	ANALYSIS (wt. in mg)				
			Cd	Ag	In	Sn	U
16-A	1800	294	178	103	9	3	<1
16-B	2200	103	1	80	20	1	<1
16-C	2400	23	<1	17	3	<1	<1

CM-16 FURNACE-DEPOSITED AEROSOLS

SAMPLE NO.	MAXIMUM TEMPERATURE (°C)	RELEASE (mg)	ANALYSIS (wt. in mg)				
			Cd	Ag	In	Sn	U
16-A	1800	345	270	73	<1	<1	
16-B	2200	175	<1	158	15	<1	
16-C	2400	218	83	108	21		6

CM-16 TOTAL AEROSOL RELEASE

ELEMENT	MASS RELEASED (g)	PERCENT OF MASS INVENTORY
Cd	0.53	53
Ag	0.54	6.1
In	0.07	5.4
Sn	0.005	0.2
U	0.006	1×10^{-3}

ORNL DWG 82-1133

CORE MELT EXPERIMENT CM-19

ELEMENT	WEIGHT OF EACH ELEMENT (gms)	PERCENT RELEASE			TOTAL RELEASE[a] (%)
		1st HEAT (1800°)	2nd HEAT (2200°)	3rd HEAT (2400°)	
UO_2	501.35	6×10^{-6}	6×10^{-6}		1×10^{-5}
Zr	178.3			1×10^{-3}	1×10^{-3}
Fe	12.11				0
Cr	2.99				0
Ni	1.32				0
Sn	2.72	2×10^{-2}	0.17	5×10^{-2}	0.23
Mn	0.16				0
Sr	0.086	5.4	5.1	0.77	11.3
Ba	0.13	2.9	3.1	1.3	7.3
Ce	0.19				0

[a] FURNACE WASH, TOTAL: Sr = 1.4 %, Ba = 2.0 % ADDITIONAL RELEASE.

ORNL DWG 82-1131R

METALS DISSOLVED IN RESIDUAL S. S. MELT[a]

FUEL BUNDLE ADDITIVES		ANALYSIS OF S. S. RESIDUE[b]			ADDITIVE TRANSFERED TO THE MELT
ELEMENT	g	mg/g	g	%	%
Zr (CLAD)	178.3	67	4.24	6.7	2.4
Sn (CLAD)	2.7	20	1.27	2.0	46.9
Mo (F.P.)	0.33	3	0.19	0.3	57.5
Ru (F.P.)	0.43	3	0.19	0.3	44.2
Te (F.P.)	0.06	0.8	0.051	0.08	84.4
I (FUEL)	551.0[c]	90.0	5.7	9.00	1.0

[a] DATA FROM CORE-MELT RUN 21.
[b] DENSITY OF S.S. WAS 8.7 g/cm^3.
[c] DENSITY OF UO_2-ZrO_2 (OXIDE PHASE) WAS 8.1 g/cm^3.

ORNL DWG 82-1132

ESTIMATE OF AEROSOL SOURCE TERM FROM 1-kg EXPERIMENTS

MIDLIFE REACTOR INVENTORY[a] (kg)			AEROSOLS RELEASED		
			MEASURED FROM 1-kg EXPERIMENTS (%)	CALCULATED FOR WHOLE CORE (kg)	
ELEMENT[b]	PWR	BWR		PWR	BWR
Sr	54.3	81.5	7.8	4.2	6.4
Mo	157.3	236	0.14	0.22	0.33
Ru	111.8	167	0.00	0.00	0.00
Te	22.8	34.2	0.00	0.00	0.00
I	11.8	17.6	100	11.8	17.6
Cs	139.1	208.7	100	139.1	208.7
Ba	69.6	104.4	6.6	4.6	6.9
Ce	155.9	233.9	0.0	0.0	0.0
Sn	380.7	808.9	1.2	4.6	9.7
Mn	40.3	374.6	12.0	4.8	45.0
Ag	2159.0	0.0	6.1	131.7	0.0
In	342.3	0.0	5.4	18.5	0.0
Cd	265.9	0.0	53.0	141.0	0.0
Fe	1410	9295.0	0.076	1.1	7.1
TOTAL				461.6	301.7

[a]STRUCTURAL MATERIALS, CONTROL RODS, AND FISSION PRODUCTS.
[b]FISSION PRODUCTS CALCULATED BY ORIGEN FOR 16,500 MWD CORE.

FISSION PRODUCT CHEMISTRY EXPERIMENTS AT SANDIA*

R. M. Elrick, R. A. Sallach, J. E. Brockmann

Sandia National Laboratories**
Albuquerque, NM 87185

SUMMARY

The scope of the High Temperature Fission Product Chemistry and Transport program is 1) to define thermodynamic data and chemical reaction characteristics of fission products of interest, 2) to examine the chemistry and transport of fission products in typical steam and hydrogen environments, and 3) to compare observed behavior of the fission products with predictions made by purely thermodynamic calculations.

A steam facility has been constructed to examine the transport and interaction of fission product species in typical steam and hydrogen environments. Other laboratory experiments are being performed to study kinetic and thermodynamic features of some of these fission product systems in greater detail.

Attention has concentrated primarily on the study of the cesium and iodine system in steam in the steam facility and in a transpiration apparatus and of the tellurium system using a microbalance. The equipment will be described along with the experiments and the experimental results.

The steam facility was designed to study the chemistry resulting from the reaction of single or multiple fission product vapors in steam at temperatures to about 1100C. This laboratory-scale facility provides residence times

*This work sponsored by the United States Nuclear Regulatory Commission.

**Operated for the United States Department of Energy under Contract No. DE-AC04-76DP00789.

from seconds to as long as several hours for chemical and physical changes to occur among the reactants. Initially the reactants include the fission product vapors, steam, hydrogen, and the materials used to constuct the steam facility.

Laser Raman spectroscopy is being developed to examine the vapor phase species produced in the steam facility and to identify the kind of species and their number concentration at the reaction temperature. Calibration relates vibrational frequency to species type and vibrational intensity to species concentration. The rotational spectrum is used to estimate species temperature. Two methods are being used to calibrate for species signatures. For those species that do not react with quartz, closed quartz cells containing known amounts of the species are used. Flow-through calibration in an alumina system is used for species that are corrosive to quartz.

The molecules iodine, tellurium, hydrogen, nitrogen, and steam have been examined for threshold level of detection and signal strength.

The reaction of CsI at 1000C in the presence of steam and hydrogen was studied in two systems. One, in which the reaction tube was lined with 304 stainless steel and the other in which the reaction tube was lined with Inconel 600. In both systems, essentially no water soluble form of cesium was deposited on the walls of the reaction tube. Also, there was very little reaction between the CsI and the surface oxides.

A series of tests was made with cesium hydroxide in a 304 ss system. One test was run without steam at 1000C; three tests were made with steam at 700C, 850C, and 1000C. Hydrogen generation rates for these four runs varied from 1×10^{-5} moles/s (background) to 5×10^{-4} moles/s depending on the operating temperature of the system and its previous history. In the 700C steam run, CsOH was physically absorbed on the 304 ss; at 1000C, essentially no CsOH was physically absorbed but some had reacted with the oxide layer on the 304 ss. The reaction caused the oxide to spall easily from the steel surface. Without steam, the CsOH reacted with the 304 ss producing a thin flaking surface layer.

Kinetic data are required to model interactions where experimental parameters change with time. Such data can conveniently be obtained by the use of a microbalance. Tellurium surface interactions were studied in this way where tellurium vapor (in an argon carrier) was flowed over metal coupons suspended from the microbalance. Coupon

materials were Ni, 304 ss, Inconel 600, preoxidized 304 ss, preoxidized Inconel 600, and silver. Reaction products were measured by x-ray diffraction and reaction kinetics were expressed as a deposition velocity estimated from the calculational program FLATDEP. Tellurium vapor reacted quite rapidly with nickel and Inconel 600 (probably diffusion limited reactions), less rapidly with 304 ss and somewhat less rapidly with preoxidized 304 ss and preoxidized Inconel 600. A very rapid reaction was observed between tellurium vapor and solid silver to form Ag_2Te whiskers. Iodine vapor (also in argon) reacted rapidly with solid silver to form AgI.

A transpiration type of apparatus was developed to study vapor-vapor or vapor-solid reactions among fission products and reactor materials at high temperature. In a two chamber apparatus, vapor concentrations can be prepared and then mixed with each other or with a solid material for reaction times of a minute or so. In a series of transpiration experiments to test the stability of cesium iodide in accident environments the following effects were observed. Either iodine or HI vapors in the presence of CsOH was found to react completely to form the more stable CsI. Cesium iodide remained stable in the presence of oxygen. Likewise, solid silver did not affect the stability of CsI vapor.

As part of the fission product program, additional experimental and analytical work is in progress to predict the characteristics of aerosols produced from the interaction of the molten core with concrete. Mechanistic models are being developed to predict aerosol mass generation rates, composition and size distributions from hypothesized mass transport, and aerosol formation mechanisms. Aerosol generation mechanisms being considered are condensation from the vapor sparging through the melt and hydrodynamic break-up of the melt. Application of the preliminary model to data from small (10 to 30 Kg of melt) melt/concrete interaction tests indicates that the model predicts the experimental results reasonably well.

On the Fission Product Release into the Environment during a PWR Core Meltdown Accident

J. Peter Hosemann
Projekt Nukleare Sicherheit
Kernforschungszentrum Karlsruhe

A reactor pressure vessel contains not only radioactive substances, all of which will be released during a core meltdown accident, but besides water contains also various steel internal structures, control rods and, of course, fuel elements. The fuel elements consists mainly of uranium dioxide, zircaloy cladding tubes, and Inconel spacers; radioactive and stable fission products and daughter products are contained in the fuel matrix i.e. in the fuel pins. Altogether this amounts to a mass of 167.2 t, subdivided as follows (after an in-pile time of 1000 d):

Fuel (UO_2)	98.8 t	59.3 %
Interior Steel Structures	31.1 t	18.6 %
Cladding Tubes (Zircaloy)	31.9 t	19.0 %
Control Rods	2.3 t	1.4 %
Fission Products	2.8 t	1.7 %

- The reactor pressure vessel (RPV) contains about 2 tonnes of silver from the control rods, almost 1.4 % of the RPV inventory is silver metal.

Revised version of a paper presented at the Kerntechnik '82 Annual Conference in Mannheim on May 5, 1982

- Only about 1.7 % of the RPV inventory,water excluded, are fission products and daughter products. Of these, in turn, 1/10 is radioactive, resulting in about 280 kg of radioactive material out of a total inventory of 167 200 kg.

This mass balance leads to the following observations:

During a core meltdown accident, most of the RPV inventory will be heated until melting occurs. Consequently, substantial portions of the different materials will be released as aerosol particles into the containment.

The rate of reduction of the water level in the core will determine the rate of fission product release from the fuel and the rate of hydrogen production from oxidation of the cladding.

This is an important consideration to assess timely the releases of both gaseous and particulate fission products and of non-radioactive material.

Nine years ago, realistic release experiments were started at the SASCHA meltdown facility of the Karlsruhe Nuclear Research Center within the framework of the Nuclear Safety Project. The program involved very sophisticated technical systems and approx. DM 13 million has been spent to date.

The results of these tests provided knowledge about maximum estimated releases into the containment of particles existing in the reactor vessel.

During a postulated loss of coolant accident and subsequent failure of all emergency cooling and when the water level drops below the top of the core a considerable axial temperature gradient develops along the core between the fuel at water level and the top of the core. Consequently, at the highest temperatures, condensing aerosol particles of less volatile materials may be produced at the top, while, at the bottom, right above the water level, more volatile material can be evaporated

at the same time, part of which may also condensate on particles generated at the top. The process becomes even more complex when considerations of melting fuel flowing down and by fuel rod particles dropping into the residual water and also by axial differences in the degree of oxidation of the cladding tubes.

Therefore, it is simply wrong to assume that, in the course of a core meltdown, first the more highly volatile and later the less volatile fission products will be released into the containment. Instead, coagulation and condensation processes largely homogenize the release of aerosols. It is not meaningful to trace the history of each individual fission product in detail. This is a basic process which, however, frequently is not followed.

The SASCHA data provided the release functions, as a function of time, for gaseous and particulate, radioactive and non-radioactive fractions of the mass inventory in the reactor pressure vessel.

An integral particle mass of about 3.5 t is discharged as airborne material into the containment when consideration is taken that, during and after meltthrough of the pressure vessel, steel fractions of the hemispherical bottom of the vessel and fractions of the melting concrete are also released as particles. This is approx. 1.5 % of the mass inventory of the pressure vessel. The control rods (Cd, In, Ag) contribute the largest portion, almost 1 600 kg mostly silver metal. The next largest portion is steel which amounts to 745 kg. Most of the steel is available as oxide. Uranium oxide contributes 490 kg, silicate and carbonate particulate from the concrete amount to some 300 kg. The next largest mass is contributed by the non-radioactive fission products and daughter products (approx. 160 kg). The cladding tube material releases some tin, but mostly zirconium as an oxide (80 kg). Only slightly less than 100 kg is radioactive material emanating from the fuel, with the largest portion being cesium-137. The material breakdown relates to a reactor

core of a typical German pressurized water reactor with 100 t of UO_2 and an average burnup of 37 GWd/t after an in-pile time of 1000 days. It should be noted that only some 2.6 % of all aerosol particles released into the containment are radioactive. Of course, 100 % of the noble gases are released from the reactor core. Under the conditions specified above, the iodine inventory at the beginning of the core melt accident is 18 kg, which is also assumed to be released by 100 %. Only some 800 g of this material are made up of the iodine 131 isotope, which is the radiologically important isotope.

After approximately one hour after a postulated double ended rupture of a main coolant pipe and hypothetical failure of sump cooling, the sinking water level in the pressure vessel will reach the top of the core. At that time, massive releases of gases and particles into the reactor pressure vessel and then subsuequently into the containment will occur. After another 50 minutes the pressure vessel is assumed to fail. Some 230 t of melt with a maximum temperature of 2400 ^{o}C will then flow into the 6 m wide concrete cavity underneath the RPV. The melt consists mainly of two phases. At the bottom, there are some 70 t of liquid metal, the rest is oxide. The oxide phase is continuously diluted by liquid concrete components. Water vapor from the concrete permeates the melt, partly oxidizing the metal phase.

Since 1974, the interaction between the molten core and the concrete basemat has been studied in close cooperation between German (BMFT) and US NRC agencies. This has led to the development of computer codes for analyses of the gas and steam production and radial and axial melting of the concrete during core melt accidents. A large number of test data had to be evaluated theoretically from laboratory tests and large-scale experiments by various disciplines of science and engineering. In general, three of the more important findings are:

(1) In the first two hours, concrete melting is a highly transient process, the temperature of the molten pool decreases quickly from 2400 °C to 1500 °C. Thereafter, the melting process slows down more and more until it reaches quasi-steady state conditions.

(2) Radial concrete melting causes the sump water to penetrate to the melt 6 to 9 hours after the melt had contacted the concrete.

(3) Currently, the solidification behavior of the melt cannot be firmly determined, because of the fast encrustation of the metal phase. It is not certain whether a concrete foundation of 5 to 7 m thickness will be penetrated at all. However, it can be concluded that melting of the concrete basemat results in sump ingression, and, hence, in a long term pressure buildup in the containment with subsequent containment failure.

The so called "Chira Syndrome" will not lead to loss of containment integrity rather the pressure build up after a few days after the accident will lead to containment overpressurization and subsequent release of fission products. Hence, Fig. 1 shows the results of more recent analyses for the so called release category 6 obtained by the COCMEL containment code on the basis of the pressure vessel evaporation analysis calculated by the BOIL code and based on concrete destruction calculations by means of the WECHSL code. The diagram is a plot, over the logarithmic time axis (scale change at 10^3 sec), of the atmospheric pressure in the containment, expressed in bar, for the 2F LOCA accompanied by failure of the sump cooling system. The containment design pressure of 6 bar and the failure pressure of 9 bar are shown in the diagram. The blowdown peak of 4.6 bar is reached after 20 sec. After 3600 sec, core heating begins and with it the release of fission products into the containment. After some 6000 sec the failure of the RPV occurs. After 30 000 sec (8.3 h) sump water breaks into the melt which creates a pressure rise. In accordance with the German Risk Study it

was assumed that overpressure of the containment failure would occur after 27 h, when the design pressure level is reached after slightly less than two days according to Fig. 1. However, overpressure failure need not to be anticipated earlier than after five days. Within these five days the aerosol system discussed above is subjected to major removal mechanisms within the containment which can be calculated reliably (perhaps too pessimistically) be means of the NAUA aerosol code.

Fig. 2 shows the airborne particle mass in the containment as computed by NAUA relative to the initial mass. Within 120 h the airborne aerosol mass decreases by six orders of magnitude. If the release factors from the core are known, the airborne particle mass of fission products can be read directly from the curve. Cesium, e.g., is released from the core by 100 %. Hence, the airborne cesium mass relative to the cesium inventory is M/M_o.

It has been sometimes assumed that even the slightest atmosphere disturbance would reagitate the aerosol masses precipitated and distributed throughout the containment. This is, of course, not true. Given 3 500 kg of aerosol mass, all surfaces in the containment, which add up to some 50 000 m^2, could be covered only with an aerosol layer 10 µm thick, hence particles once plated out will remain plated out.

The risk study experts, insist that a containment should not be considered leaktight. At least the design leakage of 0.25 vol.%/day (which is some 7 m^3/h), or rather ten times that level up to overpressure failure, would have to be anticipated. Consequently, Fig. 2 also shows, for both leakrates the particle masses which will be discharged into the annulus. It should be noted that the maximum leak rate has been reached already after about 6 hours.

Fig. 3 shows the behavior of the aerosol in the annulus and is based on the following assumptions: The annulus exhaust air handling system is in operation at a rate of 600 m^3/h, and the assumption is made that the aerosol can spread and plate out only in half the annular area. At the time of containment failure due to overpressurization the total aerosol mass which is still airborne in the containment and in the annulus is suddenly released to the outside environment (puff release). Two cases of outside leakage have been considerated: the aerosol filter of the annulus exhaust air handling system is undamaged (which results in the lower leakage mass curve in Fig. 3) or is not available for filtration (upper curve of leakage masses). The spikes in the leakage mass curves are the sudden and unfiltered releases as a result of the still airborne particle masses in the containment and in the annulus at overpressure failure.

At the top of the diagram, the integral particle release expected in the German Risk Study is shown for comparison. As can be seen from Fig. 3, the German Risk Study overestimated the releases at least by two, more probably even by three orders of magnitude.

The sudden release of all airborne masses from the containment and the annulus as soon as a pressure of 9 bar in the containment has been reached is a very unlikely event. It cannot be postulated that the concrete shell and the steel containment at that moment would burst like a balloon and all of the sump water would evaporate from the depressurization with the release of all volatile matter precipitated in the sumpf. Instead, it is more likely that overpressure failure of the containment would be a gradual process of increasing leakage. It can be seen (Fig. 1) that the gas- and steam flow causing further pressure increases above the design pressure of 6 bar is in the range of 1 m^3/h. Under critical outward flow conditions, which of course would exist at that pressure, this mass flow could be passed into the annulus through a leak cross section of only 13.5 cm^2 (which would correspond, e.g., to a circular area with a radius of 2.1 cm).

This example shows that the following concept is very probably correct:

With rising pressure in the containment above the design pressure level, leakages into the annulus increase in such a way (probably with seals and welding seams failing) that the pressure stabilizes somewhere above 6 bar. Total sump evaporation will then occur within two to three weeks. Slight resuspension (0.01 %) of the particles deposited in the sump must be expected. At the same time, the aerosol plate out mechanism continue to deposit particles both in the containment and in the annulus. The filters of the annulus exhaust air handling system will continue to be available, since there is no sizable pressure buildup in the annulus. According to first engineering estimates, the integral release to the outside in accordance with this scenario will be below that assumed pessimistically in Fig. 3. As soon as reliable leakage analyses and data about possible resuspension from the sump are available, the assumption of a sudden puff release after five days can be revised.

The reduction in the release of iodine when compared with the assumption in the German Risk Study is even more significant than it is for aerosol particles. The computer code used for estimating maximum iodine releases in core meltdown accidents postulates that all iodine existed in its radiologically most adverse and most highly volatile chemical form, namely as I_2, although this is physically not possible according to the present state of the art. It is further assumed that the containment will contain a 50 - 100-fold stoichiometric excess of silver and other metals over iodine, and this must result in the formation of metal iodide in an airborne state and in the sump water, if evaporation causes the solubility limit for ionic (non-volatile) I^- to be exceeded there. The most stable and the most frequent metal iodide will be AgI.

Fig. 4 shows the integral results of the new iodine calculations for release category 6 as the fraction of the iodine inventory released into the environment as I_2, both for single and for

ten fold design leakage levels, both with and without the activitated carbon filters available. At the time of overpressure failure it was assumed that all iodine in the sump water and all iodine in the containment atmosphere and in the annulus would be released suddenly and without filtering. In addition, the figure shows also iodine releases according to the German Risk Study. Compared to the best estimate curves for single and ten fold design leakages with the iodine filters in operation, the results of the German Risk Study are overestimated by almost five orders of magnitude. Again, a more realistic assessment must be expected for the future, which will no longer be based on sudden containment overpressure failure (puff release).

It has also been postulated that the containment at the time of the accident had an opening which acted as release path. The most serious case was the failure of containment isolation valves to close as scheduled in case of an emergency cooling signal. This case corresponds to release category 2 in the German Risk Study.

Assuming (as is done in four cases out of 1000 core melt-down accidents in the German Risk Study) that both isolation valves in the vent air line from the containment fail in open position, the containment would have a leak of 300 mm diameter, which would initially lead into the vent air ducts. These, of course, would not withstand the blowdown. It has to be assumed that the vent air ducts normally used in ventilation systems fail at less than 0.2 to 0.3 bar overpressure. Since the penetration into the reactor auxiliary building consists of a steel pipe with an inner diameter of 300 mm, and since it must be assumed that the sheet metal duct connected downstream of it will fail, the containment with the annulus and the annulus with the reactor auxiliary building will each be connected by a leak of 300 mm diameter. This leakage model is different from the respective assumptions in the Risk Study.

Since the leaks into the annulus and into the reactor auxiliary building had been assumed to be close to each other, it was assumed that aerosol and iodine propagation could occur in half the volume of the annulus. Consequently, the propagation of iodine and aerosols in the containment, in half the annulus and in the reactor auxiliary building was analyzed for release category 2. The time curves and the integral masses released depend greatly on the leak discharge rates and, hence, on the thermodynamics in the containment. Improved analysis results are presented as follows:

Fig. 5 shows the leakage mass flows (m^3/s) into the annulus according to recent thermodynamic analyses with COCMEL. Also shown, for comparison, is the leakage mass flow of the Risk Study which, according to the state of the art at that time, also represented the leakage to the outside environment. In the time between the failure of the RPV and the inrush of the sump water in the containment more steam is condensed than is supplied as gas and steam from the concrete/melt interaction, no leakage into the annulus occurs in that period, according to the new calculation. In fact, there is even an inward flow into the containment. Only the impressing of sump water will cause another steam surge, but the leak rate again will decrease because of condensation, and then, once the heat stored in the structures leads to increasingly smaller condensation rates the pressure again rises continuously.

Corresponding analyses have been made also for leakage into the reactor auxiliary building, which is of course smaller because, initially, steam can condensate also in the annulus. However, the leak rate from the reactor auxiliary building to the outside was pessimistically assumed to be identical to the inflow from the annulus.

NAUA calculations of aerosol behavior in the containment and in the annulus and calculations of the respective integral particle masses released result in values approximately five orders of magnitude higher than in release category 6 (Fig. 2). Again,

the peak of the aerosol masses escaping through the leaks is reached within a relatively short period of time (approx. 2 h after blowdown) and the mass of airborne particles in this case decreases even by eight orders of magnitude within 80 hours as a consequence of the large leakage cross section as compared to release category 6.

The behavior of the airborne particle mass in release category 2 in the reactor auxiliary building and the respective cumulated leakage mass is obtained from Fig. 6. The difference relative to the recent results is almost 1 1/2 orders of magnitude.

Fig. 7 shows the integral I_2 masses released to the outside relative to the inventory. The top curve corresponds to the release of I_2 as assumed in the German Risk Study. The lower curve is the maximum estimate calculated in accordance with the new idione model.

The transient release as incorporated in the newly calculated curve plays an important part with respect to the consequences of an accident. In the first eight hours, the iodine release is at least a factor of 400 lower than it is according to the Risk Study. The integral iodine quantities then released up until approx. 90 h amount to 39 % of the inventory according to the Risk Study and 0.64 % according to the new calculations. As in the case of the aerosols, this results in smaller releases of approx. 1 1/2 orders of magnitude.

The most probable of the credible accident sequences associated with the rupture of the main coolant pipe and with emergency cooling measures failing has been analyzed, (release category 6). The case with the severest consequences, but a correspondingly lower probability of occurence, was presented, which is release category 2.

In summary, the new PNS results will be compared with those obtained under the German Risk Study for the two release categories, broken down by the radiologically most important elements. The data quoted are the masses released of all isotopes of an element relative to the original core inventory. The radioactive post-accident decay after the blow down has not been taken into account.

	Maximum fraction of core inventory released				
	Kr-Xe	I_2-Br	Cs-Rb	Te	Ba-Sr
DRS, A	1.0	3.9E-1	2.6E-1	1.6E-1	3.0E-2
PNS (best estimate)	1.0	6.4E-3	6.9E-3	5.6E-3	6.9E-5

Release category 2 (low pressure path) leak: D_i = 300 mm

In release category 2, the new results lead to a reduction for iodine (I_2) and for cesium by 1 1/2 orders of magnitude. The difference for tellurium and especially, for barium and strontium is even greater; this is due to the improved core release data from the SASCHA program of the Nuclear Safety Project (PNS). Noble gases, of course, will be released into the environment by 100 %, but with a much greater time delay than had been assumed in the German Risk Study.

	Maximum fraction of core inventory released				
	Kr-Xe	I_2-Br	Cs-Rb	Te	Ba-Sr
DRS, A	1.0	E-2	8.7E-4	9.3E-4	9.6E-5
PNS (best estimate)	1.0	1.1E-7	9.6E-7	7.8E-7	9.6E-9

Release category 6 (low pressure path)

In release category 6, which is the most frequent release category (99.6 %) the PNS results show a reduction by five orders of magnitude with respect to iodine release. In the case of cesium and tellurium it is three, for barium and strontium four orders of magnitude.

Calculations of the accident consequences with the UFOMOD code of PNS, which was also used in the German Risk Study, show that neither early nor late fatalities must be expected to occur for release category 6. For release category 2, no early fatalities were found under almost any weather condition. Under extremely unfavorable conditons a few cases of early fatalities were calculated with UFOMOD. Late fatalities are reduced by a factor of six. More than three quarters of all cases of late fatalities in release category 2 were calculated to have resulted from radiation doses below the respective limits under Section 28 of the German Radiation Protection Ordinance. According to the UFOMOD results, almost 90 % of all cases of late fatalities are due to ingestion. With realistic treatment of the ingestion pathway and with modified dose-effect relationships it is expected to reduce the occurrences of late fatalities after a core meltdown accident in release category 2 even further.

The new results elaborated so far were mostly concerned with developments since the completion of the German Risk Study. Some of the problems still requiring further evaluation are as follows:

The analyses presented may not cover all credible scenarios of core meltdown accidents, e.g. fission product releases associated with core meltdown accidents on the high pressure pathway will have to be analyzed in detail. This work is under way at present. It is expected, however, that also in this case the loss of containment integrity will lead to the most severe effects. The solution of yet another problem is being researched in both Germany and especially in the U.S.A. with great financial and personnel expenditures. The objective is to preclude, by scientific methods, the early destruction of the safety con-

tainment by a hydrogen detonation in the case of release category 6. In the ternary diagram of air/steam/hydrogen mixtures, an ignition limit can be presented which is supported by scientific findings (Fig.8). For any composition of the mixture within the ignition limits there is a possibility of deflagration, i.e., a virulent combustion process. In most cases, such deflagration can be excluded from involving the entire containment, because the combustion flame will have been extinguished and no deflagration can jeopardize the containment. However, the case is different when the mixtures reach the so-called detonation range. A sufficiently violent H_2 detonation in the containment has the potential to breach the containment. If it is assumed that there were no steam, but only air in the containment, to which the H_2 oxidation of cladding tubes would be added, and 70 % of all cladding tubes were fully oxidized, this would lead to slightly less than 15 vol.% of H_2. If 100 % of all cladding tubes are oxidized, this leads to nearly 20 vol.% of H_2 in the containment. Theoretically, this mixture of air and H_2 is just capable of detonating. Now, in a core meltdown accident, much more water vapor than H_2 will be released, 20 t of water vapor reduce the H_2 fraction to 15 vol.%. That amount of water vapor will be present in any case.

The following statements can be made with a sufficient safety margin:

The composition of the mixture reaching the detonation range exists only if the H_2 fraction exceeds 15 % and at the same time the air fraction exceeds 40 % of the total mixture. Since vol.% behave like the corresponding partial pressures, this can be shown by the example of release category 6. Fig. 9 shows the total pressure in the containment P_g, the partial pressure of air P_L, and the hydrogen partial pressure P_{H_2}. Additionally, the curves for 40 % of the total pressure and for 15 % of the total pressure have been entered. Up to some 10^5 sec, the partial air pressure is above the 40 % curve but that of H_2 is not above the 15 % curve at the same time. After 10^5 sec, both conditions are no longer met, dispite the H_2 partial pressure

rising because of metal oxidation associated with the interaction between concrete and the melt. Since 15 vol.% of H_2 still have a safety margin relative to the range of detonation, one is not required to anticipate a detonation at any point in time according to Fig. 9. This assumes that there are no different local concentration distributions due to stratification in the containment, however this assumption is still under theoretical and experimental investigation at the present time. Existing model calculations support the expectation of a uniform mixture, at least in large subspaces of the containment. Detonations in bunkered plant compartments are not very likely to imperil the steel sphere of the safety containment.

It is not likely that the mere existence of a mixture capable of detonation would already lead to a detonation. Because a corresponding ignition power must be available, which must be orders of magnitude higher than that required to ignite a H_2 combustion. In addition, the available water vapor not only causes ignition conditions to deteriorate, but also mitigates the pressure and the reaction rate after ignition. Even in the range of detonation, combustion is therefore much mor probable than detonation. A sufficiently extensive H_2 combustion reduces the likelyhood of any subsequent detonation due to the consumption of H_2 and oxygen. The deliberate combustion of H_2 (e.g., with glow plugs) has already been successfully tested in the U.S.A. It may be assumed that the destruction of the containment by H_2 detonations can be excluded deterministically in a foreseeable time.

Finally, the following efforts are required in addition to the deterministic exclusion of destruction of the containment by steam explosions.

The maximum estimates for iodine releases as presented here must be reduced to best estimate values. This requires elucidation of the actual chemical and physical processes iodine undergoes in an interaction with the aerosol and in an interaction with the sump water composition. The corresponding programs have already been launched.

Since the decomposition of aerosols as a function of time plays such a dominating role with respect to accident consequences, a large scale experiment in the PWR model containment of Battelle in Frankfurt is expected to provide significant results although experts believe to be able to predict the results already as a result of numerous verification steps, however these tests will demonstrate that there are in fact drastic aerosol removal mechanisms and that they can be calculated in advance sufficiently accurate. The so-called BETA experiment is presently being installed at the Karlsruhe Nuclear Research Center, which is to be used to verify the corresponding German and American computer codes to predict the point in time of overpressure failure and thus on the interaction between the concrete and the melt.

All these studies are mainly carried out within the Karlsruhe Nuclear Safety Project, not as a solitary effort but with collaboration with research agencies in Germany and abroad. Hence, one may be confident that all the open questions of today will have been answered satisfactorily within roughly three years. However, it is safe to say now that the effects of core meltdown accidents so far have been overestimated by several orders of magnitude. At any rate, they will not mean a "national disaster".

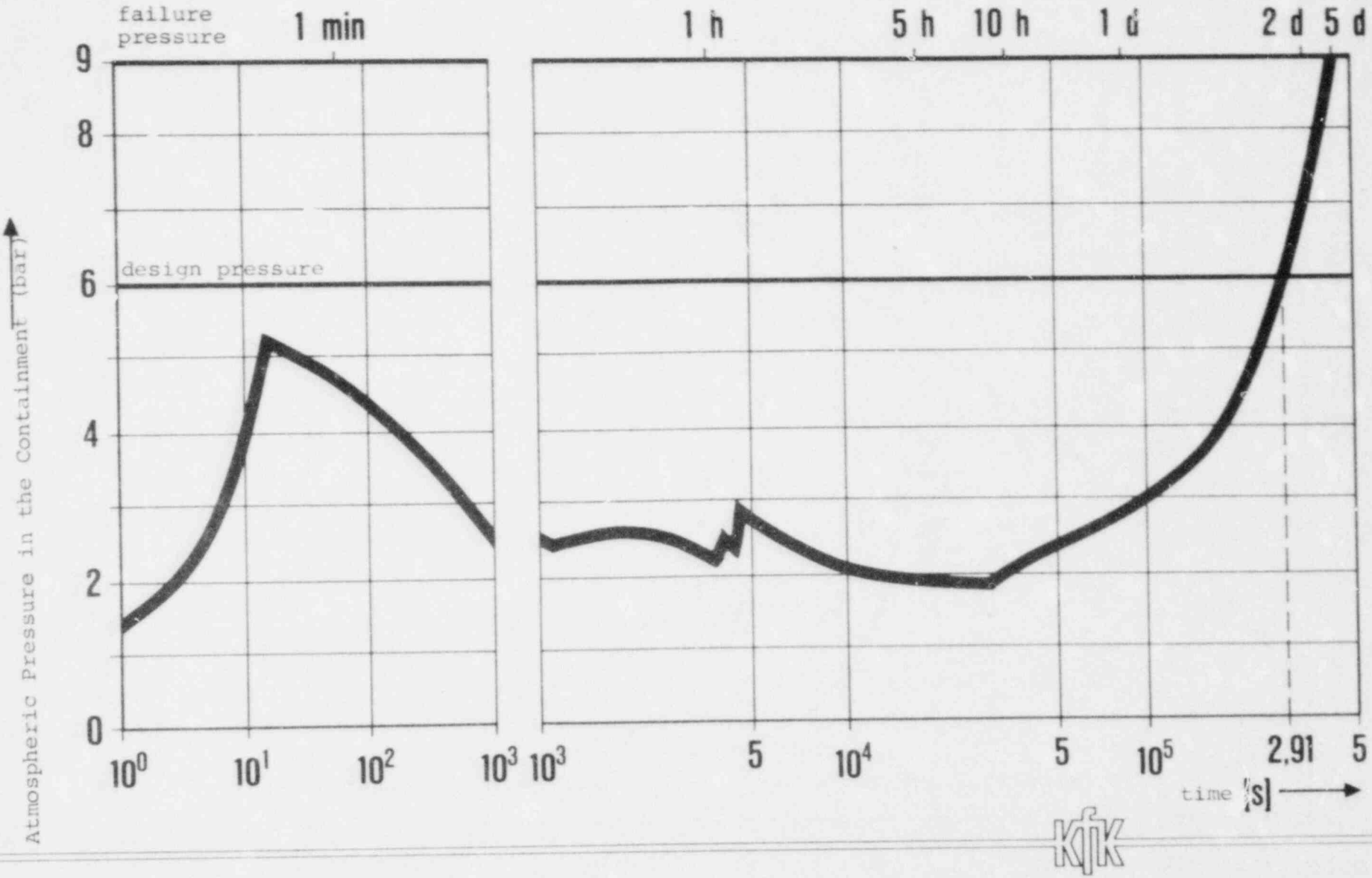

Fig. 1: Pressurization of the Containment for the 2F LOCA accompanied by Failure of the Sump Cooling System (low pressure path)

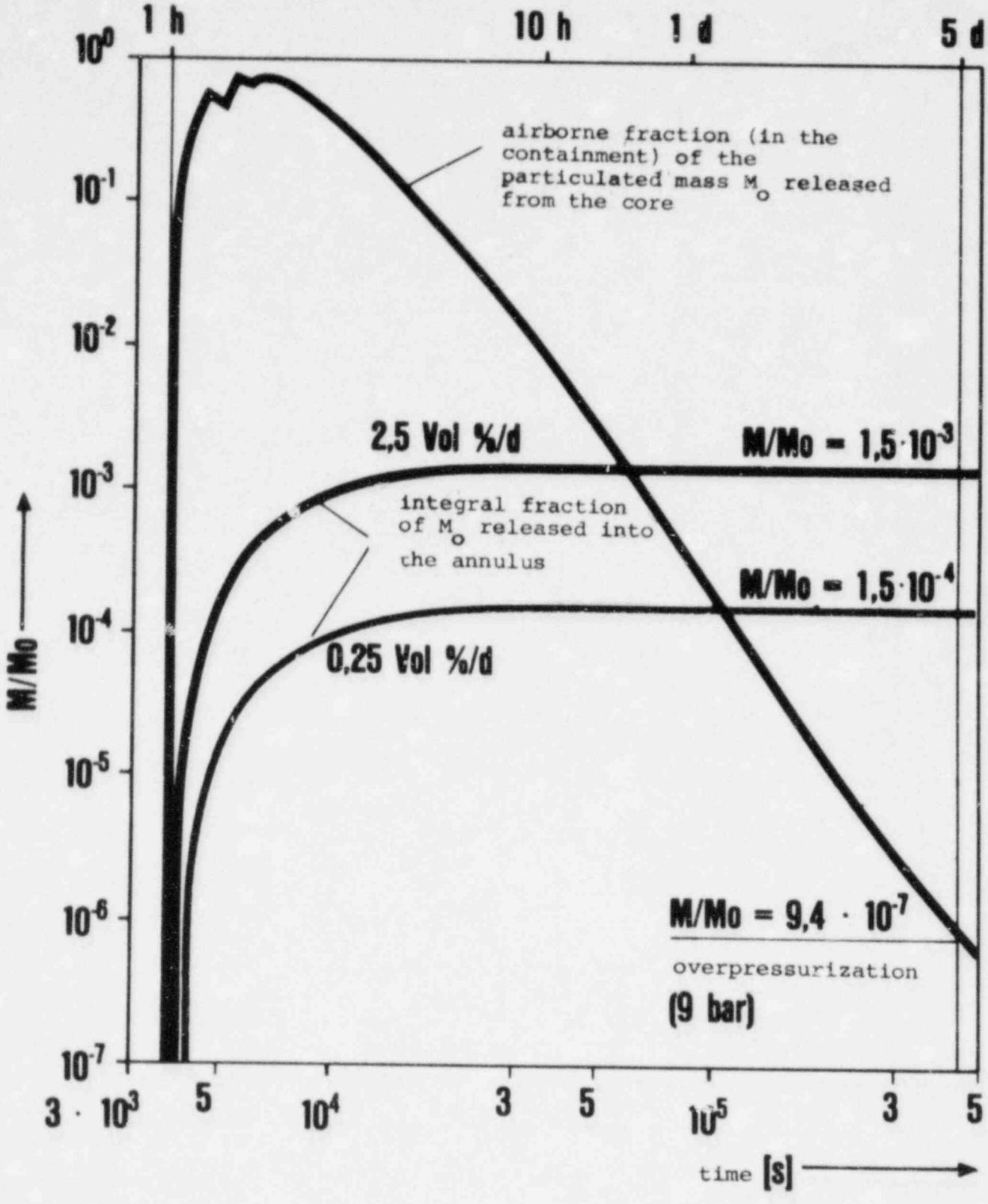

Fig. 2: FK 6 (low pressure path):Aerosol Particles in the Containment
M_o = 3.46 t (2,6 % radioactive)

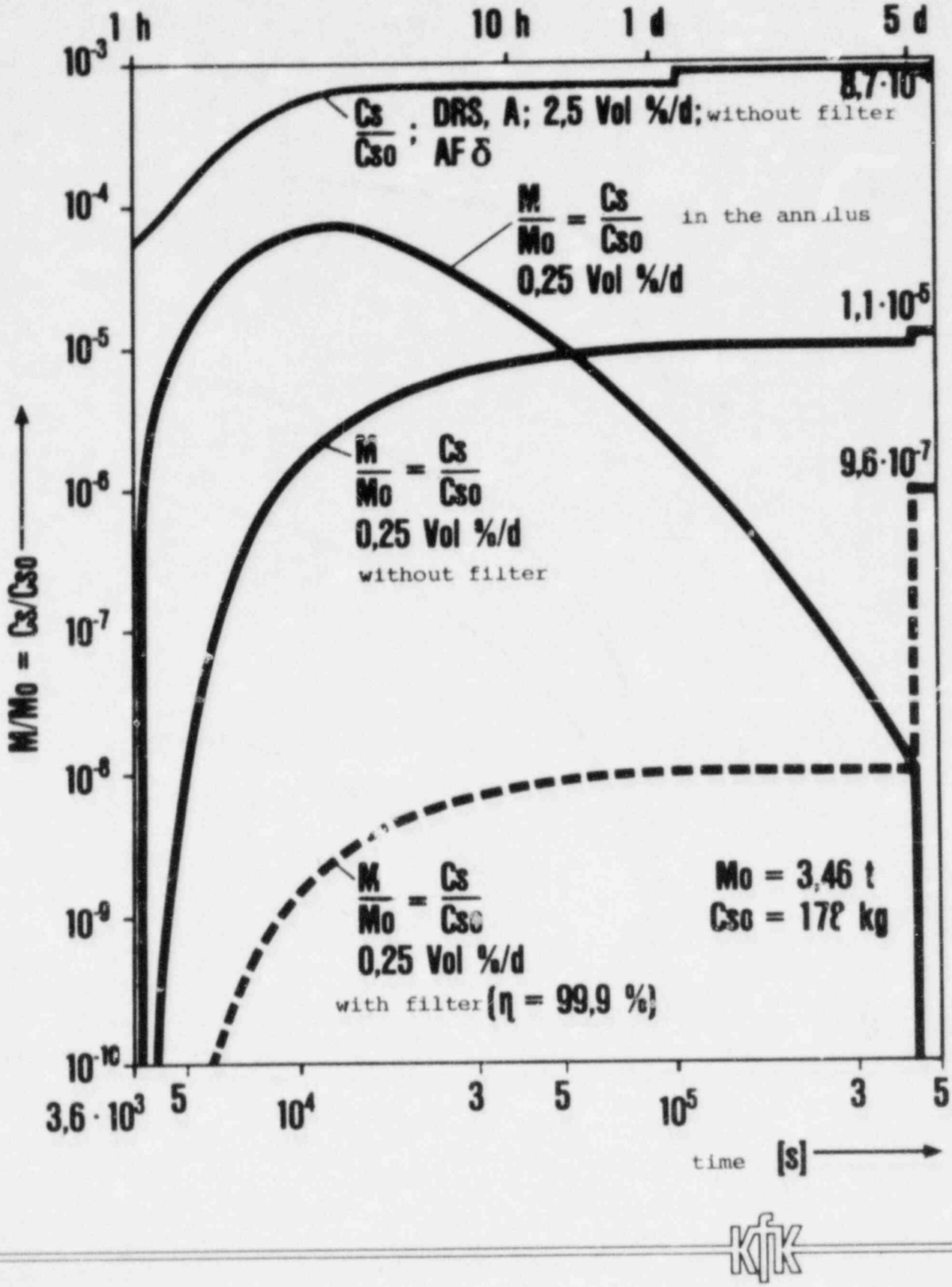

Fig. 3: FK 6 (low pressure path) Aerosol-(Cs)-Mass in the Annulus and Released Integral Fraction

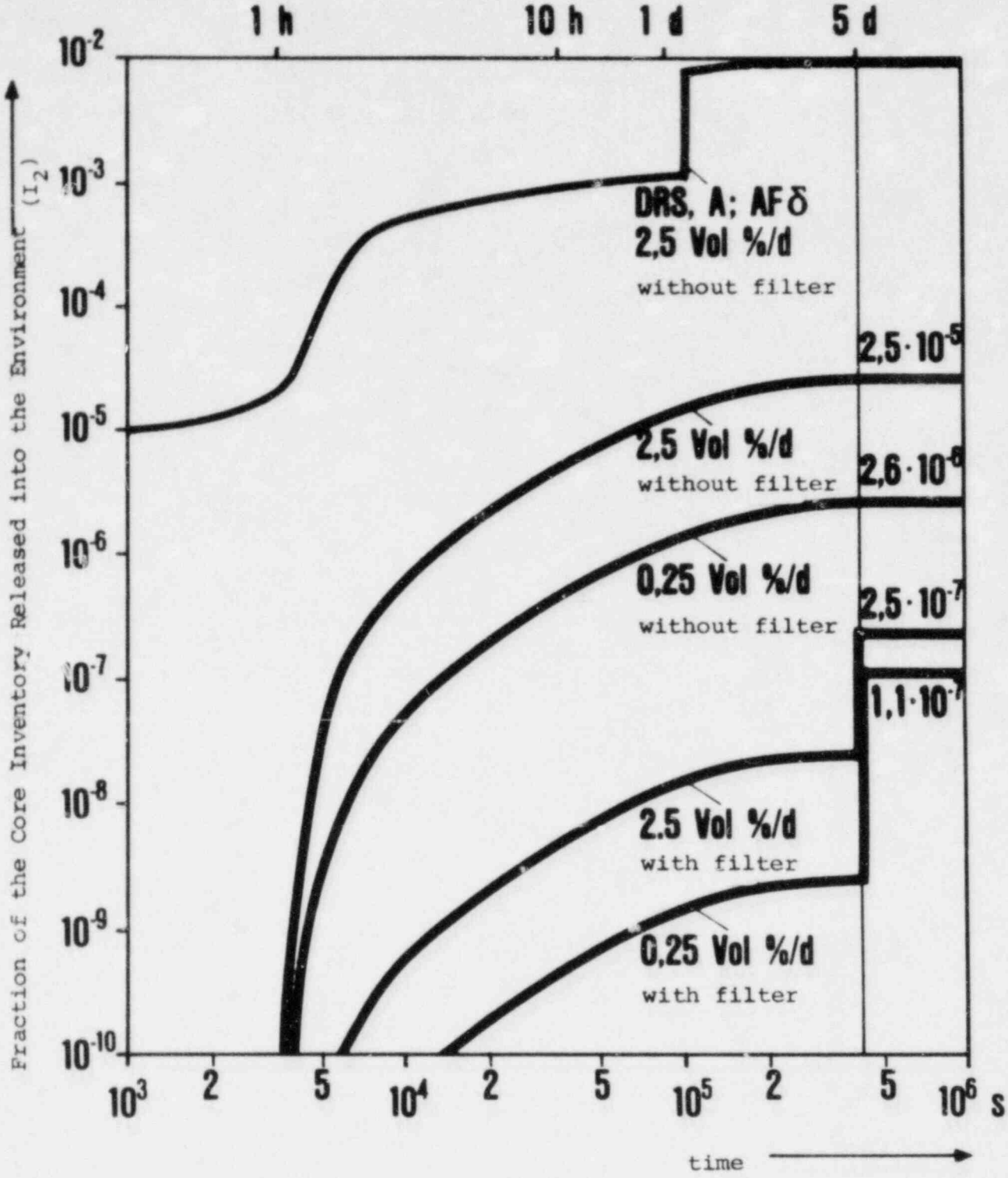

Fig. 4: FK 6 (low pressure path): I_2-Release Comparison DRS,A - PNS-Model

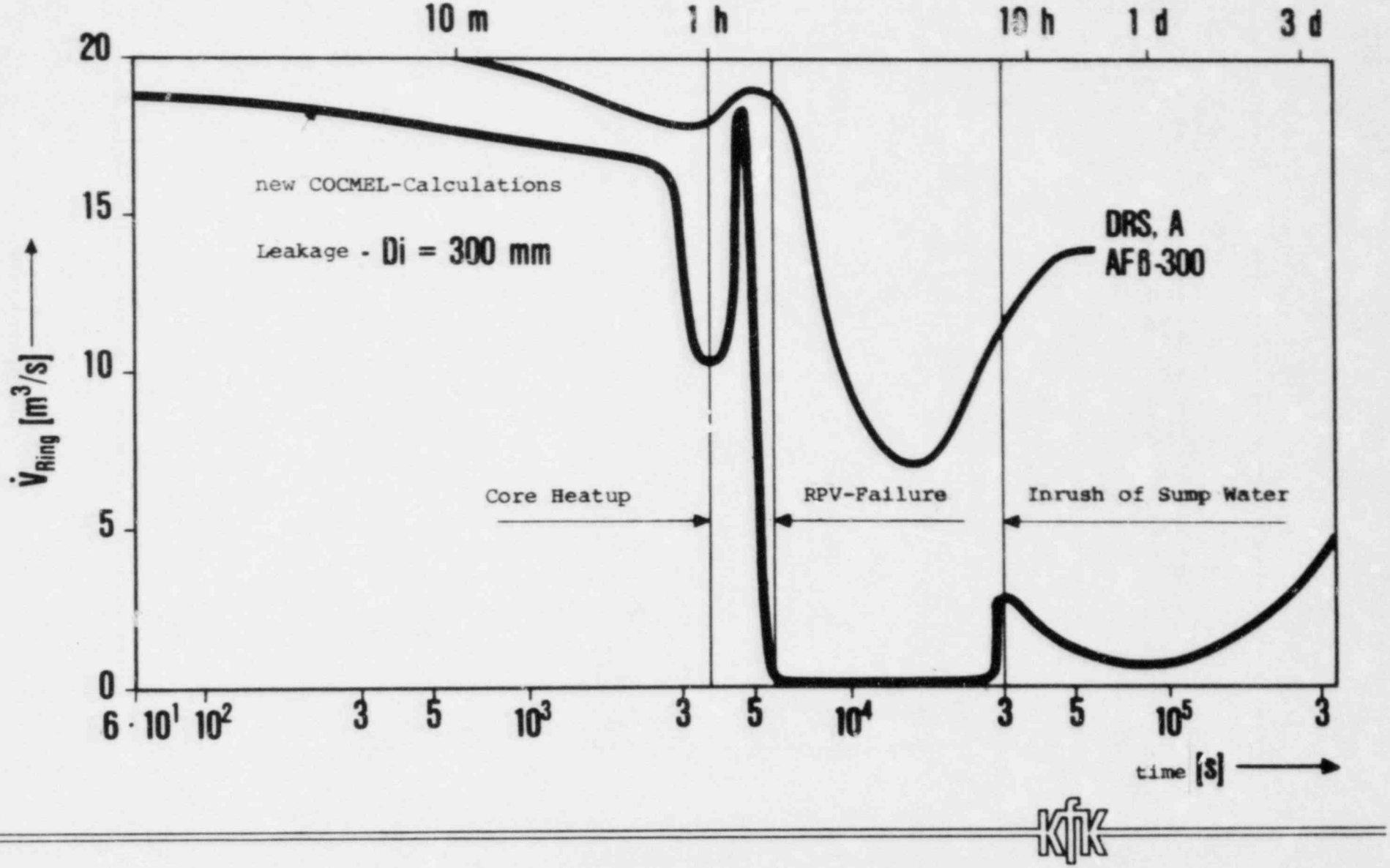

Fig. 5: FK 2 (low pressure path): Leakage Flows into the Annulus

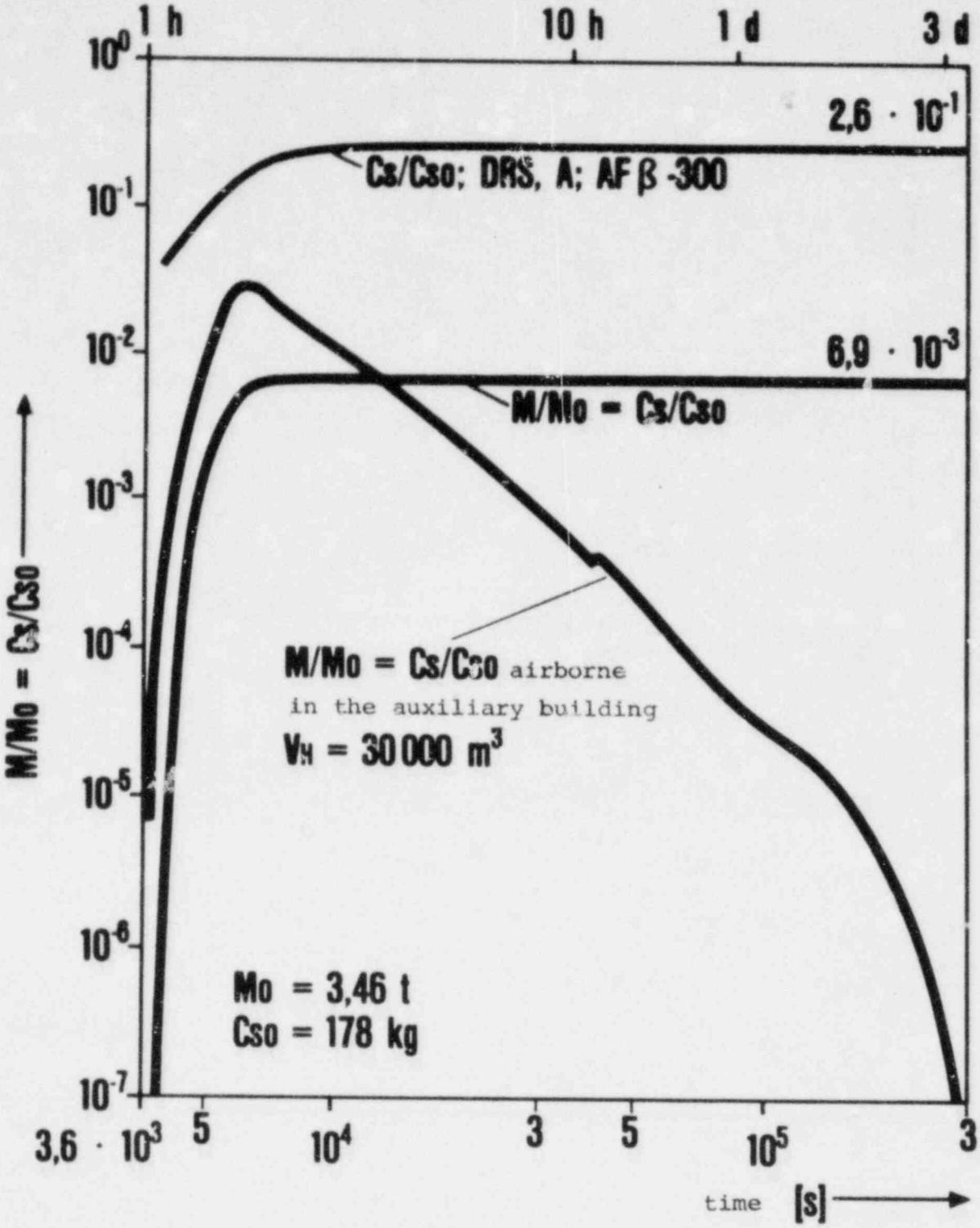

Fig. 6: FK 2 (low pressure path) Aerosol-(Cs)-Mass in the Reactor Auxiliary Building and Cumulated Leakage Mass

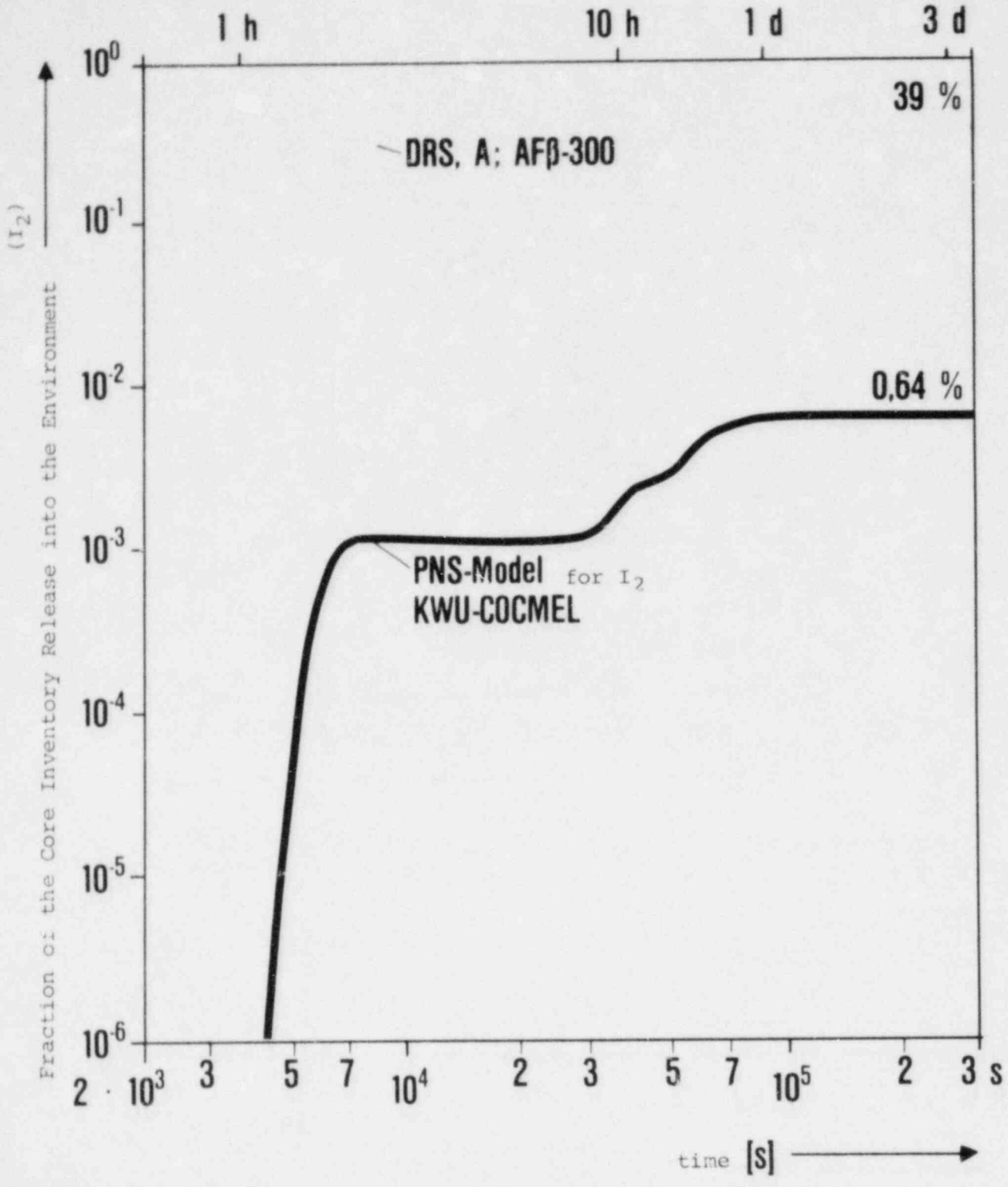

Fig. 7: FK 2 (low pressure path)
I_2-Release into the Environment

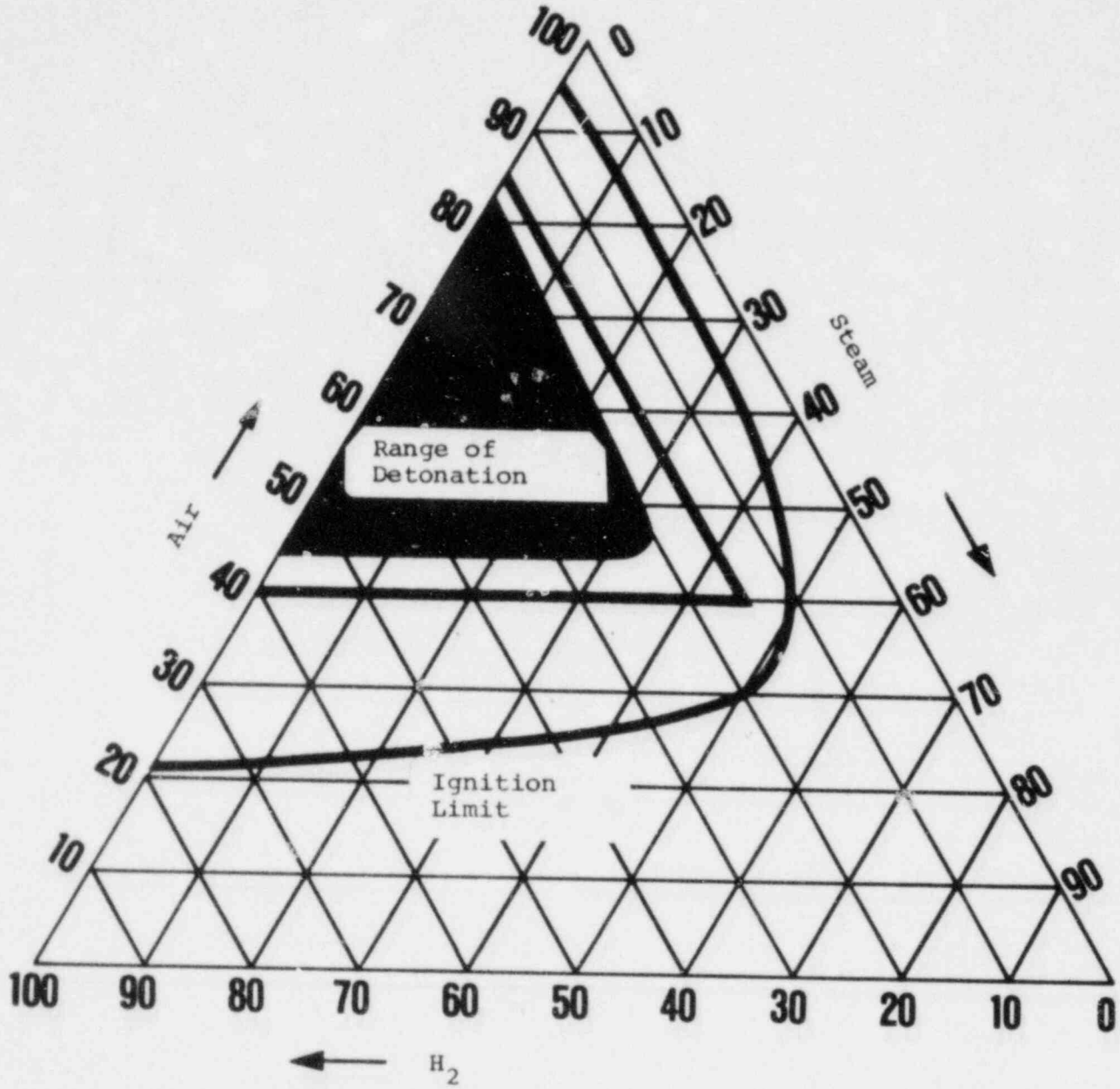

Fig. 8: Ternary Diagram of Air/Steam/H_2 (Vol.-%)

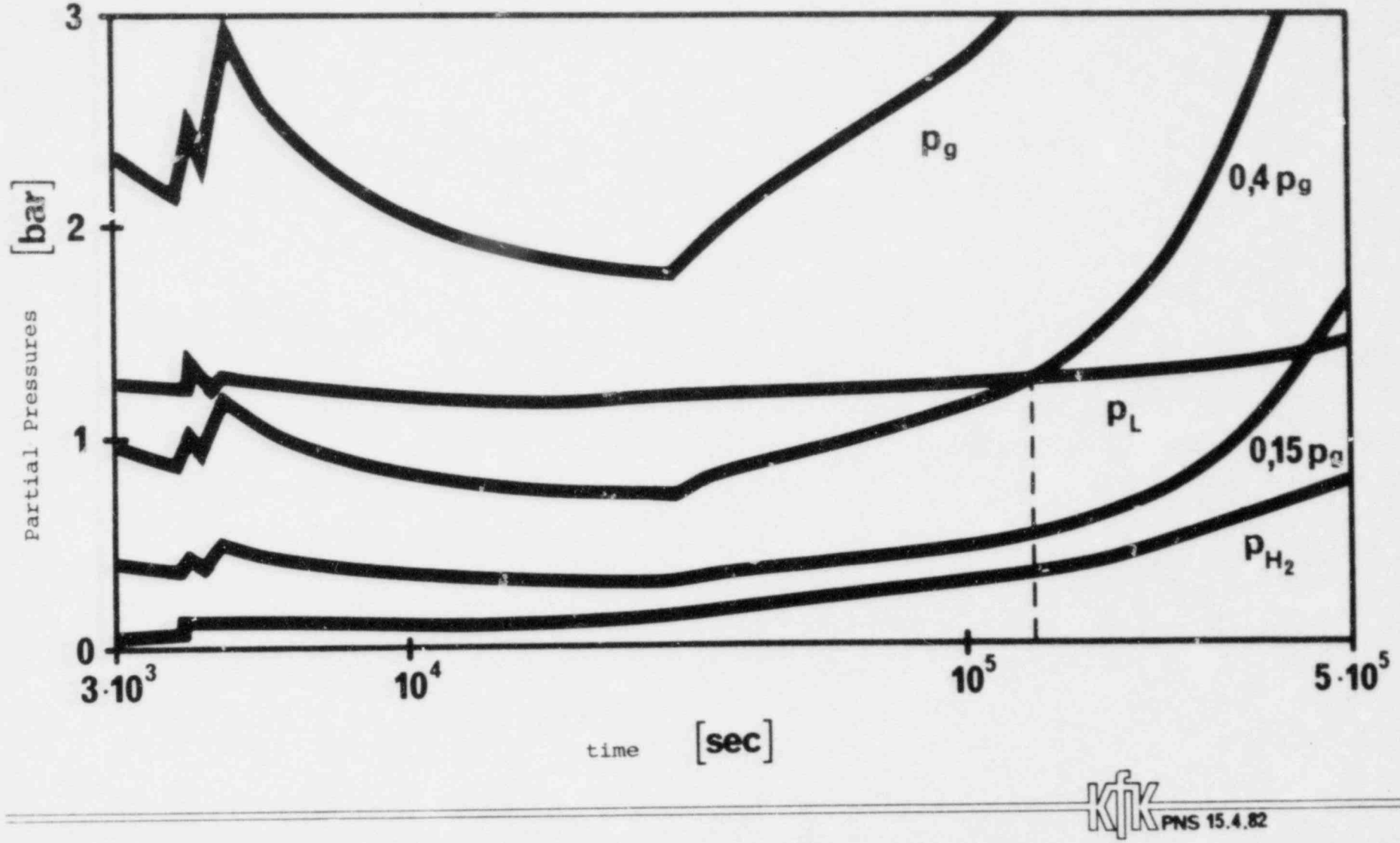

Fig. 9: FK 6 (low pressure path) Partial Pressures in the Containment

RECENT IMPROVEMENTS TO THE TRAP-MELT RCS FISSION PRODUCT TRANSPORT CODE

J. A. Gieseke, M. R. Kuhlman, R. Freeman-Kelly,
R. J. Avers and R. S. Denning

BATTELLE
Columbus Laboratories

The TRAP-MELT code is intended to provide a method for predicting the transport and deposition of radionuclides within reactor structures along flow paths between the fuel and the containment barrier. The code is currently applicable under accident conditions estimated for core meltdown accidents although in a previous version of the code, terminated LOCA conditions were considered. The radionuclide materials are modeled as transporting in both vapor and particulate forms and depositing from the gas flow as they are transported. Emphasis has been placed on transport and deposition within the reactor coolant system but the mechanistic models on which the code is based are equally adaptable to consideration of alternate flow paths. The extension to numerous species, the improvement of the deposition models based on experimental data, and the improvement of physical descriptions of radionuclide species interactions comprise the major portion of current development efforts.

Background

The TRAP-MELT code has evolved from an earlier code called TRAP-LOCA which was directed toward analyzing radionuclide transport and deposition within reactor primary coolant circuits under conditions expected for a terminated loss-of-coolant accident. In such cases, the flow is expected to be primarily two-phase, steam-water flow and temperatures near or below operating temperatures. Under these conditions, the radionuclide source term to the primary coolant flow was expected to be comprised solely of vapors or gaseous species.

As the low risk nature of such accidents became apparent, the emphasis shifted to analyses of severe core damage accidents. Under these conditions attenuation along flow paths could have a significant impact on the radiological consequences of the greater radionuclide release fractions expected from the fuel. The major meltdown conditions which required changes in the modeling were the higher temperatures, the superheated stream plus hydrogen flow, and the presence of particles as a portion of the transporting radionuclides. The TRAP-MELT code, accommodating these factors, is represented by the currently available version and that described in the "TRAP-MELT Users' Manual".[1] The models contained in this version of the code, and the revisions made subsequently and currently in progress will be described.

TRAP-MELT Code Description

The TRAP-MELT code considers a system of control volumes connected by fluid flow. Within each control volume a radionuclide species may exist in particulate or vapor form and be located on a wall surface or in the gaseous phase. In combination, the form and location define four "states" for each species. Using basic mechanisms for vapor and particle behavior, the TRAP-MELT code computes transfer of species among the four states and, in addition, predicts changes in particle size and concentration resulting from growth by agglomeration of the particles.

Several assumptions and restrictions have been imposed on the physical models to make the analysis more tractable. The vapor in each control volume is assumed to be well mixed and the flow pathway is expected to be dry. No chemical reactions or radioactive decay are treated, and the transfer rate of species between any two states is in all cases taken as being first order. The first order species transfer problem is solved separately with second order effects (particle agglomeration) and condensation being adjusted in a parallel fashion. Input in the form of species identification (with physical properties) and input rate, and time-dependent thermal hydraulic conditions are required.

The underlying transport equations of the TRAP code are:

$$\frac{dM^k_{im}}{dt} = S^k_{im} + \sum_{n\neq m} {}^{m}\beta^k_{in}\, M^k_{in} - \sum_{n\neq m} {}^{n}\beta^k_{im}\, M^k_{im} - \sum_{j\neq i} {}^{i}F_{jm}\, M^k_{jm} - \sum_{j\neq i} {}^{j}F_{im}\, M^k_{im}$$

Here M^k_{im} = Mass of radionuclide species k in volume i and state m

S^k_{im} = Source rate of species k in volume i and state m

${}^{n}\beta^k_{im}$ = Transfer coefficient for transport of species k in volume i from state m to state n

j_{F_m} = Transfer coefficient for transport of fission product in state m from volume i to vol me j.

The available TRAP-MELT code uses physical properties for three species with low, high and intermediate volatilities. Specifically, the properties of UO_2, I_2 and CsOH are incorporated into the code.

Vapor processes include adsorption onto walls and particle surfaces and condensation onto or evaporation from these surfaces. Adsorption rates are derived, where available, from measured deposition velocities, and condensation and evaporation rates are based on species vapor pressures.

Aerosol processes include inertial deposition of large particles and diffusional deposition of small particles from turbulent flows, diffusional deposition of small particles from laminar flow, and thermophoretic deposition for all particle sizes. Particle growth is also included for Brownian and turbulent agglomeration.

Subsequent to the preparation of the TRAP-MELT code described in the users' manual[1] and summarized above, revisions to the code have been made and are under way to provide an improved description of the important physical processes and to make the code more generally applicable to current expectations of conditions for severe core damage accident sequences.

TRAP-MELT Code Revisions

The code revisions have been based on new experimental results which give better physical descriptions of the vapor and aerosol processes as well as expanding the code to permit consideration of additional radionuclide species and additional processes previously not included. The additional species which are considered in the code now are CsI and Te, both of which are treated as vapors which are subject to condensation on particles and control volume surfaces in the reactor coolant system. The inclusion of these species has been made possible by recently obtained vapor pressure and vapor deposition velocity data, although preliminary data indicate that the chemical reaction of Te vapor with surfaces may be so rapid as to render condensation of this species unimportant and the deposition process to be limited by mass transfer in the vapor.

The treatment of turbulent deposition of aerosol particles in the code has been improved by implementing the empirical correlation developed by Gieseke, et al[2] and extending the treatment to more turbulent flows. More significant, however, is the inclusion of gravitational agglomeration and settling in the TRAP-MELT code. These processes were shown to be potentially very important mechanisms for retention of aerosol mass in the reactor coolant system under conditions of high aerosol concentration and long residence times.[3] Such conditions are characteristic of the so-called high pressure accident sequences such as TMLB'.

One further modification of the TRAP-MELT code, which is currently in progress, is its extension to include the containment as one of the control volumes in the simulation. When this module is incorporated with the rest of the code, it will be possible to examine the reduction of source terms brought about by the actions of filters, sprays, and natural retention mechanisms operative in the containment, including particle growth via water condensation.

TRAP-MELT Input

As discussed previously, the TRAP-MELT code requires input in the form of time-dependent thermal hydraulic conditions for all control volumes. Also, the rate of input of material into any control volume is required for all species. Because the overall results for radionuclide deposition and release to the environment are sensitively dependent on this input information, efforts parallel to the TRAP-MELT improvement activities have been carried out. Because of the importance of this information to the TRAP-MELT calculations and because the input data themselves are of interest, some examples of specific input will be described.

More detailed thermal hydraulic information than was previously available can now be obtained from a newly developed code called MERGE. This code is intended to provide better spatial resolution of temperatures and flows within the primary system, but depends on MARCH code predictions for gas composition, temperatures, and flow rates for initial conditions and continued input data for the primary system volumes being considered. As a portion of the efforts for the "NUREG-0772 Follow-on" work, thermal hydraulic conditions are being predicted for various accident sequences as a portion of the TRAP-MELT input. Results of MERGE predictions for gas and wall temperatures in a large PWR for the AB (Hot Leg) sequence are shown in Figures 1 and 2, respectively.

Similarly, source term information in the form of mass of specific radionuclide species per unit time has been predicted as TRAP-MELT input. The source term needed is as released from the fuel and is obtained with a computer code called CORSOR. This model uses the release rate coefficients presented in the "Technical Bases Report"[3] coupled with a 120-node description of core temperature as a function of time as computed with the MARCH code to derive the mass release rate for the species of interest. Results of such calculations for cesium and for all materials expected to form aerosols are shown in Figure 3 for the AB (Hot Leg). Combining these results with MARCH calculated flow rates gives the averaged concentrations in the flow leaving the core region at specified times for each species. Results for the aerosol concentration with time are given in Figure 4.

The procedures for predicting thermal hydraulic and radionuclide sources are now available to provide the necessary TRAP-MELT code input. With this ability to provide necessary input data, completion of the TRAP-MELT code revisions will then allow analyses of radionuclide release to the environment on a consistent basis for specific accident sequences.

References

(1) Jordan, H., Gieseke, J. A., and Baybutt, P., "TRAP-MELT Users' Manual", NUREG/CR-0632 (BMI 2017), February, 1979.

(2) Gieseke, J. A., Lee, K. W., and Goldenberg, M. A., "Measurement of Aerosol Deposition Rates in Turbulent Flows", NUREG/CR-1264 (BMI 2041), January, 1980.

(3) "Technical Bases for Estimating Fission Product Behavior During LWR Accidents", prepared by Battelle's Columbus Laboratories, Oak Ridge National Laboratory, Sandia National Laboratories, Office of Nuclear Regulatory Research, Office of Nuclear Reactor Regulation, NUREG-0772, June, 1981.

OBJECTIVE

TO DEVELOP METHODS FOR ANALYZING AND PREDICTING RADIONUCLIDE RELEASE AND TRANSPORT THROUGH THE PRIMARY SYSTEM AND ALONG ALTERNATE FLOW PATHS UNDER LWR ACCIDENT CONDITIONS

Battelle
Columbus Laboratories

TRAP-MELT CODE HISTORY

- ORIGINALLY TRAP-LOCA FOR RADIONUCLIDE DEPOSITION IN REACTOR COOLANT SYSTEMS UNDER TERMINATED LOCA CONDITIONS
  - -- NO PARTICLES
  - -- LOW TEMPERATURES
  - -- TWO-PHASE STEAM/WATER FLOW
- EXTENDED TO CORE MELT CONDITIONS, TRAP-MELT
  - -- PARTICLES PRESENT
  - -- HIGH TEMPERATURES
  - -- SUPERHEATED STEAM AND HYDROGEN FLOW
- REVISIONS FOR HIGH PARTICLE CONCENTRATION SOURCES AND ALTERNATE FLOW PATHS

Battelle
Columbus Laboratories

FISSION PRODUCT TRANSPORT ANALYSIS

TASKS:

1	TRAP Code Development
2	Containment Modeling
3	Source Term Modeling
4	Sensitivity Analysis
5	TRAP Verification Methods
6	Data Requirements Identification
7	NUREG/0772 Follow-on

Battelle
Columbus Laboratories

TRAP-MELT CODE BASIS AND ASSUMPTIONS

- Arbitrary interconnected control volumes
- Thermal hydraulics provided as input
- Exchanges/transfer between states are first order
- Particle growth treated parallel to first order processes
- Vapor in control volumes is well mixed
- Pathway to containment is dry
- No chemical reactions or radioactive decay

Battelle
Columbus Laboratories

MECHANISMS INCLUDED IN TRAP-MELT

- BULK TRANSPORT OF MATERIALS WITH STEAM FLOW
- VAPOR PROCESSES
- PARTICLE PROCESSES
- ARBITRARY SOURCES

(FOR I_2, INTERMEDIATE VAPOR PRESSURE MATERIAL, PARTICLES)

Battelle
Columbus Laboratories

TRANSFER PROCESSES

VAPOR PROCESSES

- ADSORPTION
- CONDENSATION/EVAPORATION
  - -- BOTH ON WALL AND PARTICLE SURFACES

PARTICLE PROCESSES

- DEPOSITION MECHANISMS
  - -- TURBULENT
  - -- DIFFUSIVE
  - -- THERMOPHORETIC
- AGGLOMERATION
  - -- BROWNIAN
  - -- TURBULENT

Battelle
Columbus Laboratories

REVISIONS TO TRAP-MELT

COMPLETED:

- GRAVITATIONAL DEPOSITION
- GRAVITATIONAL AGGLOMERATION
- ADDITIONAL SPECIES (I_2, CsOH, CsI, Te, PARTICLES

UNDERWAY:

- REVISED AGGLOMERATION TREATMENT
- WATER CONDENSATION
- TURBULENT WALL DEPOSITION
- DIFFUSIOPHORESIS
- ENGINEERED SAFEGUARDS

Battelle
Columbus Laboratories

TRAP-MELT INPUT REQUIREMENTS

- CONTROL VOLUME SPECIFICATIONS
  - -- FLOW PATHWAYS
  - -- PHYSICAL DIMENSIONS
- THERMAL HYDRAULICS (FROM MARCH/MERGE)
  - -- STEAM MASS FLOW RATES
  - -- STEAM TEMPERATURE PROFILES
  - -- SURFACE TEMPERATURE PROFILES
  - -- PRESSURE PROFILES
- SOURCE INFORMATION (FROM CORSOR)
  - -- SPECIES
  - -- VOLUME AND TIME PROFILE
  - -- MATERIAL PROPERTIES RELEVANT TO TRANSPORT (E.G., VAPOR PRESSURE DATA, SORPTION DATA)

Battelle
Columbus Laboratories

TRAP-MELT OUTPUT

FOR ANY DESIRED TIME:

- FLUID DATA AND DEPOSITION VELOCITIES (EACH VOLUME)
- CUMULATIVE MASS (EACH SPECIES, STATE, AND VOLUME)
- PARTICLE NUMBER CONCENTRATION (EACH VOLUME)
- PARTICLE GEOMETRIC MEAN RADIUS AND LOGARITHMIC STANDARD DEVIATION (EACH VOLUME)

Battelle
Columbus Laboratories

THERMAL HYDRAULICS -- TRAP-MELT INPUT

- MARCH CODE PREDICTIONS
  - -- FUEL THERMAL BEHAVIOR
  - -- STEAM FLOW RATES
  - -- CONTAINMENT CONDITIONS
- MERGE CODE PREDICTIONS
  - -- GAS TEMPERATURES
  - -- SURFACE TEMPERATURES

Battelle
Columbus Laboratories

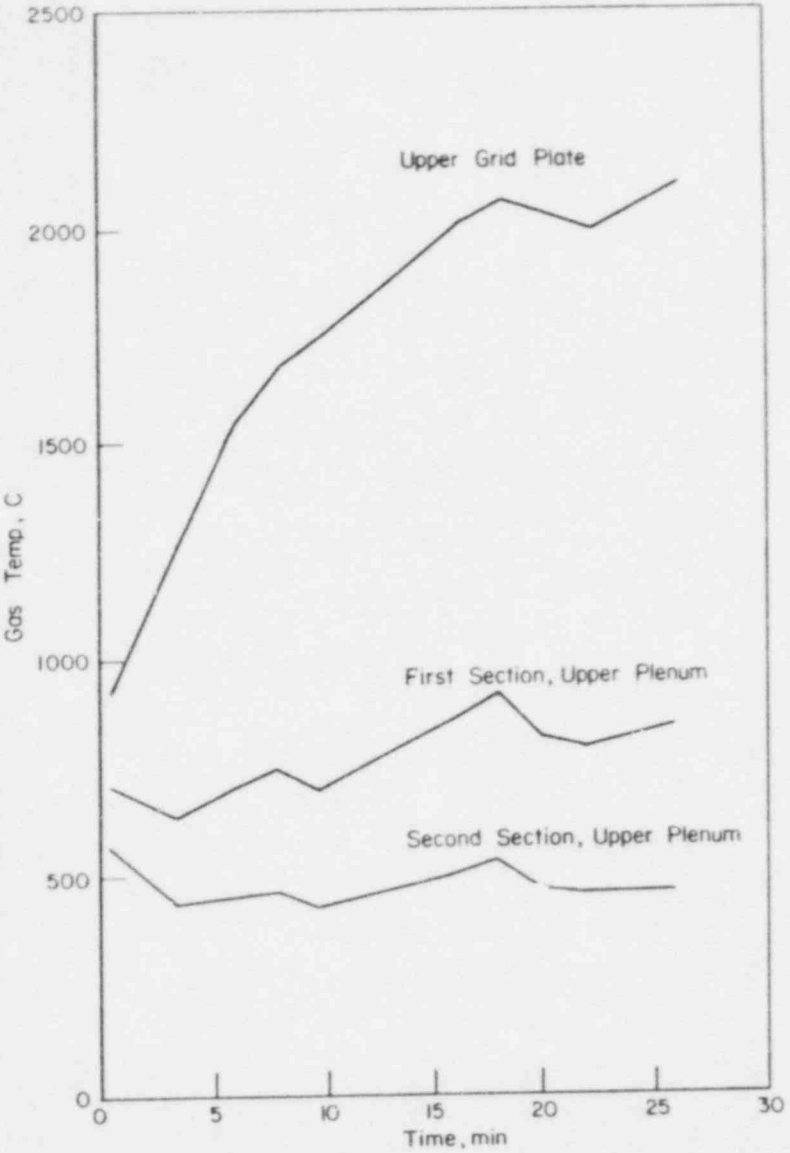

GAS TEMPERATURES FOR AB(HOT LEG)

Figure 1.

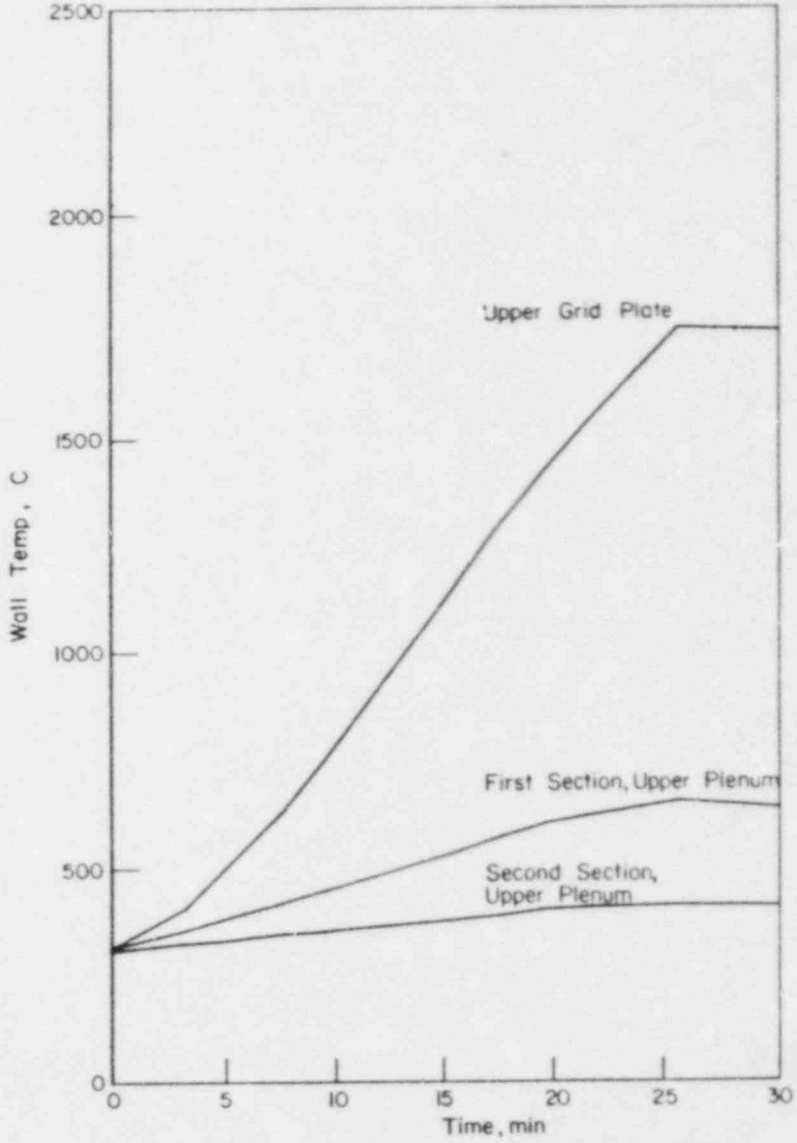

WALL TEMPERATURES FOR AB(HOT LEG)

Figure 2.

SOURCE TERM FROM FUEL -- TRAP-MELT INPUT

CORSOR CODE

- MARCH TEMPORAL FUEL TEMPERATURE PROFILES (120 NODES)
- ORNL RELEASE RATE COEFFICIENTS (NUREG 0772)
- OUTPUT IS TIME DEPENDENT AVERAGE MASS RELEASE RATE BY SPECIES

Battelle
Columbus Laboratories

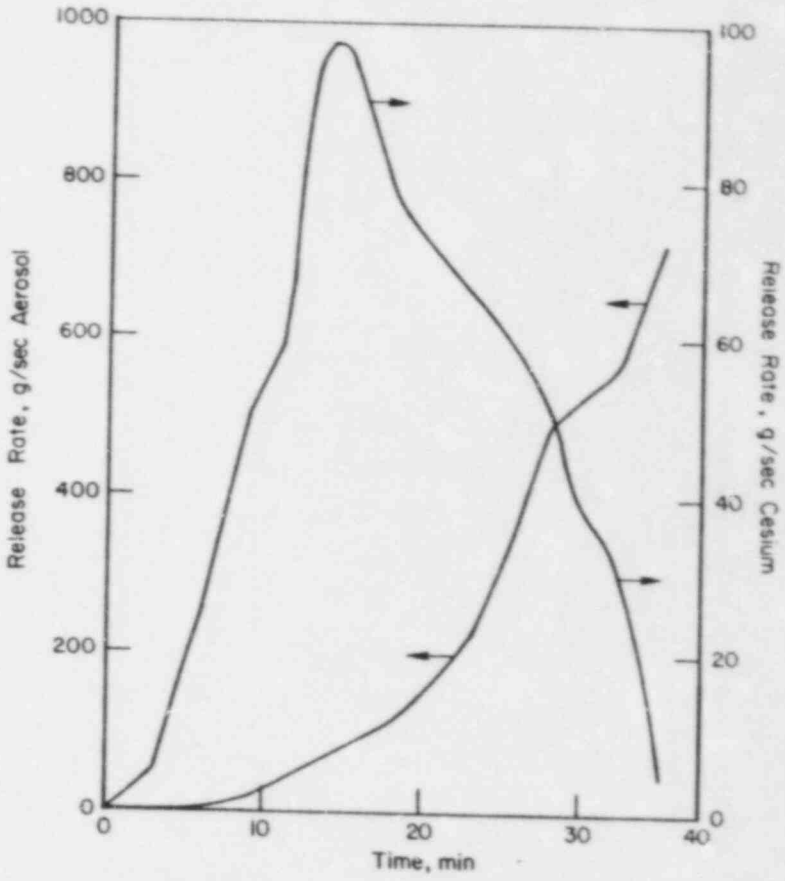

CORE RELEASE RATES OF AEROSOL AND CS FOR AB(HOT LEG)
Figure 3.

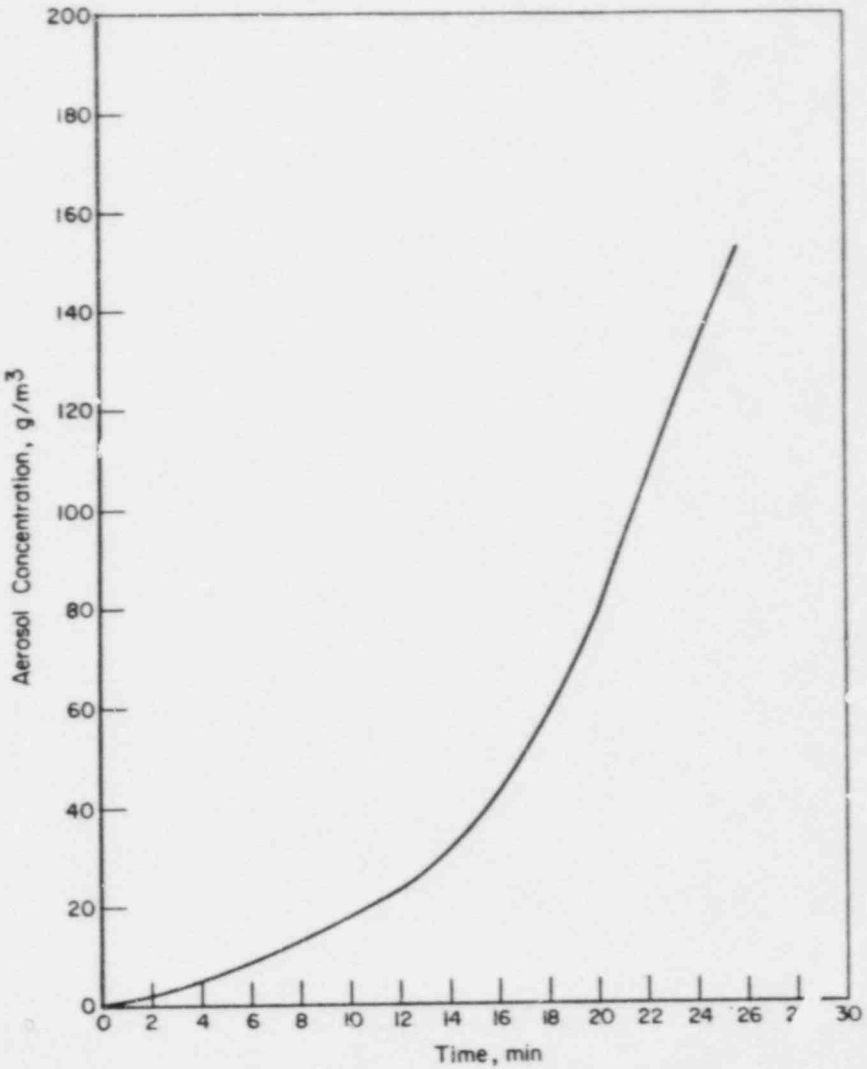

AEROSOL CONCENTRATIONS IN GAS LEAVING CORE FOR AB(HOT LEG)
Figure 4.

INITIAL SCDAP PREDICTIONS OF THE TMI-2 EVENT[a]

C. M. Allison and T. M. Howe
EG&G Idaho, Inc.

G. P. Marino
U.S. Nuclear Regulatory Commission

The Severe Core Damage Analysis Package (SCDAP) computer code is being developed at the Idaho National Engineering Laboratory under the sponsorship of the Office of Research of the United States Nuclear Regulatory Commission.[1,2,3] SCDAP models the progression of core damage including (a) core heatup, (b) core disruption and debris formation, (c) debris heatup, and (d) debris melting. SCDAP will be used to help identify and understand the phenomena that control core behavior during a severe accident, to help quantify uncertainties in risk assessment analysis, and to support planning and evaluation of severe fuel damage experiments and data.

The first version of the code, SCDAP/MOD0, is in the initial phases of assessment to determine the limitations and strengths of the code and its models when compared with the limited severe core damage data base. One of the early assessment cases was a calculation of fuel rod behavior during the TMI-2 accident. The results of these early calculations that are presented in this paper provide insights into fuel behavior during severe accidents.

The fuel rod behavior calculations were performed using the component analysis module of SCDAP, which is designated SCDCOMP. This module calculates fuel rod, control rod, and structural component behavior using thermal-hydraulic conditions provided either by the other modules in SCDAP or as input by the user. Checkout of the linkage between SCDCOMP and the

---

a. This work is supported by the U.S. Nuclear Regulatory Commission, Office of Nuclear Regulatory Research, Under DOE Contract No. DE-AC07-76ID01570.

SCDAP thermal-hydraulic models is in process. Use of the SCDAP thermal-hydraulic models should provide a better estimate of fuel rod behavior and could significantly alter the SCDCOMP results as presented in this paper. Slide 1 shows that SCDCOMP includes models that treat cladding oxidation, including steam starvation and hydrogen retardation effects, cladding liquefaction and redistribution of the molten cladding and dissolved fuel, and fuel rod fragmentation.

For these calculations, five fuel rods were analyzed and are representative of the range of assembly power levels 0.76 to 1.46, as shown in Slide 2. The analysis did not consider radiation heat transfer to the core boundaries, control and structural material behavior, or debris bed behavior. The thermal-hydraulic boundary conditions of coolant liquid levels, heat transfer coefficients, and coolant pressure were taken from two previous calculations.[4,5,6] These core uncovery scenarios roughly bound the expected core uncovery for TMI-2. The first, as shown in Slide 3, predicts the beginning of core uncovery at 113 minutes after reactor shutdown, reaching a maximum of 75% uncovery at 174 minutes. This scenario is designated "Late Uncovery." The second scenario, designated "Early Uncovery," predicts the beginning of core uncovery at 103 minutes, reaching a maximum of 75% uncovery at 135 minutes.

Differences in the assumed core uncovery scenario have a significant influence on the calculated results. Slide 3 shows that the maximum cladding temperatures for the highest powered bundle were 2180 K, and 3030 K for the late and early uncovery scenarios, respectively. As a consequence of the differences in temperature, the overall core behavior was calculated to be significantly different for the two scenarios.

For the early core uncovery scenario the following results were obtained:

1. The maximum cladding temperatures ranged from 2360 to 3030 K for the low powered bundles on the core periphery to highest power bundle in the center of the core. Slide 4 shows the approximate isotherms in the core at the time of peak cladding temperature.

2. As a consequence of the high temperatures, the unoxidized zircaloy in the upper 10% of the core was liquefied for the bundles with a radial power factor of 1.05 or greater. This molten zircaloy dissolved 0.3% of the fuel in the core and the mixture relocated to a point above the coolant as shown in Slide 4. The relocation took place at a temperature between 2200 and 2300 K. Later in the scenario, cladding in the highest powered bundle, which had completely oxidized in place at temperatures below 2170 K, relocated. These regions of liquefaction and freezing are shown in Slide 4 as the shaded areas. The percentages of cladding and fuel that liquefied and then relocated were 8 and 0.3% of the total core cladding and fuel, respectively.

3. Cladding was completely oxidized over the upper 40 to 50% of the core and, as a consequence, was calculated to fragment during the quench of the core at 210 minutes. The fragmented area is delimited by a dashed line in Slide 4. Consumption of the zircaloy due to oxidation took place in the following sequence. For the low powered bundle, the cladding was completely oxidized over the upper 40% before temperatures reached 2170 K. Thus, liquefaction of zircaloy was not calculated. For the other bundles, cladding in the upper part of the core and below the 90% elevation became fully oxidized at temperatures slightly less than 2170 K. The upper 10% of the cladding reached 2170 K prior to complete oxidation, and the zircaloy liquefied and relocated leaving a ZrO_2 shell. This critical sequence of oxidation and liquefaction is discussed in greater detail later in this paper.

4. No melting of UO_2 was predicted. However, calculated fuel temperatures were near the melting temperature of UO_2.

For the late core uncovery scenario, the following results were obtained:

1. Maximum cladding temperatures ranged from 1970 to 2180 K for the five representative bundles. Slide 5 shows the approximate isotherms in the core at the time of peak cladding temperature.

2. Cladding was completely oxidized over the upper 20 to 30% of the core height. This region was embrittled before the maximum temperature of 2180 K was reached. No liquefaction and relocation were calculated.

The balance between cladding oxidation and liquefaction is a critical factor in determining the extent and timing of relocation of liquefied cladding, ZrO_2, and dissolved UO_2. The phas diagram for zircaloy and oxygen shows this balance graphically. The phase diagram showing the liquidus and solidus temperatures for zircaloy at different oxygen atom fractions is shown along with the oxygen atom fraction-temperature curves for the high and low powered bundles for the two core uncovery scenarios in Slide 5. These curves were generated for the elevation of maximum cladding temperatures by taking the difference between the total oxygen absorbed in the cladding and the oxygen uptake in the growth of the ZrO_2 layer. This difference represents the average oxygen concentration in the unoxidized α-and β-layers of the zircaloy.

Slide 5 shows the maximum cladding temperatures never exceed the solidus temperature for the late core uncovery. As a result, liquefaction is not calculated to occur. However, the oxygen content can actually vary across the zircaloy so that thin layers of liquefied zircaloy can be formed, although the bulk of the zircaloy remains solid. For the early uncovery scenario, both cladding temperature histories exceed the solidus temperature. Thus, cladding liquefaction is calculated to occur. However, liquefied zircaloy for the low powered bundle did not break through the oxide shell and was rapidly oxidized to ZrO_2. The liquefied zircaloy for the high powered bundle does penetrate the shell and relocates.

The important results of the SCDCOMP calculations using the two different sets of coolant boundary conditions can be summarized as follows:

1. Variations in core uncovery scenarios (boundary conditions) can significantly influence calculated fuel rod behavior and result in a variation of behavior accompanying maximum temperatures from above the melting point of ZrO_2 to those below the melting point

of zircaloy. Use of the SCDAP thermal-hydraulic models should provide a better estimate of fuel rod behavior and could significantly alter these results.

2. If temperatures above the melting point of zircaloy are reached, the balance between oxygen uptake and temperature significantly influences the subsequent formation and movement of liquefied fuel rod material.

REFERENCES

1. C. M. Allison et al., Severe Core Damage Analysis Package (SCDAP) Code Conceptual Design Report, EGG-CDAP-5397, April 1981.

2. C. M. Allison and T. M. Howe, "Conceptual Design of the Severe Core Damage Analysis Package," Transactions of the American Nuclear Society, 39, 1981, pp. 369-370.

3. G. P. Marino, C. M. Allison, and D. Majumdar, "SCDAP: A Light Water Reactor Computer Code for Severe Core Damage Analysis," Transactions of the American Nuclear Society, September 1982.

4. K. H. Ardron, D. G. Cain, TMI-2 Accident Core Heat-up Analysis, NSAC-24, January 1981.

5. D. Coleman, "Fuel Rod Conditions in TMI-2 during Uncovery Using FRAP-T5," Part 1 in TMI-2 Accident Core Heat-up Analysis, A Supplement, NSAC-25, June 1981.

6. Electric Power Research Institute, Analysis of the Three Mile Island Unit 2 Accident, NSAC-1, July 1979.

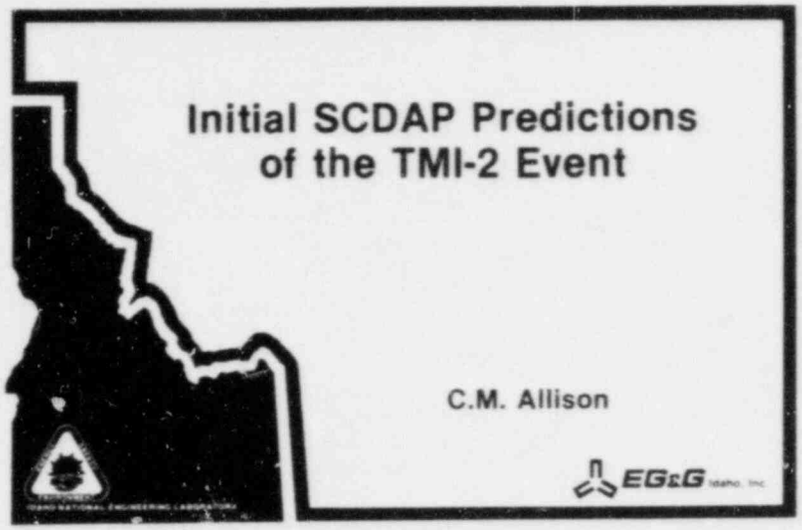

Outline

- Basis for calculations
- Core uncovery sequence
- Results
- Summary

S2 3470

Basis for Calculations

- Important effects modeled include
  - Steam/hydrogen limited oxidation
  - Fuel/cladding liquefaction and redistribution
  - Fuel/cladding fragmentation
- Limitations of these calculations
  - Control rods and other structure not considered
  - Liquid levels, heat transfer coefficients, etc.

S2 3471

Core Map of Model Region Assembly Assignment

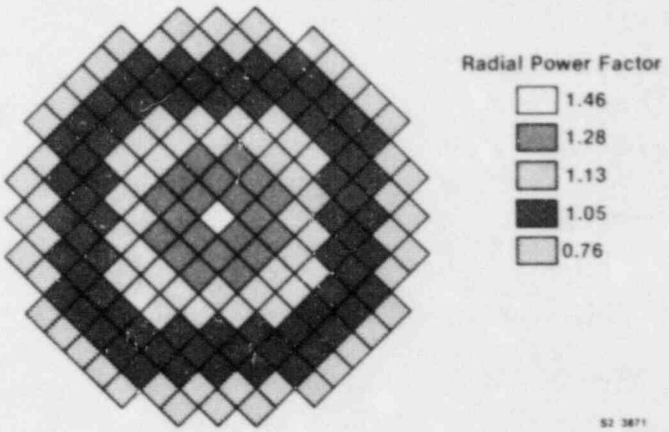

S2 3471

Core Uncovery Sequence

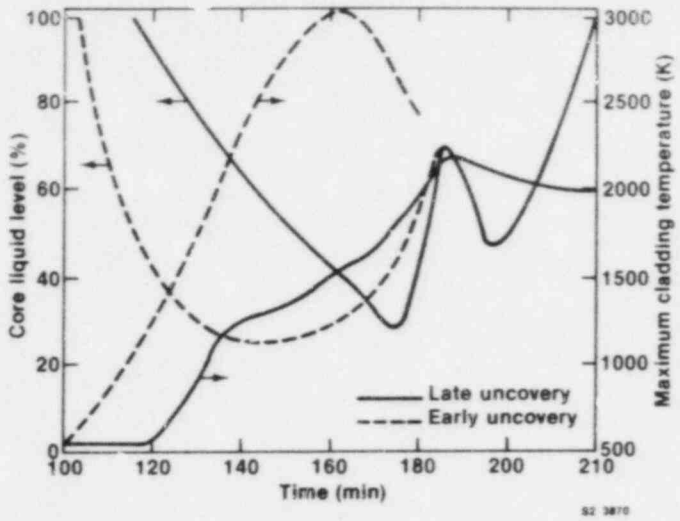

Core State for Late Uncovery Scenario

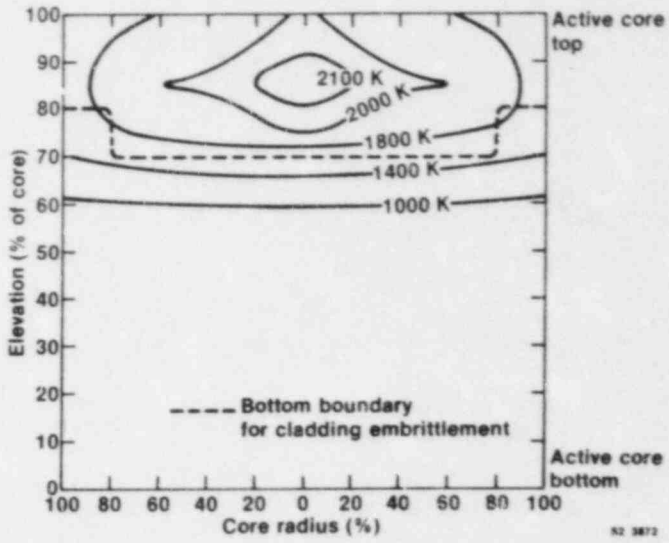

Core State for Early Uncovery Scenario

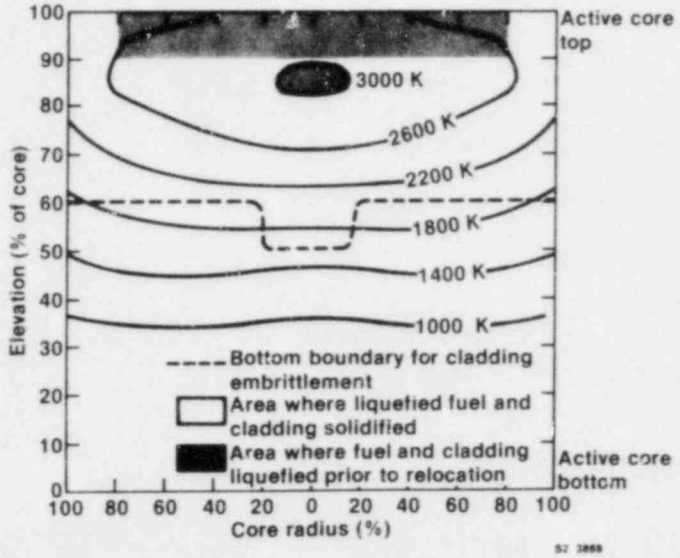

Temperature-Oxygen Uptake Behavior

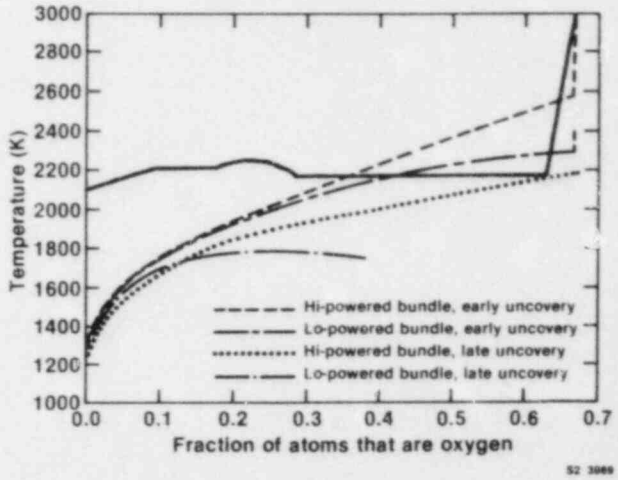

Summary

- Variations in thermal-hydraulic boundary conditions significantly influence calculated fuel rod behavior
- The balance between oxygen uptake and temperature significantly influences the formation and movement of liquefied material

SZ 3867

FUEL ELEMENT GAP IRREGULARITIES DETERMINED FROM INFRARED SCANNING

D. L. Burman (Westinghouse)
D. D. Davis (Westinghouse)
W. J. Leech (Westinghouse)
R. W. McCulloch (ORNL)

BACKGROUND

It has been hypothesized [1,2,3] that the fuel pellet column in a nuclear fuel rod will not be concentric in the cladding. The pellets will assume random offsets, and frequent contact with the tube, resulting in a series of broken spirals. Evidence for the existence and stability of spiralling pellet columns has been observed from crud patterns on fuel rods irradiated for one and two cycles [2] in commercial reactors.

Such behavior has important implications on the pellet to cladding thermal conductivity under both normal and accident conditions and on the swelling and burst behavior of cladding under LOCA conditions.

An experimental program to verify and quantify the pellet offset behavior in an unirradiated commercial fuel rod was undertaken at ORNL under the sponsorship of the Central Electricity Generating Board and Westinghouse Electric Co. The results of the experimental program were used to develop a model to predict the burst strain behavior of the NRU test rods and were compared with the empirical correlation of the gap conductances inferred from instrumented Halden rods.

EXPERIMENTAL PROGRAM

The tests were performed on a Westinghouse 17x17 fuel rod made to the same specifications as commercial fuel except that the fuel pellets were made from depleted UO_2. The rod was mounted in the vertical position and electrical leads clamped in positions such that the central 4 ft. of the 12 ft. rod could be heated by direct resistance heating of the Zircaloy cladding. The area of the rod to be scanned was painted with a flat black paint to provide a uniform emissivity. The scanning was performed with the infra-red camera previously used to characterize electric heating rods for the MRBT, FLECHT-SEASET and other programs. Additional information on this equipment can be found in a report by Simpson, Snyder and Cook [4]. Vertical scans were performed at eight 45°

degree increments around the rod. For each vertical scan the rod was heated from approximately room temperature to about 130°C in three seconds and the scan performed at the peak temperature. At the completion of the eight 45 degree increment scans the rod was dismounted, laid flat on the floor, rolled six times over a two foot distance, remounted and re-scanned. After the second scanning the rod was again dismounted, rolled an additional six times with sudden stops, remounted and re-scanned.

As a final test the central portion of the fuel rod was cut out, the pellets removed and the empty cladding scanned to provide assurance that the observed temperature patterns were indeed caused by pellet effects and not by the cladding itself.

THEORY AND ANALYSIS

Because of the transient nature of the rod heat-up, the UO_2 pellets lag the cladding in temperature and thus act as heat sinks. The rate at which heat is locally transferred from the cladding to the pellet depends on the local width of the gap. Thus, where the gap is narrow, the rate heat transfer to the pellet will be high and a cool spot in the cladding will result.

Burman and Kuchirka [5] have shown that, for an eccentric pellet, the clad temperature at any azimuth θ can be described by

$$T_\theta = T\alpha + \frac{\Delta Tm}{2} [1-\text{Cos}(\theta-\alpha)] \qquad (1)$$

where: $T\alpha$ is the temperature at the minimum gap
ΔT_m is the maximum temperature difference around the clad
α is the azimuth of minimum gap

They have also shown that the maximum temperature difference across the cladding is linearly proportional to the fraction of pellet offset, all

other parameters constant, i.e.

$$\Delta T_m = A\frac{d}{g} \qquad (2)$$

where d is the distance from the center of the pellet to the center of the cladding, and
g is the average radial gap

For each set of scans the temperatures measured at each 45 degree orientation were evaluated at axial increments of about 1.4 cm. A least squares fitting routine was used to determine d and ΔT_m from the temperature data using equation (1).

The TAPSWEL program[6], a finite difference program for determining heat transfer and cladding strain for non-uniform heat transfer conditions, was used to determine the circumferential temperature distribution arising from the heatup transient conditions used in the test program for different assumed pellet offsets and average gaps. The least squares fits of the data for ΔT_m were then matched to the TAPSWEL results to determine the offset for each axial location.

RESULTS

Figure 1A shows the axial distribution of temperatures from the first of the three sets of measurements for each of the eight 45 degree scans. The range of the temperature variations is about 40°C along any one scan. Figure 1B shows a similar scan from the empty tube.

Tables 1-3 show the calculated results for the three sets of tests. The nominal diametral gap for the rod tested was 6.5 mils; however, to obtain a fit to the observed temperature distribution it was occasionally necessary to assume a larger local gap within the design tolerance levels. If a smaller than nominal gap existed at any level, then the results would be interpreted as a smaller than actual relative pellet offset. These uncertainties result in a slight underprediction of pellet offset.

Table 4 shows the mean and standard deviations for the relative pellet offset. Figure 2 is a cumulative frequency plot of the relative pellet

offset for the three sets of measurements. The solid line is the theoretical relationship based on random pellet location within the clad boundary. Good agreement is observed. The mean of the measured values ranged from .65 to .68 as compared to .71 from theoretical considerations. As indicated above, uncertainties in the local gap size will tend to result in a lower calculated offset.

Figures 3-5 show the degree of pellet offset at each elevation analyzed for each of the three sets of measurements. Figures 6-8 show the angle of the minimum gap. A general spiralling pattern can be observed which is consistent with our observations of inpile crud patterns.

IMPLICATION AND APPLICATIONS OF RESULTS

The observations of pellet offset have important implications in at least two areas; gap conductance under either normal or accident conditions, and burst strain and blockage under LOCA conditions.

Gap Conductance

It has long been observed that the gap conductance in nuclear fuel rods is greaterthan would be calculated using concentric gap models. Many have attributed the enhancement to pellet cracking and relocation. However,the occurrence of gap enhancement on initial rise to power and an inability to rationalize gap enhancement as a function of gap size casts a measure of doubt on relocation models. Furthermore there is a growing body of evidence, arising particularly from LOCA related work, which indicates that pellet relocation does not readily occur and cannot be counted on to justify gap conductance models.

At Westinghouse, Leech, et. al have correlated the temperature data from three Halden instrumented assemblies IFA-431, IFA-432, and IFA-513 using an underlying assumption of random pellet offset. Figure 9 shows the gap conductance enhancement factors used to correlate the data compared to calculated curves for the mean and median enhancement due to pellet

offsets. Figure 10 shows predicted vs measured centerline temperatures. Figures 11-13 show the bias between predicted and measured centerline temperature vs gap size, power and burnup respectively for the upper TC of 13 IFA rods.

LOCA Burst Strain And Blockage

Erbacher[3] has shown that the effective burst strain of a Zircaloy tubing under simulated LOCA conditions is related to the circumferential temperature distribution and that this distribution, for specimens internally heated by rigid heaters is due to the eccentricity of heaters and cladding. Burman and Kuchirka have shown similar temperature distributions for directly heated clad specimens with either alumina pellets or mandrels acting as heat sinks. Thermocouple data from the EOLO-JR tests show that, at least for previously unirradiated and uncracked nuclear rods tested in pile, circumferential temperature differences consistent with a spiralling offset pellet column existed and, in general, increased in magnitude during the test. The German FR-2 inpile LOCA tests showed no significant difference between unirradiated test rods and rods previously irradiated up to ~ 30,000 MWD/MTU. Furthermore thermocouples near the top of the fuel columns showed a sudden drop in temperature at the instance of burst. This demonstrates that the fuel column did not relocate until the rather violent motion which accompanies burst.

Burman, et. al. under programs funded in part by CEGB have developed a model for burst strain based on random pellet offsets and constant relative eccentricity throughout the straining period. This model was applied to the NRU MT3 and MT4 test results. Although the model slightly underpredicted burst strains for both MT3 and MT4, the relative strain difference from one test to the other and the distribution of the individual rod strains were well reproduced as shown in Figure 14. The reason for the underprediction in the values of the strains is believed to be due principally to the assumption of isotropic strain. If anisotropic strain, with the attendant lesser clad thinning in the high strain areas, were used the resulting burst strains would be greater and agreement with data much improved.

SUMMARY

The infra-red scanning of a Westinghouse 17x17 fuel rod has verified the pellet-cladding offset distributions predicted from random pellet locations. It has shown pellet column spirally consistent with observations of crud pattern after up to two reactor cycles of operation.

The tendency for pellets to be offset and the random statistics for such offsets provide an excellent basis for correlation of both fuel-cladding gap thermal conductance and LOCA burst strains.

References

1. Burman, D. L., "Role of Fuel-Clad Gap Heat Flux In Determining Clad Ballooning Strain in LOCA," ANS Topical Meeting, Sun Valley, Idaho, August 1981.

2. Burman, D. L. et. al., "Comparison of Westinghouse LOCA Burst Test Results with ORNL And Other Program Results," Specialists Meeting on the Behavior of Water Reactor Fuel Elements Under Accident Conditions. CSNI, Helsinki, Finland, September 1-4, 1980.

3. Erbacher, F. J., "LWR Fuel Cladding Deformation in a LOCA And Its Interaction With The Emergency Core Cooling," ANS Topical Meeting, Sun Valley, Idaho, August 1981.

4. Simpson, W. A, Jr., "Infared Inspection and Characterization of Fuel-Pin Simulators," ORNL/NUREG/TM-55, Novermber 1976.

5. Burman, D. L. and Kuchirka, P. J. "A Temperature Sensitivity Study Of Single Rod Burst Tests," WCAP-8289 Addendum 1, November, 1975.

6. Burman, D. L. et. al., "Tapswel-A Finite Difference Program for Evaluating Fuel Rod Temperature Distributions and Clad Strain for Non-Symmetrical Heat Transfer Conditions," WCAP-10057 Westinghouse Electric Corp., March 1982.

TABLE 1: ANALYSIS OF ORNL IR SCANNING RESULTS: PHASE I

Elevation (in)	ΔT_m (°F)	α (DEG)	Offset	Min Radial Gap (in)	Av. Diametral Gap
.04	13.4	100.7	.2685	.0024	6.5 MILS
.60	30.3	178.7	.5922	.0013	6.5 MILS
1.17	9.9	140.1	.2010	.0026	6.5 MILS
1.72	11.5	91.1	.2314	.0025	6.5 MILS
2.28	30.2	131.4	.5706	.0013	6.5 MILS
2.85	7.8	277.4	.1000	.0027	6.5 MILS
3.40	16.8	175.7	.3327	.0022	6.5 MILS
3.95	31.7	170.9	.6199	.0012	6.5 MILS
4.51	15.0	199.2	.2997	.0023	6.5 MILS
5.06	26.0	33.7	.5096	.0016	6.5 MILS
5.62	57.6	5.8	1.0000	0.0000	>6.5 MILS
6.18	35.9	11.5	.7162	.0009	6.5 MILS
6.71	49.3	73.0	.9563	.0001	6.5 MILS
7.27	62.3	120.0	1.0000	0.0000	>6.5 MILS
7.83	66.6	101.1	1.0000	0.0000	>6.5 MILS
8.40	63.5	76.8	1.0000	0.0000	>6.5 MILS
8.98	27.9	23.5	.5471	.0015	6.5 MILS
9.56	27.2	279.5	.5331	.0015	6.5 MILS
10.10	46.2	243.3	.8982	.0003	6.5 MILS
10.65	15.0	245.4	.2992	.0023	6.5 MILS
11.19	38.9	152.7	.7567	.0008	6.5 MILS
11.75	32.5	67.7	.6338	.0012	6.5 MILS
12.30	39.5	23.3	.7697	.0007	6.5 MILS
12.86	28.9	80.8	.5662	.0014	6.5 MILS
13.43	32.9	52.4	.6422	.0012	6.5 MILS
13.99	37.9	40.8	.7382	.0009	6.5 MILS
14.56	36.1	122.8	.7036	.0010	6.5 MILS
15.14	49.3	147.9	.9563	.0001	6.5 MILS
15.71	57.6	116.0	1.0000	0.0000	>6.5 MILS
16.29	39.5	127.7	.7698	.0007	6.5 MILS
16.87	38.3	127.7	.7453	.0008	6.5 MILS
17.45	35.8	145.1	.6972	.0010	6.5 MILS
17.99	14.1	174.2	.2612	.0023	6.5 MILS
18.57	13.4	116.9	.2580	.0024	6.5 MILS
19.11	35.5	49.5	.6931	.0010	6.5 MILS
19.70	48.6	58.5	.9433	.0002	6.5 MILS
20.24	20.9	200.7	.4117	.0019	6.5 MILS
20.83	64.9	202.1	1.0000	0.0000	>6.5 MILS
21.37	41.3	199.6	.8032	.0006	6.5 MILS
21.91	47.7	148.6	.9267	.0002	6.5 MILS
22.45	29.7	143.0	.5809	.0014	6.5 MILS
22.99	42.0	86.8	.8178	.0006	6.5 MILS
23.53	49.6	45.0	.9626	.0001	6.5 MILS
24.07	32.5	74.9	.6349	.0012	6.5 MILS
24.61	43.0	59.4	.8354	.0005	6.5 MILS
25.15	34.9	142.1	.6806	.0010	6.5 MILS

TABLE 1(CON'D): ANALYSIS OF ORNL IR SCANNING RESULTS: PHASE I

Elevation (in)	ΔT_m °F	α (Deg)	Offset	Min Radial Gap(in)	Av. Diametral Gap
25.69	26.3	245.3	.5159	.0016	6.5 MILS
26.23	50.8	220.3	.9850	.0000	6.5 MILS
26.77	61.6	182.1	1.0000	0.0000	>6.5 MILS
27.31	57.7	185.9	1.0000	0.0000	>6.5 MILS
27.90	54.1	191.6	1.0000	0.0000	>6.5 MILS
28.48	35.8	159.0	.6977	.0010	6.5 MILS
29.02	51.6	111.6	1.0000	0.0000	6.5 MILS
29.60	52.7	44.9	1.0000	0.0000	>6.5 MILS
30.14	57.4	16.7	1.0000	0.0000	>6.5 MILS
30.72	58.9	.8	1.0000	0.0000	>6.5 MILS
31.30	19.2	23.5	.3786	.0020	6.5 MILS
31.87	26.2	179.2	.5142	.0016	6.5 MILS
32.45	35.3	202.0	.6875	.0010	6.5 MILS
33.02	42.8	262.6	.8325	.0005	6.5 MILS
33.59	37.3	209.3	.7274	.0009	6.5 MILS
34.15	31.2	287.6	.6098	.0013	6.5 MILS
34.72	44.4	253.9	.8636	.0004	6.5 MILS
35.27	32.5	314.1	.6345	.0012	6.5 MILS
35.83	30.2	134.2	.5904	.0013	6.5 MILS
36.38	39.1	166.2	.7617	.0008	6.5 MILS
36.92	20.1	71.0	.3969	.0020	6.5 MILS
37.46	26.9	54.7	.5269	.0015	6.5 MILS
38.00	46.3	81.8	.8997	.0003	6.5 MILS
38.58	23.5	15.3	.4623	.0017	6.5 MILS
39.15	16.9	319.7	.3349	.0022	6.5 MILS
SOLUTION DIVERGES					
40.28	33.4	127.6	.6527	.0011	6.5 MILS
40.83	33.5	102.9	.6543	.0011	6.5 MILS
41.38	40.9	134.1	.7959	.0007	6.5 MILS
41.92	32.4	158.5	.6319	.0012	6.5 MILS
42.50	45.3	298.8	.8809	.0004	6.5 MILS
43.06	58.9	321.2	1.0000	0.0000	>6.5 MILS
43.62	45.8	295.5	.8890	.0004	6.5 MILS
44.17	37.7	306.1	.7337	.0009	6.5 MILS
44.71	36.8	301.6	.7173	.0009	6.5 MILS
45.27	11.2	227.5	.2251	.0025	6.5 MILS
45.83	19.8	139.3	.3914	.0020	6.5 MILS
46.37	17.6	196.3	.3494	.0021	6.5 MILS
46.93	49.8	264.3	.9666	.0001	6.5 MILS
47.48	13.1	193.5	.2627	.0024	6.5 MILS
48.02	3.6	150.9	.0810	.0030	6.5 MILS

TABLE 2: ANALYSIS OF ORNL IR SCANNING RESULTS: PHASE II

Elevation (in)	ΔT_m (°F)	α (DEG)	Offset	Min Radial Gap (in)	Av. Diametral Gap
.04	7.2	82.8	.1497	.0028	6.5 MILS
.60	30.0	190.4	.5866	.0013	6.5 MILS
1.17	12.5	183.5	.2513	.0024	6.5 MILS
1.72	12.5	111.4	.2502	.0024	6.5 MILS
2.28	27.1	135.6	.5310	.0015	6.5 MILS
2.85	9.8	255.0	.1988	.0026	6.5 MILS
3.40	18.1	182.4	.3577	.0021	6.5 MILS
3.95	31.2	189.4	.6105	.0013	6.5 MILS
4.51	16.5	219.6	.3277	.0022	6.5 MILS
5.08	16.7	22.6	.3307	.0022	6.5 MILS
5.62	50.3	349.0	.9753	.0001	6.5 MILS
6.16	24.4	351.5	.4797	.0017	6.5 MILS
6.71	39.6	87.8	.7701	.0007	6.5 MILS
7.27	62.7	127.6	1.0000	0.0000	>6.5 MILS
7.83	63.1	99.3	1.0000	0.0000	>6.5 MILS
8.40	57.8	74.9	1.0000	0.0000	>6.5 MILS
8.98	26.7	357.6	.5237	.0015	6.5 MILS
9.56	30.2	274.1	.5913	.0013	6.5 MILS
10.10	54.1	250.6	1.0000	0.0000	>6.5 MILS
10.65	20.6	241.9	.4056	.0019	6.5 MILS
11.19	38.0	182.7	.7398	.0008	6.5 MILS
11.75	27.5	29.1	.5397	.0015	6.5 MILS
12.30	26.5	20.4	.5202	.0016	6.5 MILS
12.86	15.7	112.1	.3122	.0022	6.5 MILS
13.43	19.9	20.9	.3928	.0020	6.5 MILS
13.99	25.5	36.4	.5001	.0016	6.5 MILS
14.56	26.3	156.3	.5165	.0016	6.5 MILS
15.14	50.7	166.4	.9843	.0001	6.5 MILS
15.71	48.1	117.0	.9345	.0002	6.5 MILS
16.29	28.0	150.2	.5480	.0015	6.5 MILS
16.87	28.1	155.4	.5503	.0015	6.5 MILS
17.45	28.5	158.1	.5572	.0014	6.5 MILS
17.99	23.0	250.7	.4526	.0018	6.5 MILS
18.57	13.9	221.9	.2774	.0023	6.5 MILS
19.11	31.3	40.3	.6112	.0013	6.5 MILS
19.70	37.7	56.7	.7344	.0009	6.5 MILS
20.24	38.0	222.1	.7411	.0008	6.5 MILS
20.83	67.1	207.4	1.0000	0.0000	>6.5 MILS
21.37	40.2	201.4	.7821	.0007	6.5 MILS
21.91	48.9	140.1	.9493	.0002	6.5 MILS
22.45	28.1	131.6	.5505	.0015	6.5 MILS
22.99	42.6	68.1	.8290	.0006	6.5 MILS
23.53	50.2	50.1	.9742	.0001	6.5 MILS
24.07	36.7	77.4	.7149	.0009	6.5 MILS
24.61	33.0	87.1	.6449	.0012	6.5 MILS
25.15	29.9	180.2	.5856	.0013	6.5 MILS

TABLE 2 (CON'D): ANALYSIS OF ORNL IR SCANNING RESULTS: PHASE II

Elevation (in)	ΔT_m (°F)	α (Deg)	Offset	Min Radial Gap(in)	Av. Diametral Gap
25.69	39.4	251.8	.7672	.0008	6.5 MILS
26.23	56.3	208.4	1.0000	0.0000	>6.5 MILS
26.77	65.4	185.5	1.0000	0.0000	>6.5 MILS
27.31	62.5	196.6	1.0000	0.0000	>6.5 MILS
27.90	61.4	198.8	1.0000	0.0000	>6.5 MILS
28.48	39.9	161.7	.7771	.0007	6.5 MILS
29.02	46.3	99.3	.8999	.0003	6.5 MILS
29.60	48.6	29.2	.9438	.0002	6.5 MILS
30.14	56.4	358.4	1.0000	0.0000	>6.5 MILS
30.72	52.5	354.7	1.0000	0.0000	>6.5 MILS
31.30	9.6	8.3	.1950	.0026	6.5 MILS
31.87	35.9	189.4	.7006	.0010	6.5 MILS
32.45	41.6	240.8	.8092	.0006	6.5 MILS
33.02	49.7	280.0	.9645	.0001	6.5 MILS
33.59	24.7	280.2	.4856	.0017	6.5 MILS
34.15	36.2	277.1	.7060	.0010	6.5 MILS
34.72	48.3	260.6	.9386	.0002	6.5 MILS
35.27	17.4	352.2	.3445	.0021	6.5 MILS
35.83	32.9	142.5	.6424	.0012	6.5 MILS
36.38	18.9	160.6	.3735	.0020	6.5 MILS
36.92	33.0	34.0	.6449	.0012	6.5 MILS
37.46	29.4	55.7	.5751	.0014	6.5 MILS
38.00	43.9	67.1	.8530	.0005	6.5 MILS
38.58	14.3	350.6	.2846	.0023	6.5 MILS
39.15	20.3	289.4	.4010	.0019	6.5 MILS
39.72	14.0	154.2	.2804	.0023	6.5 MILS
40.28	41.4	140.1	.8056	.0006	6.5 MILS
40.83	33.0	90.5	.6449	.0012	6.5 MILS
41.38	42.0	157.3	.8162	.0006	6.5 MILS
41.92	29.8	255.8	.5830	.0014	6.5 MILS
42.50	58.2	299.5	1.0000	0.0000	>6.5 MILS
43.06	52.5	315.5	1.0000	0.0000	>6.5 MILS
43.62	46.0	304.2	.8941	.0003	6.5 MILS
44.17	37.4	315.8	.7283	.0009	6.5 MILS
44.71	39.4	319.1	.7662	.0008	6.5 MILS
45.27	15.0	35.6	.2995	.0023	6.5 MILS
45.83	22.7	55.2	.4476	.0018	6.5 MILS
46.37	21.4	313.1	.4220	.0019	6.5 MILS
46.93	38.0	286.5	.7392	.0008	6.5 MILS
47.48	24.2	95.3	.4750	.0017	6.5 MILS
48.02	3.3	189.0	.0750	.0030	6.5 MILS

TABLE 3 : ANALYSIS OF ORNL IR SCANNING RESULTS: PHASE III

Elevation (in)	ΔT_m (°F)	α (Deg)	Offset	Min Radial Gap (in)	Av Diametral Gap
.04	7.6	153.3	.1574	.0027	6.5 MILS
.60	31.4	194.9	.6136	.0013	6.5 MILS
1.17	9.4	201.8	.1909	.0026	6.5 MILS
1.72	5.6	191.8	.1180	.0029	6.5 MILS
2.28	26.3	128.1	.5162	.0016	6.5 MILS
2.85	12.9	279.9	.2590	.0024	6.5 MILS
3.40	17.8	201.0	.3534	.0021	6.5 MILS
3.95	34.8	190.4	.6793	.0010	6.5 MILS
4.51	12.2	217.9	.2448	.0025	6.5 MILS
5.08	16.1	26.6	.3201	.0022	6.5 MILS
5.62	51.8	344.4	1.0000	0.0000	6.5 MILS
6.16	26.5	336.1	.5192	.0016	6.5 MILS
6.71	34.8	91.5	.6797	.0010	6.5 MILS
7.27	62.4	128.1	1.0000	0.0000	>6.5 MILS
7.83	65.0	101.4	1.0000	0.0000	>6.5 MILS
8.40	58.5	78.0	1.0000	0.0000	>6.5 MILS
8.96	28.1	357.2	.5506	.0015	6.5 MILS
9.56	36.4	282.2	.7096	.0009	6.5 MILS
10.10	50.8	247.5	.9854	.0000	6.5 MILS
10.65	20.1	252.0	.3961	.0020	6.5 MILS
11.19	40.4	162.9	.7861	.0007	6.5 MILS
11.75	25.2	43.3	.4938	.0016	6.5 MILS
12.30	24.0	13.9	.4723	.0017	6.5 MILS
12.86	18.0	89.3	.3569	.0021	6.5 MILS
13.43	23.0	38.3	.4521	.0018	6.5 MILS
13.99	28.2	42.9	.5520	.0015	6.5 MILS
14.56	31.4	134.5	.6136	.0013	6.5 MILS
15.14	52.6	158.1	1.0000	0.0000	>6.5 MILS
15.71	57.8	127.6	1.0000	0.0000	>6.5 MILS
16.29	36.0	146.4	.7027	.0010	6.5 MILS
16.87	32.9	146.6	.6427	.0012	6.5 MILS
17.45	33.7	150.0	.6575	.0011	6.5 MILS
17.99	18.8	192.3	.3711	.0020	6.5 MILS
18.57	14.4	175.7	.2883	.0023	6.5 MILS
19.11	30.7	50.9	.5994	.0013	6.5 MILS
19.70	40.9	61.7	.7960	.0007	6.5 MILS
20.24	31.0	212.1	.6051	.0013	6.5 MILS
20.83	61.3	208.0	1.0000	0.0000	>6.5 MILS
21.37	27.5	212.3	.5384	.0015	6.5 MILS
21.91	42.3	128.7	.8219	.0006	6.5 MILS
22.45	33.4	117.7	.6520	.0011	6.5 MILS
22.99	43.7	68.5	.8504	.0005	6.5 MILS
23.53	48.5	47.1	.9422	.0002	6.5 MILS
24.07	40.2	76.1	.7817	.0007	6.5 MILS
24.61	36.3	78.5	.7079	.0009	6.5 MILS
25.15	32.5	157.2	.6354	.0012	6.5 MILS

TABLE 3 (CON'D): ANALYSIS OF ORNL IR SCANNING RESULTS: PHASE III

Elevation (in)	ΔTm (°F)	α (Deg)	Offset	Min Radial Gap(in)	Av Diametral Gap
25.69	22.3	238.4	.4392	.0018	6.5 MILS
26.23	55.5	201.8	1.0000	0.0000	>6.5 MILS
26.77	64.3	180.8	1.0000	0.0000	>6.5 MILS
27.31	60.6	188.8	1.0000	0.0000	>6.5 MILS
27.90	57.7	194.0	1.0000	0.0000	>6.5 MILS
28.48	38.9	165.2	.7567	.0008	6.5 MILS
29.02	49.2	111.9	.9557	.0001	6.5 MILS
29.60	45.4	33.9	.8819	.0004	6.5 MILS
30.14	54.3	3.7	1.0000	0.0000	>6.5 MILS
30.72	54.9	351.7	1.0000	0.0000	>6.5 MILS
31.30	8.9	3.0	.1827	.0027	6.5 MILS
31.87	38.3	179.5	.7467	.0008	6.5 MILS
32.45	38.2	209.2	.7447	.0008	6.5 MILS
33.02	41.8	268.7	.8131	.0006	6.5 MILS
33.59	24.9	268.5	.4898	.0017	6.5 MILS
34.15	29.1	284.4	.5656	.0014	6.5 MILS
34.72	47.6	258.7	.9237	.0002	6.5 MILS
35.27	32.6	326.3	.6365	.0012	6.5 MILS
35.83	28.8	125.0	.5644	.0014	6.5 MILS
36.38	29.3	143.8	.5731	.0014	6.5 MILS
36.92	25.3	46.3	.4973	.0016	6.5 MILS
37.46	25.0	40.5	.4905	.0017	6.5 MILS
38.00	45.4	89.3	.8827	.0004	6.5 MILS
38.58	6.5	8.8	.1356	.0028	6.5 MILS
39.15	17.0	261.9	.3380	.0022	6.5 MILS
39.72	18.0	181.0	.3555	.0021	6.5 MILS
40.28	37.3	152.9	.7262	.0009	6.5 MILS
40.83	23.1	108.0	.4552	.0018	6.5 MILS
41.38	50.5	144.1	.9885	.0000	6.5 MILS
41.92	29.4	183.0	.5757	.0014	6.5 MILS
42.50	48.5	288.2	.9416	.0002	6.5 MILS
43.06	52.0	310.7	1.0000	0.0000	6.5 MILS
43.62	44.1	279.9	.8572	.0005	6.5 MILS
44.17	30.0	293.2	.5870	.0013	6.5 MILS
44.71	31.3	289.5	.6114	.0013	6.5 MILS
45.27	11.4	151.8	.2290	.0025	6.5 MILS
45.83	32.7	118.1	.6391	.0012	6.5 MILS
46.37	17.8	148.2	.3535	.0021	6.5 MILS
46.93	38.0	263.8	.7358	.0008	6.5 MILS
47.48	30.6	125.0	.5985	.0013	6.5 MILS

SOLUTION DIVERGES

Table 4

PELLET OFFSET

	MEAN	STANDARD DEVIATION
PHASE I	.6771	.2541
PHASE II	.6502	.2583
PHASE III	.6499	.2553

Figure 1: Phase I Infrared Scans /A/ ; Empty Tube Infrared Scan /B/

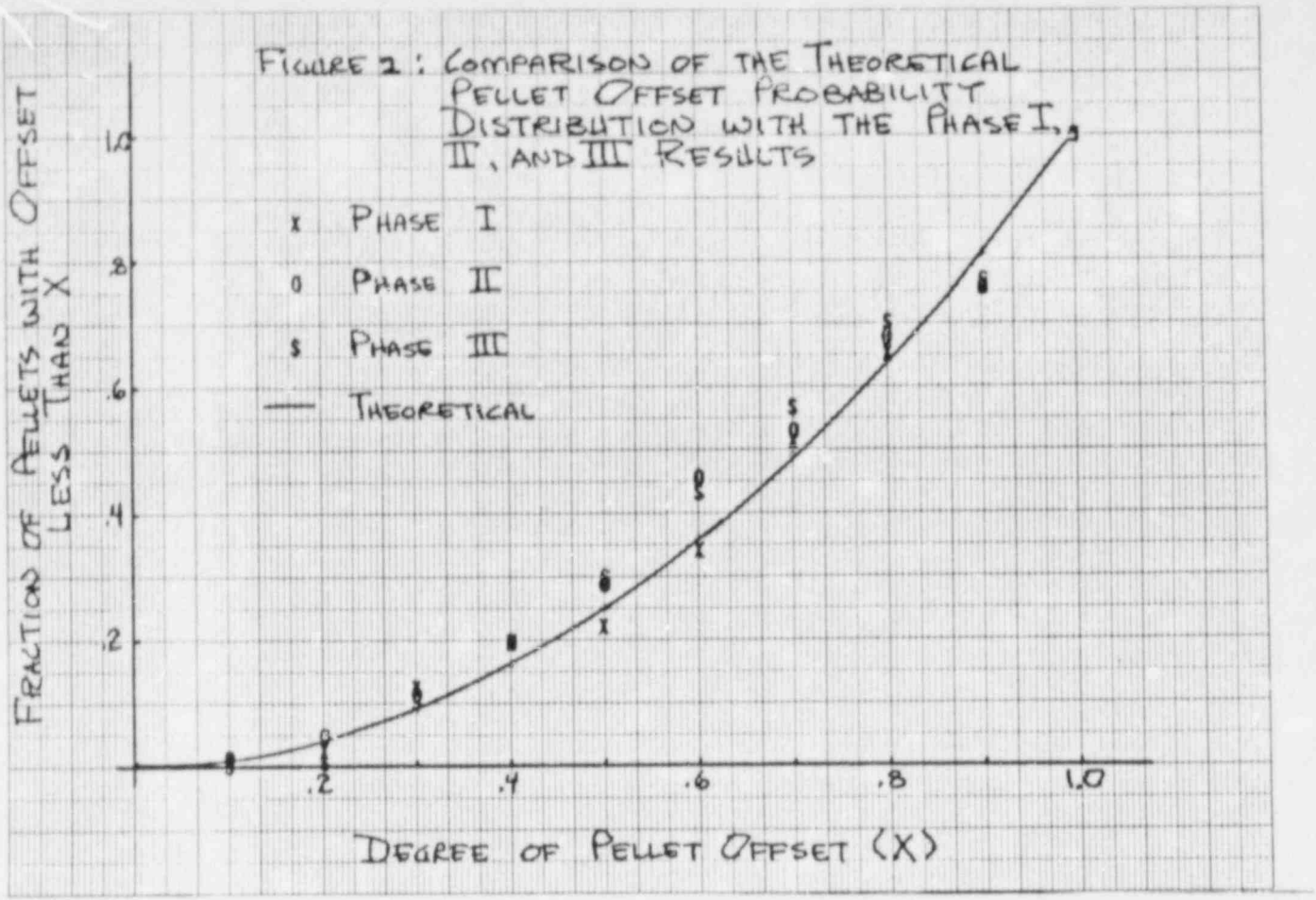
FIGURE 2: COMPARISON OF THE THEORETICAL PELLET OFFSET PROBABILITY DISTRIBUTION WITH THE PHASE I, II, AND III RESULTS
x PHASE I
0 PHASE II
$ PHASE III
— THEORETICAL
FRACTION OF PELLETS WITH OFFSET LESS THAN X
1.0
.8
.6
.4
.2
.2
.4
.6
.8
1.0
DEGREE OF PELLET OFFSET (X)

Figure 3

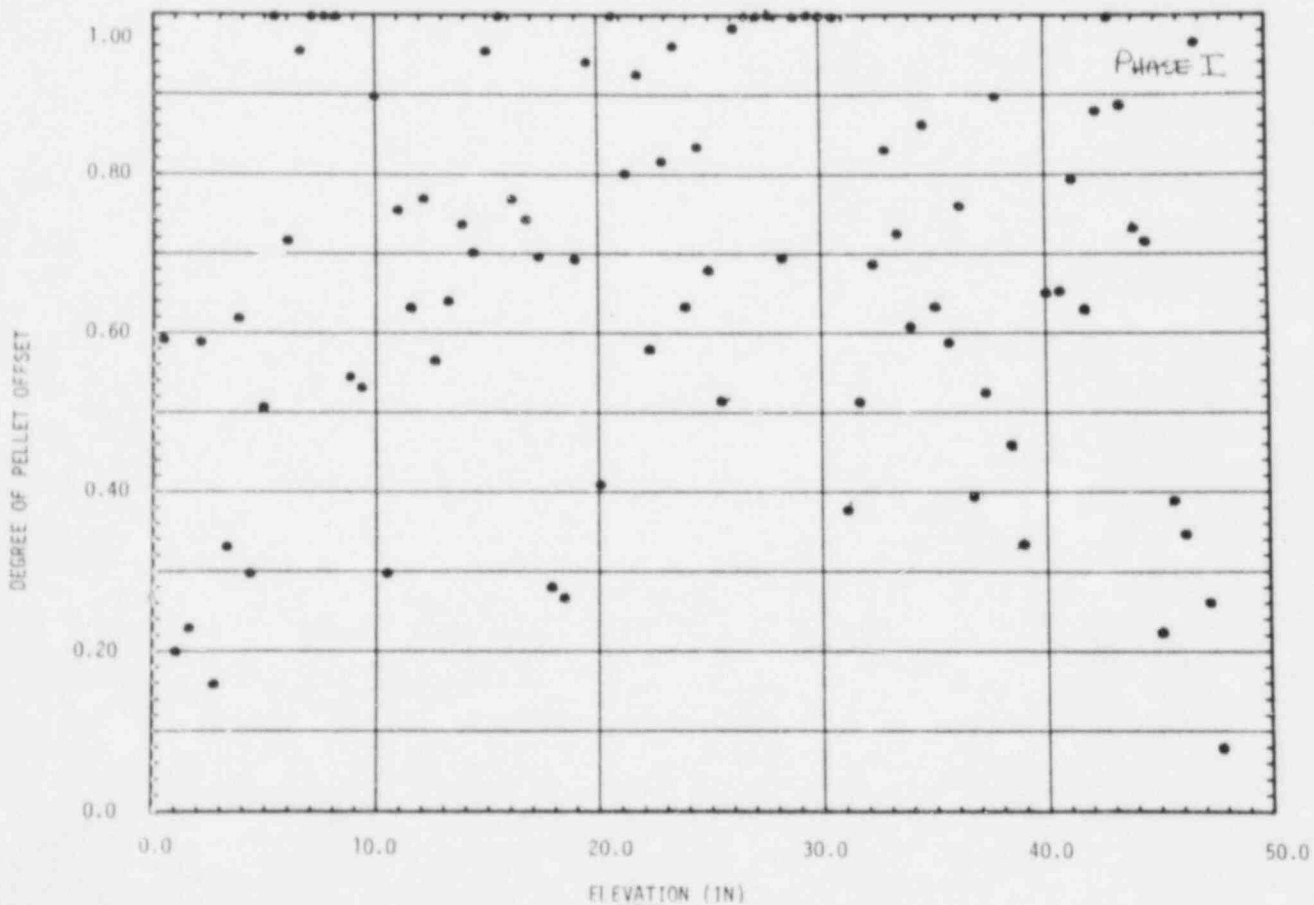
PHASE I
1.00
0.80
0.60
0.40
0.20
0.0
DEGREE OF PELLET OFFSET
0.0
10.0
20.0
30.0
40.0
50.0
ELEVATION (IN)

Figure 4

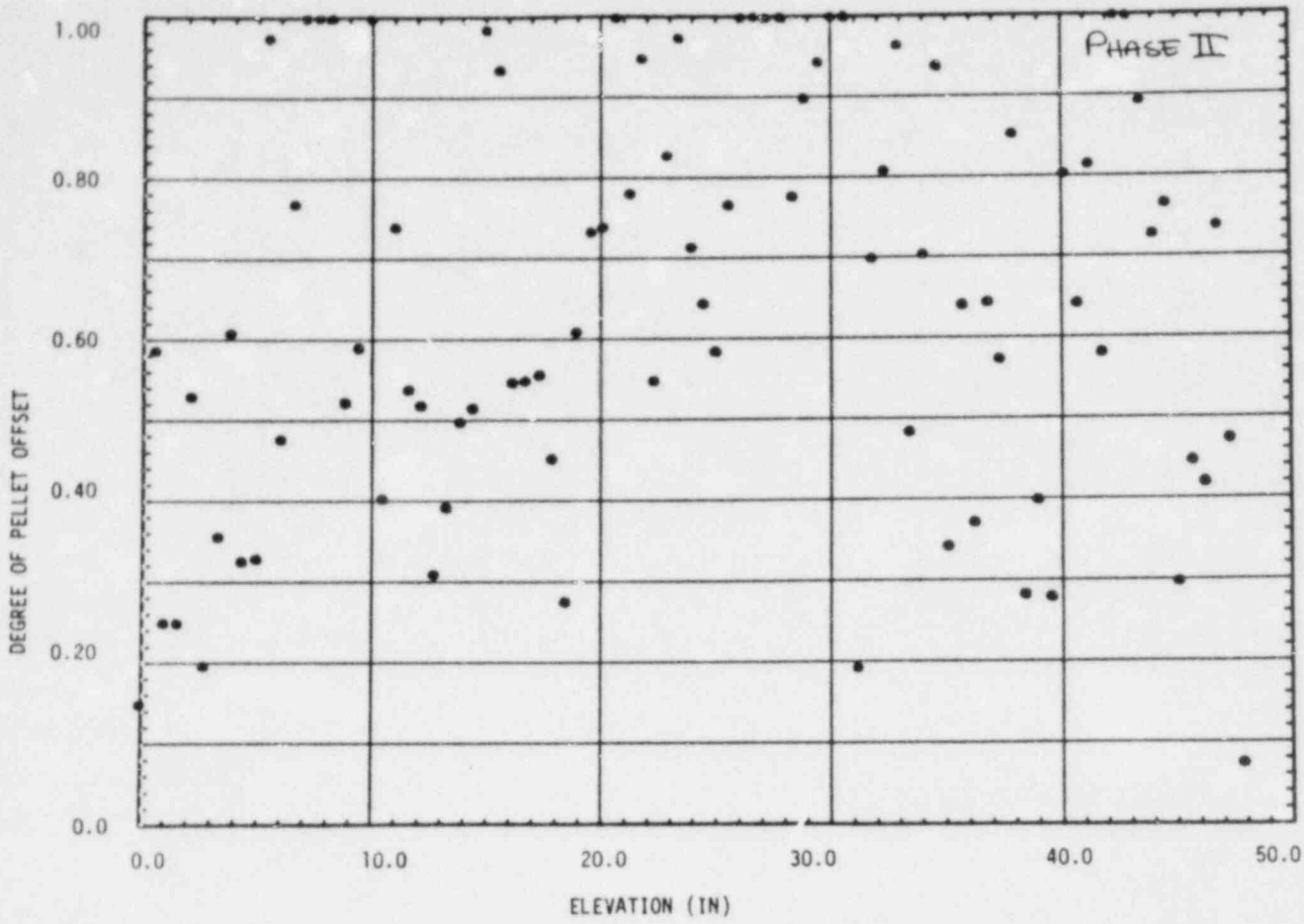

Figure 5

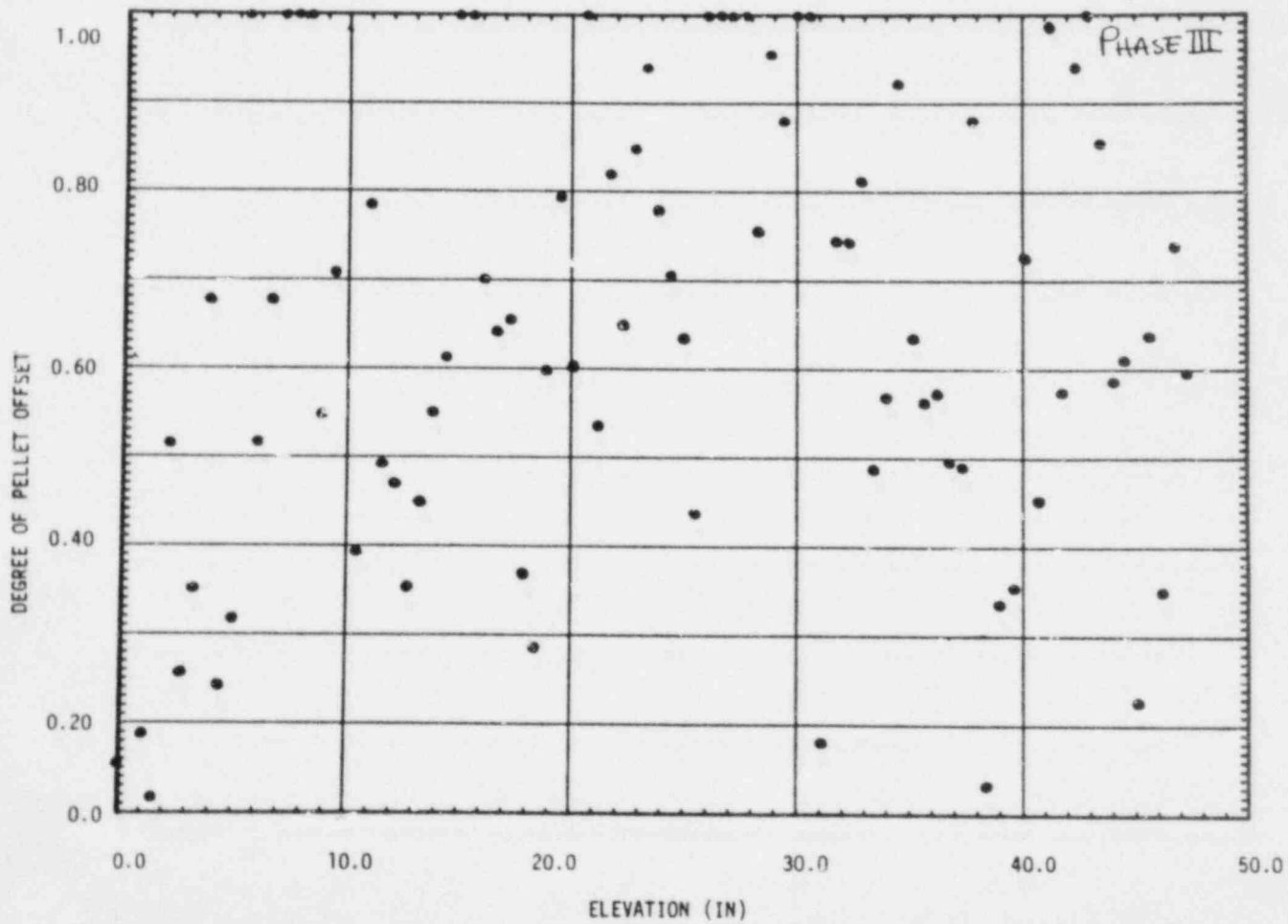

Figure 6

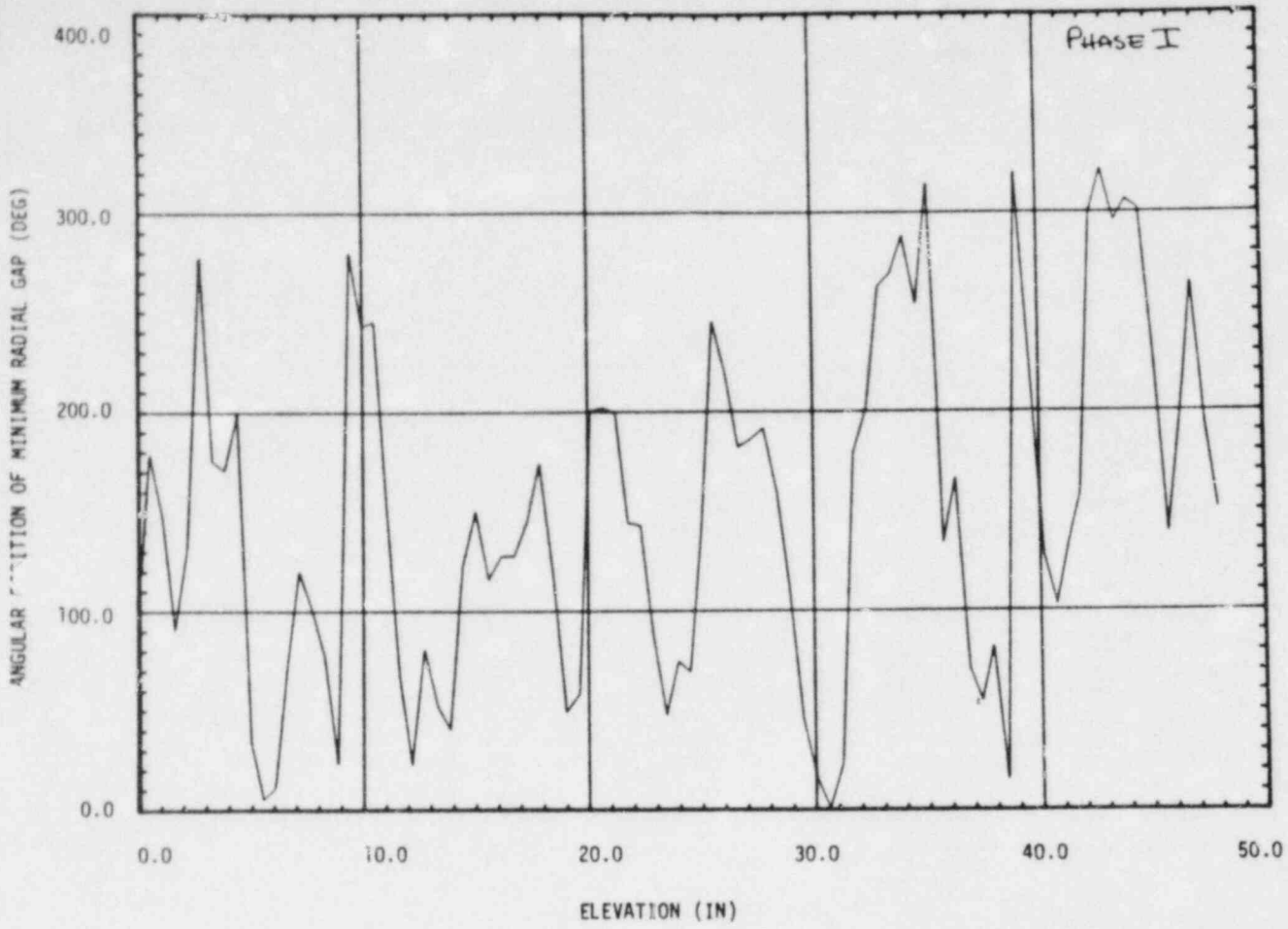

Figure 7

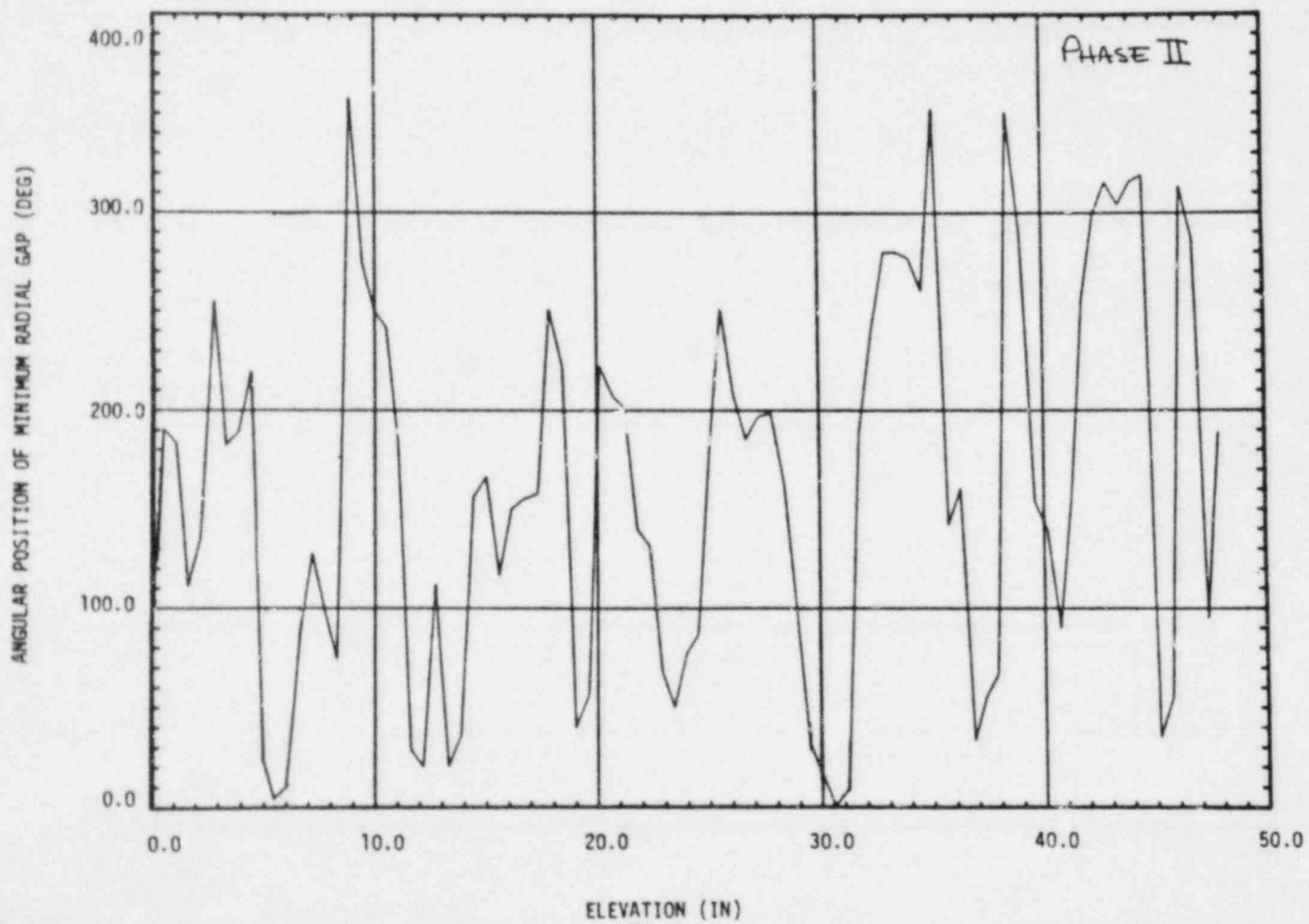

Figure 8

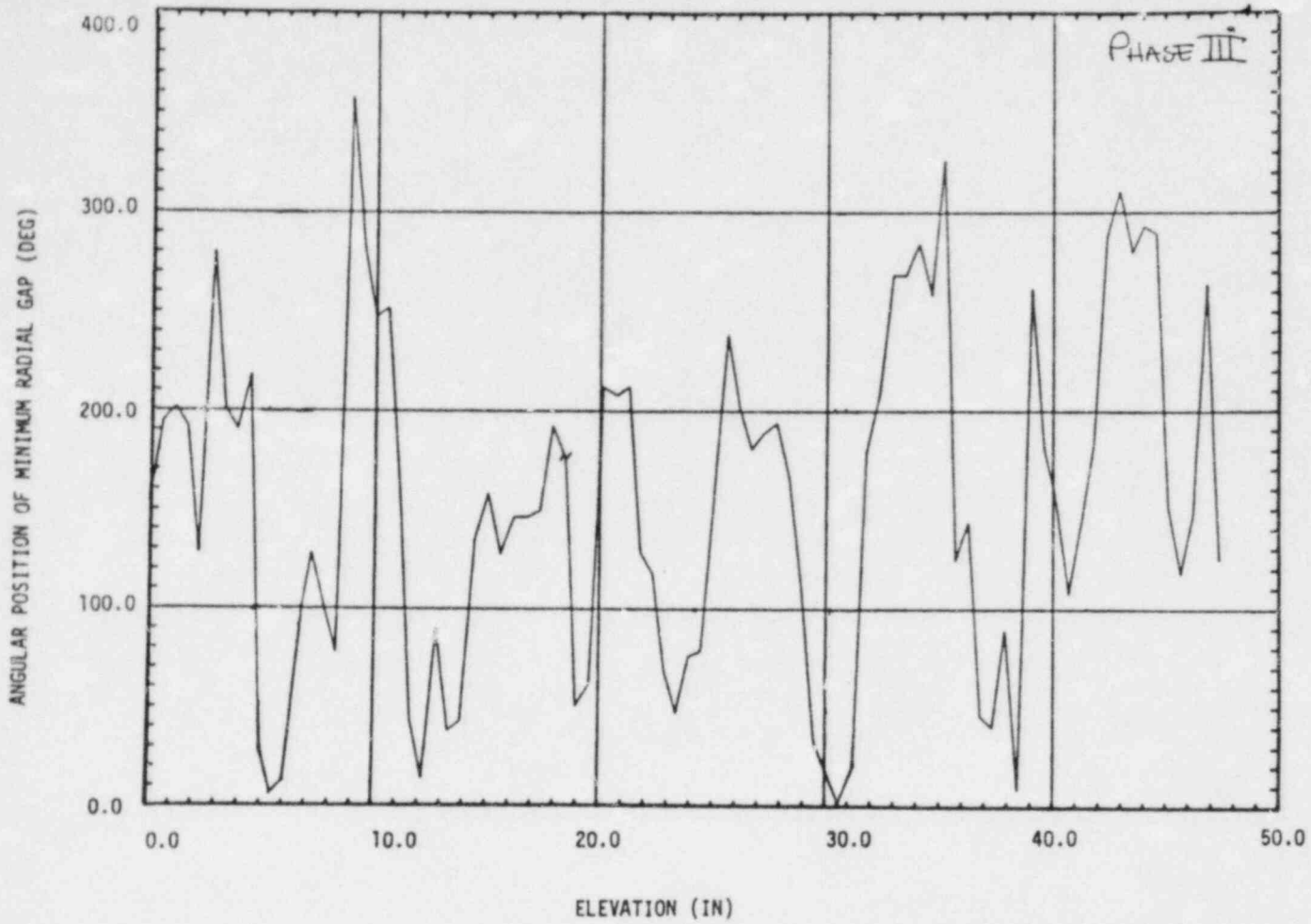

Figure 9

Ratio of Eccentric To Concentric Gap Conductance vs. Diametral Gap

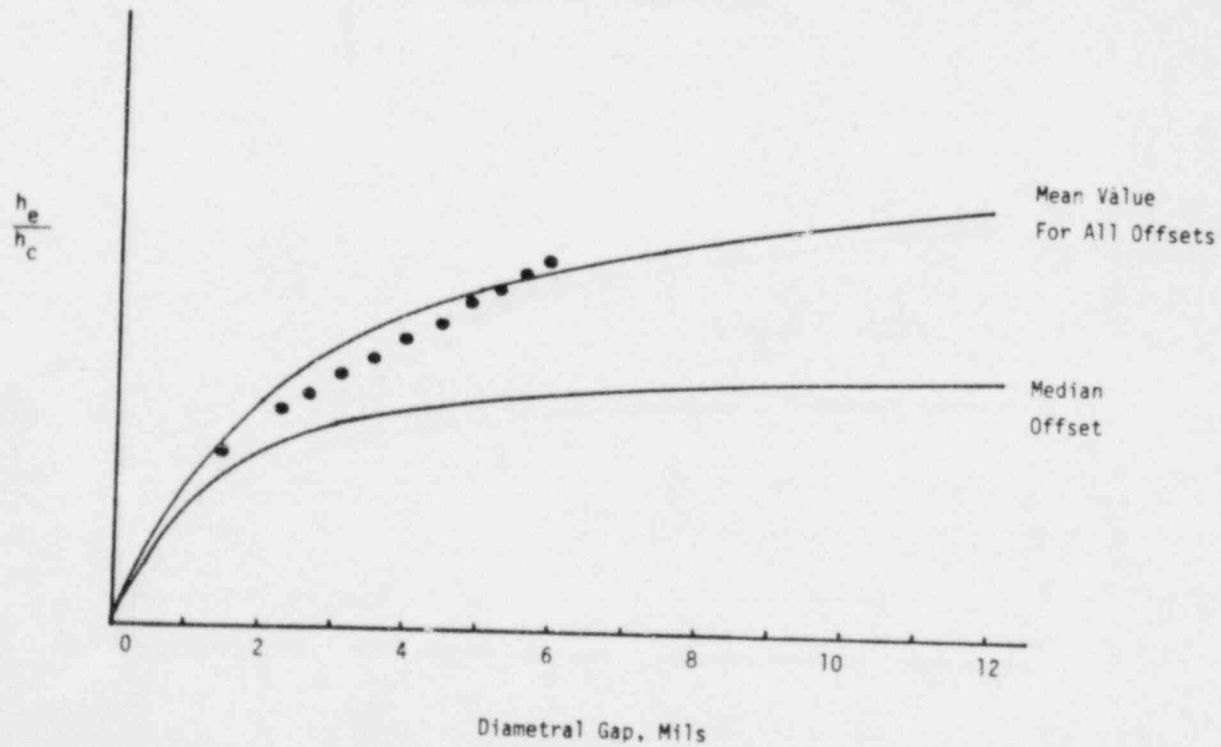

Figure 10

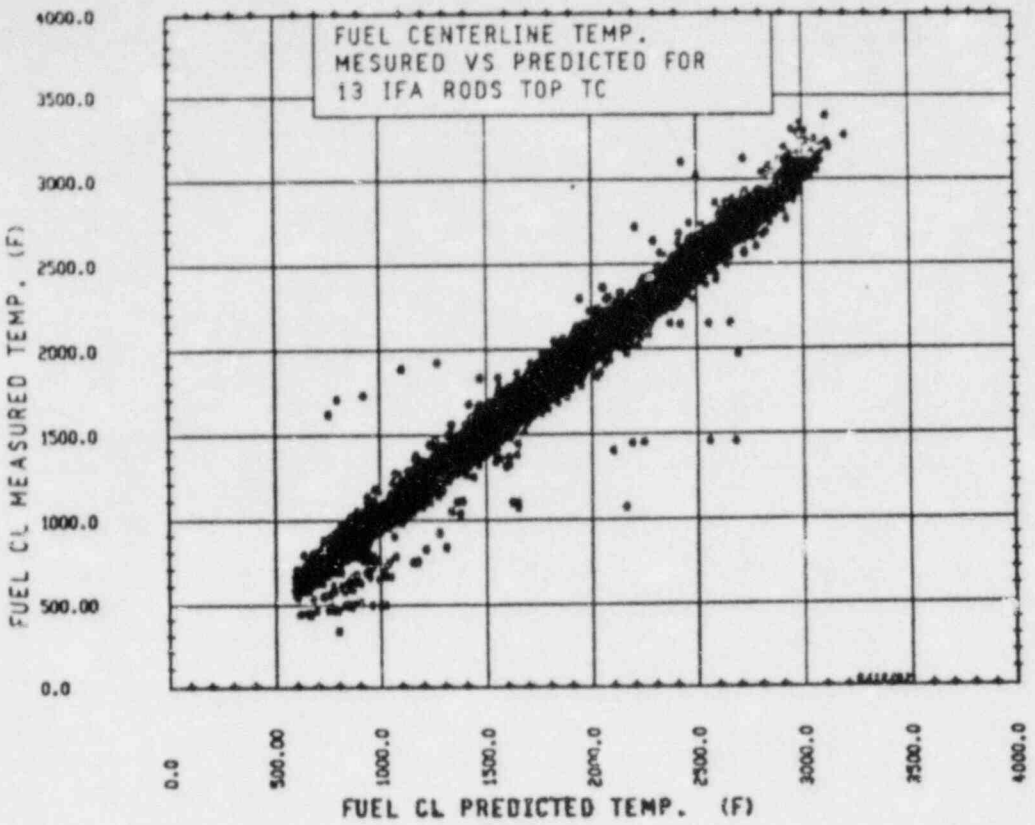

Figure 11

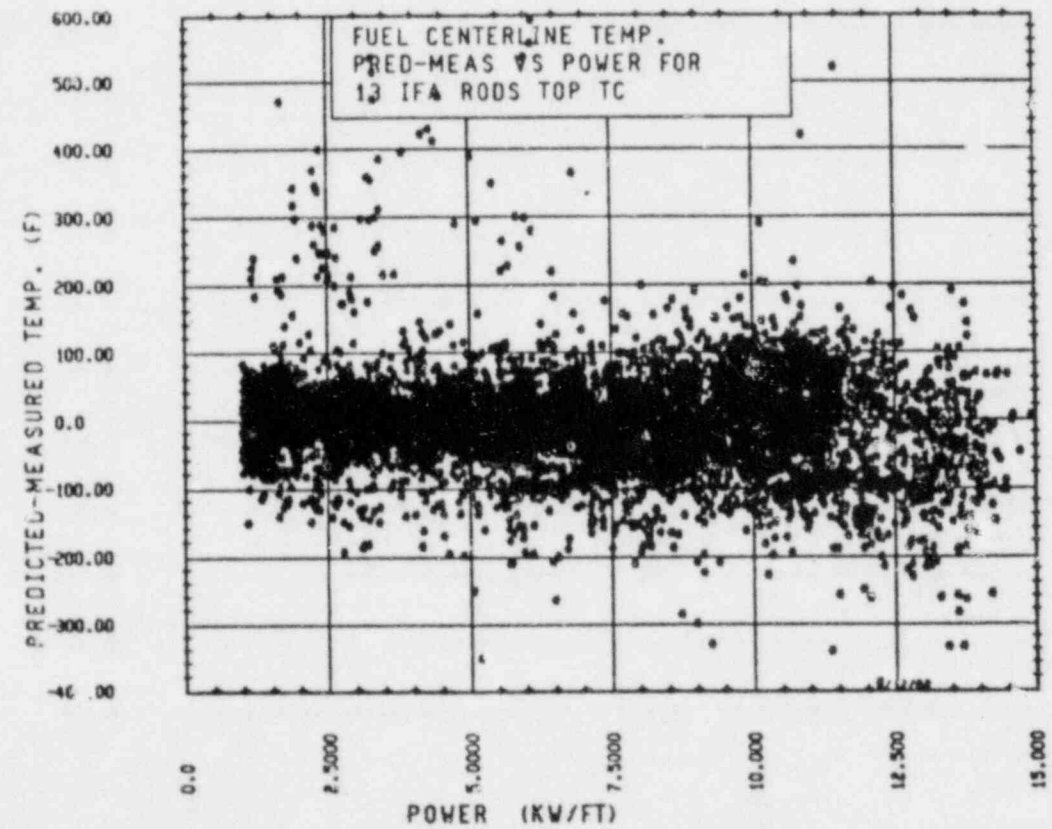

Figure 12

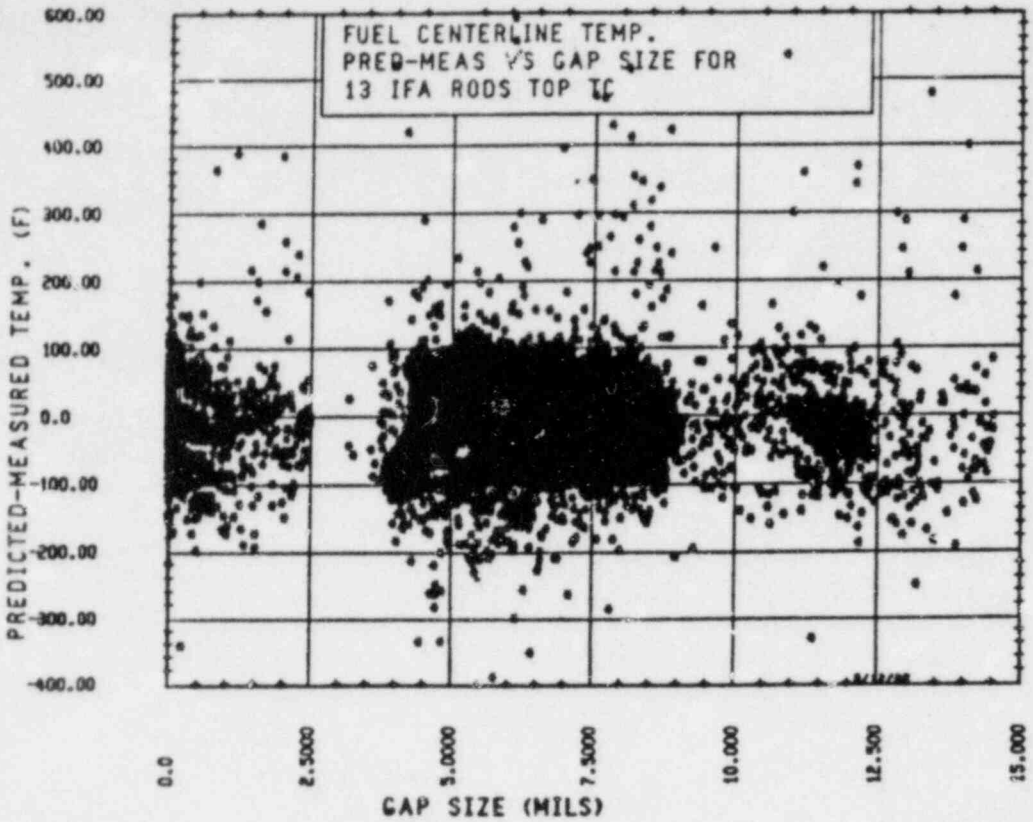

Figure 13

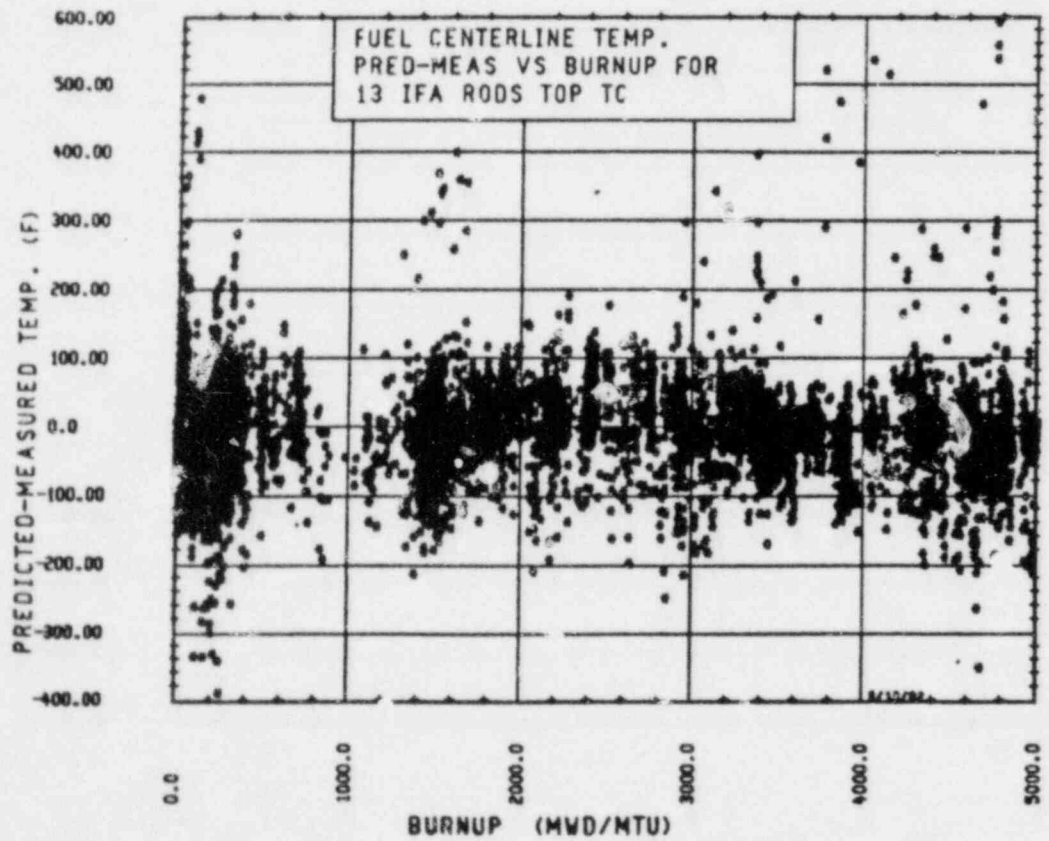

Figure 14

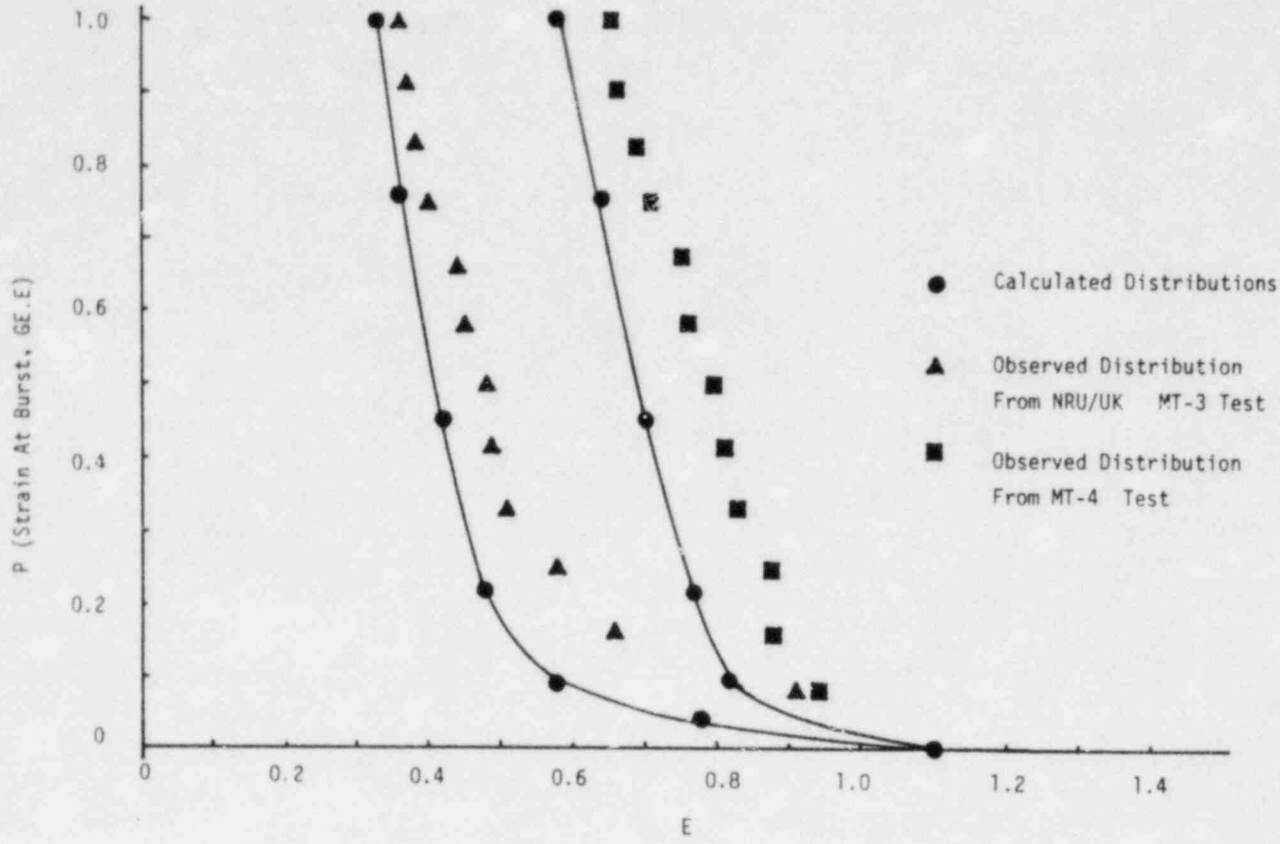
1.0
0.8
0.6
0.4
0.2
0
P (Strain At Burst, GE.E)
0
0.2
0.4
0.6
0.8
1.0
1.2
1.4
E
Calculated Distributions
Observed Distribution From NRU/UK MT-3 Test
Observed Distribution From MT-4 Test

TEST OPTRAN 1-1 RESULTS[a]

Z. R. Martinson and P. E. MacDonald
EG&G Idaho, Inc.

Anticipated transients are deviations from normal operating conditions that result from system component malfunctions which may occur one or more times during the service life of a reactor and are accompanied by a scram. Examples of anticipated transients are total loss of feedwater in a pressurized water reactor (PWR), uncontrolled control rod withdrawal in a PWR, a boiling water reactor (BWR) turbine trip without steam bypass, and BWR generator load rejection with steam bypass. Frequently, the effect of the malfunction that initiates the transient results in a loss of secondary heat sink and a subsequent increase in system pressure, which causes a positive reactivity feedback and associated power increase. Dryout and severe cladding temperatare excursions are not expected during anticipated transients in either a BWR or PWR and, therefore, the damage mechanism of concern is cladding fracture due to pellet-cladding mechanical interaction (PCI).

Since the first indication that zircaloy cladding might be susceptible to failure caused by a pellet-cladding interactive mechanism, the phenomenon has received considerable attention. Pellet-cladding interaction failures during slow power increases are apparently induced after sufficiently high burnup is attained to allow fission product release. However, PCI failures may also occur during very fast power increases due to high strain rate tearing or fracture of irradiation embrittled zircaloy cladding. A number of experimental programs have been completed or are underway to determine the power, ramp rate, and burnup dependency of PCI failures during relatively slow power ramps. Results

---

a. Work supported by the U.S. Nuclear Regulatory Commission, Office of Nuclear Regulatory Research, under DOE Contract No. DE-AC07-76ID01570.

from these programs indicate that incipient cladding cracks may occur in some fuel designs at power levels within commercial reactor operating ranges. Such cladding cracking is usually prevented during normal operation by using very slow rates of reactor power increase. However, certain anticipated transients cause a very rapid change in power. Since the most severe anticipated transients have not actually occurred and applicable data are not available, the Nuclear Regulatory Commission (NRC) was uncertain whether light water reactor (LWR) irradiated fuel rods would fail or even be damaged as a result of these transients. Therefore, NRC requested that transient testing be performed for the primary purpose of evaluating the probability of cladding failure occurrence during anticipated transients in order to assess the accuracy of licensee radiation dose calculations for such transients. Two other NRC concerns are, (a) should a reactor be derated following a severe anticipated transient, and (b) should regulations be imposed to limit pellet-cladding interaction in irradiated fuel rods? Accordingly, the Operational Transient (OPT) 1-1 Test Series was conducted in the Power Burst Facility (PBF) at the Idaho National Engineering Laboratory by EG&G Idaho, Inc.

The objective of the OPT 1-1 Test Series was to evaluate the extent of damage and the threshold for failure during simulated BWR anticipated transients. Four power transient tests with progressively higher power levels were performed with preirradiated fuel rods at power ramp rates as high as 550 kW/m per second. Six separately shrouded fuel rods fabricated by the General Electric Co., and preirradiated in the Monticello BWR to burnups of about 5000 to 23,000 MWd/t were tested, four at a time. Four of the fuel rods were of typical GE 8 x 8 design, except for fuel length (0.75 m). Two of the rods included design modifications to improve their PCI-resistant characteristics. A lengthy fuel conditioning preceded the transient testing of the fuel rods.

The first test simulated the power transient predicted to occur during a BWR turbine trip without steam bypass, with the fuel rods operating at BWR-6 core-average rod powers. Two test fuel rods were replaced following the first transient so that the possible occurrence of incipient cracks on the inside surface of the cladding exposed to only one transient could be

investigated during postirradiation examination. The results of slower power ramp tests performed elsewhere suggest that incipient cracks may be initiated at test rod linear powers considerably lower than the 92 kW/m that was reached during the first transient. The second transient simulated the power peak predicted to occur during a BWR generator load rejection without steam bypass, with fuel rods operating somewhat above the core-average rod power. The maximum test rod linear power for the second test was 177 kW/m. The third and fourth tests were performed at higher transient powers (206 and 261 kW/m, respectively) than current safety analysis predicts to be possible in a BWR in order to determine the cladding failure threshold margin.

The radially averaged peak fuel enthalpy increased from 47 to 87 cal/g UO_2 during the fourth transient, and the fuel centerline temperature increased from 1350 to 2005 K following the transient. A maximum cladding axial elongation change of 2.6 mm was measured during the fourth transient. Hard pellet-cladding contact was calculated to result in a maximum cladding hoop strain of 0.44% and a hoop stress of 183 MPa. As expected, boiling transition did not occur on any of the fuel rods.

Fission products were not released during or after any of the four power transients and posttest analysis of the plenum gases confirmed that none of the fuel rods leaked. Metallurgical examination of the rods has not indicated any damage or change in these rods which could have been caused by the PBF testing.

Even though only six fuel rods were tested during the OPT 1-1 Test Series, the peak transient fuel rod powers were twice that expected for a design average power rod (26 kW/m) subjected to the worst anticipated transient presently considered credible for a BWR, and none of the test rods failed. Although postirradiation examinations are continuing, the lack of any evidence of cladding through-wall cracks strongly suggests that BWR fuel rods will not fail during brief power transients. The severity of the tests compensates somewhat for the lack of redundancy in test rods with regard to possible interpretation of the significance of these results. However, the fuel rods used in the OPT 1-1 tests and the PBF test

conditions are not entirely typical of those in commercial reactors. For instance, the short rod length may have affected the fission product release and transport and the axial loading of the cladding due to pellet-cladding mechanical interactions. Therefore, further evaluation of the question may be required.

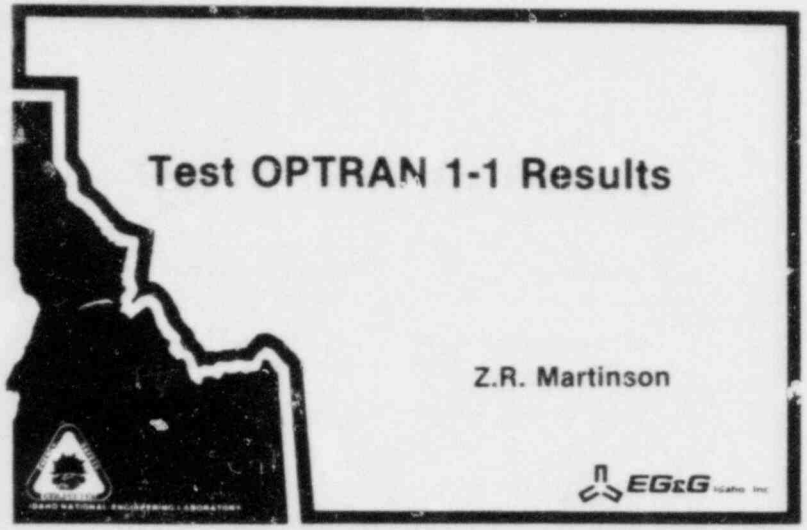

Anticipated Transients With Scram

- Anticipated transients occur with frequencies up to once per reactor year
- Consequences of most severe anticipated transients may be somewhat greater for BWRs than for PWRs
- Worst case BWR anticipated transient reaches 495% power in about 1 second
- Dryout and severe cladding temperature excursions are not expected. The damage mechanism of concern is cladding fracture due to pellet-cladding mechanical and chemical interactions

NRR Concerns

- Are the failure probabilities used in dose calculations for anticipated transients conservative?
  - — Should a reactor be derated following a severe operational transient?
  - — Should regulations be imposed to limit pellet-cladding interactions in irradiated rods?

Test OPT 1-1 Objectives

- Determine threshold at which LWR fuel rods are likely to fail
- Identify the damage mechanisms which may occur during a severe BWR anticipated transient with SCRAM

OPT 1-1 Test Fuel Rods

Fuel rod type	Burnup MWd/t
4 reference	12,000-23,000
1 zirconium liner	5000
1 fuel additive	5000

S2 10 337

Schematic of 4x Hardware

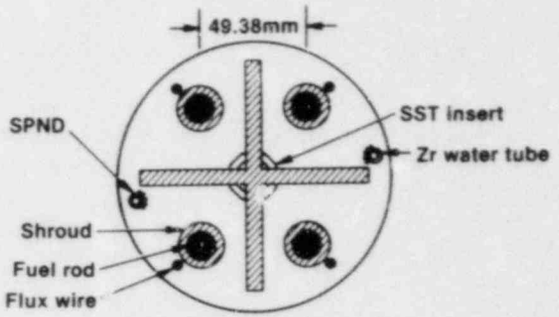

S2 10 341

Test OPT 1-1 Transients

- Four progressively higher power transients
- Transient A simulated a turbine trip without steam bypass (TT w/o BP) for rods operating at BWR average rod power
- Transient B simulated a generator load rejection without steam bypass for rods operating above BWR average rod powers
- Transients C and D performed at higher transient powers than current safety analysis predicts to be possible in a commercial BWR to determine failure threshold margins

S2 10 342

Test OPT 1-1

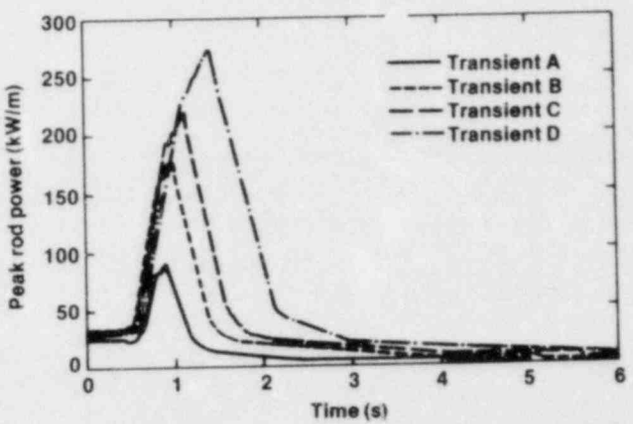

S2 10 339

OPT 1-1 Power Transients

Transient	Initial peak rod power (kW/m)	Peak fuel rod power (kW/m)	Initial fuel enthalpy (Cal/g)	Transient energy input (Cal/g)	Peak fuel enthalpy (Cal/g)
A	26.0	92	45	6	49
B	28.4	177	48	18	63
C	28.5	206	48	28	69
D	28.2	261	47	56	87

S2 10 338

Test OPT 1-1 Transient A

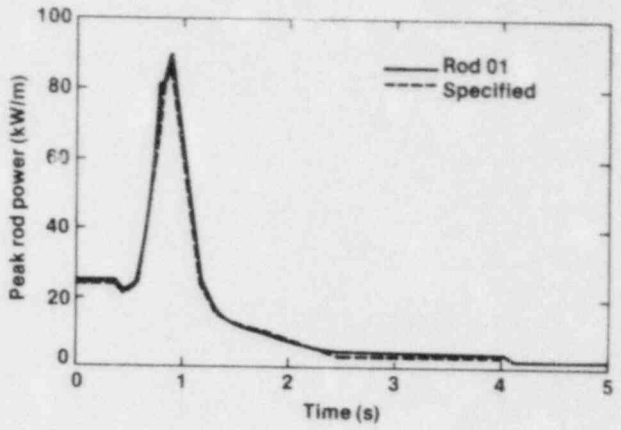

S2 10 340

Cross Section of Rod 901-3

T-2175 82B-19

S2 2860

Typical Cladding Structure of Rod 901-3

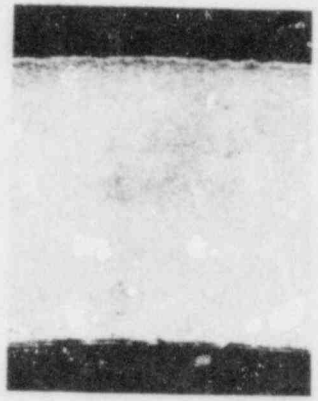

T-2175 100 μm 82B-31

S2 2860

OPTRAN 1-1

Rod #	Total gas in std CC(1)	Void area in CC(2)	MOL %		
			He	Kr	Xe
1	13.4	14.4	97.5	0.24	1.83
2	37.9	13.8	99.3	0.07	0.51
3	13.4	13.8	96.6	0.33	2.79
4*	35.1	14.1	97.4	0.15	0.77
5	13.3	13.7	94.6	0.53	4.14
6	12.8	13.3	94.7	0.44	3.40

* Small water leak into sample
(1) ± 0.1 to 0.3 accuracy
(2) ± 0.2 accuracy

S2 10 336

Summary

- No fuel rod failures during or after any of the OPT 1-1 transients
- The results of these tests suggest that LWR fuel rods will not fail or be severely damaged during anticipated transients

S2 10 343

EXPERIMENTAL EVIDENCE FOR THE DEPENDENCE OF FUEL RELOCATION UPON THE MAXIMUM LOCAL POWER ATTAINED *

D. D. Lanning
Pacific Northwest Laboratory

INTRODUCTION

A paper presented in 1981 at the Ninth NRC Light-Water Reactor Safety Meeting reviewed trends in fuel rod behavior modeling during the past decade.(1) The major trend cited was the inclusion of the effects of pellet cracking and relocation within fuel rod performance computer programs. The inclusion of relocation has resulted in lower and more realistic calculated fuel temperatures and stored energy, even when the effective fuel thermal conductivity is degraded to account for the thermal resistance of the cracks. The relocation effect is usually applied as a "prompt" fraction of the fabricated gap plus a time or burnup-dependent rate of relocation to a maximum value. The NRC fuel performance codes(2,3,4) and others, have no power dependence for the relocation, or at most a weak dependence.

Experimental evidence that indicates a definite power dependence for fuel cracking and relocation is presented. (The evidence consists of fuel centerline thermocouple measurements and metallographic cross sections from Halden Reactor test assembly IFA-527.) The implications of such a dependence for fuel modeling and calculated fuel temperatures are discussed.

---

*This paper was prepared for the report on the proceedings of the Tenth Water Reactor Safety Research Information Meeting and was not listed in the agenda for this meeting.

II - BACKGROUND ON FUEL RELOCATION ESTIMATES

There are at least two ways to investigate fuel relocation: the observation of residual gaps in metallographic cross-sections of irradiated rods; and inference of gap size from measured fuel temperatures.* The latter involves more analysis and assumptions, but holds the promise for through-life determination of gap size changes, rather than end-of-life data only.

The NRC-sponsored instrumented tests which have been studied most thoroughly with respect to gap size and fuel relocation have been the PBF "Gap Conductance" GC-2 Tests[5] and the Halden Reactor assemblies IFA-431/432[6,7] IFA-513,[8] and IFA-527.[9] With the important exception of IFA-527, these tests have all featured BOL peak powers in excess of 30 kW/m (10 kW/ft). In these tests, fuel cracking and relocation was extensive even for short irradiations, as shown in Figures 1 and 2. Note that the PBF test for example ran for only about 70 hours, and that the HBWR rod IFA-431-6 had a peak burnup of only 5,000 MWd/MTM. On the basis of such tests, fuel is assumed in various codes to have a substantial "prompt fraction" to the relocation; this varies from approximately 10% (of the fabricated gap) in GAPCON THERMAL-2 to approximately 100% in FRAPCON-2 (PELET mechanical subcode). Many codes use a prompt fraction of about 40-50%.

The low-powered IFA-527 assembly, however, which operated at less than 20 kW/m (6 kW/ft) lifetime peak, has just been examined in PIE, and its fuel cross-sections reveal minimal cracking and relocation, as discussed in the next section.

---

*In the Halden Project, a third way is being investigated, which consists of squeezing the rod between two knife edges and recording load-deflection curves. This has been done both in hot cells and in-reactor.

III - IFA-527 DESCRIPTION AND PERFORMANCE

IFA-527 was an instrumented Halden Reactor test assembly, fabricated and operated for the purpose of monitoring the progress of fuel relocation. The BWR-sized rods were filled with xenon gas to prevent the fission gas release thermal feedback mechanism from interfering with estimation of gap size changes with time. The gap size changes were inferred from measured fuel centerline temperatures. In order to obtain representative fuel temperatures with the low-conducting xenon fill gas, the powers were held low. This provided a check on the effect local linear power upon the degree of fuel pellet cracking. A cross-section of a typical IFA-527 rod (230 μm fabricated diametral gap, BWR 8 x 8 sized pellet) is presented in Figure 3. The degree of cracking is minimal and it is apparent that the relocation was also minimal.

The measured temperatures in the IFA-527 rods also support the conclusion that, at least over the first month of operation, the relocation was minimal. This is emphasized in Figure 4, where measured fuel temperatures are compared against calculated temperatures from a fairly standard fuel performance code GAPCON-THERMAL-2 (GT-2). Two degrees of fuel relocation were assumed for the calculations. Both the magnitude and the slope of the observed temperature versus power curves are poorly predicted by the calculations. The gap size associated with calculated power/temperature points is output by GT-2. A similar effective gap size may be inferred from the measured temperatures by making assumptions (fuel conductivity, flux depression, etc.) similar to those used in the code. The gap size inferred from this data is plotted in Figure 5, and is clearly much larger than that obtained from the commonly applied "prompt fraction" of relocation equal to approximately 50% of as-fabricated gap.

Finally, Figure 6 is presented to demonstrate the lack of time/burnup dependence for the relocation in these low-powered rods. Over the first month of operation, the IFA-527 fuel temperatures (measured in five replicate rods containing 10 thermocouples) failed to significantly decrease at all. However, many fuel modeling codes would predict a temperature decrease (due to a time-dependent increase in fuel relocation) similar to the one indicated. There is apparently a power dependence to the speed of relocation as well as to the value of the "prompt fraction" of relocation.

IV - IMPLICATIONS FOR FUEL ROD PERFORMANCE COMPUTER PROGRAMS

The idea of a power dependence for fuel cracking and relocation is certainly not new. A weak dependence was discernible even within the highly scattered data on cold post-irradiation residual gap sizes which formed the basis of the original GAPCON-THERMAL-2 relocation model.[10] The data presented here from IFA-527, however, point toward a stronger power dependence, and one that is of a "threshold" nature rather than a continuous function. The current data indicate a threshold for fuel relocation in BWR-size rods, with the rods quickly attaining significant relocation (approximately 40-50% of the as-fabricated gap) if the local power exceeds 25-30 kW/m, but attaining much less relocation if the local power does not exceed approximately 20 kW/m.

Furthermore, time dependence of fuel relocation appears to be dependent upon the operating power level. A definite decrease in centerline temperature in the first two months of operation was observed in tests where local power exceeds 30 kW/m[7] and was attributed to continued fuel relocation. No such decrease was observed in the IFA-527 rods, which may indicate a threshold power dependence to the rate as well as the magnitude of relocation. If these trends are verified by additional evaluation of data, then NRC relocation models should be altered to decrease the predicted relocation for fuel segments with powers below 20 kW/m. There will be a commensurate increase in temperature and stored energy for these cases). However, the predictions for rod segments with powers above 30 kW/m should remain unchanged.

V - RECOMMENDATIONS FOR FUTURE ACTION

There are several questions which follow from the data and ideas presented here, and which should be answered before modification of existing fuel performance codes is undertaken. For example, do prepressurized, PWR sized rods exhibit the same power range for the relocation threshold that apparently applies to BWR sized rods? It may be, however, that such questions can be answered by careful analysis of existing fuel temperature data and mirostructure data, such that no new tests are actually required.

In any case, the potential impact upon calculated fuel temperatures for "real-world" commercial reactor fuel rods at nominal power is significant enough that a reasoned modification of the NRC fuel performance codes should be made to incorporate the power dependency of fuel relocation.

REFERENCES

1. D. D. Lanning and M. E. Cunningham, "Trends in Thermal Calculations for Light Water Reactor Fuel," (PNL-SA-9938) presented at the Ninth Water Reactor Safety Research Information Meeting, Gaithersburg, MD, October 26-30, 1981.

2. G. A. Berna, et al., FRAPCON-2: A Computer Code for the Calculation of Steady-State Thermal-Mechanical Behavior of Oxide Fuel Rods, NUREG/CR-1845, January 1981.

3. C. E. Beyer, et al., GAPCON-THERMAL-2: A Computer Program for Calculating the Thermal Behavior of an Ocide Fuel Rod, BNWL-1898, November 1975.

4. L. J. Siefken, et al., FRAP-T5 - A Computer Code for the Transient Analysis of Oxide Fuel Rods, NUREG/CR-0840, TREE 1231, June 1979.

5. R. W. Garner, et al., Gap Conductance Test Series-2: Test Results Report for Tests GC 2-1, GC 2-2, and GC 2-3, NUREG/CR-0300, TREE-1268, November 1978.

6. M. E. Cunningham, et al., The Thermal and Mechanical Behavior of a Xenon-Filled Fuel Rod as a Function of Burnup, NUREG/CR-0749, PNL-3075, September 1979.

7. R. E. Williford, et al., The Analysis of Fuel Relocation for the NRC/PNL Halden Assemblies IFA-431, IFA-432, and IFA-513, NUREG/CR-0588 PNL-2709, April 1980.

8. D. D. Lanning and M. E. Cunningham, Startup Data Report for NRC/PNL Halden Assembly IFA-513, NUREG/CR-0862, PNL-2948, July 1979.

9. D. D. Lanning, Beginning-of-Life Data Report for the Instrumented Fuel Assembly (IFA) -527, NUREG/CR-2167, PNL-3831, September 1981.

10. K. P. Galbraith, Pellet-to-Cladding Gap Closure from Pellet Cracking: Data and Analysis, XN-73-17, August 1973.

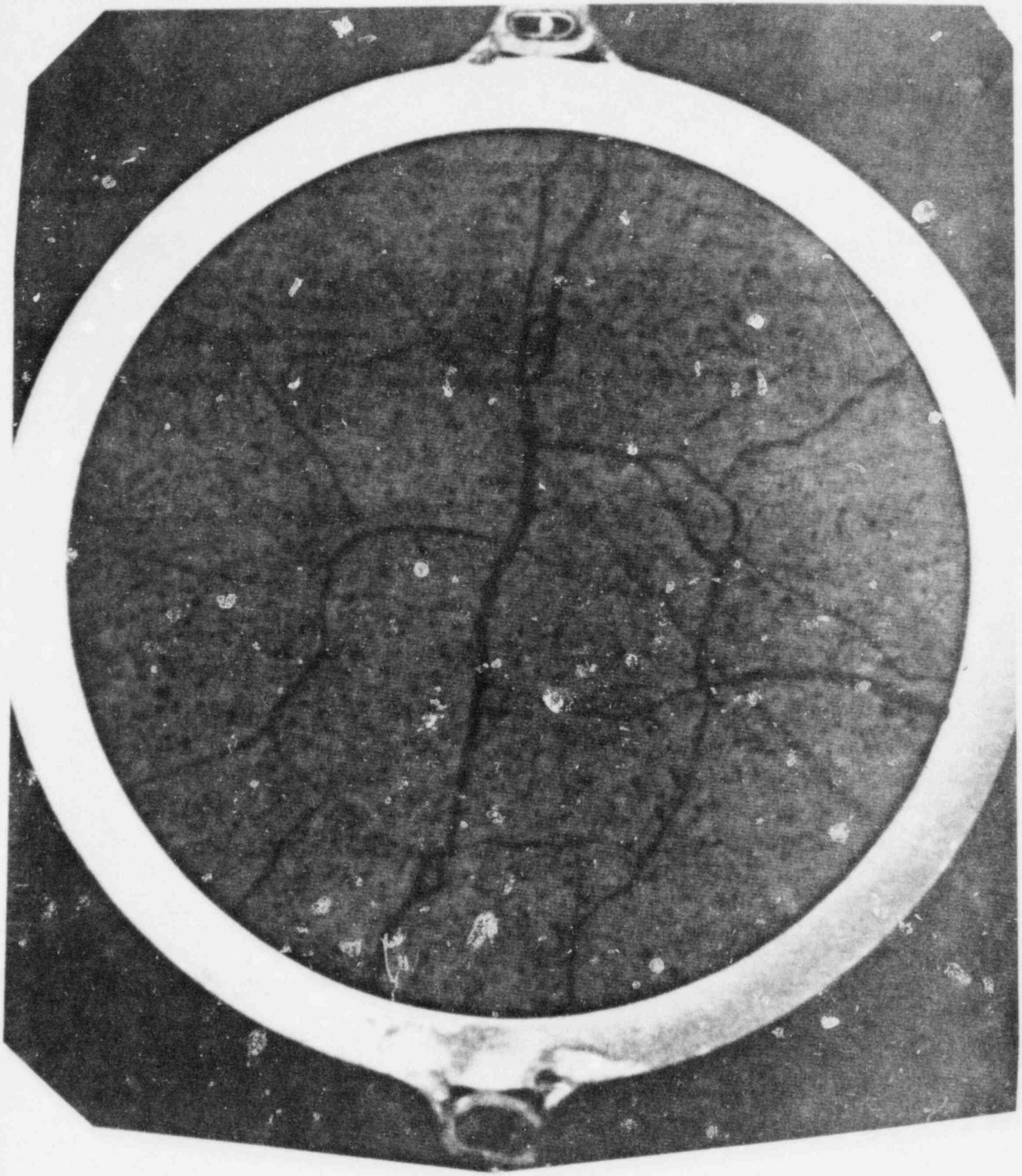

FIGURE 1. Cross Section from Rod 503 of the PBF GC-2 Gap Conductance Test.[5] The peak local power at this elevation was about 30 kW/m; this was a He-filled rod with a 0.23 mm diametral gap.

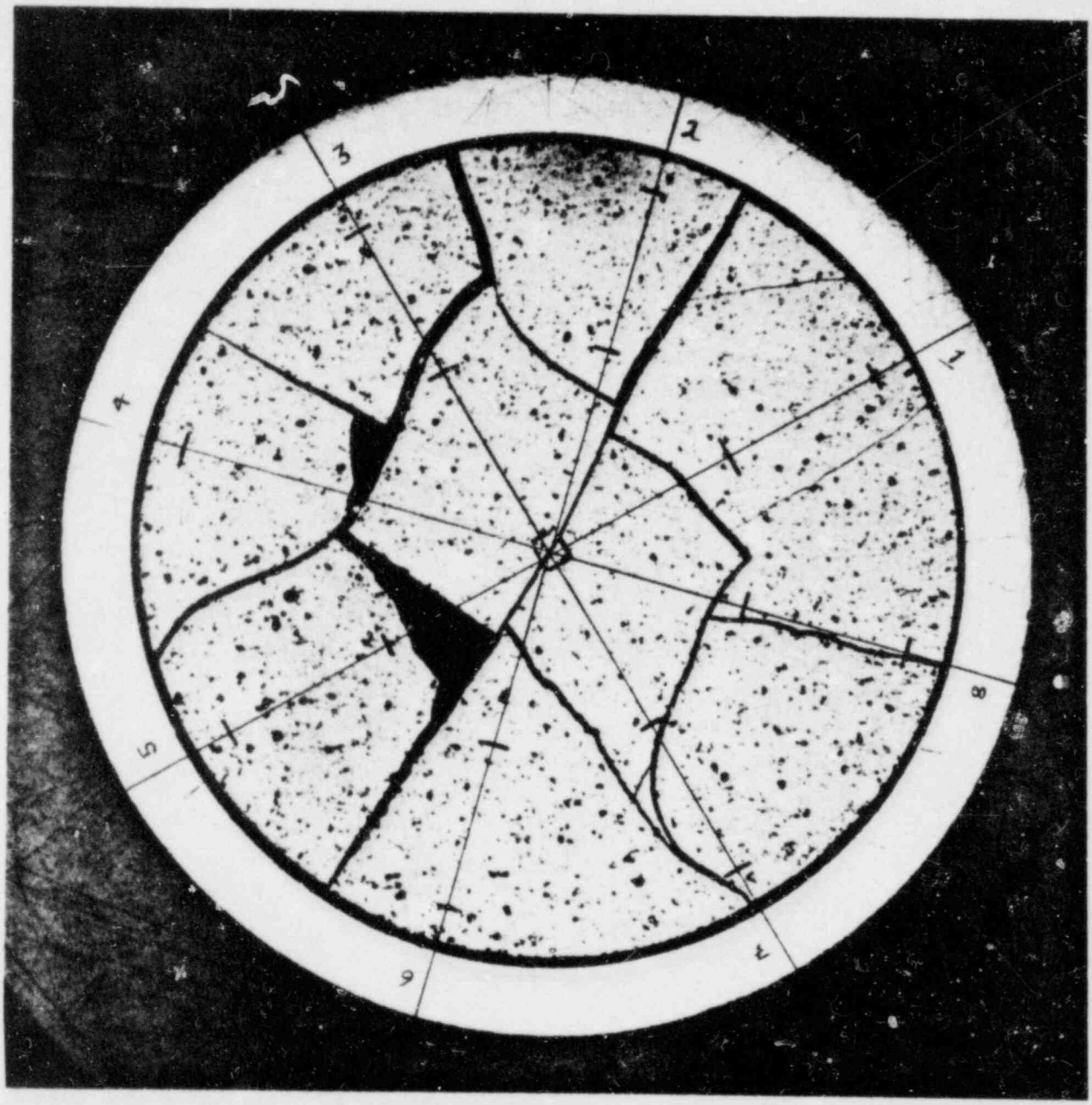

FIGURE 2. Cross Section from Lower End of Halden Test Rod 6 IFA 431. This was a He-filled rod with a 230 μm diametral gap. The peak power at this elevation was about 25 kW/m, and the local burnup was about 3.6 GWd/MTM.

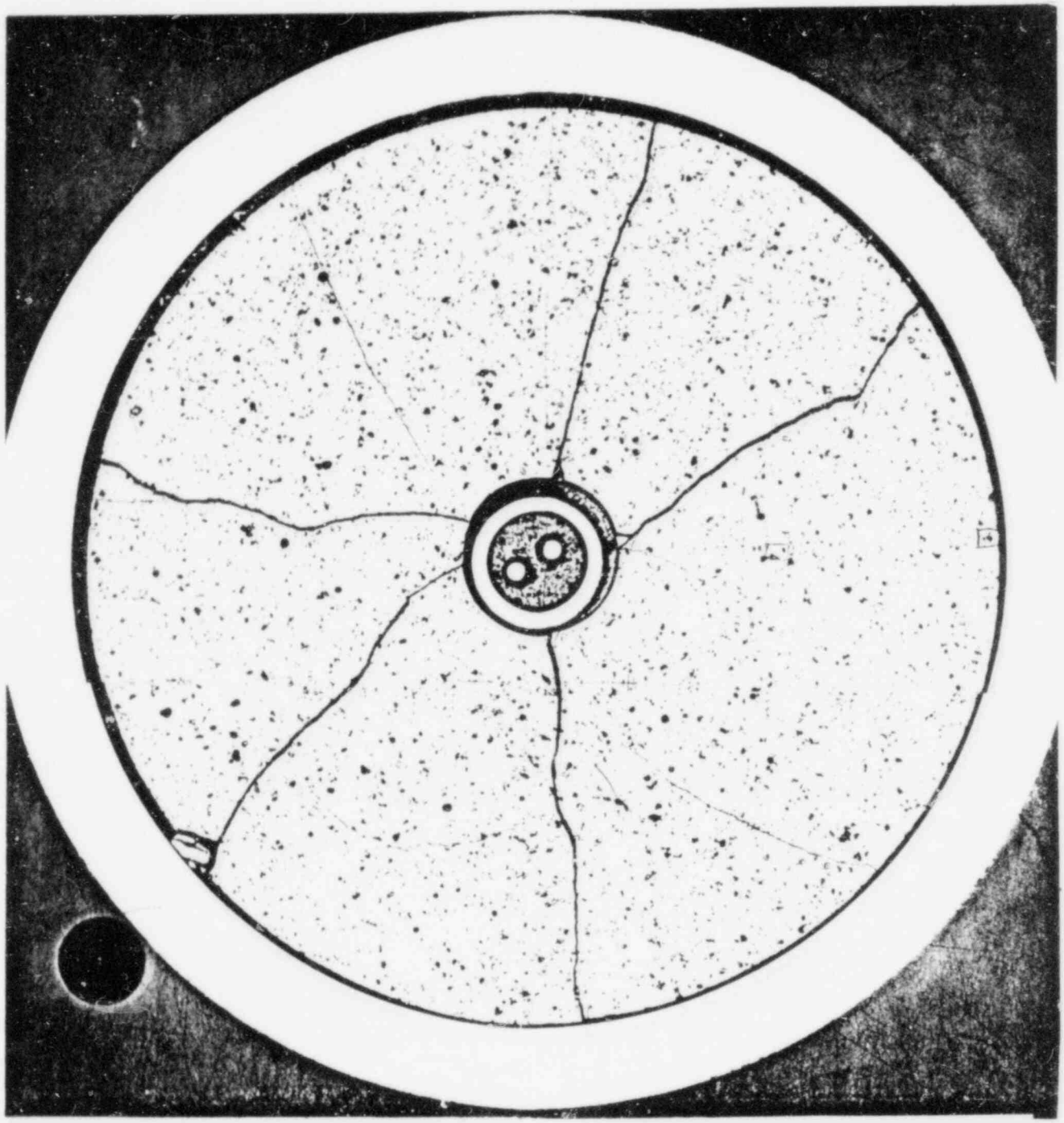

FIGURE 3. Cross Section from IFA-527. The maximum local power attained was 18 kW/m.

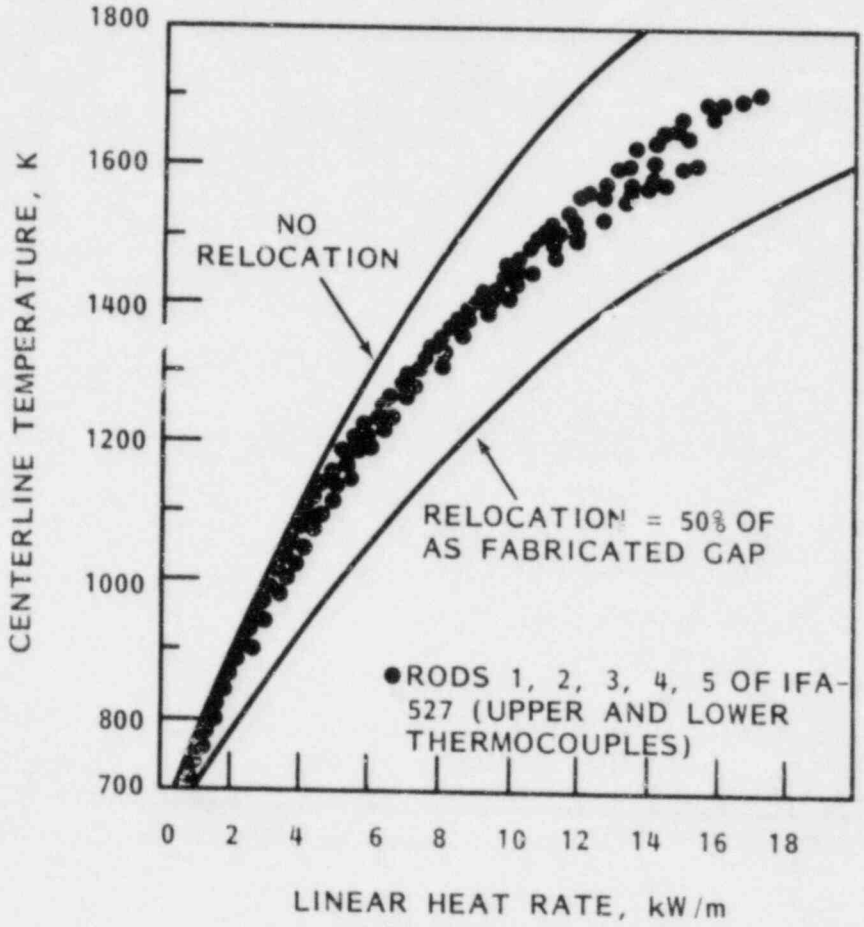

FIGURE 4. Early-in-Life Temperature Versus Power Data for IFA-527 Xe-Filled Rods, Compared to Calculated Temperatures Assuming Two Different Levels of Fuel Relocation

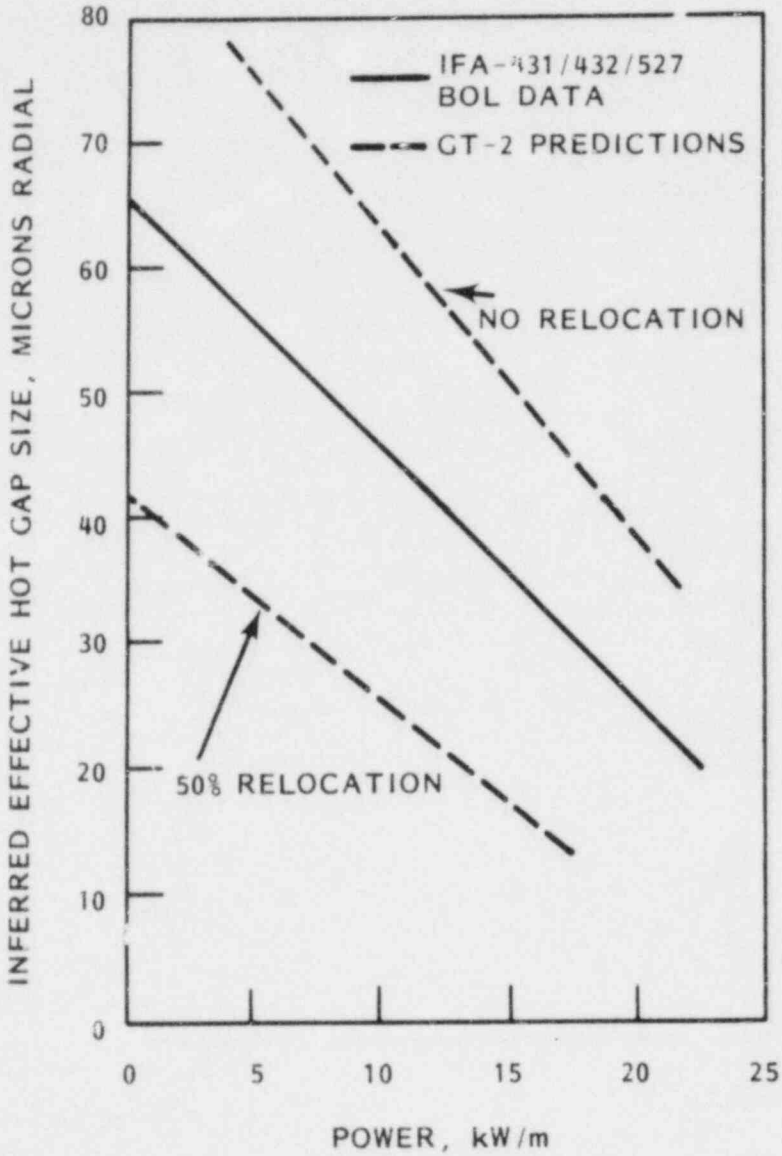

FIGURE 5. Inferred Gap Sizes from the Centerline Temperatures in Figure 4 for Xenon-Filled NRC/Halden Test Rods

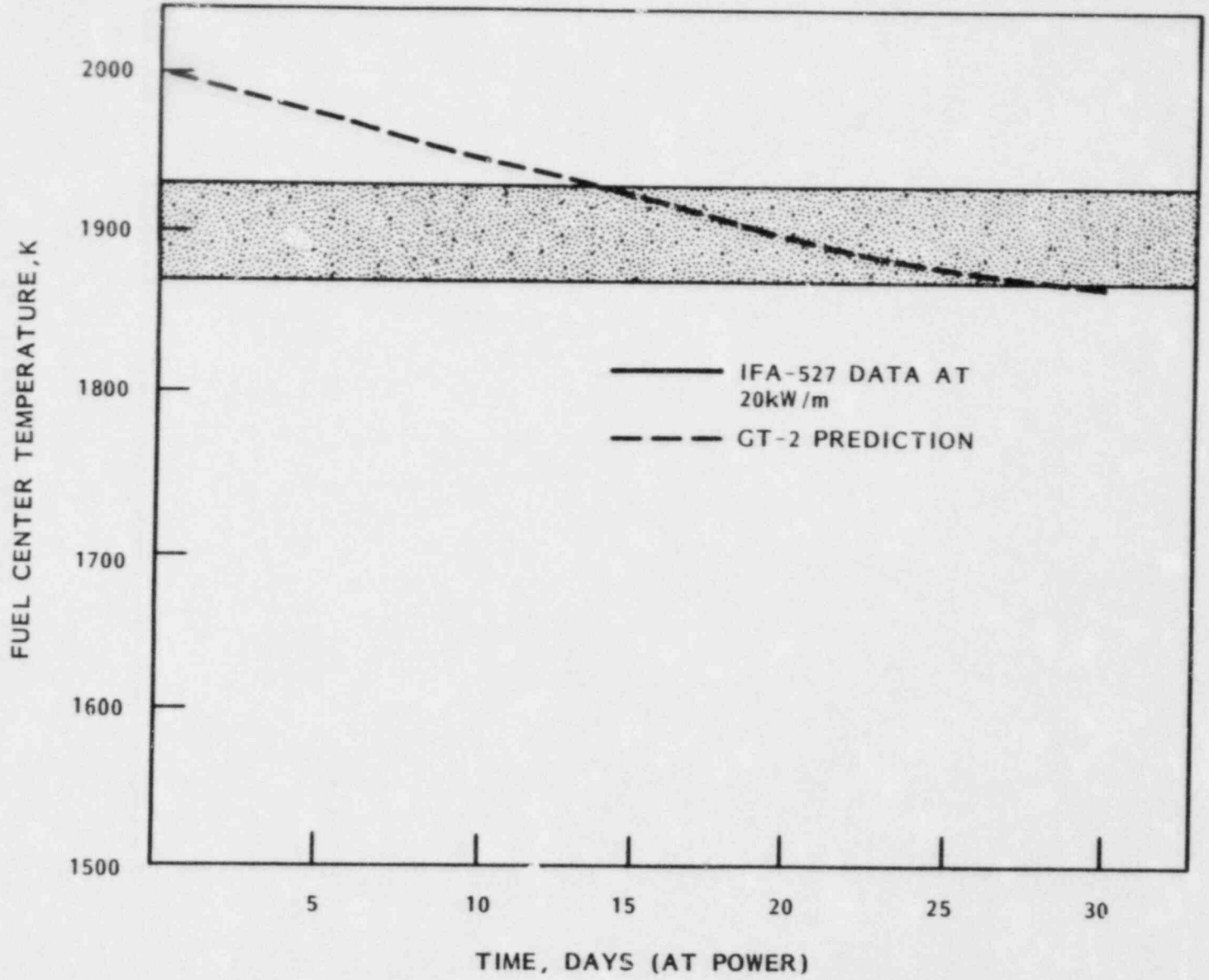

FIGURE 6. Time Dependence of Centerline Temperature for IFA-527 Rods Versus Calculated Behavior from GT-2. Note that it is progressive fuel relocation which causes the calculated temperature decrease. Fuel densification is assumed to be negligible for these highly stable fuel pellets.

CORE RETENTION CONCEPT ASSESSMENT: ALUMINA PARTICLE BEDS*

J. D. Fish

Sandia National Laboratories**
Albuquerque, NM 87185 USA

ABSTRACT

Investigations of the particle-bed core retention concept have shown that molten core material can be retained in a coolable configuration for an extended period of time on a properly designed layered bed. Test results also have shown that coolant is neither necessary nor sufficient to stop initial penetration of the bed by a superheated melt. In fact, delaying the introduction of coolant may have significant advantages in that the production of aerosols and combustible gases is reduced by lowering the temperature at which core/coolant interactions take place.

INTRODUCTION

Both experimental and analytical investigations of various core retention concepts are being carried out at Sandia National Laboratories under the auspices of the U. S. Nuclear Regulatory Commission (NRC), Office of Nuclear Regulatory Research. The objectives of the program at Sandia are to determine the fundamental limitations of the various concepts and to develop a data base for use by the NRC in licensing review of proposed ex-vessel core retention designs.

The primary functional requirement of a core retention device is to prevent the contact of either molten or hot solid core debris with the basemat of the reactor. The core retention device should contain the debris in such a manner that the decay heat can be dissipated without introducing further hazards to the integrity of the reactor containment structure. Specifically, the interaction of core debris with the core retention device should not produce large amounts of hydrogen, aerosols, or energy (from exothermic chemical reactions). Reducing these various source terms instead of attempting to handle them after their generation is a unique feature of core retention when compared to other mitigation concepts, such as filtered vents and hydrogen burners. In fact, core retention can play a synergistic role to such devices by reducing the load to them.

Results of scoping tests on concepts based on castable ceramics, steel liners, sacrificial beds, refractory brick crucibles, and particle beds were reported earlier [1]. Over the past year, the particle-bed concept has been the focus of more detailed considerations

*This work sponsored by the United States Nuclear Regulatory Commission

**Operated for the United States Department of Energy under Contract number DE-AC04-76DP00789

[2,3]. A summary of the investigations of the particle-bed concept is presented here.

A particle-bed core retention device, in its simplest form, is a bed of loose refractory particles poured into the cavity of a reactor between the primary vessel and the concrete basemat. Based on the advantage that such a device could be installed easily and quickly into existing reactor cavities where space is minimal and radiation levels preclude extensive modifications, particle-bed retention devices were originally proposed for retrofit of existing reactors. Results of testing at Sandia indicate that a particle bed can retain molten core debris and protect the basemat of a reactor for a short period of time (few hours) with no cooling and for an extended period of time with only passive cooling. The tests showed, however, that the minimum configurational requirement on a particle-bed core retention device that meets the functional requirements described above is a layer of smaller particles sandwiched between layers of larger particles. The role of each layer is discussed with the test results below.

TEST RESULTS

Eleven tests of the particle-bed concept were conducted. The test bed was composed of thoria particles in two of the tests, alumina particles in eight of the tests, and a combination of thoria and alumina in one test. Melts ranging from 2.8 kg to 25 kg were generated either by inductive heating of stainless steel slugs or by iron oxide/aluminum thermite reactions. In the former case, the melts were generated in place on top of the beds. In the latter case, the melts were dropped onto the beds from the reaction vessel. Two of the thermite tests involved sustained heating by inductive coupling to the iron phase of the melts. The thermite reaction produces a melt temperature of approximately 2700 K. With inductive heating at 1.0 W/g, melts were sustained at approximately 1700 K for up to several hours. Three of the tests, including one of the sustained thermite tests, were water cooled. Two of the tests involved the ejection of thermite melt from a vessel at high pressure.

The importance of a layered bed was clearly demonstrated by the tests. To assure long-term removal of decay heat from debris contained by a particle-bed device, the particles in the lower portion of the bed must be sufficiently large (> 1-2 cm) to allow flow of coolant under and around the debris. The ability to cool the bottom of contained debris is an inherent advantage of the particle-bed concept over those in which the debris is contained on a non-porous structure where only the top of the debris can be cooled. If the entire bed were composed of large particles, however, a superheated melt would rapidly penetrate the bed--even if the bed were completely filled with coolant. Both the rate and the depth of melt penetration into water-filled beds were the same as those measured with dry beds of particles of the same size. See Figure 1. On the other hand, in agreement with the PLUGM code predictions [4], thin layers of small particles (< 0.3-0.4 cm) effectively stopped the melt by a combination of surface tension effects and conduction freezing in both dry and water-filled beds. Stopping the melt before it reaches the large coolant pathways in the lower level is critical if the core retention device is to serve its purpose of preventing core/concrete interactions.

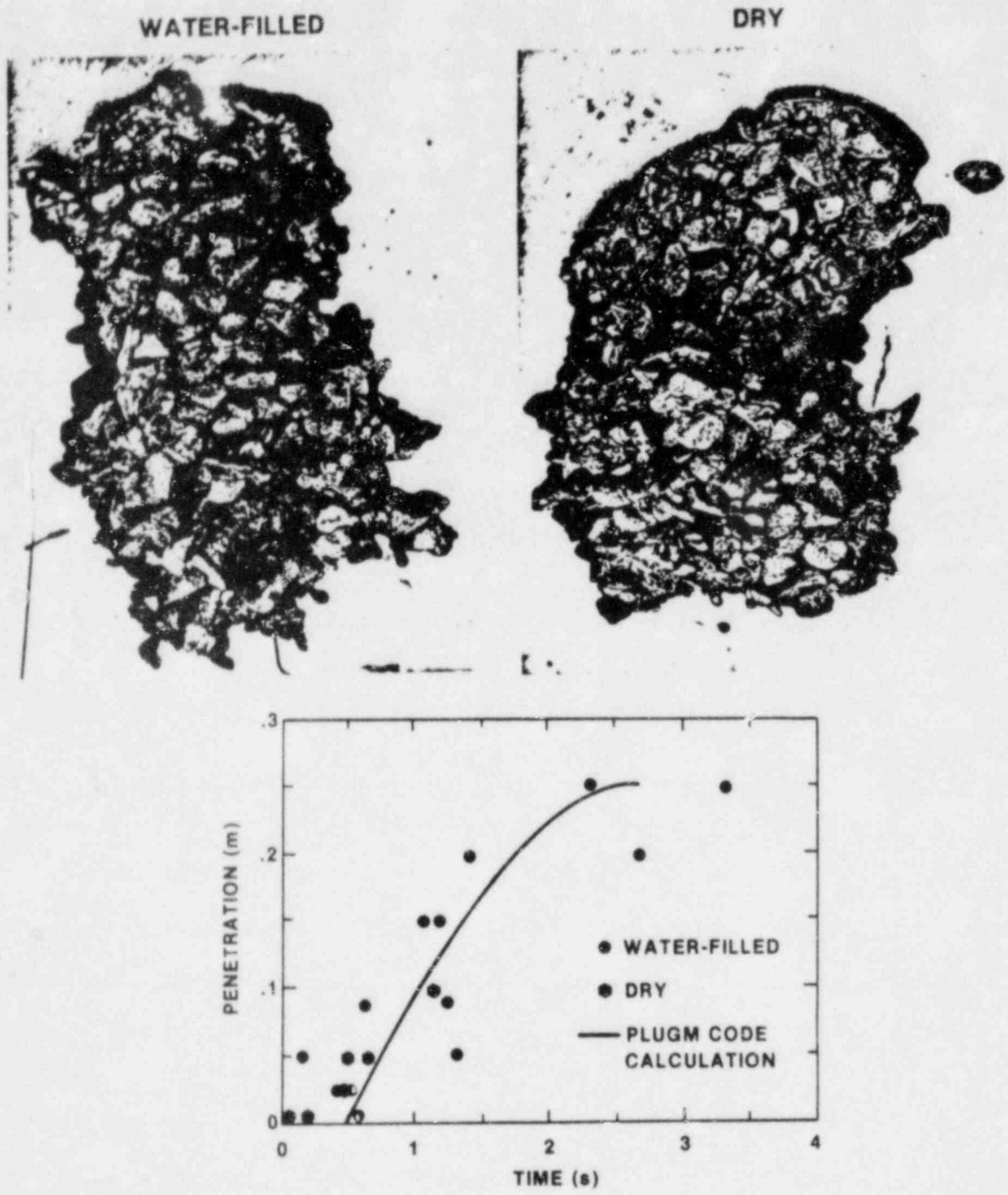

Figure 1.
Penetration of large particles by superheated melt

The role of the top layer of large particles, which is readily penetrated by a superheated melt, is to dilute and quench the core debris. Tests have shown that a superheated melt not only penetrates the large particles downward but also spreads laterally through them. Heat flux from the debris is reduced both by the increase in the surface to volume ratio and by the reduction in temperature.

The top layer of large particles also addresses one of the possible failure modes for a particle-bed device: sweep-out of the loose particles by some event in the accident sequence. Such events include 1) high velocity melt streaming which might occur as a result of failure of a small section in the bottom of the pressurized primary vessel of a light water reactor, and 2) energetic fragmentation resulting from the contact of molten reactor material and coolant in either light water or liquid metal reactors. Resistance to sweep-out is directly related to the size of the particles. Furthermore, penetration of a layer of large particles by melt may be instrumental in preventing an energetic fragmentation of the melt from occurring ex-vessel. The matrix of melt and particles prevents the intimate intermixing of melt and coolant that is required for such an event. In none of the tests in which thermite melts at 2700 K were dropped onto water-filled beds was there any indication of a violent interaction between the melt and the water. There was no steam explosion, no disruption of the bed, and little fragmentation of the melt. The melt simply pushed the water through the large particles ahead of it.

Tests are currently underway to determine the quantitative relationship between resistance to sweep-out and such parameters as particle size, bed depth, and physical constraints. Two recent tests in which melt was ejected onto particle beds from pressure vessels at 700 and at 1100 psi indicate that several thicknesses of particles larger than a few centimeters in diameter may be sufficient to prevent gross failure of a particle bed.

Finally, results of the tests on the particle-bed concept and of preliminary design calculations based on these results, suggest that a viable strategy for mitigation of the early stages of an ex-vessel accident in an LWR reactor outfitted with a particle-bed core retention device is to maintain a dry cavity. Ex-vessel quenching of the core debris simultaneously with blowdown of the primary vessel would further aggravate the threat to containment posed by the steam and the hydrogen produced in-vessel. Furthermore, delaying the introduction of water until the debris has had time to come to thermal equilibrium with the large particles would reduce the rate of the hydrogen producing reactions between the water and the metal components of the debris. Likewise, the rate of aerosol production would be reduced. The relative hydrogen concentration as a function of time for one of the tests in which thermite was dropped onto a water-filled bed is shown in Figure 2. Note how quickly the concentration of hydrogen decreases as the melt is quenched. These data were obtained from grab samples taken directly above the particle bed. The concentration of hydrogen in a sample, therefore, is a direct indication of the rate of hydrogen production. Similar results* were obtained in a test in which the melt was sustained by induction heating. Even with continued heating, the rate of hydrogen production remained low after the initial quench.

*See Reference 2 for a plot of these results.

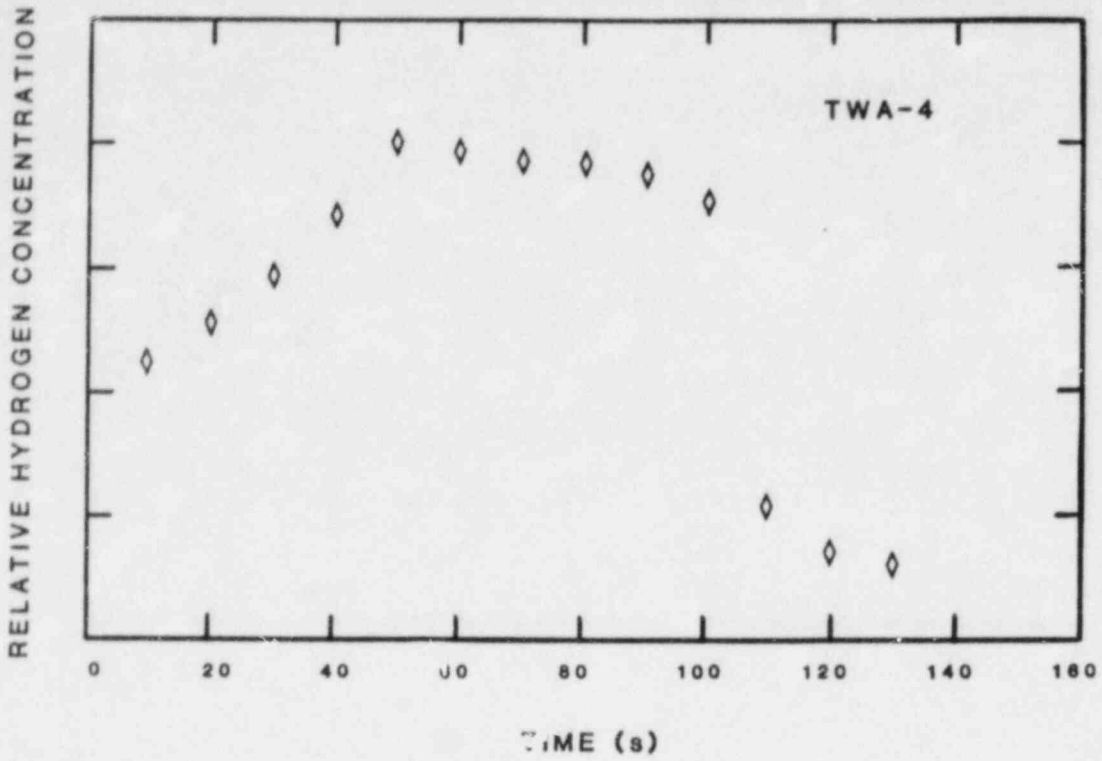

Figure 2.
Hydrogen production from a thermite melt on a water-filled bed

The test results shown in Figure 3 illustrate the possibility for delaying the introduction of water. In this test, a 10 kg thermite-generated melt was dropped onto a dry, layered alumina bed. The melt was sustained after deposition by inductive heating at a power into the melt of approximately 1 W/g. As indicated in the figure, the melt quickly penetrated the top layer of large (1-2 cm dia.) particles and was stopped by conduction freezing at the interface with the layer of small (0.3-0.4 cm) particles. Over the next half hour the top portion of the bed heated up to the melting point of the iron phase of the charge. Penetration then proceeded through the layer of small particles with the location of the melt front at a given time corresponding roughly to the point at which the particles had locally reached the melting point of iron. Once the melt reached the bottom layer of large particles, it quickly dropped to the bottom of the test bed. This test was repeated with water flowing through the bottom layer of large particles. Although heating was continued for approximately 10 hours, the melt never moved beyond the boundary between the top layer of large particles and the middle layer of small particles. The melt did spread laterally in the top layer. Together, these two tests indicate that coolant is not necessary in the short-term but must be added at some point to prevent the eventual penetration of the particle bed.

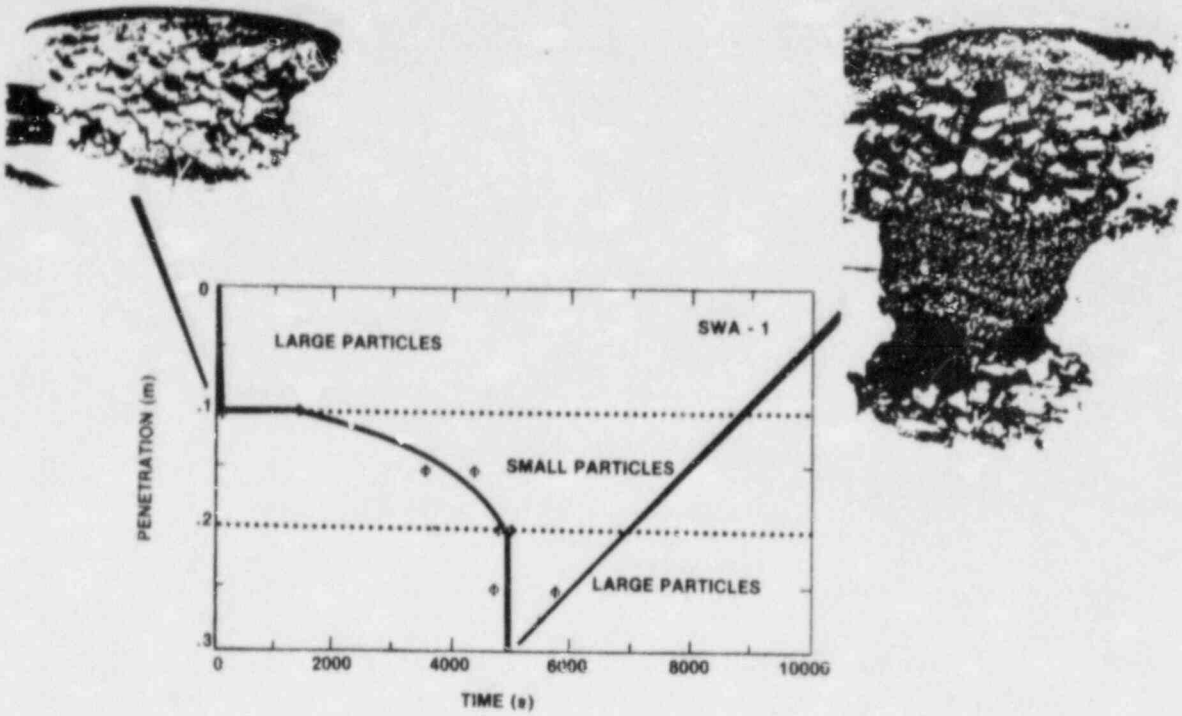

Figure 3.
Penetration through a layered bed with sustained heating (1 W/g)

Currently, calculations are underway to extrapolate the results of these tests to reactor conditions in a full-scale core retention device. The preliminary results shown in Figures 4 and 5 are for the bounding assumptions 1) that all of the urania (98,000 kg) drops onto the layered alumina bed, and 2) that all of the heat stays in the bed (i.e., no account is taken of loss of heat to overhead structures or the sidewalls of the cavity). The calculations will be expanded soon to account both for heat losses and for the actual composition and temperature of the melt. Both effects will extend the times at which the indicated events occur. The decay heat input to the debris in these calculations is based on a delay of one hour between reactor scram and deposition of the melt onto the bed. This assumption corresponds to a decay heat at time of deposition of 0.4 W/g.

Figure 4 shows the temperature history and melt progression for a top layer thickness of 0.5 m averaged over an area corresponding to that available in a typical LWR cavity. The penetration follows the same trend as that shown in Figure 3. In this case, the bed slowly heats up to the eutectic temperature of urania and alumina (2200 K) at which point the top layer starts melting. Once the top layer is molten and the middle layer has heated up, the molten pool starts working its way down through the bed. Assuming that the particles in the middle layer are sufficiently small, this penetration is by melting and not by flow.

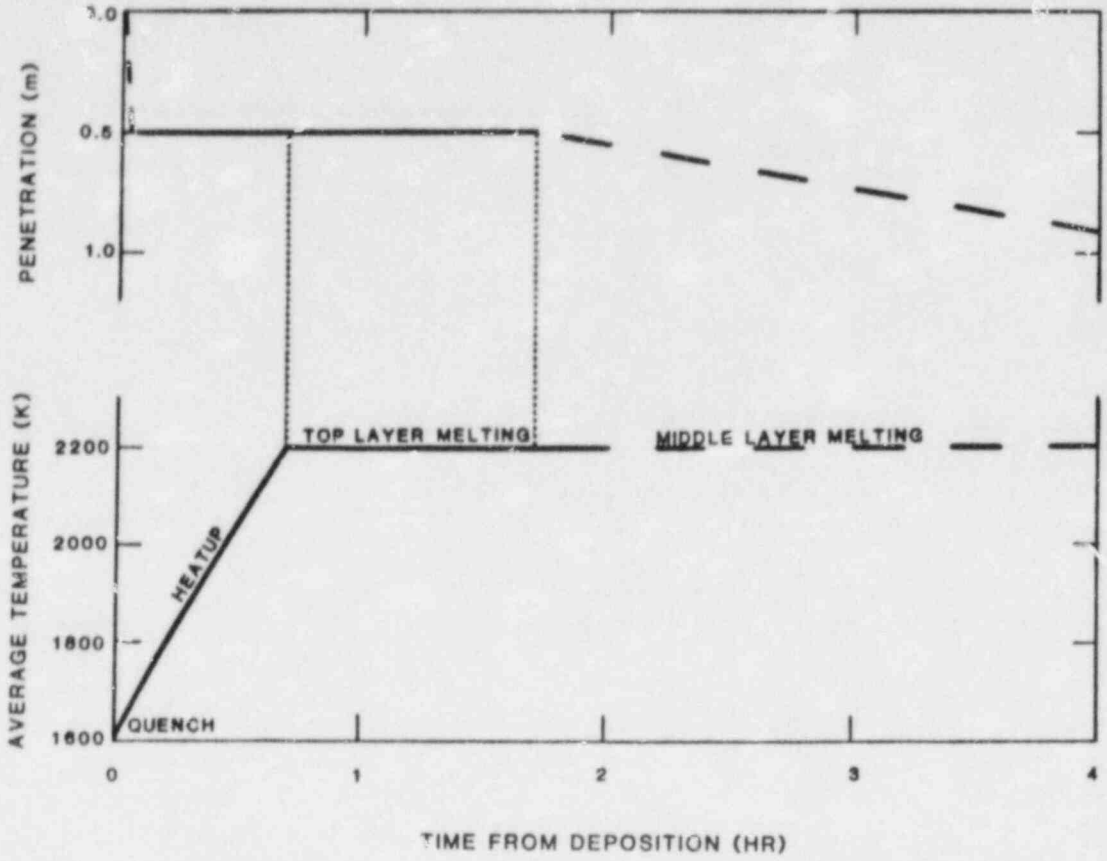

Figure 4.
Example: Molten urania onto a layered alumina bed
0.5 m top layer

Figure 5 is a generalized curve for an arbitrary top layer thickness followed by a 0.25 m layer of small particles and a layer of large particles of some thickness (for coolant flow). Depending on the space available between the primary vessel and the basemat, considerable time can elapse before it becomes necessary to add water to prevent further penetration.

SUMMARY

Although the results of the tests described above need to be scaled up before definitive conclusions can be drawn, the particle-bed core retention concept appears to offer a number of possibilities for severe accident mitigation. Indications are 1) that a properly designed bed can control the initial location of ex-vessel debris without a requirement for coolant, and 2) that a significant amount of time would be available before it becomes necessary to add coolant to prevent further penetration of the bed by the decay-heated debris.

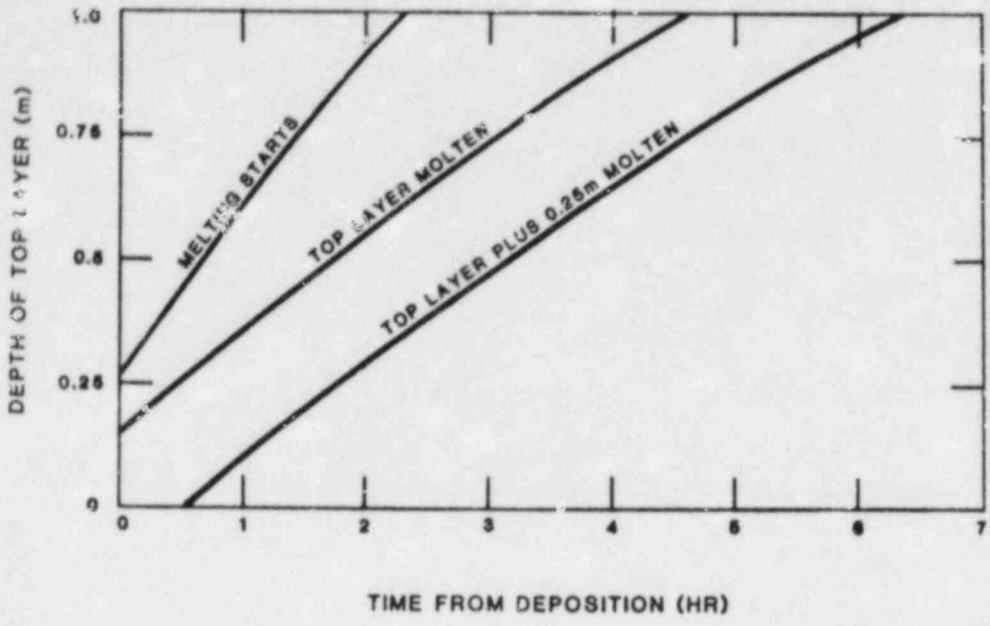

Figure 5.
Example: Molten urania onto a layered alumina bed
Top layer from 0 to 1 m thick

REFERENCES

1. J. D. Fish, "Core Retention Assessment Program at Sandia National Laboratories," presented at Ninth Water Reactor Safety Research Information Meeting, Gaithersburg, MD, USA, 26-30 October 1981.

2. J. D. Fish, M. Pilch, and F. E. Arellano, "Demonstration of Passively-Cooled Particle-Bed Core Retention," presented at International Topical Meeting on Liquid Metal Fast Breeder Reactor Safety and Related Design and Operational Aspects, Lyon, France, 19-23 July 1982.

3. J. D. Fish, M. Pilch, and F. E. Arellano, "Particle-Bed Core Retention Concept Assessment," presented at Information Exchange Meeting on Post Accident Debris Cooling, Karlsruhe Nuclear Research Center, Germany, 28-30 July 1982.

4. M. Pilch and P. K. Mast, "PLUGM: A Coupled Thermal-Hydraulic Computer Model For Freezing Melt Flow in a Channel," SAND82-1580, Sandia National Laboratories, (In Press).

PLUGM: A Coupled Thermal-Hydraulic Computer Model For Freezing Melt Flow In a Channel*

Marty Pilch
Sandia National Laboratories**
Albuquerque, NM 87185
Division 9425

1. Introduction

PLUGM[1] is a coupled thermal-hydraulic computer model for freezing liquid flow and plugging in a cold channel. PLUGM is being developed at Sandia National Laboratories for applications in Sandia's ex-vessel Core Retention Concept Assessment Program and in Sandia's LMFBR Transition Phase Program. The purpose of this paper is to introduce PLUGM and demonstrate how it can be used in the analysis of two of the core retention concepts under investigation at Sandia: refractory brick crucibles and particle beds.

A magnesia brick crucible has been proposed for floating nuclear plants. The refractory brick concept has also been suggested for LMFBR plants, including Clinch River. One disadvantage of the brick crucible concept is the design requirement for some spacing between bricks to allow for thermal expansion. This spacing introduces a major failure mode. Penetration of the spaces by melt could initiate catastropic and rapid failure of the crucible by eroding the interlocking network and freeing bricks to float away. Even without gross failure, penetration of the spaces could lead to premature contact of themelt with the underlying concrete or with cooling channels placed in the brick structure. Failure of brick core retention devices by gap flow is not treated in current thermal modeling of these devices because the structure is assumed monolithic. In Section 4, three sample problems involving steel melt seepage into a Harklase (MgO) core retention device are used to illustrate some of PLUGM's capabilities in this area.

For near-term retrofit of existing reactors, the particle-bed concept appears particularly attractive. This type of protection, consisting of layers of loose particles, could be installed easily and quickly into reactor cavities where space is minimal and radiation levels preclude extensive modifications. The major

* This work sponsored by the United States Nuclear Regulatory Commission.

** Operated for the United States Department of Energy under Contract No. DE-AC04-76DP00789.

advantage of the particle-bed concept for both new and existing reactors is the inherent coolability of debris contained on a porous support. Coolant can flow under and around the debris as well as across the top. Design of the particle bed, however, must be such that molten debris does not rapidly flow through the bed downward to the concrete basement or horizontally to the sidewalls of the cavity. PLUGM is the only analytic tool which models melt flow and freezing in a particle bed. Comparison of PLUGM calculations with experimental data has been reported earlier [2,3].

2. PLUGM Code Description

Conceptually, PLUGM models time dependent melt flow from a reservoir, through a channel, and possibly into a dump tank. Convective heat transfer to the wall or crust (solidified melt) cools the melt as it flows along the channel. Crust deposition on the channel wall is controlled by the competing effects of convective heat transfer from the bulk liquid to the crust surface and the conduction limited removal of heat from the crust surface into the wall substrate. Heat conducted through the crust causes the wall to heatup. An external coolant cools the wall should the wall thermal front reach the outer wall surface.

PLUGM's geometry capabilities enable realistic modeling of many problems. Three user specified channel geometry options currently exist: 1) tube, 2) thin slit, and 3) particle bed. Axial variation (i.e., in directions of flow) of five channel parameters is possible by breaking the channel into an arbitrary number of regions. The five channel parameters which can be varied axially are 1) flow direction i.e. with gravity, against gravity, or horizontal, 2) channel diameter, 3) channel wall thickness, 4) initial wall temperature, and 5) external coolant heat transfer coefficient.

PLUGM's hydrodynamics calculations are based on a finite-difference axial formulation. Inertial effects are included by solving the complete one dimensional momentum equation. Available is an alternate option which assumes quasi-steady flow; a modified Bernoulli equation is used to calculate consistent velocities at the end of each time step.

Melt flow is driven by one or more of the following: 1) applied pressure, 2) gravity, or 3) capillary pressure. Note that any of these can also be a retarding force depending on the problem. PLUGM's hydrodynamics also account for 1) friction losses (laminar or turbulent flow), 2) recoverable Bernoulli losses due to flow area changes, and 3) non recoverable losses due to sudden expansions, contractions, or changes in flow direction (i.e., elbow losses).

PLUGM allows for arbitrary mass addition to the reservoir or trailing edge node. PLUGM also accounts for the film deposition at the trailing edge of the flow in the event that mass addition is insufficient to prevent draining of the inlet reservoir. Thus,

mass depletion of the liquid material by crust and liquid-film deposition is calculated.

PLUGM models time-dependent convective heat transfer from the melt to the crust or directly to the channel wall if no crust exists. An axial finite-difference formulation is used. The melt can be saturated or superheated, and the flow can be laminar or turbulent. The fluid can be a normal fluid or a liquid metal.

Coupled crust-growth (or decay) and wall-heatup parameters are obtained from numerical solution of coupled first-order differential equations at each axial node. The differential equations are obtained from an energy integral analysis in which temperature profiles in the crust and wall are assumed to be a time-dependent combination of first-order and second-order spacial terms. The equations fully account for the time-dependent heat flux from the melt into the growing crust at each axial node. The influence of an external coolant is included when the wall thermal layer passes through a channel wall of finite thickness. The time-dependent crust/wall contact temperature is uniquely defined by the coupled equations. Wall melting solutions, which are required when the crust/wall contact temperature exceeds the wall melting temperature, are not currently available, however, their addition is planned.

The following time-dependent information is calculated at each melt-containing channel node: 1) bulk melt temperature, 2) crust thickness, 3) crust temperature profile, 4) crust/wall or melt/wall contact temperature, 5) wall thermal layer thickness, 6) wall temperature profile, 7) external-coolant/wall contact temperature, and 8) velocity. From this information, the complete history of melt penetration into the channel can be constructed. Integral information such as final total penetration and total plugging time are also provided to the user.

3. PLUGM Code Verification

Efforts are currently under way to find applicable experiment data and test problems that are suitable for PLUGM code verification. Data published by Chun[4] et al from BNL has been used in the initial code verification effort.

Chun et al's experiment apparatus is shown in Figure 1. Molten Wood's metal ($T_m=73^{\circ}C$) is heated until a superheat of $22^{\circ}C$ is obtained. A plug is pulled, and the molten Wood's metal passes through a 74.5 cm long brass tube (ID = 1.107 cm) into a dump tank. Surrounding part of the brass tube flow channel is a 60 cm long counter flow cooling jacket; the coolant (water) inlet temperature is about $15.5^{\circ}C$.

Chun et al measured the time-dependent mass collected in the dump tank. Their experiment data is shown in Figure 2. Immediately obvious is the relatively large amount of scatter in the mass displacement histories, total displaced mass, and total

flow times. The source of this scatter is not known since each experiment was run under nominally identical conditions.

PLUGM used a six region representation of Chen et al's experiment. The first region was the reservoir and the second region was an adiabatic channel section penetrating the reservoir tank, heater coil, and insulation. The initial wall temperature in each of the first two regions was set equal to the Wood's metal temperature in the reservoir. The third region had an adiabatic external surface; the initial wall temperature was taken as the average of the regions above and below it. The fourth region was in the coolant jacket; time dependent heatup of the external counter flow coolant was modeled. The initial wall temperature was set equal to the coolant inlet temperature. The fifth region was a short adiabatic section; the initial wall temperature equal to the coolant inlet temperature. The sixth region was the dump tank.

The results of two PLUGM calculations are shown in Figure 2; a fully coupled thermal-hydraulic calculation for comparison with the data, and a pure hydrodynamic calculation (no crust growth or plugging) for reference. Also shown in Figure 2 are the results of three models that Chun et al compared to their data.

PLUGM does an excellent job of predicting the observed mass displacement history. PLUGM predicted total displaced mass and total flow time are also consistent with several of the experiment runs shown. Further modeling improvement can only be made, if needed, when the source of the data scatter is understood.

4. Ex-Vessel Core Retention

This section presents three sample problems that illustrate how PLUGM can be used in the assessment of ex-vessel core retention devices composed of Harklase (MgO) bricks. The first example considers a .1 m pool of molten steel over a vertical crack. Such a crack might be formed by thermal or mechanical stresses when the melt falls onto the core retention device. The intial wall temperature in the channel is taken as 300 K.

Figure 3 shows the expected penetration for various crack spacings. First note that no penetration is predicted for crack spacings less then .5 mm; surface tension prevents flow into these small cracks. Note also that the penetration distance significantly increases with melt superheat. PLUGM predicts that the initial channel constriction occurs at that point in the channel where all superheat is stripped from the bulk melt. This is at the channel entrance for a saturated melt, and progressively further downstream of the channel entrance for increasing melt superheats.

The second sample problem considers a .1 m pool of molten steel over a brick matrix (initially T = 300 K) with uniform spacing, D. This problem illustrates melt flow and plugging in

tortuous channels. Penetration depths for various brick spacing are shown in Figure 4.

Three features distinquish this problem from the previous one. First, pressure losses due to sudden changes in flow direction impede flow into the brick stack. Secondly, an increment of melt flow along a horizontal brick surface does not result in an increment in the total gravity head; this also results in less flow. Thirdly, horizontal flow does not contribute to an increase in the actual depth of penetration. This later point is represented by the horizontal curve segments shown in Figure 4.

The third sample problem considers plug remelt followed by secondary flow and plugging. Again, consider a .1 m pool of molten steel (2000 K) over a brick stack with 1 mm spacing. Initial penetration into the cold (300 K) brick stack is .049 m; this is illustrated in Figure 5.

As time passes, the brick stack heats up. After 4.8 h the melt isotherm (T = 1700 K) reaches the leading edge of the initial plug, and the melt can once again flow. Just prior to remelt, the melt slug and the wall have the temperature distribution shown in Figure 6; these temperature distributions can be modeled by PLUGM. Following remelt, the steel penetrates an additional .115 m into the brick stack before plugging is again calculated. This is illustrated in Figure 6.

IV. Conclusions

PLUGM is a tool which can now be used to investigate melt seepage and plugging in complex geometries such as a brick matrix or a particle bed. Code verification, required to achieve confidence in PLUGM's predictions, is continuing.

References

1) M. Pilch and P. K. Mast, PLUGM: A Coupled Thermal-Hydraulic Computer Model For Freezing Melt Flow In a Channel, SAND82-1580, to be published.

2) J. D. Fish, M. Pilch, and F. E.Arellano, "Demonstration of Passively-Cooled Particle-Bed Core Retention," presented at International Topical Meeting on Liquid Metal Fast Breeder Reactor Safety and Related Design and Operational Aspects, Lyon, France, 19-23 July 1982.

3) J. D. Fish, M. Pilch, and F. E. Arellano, "Particle-Bed Core Retention Concept Assessment," presented at Information Exchange Meeting on Post Accident Debris Cooling, Karlsruhe Nuclear Research Center, Germany, 28-30 July 1982.

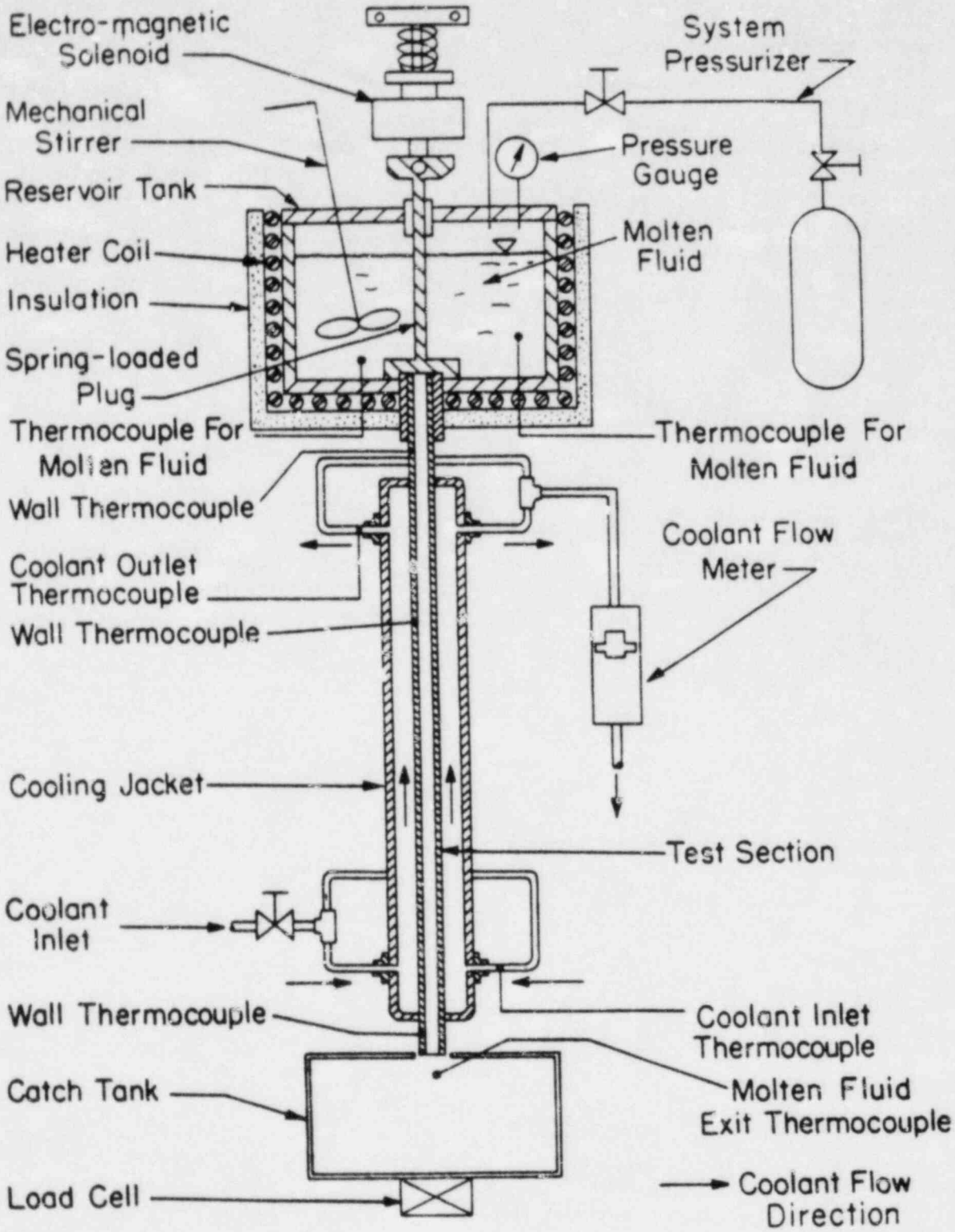

Figure 1: Chun et al.'s test apparatus for transient mass displacement measurements

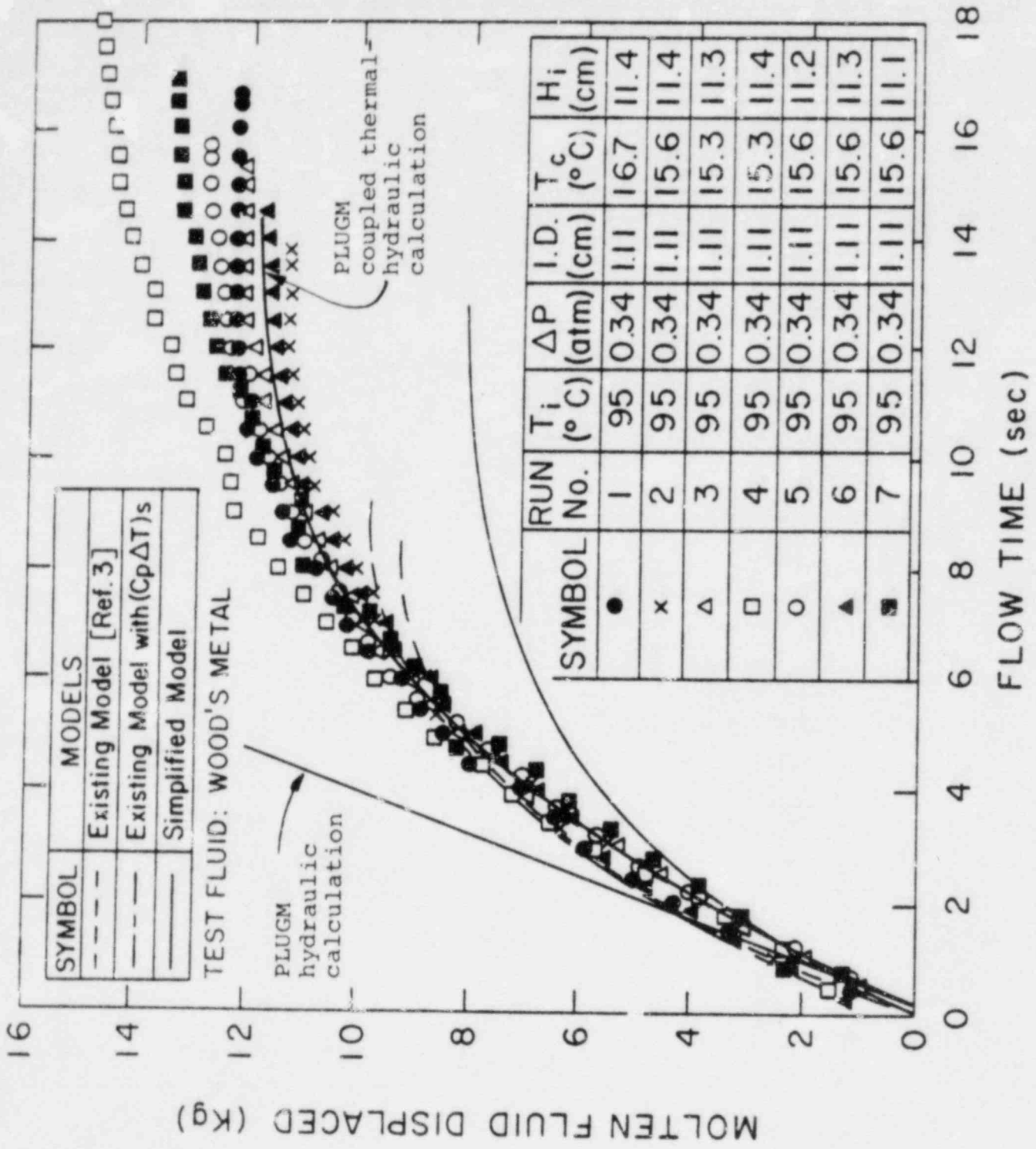

Figure 2: Comparison of PLUGM predictions with experiment data of Chun et al.

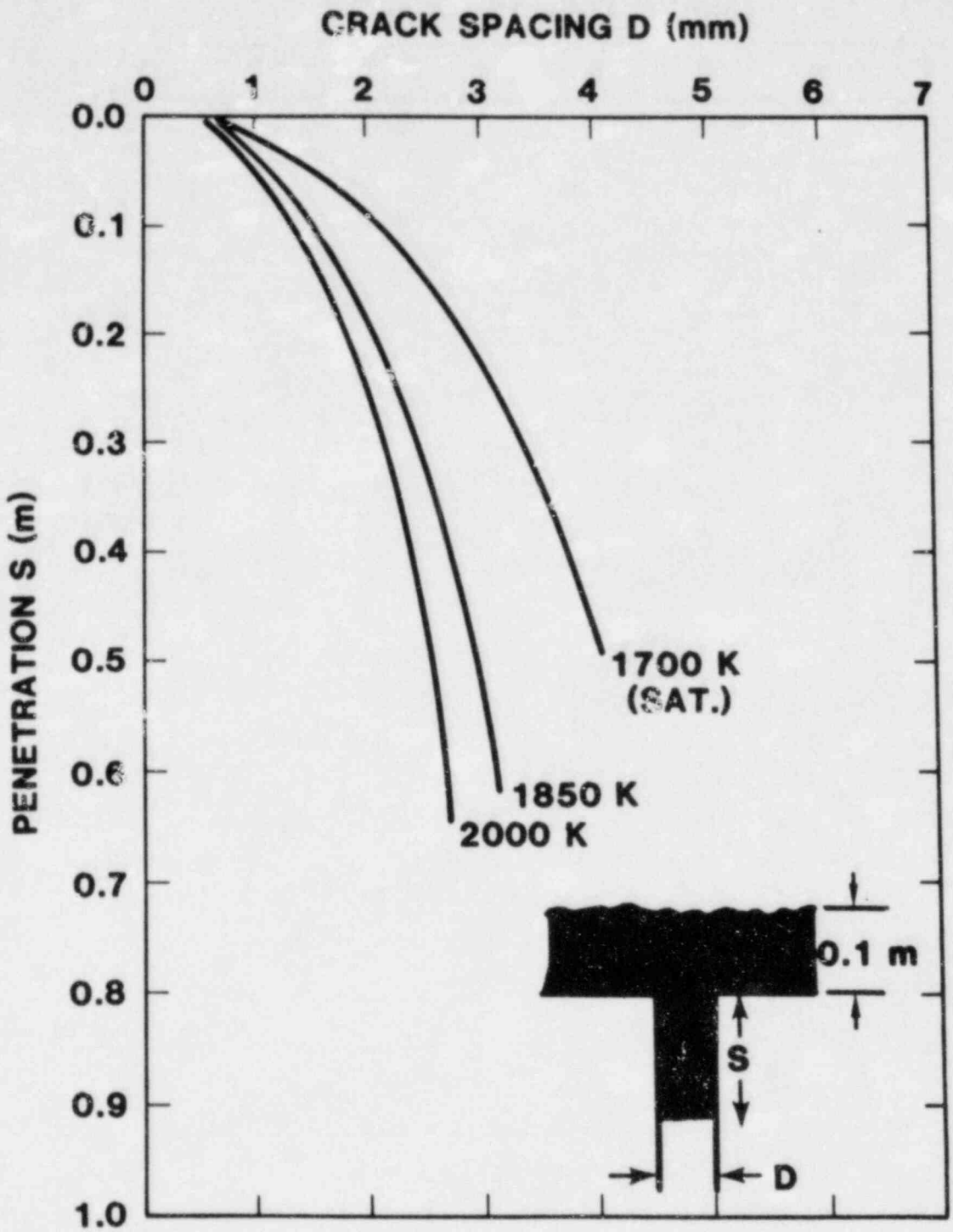

Figure 3: Steel Melt Penetration into Vertical Cracks in Harklase Brick

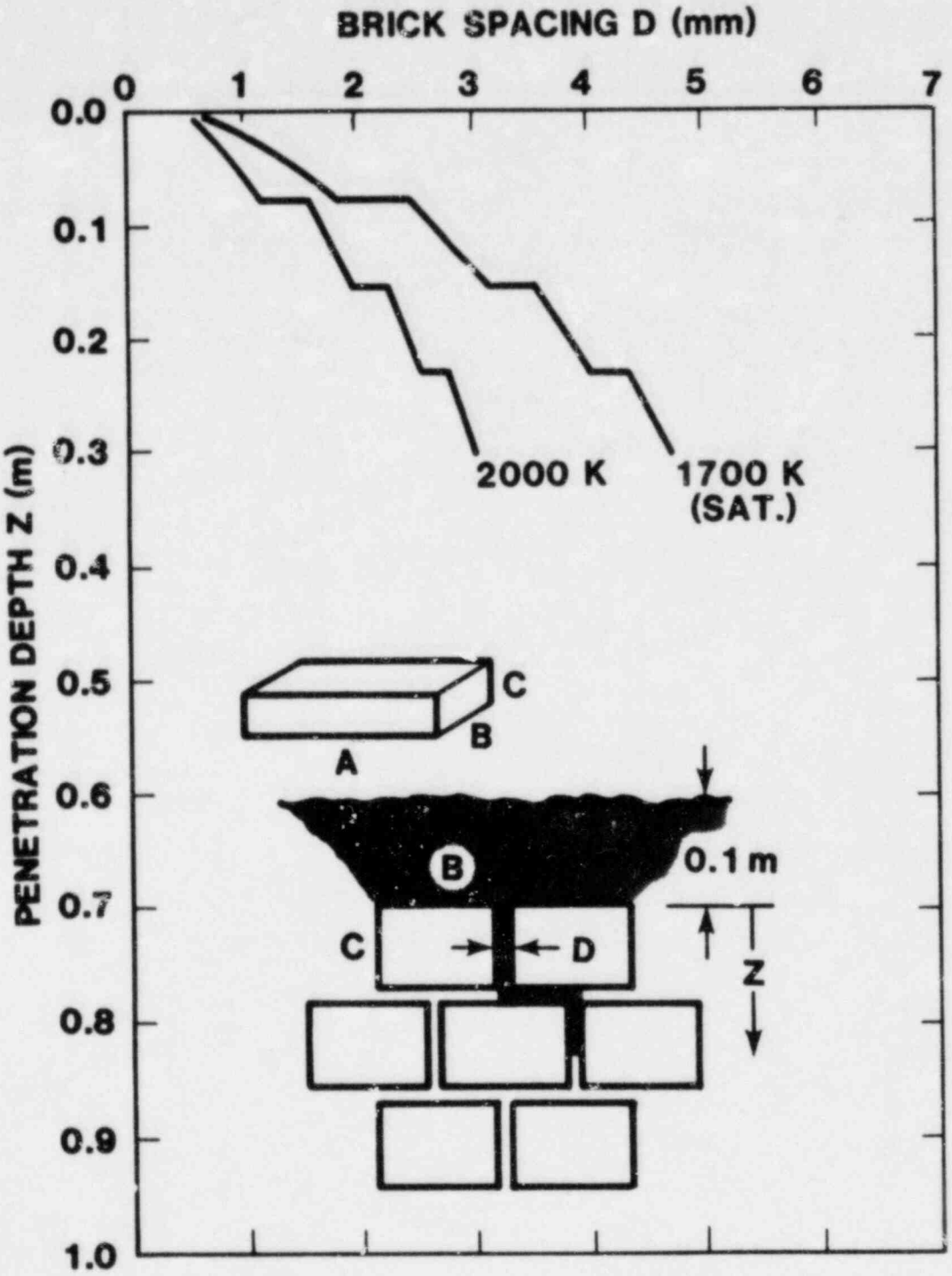

Figure 4. Steel Melt Penetration into a Harklase Brick Matrix

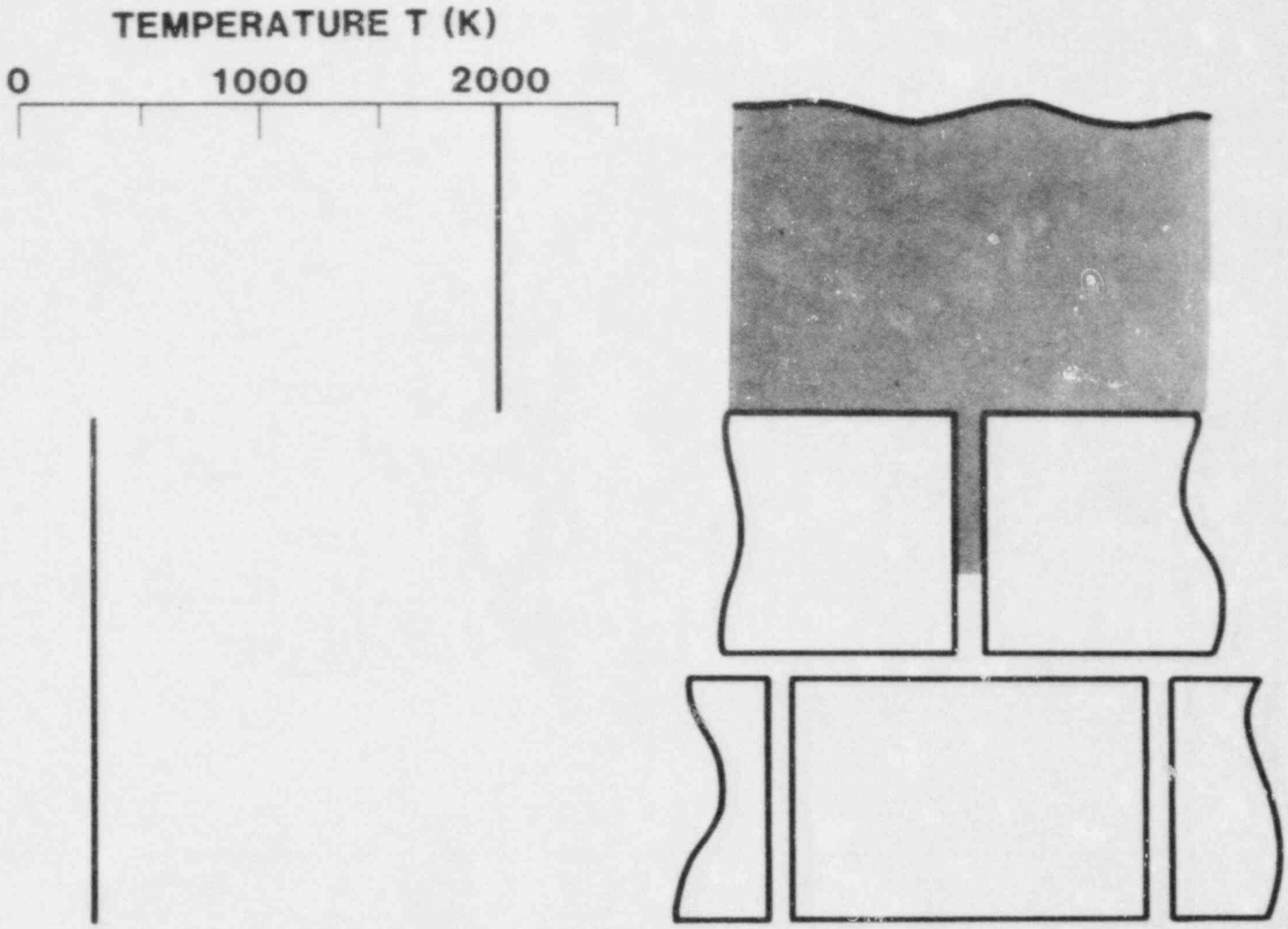

Figure 5: Initial Penetration of a Steel Melt into a Harklase Brick Matrix with a 1 mm Brick Spacing

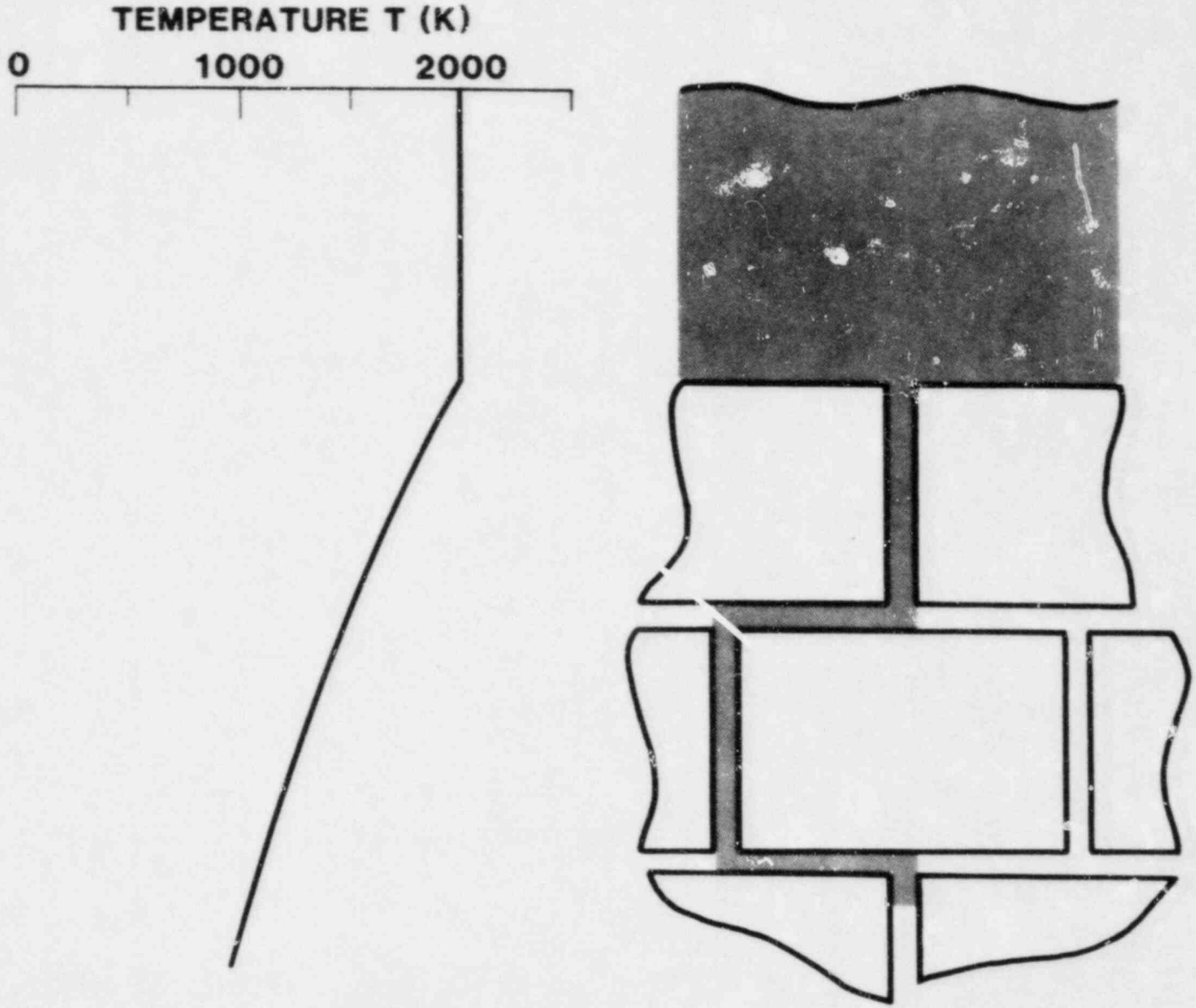

Figure 6: Penetration of a Steel Melt into a Harklase Brick Matrix with a 1 mm Brick Spacing Following Initial Plug Remelt and Subsequent Refreezing

Attack of Fragmented Core Debris On Concrete in the Presence of Water

William W. Tarbell
Ktech Corp., Under Contract to SNL

David R. Bradley
Sandia National Laboratories

Background

In the unlikely event that core debris escapes the reactor pressure vessel, the interactionns of the debris with concrete, structural materials, and coolant become the driving force for severe accident phenomena. The Ex-Vessel Core Debris Interactions Program at Sandia Laboratories is an experimental research effort to characterize the nature of these interactions and the magnitude of safety-related phenomena such as flammable gas generation, aerosol production, fission product release, and concrete attack.

Major efforts within the program include molten core simulants in contact with concrete, high pressure melt streaming into scaled cavities, the addition of coolant to a high-temperature melt/concrete interaction, and the attack of hot, solid core debris on concrete. This paper describes results from the last of these efforts, i.e., the attack of hot, but not molten debris on concrete.

Figure 1 shows the temperature of debris during a hypothetical accident sequence that can lead to hot, fragmented core debris attacking the concrete basemat. In this sequence, the core material ejected from the vessel undergoes an energetic reaction with water in the cavity to cause fragmentation and quenching of the debris. Decay heating causes the coolant to boil off and the debris to increase in temperature. Depending on the condition of the plant at the time of the accident and subsequent operator actions, the interaction can follow any of the three paths depicted. If path 2 is followed, the result is fragmented core debris at a temperature above the concrete ablation in contact with the basemat. Because the power densities involved are low, this situation may be maintained for many days.

Description of Tests

The four experiments that have been conducted are described in Table 1. The two characteristics that are addressed are the type of concrete and the absence or presence of water overlying the debris. Basalt and limestone-common sand are both generic reactor concretes found in the USA. The principal differences in composition is in the CaO and SiO_2 ratios and the large CO_2 fraction present in the limestone aggregate. The test apparatus consists of a concrete crucible with an internal cavity containing the debris material. Nominal dimensions are 41 cm diameter and 75 cm height by 22 cm inner diameter and 60 cm deep. Mild steel spheres (approximately 3 mm diameter) are placed into the cavity to a height of 25 cm. Thermocouples in the spheres and in the concrete allow monitoring temperature thoughout the fixture.

An induction coil placed about the crucible is used to generate a magnetic field within the debris (3000 hz) to cause magnetic currents to circulate and heat the metallic debris. The crucible is capped by an insulated and heated instrumentation tower to channel and measure the by-products of the interaction. Diagnostics for measuring flow, temperature, gas species, aerosols and heat flux are used in addition to video and framing camera documentation.

The test is initiated with the debris and concrete at ambient temperature. The strength of the magnetic field is varied to control the temperature of the debris. The concrete surfaces exposed to the debris increase in temperature due to conduction at the sphere/concrete interface. When melting of the concrete occurs, the heat transfer becomes more complicated due to the liquid/solid interface and the movement of molten concrete through the debris. Once melted, the hydrostatic force exerted by the debris causes the molten concrete material to flow through and around the debris. As the material moves upward, it reaches a location where it solidifies and forms an intact, solid crust adhered to the crucible sidewalls. Each test was terminated when the debris attack breached the bottom or sidewall surface of the crucible.

Test Results

The strategy in the tests was to heat the debris until a steady state nominal temperature of 1300 - 1400°C was obtained. These temperatures were sufficient to cause decomposition and melting of the exposed concrete surfaces. For tests FRAG 3 and FRAG 4, this interaction proceeded for a short period of time (30 to 60 mins) before tap water was flooded into the cavity from above. The water pool was then maintained at a height of approximately 15 cm above the original debris surface for the remainder of the test.

The thermally induced decomposition of both concrete types is quantitatively similar. Upon heating, evaporable water within the concrete structure and molecular water in the cementitious species is lost over the temperature range 30 to 240°C. This is followed by a second release of bound water with the decomposition of hydroxide-species over the range 360 - 485°C. The magnitudes of these two losses are similar for both concrete types. Above 600°C another loss occurs due to the decomposition of calcareous species and the decarboxylation of the limestone aggregate.

The release of water and carbon dioxide from the concrete allows these gases to bubble through and react with the melt species. Of primary interest in the accident situation is the type and amount of flammable gas species produced during these interactions. The equilibrium reaction of interest in the gas phase is:

$$CO_2 + H_2 \rightleftharpoons CO + H_2O$$

where the H_2 and CO are produced by the reaction with the metallic steel.

Gas specimens were obtained in all tests using "grab" samples of the gas stream within the interaction chamber. Some impurities such as air and water vapor are also present in these samples. If the data are corrected for these impurities, the values obtained effectively become a measure of the molar ratios of H_2, CO_2 and CO. The ratios can then be inserted into an equation representing the thermodynamics of the reaction to obtain the partial pressure of each constituent. These data are given in Figures 2 and 3 for tests FRAG 1 and 2A.

The results of Figures 2 and 3 suggest that the evolved gas is being reduced to form the flammable gas species, H_2 and CO. The extent of the reduction is

not complete, as evidenced by the amount of CO_2 and H_2O remaining in the stream. These inert components will affect the flammability detonation characteristics of the gas accumulation.

The data from FRAG 3 and 4 provide the opportunity to study the effect of an overlying water pool on the evolution of gas. Data from thermocouples placed in the debris of FRAG 3 (Figure 4) show how the coolant addition affects bed temperature. In this figure, the initial 340 minutes represent the period following fragmentation where the debris bed was flooded, this is followed by a heating period of 175 minutes after the bed was allowed to boil dry. At 515 minutes, coolant was added causing penetration of water into the top portions of the bed. The thermocouple records clearly indicate that the upper region of the bed rapidly quenches while the lower region remains at elevated temperature.

The addition of water to the debris may provide an additional source of hydrogen generation. If this were the case, then the fraction of flammable gas species in the gas samples would increase dramatically upon the introduction of water. Figure 5 represents a plot of the flammable gas volume fraction versus time. The results are remarkably constant before and after the addition of water. These results are significant because they indicate that the coolant is not entering into hot spaces in the debris to generate additional hydrogen. In addition, the quenching of approximately one-third of the bed height without affecting the composition of the evolved concrete gases means that the reduction reactions must be occurring readily. This result would suggest the gas reaction process can be modeled thermodynamically rather than the more complicated kinetic formalism.

The gas production process is dependent on the dehydration and decarboxylation reactions occurring within the concrete structure. These processes can be evaluated by inspection of the temperatures recorded by the sensors in the crucible base and sidewalls. An example of these data in the form of temperature versus depth are given in Figure 6 (for FRAG 1). Comparing isotherm velocities calculated from this figure indicates that the free water loss is occurring at a rate of propagation through the concrete greater than 12 cm/hr. The bound water dehydration front proceeds at a velocity of 3 to 5 cm/hr and the decarboxylation process represented by an 800°C isotherm moves at a rate of 2 to 4 cm/hr. These results demonstrate that the gas evolution process is non-stoichiometric in that the free water is consumed much more quickly than either the bound water loss or carbon dioxide evolution. Assuming that this same behavior holds for an accident situation, the reactor basemat provides a near-infinite source of water. Predictive models that invoke stoichiometric proportions in the gas evolution will then underpredict the actual amount.

Basalt and limestone-common sand concrete have been observed to form characteristically different crust formation patterns. The basalt crust typically forms above the debris in a series of thin, glass-like layers containing significant void volume. The formation process appears to be independent of debris location, in that there was not a propensity to form at the boundry of the debris. The molten material did not seem to be hindered by the relatively cool temperature (700 - 800°C) of the upper debris layers so that the material did not solidify until exposed to the atmosphere within the chamber. Prior to solidification, emerging gas causes the crust layers to levitate and collapse.

The limestone-common sand crust forms intermediate to the debris bed at a location nominally two-thirds of the bed height. Unlike the thin layers seen in the basalt tests, the limestone crust consists of a thick, granular layer of material surrounding the particles. The crust is approximately 4 cm thick at thecenterline of the crucible and slightly thinner where it attaches to the sidewall. The decomposed concrete material is much denser at the top and bottom crust surfaces leaving the center region comprised mostly of debris. These denser regions are sufficiently intact to provide an effective barrier to the penetration of water.

The results from FRAG 4 have not been completely analyzed. Initial indications are that the crust formed above the debris appears also to prevent the penetration of water into the debris bed.

Erosion is caused by the decomposition and removal of the concrete by-products. The results from the two types of concrete tested provide an interesting comparison. The basalt attack appears to be predominantly downward with only minimal amounts of sideward movement. Conversely, the limestone concrete erosion is nearly equivalent in the vertical and horizontal directions. The rate at which the erosion proceeds is comparable for the two concretes at nominally 5 cm/hr.

Conclusion

The FRAG test series is a quantitative evaluation of the attack of fragmented, hot debris on concrete. The results show that water and carbon dioxide liberated from the concrete are reduced to form the flammable species, hydrogen and carbon monoxide. The gas analyses suggest that the reduction process is not complete and that a large inert contribution remains. The reaction appears to proceed rapidly indicating the process is thermodynamic rather than kinetic controlled.

Inspection of the isotherms associated with the dehydration and decarboxylation processes shows that the evolved gases are not in stoichiometric proportions. The lower temperature free water evolution occurs much more rapdily than either of the other two processes.

Both concrete types form characteristic crusts of decomposed concrete byproducts. Although different in structure and location, the two crust types appear to be effective barriers preventing the penetration of coolant into the debris bed. Gas transport out of the bed is not similarly affected.

Both concrete types are attacked and eroded by the hot debris. The basalt attack is primarily downward while the limestone concrete erodes both horizontally and vertically. The rate at which the attack proceeds is nominally the same for both material types.

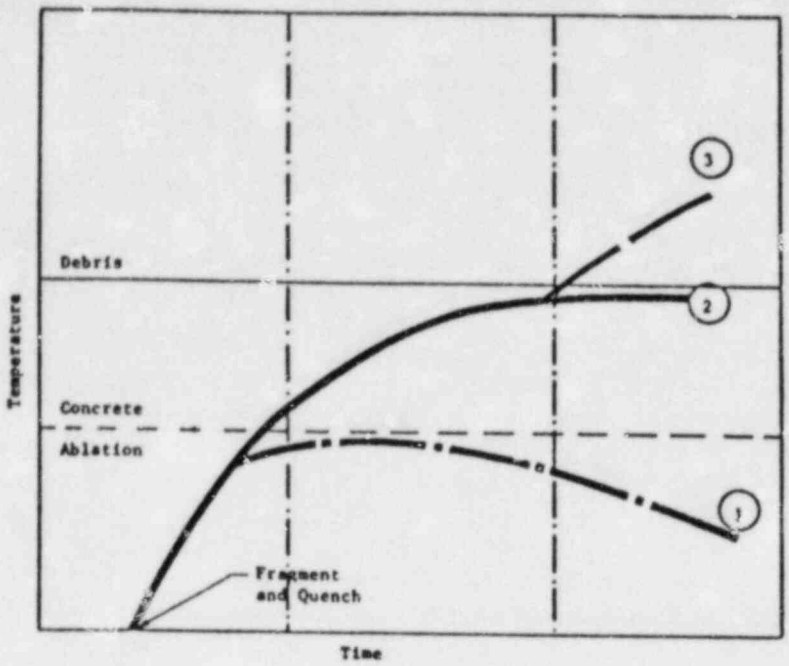

Fig. 1 Accident Sequence Leading to Hot, Fragmented Debris

TABLE 1
Fragmented Debris Test Description

Test Name	Concrete Type	Debris Size (mm)	Debris Quantity (kg)	Water In Cavity
FRAG 1	Basalt	3.4	44.5	No
FRAG 2A	Limestone-common sand	3.4	45.0	No
FRAG 3	Limestone - common sand	3.8	45.5	Yes
FRAG 4	Basalt	3.8	45.5	Yes

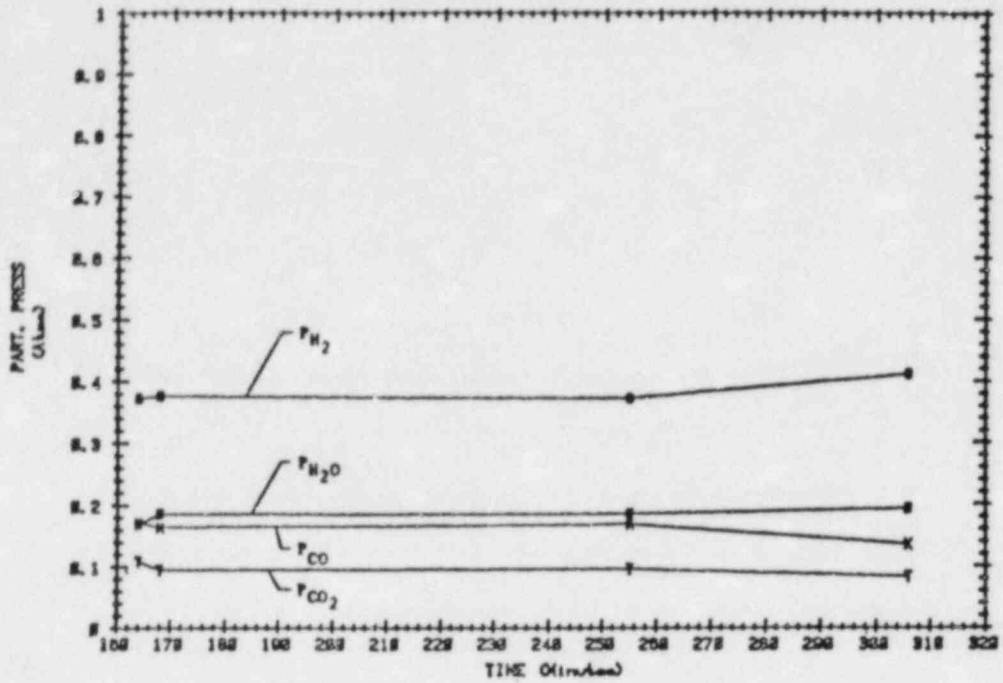

Fig. 2 FRAG 1 Gas Composition Results

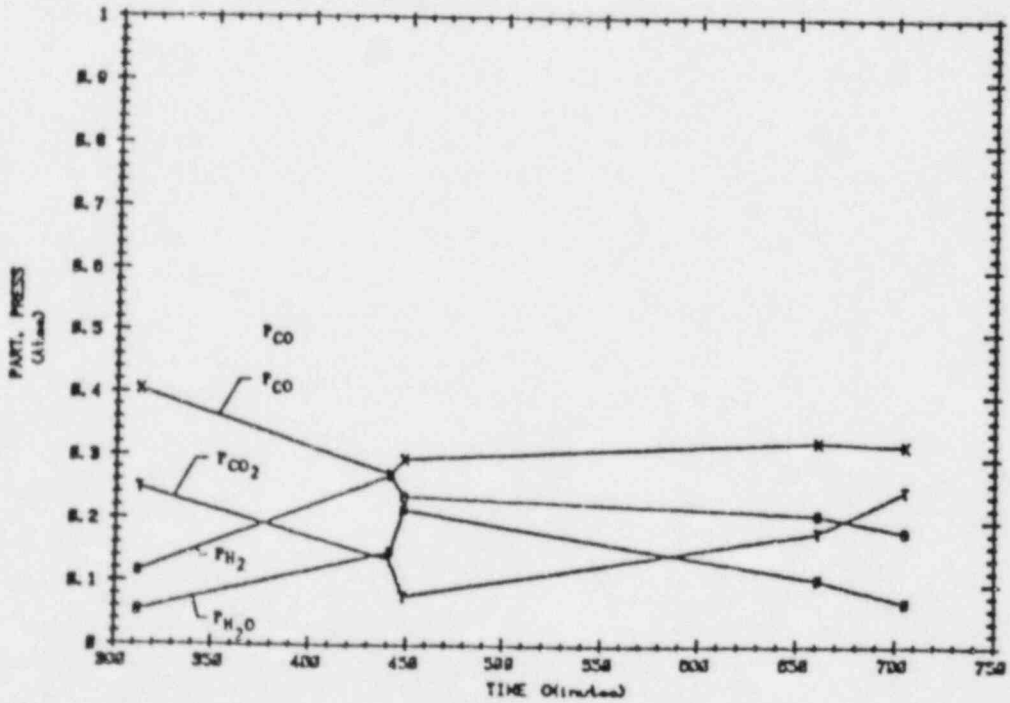

Fig. 3 FRAG 2A Gas Composition Results

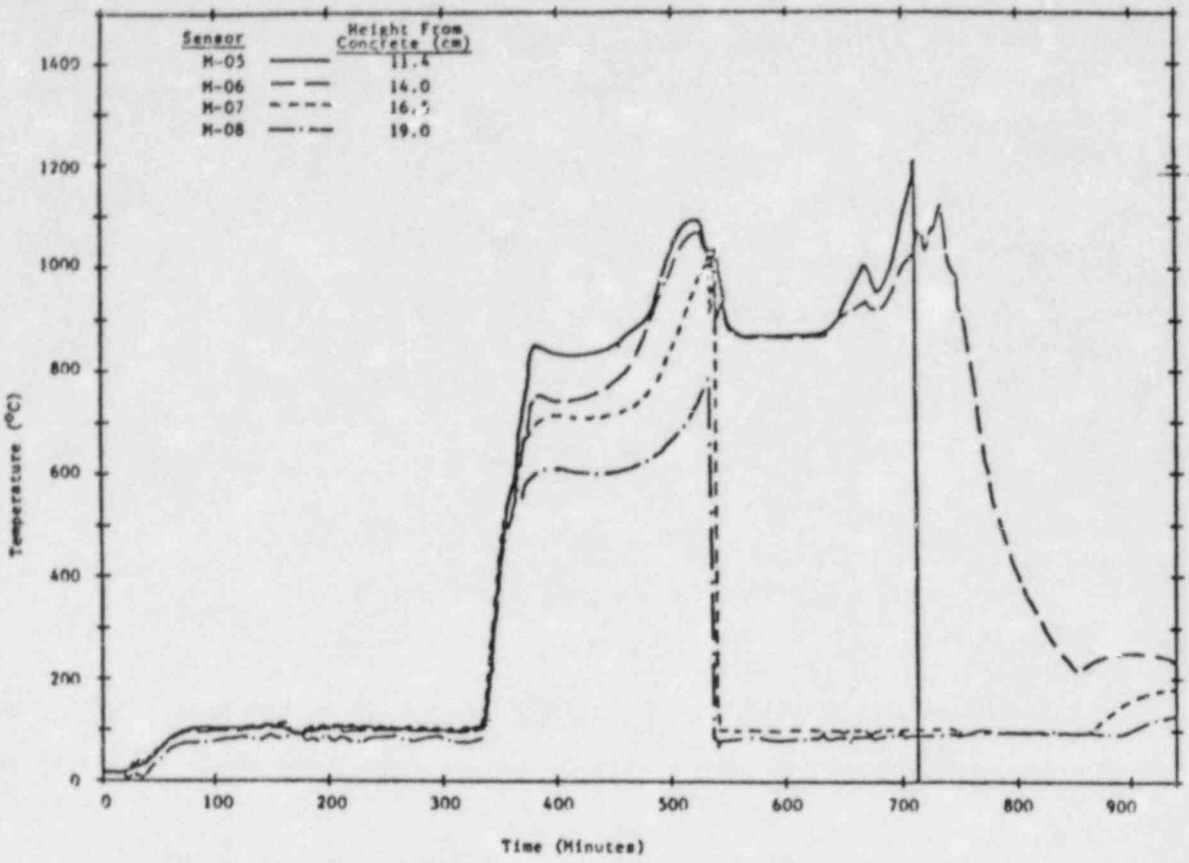

Fig. 4 Debris Thermocouple Temperature Histories for FRAG 3 Test

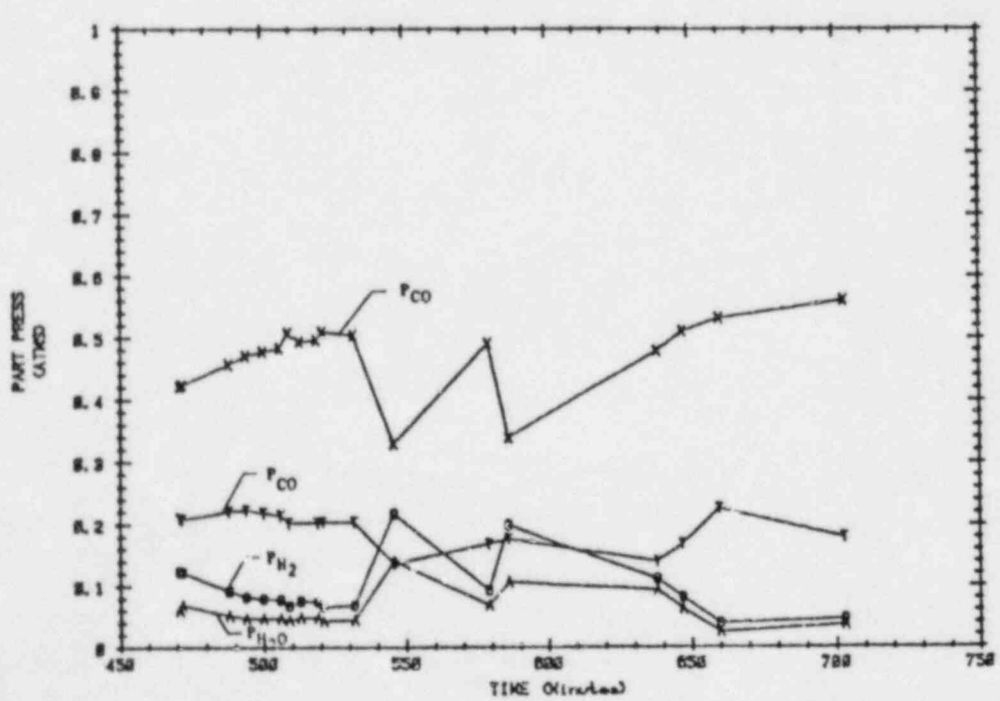

Fig. 5 FRAG 3 Gas Composition Results

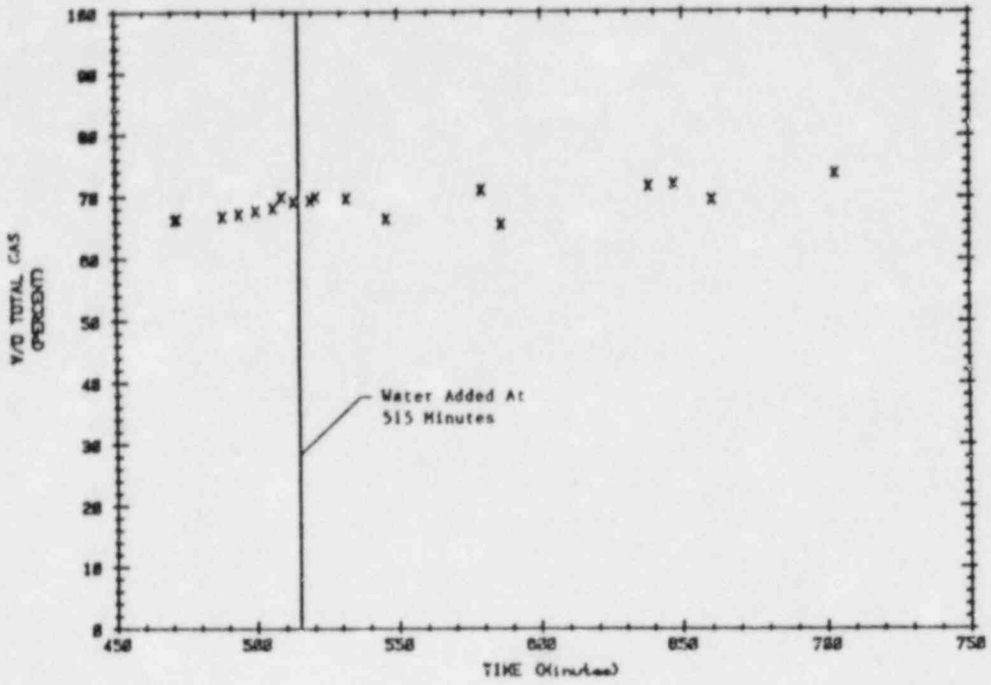

Fig. 6 FRAG 3 Volume Fraction of Flammable Gas Species

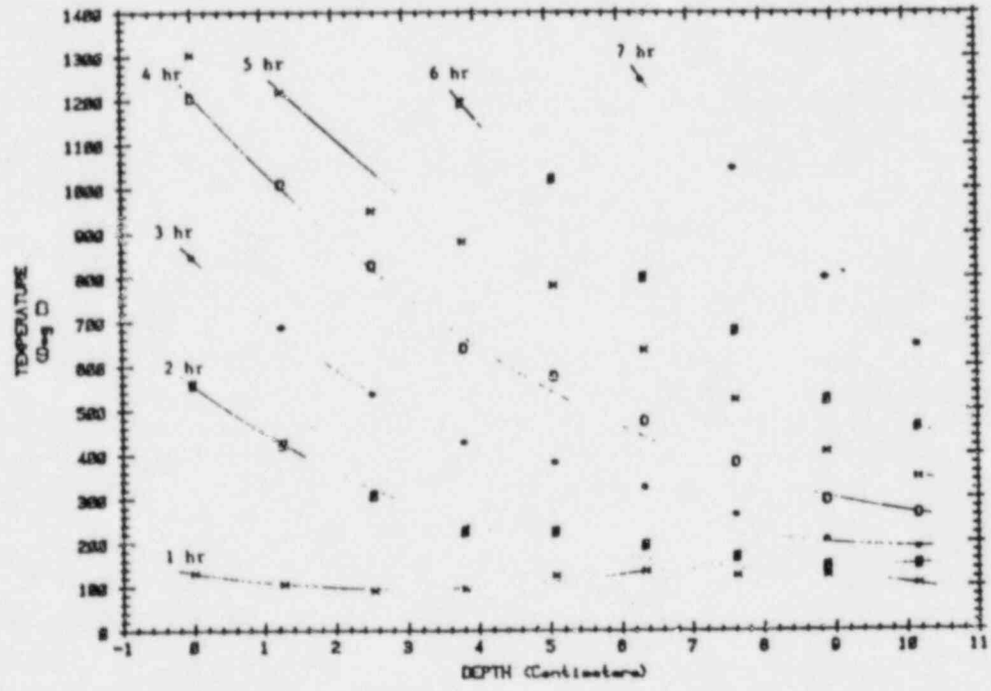

Fig. 7 FRAG 1 Temperature Versus Depth Histories

INFLUENCE OF STEAM ON THE BEHAVIOR OF U_3O_8 AEROSOLS

R. E. Adams
M. L. Tobias T. S. Kress

OAK RIDGE NATIONAL LABORATORY
Oak Ridge, Tennessee

A project is being conducted in the Nuclear Safety Pilot Plant (NSPP), located at the Oak Ridge National Laboratory (ORNL), to study the behavior of aerosols assumed to be generated during LWR reactor accident sequences and released into containment. This project, which is part of the ORNL Aerosol Release and Transport (ART) Program, is sponsored by the Nuclear Regulatory Commission and its purpose is to provide experimental qualification for LWR aerosol behavioral codes being developed independently by other NRC-sponsored programs.

The program plan for the NSPP aerosol project provides for the study of the behavior of LWR accident aerosols emanating from fuel, reactor core structural materials, and from concrete-molten metal reactions. The behavior of each of these aerosols is being studied individually to establish their characteristics; future experiments will involve mixtures of these aerosols to establish their interaction and collective behavior within containment.

The NSPP facility diagramed schematically in Fig. 1 includes a test containment vessel, aerosol generating equipment, analytical sampling and system parameter measuring equipment, and an in-vessel liquid spray decontamination system. The NSPP vessel is a stainless steel cylinder with dished ends having a diameter of 3.05 m, a total height of 5.49 m, and a volume of 38.3 m^3. The floor area is 7.7 m^2 and the internal surface area (including top, bottom, and structural items) is 68.9 m^2. The equipment for the measurement of aerosol parameters includes filter samplers for measuring the aerosol mass concentration, coupon samplers for aerosol fallout and plateout measurements, cascade impactors and a centrifuge sampler for determining the aerodynamic particle size distribution of the aerosol, and devices for collecting samples for electron microscopy. System parameters measured are moisture content of the vessel atmosphere, steam condensation rates on the vessel wall, vessel atmosphere temperature, wall temperature gradients, and vessel pressure.

The purpose of this paper is to document observations illustrating the influence that steam has on the behavior of U_3O_8 aerosols within

the NSPP vessel. In a previous study, a number of U_3O_8 aerosol behavior experiments were conducted in a relatively dry air environment (RH<20%); these experiments serve as a basis for comparison in observing the changes in U_3O_8 aerosol behavior induced by the presence of steam. Under dry conditions the experimentally-observed change in U_3O_8 aerosol mass concentration within the NSPP vessel as a function of time (Fig. 2) is modeled reasonably well by the HAARM-3 aerosol code. As predicted by theory and illustrated by the results of this set of experiments, the aerodynamic behavior of U_3O_8 aerosol in a closed vessel is influenced by the initial aerosol mass concentration. At the lower mass concentrations, a longer period of time is required for small particle agglomeration to produce larger particles which are more subject to removal through the process of gravitational settling. Scanning electron microscopy revealed the U_3O_8 aerosol to be in the form of very small spherical particles agglomerated into intermingled branched chains characteristic of vapor-condensed aerosols formed through high temperature oxidation processes (see Test 207, Fig. 6).

As a preamble to the aerosol experiments in a steam environment, two U_3O_8 aerosol experiments were conducted in a relatively moist environment. Water was evaporated into the NSPP vessel to produce an environment with a relative humidity of >95% at a temperature of approximately 323 K. The U_3O_8 aerosol was then generated and introduced into this atmosphere; aerosol mass concentration as a function of time for these two experiments is contained in Fig. 3. The aerodynamic behavior of the U_3O_8 aerosol in the vessel was not greatly different from that observed in the dry atmosphere experiments. However, scanning electron microscopy revealed that the aerosol no longer existed as intermingled branched chains but as spherical clumps of particles (see Test 208, Fig. 6).

Five experiments were conducted to investigate the behavior of U_3O_8 aerosols in a steam environment. The vessel was heated and the steam environment was produced by injecting steam for a period of about one hour. When the desired temperature was reached, the steam injection rate was reduced and the accumulated steam condensate was drained from the vessel. Steam injection at the low rate was continued for either two or six hours to replace steam losses to the vessel walls. U_3O_8 aerosol was generated and introduced into this quasi-steady state environment. In the first three experiments an aerosol concentration gradient was noted during the early stages of the experiment; the aerosol mass concentration was greater by a factor of 2-3 in the upper region of the vessel than in the lower region. A small fan-mixer was installed near the bottom of the vessel and utilized during the last two experiments. Mixing of the U_3O_8 aerosol within the steam atmosphere was enhanced. The initial aerosol mass concentration was varied from about 5 to 26 $\mu g/cm^3$ over the five experiments. After the first hour the aerodynamic behavior of U_3O_8 aerosol was essentially the same in all five experiments; the rate of aerosol disappearance from the vessel atmosphere was very similar. The aerosol mass concentration as a function of time for three of these five experiments is given in Fig. 4. Scanning electron microscopy

showed the aerosol to be in the form of spherical clumps of particles much the same as noted during the humid atmosphere experiments (see Test 404, Fig. 6).

Comparison of the aerosol behavior in the three environments reveals that the rate of aerosol disappearance from the steam environment is larger than in the dry or moist environments. The data contained in Fig. 5 support this observation. The times required for 90% of the maximum aerosol mass to disappear from the NSPP vessel atmosphere in these three experiments are approximately: 100 min in the dry environment; 107 min from the moist environment; and 75 min in the steam environment. The times required for 99% of the aerosol mass to disappear would be approximately 340 min, 270 min, and 115 min, respectively.

It is clear that under the influence of a condensing steam environment, as would be present in LWR containment during and following an accident, the U_3O_8 aerosol behaves in a manner different from that in a dry or moist environment. This change in behavior could be the result of several factors, or combinations of these factors: a change in aerosol morphology enhancing gravitational settling; influence of steam flux toward the walls enhancing plateout; thermal factors influencing particle agglomeration; or currently unrecognized influences of steam condensation.

Computer modeling of U_3O_8 aerosol behavior in a steam environment is underway, both in this country and abroad, but no code is yet fully operational that can account for the experimentally observed influence of steam on the behavior of U_3O_8 aerosol in containment.

The results of this study may have several implications in the field of nuclear safety. Removal of U_3O_8 (fuel) aerosols from reactor containment following an accident should be beneficially enhanced. Filtration of aerosols from the containment environment may be degraded because of the change in aerosol shape from chain-agglomerate to spherical. Coagglomeration of aerosols and fission products may be influenced both by the steam environment and the change in shape of the aerosol. Finally, experimental observations of aerosol behavior in dry atmospheres should not be construed to be the same in steam environments.

Bibliography

R. E. Adams et al, "Uranium and Sodium Oxide Aerosol Experiments: NSPP Tests 201-203 and Tests 301-302, Data Record Report," NUREG/CR-1002 (ORNL/NUREG/TM-343) November 1979.

R. E. Adams et al, "Sodium Oxide and Uranium Oxide Aerosol Experiments: NSPP Tests 106-108 and Tests 204-207, Data Record Report," NUREG/CR-1767 (ORNL/NUREG/TM-408) March 1981.

T. S. Kress (compiler), "Proceedings of the CSNI Specialists Meeting on Nuclear Aerosols in Reactor Safety," Gatlinburg, Tenn., NUREG/CR-1724 (ORNL/NUREG/TM-404) CSNI-45, October 1980.

Results from the various experiments also reported in quarterly progress reports:

LMFBR Aerosol Release and Transport Program Quarterly Progress Report for:

January-March 1979, NUREG/CR-0844 (ORNL/NUREG/TM-329)
April-June 1979, NUREG/CR-1062 (ORNL/NUREG/TM-354)
July-September 1979, NUREG/CR-1296 (ORNL/NUREG/TM-376)
October-December 1979, NUREG/CR-1449 (ORNL/NUREG/TM-391)
January-March 1980, NUREG/CR-1790 (ORNL/NUREG/TM-416)
April-June 1980, NUREG/CR-1791 (ORNL/NUREG/TM-417)
July-September 1980, NUREG/CR-2117 (ORNL/TM-7806)
October-December 1980, NUREG/CR-2215 (ORNL/TM-7884)
January-March 1981, NUREG/CR-2299, Vol. 1 (ORNL/TM-7946)
April-June 1981, NUREG/CR-2299, Vol. 2 (ORNL/TM-7974)
July-September 1981, NUREG/CR-2299, Vol. 3 (ORNL/TM-8149)
October-December 1981, NUREG/CR-2299, Vol. 4 (ORNL/TM-8307)

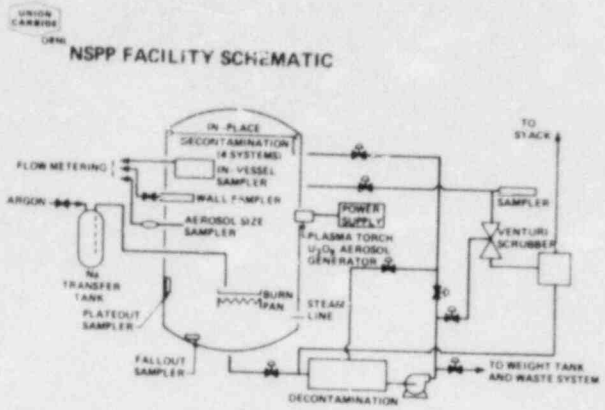

Figure 1

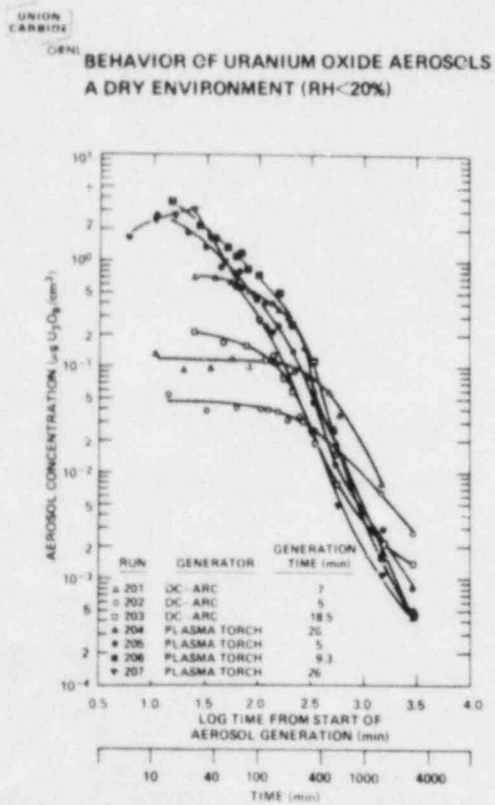

Figure 2

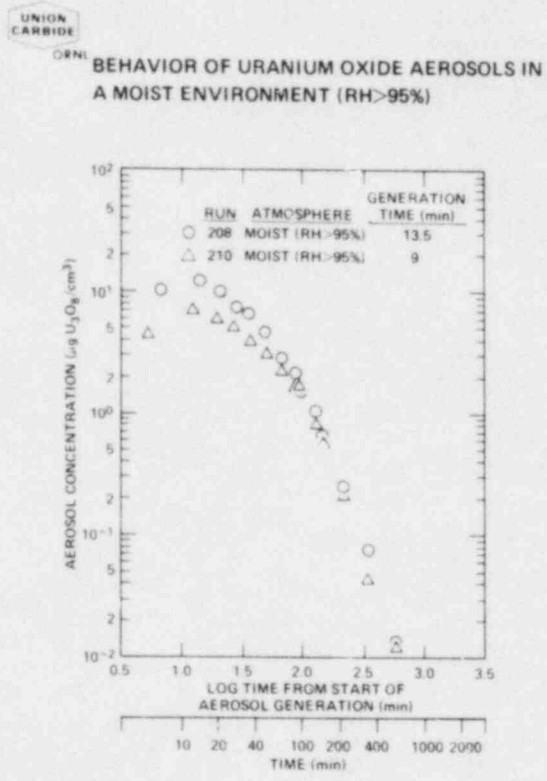

Figure 3

UNION CARBIDE
ORNL

BEHAVIOR OF URANIUM OXIDE AEROSOLS IN A STEAM-AIR ENVIRONMENT (RH ~ 100%)

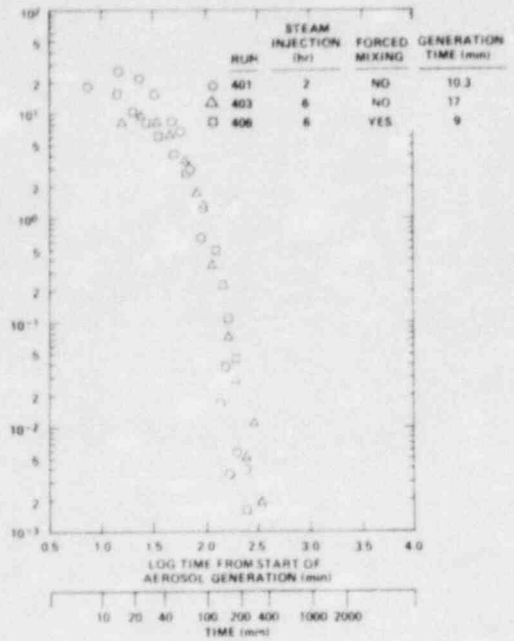

Figure 4

UNION CARBIDE
ORNL

COMPARISON OF THE INFLUENCE OF MOISTURE ON THE BEHAVIOR OF URANIUM OXIDE AEROSOLS IN A CLOSED VESSEL

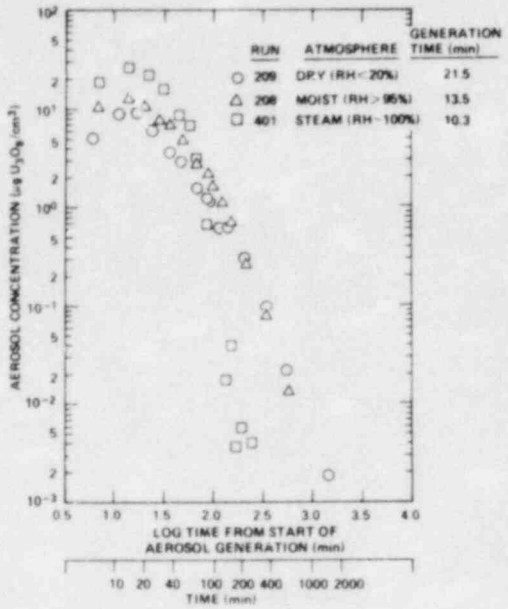

Figure 5

UNION CARBIDE ORNL

SEM PHOTOGRAPHS ILLUSTRATING INFLUENCE OF MOISTURE ON PHYSICAL APPEARANCE OF U_3O_8 AEROSOL

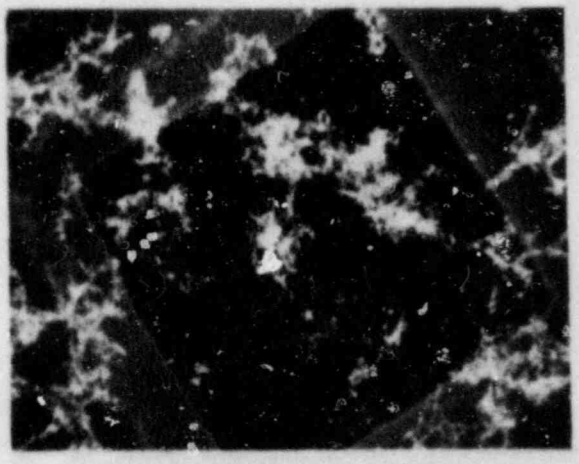

TEST 207; U_3O_8 AEROSOL IN A DRY ATMOSPHERE (RH<20%); SAMPLED AT 313 (min), 313 (K); Mag. 2000X (1 cm = 5 μm)

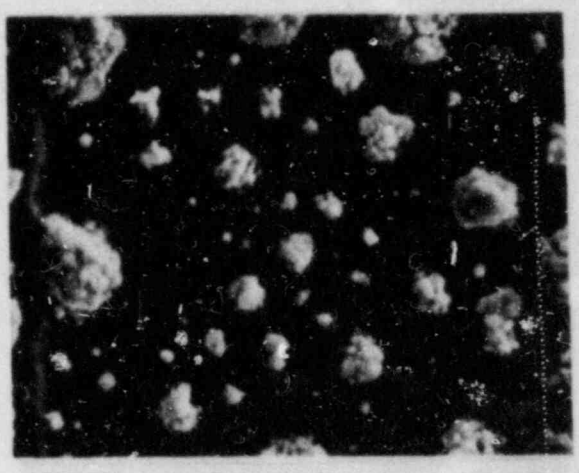

TEST 208; U_3O_8 AEROSOL IN A MOIST ATMOSPHERE (RH>95%); SAMPLED AT 73 (min), 323 (K); Mag. 2000X (1 cm = 5 μm)

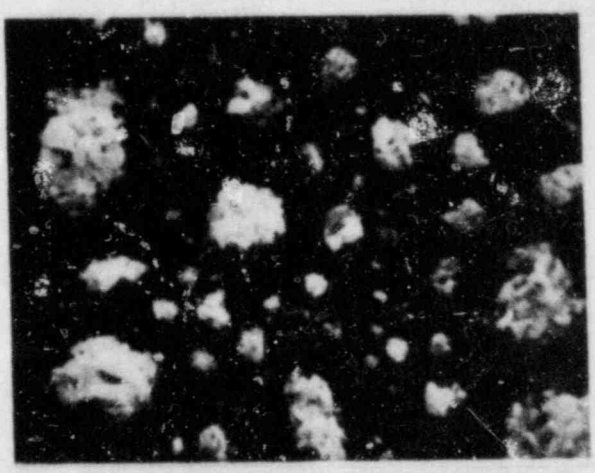

TEST 404; U_3O_8 AEROSOL IN A STEAM–AIR ATMOSPHERE (RH~100%); SAMPLED AT 46 (min), 385 (K); Mag. 4000X (1 cm = 2.5 μm)

NOTE: REDUCTION 68% OF ORIGINAL

Figure 6

HYDROGEN BEHAVIOR AND CONTROL PROGRAM

JOHN C. CUMMINGS AND MARSHALL BERMAN
SANDIA NATIONAL LABORATORIES
ALBUQUERQUE, NEW MEXICO

SUMMARY

Sandia National Laboratories is conducting a hydrogen research program for the Office of Research of the U. S. Nuclear Regulatory Commission. Our program has two major objectives: assessment of the threat to nuclear power plants (containment structure, safety and control equipment, and the primary system) posed by hydrogen combustion; assessment of proposed hydrogen control and disposal methods, and development of new concepts.

A number of fundamental questions and issues arise when examining the hydrogen problem for light water reactor (LWR) plants. These questions and issues are related to the four natural divisions of the problem: hydrogen production; hydrogen transport, release, and mixing; hydrogen combustion; and prevention or mitigation of hydrogen combustion. Unknowns and uncertainties exist in each of the four problem areas. For example, the rate of hydrogen production during a degraded-core or molten-core accident, hydrogen-water solubility dynamics, the rate of hydrogen mixing, the effect of geometrical structures and scale on combustion, flame speeds, combustion completeness, and mitigation-scheme effectiveness, are all important issues with significant uncertainties. Our approach to resolving the uncertainties includes analytical modelling, computer simulation, and experimentation on several scales. The products of this research program will include:

1. Assessment of the threat for several classes of reactors and containment designs;

2. Assessment of the adequacy of existing safety systems and mitigation strategies;

3. Identification and concept demonstration of improved mitigation and detection systems;

4. Publication of manuals and reports on: evaluation of the state-of-the-art; phenomena important to threat assessment; operator strategies and training; and reactor safety issues;

5. Development and application of computer codes for addressing the generation, transport, combustion and mitigation of hydrogen during hypothetical reactor accidents.

From its inception, this program has been planned and executed in close cooperation with the Office of Nuclear Reactor Regulation and with the industry research effort conducted by the Electric Power Research Institute and various interested utilities.

Considering the large diversity of issues related to the hydrogen problem, the elements of the various research programs have remained, to a large extent, complementary to each other, as can be seen from the papers at this meeting. Even in some areas where overlap has occurred, the data have frequently supported each other and raised our confidence in the accuracy and reliability of the results; in some cases, possible discrepancies have arisen, and further research will be required to resolve these questions.

Research Program Elements and Results

There are several aspects to the hydrogen issue: hydrogen generation (sources), detection, transport and mixing, combustion, and ultimately mitigation and control. Figure 1 illustrates the interdependence of these aspects; phenomenological information from these areas must eventually be incorporated into models which can predict reactor and containment responses during hypothetical accidents. The NRC research program is addressing many areas within each of these groups; current research emphasizes those aspects of the problem which are considered to be most urgent, based on current information; future research directions will obviously depend on information produced from the current research.

The Hydrogen Behavior program (A-1246) is the first, the largest, and the most comprehensive of the NRC hydrogen programs. It addresses most of the items shown in Fig. 1 which are not specifically addressed by the other programs. The primary emphasis of this program is on the combustion aspects of the hydrogen problem; it also ensures that the research elements are well organized, and integrates these elements into the reactor accident analysis tasks.

Several philosophies have been incorporated into the various hydrogen programs to maximize their utility to the NRC. First, the programs contain both experimental and analytical elements. This facilitates the use of the experimental data, as well as providing guidance to and assessment of the code-development efforts. Secondly, the programs are designed to provide interim, scoping information to assist in current decision-making processes and in answering urgent licensing questions. The programs are also designed to address long-term research goals (i.e., experimental facilities of broad scope and equipped with adequate instrumentation are being designed and built to comprehensively address important reactor safety issues, these facilities will be intimately coupled with longer-term code-development activities). This two-pronged approach is consistent with meeting urgent licensing needs, without compromising the

more detailed information that will be needed in the long-term evaluation of the consequences of severe reactor accidents.

Figure 2 illustrates the relationships between the various code-development tasks and their applications. The HECTR code (see Fig. 3) is intended to be a fast-running reactor accident analysis tool which will calculate the transport and combustion of the fuel and oxidant gases during hypothetical reactor accidents. It is a one-dimensional, multicompartment, control-volume code, which will model the various engineered safety features in different containments. It includes heat transfer (radiation, convection, conduction, droplet evaporation), flame initiation and propagation, and a rudimentary model for transport and mixing (see Fig. 4). It employs other codes for the definition of the source term (e.g., MARCH, CORCON, MELCOR, etc.), or internally calculates this term by means of tables or simple formulas. It may also incorporate simplified versions of more complex flame-propagation codes. HECTR has been and will continue to be used for reactor accident calculations (see Figs. 5-8); it may also provide models for incorporation into the large, second-generation accident analysis codes such as MELCOR. A version of HECTR called HECTR-ES is being used to provide pressure and temperature histories for the evaluation of equipment survival. These histories are used directly in heat transfer codes to predict the response of equipment to hydrogen burns; they are also being used to guide the design of experimental facilities which will simulate temperature histories at reactor scales.

An analytic effort is underway at Sandia Livermore (SNLL) to predict the possibility and consequences of flame acceleration in reactor accidents. This effort includes the modification and application of complex vortex-dynamics codes (Figs. 9-10) as well as simpler codes, and even empirical correlations when appropriate. This code development effort is closely coupled to the experimental study of accelerated flames at Sandia Albuquerque (SNLA) and at McGill University.

Under NRC sponsorship, several hydrogen transport codes are currently being evaluated. The best of these codes will be pursued, both for comparisons to experiments, and to provide benchmark calculations. However, with the extension of HECTR's capability to the modelling of transport and mixing, the need for simplified 1-D pure transport codes will diminish. Code storage limitations and run-time constraints, however, may extend the utility of RALOC or similar codes for pure transport calculations.

Detonation loads have been calculated by a modified version of the Sandia CSQ code for several plants (Figs. 11-12). The code can sometimes calculate non-conservative loads (i.e., less than the classical Chapman-Jouguet predictions), because it

empirically assumes a finite run distance for transition to detonation. Nevertheless, it provides pressure-time behavior for calculating impulses delivered to structures (which are needed for structural failure calculations). The calculated impulses, (i.e., the time integrals of pressure), however, are generally quite accurate. Although refinement and improvement of CSQ for these calculations is quite possible, it is not planned for the immediate future.

Figure 13 lists the various experimental facilities available for the hydrogen research effort. A large pre-existing capability has been tapped for this work (e.g., the VGES 16-ft tank, the FITS tank, two large sites for detonation testing at SNLA, and 10 tubes and channels of various lengths and diameters at McGill University). Some new facilities have been built (e.g., steam: hydrogen jet facility), or will be built shortly (FLAME). These facilities, together with those employed by EPRI and the utilities should suffice for most experimental investigations. Figure 14 shows those facilities which are being used to address questions dealing with deflagration phenomena. Figures 15 and 16 connect the appropriate facilities to studies of detonations and accelerated flames, respectively.

Deflagration experiments in the VGES burn tank (Fig. 17) and in the FITS burn tank (Fig. 18) have addressed the following issues: flame shape and speed; combustion completeness; effects of igniter type and location; quiescent versus dynamic (turbulent) initial conditions; effects of steam, carbon dioxide and water foams; equipment survivability; and the effects of initial pressure, temperature, and gas concentrations. Some very important conclusions can be drawn from this body of experimental data, many of which have also been confirmed in studies conducted by EPRI and the utilities. It is important now to understand that the earlier concept of "flammability limits" is insufficient (and sometimes misleading) for reactor safety applications. The experiments show that such limits are not based on physical and chemical properties of the component gases alone; rather, they depend on ignition type and strength, vessel geometry and size, the nature and geometry of obstacles which may be present (and their heat transfer properties), and the velocity of the gases (quiescent versus moving). In addition, flame ignition must clearly be distinguished from flame propagation; e.g., hydrogen can be burned in the neighborhood of an igniter or on the surface of a catalyst, without any flame propagation occurring. This clearly complicates the job of the reactor safety analyst. If he wishes to know if a particular mixture of gases will sustain a propagating deflagration (and to know the resulting pressure rise), he will need to describe the initial and boundary conditions of the problem sufficiently accurately to determine flame speeds, combustion completeness, and the important heat transfer mechanisms.

The steam:hydrogen jet facility (Fig. 19) has two major objectives: to understand the behavior of such jets issuing from breaks in the primary system as a function of hydrogen and steam concentrations, flow velocities, gas temperatures, break size, and the nature and placement of flameholders (i.e., obstacles); and to examine deliberate flaring through high-point vents as a mitigation concept. The facility is operational.

Our research has already shown that "detonability limits" (in the classical sense of specific numbers independent of geometry and size) are no more fundamental properties of nature than were "flammability limits". A very extensive program at McGill University (using hydrocarbons as well as hydrogen) coupled with large-scale critical-tube-diameter experiments (Fig. 20) at the VGES site, has led to the production of U-shaped curves as shown in Figs. 21-22. The detonation cell width, λ, appears to be a fundamental parameter of detonations. Small values of λ correspond to highly detonable gases (such as acetylene and hydrogen) or to near-stoichiometric mixtures. The larger the value of λ, the more difficult it is to establish and maintain a steady detonation wave. It now appears that the cell width can be related to other important parameters of detonations such as initiation energy, critical tube diameter, and detonability limits. The critical tube diameter d_c, is the minimum diameter which will permit a steady planar detonation wave to propagate into an open volume (i.e., become a spherically expanding wave). The solid curve in Fig. 21 shows the critical tube diameter as a function of hydrogen concentration (in air) calculated by the empirical equation, $d_c = 13\ \lambda$; the specific points refer to direct measurements of d_c. A similar curve can be drawn where the ordinate is the critical energy for direct initiation of a detonation. Hence, Fig. 21 relates detonability limits to geometry, size, and the relative concentrations of the gases. Figure 22 is a direct plot of detonation cell width, λ, as a function of the relative fractions of hydrogen and air, and including additions of carbon dioxide gas. This curve can again be employed to indicate detonability limits. As the concentrations move away from stoichiometric conditions (29.6% hydrogen in air), the establishment of steady propagating detonation waves requires larger volumes; i.e., λ, and also d_c, become larger, indicating that the mixture is becoming less detonable. Similarly, the addition of carbon dioxide also reduces the detonability of the mixture.

An extensive experimental investigation of flame acceleration has been underway at McGill University for many years, primarily studying various hydrocarbons. The NRC is supporting part of this effort, which is aimed specifically at reactor accident simulations using hydrogen. The small-scale experimental effort at McGill is strongly coupled to the larger-scale program at

SNLA, where the FLAME (Flame Acceleration Measurements and Experiments) facility is being built (Fig. 23). The McGill experimental program has already produced a significant body of data with important applications to reactor safety. It now appears that hydrogen is very sensitive to flame acceleration (as is acetylene). Significant flame acceleration (flame speeds on the order of hundreds of m/s) has been observed in hydrogen:air mixtures as lean as 10% H_2. The degree of acceleration depends strongly on tube geometry and size, obstacle nature and blockage ratio, and gas concentrations. Recent data have also shown an extreme sensitivity to the degree of confinement along a channel· e.g., vent areas representing about 10% of the top face of the channel can lead to order-of-magnitude reductions in flame speed. If this strong dependency on venting persists in the large-scale tests in the FLAME facility, it would indicate that flame acceleration in large channels (e.g., the ice condenser upper plenum) could be significantly moderated by partial venting.

Experiments to date indicate that the mechanisms governing flame acceleration may represent a precarious balance of positive and negative factors associated with flame folding and turbulence. Two positive factors that lead to an increase in burning rate are the increase in flame area due to folding, and the increase in the local burning velocity of the folds due to higher turbulent diffusivities associated with fine-scale turbulence; the increase in flame areas is a result of the gas flow ahead of the flame being greatly perturbed by the presence of obstacles. In the absence of negative factors, the volumetric burning rate would continue to increase until a transition to detonation occurred. The negative factors that lead to a decrease in the burning rate are reaction quenching due to excessive flame stretching, and rapid cooling due to turbulent mixing. If the negative factors are strong enough, the flame may be quenched; if they are of intermediate strength, then a steady, strong flame can be produced which does not undergo transition; if the factors are sufficiently weak, then transition to detonation may take place.

Conclusions

It is clear from the preceding discussion that the current research program has already produced results of significant value to reactor safety analyses. Several other programs supported by the Office of Research (Fig. 24) are also contributing to the resolution of hydrogen-related questions. The Hydrogen Combustion Mitigative and Preventive Schemes program (A-1336) and the Hydrogen Burn Survival program (A-1270, A-1306) will be discussed in detail at this conference. The Combustible Gas in Containment program (A-1255) has two goals: to determine the rates and total quantities of hydrogen which could be

generated from corrosion of coatings (galvanized material, aluminum, paints, etc.) in containments during reactor accidents; and to determine the quantity and morphology of debris and residues which might be produced during the corrosion reactions. The Molten Core-Concrete Interactions program (A-1019) and the Core Melt Technology program (A-1218) will provide information on the production of combustible gases (carbon monoxide and hydrogen) due to core-concrete reactions. The Molten Core-Coolant Interactions program (A-1030) can provide information on the amounts and rates of hydrogen generated by the explosive and nonexplosive interactions of molten metals and water.

The primary objective of the Code Assessment and Applications program (A-1205) is to evaluate several thermalhydraulic computer codes (TRAC, RELAP4 and 5, etc.). A major subtask, however, is the assessment of the German (GRS) hydrogen transport code, RALOC. This code has been used to evaluate hydrogen transport and mixing times in various containments as a function of source rates and other initial conditions.

There are also several research programs that will use the codes and experimental data generated by the hydrogen programs. The Safety Margins for Containment program (A-1219) will use the predictions for mechanical loads resulting from combustion. The Containment Analysis (A-1198), MELCOR (A-1339), and SASA (A-1258) programs will all use the models and codes developed for hydrogen behavior analyses.

In the short time that the hydrogen research programs have been in place, we have already advanced our understanding of many hydrogen-related phenomena pertinent to reactor safety questions. We are quite optimistic that the ultimate result of these research efforts will be the resolution of hydrogen-related issues to the satisfaction of the NRC and most other affected parties, including the utilities, the industry, and the general public.

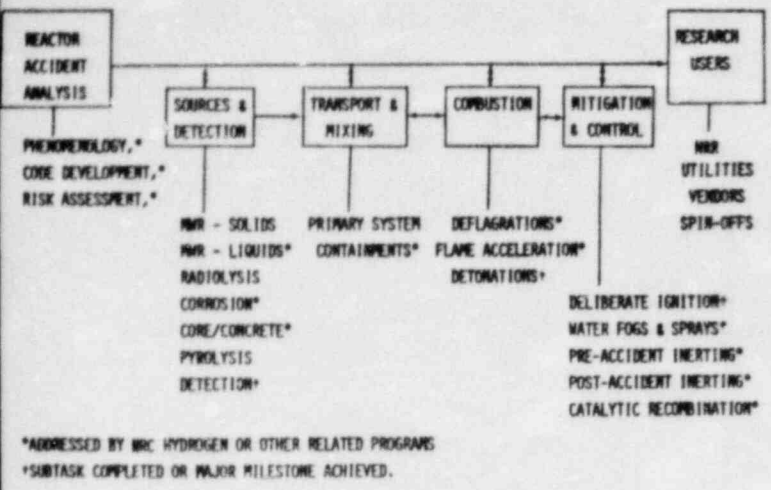

Figure 1. Aspects of the Hydrogen Behavior and Control problem for LWRs.

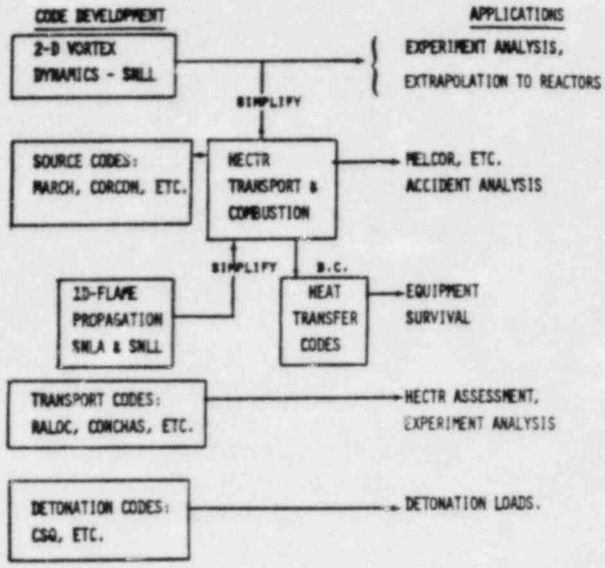

Figure 2. Relationship between the Various Code Development Tasks and their Applications.

HECTR

(HYDROGEN EVENT - CONTAINMENT TRANSIENT RESPONSE)

PURPOSE - CALCULATE TEMPERATURES, PRESSURES, GAS COMPOSITION, AND WALL TEMPERATURES AS A FUNCTION OF TIME IN MULTICOMPARTMENT REACTOR CONTAINMENTS.

Figure 3. The HECTR Computer Code.

EFFECTS INCLUDED IN HECTR

- FLAME INITIATION AND PROPAGATION
- GAS FLOW BETWEEN COMPARTMENTS
- RADIATIVE HEAT TRANSFER
- CONVECTIVE HEAT TRANSFER
- WALL CONDENSATION
- WALL HEAT CONDUCTION
- CONTAINMENT SPRAYS
- INTERCOMPARTMENT FANS
- ICE CONDENSERS

Figure 4. List of the Features Included in the Present Version of HECTR.

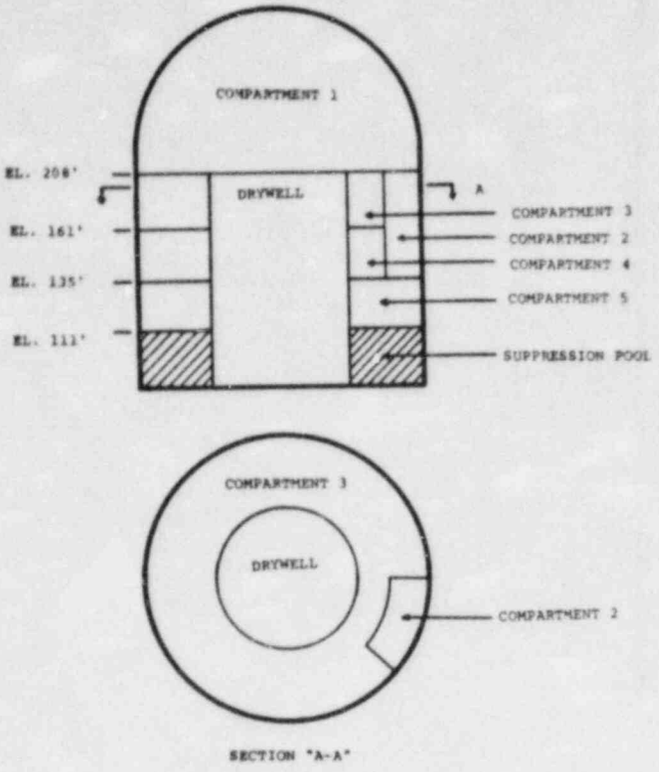

Figure 5. Five-Compartment Model of Grand Gulf used for some of the HECTR Calculations.

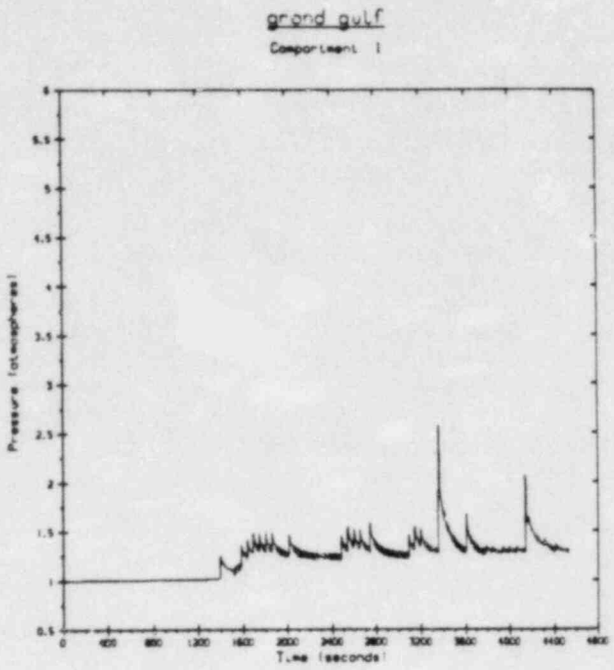

Figure 6. HECTR Calculation of Pressure in Grand Gulf (5-Compartment Model) for One Accident Scenario.

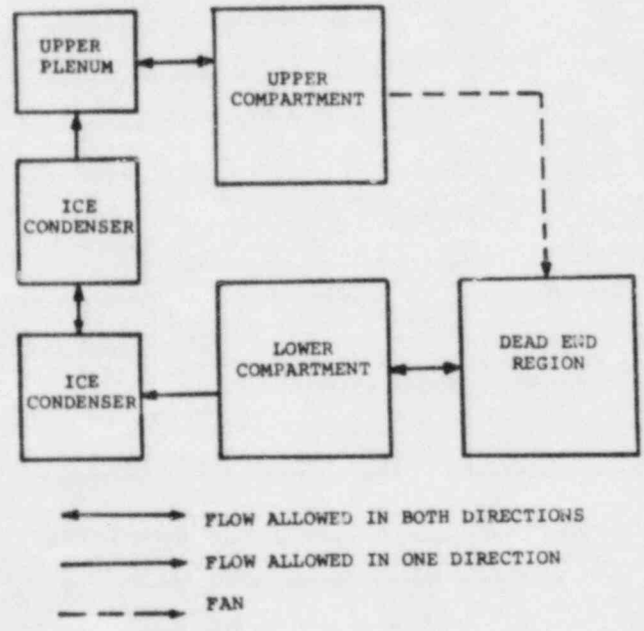

Figure 7. Six-Compartment Model of an Ice-Condenser Plant Used for HECTR Calculations.

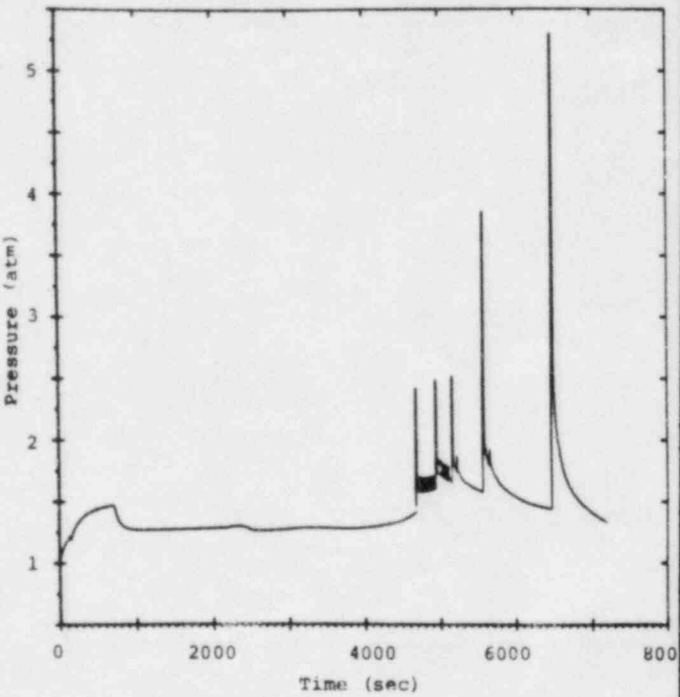

Figure 8. HECTR Calculation of Pressure in an Ice-Condenser Plant (6-Compartment Model).

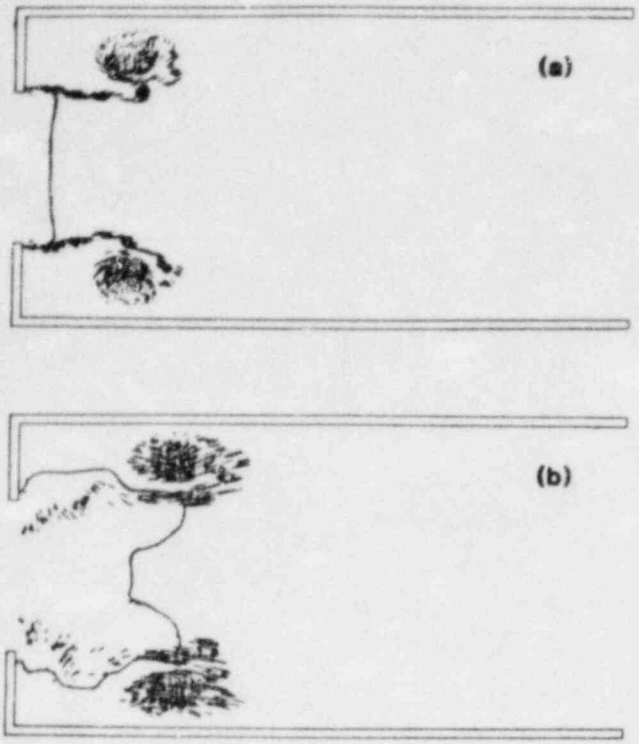

Figure 9. Vortex-Dynamics Calculation of Flame Propagation from a 2-D Orifice Slot.

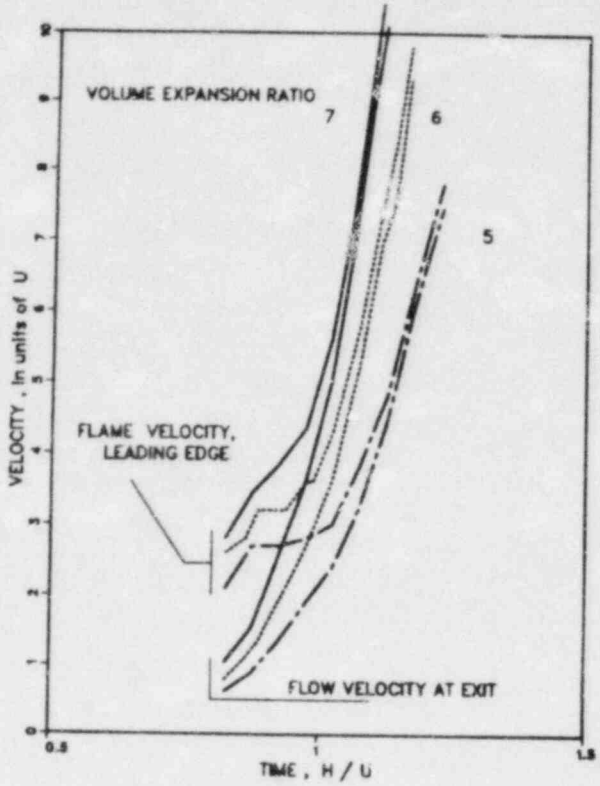

Figure 10. Vortex-Dynamics Calculation of Flame Acceleration due to an Orifice in a Channel.

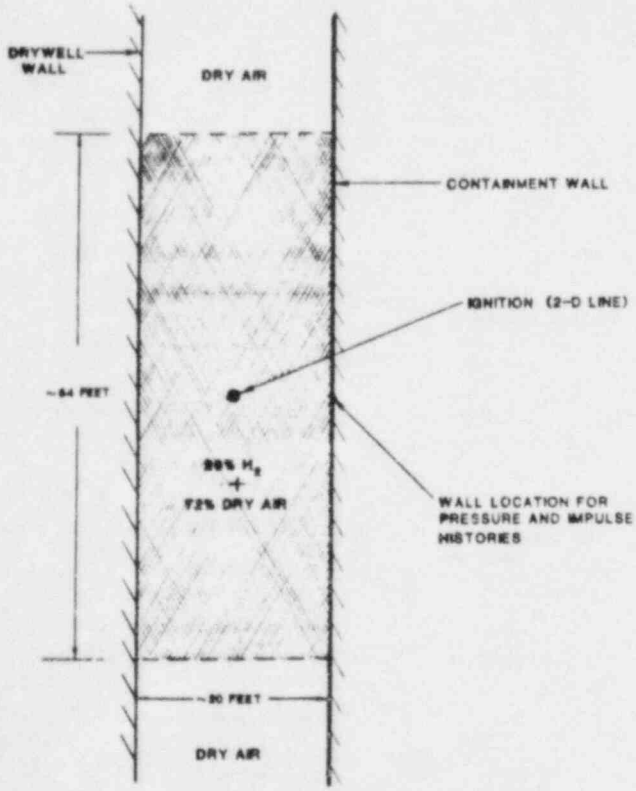

Figure 11. Grand Gulf Wetwell Geometry (2-D) Used for CSQ Detonation Calculation.

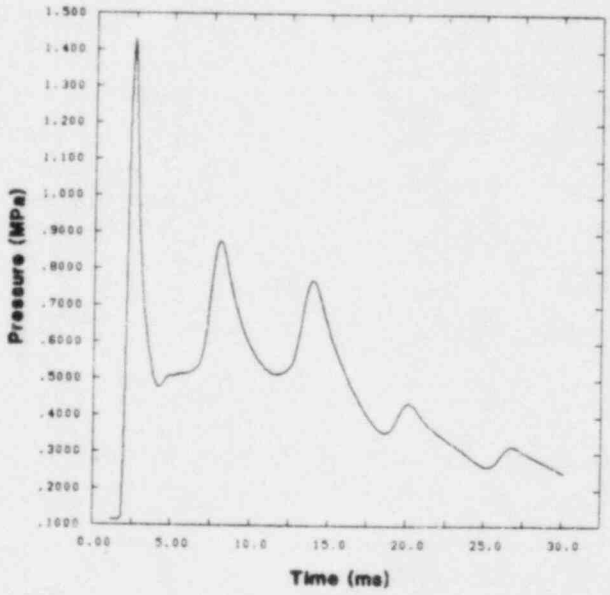

Figure 12. Pressure History Calculated by CSQ Using Geometry Shown in Fig. 11.

OPERATIONAL:

- LABORATORY-SCALE (FOG & FOAM)
- VGES 16-FT TANK
- McGILL TESTS
- FITS TANK
- STEAM:HYDROGEN JET
- VGES PLASTIC BAG DETONATIONS

OPERATIONAL IN FY83:

- VGES ACCELERATED FLAME FACILITY, "FLAME"
- VGES 18" STEAM:HYDROGEN DETONATION TUBE

PLANNED ACCORDING TO NEED:

- CHARGED DROPLET APPARATUS
- VERY LARGE SCALE TRENCH (MAY NOT BE NEEDED IF EPRI/NTS 52' SPHERE IS ADEQUATE)

Figure 13. Experimental Facilities Available for the Hydrogen Research Effort.

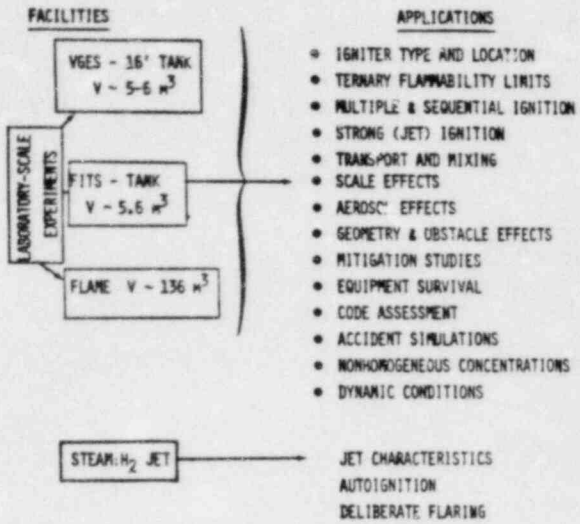

Figure 14. Experimental Facilities for Deflagration Tests.

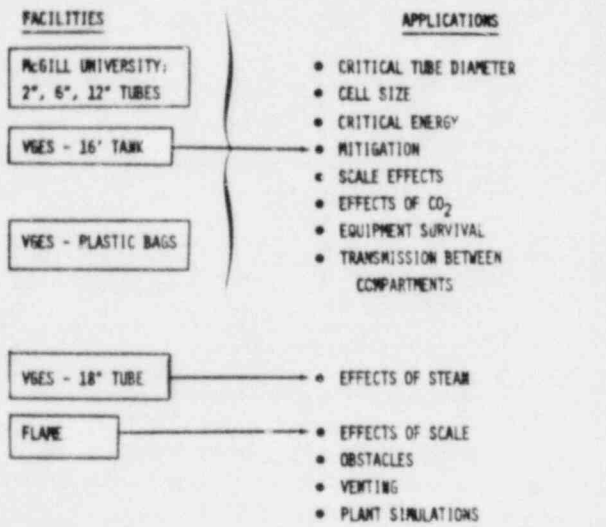

Figure 15. Experimental Facilities for Detonation Tests.

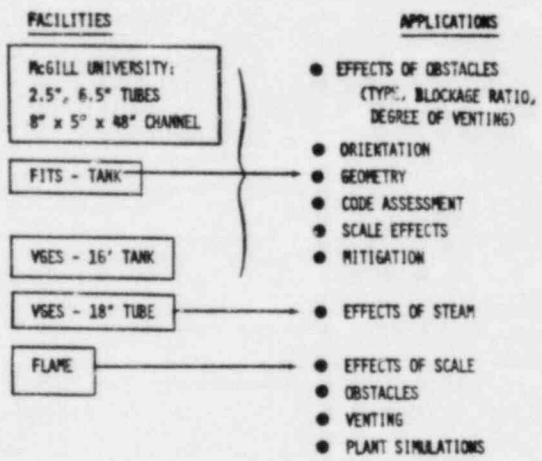

Figure 16. Experimental Facilities for Flame-Acceleration Tests.

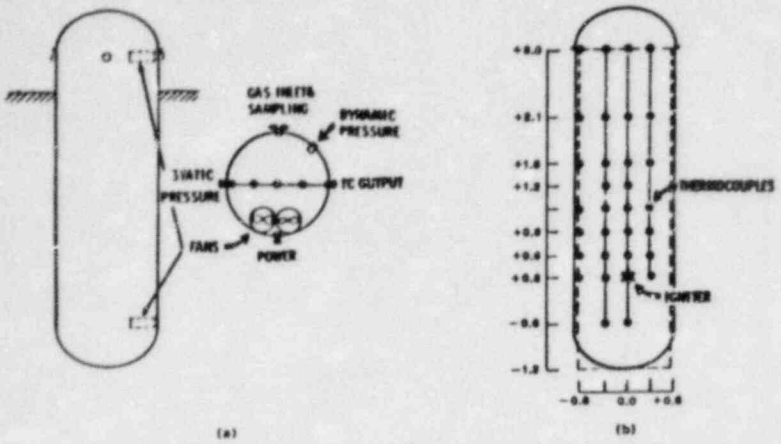

Figure 17. VGES Burn Tank: (a) Layout, (b) Thermocouple Instrumentation.

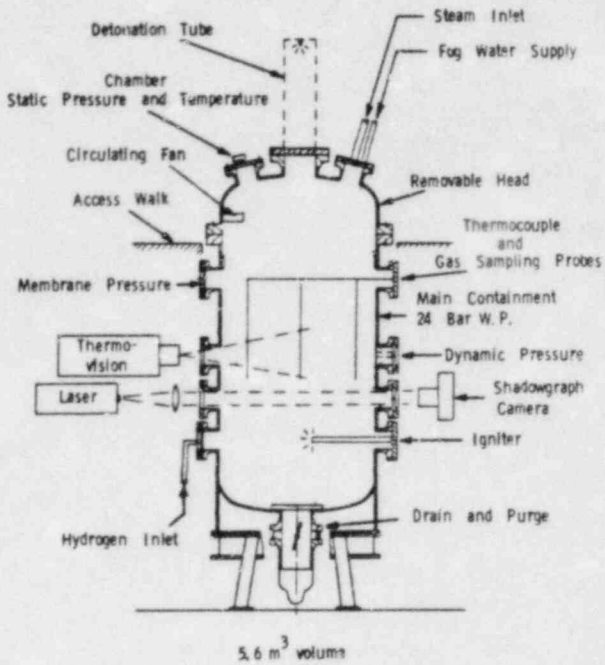

Figure 18. FITS Burn Tank (Modified for Heating to ~100°C).

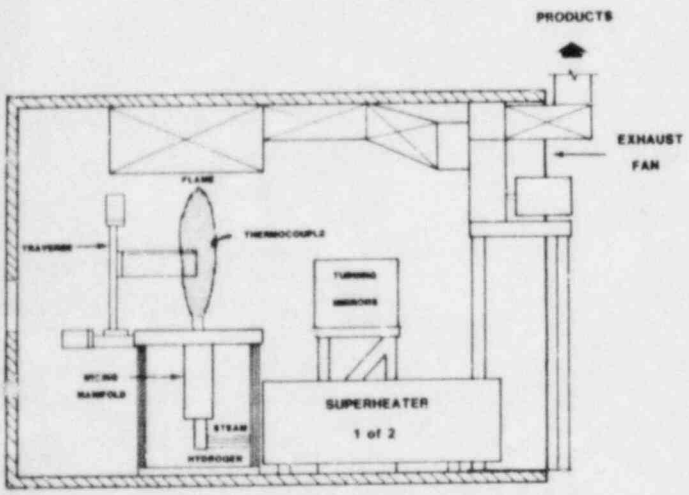

Figure 19. Steam:Hydrogen Jet Facility.

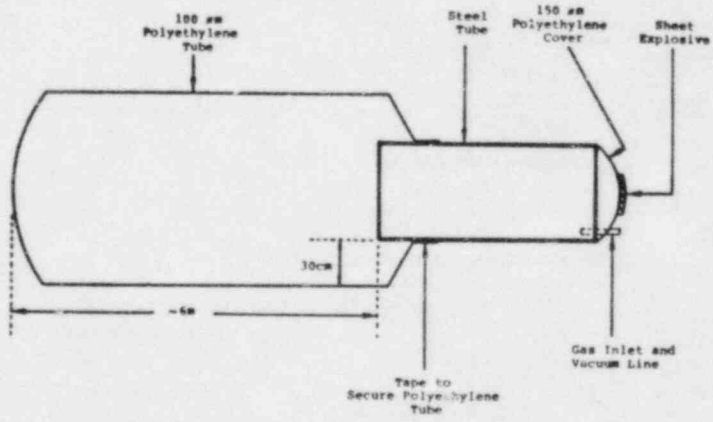

Figure 20. Critical-Tube-Diameter Test Facility.

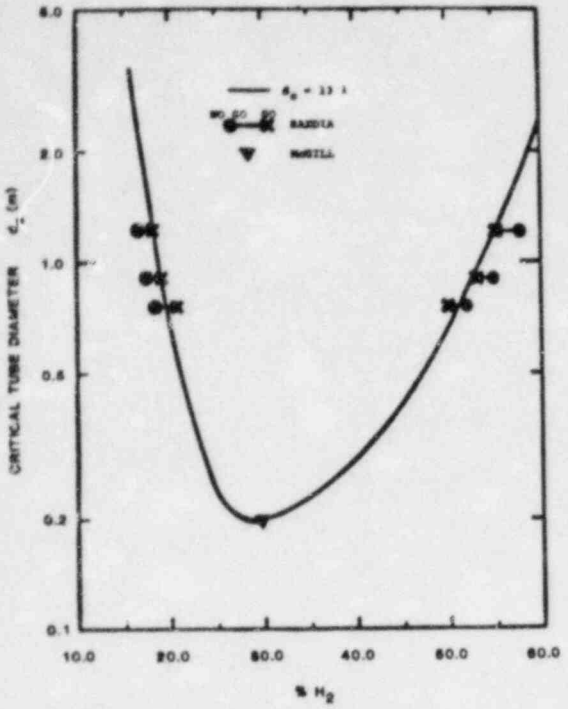

Figure 21. Critical-Tube-Diameter Measurements at Sandia and McGill Compared to the 13λ Correlation.

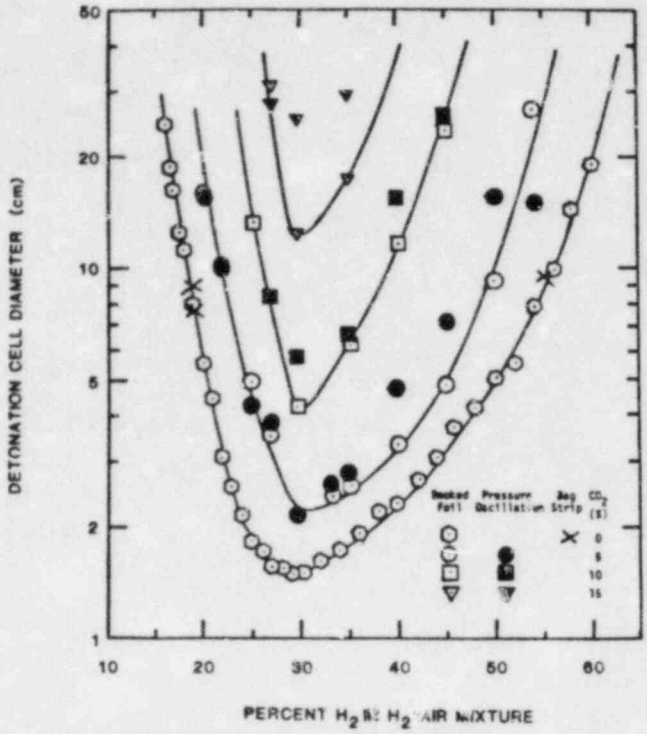

Figure 22. Detonation Cell Diameter Measurements for Various H_2:air:CO_2 Mixtures.

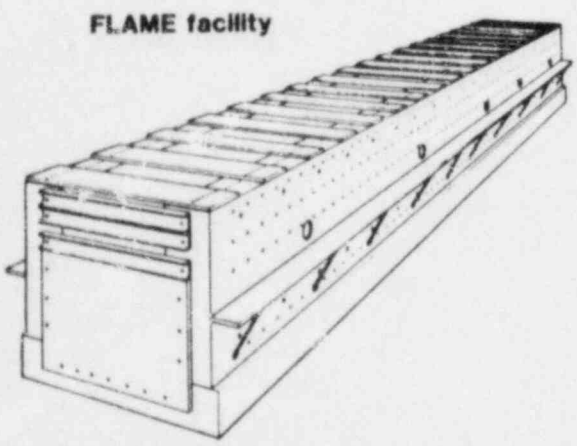

Figure 23. Artist's Drawing of the FLAME Facility (Channel width 6', height 8', length 100').

- HYDROGEN BEHAVIOR (A-1246)
- HYDROGEN COMBUSTION MITIGATIVE AND PREVENTIVE SCHEMES (A-1336)
- HYDROGEN BURN SURVIVAL (A-1270, A-1306)
- COMBUSTIBLE GAS IN CONTAINMENT (A-1255)
- REVIEW OF THE GRAND GULF HYDROGEN IGNITER SYSTEM (A-1301)

- MOLTEN CORE-CONCRETE INTERACTIONS (A-1019)
- CORE MELT TECHNOLOGY (A-1218)
- MOLTEN CORE-COOLANT INTERACTIONS (A-1030)
- CODE ASSESSMENT AND APPLICATIONS (A-1205)
- SAFETY MARGINS FOR CONTAINMENT (A-1219)
- CONTAINMENT ANALYSIS (A-1198)
- MELCOR (A-1339)
- SASA (A-1258)

- EPRI
- IDCOR
- HCOG

- FOREIGN RESEARCH PROGRAMS AND STUDIES

Figure 24. Hydrogen Research Programs at Present.

Hydrogen Burn Survival Program

W. H. McCulloch
Sandia National Laboratories
Albuquerque, New Mexico

SUMMARY

1.0 INTRODUCTION

In severe nuclear power station accidents, there is a possibility that substantial quantities of hydrogen may be released into the containment building. Analyses have indicated that under some circumstances in some containments there is the potential for the release of enough hydrogen to threaten the integrity of the containment building should the hydrogen be ignited. To prevent the accumulation of dangerous concentrations of hydrogen, some plants and plant designs now include systems to deliberately ignite the hydrogen before potentially damaging levels are reached. This protects the containment building but presents a challenge to equipment which might be subjected to repeated hydrogen burns. Of particular concern is the exposure of components vital to the safe operation of the plant.

As part of the response to this issue, the Hydrogen Burn Survival (HBS) Program was initiated at Sandia National Laboratories in Albuquerque, NM, (SNLA) by the Offices of Nuclear Reactor Regulation (NRR) and Nuclear Reactor Research (RES) of the Nuclear Regulatory Commission (NRC) late in FY 1981. The near-term goal of the HBS Program is to provide to the NRC, specifically to NRR, an analytical procedure whereby equipment survivability analyses submitted by license applicants may be evaluated. In the course of generating this analytical procedure, a more general purpose is being served, i.e., the development of a more definitive understanding of the phenomena of hydrogen combustion in reactor containments and the responses of safety-related equipment to hydrogen burn environments.

2.0 PROGRAM PLAN

The plan for reaching the objectives of the HBS Program involves the utilization of existing capabilities at SNLA, namely, applicable test facilities and related analytical efforts in heat transfer and hydrogen combustion. Experiments are designed to identify pertinent parameters and physical mechanisms. New insight from the experiments are incorporated in analytical models which, in turn, are verified by additional experiments. When the credibility of the models is established (to the degree possible in sub-scale tests), the responses of components to full-scale hydrogen burns can be calculated. These calculations can also provide descriptions of the environments seen by the components, making possible the specification of test conditions to simulate full-scale hydrogen burn exposures. Thus the responses of actual components to these environments can and will be demonstrated experimentally.

To date, experiments have included test series at the Variable Geometry Experimental System (VGES) and the Fully Instrumented Test System (FITS). Both of these facilities consist of vertical cylindrical tanks, 5.7 m^3 and 5.6 m^3, respectively, and associated controls and instrumentation to conduct tests over a range of gas mixture compositions.

Shortly, we will begin tests at the Central Receiver Test Facility (CRTF), a solar facility also located at SNLA. The CRTF offers the capability of a programmed thermal flux input to test specimen. We plan to simulate heat flux profiles from both the test facilities and full-scale reactor containment burns. Data from these tests will corroborate the results from analytical models and show the impacts of hydrogen burn environments on components.

3.0 FUTURE ACTIVITIES

The outgrowth of these activities is expected to be an experimentally verified analytical representation of the physical phenomena involved in the exposure of safety-related equipment to hydrogen burn environments. This involves somewhat elaborate heat transfer and hydrogen combustion computer codes. Our intent is to use the complex models to develop analytical tools that do not require the use of large computer systems. These general tools will be used by NRR to evaluate analyses submitted by license applicants.

4.0 OBSERVATIONS TO DATE

Although the general analytical tools will not be developed until next year, the experimental and analytical activities to date have provided some significant insights.

Comparison of VGES and FITS test data with calculations for ice condenser pressurized water reactors indicates that gas temperatures in full-scale containments remain elevated for much longer times than for similar burns in smaller vessels. One implication of this fact is that responses of components in test facility (i.e., small) environments cannot be taken directly as indications of responses to burns in larger containment volumes since these burns will produce significantly higher component temperatures.

Preliminary single burn analyses indicated that, depending on location in containment, thermal mass, and accident scenario, components may reach temperatures in excess of LOCA qualification guidelines. It must be noted that in these analyses components were treated as being fully exposed to the environment. No consideration was given to the thermal protection provided by structures attached to or near the components. Cable exposed in the FITS tests and equipment removed from the TMI containment have shown that the effects of such protection can be significant.

Recent calculations using an improved code have shown component temperatures in response to hydrogen burns somewhat higher than those predicted earlier. In addition, these analyses have shown that a series of burns, as is expected in some accident sequences, produces a "ratcheting" effect in component temperature, i.e., there is not enough time between burns for components to cool back to the initial temperature so that each burn in the series produces higher component temperatures. Therefore, multiple burns can be expected to produce substantially higher peak component temperatures than single burns in a given situation.

CORCON Molten Fuel-Concrete Interactions Code

Randall K. Cole, Jr.
Sandia National Laboratories
Albuquerque, New Mexico

INTRODUCTION

The CORCON code[1] is being developed at Sandia National Laboratories to model the interaction of molten core materials with concrete during a hypothetical core-melt accident. A MOD1 version of the code has been available since late 1980. This version is applicable to the early stages of the interaction; crusting and freezing are not considered. Also, interaction with water in the reactor cavity is not allowed. We are currently developing a MOD2 version of the code in which these restrictions will be removed. In addition to developing new models, we are supplying user support for MOD1, and are assessing the importance and suitability of models contained in it. In several cases, this has led to improvements which will be included in MOD2. We expect this new version of the code to be available for testing early in 1983.

CRUSTING/FREEZING MODEL

The major new model to be included in CORCON-MOD2 is a crusting/freezing model. An important assumption in MOD1 is that the pool remains liquid. Each phase (metallic or oxidic) is considered to be well-stirred and isothermal, except for thin thermal boundary layers, and convective heat-transfer correlations are used to calculate the heat flux at each surface. When a calculated interface temperature falls below the solidification temperature, a two-phase multiplier greatly increases the calculated viscosity. This reduces the corresponding heat-transfer coefficient, simulating the effect of a conductive crust. Once the bulk of the layer falls below the solidification temperature, however, the model is clearly invalid, although it probably provides an upper bound on the erosion of concrete and the generation of combustible gases.

A significant improvement in MOD2 will be the inclusion of a crust and freezing model, which will provide a more realistic treatment of crust formation and allow the calculation to continue through to the eventual solidification of the debris. This will require consideration of heat transfer by conduction in solid regions and by bubble-enhanced or natural convection (with a conduction limit) in liquid regions of an axisymmetric domain with volumetric heating. Because conditions are slowly changing, with a time scale of hours to days, we have chosen to neglect transient effects, and are developing a quasi-steady model.

In the version currently being tested, the two-dimensional problem has been further simplified by averaging over horizontal areas for axial heat transfer, and over vertical areas for radial heat transfer, within each layer of the pool. The result is that the two-dimensional problem is replaced by two independent one-dimensional ones formulated in terms of the average layer temperature and the average boundary temperatures. In each direction, an effective volumetric source is determined for which the corresponding one-dimensional, steady temperature profile has the desired average, and the resulting heat fluxes are used. This profile can have liquid and solid regions, and can include convective and conductive heat transfer. The method therefore provides a general solution for fully liquid, crusted, or fully frozen layers, with natural transitions between layer regimes. The two one-dimensional solutions are coupled only indirectly, through their effects on the average temperature of the layer as determined by the layer energy equation.

This model is incorporated into CORCON's multilayer geometry by solving for the axial heat transport in each layer for assumed interface temperatures which are then adjusted to obtain continuity of heat fluxes at the interfaces. Because the heat flux at

the top (bottom) of a layer may depend on the temperature of the bottom (top), this is rather more complicated than in MOD1, and requires an iteration. Radial transport is independent of axial, and involves only one layer at a time; therefore, no such iteration is required.

A layer may be entirely liquid, entirely solid, or crusted on one or more surfaces. Therefore, a one-dimensional calculation may involve as many as three subregions. While the temperatures of any internal interfaces are known (the solidification temperature), the positions are not and must be determined from the requirements of constant volumetric heat source, continuous heat flux, and desired average temperature. This requires another iteration.

Coding of the model involves three levels of subroutines. The highest solves iteratively for the temperatures of interfaces between layers, given the heat transfer within each layer. The second evaluates single-layer heat transfer, determining the positions of solid/liquid interfaces if present. This may require calling a third-level subroutine to calculate the heat transfer within a liquid (sub) layer. Here, bubble-driven and natural convection are considered, subject to a conduction limit; the regime is chosen based on the greatest Nusselt number.

The various sub-models have been tested independently, outside of CORCON, and found to perform as expected. Concurrent with this, we have modified the calculational structure of CORCON to take the new form just described, while maintaining MOD1 models. This has allowed us to verify that the old results could be obtained from the new structure, before new heat-transfer models were added. The final step, installation of the crusting/freezing model into CORCON is now under way, and no major difficulties are expected.

The process of crust formation and freezing in the presence of high gas fluxes is not well understood. Various concepts have been proposed including: the formation of fumaroles which allow gas venting during the freezing process; the formation of a frothy but permeable solid; the formation of a frothy but impenetrable solid; the formation of a dense solid. The last two cases would indicate that the only path available for gas release would be through the film between the melt and the solid concrete. A qualitative set of experiments is being performed to investigate the freezing process at small scale. Simulant pairs have so far included dry ice with water, mercury and solder. This investigation is continuing.

OXIDIC-PHASE VISCOSITY MODEL

In CORCON-MOD1, the viscosity of oxidic mixtures is calculated from a Kendell-Monroe[2] relation if the silica content is low, and from the VISRHO model if it is high. Our assessment effort has revealed a number of problems with this. For one thing, the calculated viscosity is not a continuous function of silica content. This could, of course, be corrected by a suitable smoothing or interpolation. However, and more importantly, the model was also seen to give unrealistically high viscosities for some compositions at high temperatures. The VISRHO[3] model is based on a correlation developed by Bottinga and Weill[4] for magmatic materials. Application to many situations occurring in core melt accidents requires aliasing of constituents (magmas contain no significant amounts of UO_2 or ZrO_2) and extrapolation in temperature (the original correlation is limited to temperatures below 1800°C). The accuracy of the results is questionable.

H. R. Shaw,[5] working from the Bottinga-Weill correlation, observed that all plots of log-viscosity against inverse temperature yielded straight lines which passed through or near a single convergence point. If this point is taken as fixed, viscosity is fully determined by the slope, s, of the line in the form

$$\ell n\ \mu = A + s(10^4/T-C)$$

Finally, Shaw correlated s as proportional to the silica content of the mixture, with a proportionality constant which is determined linearly by the non-silica composition.

Shaw's model is limited to mixtures with moderate-to-high silica content. At low silica contents it gives unreasonably low values. We are currently testing a formulation which uses the greater of the values calculated from the Kendell-Monroe and Shaw models. As a function of silica content, the cross-over always occurs near 30 mole percent silica.

A significant structural change in the liquid takes place at the orthosilicate point (33 mole percent silica), which is the threshold for cross-linking of silicate tetrahedra. Therefore, it is not surprising that a change in the viscosity model should occur at or near this composition.

REFERENCES

1. J. F. Muir, et al., CORCON-MOD1: An Improved Model for Molten-Core/Concrete Interactions, July 1981, NUREG/CR-2142, SAND80-2415.
2. J. Kendell and K. P. Monroe, "The Viscosity of Liquids, III Ideal Solutions of Solids in Liquids," Journal of the American Chem. Soc., Vol. 30, No. 9, P. 1802, September 1917.
3. D. A. Powers, A. W. Frazier, VISRHO: A Computer Subroutine for Estimating the Viscosity and Density of Complex Silicate Melts, SAND76-0649, Sandia National Laboratories, Albuquerque, NM (June 1977).
4. Y. Bottinga and D. F. Weill, "The Viscosity of Magmatic Silicate Liquids: A Model for Calculation," American Journal of Science, Vol. 272, pp. 438-475, 1972.
5. H. R. Shaw, "Viscosities of Magmatic Silicate Liquids: An Empirical Method of Prediction," American Journal of Science, Vol. 272, November 1972, pp. 870-893.

CORCON

MOLTEN FUEL-CONCRETE INTERACTIONS CODE

R. K. COLE, JR.
D. P. KELLY
M. A. ELLIS
M. BERMAN

Sandia National Laboratories

CORCON DEVELOPMENT

OBJECTIVE

DEVELOP AND VERIFY A CODE FOR CALCULATION OF THE INTERACTIONS OF MOLTEN CORE MATERIALS WITH CONCRETE. PRINCIPAL CONCERNS INCLUDE

- RATE AND GEOMETRY OF MELT PENETRATION
- RATE AND NATURE OF GAS EVOLUTION
- OTHER SOURCE TERMS TO CONTAINMENT

CORCON DEVELOPMENT

MOD1 VERSION

- AVAILABLE SINCE NOVEMBER 1980
  "FROZEN" APRIL 1981
  MAINTENANCE LIMITED TO ERROR CORRECTION
- APPLICABLE TO EARLY STAGES OF INTERACTION IN DRY CAVITY
  NO CRUST OR FREEZING MODEL
  NO COOLANT LAYER PERMITTED

CORCON DEVELOPMENT

MOD2 VERSION

- TO BE AVAILABLE EARLY 1983
  WILL BE "FROZEN" AFTER INITIAL FIELD TEST
- MORE GENERAL APPLICABILITY THAN MOD1
  INITIAL CRUST/FREEZING MODEL
  ADDITION OF COOLANT LAYER
- RESTRUCTURED FOR EASIER COUPLING TO CONTAINMENT CODES

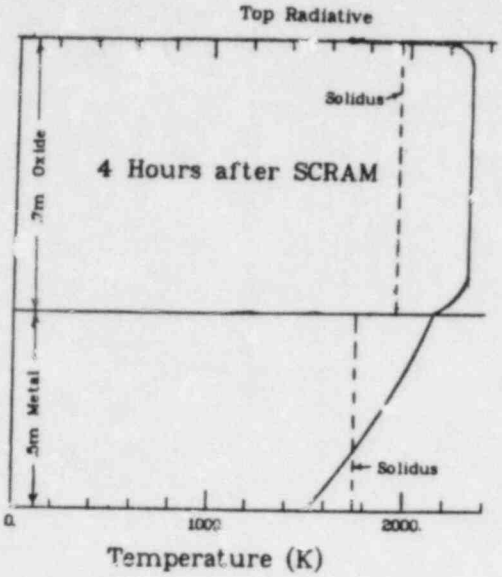

CORCON DEVELOPMENT

CRUST/FREEZING MODEL

- QUASI-STEADY (NON-DYNAMIC)
- 2-D PROBLEM REDUCED BY SPATIAL AVERAGING TO
  - 1-D AVERAGE AXIAL HEAT FLOW
  - 1-D AVERAGE RADIAL HEAT FLOW
- AXIAL AND RADIAL HEAT TRANSFER COUPLED ONLY THROUGH ENERGY EQUATION
- AXIAL (HORIZONTAL) INTERFACE TEMPERATURES DETERMINED BY CONTINUITY OF HEAT FLUX

CORCON DEVELOPMENT

SINGLE-LAYER HEAT TRANSFER

- INDEPENDENT 1-D AXIAL AND RADIAL SOLUTIONS
- FORMULATED IN TERMS OF AVERAGE LAYER AND BOUNDARY TEMPERATURES
- EACH LAYER MAY CONTAIN LIQUID AND/OR SOLID REGIONS
- REQUIRE (SPATIALLY) CONSTANT VOLUMETRIC HEATING AND CONTINUOUS HEAT FLUX

CORCON DEVELOPMENT

HEAT TRANSFER MECHANISMS

- IN LIQUID
  1. BUBBLE DRIVEN CONVECTION
  2. NATURAL CONVECTION
  3. CONDUCTION

  REGIME DETERMINED BY LARGEST NUSSELT NUMBER
- IN SOLID
  1. CONDUCTION (INCLUDING EFFECTS OF VOLUMETRIC HEATING)

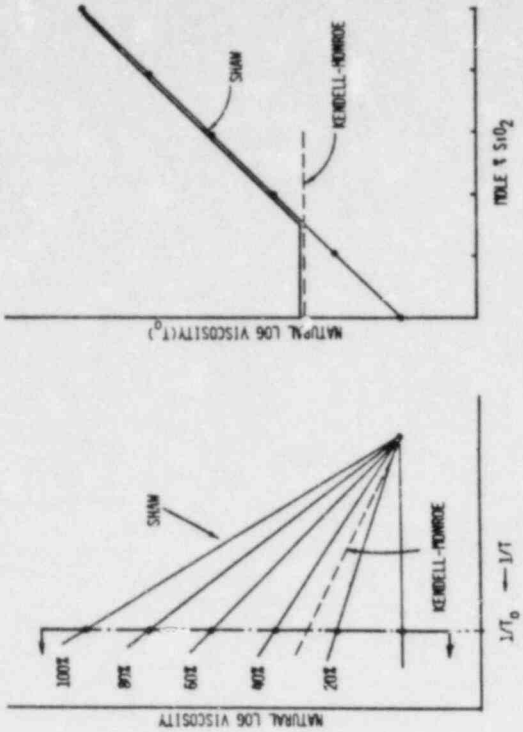
SHAW
KENDELL-MONROE
MOLE % SiO_2
NATURAL LOG VISCOSITY (T_0)

SHAW
KENDELL-MONROE
100%
80%
50%
40%
20%
$1/T_0$ — $1/T$
NATURAL LOG VISCOSITY

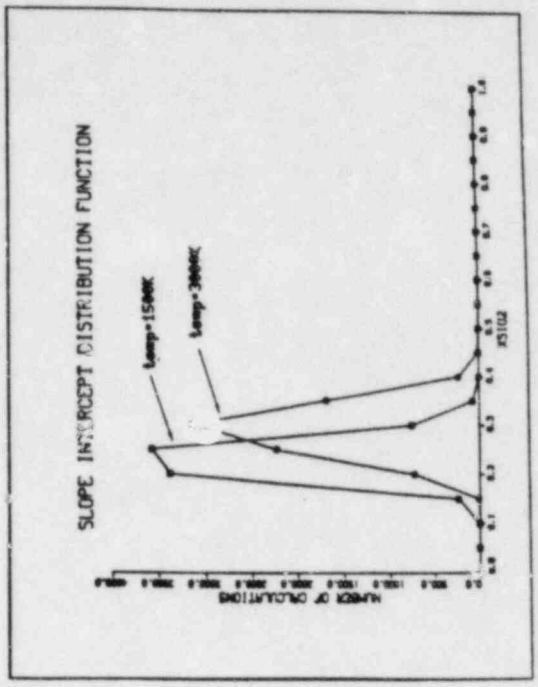
SLOPE INTERCEPT DISTRIBUTION FUNCTION
Lamp=1540K
Lamp=3000K
NUMBER OF CALCULATIONS

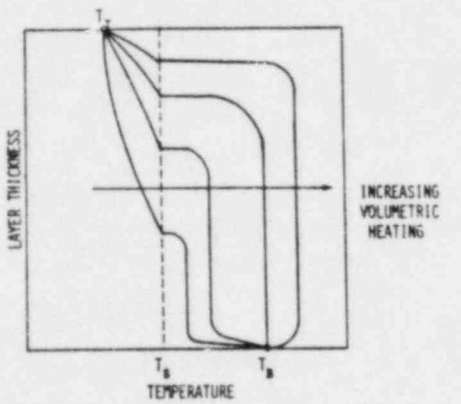
LAYER THICKNESS
INCREASING VOLUMETRIC HEATING
T_s
T_b
TEMPERATURE

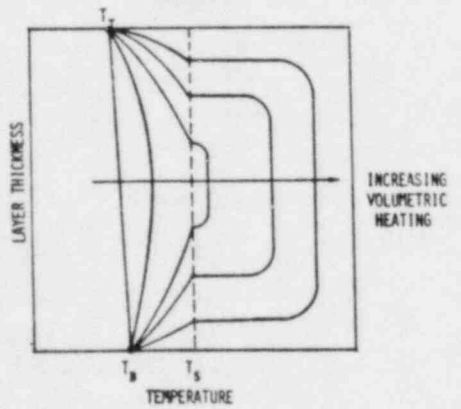
LAYER THICKNESS
INCREASING VOLUMETRIC HEATING
T_b
T_s
TEMPERATURE

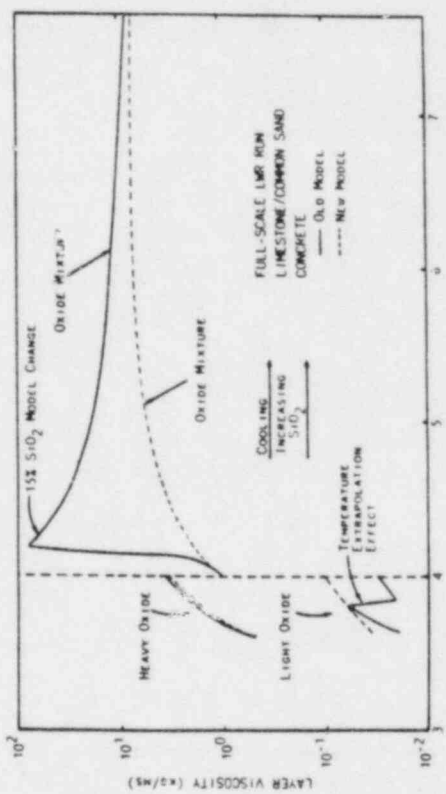
15% SiO_2 Model Change
Oxide Mixture
Oxide Mixture
Cooling
Increasing SiO_2
Temperature Extrapolation Effect
Heavy Oxide
Light Oxide
Full-Scale LMR Run
Limestone/Common Sand Concrete
Old Model
New Model
Layer Viscosity (x0/ms)
Time After Scram (hr)

The Status of the CONTAIN Computer Code for LWR Containment Analysis[+]

K. D. Bergeron, K. K. Murata, P. E. Rexroth, M. J. Clauser, H. E. Senglaub, F. W. Sciacca*, and W. Trebilcock

Division 9424, Sandia National Laboratories[++], Albuquerque, N.M. 87185

ABSTRACT

The current status of the CONTAIN code for LWR safety analysis is reviewed. Three example calculations are discussed as illustrations of the code's capabilities: (1) a demonstration of the spray model in a realistic PWR problem, and a comparison with CONTEMPT results; (2) a comparison of CONTAIN results for a major aerosol experiment against experimental results and predictions of the HAARM aerosol code; and (3) an LWR sample problem, involving a TMLB' sequence for the Zion reactor containment.

INTRODUCTION

The CONTAIN computer code is a highly mechanistic treatment of phenomena occuring in the containment building during a hypothetical severe reactor accident. It is designed to model any type of commercial power reactor, but at present it is limited to LMFBRs and LWRs. This paper reports on the status of CONTAIN for LWR accident analysis.

The code is very modular and flexible. Currently operational features include two-phase water thermodynamics, heat transfer to structures (including condensation and evaporation), aerosol particle distribution evolution, (including deposition, agglomeration, condensation, and evaporation), radioisotope transport and decay (for any number of isotope chains), hydrogen burn, intercell flow (including

+This work supported by the U.S. Nuclear Regulatory Commission.

*Under contract from Energy, Inc.

++Operated for the U.S. Department of Energy under contract number DE-AC-04-76DP00789.

release from containment) engineered safety features, and a number of phenomena occuring in the reactor cavity pool.

RECENT PROGRESS

In January, 1982, a CONTAIN code review was held by NRC. This was followed shortly by the release of an interim version of the code to selected users in order to obtain feedback concerning the use of the code for practical applications. A stand-alone version of the aerosol module, called MAEROS, has also been made available to the code centers.

In parallel with these releases, a substantial amount of effort in the past year has gone into making the code useful for practical applications. An organized program of testing has been initiated, encompassing tests of the logic and physics of individual modules, as well as verification and validation efforts for more integrated applications. A document has been written describing guidelines for standardized testing procedures. Each test is given a test index, and the results of the tests, successful or not, are reported in a Test Summary Report, which is kept in a computerized file. The input data set is also archived in a computer file so that the tests can be rerun on new versions of the code. There are over fifty tests which have been archived in this way. Separate effects tests have been conducted for all the features described earlier, though in some cases, not all facets of the models have been exhaustively tested.

In addition, there are two major validation exercises underway, involving comparison of the code's predictions against experimental results. The first is the ABCOVE experimental series, which provides an opportunity to compare CONTAIN's aerosol behavior predictions against large scale experiments and other aerosol codes. The second is the HDR experimental series in Germany, involving steam and water blowdowns in a full-size reactor containment building. These programs require "blind" predictions of experimental results and will be a serious test of the models which CONTAIN uses for the relevant phenomena.

In addition to the testing, there has been a considerable amount of development of new capabilities for CONTAIN. For example, improvements have been made to the aerosol and structure heat transfer models to include evaporation as well as condensation of steam.

The most important of the new modelling efforts for LWR applications has been the development of a framework for engineered safety features (ESF's) and the inclusion therein of containment spray and fan cooler models. The framework comprises the input, output, data transfer, and operational control functions for major engineered safety systems as well as various supporting components that direct flow into and out of these systems. The framework provides a modular structure for the insertion of physical models for each of the various systems and components. The major systems for which support is provided are 1) containment sprays, 2) fan coolers, 3) ice condensers, 4) suppression pools, and 5) filtered vents. Supporting components include pipes, valves, orifices, heat exchangers, pumps, and storage tanks.

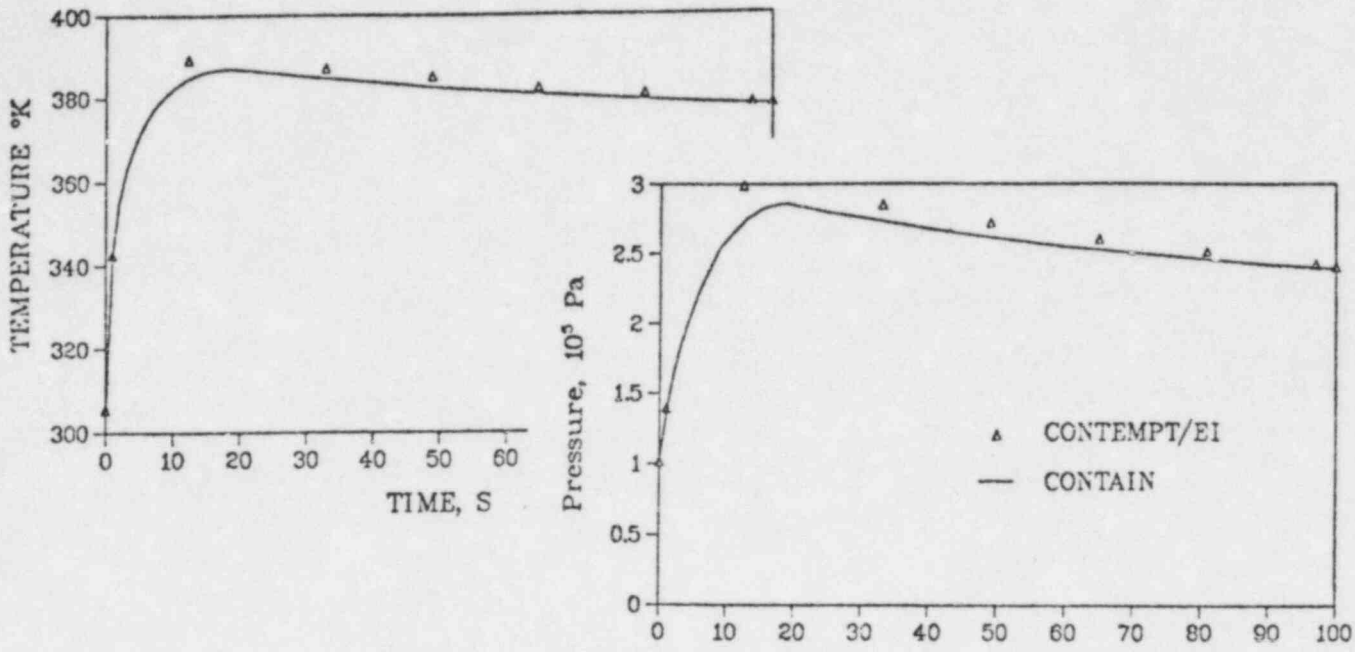

Figure 1. Containment spray test problem, based on the H. B. Robinson PWR.

Mechanistic models for each of these elements have been or will be developed.

Models for containment sprays and fan coolers have been implemented and undergone preliminary testing. The fan cooler model is based on a simple temperature-dependent heat transfer function, but the spray model is much more mechanistic. It assumes a single initial sized droplet falling vertically at terminal velocity through a homogeneous atmosphere. Heat and mass transfer rates to or from the droplet are determined using appropriate semi-empirical heat and mass transfer correlations (1). The equations of mass and enthalpy conservation are integrated simultaneously using a Runge-Kutta numerical scheme. At each integrating time step the droplet terminal velocity and physical properties are updated. The motion of the droplet is tracked until it either reaches the bottom of the cell or comes to thermodynamic equilibrium with the atmosphere.

To illustrate the operation of the ESF framework, a demonstration problem was run involving a large loss-of-coolant blowdown in a typical PWR plant. The problem is modeled after a sample case presented in the

CONTEMPT/EI user's manual (2). The containment sprays are activated at eight seconds into the blowdown, and the fan coolers come on at forty seconds. Comparisons of the CONTAIN and CONTEMPT/EI temperature and pressure histories are shown in Fig. 1. The agreement between the two codes is quite good. The lower values provided by CONTAIN at early times are probably the result of the more mechanistic (and best-estimate) models for structure condensation and containment sprays (CONTAIN treats steam condensation on droplets whereas CONTEMPT/EI does not).

To provide a test of the aerosol model in CONTAIN, calculations of an uranium oxide aerosol experiment in NSPP were made (5). In the experiment (NSPP Test 207) uranium oxide aerosols were injected into the experimental chamber for about 28 minutes. The source was then turned off, and the aerosols agglomerated and settled out. A fit to this experiment with HAARM-3 has previously been reported (5), and the results are reproduced in Figure 2. One CONTAIN calculation (Run A in Figure 2) used the same aerosol parameters as in the HAARM-3 calculation (aerodynamic shape factor $\chi = 3$, and agglomeration shape

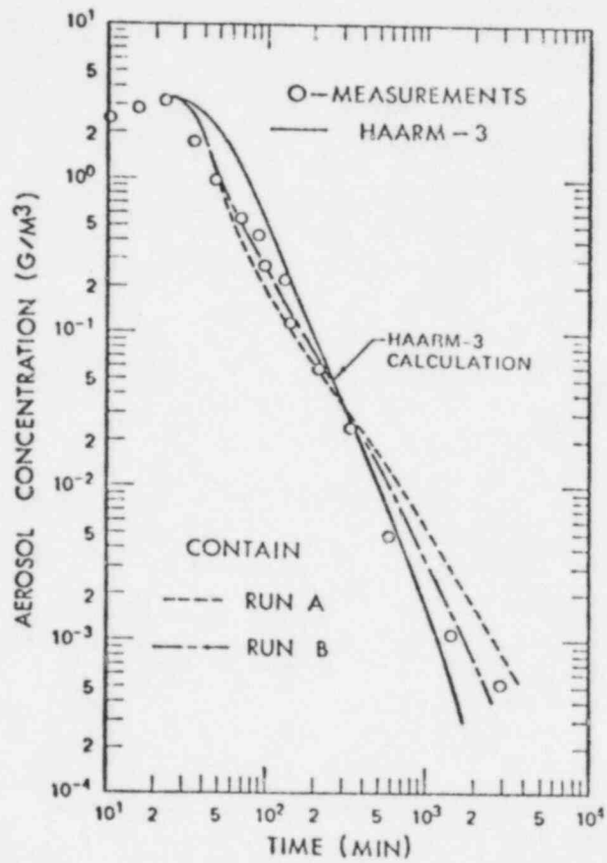

Figure 2. Measurements in NSPP test 207 with uranium oxide aerosols, and comparisons with CONTAIN and HAARM-3. Run A used the same shape factors as the HAARM calculation. Run B was a best fit to the shape factors.

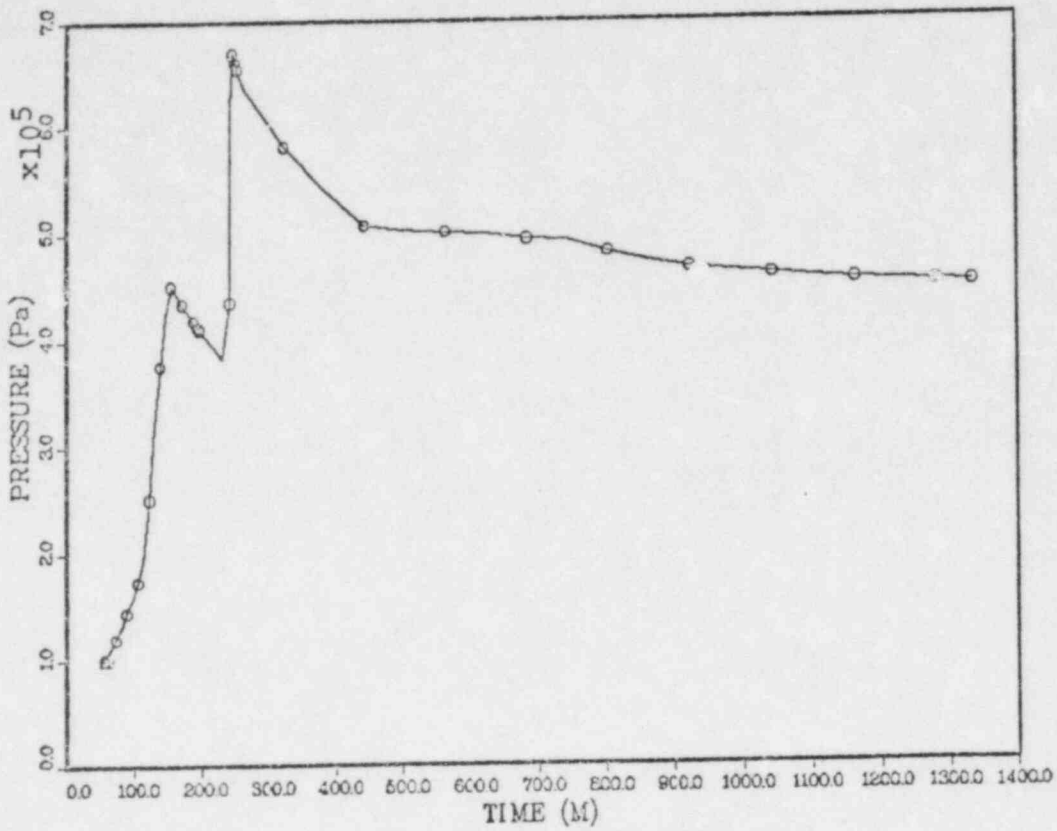

Figure 3. Pressure history from CONTAIN LWR sample problem, involving a TMLB' sequence in a Zion-like containment. Blowdown occurs at 55 minutes and vessel melt-through occurs at 240 minutes

factor Υ = 10.) Both the CONTAIN and HAARM runs started with an aerosol concentration of 3.4 g/m^3 (5) and used an initial mean radius of 0.43 μm. As can be seen, the two calculations are about equally consistent with the data.

A best fit to the experimental data using CONTAIN was also obtained (Run B). The aerodynamic shape factor used was χ =1.5 and the coagulation shape factor was Υ = 7.0. Since the median radius is obtained from the measured aerodynamic radius as the radius of a sphere of equivalent mass, it depends on the aerodynamic shape factor. For χ =1.5, the equivalent median radius is 0.53 μm. (To be consistent with χ =3, the radius in the first two calculations should have been 0.72 μm, not 0.43 μm.) As can be seen, excellent agreement with experiment can be obtained with the new parameters. The difference between CONTAIN and HAARM-3 in the first two calculations is believed due to the fact that CONTAIN uses a general histogram (or discrete) representation of the particle distribution function, whereas HAARM-3 makes the assumption of a lognormal distribution at all times. The fact that HAARM-3 predicts too large an aerosol concentration at early times and too small a concentration at late times is characteristic of lognormal codes (5).

A third and final example of the use of CONTAIN is a sample problem for LWR's which has recently been developed. A TMLB' sequence in a large dry containment (similar to Zion) is simulated. Source tables are used for 1) steam, fission product, and hydrogen release during the blowdown phase, 2) water and hydrogen release at vessel failure, and 3) non-condensible gases and aerosols (with associated radioisotopes) from a dry core-concrete interaction. These sources were obtained from MARCH (8) and CORCON (9) runs (i.e., neither the pool model nor the explicit CONTAIN-CORCON link was used.) The containment building was modeled as a single cell, while a second cell was used to follow releases from containment (e.g., to the auxilliary buildings.)

The purpose of the sample problem is to demonstrate the operation of as many of the features of the code as possible in a realistic application, rather then to provide a benchmark for comparison with other codes. Operational features include condensation and heat

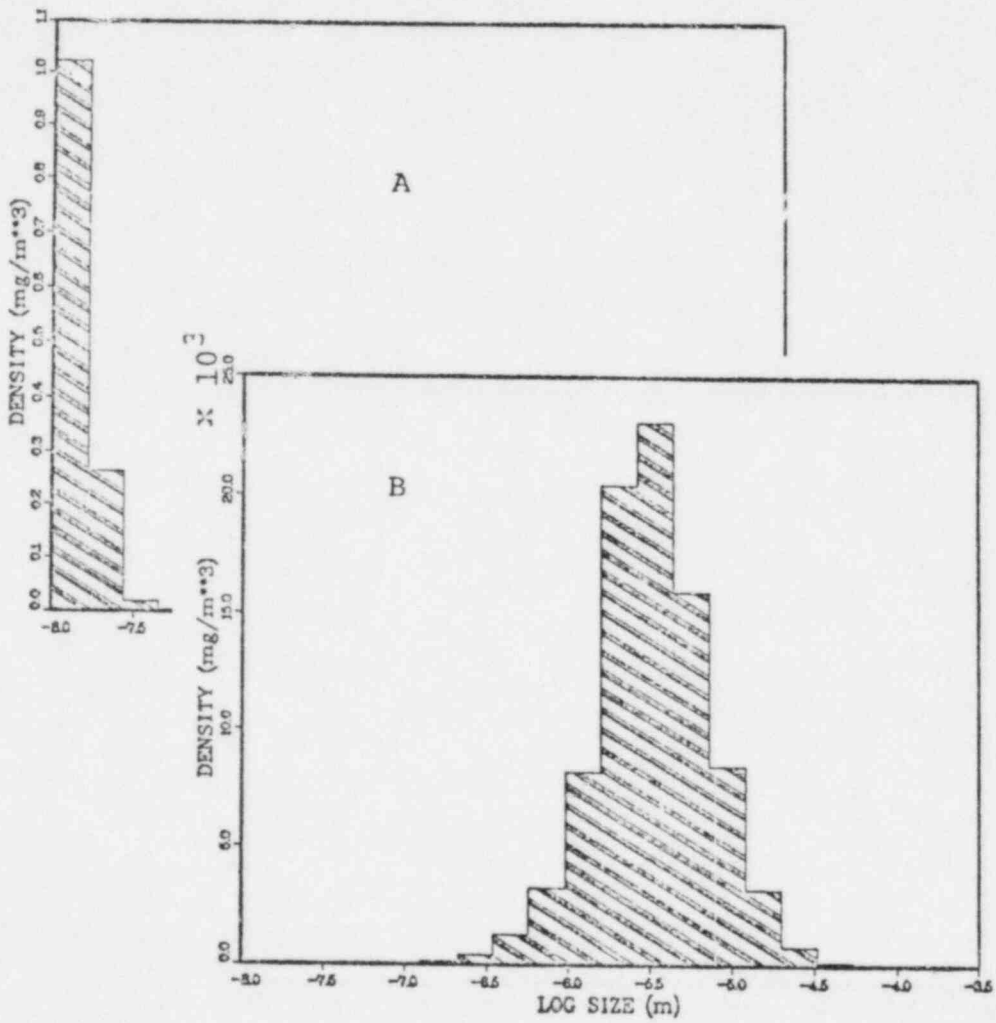

Figure 4. Aerosol size distribution for liquid water in containment atmosphere; a) seed distribution used for homogeneous condensation of blowdown steam; b) 17 minutes after the start of blowdown. Note increase in mass density and particle sizes due to condensation on the aerosols.

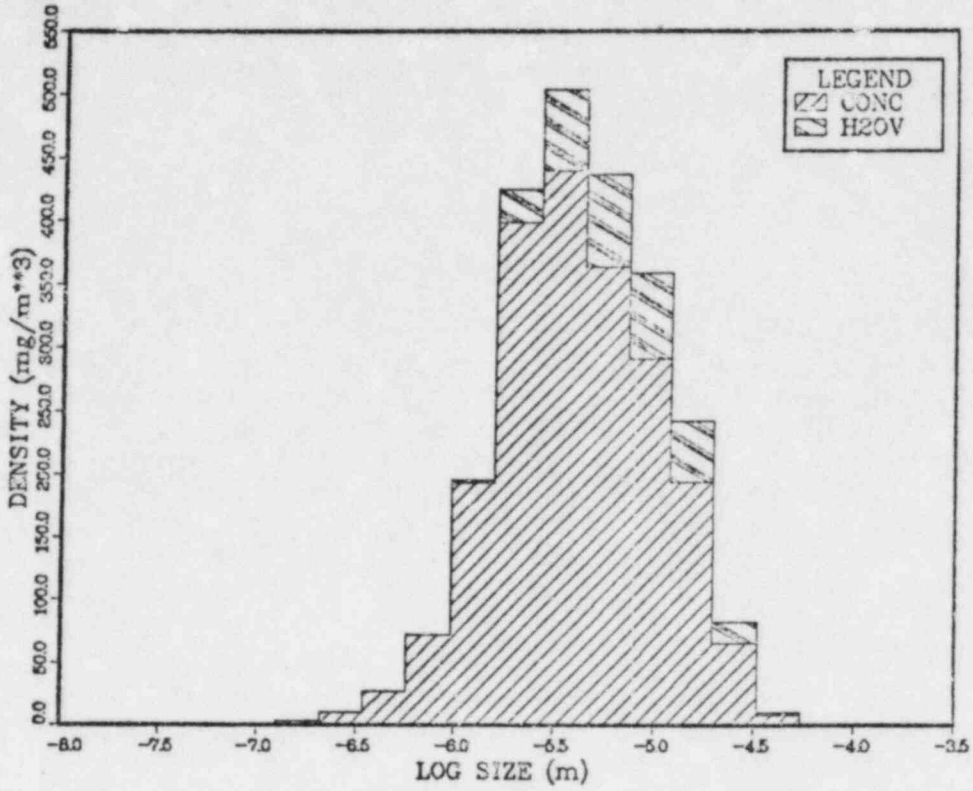

Figure 5. Aerosol distribution approximately 8 hours following vessel breach.

transfer in structures; two-phase atmosphere thermodynamics; deposition, condensation, and agglomeration of aerosols; intercell flow; transport and decay of radioisotopes; and hydrogen burn.

Selected results are shown in Figures 3-6. Containment pressure as a function of time is shown in Figure 3. The second peak occuring at 240 minutes is due to accumulator water and non-condensible gas released upon vessel breach. Of particular interest is the use of the aerosol model (MAEROS) for the homogeneous condensation of the blowdown steam, illustrated in Figures 4a and b. Rapid condensation on the aerosolized water causes the particle distribution to shift to the left, at the same time that the mass density increases sharply. The aerosol distribution much later in time (Figure 5) shows that most of the aerosolized water has settled out, and the aerosol is primarily concrete from the core-concrete interaction.

A very small flow path was modelled, corresponding to a design leak rate of 1 g/sec gas flow, which had no effect on containment pressure. In Figure 6 the cumulative mass of a representative fission product (Xe^{133}) outside of containment is plotted. For this calculation, Xe^{133} was not a source itself, but only a daughter of one

of the species (I^{133}) used as a representative source. Thus, the plotted quantity illustrates both the flow and radioisotope decay features of the code. It was not possible to obtain a sufficiently high concentration of hydrogen for a burn in the nominal TMLB' sequence, so a variation of the sequence was run with an (unrealistic) increase in the leak rate to 1.7 kg/sec. This depleted the containment of the early H_2O, allowing a hydrogen burn due to core-concrete-generated hydrogen late in the sequence (at about 14.5 hours into the sequence.)

CONCLUSION

The CONTAIN code is reaching the point of development that it can be used for many realistic LWR safety calculations. The principal focus at present is validation and verification of the code before an operational version is widely distributed. A series of example runs have been presented illustrating the operational status of the code, and the nature of some of the validation exercises.

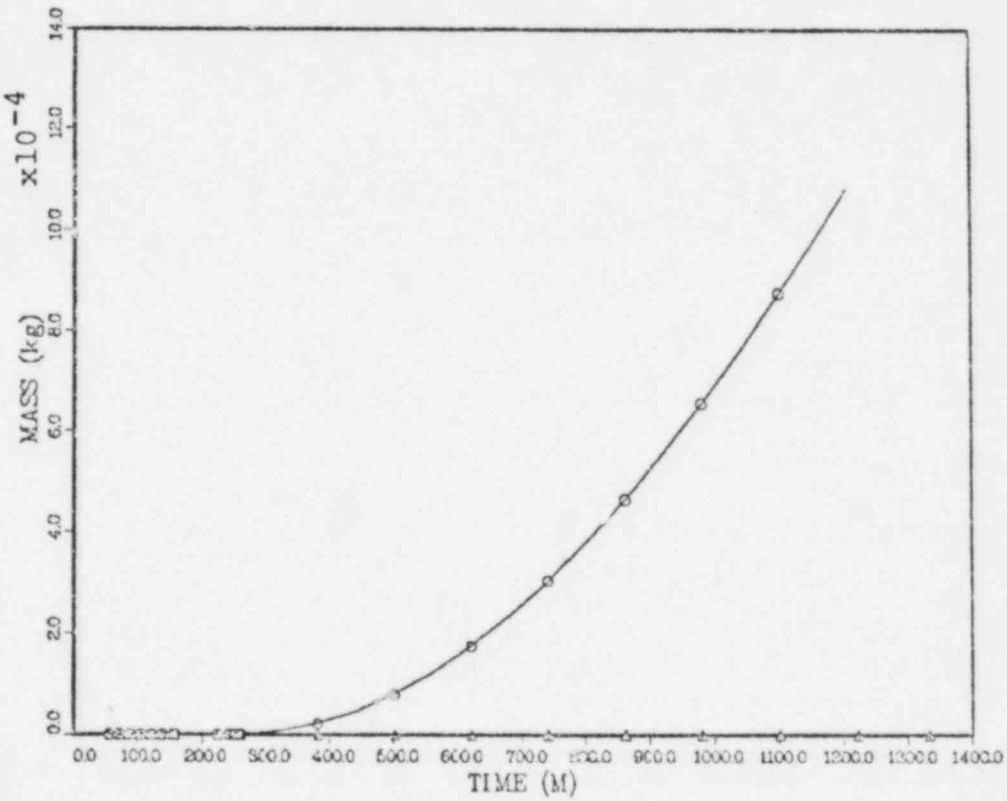

Figure 6. Representative radioisotope mass released from containment, resulting from transport out of containment both before and after radioactive decay.

Future plans include continued development of engineered safety features models, as well as additional testing efforts. Also, the ABCOVE and HDR validation exercises should be completed within the next year. Another important development is the MEDICI module, which will model interactions of molten debris released into the cavity when a pool of water is present (including steam explosions and related phenomena.)

REFERENCES

1. M. E. Senglaub, J. P. Odom, M. J. Clauser, J. E. Kelly, and P. S. Pickard, CONTAIN, A Computer Code for the Analysis of Containment Response to Reactor Accidents - Version 1A, NUREG/CR-2224, SAND81-1495, Sandia National Laboratories, draft report.

2. K. D. Bergeron, Standardized Test Procedures for the CONTAIN Computer Code, RS 4450/82/42, Sandia National Laboratories, Albuquerque, N.M. 87112.

3. R. B. Bird, W. E. Stewart, and E. N. Lightfoot, Transport Phenomena, New York, John Wiley and Sons, Inc., 1960.

4. G. F. Niederauer, R. J. Breeding, and D. R. Meier, CONTEMPT-EI/28A A Computer Program for Predicting Containment Pressure-Temperature Transients, EI-81-03, Energy Incorporated Report, February 1981.

5. R. E. Adams, T. S. Kress, J. T. Han, M. Silberberg, "Behavior of Sodium Oxide, Uranium Oxide and Mixed Sodium Oxide-Uranium Oxide Aerosols in a Large Vessel", Proceedings of the CSNI Specialists Meeeting on Nuclear Aerosols in Reactor Safety, NUREG/CR-1724, ORNL/NUREG/TM-404, CSNI-45, Gatlinburg, TN, April 1980

6. M. J. Clauser, F. W. Sciacca, M. E. Senglaub, K. K. Murata, K. D. Bergeron, P. E. Rexroth, J. E. Kelly, M. F. Young, and P. J. Cooper, CONTAIN, A Code For Analysis of Breeder Reactor Containment Response to Hypothetical Severe Accidents, International Topical Meeting on LMFBR Safety, Lyon, France, July, 1982.

7. H. Jordan, P. M. Schumacher, J. A. Gieseke, and K. W. Lee, "Aerosol Behavior Modeling", Proceedings of the CSNI Specialists Meeting on Nuclear Aerosols in Reactor Safety, NUREG/CR-1724, ORNL/NUREG/TM-404, CSNI-45, Gatlinburg, TN, April 1980.

8. R. O. Wooton, H. I. Avci, MARCH Code Description and User's Manual, NUREG/CR1711, BMI-2064 Battelle Columbus Laboratories, October, 1980.

9. J. F. Muir, R. K. Cole, M. L. Corradini, and M. A. Ellis, CORCON-MOD1: An Improved Model for Molten-Core/Concrete Interactions, NUREG/CR-2142, SAND80-2415, Sandia National Laboratories, 1980.

BNL PROGRAM IN SUPPORT OF LWR DEGRADED CORE ACCIDENT ANALYSIS

by

T. Ginsberg and G. A. Greene

Program Contributors: J. Klages, J. Klein, C. L. Schwarz, Y. Sanborn, N. Tutu

Consultants: J. C. Chen, T. F. Irvine

Brookhaven National Laboratory
Department of Nuclear Energy
Experimental Modeling Group
Upton, NY 11973

BNL PROGRAM IN SUPPORT OF LWR DEGRADED CORE ACCIDENT ANALYSIS

T. Ginsberg and G. A. Greene

1. INTRODUCTION

The U.S. Nuclear Regulatory Commission currently sponsors analyses of the response of light water reactor containment buildings to degraded core accidents (Murfur, 1980; Meyer, 1981; Pratt, 1981). Two major sources of loading on dry pressurized water reactor containments are:

(i) Steam generation from core debris water thermal interactions.

Quenching of hot debris by cooling water leads to steam generation and containment pressurization. Interaction of hot, unquenched debris with concrete can lead to simultaneous gas release. Hydrogen continues to be generated until debris is finally quenched.

(ii) Molten core-concrete interactions.

The interactions lead to pressurization of the containment as a result of generation of concrete decomposition products and potential combustion of flammable gaseous products. In addition these interactions lead to penetration of the core melt into the containment basemat.

Experiments are in progress at BNL in support of analytical model development related to aspects of the above containment loading mechanisms. The work supports development and evaluation of the CORCON (Muir, 1981) and MARCH (Wooton, 1980) computer codes. Progress in the two programs is described below.

2. CORE DEBRIS THERMAL-HYDRAULIC PHENOMENOLOGY

Light water reactor degraded core accident sequence studies have been performed which postulate the existence of a high temperature core debris bed within the reactor cavity (Meyer, 1981). The debris bed would be cooled by an overlying pool of water. Two models have been used to characterize the interaction between hot core debris and water. The MARCH code's "HOTDROP" model (Wooton, 1980) assumes that the core debris is suspended in an infinite sea of water and that heat transfer is limited by the particle debris internal and external thermal resistances. Steam production is governed by the total surface area of the fragments. On the other hand, steady state debris bed cooling models have been used to predict the steam production rate resulting from quenching of packed beds of solid core debris (Yang, 1981). The containment pressurization rates based upon the two models are significantly different (Yang, 1981). The validity of these models when applied to the transient cooling of debris beds has not been established by comparison with suitable

transient quench experiments.

Presented below are recent results of an experimental investigation whose objective is to provide an understanding of the thermal interaction between superheated core debris and water during postulated light water reactor degraded core accidents. The experiment was designed to study the heat transfer characteristics of superheated spheres as they are quenched in a packed bed configuration by an overlying pool of water. A model based upon the experimental results is presented and implications with respect to reactor safety are discussed.

The test apparatus is shown in Figure 1. Stainless steel spheres, 3 mm in diameter, were heated in the oven shown at the top of Figure 1 to temperatures between 533 K and 97. K. They were subsequently transferred to a vertical 108.2 mm i.d. stainless steel pipe, flanged at the lower end. Water at temperatures between 274 K and 360 K was released on to the spheres and the resulting thermal interaction was observed. Packed beds of 40% porosity were studied, whose nominal heights were in the range 200 mm to 400 mm. The experiments were carried out at constant pressure, with the steam vented to the atmosphere. The wall of the test vessel could be preheated, if desired, to match the initial sphere temperature. The test section was instrumented with an array of thermocouples, both within the pipe and on its outside wall. A pressure transducer was mounted on the test vessel wall to monitor pressure fluctuations indicative of continued boiling within the vessel. In the early stages of the work the steam was vented to the atmosphere via the steam vent shown in Figure 1. The apparatus was subsequently modified to incorporate the turbine flowmeter shown in Figure 1(b). This flowmeter was used to monitor the flow of steam during the particle quench process. In these latter experiments all of the piping which led to the flowmeter was preheated to the water saturation temperature prior to a run.

A typical set of bed temperature traces is shown for Run. No. 116 in Figure 2. The temperature traces are labeled by the thermocouple (TC) identification number. TC2 was located at the base of the bed. The remaining thermocouples were spaced in ascending order every 50 mm. TC8 was the uppermost thermocouple located 300 mm from the base of the bed. The key feature of Figure 2 is the sequence of step changes in temperature, beginning with TC8 located near the top of the bed. This sequence proceeded in the downward direction to each thermocouple in the bed. The temperature at each position suddenly fell from the initial sphere temperature to the liquid saturation temperature. Figure 2 also indicates that several of the thermocouples partially recovered their superheated temperatures subsequent to the first arrival of liquid. In this case four channels (TC Nos. 4, 6, 7, 8) exhibit this behavior. The temperature recovery characteristic of Run No. 116 occurred in many, though not all, of the experiments. These four thermocouples were finally quenched in a sequential pattern from the bottom upwards. A sequential pattern of wall quenching was also observed to proceed from the bottom upwards (not shown).

Three "frontal" particle bed cooling patterns are suggested by the bed and wall temperature traces. The times of arrival of each of the three cooling fronts are presented in Figure 3 as a function of axial position in the test column. Figure 3 shows the advance of a downward-propagating front which

reaches the bottom of the bed at 165 seconds after initial water/bed contact. At this point an upward-propagating front is observed which is responsible for "final" cooling of the particle bed as well as the test wall (third front was wall quench).

Prior to installation of the turbine flowmeter system for the steam flow-rate measurement, an estimate of the time-average bed heat transfer rate was made. The time period during which boiling was observed in the test vessel wa' determined from the piezoelectric transducer traces.

The average bed heat flux was computed from the known initial bed stored energy (temperature), the boiling time and the bed cross-sectional area. The results of these calculations are shown in Figure 4. They indicate that the time-average rate of heat transfer from the particles to the water was approximately 10^6 W/m^2. The heat transfer rate was independent of bed temperature for initial bed temperatures in the range 530 K to 970 K.

The turbine flowmeter data substantiate the magnitude of the heat flux determined as described above. In addition the flowmeter data indicate that the bed cooling rate is identical during the downward and upward frontal time periods.

The frontal progression speeds were obtained from the frontal propagation data (such as Figure 3) for each set of experimental conditions. These data, calculated using a linear least squares analysis, are shown in Figure 5. Data from Armstrong, et al (1982) are also presented. The results indicate that the frontal speeds decrease with increasing temperature and that the downward frontal speed is consistently larger than the corresponding upward frontal speed.

A model has been developed to characterize the debris bed quench behavior as observed in the experiments. Based upon the above observations it is assumed that the packed bed heat transfer occurred at the quench front during both the downward and upward frontal periods. The rate of heat transfer with liquid supplied from an overlying pool is assumed to be limited by maximum rate at which vapor can be removed from the bed under conditions of countercurrent two-phase vapor-liquid flow in or to the packed bed. A coupled set of equations were developed which include (i) a lumped parameter bed energy equation and (ii) countercurrent flow hydrodynamics equations. Three hydrodynamics models were used to characterize the two phase countercurrent flow processes: (i) the Zuber "CHF" model (Zuber, 1959), (ii) a modified version of the Lipinski debris bed model (Lipinski, 1981) and (iii) a modified version of the Ostenson flooding model (Ostenson, 1981). The set of equations was solved simultaneously for the particle bed heat flux and the downward- and upward-frontal speeds.

The data are compared with model predictions in Figures 4 and 5. Figure 4 indicates that the heat transfer rate is characterized reasonably well by either the CHF model or the TRANSBED (quasi-steady Lipinski) model. The cooling front data shown in Figure 5 agree with the model over the entire range of temperature with the possible exception of the lowest bed temperature.

The results of the program suggest that:

(i) A superheated particle bed quenches in a two-step bi-frontal process. A partial quench front first propagates downward removing a fraction (f_d) of the stored sensible heat of the bed. A second upward-directed quench front starts when the downfront reaches the bed bottom. The upward front removes the balance ($1-f_d$) of the stored energy. Experimental data suggest that $f_d = 0.3-0.4$.

(ii) The net rate of energy removal from the bed is, within the scatter of the data, independent of initial bed temperature and is identical during both the downward and upward frontal periods.

(iii) The above observations strongly suggest that the phenomenon which limits the net heat removal from a superheated bed is hydrodynamic in nature. This is consistent with the hypothesis that the heat transfer is limited by the hydrodynamics of countercurrent two-phase flow, either just above the bed or within the bed.

Major implications of the results with respect to LWR reactor safety are:

(i) The rate of containment building pressurization resulting from quenching of superheated beds of core debris by overlying pools of liquid would be limited by the hydrodynamics of countercurrent two phase flow to or within the beds. The data and models indicate that this conclusion is independent of initial bed temperature.

(ii) The observed frontal characteristics, however, suggest that the debris ahead of the initial cooling front would remain dry until arrival of the downward front. Attack of the concrete by the hot solid debris must be considered during this time period.

3. HEAT TRANSFER IN CORE-CONCRETE INTERACTIONS

The phenomena of core-concrete interactions impact upon containment integrity of a light water reactor (LWR) following postulated complete meltdown of the core by containment pressurization due to condensable and non-condensable gas generation, possible ignition of combustible gases, and concrete basemat penetration. In order to develop a predictive capability to analyze such complicated interactions, the CORCON code (Muir, 1981) has been developed at Sandia Laboratory under USNRC sponsorship. Modeling of core-concrete interactions involves many poorly understood and complicated heat transfer phenomena for which there exists a sparse data base. In support of the CORCON code, one heat transfer aspect of core-concrete interactions has been investigated which had been found to have significant impact upon the results of generic code calculations, namely the phenomenon of heat transfer between overlying immiscible liquid layers whose interface is agitated by gases liberated from the underlying concrete.

The model used in CORCON to characterize liquid-liquid heat transfer to an interface agitated by transverse gas flow is a correlation developed by Konsetov (1966) to model heat transfer from a horizontal surface with gas injection. Other models which have been applied to liquid-liquid interfacial

heat transfer with bubble agitation are a model by Grief (1965) as well as the surface renewal model of Szekeley (1963). When these models were compared to a limited amount of experimental data taken with an oil-water fluid pair (Werle, 1978), it was found that the models seriously underpredicted both the magnitude and the trend of the heat transfer data, deviating from the data by as much as two orders of magnitude at a superficial gas velocity of only 1 cm/sec. As a result of this poor agreement between the data and the models, a parametric sensitivity analysis was performed to determine the impact of this phenomena upon integrated code calculations of core-concrete interactions.

The effect of interfacial heat transfer was examined parametrically, by increasing the heat transfer coefficient by a factor of 10 and 100, chosen on the basis of comparison of the heat transfer models to the limited experimental data. It was found that the integrated results of the core-concrete interactions were significantly affected by these parametric variations on the interfacial heat transfer coefficient. The Konsetov heat transfer model in CORCON always resulted in an upper bound to the generation rates of combustible, condensable and non-condensable gases from the concrete. However, increasing this magnitude of the coefficient by factors of 10 and 100 reduced these gas generation rates by as much as a factor of from two to five (Greene, 1982).

The reason for this effect on the gas release rates from the concrete is that the downward heat flux into the concrete from the heavy core oxide layer was reduced due to the increased upward heat flux into the overlying lighter metallic layer. This reduced downward heat flux similarly reduced the concrete ablation rate and reduced the rate of dilution of the lower oxide layer by concrete slag. Accompanying the reduced gas generation rates and reduced concrete ablation rate by increasing the interfacial liquid-liquid heat transfer coefficient, it was found that the layer temperatures themselves would decrease significantly faster with the increase in the magnitude of the interfacial liquid-liquid heat transfer coefficient. An example of the reduced gas generation rates and reduced layer temperatures due to enhancing the interfacial heat transfer coefficient is shown in Figure 6a-f. On the basis of these observations, the experimental and analytical program about to be described was performed.

Mercury-Water Bubbling Interfacial Heat Transfer: Non-Entraining

Two sets of bubbling heat transfer data were taken with mercury-water fluid pairs, Series 300 and Series 400 data. The bubble radii were in the range 0.3 to 0.5 cm and the superficial gas velocity was varied over the range from zero to 1.4 cm/sec. These data are presented in Figure 7 along with the Wood's metal-oil data of Werle (1978, 1981). In the limit of zero gas flow rate, these data converged asymptotically to a lower limit calculated by the natural convection model of Haberstroh (1974). As the superficial gas velocity increased, the heat transfer coefficient similarly increased due to the periodic bubble-induced disturbances at the liquid-liquid interface. The vertical temperature distribution demonstrated a sharp gradient in the vicinity of the fluid-fluid interface, suggesting that the interface did maintain its approximate spatial integrity and that mixing and entrainment were absent. These observations were further supported by visual and photographic evidence

of the absence of entrainment of mercury even under intense interfacial disturbance.

The mercury-water heat transfer data were found to be greater in magnitude than the Wood's metal-oil data (Werle, 1978; 1981) by a significant margin. The observed superiority of the water layer to the oil layer in transferring heat is evident from the data in Figure 8 and the ratio is roughly a factor of five increasing to as much as ten. On the basis of the surface renewal formulation shown in Figure 7, this ratio should be approximately four. However, as will become evident in the discussion, there are factors absent from this formulation which, when included, may account for this discrepancy.

The regime of heat transfer between two fluid layers enhanced by interfacial disturbances generated at their interface by rising bubbles with the absence of entrainment is referred to as the surface renewal regime. When the gas flux is initiated, the interfacial heat transfer coefficient is found to increase above the value characteristic of pure steady natural convection. For the mercury-water case, no large scale entrainment of the mercury is observed into the overlying water layer. In this case, the bubble acts only to disrupt the temperature gradients at the interface and transient conduction acts to renew the gradients until the arrival of a subsequent bubble. The mercury-water and Wood's metal-oil data are characterized by the surface renewal model.

The major assumptions of the surface renewal model are that a rising bubble totally destroys the temperature gradients on both sides of the interface only in the area of impact projected by the bubble, no influence is felt outside the bubble area, and surface distrubances do not enhance the transport mechanisms or the interfacial surface area. As is evident from Figure 7, the surface renewal heat transfer model of Szekeley (1963), modified by Blottner (1979),

$$h_{SZE} = 1.69\ k\ (j_g/\kappa r_b)^{1/2} \qquad (1)$$

where k is the thermal conductivity, κ is the thermal diffusivity, and r_b is the bubble radius, represents a lower bound to both the mercury-water data as well as the Wood's metal-oil data. In both cases the deviation between the measured and calculated heat transfer coefficient increases with increasing superficial gas velocity, indicating the effect of the increasing disturbance intensity and interfacial wave propagation on the magnitude of the heat transfer. The fact that the discrepancy is greater for the water-mercury data than for the oil-Wood's metal data may indicate the presence of a Prandtl number effect in addition to the hydrodynamic interfacial stretching mechanism due to surface waves.

Nevertheless, for fluid pairs that do not mix or entrain even under the influence of transverse gas bubbling through their interface, the simple transient conduction surface renewal model is found to predict a lower limit to the magnitude of the interfacial heat transfer coefficient, differing from the measured data by up to a factor of four over the range of conditions cov-

ered by these experiments.

Water-Oil Bubbling Interfacial Heat Transfer: Entraining

In addition to the liquid metal-oil/water interfacial heat transfer experiments which did not exhibit entrainment over the entire range of gas velocity covered, experiments were also performed with zinc sulfate-silicone oil (Series 100) and copper sulfate-silicone oil (Series 200) fluid pairs which demonstrated entrainment and mixing when their interface was agitated by rising bubbles from below. The bubble radii and superficial gas velocity were in the same range as for the liquid metal-oil/water experiments. The data for the Series 100 and 200 oil-water experiments are presented in Figure 8 along with the oil-water data of Werle. These experiments, all experiencing liquid-liquid entrainment effects, are compared to the Wood's metal-oil data previously discussed.

In the limit that the superficial gas velocity asymptotically goes to zero, these data converge to the natural convection limit represented by the Haberstroh model. As the superficial gas velocity was increased, a dramatically different behavior was observed than for the fluid pairs which did not exhibit entrainment. Instead of a gradual increase in magnitude, the heat transfer coefficient is seen to suddenly jump almost a factor of ten at the onset of bubbling and steeply increase until, at a gas velocity of 1 cm/s, it is greater than the silicone oil-Wood's metal data by more than two orders of magnitude. The measured vertical temperature distribution exhibited characteristics of an intermediate mixing zone in which the temperature gradually changed from one layer to the other. This is in contrast to the sharp temperature gradient measured with non-entraining fluids previously. These observations were further supported by visual and photographic evidence of the severe mass entrainment rate even at modest superficial gas velocities below 1 cm/sec.

The significant increase in interfacial heat transfer for the silicone oil-water fluid pair over that measured for the silicone oil-Wood's metal fluid pair (KFK) is attributed directly to the effect of mass entrainment of the hot lower fluid across the interface into the cold upper fluid. This regime of heat transfer is referred to as the entrainment heat transfer regime (Greene, 1982).

As the bubble penetrates the liquid-liquid interface, a finger of the lower heavy fluid is sucked upward into the upper layer in the bubble wake. At some location, this liquid finger is observed to pinch off; the fluid below the point of the break returns downward through the interface, while the fluid above this point continues to entrain upwards in the wake region of the bubble. In the case of large entrained drops, they are also observed to fragment in the vortex region behind the bubble into smaller droplets, greatly increasing the surface area for heat transfer. On the basis of simple analysis of transient convective heat transfer around a sphere, it can be shown that for the conditions of these experiments, the droplets essentially transfer all their excess enthalpy to the upper fluid prior to settling back to the lower fluid layer from whence they came. On the basis of these observations, it is argued that one only need to know the liquid entrainment rate in order to

calculate the entrainment heat transfer rate. In this fashion, the overall heat transfer coefficient can be written as the sum of the interfacial surface renewal contribution and the entrainment contribution as

$$h_{eff} = h_{SZE} + j_2 \rho_2 C_{p2} \quad (2)$$

where ρ_2 and C_{p2} are the density and specific heat of the entrained phase, respectively, and j_2 is the volumetric entrainment rate of the lower fluid per unit cross sectional area. At present, calculation of the entrainment rate, j_2, is treated parametrically as a function of the gas superficial velocity, $j_2 = C_2 j_g$. In reality it is recognized that C_2 is not a constant but is a function of j_g itself. For this discussion, C_2 is assigned the values 0.3 and 1.0 awaiting further attempts to improve the entrainment rate model which are currently underway in recognition of the obvious nonlinear relationship between j_g and j_2.

The results of the comparison of Equation (2) to the oil-water entrainment data are shown in Figure 8. Note that the choice of C_2 in the range of 0.3 to 1.0 appears to bracket the available data. The development of a more refined entrainment rate model will enable a more mechanistic calculation of entrainment heat transfer rate.

Nevertheless, for fluid pairs that exhibit interfacial mixing and entrainment under the influence of transverse gas bubbling through their interface, a simple entrainment rate heat transfer model is seen to reasonably bracket the available experimental data when appropriate assumptions regarding the mass transfer rate are incorporated. This limitation is expected to be relaxed when a mechanistic entrainment rate model for j_2 is available.

ACKNOWLEDGEMENTS

This work was performed under the auspices of the United States Nuclear Regulatory Commission, Office of Nuclear Regulatory Research, Division of Severe Accident Evaluation.

The authors acknowledge the help of Ms. Linda Hanlon in preparation of this manuscript for publication.

REFERENCES

Armstrong, D. R., D. H. Cho and L. Bova, "Formation of Dry Pockets During Penetration into a Hot Particle Bed," Trans. Am. Nucl. Soc., 41, 418-419 (June 1982).

Blottner, F. G., "Hydrodynamics and Heat Transfer Characteristics of Liquid Pools with Bubble Agitation," SAND 79-1132 (1979).

Greene, G. A. and C. E. Schwarz, "An Approximate Model for Calculating Overall Heat Transfer Between Overlying Immiscible Liquid Layers With Bubble-Induced Liquid Entrainment," Information Exchange Meeting on Post-Accident Debris Cooling, Karlsruhe, Federal Republic of Germany (1982).

Greene, G. A., C. E. Schwarz, J. Klages and J. Klein, "Heat Transfer Between Immiscible Liquids Enhanced by Gas Bubbling," International Meeting on Thermal Reactor Safety, Chicago, Illinois (September 1982).

Grief, R., "Heat Transfer with Gas Injected at the Surface," Int. J. Heat Mass Transfer, 8, pp. 1253-1254 (1965).

Haberstroh, R. D., and R. D. Reinders, "Conducting Sheet Model for Natural Convection Through a Density Stratified Interface," Int. J. Heat Mass Transfer, 17, pp. 307-311 (1974).

Konsetov, V. V., "Heat Transfer During Bubbling of Gas Through Liquid," Int. J. Heat Mass Transfer, 9, pp. 1103-1108 (1966).

Lipinski, R., et al., "Advanced Reactor Safety Research Quarterly Report January-March 1980," Sandia National Laboratories, NUREG/CR-1594, 13, 1, 88 (April 1981).

Meyer, J. F., "Preliminary Assessment of Core Melt Accidents at the Zion and Indian Point Nuclear Power Plants and Strategies for Mitigating Their Effects," Vol. 1, U. S. Nuclear Regulatory Commission Report, NUREG-0850 (November 1981).

Muir, J. F., et al., "CORCON-MOD1: An Improved Model for Molten Core-Concrete Interactions," SAND 80-2415 (1981).

Murfin, W. F., "Report of the Zion/Indian Point Study: Volume 1," Sandia National Laboratory, SAND 80-0617/1 (August 1980).

Ostenson, R. W. and R. J. Lipinski, "A Particle Bed Dryout Model Based on Flooding," Nuc. Sci. & Eng., 79, 110-113 (1981).

Pratt, W. T. and R. A Bari, "Containment Response During Degraded Core Accidents Initiated by Transients and Small Break LOCA in the Zion/Indian Point Reactor Plants," Brookhaven National Laboratory, BNL-NUREG-51415 (July 1981).

Szekeley, J., "Mathematical Model For Heat or Mass Transfer at the Bubble-Stirred Interface of Two Immiscible Liquids," Int. J. Heat Mass Transfer, 6, pp. 417-422 (1963).

Werle, H. "Modellexperimente zum Kernschmelzen," Halbjahresbericht 1978/1, PNS 4332, Kerforschungszentrum Karlsruhe FRG (1978).

Werle, H. "Modellexperimente zum Kernschmelzen-Einfluss eines Gasstroms auf den Warmeubergang Zwischenzwei Flussigkeitsschichten," Halbjahresbericht 1978/2, pp. 4300-79-4300-82, KFK (1978).

Werle, H. "Enhancement of Heat Transfer Between Two Horizontal Liquid Layers by Gas Injection at the Bottom," KFK 3223 (1981).

Wooton, R. O. and H. I. Avci, "MARCH (Meltdown Accident Response Characteristics) Code Description and User's Manual," Battelle Columbus Laboratories, NUREG/CR-1711 (October 1980).

Yang, J. W., "Cooling of Core Debris and the Impact on Containment Pressure," Brookhaven National Laboratory, NUREG/CR-2066 (July 1981).

Zuber, N., "Hydrodynamic Aspects of Boiling," Dissertation, Univ. of California, AECU-4439 (1959).

RECENT PUBLICATIONS AND FORMAL REPORTS

1. Greene, G. A. and C. E. Schwarz, "Interfacial Heat Transfer Between Overlying Liquid Layers with Gas Agitations," Trans. Am. Nucl. Soc., 39, (November 1981).

2. Moszynski, J. R. and T. Ginsberg, "Effect of Dispersed Particulate or Droplet Phase on the Rayleigh-Taylor Instability of a Gas-Liquid Interface," Brookhaven National Laboratory, BNL-NUREG-51533 (March 1982).

3. Ginsberg, T., et al., "Phenomenology of Transient Debris Bed Heat Removal," to be published in proceedings of Information Exchange Meeting on Post-Accident Debris Cooling, Karlsruhe, W. Germany (July 1982).

4. Greene, G. A. and C. E. Schwarz, "An Approximate Model For Calculating Overall Heat Transfer Between Overlying Immiscible Liquid Layers with Bubble-Induced Liquid Entrainment," Information Exchange Meeting on Post Accident Debris Cooling, Karlsruhe, Federal Republic of Germany (July 1982).

5. Ginsberg, T., et al., "Transient Core Debris Heat Removal Experiments and Analysis," Presented at International Meeting on Thermal Nuclear Reactor Safety, Chicago, Illinois (August 1982).

6. Greene, G. A., "Experimental and Analaytical Study of Natural Convection Heat Transfer of Internally Heated Liquids," Ph.D. Thesis, BNL-NUREG 51585, NUREG/CR 2939 (August 1982).

7. Greene, G. A., C. E. Schwarz, J. Klages and J. Klein, "Heat Transfer Between Immiscible Liquids Enhanced by Gas Bubbling," International Meeting on Thermal Nuclear Reactor Safety, Chicago, Illinois (August 1982).

8. Greene, G. A., T. F. Irvine, Jr. and O. C. Jones, Jr., "Experimental and Analytical Study of Natural Convection Heat Transfer of Internally Heated Fluids," Seventh International Heat Transfer Conference, Munich, Federal Republic of Germany (September 1982).

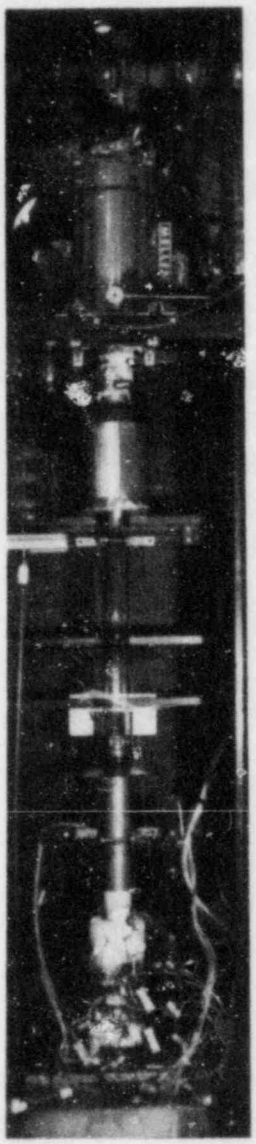

(a)

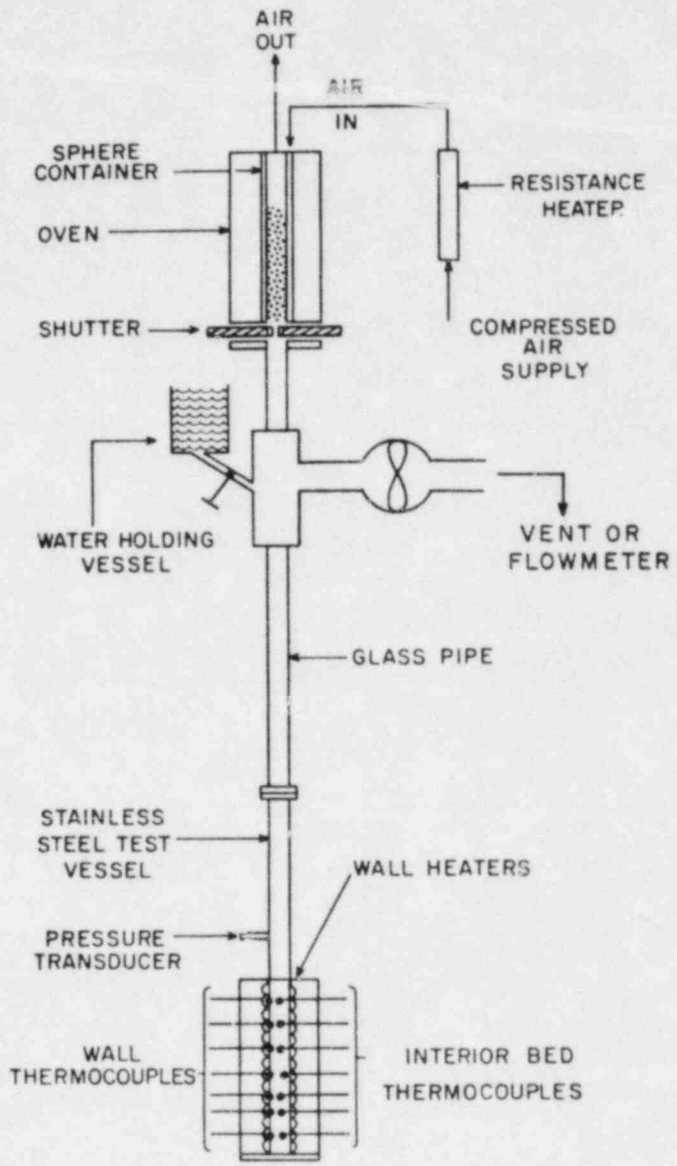

(b)

FIGURE 1-(a) Photograph and (b) Schematic Diagram of Test Apparatus

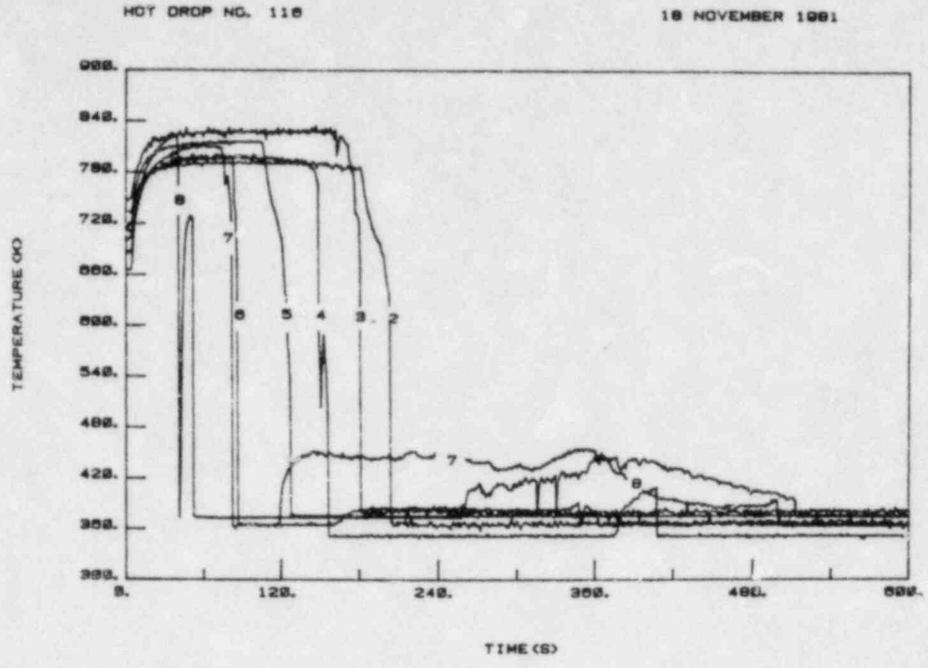

FIGURE 2 - Bed Temperature Traces: T_0=800K; Bed Height-327 mm

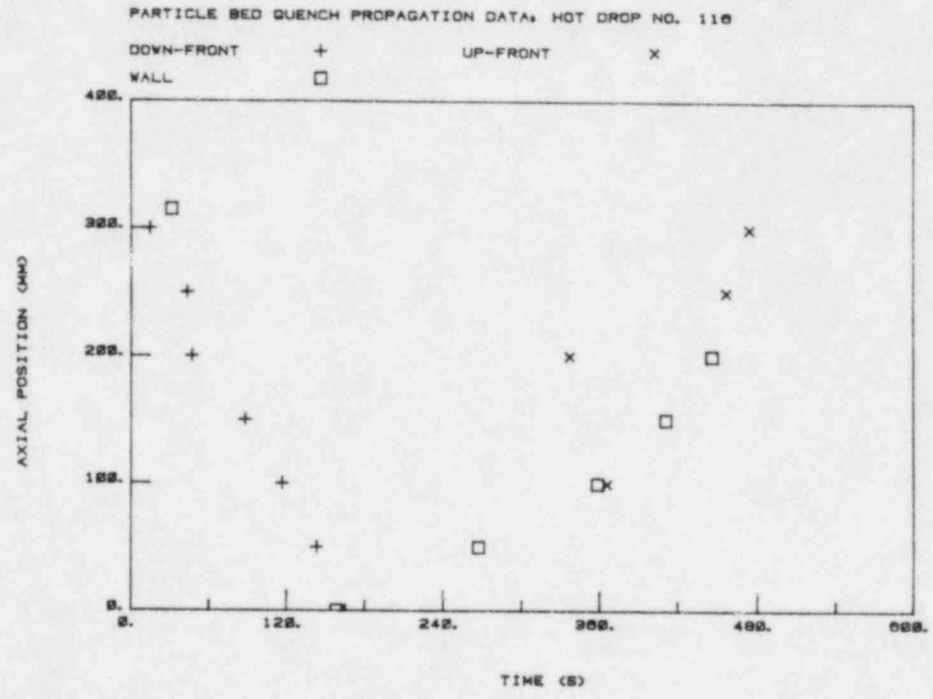

FIGURE 3 - Frontal Propagation Results: T_0=800K; Bed Height=327 mm

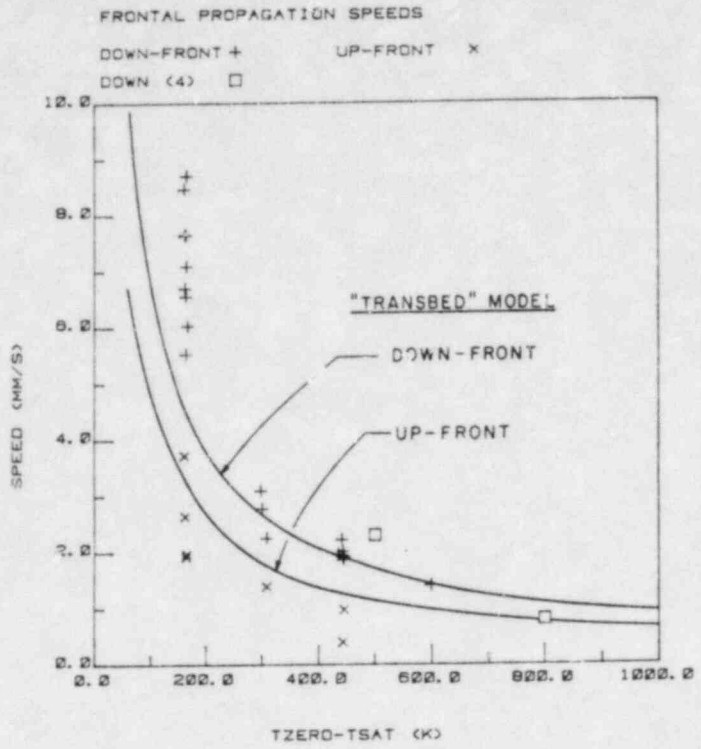

FIGURE 4 - Frontal Progression Speeds

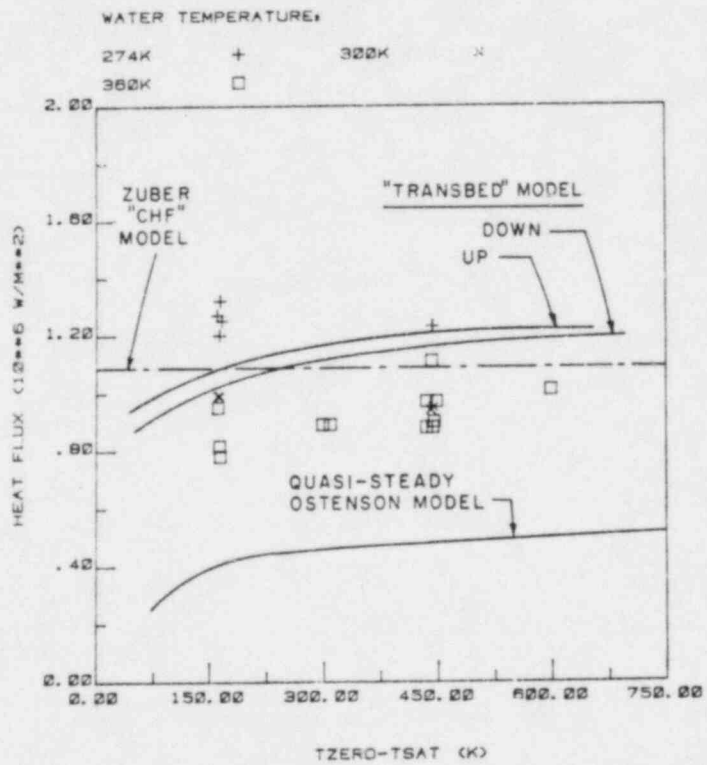

FIGURE 5 - Particle Bed Heat Transfer Rate: Measured and Calculated

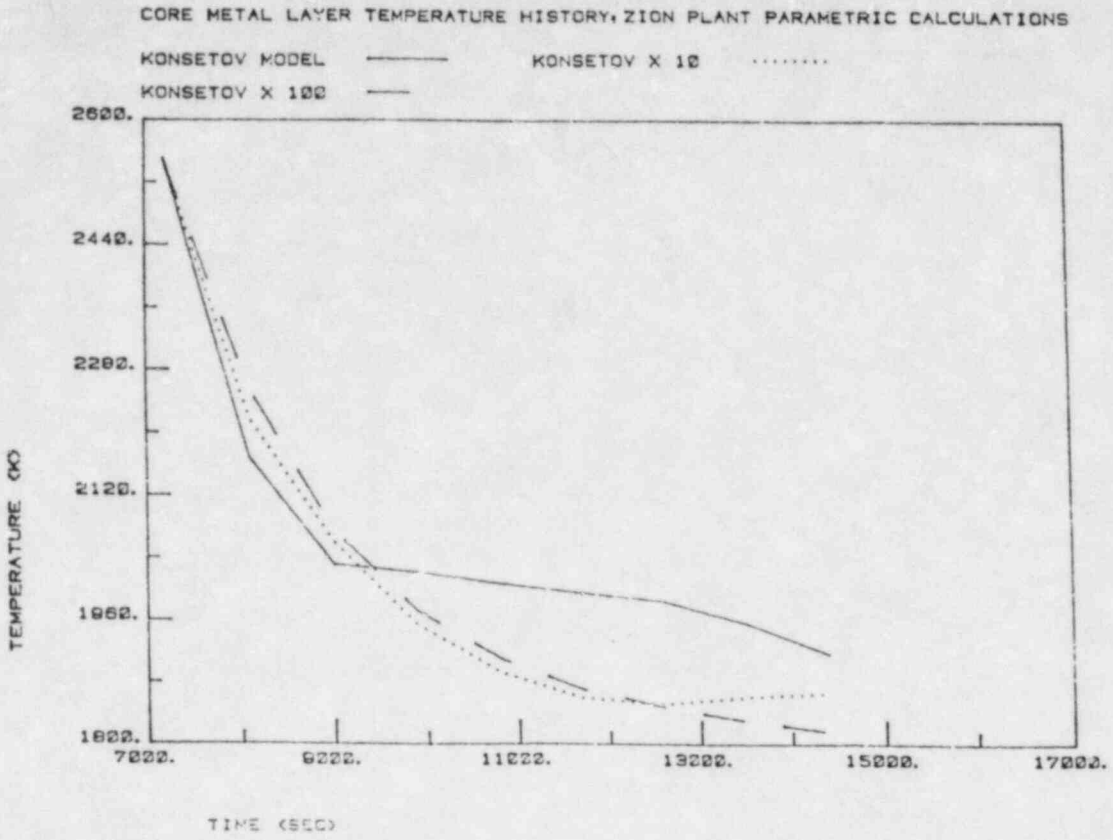

FIGURE 6a

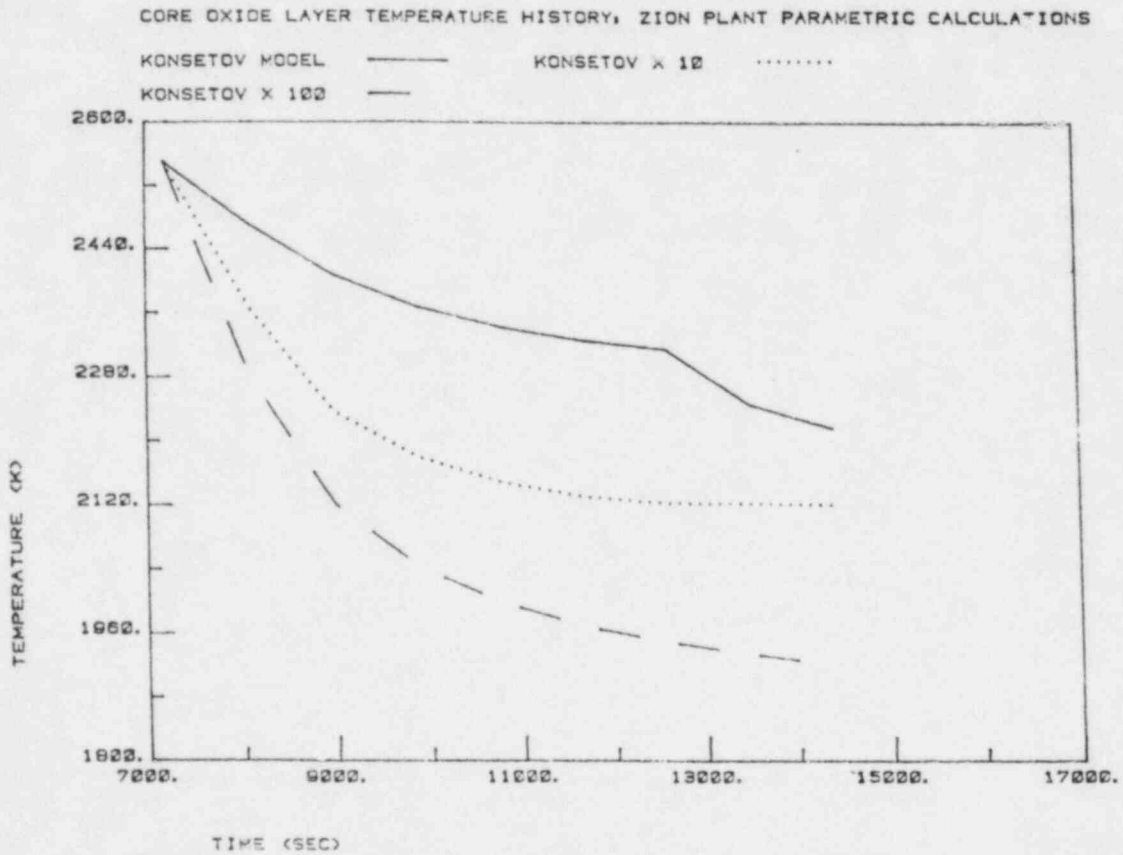

FIGURE 6b

FIGURES 6a-f - Sensitivity of CORCON Calculations to Interfacial Liquid-Liquid Heat Transfer

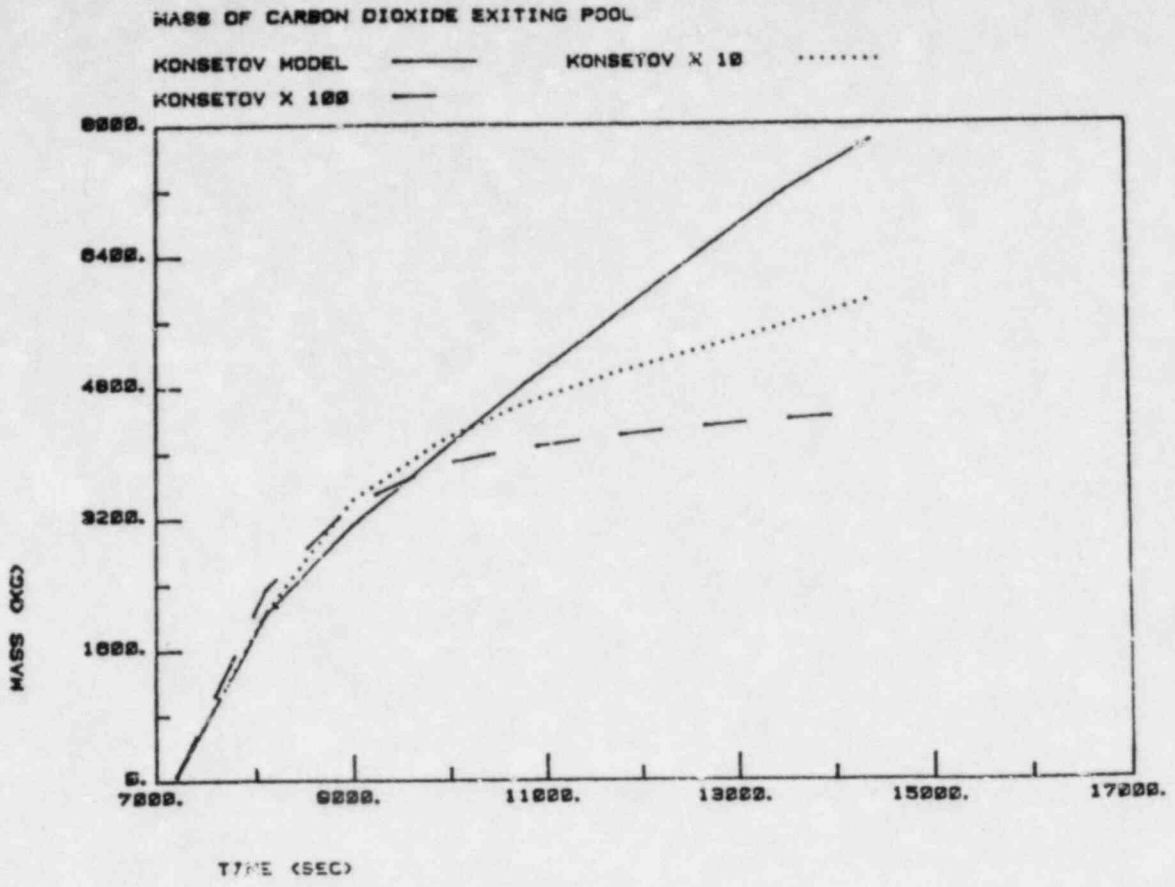

FIGURE 6c

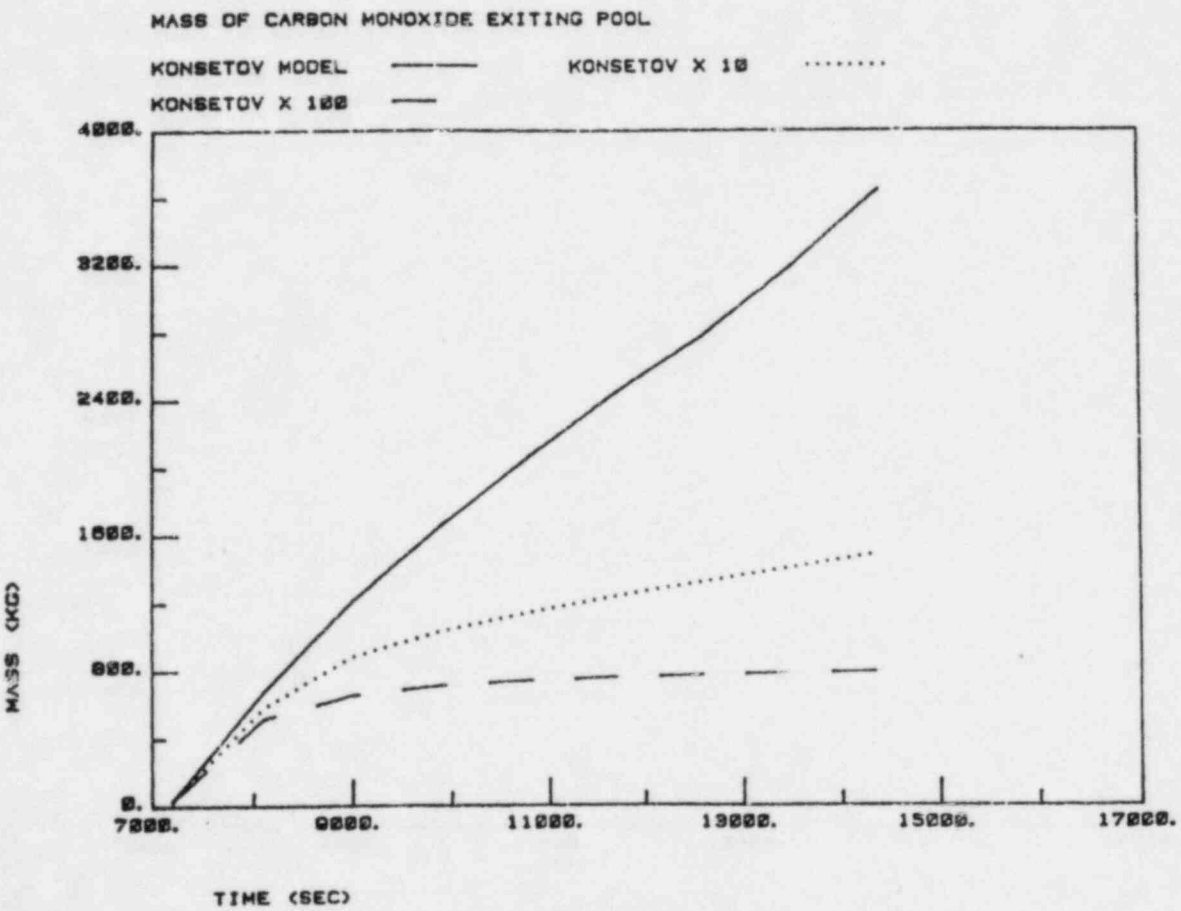

FIGURE 6d

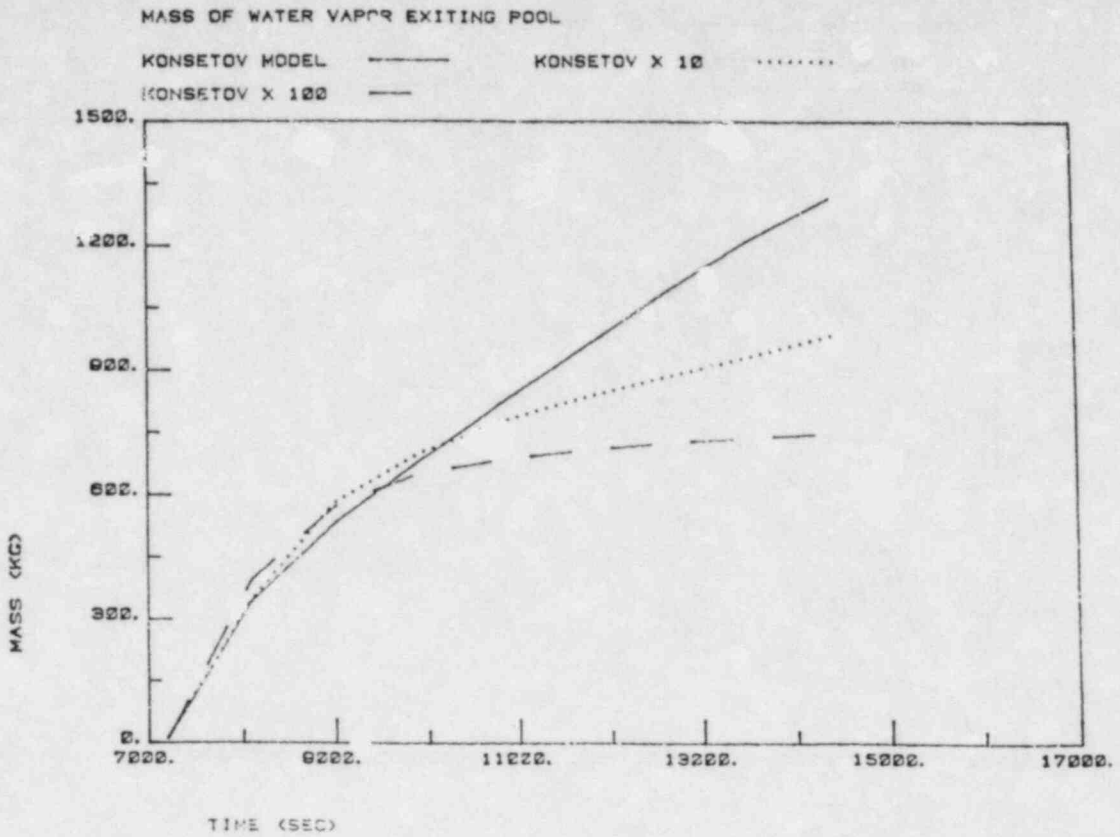

FIGURE 6e

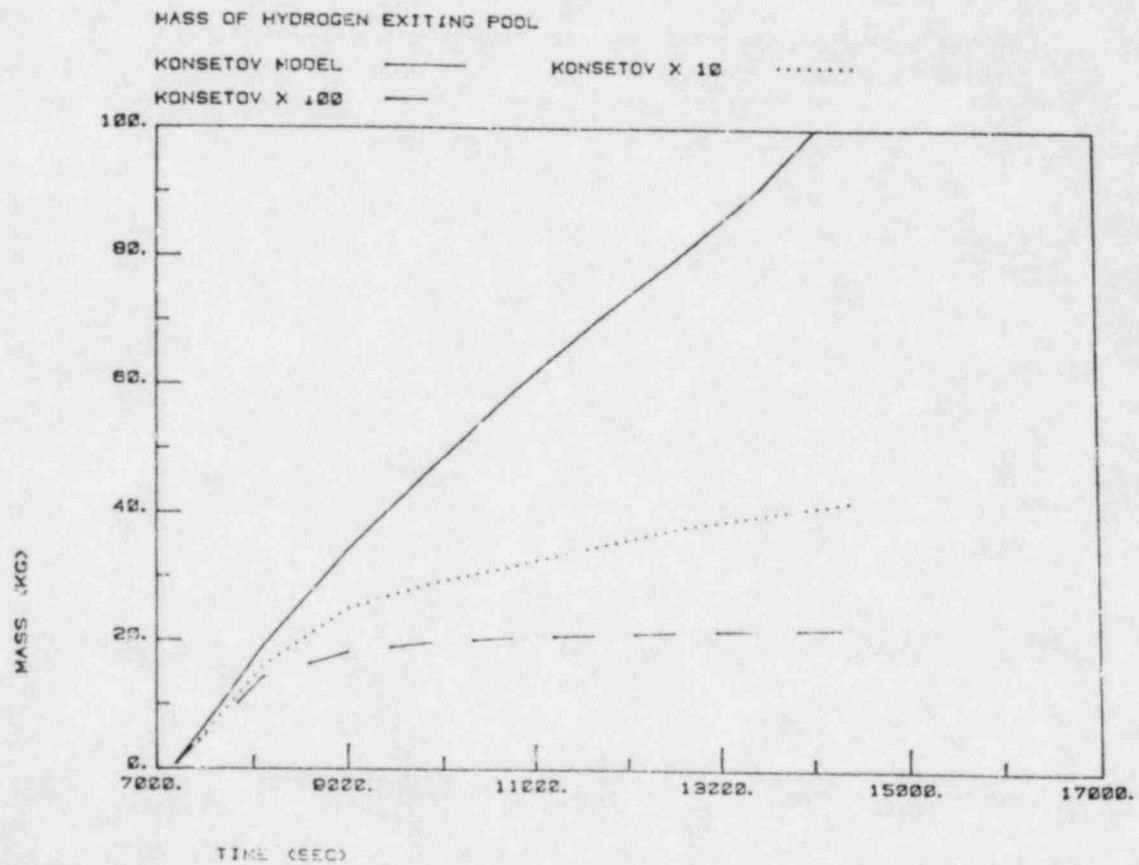

FIGURE 6f

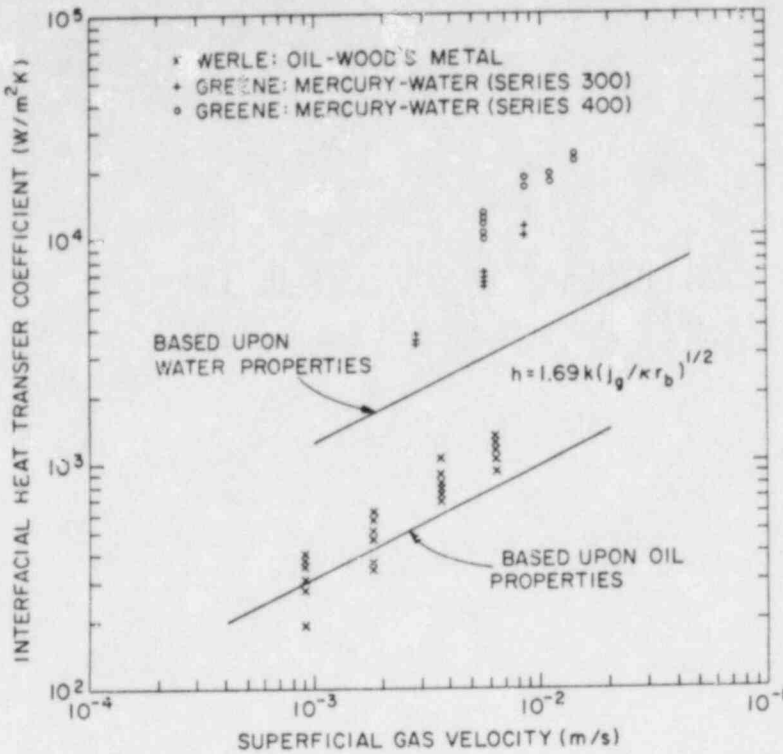

FIGURE 7 - Interfacial Heat Transfer Coefficient vs. Superficial Gas Velocity: Non-Entrainment Regime

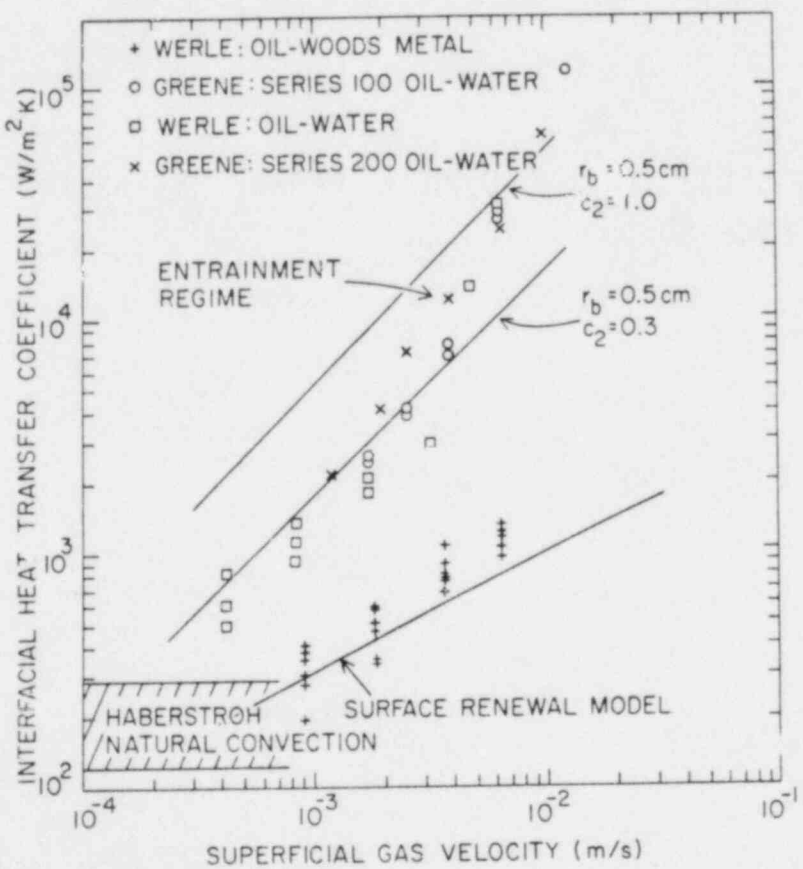

FIGURE 8 - Interfacial Heat Transfer Coefficient vs. Superficial Gas Velocity: Entrainment Regime

BNL PROGRAM IN SUPPORT OF LWR DEGRADED CORE ACCIDENT ANALYSIS

- SCOPE AND PURPOSE OF PROGRAMS
- PROGRESS IN HEAT TRANSFER IN CORE-CONCRETE INTERACTIONS RESEARCH
- PROGRESS IN CORE DEBRIS THERMAL-HYDRAULIC PHENOMENOLOGY RESEARCH
- FUTURE PLANS

SCOPE OF BNL LWR PROGRAM

LWR TASK	ACCIDENT PHASE	ISSUE	RELEVANT CODES
• HEAT TRANSFER IN CORE-CONCRETE INTERACTIONS	CORE MELT-CONCRETE THERMAL INTERACTION	CONTAINMENT INTEGRITY	CORCON
• CORE DEBRIS THERMAL-HYDRAULIC PHENOMENOLOGY	CORE MELT-WATER THERMAL INTERACTIONS IN LOWER PLENUM REACTOR CAVITY, CORE	CONTAINMENT INTEGRITY DEBRIS COOLABILITY	MARCH SCDAP

PROGRESS IN HEAT TRANSFER IN CORE-CONCRETE INTERACTIONS

- OBJECTIVE

  - SUPPORT CORCON CODE DEVELOPMENT

- SCENARIO

  - UNCOOLABLE MOLTEN DEBRIS IN REACTOR CAVITY
  - OXIDE AND METALLIC LAYERS SEPARATE AND ATTACK CONCRETE
  - GAS RELEASE FROM CONCRETE

- EXPERIMENTAL OBJECTIVE

  - DEVELOP DATA BASE FOR MODEL OF INTERFACIAL HEAT TRANSFER WITH BUBBLE AGITATION

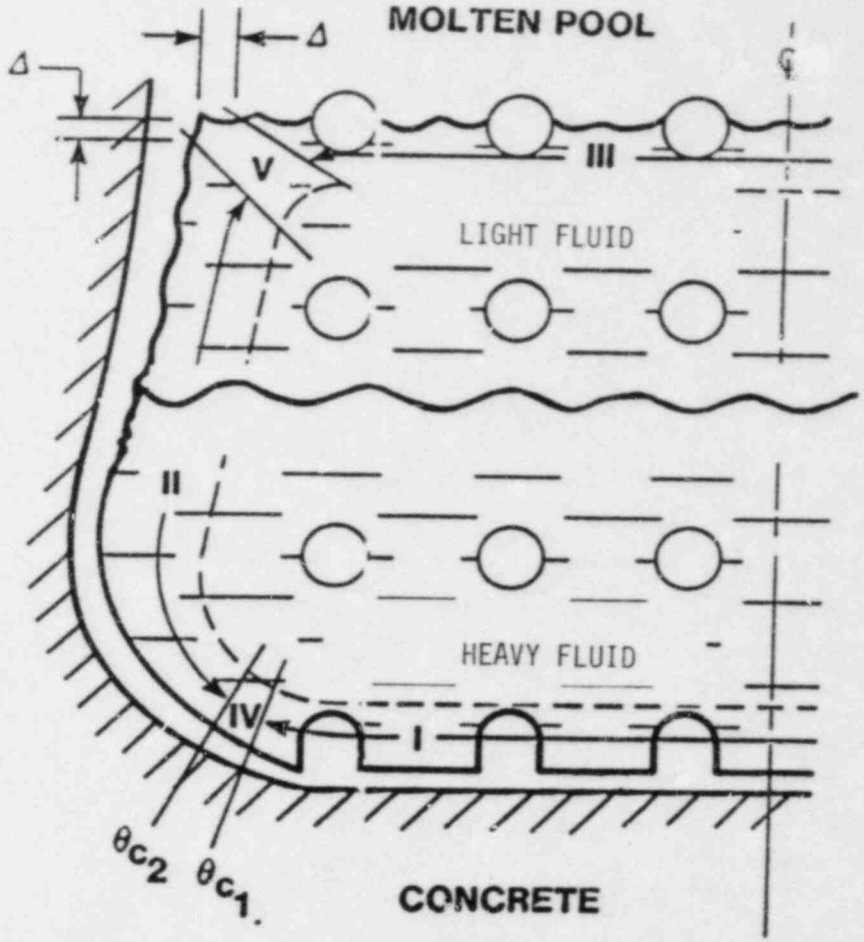

CORE-CONCRETE HEAT TRANSFER EXPERIMENTS

- APPARATUS
  - INSULATED LIQUID POOL
  - POROUS BASE FOR GAS FLUX
  - ELECTRODES FOR HEAT SOURCE
  - THERMOCOUPLE RAKE
- PROCEDURE
  - VARY FLUID DENSITY RATIO
  - MEASURE INTERFACIAL HEAT TRANSFER VS. GAS FLUX
- RESULTS
  - NON-ENTRAINING REGIME
  - ENTRAINING REGIME

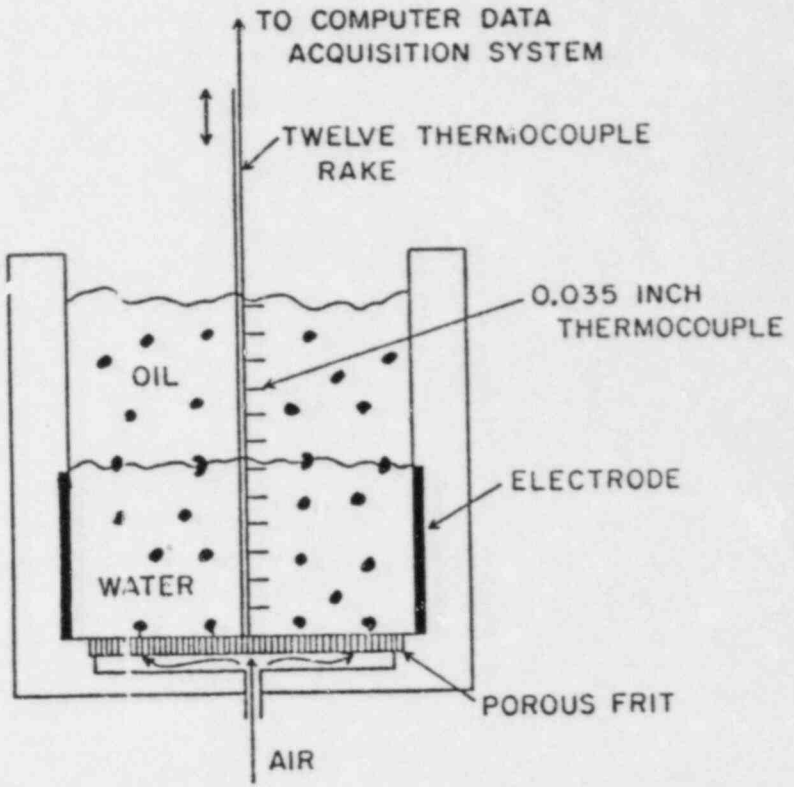

CORE CONCRETE HEAT TRANSFER RESULTS

- DENSITY RATIO: 0.1
- NON-ENTRAINING REGIME DATA
- SURFACE RENEWAL MODEL

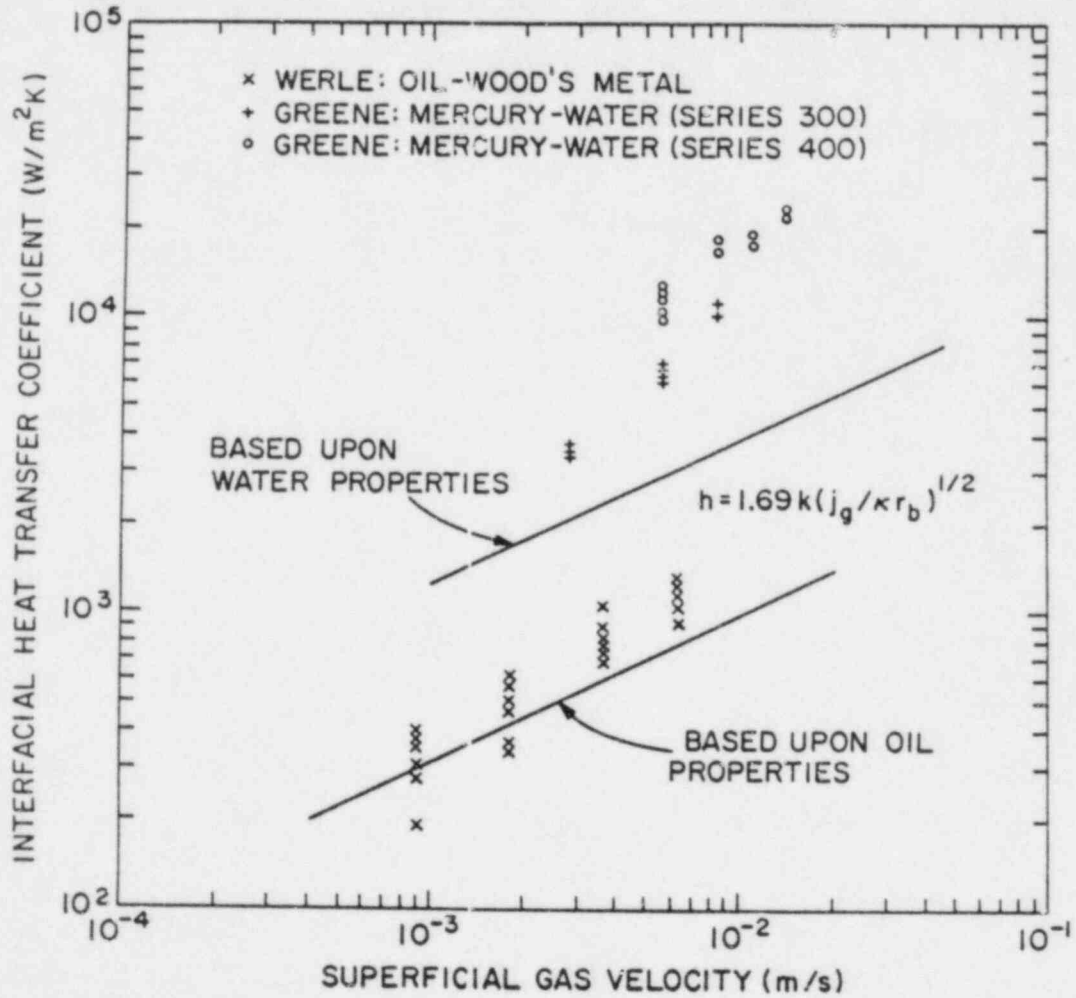

CORE-CONCRETE HEAT TRANSFER RESULTS

- DENSITY RATIO: 0.9
- ENTRAINMENT REGIME
- ENTRAINMENT PLUS SURFACE RENEWAL MODELS

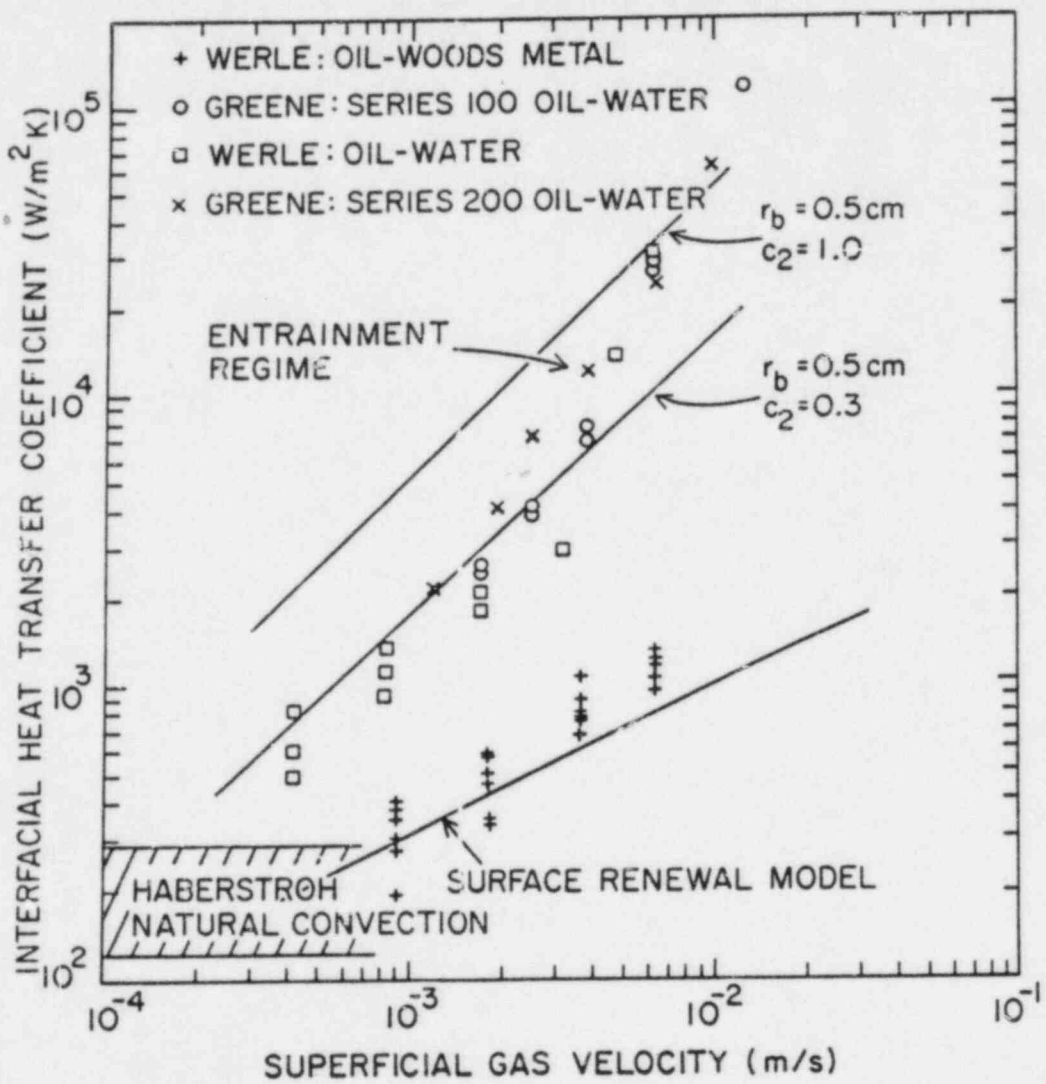

BROOKHAVEN NATIONAL LABORATORY
ASSOCIATED UNIVERSITIES, INC.

CORE-CONCRETE HEAT TRANSFER: SUMMARY

- EXPERIMENTAL

  - HEAT TRANSFER EXPERIMENTS WITH LIQUID PAIRS OF DENSITY RATIOS 0.1-0.9 PERFORMED
  - ENTRAINMENT AND NON-ENTRAINMENT REGIMES OBSERVED
  - EXPERIMENTS PERFORMED TO STUDY ONSET OF ENTRAINMENT

- ANALYTICAL

  - NON-ENTRAINMENT REGIME MODEL APPLIED
  - ONSET OF ENTRAINMENT MODEL DEVELOPED
  - MODEL DEVELOPED FOR ENTRAINMENT REGIME

- WORK CONTINUING ON MODEL DEVELOPMENT AND EVALUATION (ADDITIONAL FLUID PAIRS)

PROGRESS IN CORE DEBRIS THERMAL-HYDRAULIC PHENOMENOLOGY

- OBJECTIVE
  - SUPPORT MARCH CODE DEVELOPMENT
- SCENARIO
  - SUPERHEATED CORE DEBRIS BED IN REACTOR CAVITY
  - DEBRIS COOLED AND QUENCHED BY OVERLYING POOL OF WATER
- EXPERIMENTAL OBJECTIVE
  - DEVELOP DATA BASE FOR MODELS OF STEAM GENERATION RATE AND DEBRIS BED QUENCH CHARACTERISTICS

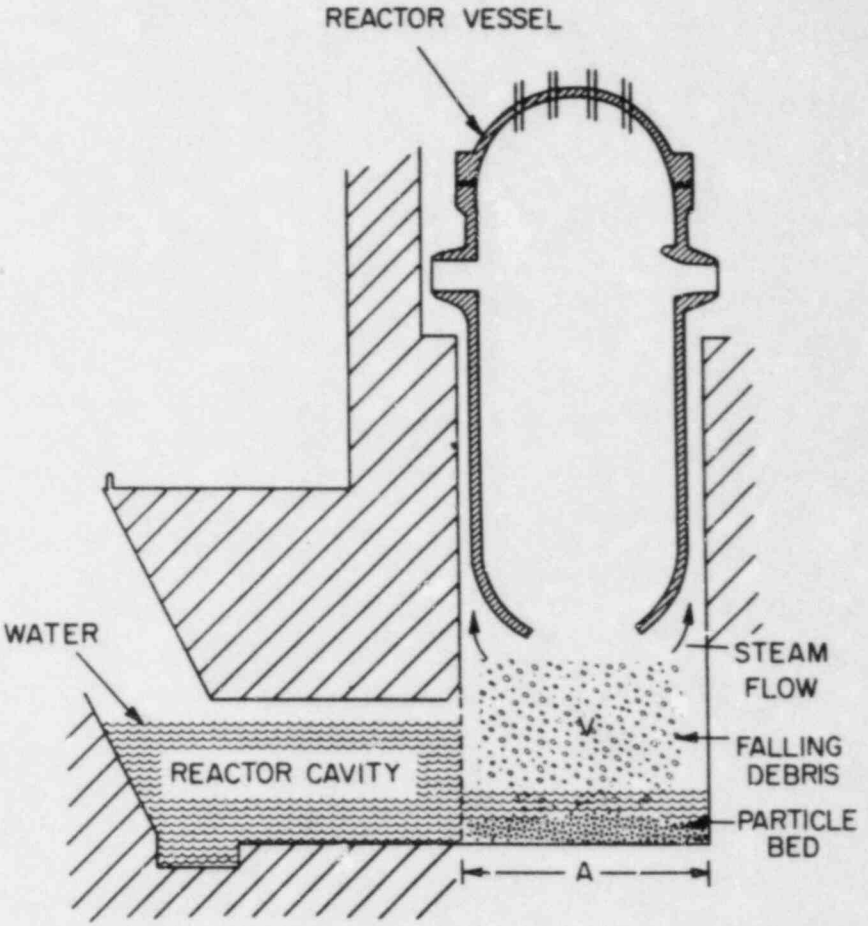

CORE DEBRIS THERMAL-HYDRAULIC (QUENCH) EXPERIMENTS

- APPARATUS

- PROCEDURE

  - HEAT PARTICLES
  - FORM DEBRIS BED
  - DROP WATER OVER BED
  - MEASURE TEMPERATURES, STEAM FLOW, PRESSURE

- PARAMETERS

  - PARTICLE SIZE (3-12MM)
  - TEMPERATURE (533-977K)
  - BED HEIGHT (200-400MM)
  - STAINLESS STEEL PARTICLES

- RESULTS

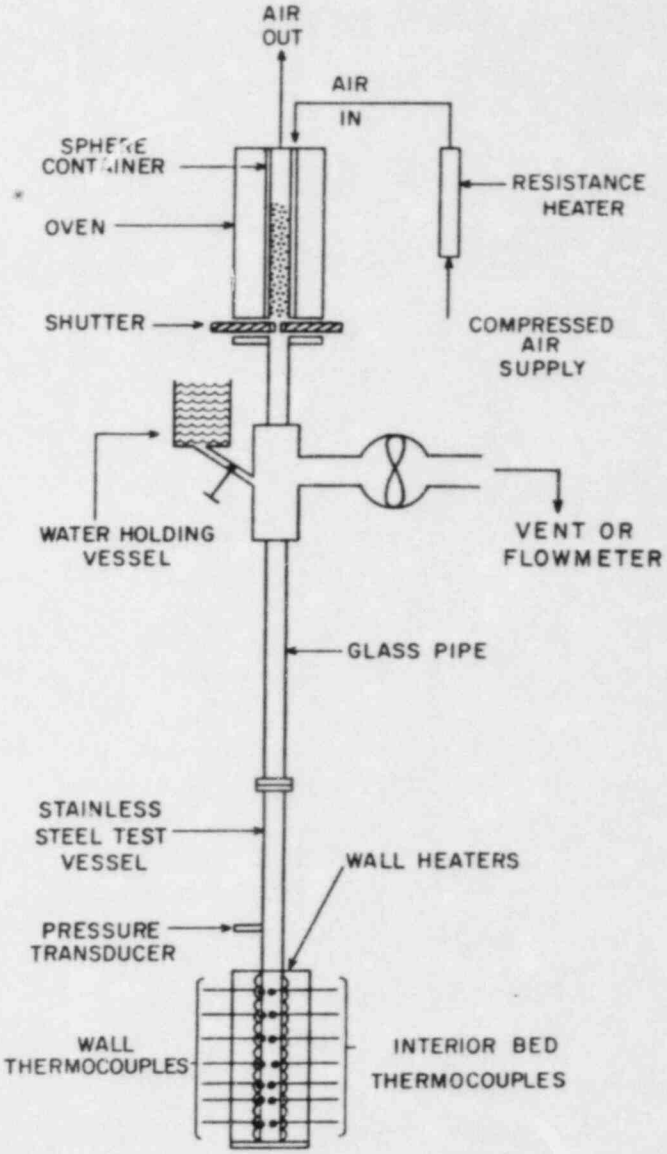

BROOKHAVEN NATIONAL LABORATORY
ASSOCIATED UNIVERSITIES, INC.

CORE DEBRIS THERMAL-HYDRAULIC EXPERIMENT RESULTS
"OBSERVED" DEBRIS BED QUENCH BEHAVIOR

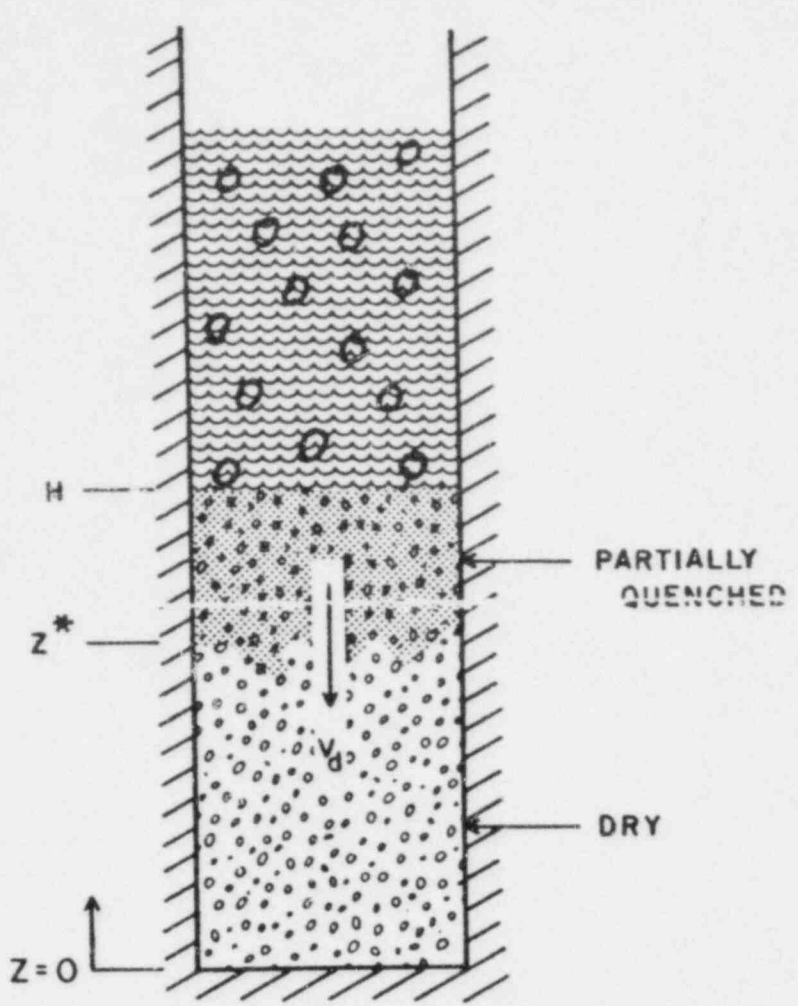

DOWNWARD FRONT

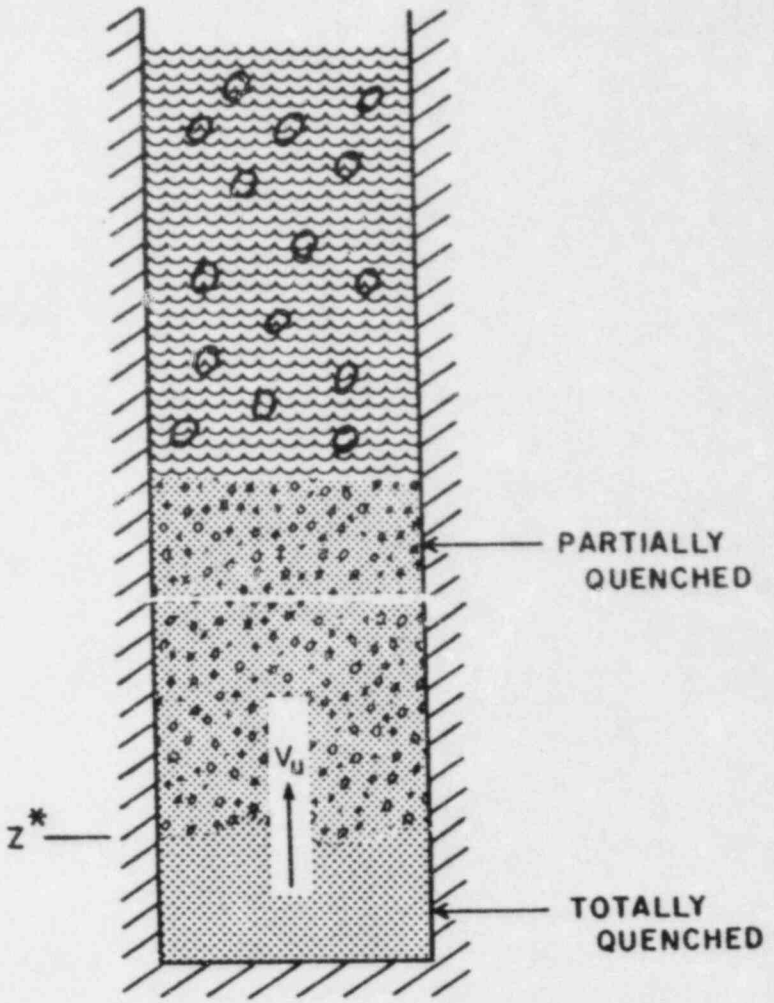

UPWARD FRONT

BROOKHAVEN NATIONAL LABORATORY
ASSOCIATED UNIVERSITIES, INC.

CORE DEBRIS THERMAL-HYDRAULIC EXPERIMENTS

ANALYTICAL MODEL

- QUENCH-FRONT HEAT TRANSFER MODE

- TWO-STEP COOLING PROCESS
  - DOWNWARD PROPAGATION
  - UPWARD PROPAGATION

- COOLING RATE LIMITED BY COUNTERCURRENT TWO-PHASE FLOW
  - QUASI-STEADY BED MODEL
  - FLAT PLATE "CHF" MODEL

- EQUATION SET
  - LUMPED PARAMETER BED ENERGY EQUATION
  - COUNTERCURRENT FLOW HYDRODYNAMICS EQUATIONS

CORE DEBRIS THERMAL-HYDRAULIC EXPERIMENTS

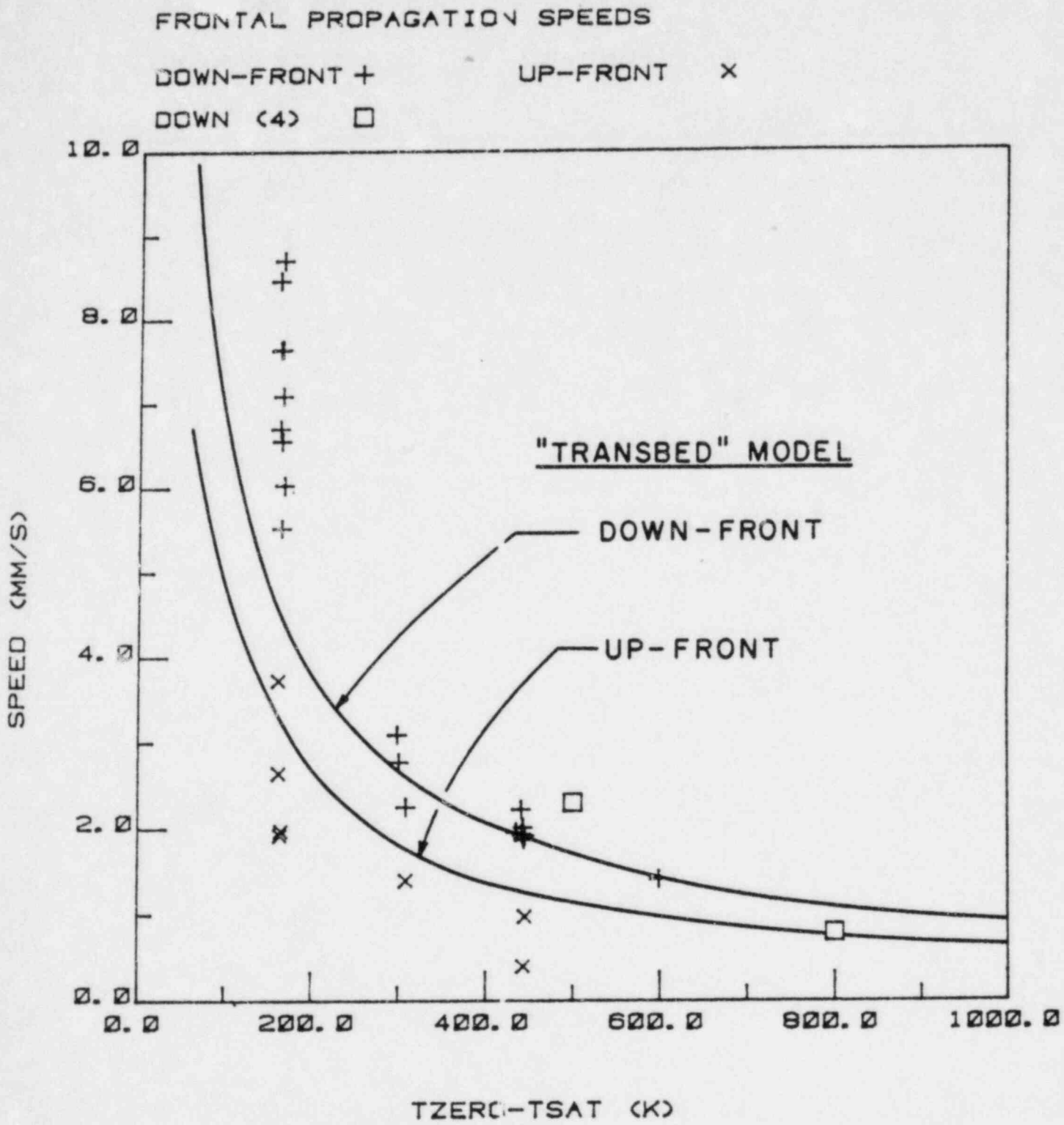

BROOKHAVEN NATIONAL LABORATORY
ASSOCIATED UNIVERSITIES, INC.

CORE DEBRIS THERMAL-HYDRAULIC PHENOMENOLOGY: SUMMARY

- EXPERIMENTAL
  - QUENCH EXPERIMENTS CARRIED OUT FOR BED OF 3MM SPHERES. BED HEIGHT, TEMPERATURE VARIED
  - SUPERHEATED BED TOP-QUENCH IS TWO-STAGE FRONTAL PROCESS
  - INITIAL WATER PENETRATION REMOVES ONLY 40% OF STORED ENERGY
- ANALYTICAL
  - "TRANSBED" MODEL LEADS TO GOOD PREDICTIONS OF MAJOR QUENCH CHARACTERISTICS
  - QUASI STEADY LIPINSKI AND ZUBER CHF MODELS PROVIDE GOOD AGREEMENT WITH 3MM HEAT REMOVAL DATA (COUNTERCURRENT FLOW LIMITED)
- WORK CONTINUING FOR MODEL DEVELOPMENT FOR BROADER RANGE OF PARTICLE SIZE

FUTURE PLANS FOR
BNL DEGRADED CORE RESEARCH

TASK	PHENOMENON	RELEVANT CODES
• HEAT TRANSFER IN CORE-CONCRETE INTERACTIONS	FILM BOILING IN LIQUID/LIQUID SYSTEMS	CORCON
• CORE DEBRIS THERMAL-HYDRAULIC PHENOMENOLOGY	BOTTOM REFLOOD	SCDAP
	DEBRIS QUENCH	
	FALLING PARTICLE	MARCH
	SYSTEM QUENCH	

BROOKHAVEN NATIONAL LABORATORY
ASSOCIATED UNIVERSITIES, INC.

SAND82-2269C

RECENT RESULTS FROM THE SANDIA STEAM EXPLOSION PROGRAM

N. A. Evans, D. E. Mitchell, L. S. Nelson
Sandia National Laboratories
Albuquerque, New Mexico

M. L. Corradini
University of Wisconsin
Madison, Wisconsin

ABSTRACT

The Sandia steam explosion program involves experiments at small and intermediate scale, and modelling and analysis, including estimates for the failure probability of the reactor pressure vessel and the containment building. Recent intermediate scale results show that molten corium A+R is as explosive as the molten simulant iron-alumina, with an average kinetic energy conversion ratio of approximately 2%. In addition, several iron-alumina tests produced rapidly sequential double steam explosions in which it appeared that the first explosion enhanced the coarse mixing process. Results at small scale indicate that the maximum pressure-volume product (the net work output) from the steam explosion of a single melt droplet increased four to five times for a ten-fold increase in ambient pressure.

With the initial assumption that contact between molten core and coolant will produce a steam explosion, and further assuming that such contact occurs in-vessel in the lower plenum, a Monte Carlo technique was used to calculate failure probabilities for a typical PWR. Inserting the latest estimates from reduced scale experiments for the kinetic energy conversion ratio, the conditional failure probability of the lower plenun is of the order of 0.4, and the failure probability of containment by large mass missiles is of the order of 5×10^{-4}. For a full scale reactor, these results are subject to changes that may be produced by effects due to scale, geometry, structure, and the prevailing thermodynamic conditions, such as (possibly) high pressure.

A start has been made on the development of coarse mixing models based on photographic data from intermediate scale experiments. Other experimental results include the effects of water to melt mass ratio and water depth on energy conversion ratio, and the rates of steam oxidation (with concurrent hydrogen production) of melts of varying oxidic content.

INTRODUCTION

A loss-of-coolant accident in an LWR may lead to a molten core-coolant interaction, which may threaten the integrity of the reactor pressure vessel or the containment building. The interaction may be non-explosive, or explosive, as distinguished by the times to achieve the maximum pressures which are, respectively, of the order of milliseconds, or seconds. In the typical steam explosion case, the molten core is initially coarsely mixed with coolant in stable film boiling; after film collapse by a triggering pressure pulse, a fine fragmentation process produces a significant surface area increases to promote rapid heat transfer and the production, at essentially constant volume, of high pressure vapor; this process propagates through the mixture at a speed of several hundred meters per second. Expansion of this vapor produces work which appears principally as kinetic energy of the coolant and quenched fuel, and as energy for shock wave pressurization of the air medium between the coolant boundary and the vessel wall. The energetic fluid slug may produce a large mass missile by failing the upper head of the vessel and thus threaten containment; the shock wave in the liquid coolant phase may cause failure of the lower plenum.

The work at Sandia has proceeded along three paths. In small scale experiments, a single droplet of molten material (typically a ferrous oxide or metal with a diameter of several millimeters) is dropped into water, and an explosive interaction is triggered in front of high speed movie cameras by a small exploding bridge wire. Pressure data are obtained from a nearby fast-response transducer. These experiments allow close control of the many parameters involved, are relatively inexpensive to perform, and have produced a significant amount of information on the basic physics of the steam explosion process.

The second path, intermediate scale experiments, involves the dropping of melt masses up to 20 kg into water containers of various shapes and volumes. These experiments are conducted both in a closed (FITS) chamber, and in the open air (EXO-FITS). Both types of experiment allow easy study of the effects of some parameters (e.g., melt composition, water depth and subcooling, etc.), while, in the enclosed FITS experiments, the pressure and composition of the ambient medium can be controlled, and the post-interaction debris can be collected for analysis. Better photographic coverage is possible with the EXO-FITS experiments.

Since the quantities of molten fuel that are available to participate in an interaction can be of the order of many metric tons in an LWR, and most of the experiments are conducted with

much smaller quantities, it is not clear to what extent the results from these reduced scale experiments can be validly extrapolated to reactor scale.

The third work path is attempting to address the scaling issue both by analyzing the experiments to better quantify the initial conditions leading to a steam explosion, and by providing data to construct mathematical models of the processes involved that would aid in extending the results to reactor scale.

PROCEDURE AND RESULTS

1. Small Scale Experiments

Single oxidic droplets ($FeO_{1.0}$, $FeO_{1.2}$) were melted by CO_2 laser heating (as in Fig. 1) or, in the case of ferrous metal droplets, by induction heating, and then dropped into a transparent plastic tank of water. The strength of the trigger used to induce a steam explosion was varied both by raising or lowering the bridge wire, and by changing the firing voltage. After the interaction, the debris was typically analyzed for particle number, mass, and area characteristics.

The high speed motion pictures clearly showed the luminous melt drop in film boiling as it fell through the water. An important observation was the immediate formation of a large bubble of noncondensing gas around a metallic iron droplet when it entered the water. A much smaller bubble was formed around a droplet of $FeO_{1.0}$, and essentially none around a droplet of $FeO_{1.2}$, as shown in Fig. 2. We consistently observed that the trigger pressure level necessary to cause a steam explosion increased as the volume of the bubble increased, presumably due to the increased cushioning effect from the noncondensable gas.

Assuming that the bubble contained mostly hydrogen produced by the oxidation of the metal or oxide by high temperature steam, measurement of the bubble size allowed the following preliminary estimates to be made for the oxidation rates:

$$R\ (Fe) = 1.6 \pm 0.2 \text{ mg } 0\ \text{cm}^{-2}\ \text{s}^{-1} \text{ at } T = 1800\ \text{K}$$

$$R\ (FeO_{1.0}) = 0.6 \text{ mg } 0\ \text{cm}^{-2}\ \text{s}^{-1} \text{ at } T = 2000\ \text{K}$$

$$R\ (FeO_{1-2})\ 0 \text{ at } T = 2000\ \text{K}$$

An investigation has been started of the behavior of other corium constituents. A noncondensable gas bubble is shown in Fig. 2 around a droplet of ZrO_2 in water. In this case, it would appear that the much higher temperature of the droplet (> 2700 K) caused thermal dissociation of the water, so that the bubble contained both hydrogen and oxygen, with consequent increased difficulty for triggering a steam explosion.

Further analysis of earlier test results using $FeO_{1.2}$ droplets shows (Fig. 3) that increased ambient pressure, P_∞, caused the net work output $P_\infty V_{max}$ (where V_{max} is the maximum steam explosion bubble volume) to increase significantly. This behavior is contrary to the prediction from the applicable current model, and the strength and importance of this result has prompted additional modelling effort on this aspect. Additional experimental support for this result is obtained from the corresponding plot (Fig. 4) for the number of fine fragments produced during the explosion for a constant initial droplet size: the overall increase factor in the number of particles was approximately the same as the increase factor in the $P_\infty V_{max}$ product.

2. Intermediate Scale Experiments

In-chamber FITS experiments using melt masses up to 20 kg were performed in the apparatus shown in Fig. 5. Iron-alumina and corium melts were prepared by a thermite process in the top crucible which was automatically released by melt sensors. This allowed the melt to fall into the water vessel where the interaction was recorded by high speed motion picture cameras, with pressures and temperatures measured by transducers at various locations. EXO-FITS tests were performed in approximately the same manner, but without the benefit of the surrounding chamber.

A generalized pressure-time trace is shown in Fig. 6 for the FITSB test series, using an iron-alumina melt. The two rapid pressurizing events corresponded to steam explosions approximately 100 ms apart, followed by possible steam or hydrogen generation, and final quenching of the settled debris. Such double explosions were observed in three of the nine FITSB tests in the melt-to-coolant ratio range $12 \leq M_w/M_f \leq 15$; an example of an actual pressure trace (for test 1B) is shown in Fig. 7. Sketches from movie frames are shown in Fig. 8. It appears that the first explosion, with only part of the melt submerged, was effective in fragmenting the remaining melt, and enhancing the mixing prior to the second explosion. Other tests in the series produced a single explosion, or, in the case of low water subcooling (test 5B), a very weak partial reaction. Triggers were observed occurring randomly in location, as opposed to the more common base triggers in earlier tests using 2 to 5 kg of melt.

In a steam explosion, the rapidly converted melt thermal energy appears principally in two forms: the kinetic energy imparted both to the liquid water initially adjacent to the fuel-coolant mixture explosion region and to the quenched fuel; and the work done by the outwardly propagating shock wave to store energy by pressurizing the FITS chamber air beyond the outer boundary of the water region. Hence, an energy conversion ratio η_{KE}, based on kinetic energy observations, will be, to a large

extent, distinct and separate from the stored energy conversion ratio, η_D, based on chamber air pressurization. Although the two energy terms are additive for a given experiment, they are not completely decoupled: different geometries and degrees of confinement can alter the partition of available energy. For LWR safety considerations with an in-vessel explosion, the kinetic energy term may be related to water slug missile production, which may cause failure of the reactor pressure vessel head, while the shock wave through the water initially surrounding the explosion may induce lower plenum failure.

To emphasize the concept of energy conversion partition, the total mechanical utilization of the rapidly transferred melt thermal energy is given to first order by

$$\eta_{TOT} = \eta_{KE} + \eta_D \tag{1}$$

with

$$\eta_{KE} = \frac{KE}{Q_m} \tag{2}$$

and

$$\eta_D = \frac{\Delta PV}{(\gamma-1)\ Q_m} \tag{3}$$

where KE = kinetic energy produced
Q_m = melt thermal energy
ΔP = chamber air pressure rise after shock wave equilibration
V = chamber volume
γ = specific heat ratio for air

The values for η_{KE} and η_D obtained from the FITSB experimental data are shown plotted against water-to-melt mass ratio in Fig. 9, and against water depth in Fig. 10. These figures show that the conversion ratio η_{KE} did not vary significantly with either mass ratio or water depth, with the exception of an extremely lean mass ratio (FITS7B). However, the values calculated from chamber pressure data for η_D show a dependence on these two parameters. Although the test matrix was rather sparse, this result suggests that, as the water-to-melt mass ratio increased, the associated tamping increased the total utilization of the converted thermal energy. Then, since the kinetic energy remained roughly constant, it would follow that the stored energy conversion ratio would increase. From Fig. 11 it is seen that, as η_{TOT} increased, the mass median particle size decreased to provide more area for the associated increase in heat transfer rate from melt to coolant.

In Table 1 the results from several test series are collected, including some using corium A+R as the melt. These corium results, together with the result for the corium test MDC-12 are repeated in Table 2; they indicate that, provided the corium mass delivered exceeds a threshold value of about 4 kg, the explosion is likely to occur spontaneously with a value for η_{KE} that is very similar to values obtained with iron-alumina (see Table 1). From this table of values, we currently consider the conservative best estimate value for η_{KE} for both iron-alumina and corium, is 2% within a multiplying or dividing factor of 3 either way. It is interesting to note that, since the mass threshold for iron-alumina (about half as dense as corium) appeared from previous tests to be about 2 kg, the mass threshold may be more physically linked to a particular volume threshold (in these cases, approximately 0.5ℓ, or 1 pint, for each melt).

Figure 12 shows the current status of the combined Sandia analytical and experimental efforts. While, as described below, the mixing model is now under development, the remaining models give a fairly complete understanding of the experimental observations obtained so far to intermediate scale (typically 20 kg of melt). An individual model has a certain level of empirical input (given by the EN designation on Fig. 12), but in no case is the level considered to represent a serious deficiency in understanding. A particularly important question remaining to be answered is whether, and how, the current results can be validly extended to the full scale reactor condition.

3. Modelling and Analysis

A. Mixing Models

The photographic records from several FITS experiments have been studied in detail, and it appears that the coarse mixing process can be related to Weber-type liquid-liquid break-up, and in the current case the additional feature of steam generation may be assisting the mixing process. From the films it would appear that liquid entered the mixing region from the bottom and sides, and that steam left from the top.

As with previous work in liquid-liquid mixing, an appropriate non-dimensional time parameter is

$$T^+ = \frac{tv_1}{D_o} \left(\frac{\rho_w}{\rho_f}\right)^{1/2}$$

where D_o = initial melt mass diameter

v_i = melt entry velocity into coolant

ρ_w = coolant density

ρ_f = melt density

From the film data, the following correlations have been obtained for the melt vertical penetration, H, the melt horizontal dispersion, D, and the melt fragment median diameter, D_f:

$$\frac{H}{D_o} = 1.2\ T^+ \tag{4}$$

$$\frac{D}{D_o} = 1 + 0.72T^+ \tag{5}$$

$$\frac{D_f}{D_o} = e^{-0.6T^+} \quad \text{- mass median} \tag{6}$$

$$\frac{D_f}{D_o} = e^{-T^+} \quad \text{- number median} \tag{7}$$

Although these expressions should be regarded as preliminary while the analysis continues, their potential application can be illustrated as follows. Consider a full scale reactor with a lower plenum containing a water depth, H = 3 m. If, with triggering on bottom contact, an explosible mixture is considered formed when the fragmented fuel diameter (number median) is 2 cm, the maximum mass of corium (ρ_f = 7000 kg/m^3) that could mix would be $M_f \simeq 8000$ kg (approximately 6% of a typical PWR core). This maximum mass is calculated from a pouring column of height H and diameter D_o (obtained from Eq. 4 and 7 after eliminating T^+). Similarly, for a reactor cavity containing water to a depth of 5 m, the maximum mass of corium that could mix would be $M_f \simeq 30{,}000$ kg (approximately 23% of a typical PWR core). It should be noted that available space is an important mixing requirement since these expressions show that an increase in water depth of approximately 70% will allow approximately 400% more corium to mix.

B. Monte Carlo Calculations for Failure Probability

Earlier work,[1] using a Monte Carlo technique to estimate containment failure probability by an in-vessel steam explosion producing a large mass missile, has been revised. The previous triangular distribution of energy conversion ratio

(ranging from 0 to 3%, with a maximum probability at 1%) was replaced by one with doubled values; i.e., the new maximum probability occurs at $\eta_{KE,p}$ = 2% to reflect the latest conservative best estimate value given above in sub-section 2. With all other features remaining the same as before, the results of 10,000 cases are shown in the second row of Table 3, and can be compared with the earlier results which are given in the first row. For a full scale reactor, these results are subject to changes that may be produced by effects due to scale, geometry, structure, and the prevailing thermodynamic conditions, such as (possibly) high pressure. For the current case, there was a total of 9 upper head failures, but only 5 produced large mass missiles (upper head plus flange plus impacting water slug) with initial velocities exceeding 60 m/s. For a typical PWR geometry, this velocity was considered the minimum necessary just to reach the underside of containment after the slug picked up additional mass from the penetrated missile shield equal to its own mass.

For initial velocities exceeding 60 m/s, the severity of the threat to containment has been classified according to the average, idealized breach diameter, d_h, which was calculated from a simple shear stress failure of the PWR containment concrete; the threat was considered severe when $d_h > 4.5$ ft, the approximate concrete thickness. The total of 5 failing cases represent a containment failure probability of 0.0005, compared with the previous value of < 0.0001 when using $\eta_{KE,p}$ = 1%. In addition, the latest calculation indicates that the lower plenum has a failure probability of 0.37; such a failure was considered possible when the initial steam explosion energy exceeded 1000 MJ, as judged from a separate set of calculations.

For completeness, the third row in Table 3 gives the results for $\eta_{KE,p}$ = 3%. The high sensitivity of conversion ratio is shown by the fact that an increase of 50% in $\eta_{KE,p}$ (row 2 to row 3 in Table 2) increases the containment failure probability by an order of magnitude, and emphasizes the need to obtain improved values for this parameter. (Note, however, that this probability is bounded (1.3×10^{-2}) by the maximum, thermodynamically achievable, conversion ratio.)

FUTURE PROGRAM INTENTIONS

For the coming year, the intermediate scale experiments will be continued with additional tests using corium in the FITS chamber to investigate possible hydrogen production and the effect of increased ambient pressure, for comparison with previous work using the iron-alumina simulant. A longer series of tests will be run EXO-FITS, using up to 50 kg of iron-alumina melt, to investigate the effects of low subcooling, mass ratio and water depth. In addition, a few tests will be performed in

an attempt to obtain a better measurement of energy conversion ratio with a rigid steel, rather than a lucite, water tank; this will provide a more realistic inertial confinement, but will prevent detailed photographic recording of the interaction.

Modelling and analysis will involve development of more refined mixing and triggering models (especially with respect to the mass threshold effect), and further adaptation of the CSQ hydrocode to analyze the experimental observations, and perform computer experiments on the effects of confinement and geometry. The objective is to provide a set of analytical tools that can be utilized to support regulatory and specific licensing decisions.

REFERENCES

1. D. V. Swenson, M. L. Corradini, Monte Carlo Analysis of LWR Steam Explosions, SAND81-1092, NUREG/CR-2307, Sandia National Laboratories, October 1981.

REPORTS PUBLISHED IN FY82

1. Monte Carlo Analysis of LWR Steam Explosions, D. V. Swenson, M. L. Corradini, NUREG/CR-2307, October 1981.

2. Recent Experiments and Analysis Regarding Steam Explosions with Simulant Molten Reactor Fuels, M. L. Corradini, D. E. Mitchell, L. S. Nelson, Fuel-Coolant Interactions, HTD Vol. 19, Winter Annual Meeting, ASME, Washington, DC, November 1981.

3. Light Water Reactor Safety Research Program Semiannual Report, April-September 1981, M. Berman, NUREG/CR-2481, February 1982.

4. Core Melt Coolant Interactions, M. Berman, M. L. Corradini, N. A. Evans, D. E. Mitchell, L. S. Nelson, D. V. Swenson, NUREG/CR-0024, Vol. 2, Ninth Water Reactor Safety Research Information Meeting, Gaithersburg, October 1981.

5. Steam Explosions of Molten Iron Oxide Droplets, L. S. Nelson, P. M. Duda, Easier Initiation at Small Pressurization, Nature, 296, 844-845, 29 April 1982.

6. Zinc Selenide Window for Transmission of CO_2 Laser Radiation into Moist Gas at Elevated Pressures, L. S. Nelson, P. M. Duda, Review of Scientific Instruments, 53, 259-260, 1982.

7. Steam Explosions of a Metallic Melt as its Degree of Oxidation Increases: Fe, $FeO_{1.0}$, and $FeO_{1.2}$; L. S. Nelson, P. M. Duda, Int. Meeting on Thermal Nuclear Reactor Safety, ANS/ENS, Chicago, August 1982.

8. The Effect of Water to Fuel Mass Ratio and Geometry on the Behavior of Molten Core-Coolant Interactions, D. E. Mitchell, N. A. Evans, Int. Meeting on Thermal Nuclear Reactor Safety, ANS/ENS, Chicago, August 1982.

9. A Proposed Model for Fuel-Coolant Mixing During a Core-Melt Accident, M. L. Corradini, Int. Meeting on Thermal Nuclear Reactor Safety, ANS/ENS, Chicago, August 1982.

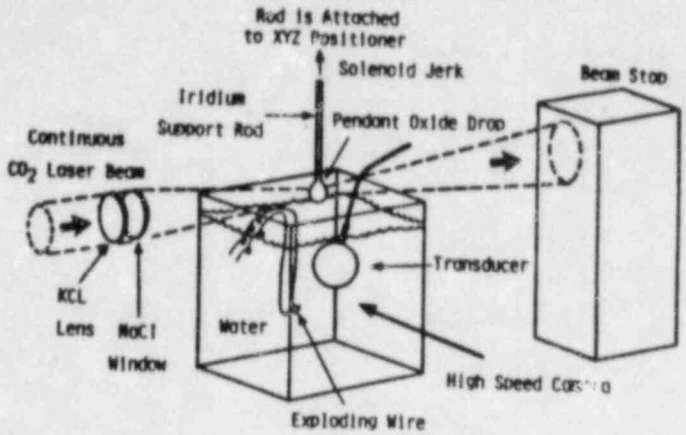

Figure 1. Small-Scale Single Droplet Apparatus with CO_2 Laser Heating. Melt Mass ~0.05 g.

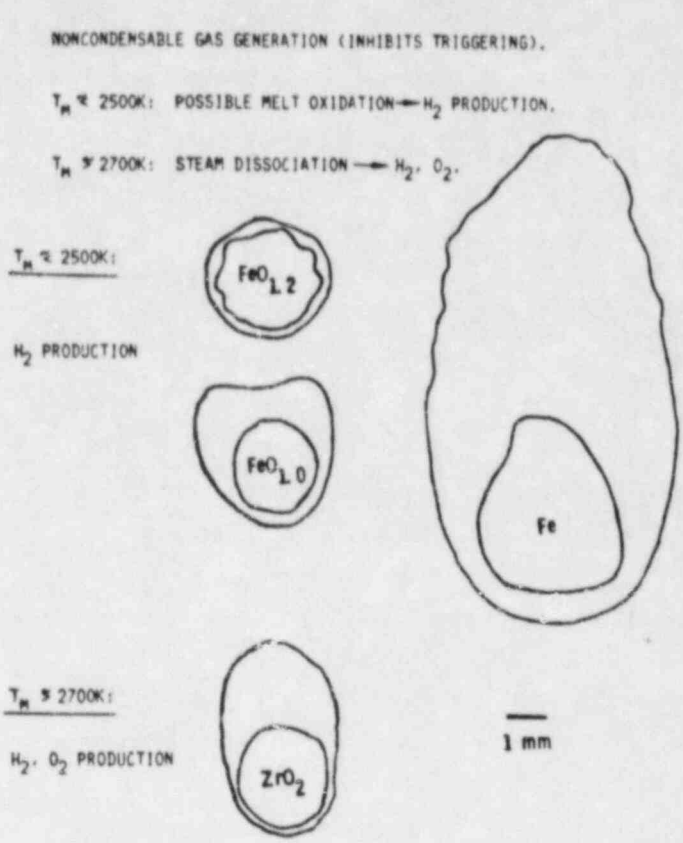

Figure 2. Effect of Melt Composition.

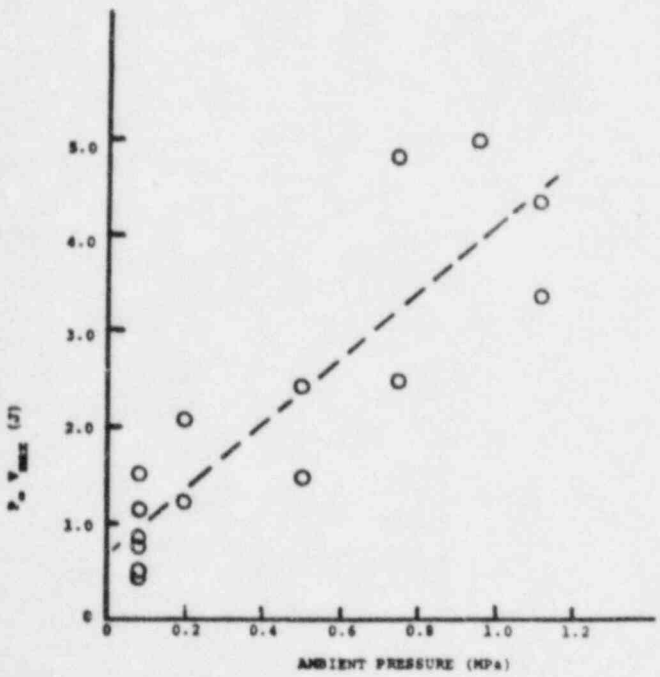

Figure 3. Effect of Pressure on Yield.

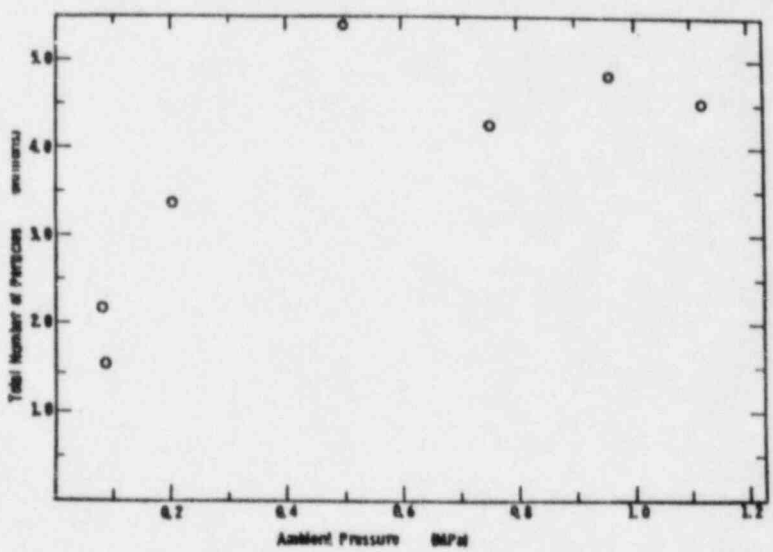

Figure 4. Effect of Pressure on Fragmentation.

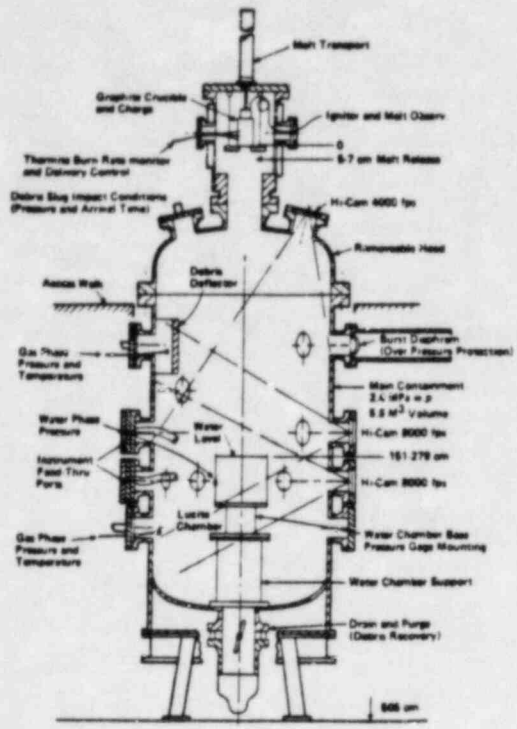

Figure 5. Intermediate Scale Apparatus - Melt Mass ~ 20 kg Full Instrumented Test Series (FITS) Chamber.

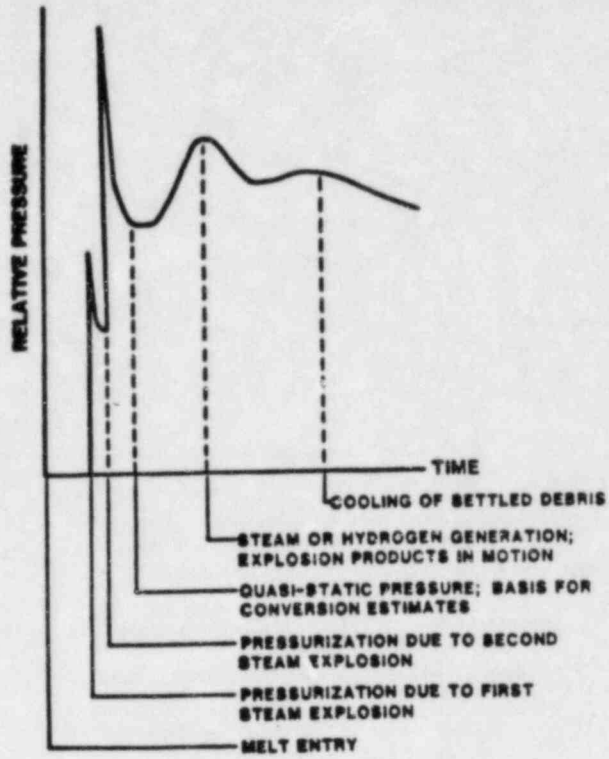

Figure 6. Typical FITS Chamber Air Pressure-Time Plot.

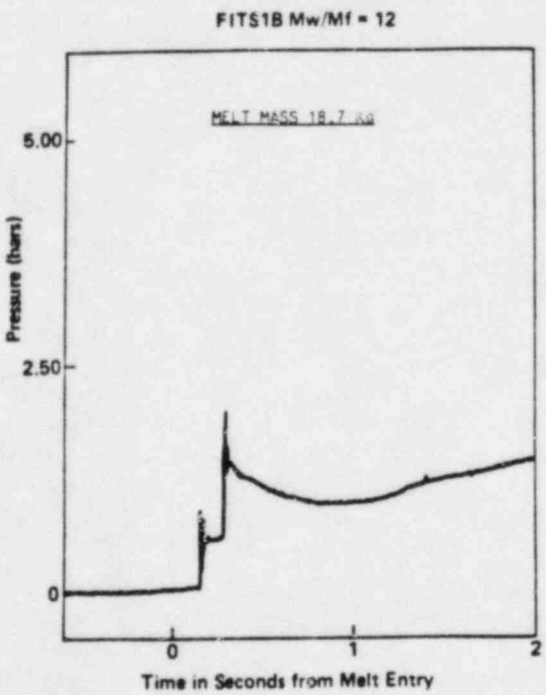

Figure 7. Double Explosion using $Fe/A\ell_2O_3$.

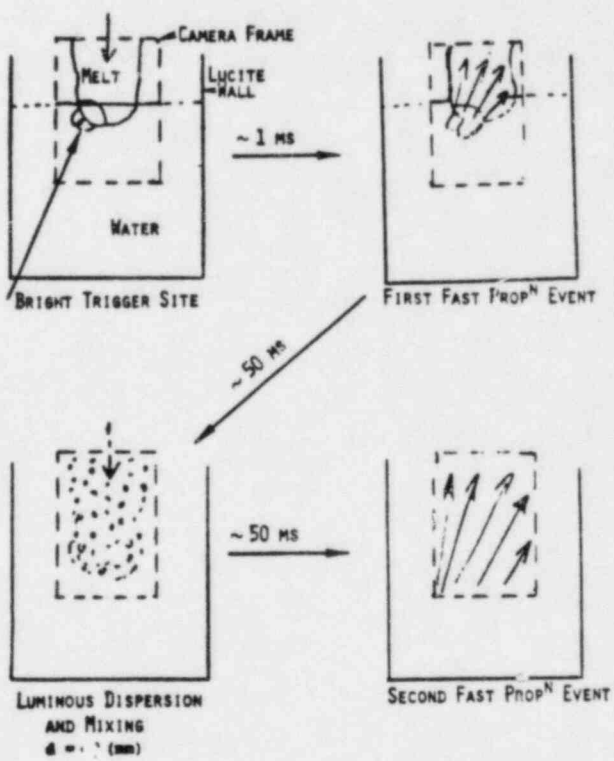

Figure 8. Sketches from Movie Film of Double Explosion.

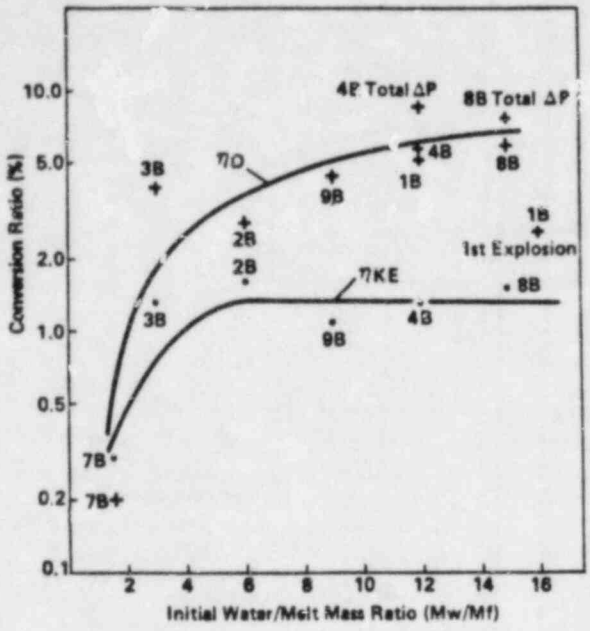

Figure 9. Conversion Ratio versus Initial Water/Melt Mass Ratio, Melt Mass 18.7 kg.

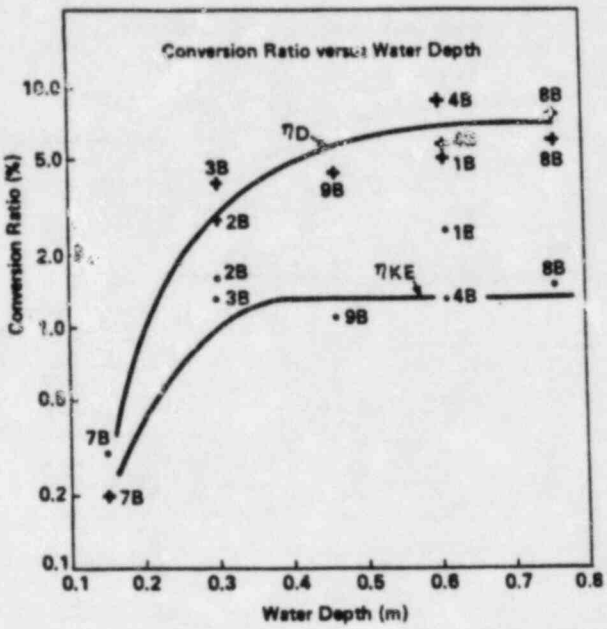

Figure 10. Conversion Ratio versus Water Depth, Melt Mass 18.7 kg.

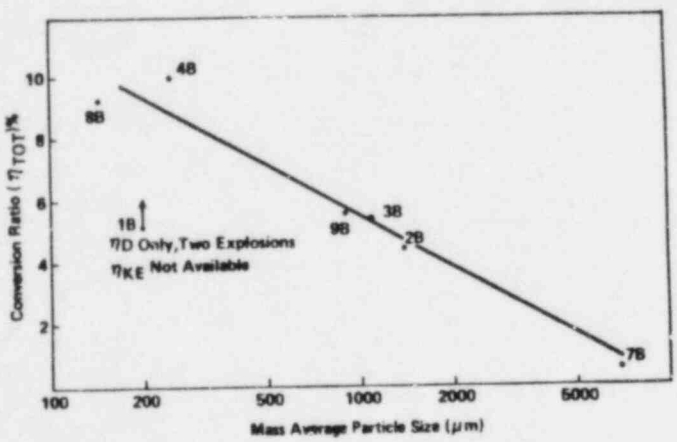

Figure 11. Total Conversion Ratio Versus Mass Median Particle Size for FITSB Post-Test Debris.

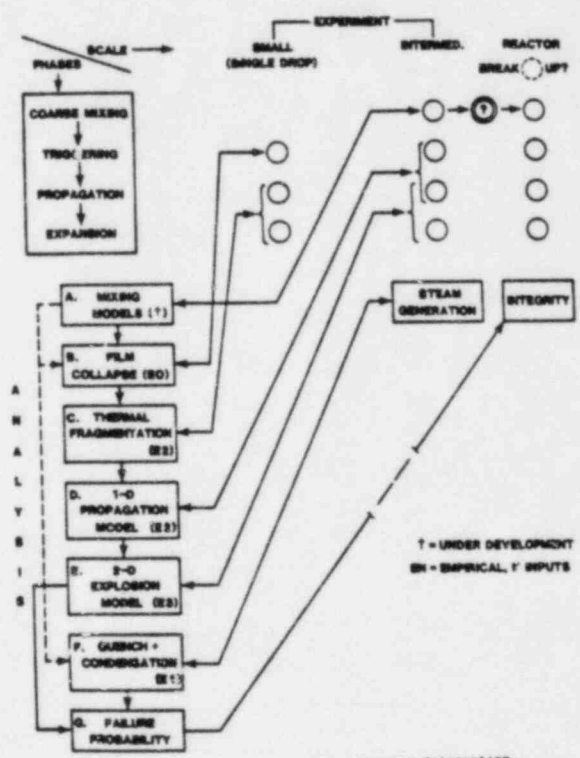

Figure 12. Program Integration.

Expt.	Melt Mass kg	Mass Ratio M_M/M_F	η_D %	η_{XX} %	$\eta_{XX} \cdot \eta_D = \eta_{TOT}$ %	Comment
MD						
Series	1.9-5.1	44-57	-	2.4	-	Average of all MD Series EXO-FITS
MDC2	4.3	36	-	2.3	-	CORIUM A+B EXO-FITS
MDC14[1]	8.0	13.5	-	1.0	-	
MDC16	8.2	18.5	-	2.4	-	
MDC17[2]	9-18	31-15	-	1.3-2.6	-	
FIT01B	16	16	2.6	1.1	3.7	First explosion
	18.7	12	5.1	-	-	η_{XX} not available
FIT02B	18.6	6	2.8	1.6	4.4	
FIT03B	18.6	3	4.0	1.3	5.3	
FIT04B	18.6	12	5.7	1.3	7.0	ΔP from ramp to Plateau
			8.6	1.3	9.9	Total ΔP
FIT07B[3]	13	1.5	0.2	-	-	
FIT07BR[3]	12	1.5	-	0.3	-	Repeat of 7B EXO-FITS
FIT05B	18.7	15	5.9	.5	7.4	ΔP from ramp to plateau
			7.7	1.5	9.2	Total ΔP
FIT09B	18.7	9	4.4	1.1	5.5	
FIT03A[4]	5.3	43	1.5-5.8	2.0	3.5-7.8	
FIT05A	5.4	42	1.0	-	-	η_{XX} not available

NOTES: (1) Premature detonator firing caused water loss prior to melt entry.

(2) Melt loss during thermite burn. Resulted in dispersed melt at water entry. Melt mass delivered estimated.

(3) Melt mass estimated from post-test debris. Only fragmented debris used in the estimate. 7BR assumed to be the same.

(4) Pressure measurement affected by premature chamber venting.

Table 1. Summary of Conversion Ratio Calculations
FITS Experiments

EXO-FITS RESULTS

ALL SPONTANEOUSLY TRIGGERED

Test	Mass, kg	$\eta_{K.E.}$ %	Remarks
MDC-2	4.3	2.3	Base triggered
MDC-12	3.9	~0	Partial reaction
MDC-14	8.0	<1.0	Base triggered
MDC-16	8.2	2.4	Base triggered
MDC-17	9-18	1.3 to 2.6	Fast burn rate

Table 2. Corium Explosibility

Mode / η-Distribution	Lower Plenum Failures	Vessel Failures in 10,000 cases: Upper Head Failure => Large Mass Missiles Containment Threat — None V_1<60m/s no impact	Slight 60<V_1<65 d_h<1.0 ft	Moderate 65<V_1<80 1.0<d_h<4.5	Severe V_1>80 d_h>4.5	Vessel Failure Probability	Total Containment Threat Probability
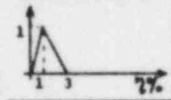	2586	0	0	0	0	0.26	< 0.0001
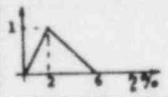	3729	4	2	2	1	0.37	0.0005
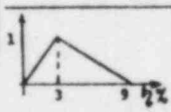	7849	11	5	13	33	0.79	0.005

NORMALIZED FREQUENCY

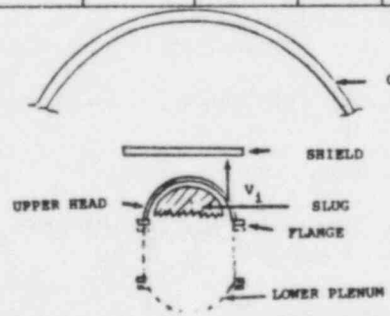

Table 3. Monte Carlo Calculations

RETROFITTING NUCLEAR PLANTS FOR THE MITIGATION OF CORE MELT EFFECTS

by R. Philip Hammond*
James L. Dooley*

The protective containment building that surrounds all U.S. power reactors is required to cope with several kinds of internal accidents and disruptions, including release of all the primary coolant. However, present requirements do not include coping with a "Class IX" accident in which all emergency cooling systems fail, and molten core material escapes from the reactor vessel. In the past, it has been assumed that such an event would be too rare to justify the requirement of a "core-catcher" or core retention device. If it did occur, the containment would fail.

The anti-nuclear activists have been quick to seize upon the point that utilities were required to protect the public against all accidents except the "Big One", and that the distinction between Class VIII and Class IX accidents was only a matter of degree, of a few minutes delay, or a small additional failure. Thus inevitably each minor incident in a nuclear plant became a "near miss", a disaster narrowly averted.

On top of this, there have been several events that really were "near misses"--that had the potential of developing into a full-fledged Class IX failure. It is clear that the public is poised to bring endless lawsuits for psychological stress or imputed damage against any utility unlucky enough to emit a few puffs of radioactivity. Such suits, on top of a plant failure, would spell financial ruin for any utility. Small wonder that financing for new plants is vitually unobtainable.

---

*R & D Associates, Marina del Rey, CA 90291

In this situation, there has lately been renewed interest in the fact that the containment is almost capable of sustaining any internal failure--that a relatively modest improvement would completely remove the threat of public exposure. Work has progressed on hydrogen control, on passive containment cooling, and on melt-down phenomena. However, a missing element has been a suitable core catchment device, information on its cost, and assurance that any such device would reliably survive the violent events accompanying destruction of the reactor. Also, while a core retention device suitable for new construction would be of interest, it would be somewhat academic; with no new reactors being ordered, what was needed was a safe way to retrofit a core catcher to existing plants.

In the spring of 1980, NRC officials learned from RDA of Marina del Rey, California, that a blast-proof, retrofittable core retention system had been devised. This concept was further discussed in a presentation at NRC headquarters in May, 1980. The complete concept proposed by RDA included the retention device, passive means of heat removal, and a method of installation for existing reactors by tunneling under the foundation.

To persons unfamiliar with the science of underground structures the idea of digging under the foundations of an operating plant seems fraught with risk and uncertainty. NRC selected this portion of the overall concept for a preliminary feasibility study, conducted over the past year. (Ref. 1). A unique construction sequence has been worked out that is feasible, entirely safe, and reasonably low in cost.

Figure 1 shows the overall RDA core-catcher concept after installation in a PWR plant. The long tapered entrance funnel is carefully designed as a blast attenuator and to prevent water from preceding the melt down the tube. Figure 2 shows

the melt in its final location at the bottom of the crucible. The actual container for the uranium oxide is a thin layer of frozen oxide, maintained by contact with the water cooled steel wall. The area of frozen skin is large enough to transfer all the decay heat at the rate it is produced in the melt. As the heat evolution decreases, the skin gradually thickens, until the entire mass is solid. The cooling water circulates by natural convection.

If all reactors were sited upon sound, competent rock, the tunneling operations would be simple indeed. However, the majority are located on river banks or seashores, and often upon very weak or sandy sediments. The problem is to devise a way to excavate under these heavy structures without the slightest risk of settlement, cave-in, or loss of support. The method to be illustrated will work in almost any kind of soil, sand, or rock. Minor modifications would be made to suit the actual conditions, and no one site would likely need all the precautions shown.

Figure 3 shows the general scheme of the excavation. Where the reactor is situated on water-saturated ground, the first step is to introduce control over water flow and produce ground stability for the excavation. The process is planned using test borings and surveys. In some cases it is sufficient to drill wells around the excavation site and install pumps to lower the water level. Where the porosity is too high for pumps to control the flow, a curtain of grout will be injected around and ahead of the excavation to displace the water. When the grout sets, the porous ground has become solid rock. By drilling ahead of the tunnel as it advances and injecting grout, the tunnel boring equipment can work in the center of a cylinder of good rock.

Starting about 600 to 1000 feet from the reactor at a convenient point away from plant activity, the tunnel advances

until it has reached the sub-reactor point about 140 feet underground. From here a large array of small core holes is drilled and used to inject grout until the entire reactor containment building is situated upon sound material from which all water has been displaced by grout. A part of this process is to drill back through the grouted area and take core samples to confirm the quality of the rock that has been produced. In some locations a vertical shaft and horizontal tunnel would be used instead of the inclined tunnel.

Figure 4 shows the next step, the construction of a strong-room--a reinforced concrete, steel lined working area beneath the reactor. Here an elevator is installed and a vertical raise boring machine mounted upon it. These machines are well known in the mining and tunneling industry. They have the ability to cut their way up through solid rock at about two to six feet per hour, while maintaining steady pressure on the overhead face. As they are normally used, on ground that has not been pregrouted to a stable form, this overhead pressure helps prevent collapse of the shaft. In our case, it is not essential but is used as a secondary precaution.

Boring upward from the strong room to the reactor base mat is done in short stages or lifts. Figure 5 shows the boring machine stopped but maintaining overhead pressure while reinforcing bar, steel liner and finally concrete are added to the shaft walls. With this method the sidewalls of the shaft are also supported almost continuously, as well as the overhead.

Figure 6 shows the structure, called a caisson, completed and attached by rock bolts to the reactor base mat. The structure is built with a continous steel liner having fully inspected welds and with a pressure-tight door to seal off the access tunnel. This strong silo is pressure-tested and qualified as an extension of the containment building, although it

is not yet interconnected. The dotted lines in Figure 6 show where this connection will be made.

The next step is to drill an accurately located ring of about 80 holes about 4-6 inches in diameter up into the base mat, using a diamond core-drill. Figure 7 shows that such a drill can cut accurately and smoothly through concrete, aggregate, and reinforcing bar. Figure 8 shows how the drill is constructed. At first the holes are drilled only about 3/4 of the way through the basemat. Then, after waiting until a normal reactor refueling shutdown has occurred, the weight of the basemat plug is taken by the elevator and the holes are rapidly completed through to the reactor pit space. The webs between holes are cut out with a mechanized torch or grinder, and short lead plugs placed in each hole as it is finished. The weight of the plug is now resting upon the elevator. The hole-cutting would require about 8 days.

The operations of lowering the old plug, placing it in its storage alcove, and raising the previously completed new plug in place are done by remote control from a station in the tunnel. Figure 9 shows part of the exchange operation, and Figure 10 shows the new plug in place and being grouted. The new plug contains the upper part of the entrance funnel for the core-catcher, and is also shielded sufficiently that as soon as the grout is in place the reactor can be restarted upon completion of refueling.

The remainder of the core-catcher installation is made by standard industrial techniques while the reactor is in operation. When it is complete, the pressure door is closed and the tunnel back-filled. The entrance portal is removed. If the site contains two units, the tunnel is extended under both, and the furthermost caisson completed first.

The cost of a complete core-catcher system in a new reactor would be about $3 million. For a two unit plant served from the tunnel, the retrofit core catcher would cost about $11 million per unit.

Detailed assessment of the risk to the public from the backfit core-catcher installation, compared to the risk from the original undisturbed plant, shows that even the initial steps of lowering the ground water reduce public risk somewhat, while the later steps of caisson construction substantially reduce the consequences of a core-melt accident. Once the device is complete a core melt accident does not cause any risk to the public.

REFERENCE

Hammond, R. Philip, Dooley, James L., "Retrofitting Core Catchers to Nuclear Plants", Final Report, NUREG/CR-2941, September 1982.

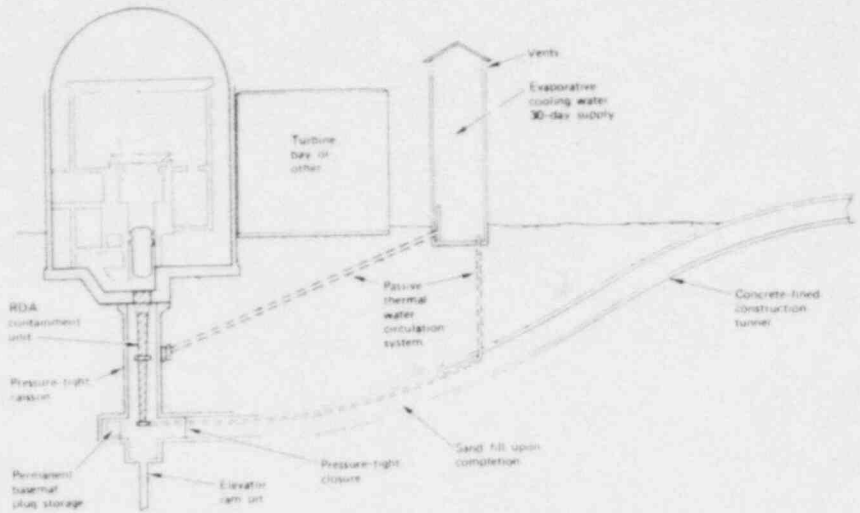

Figure 1.

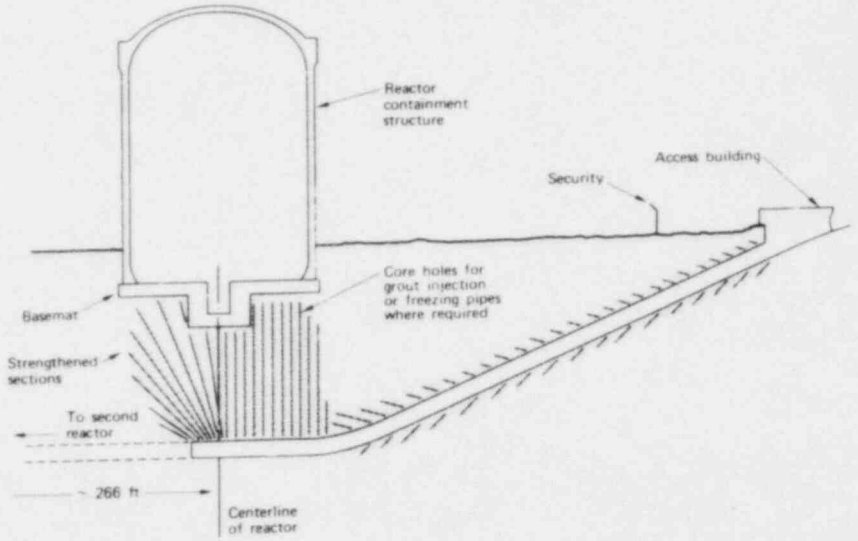

Figure 3.

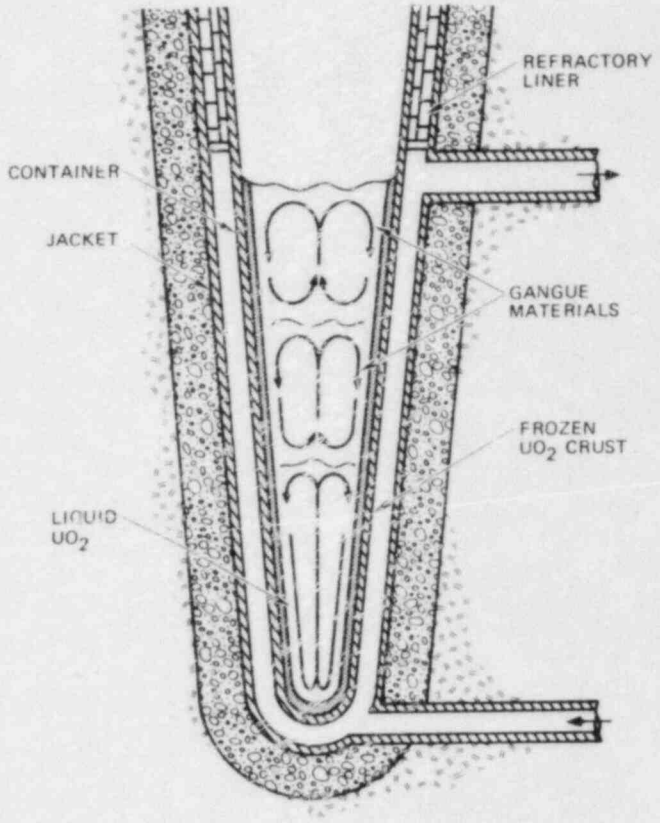

Figure 2.

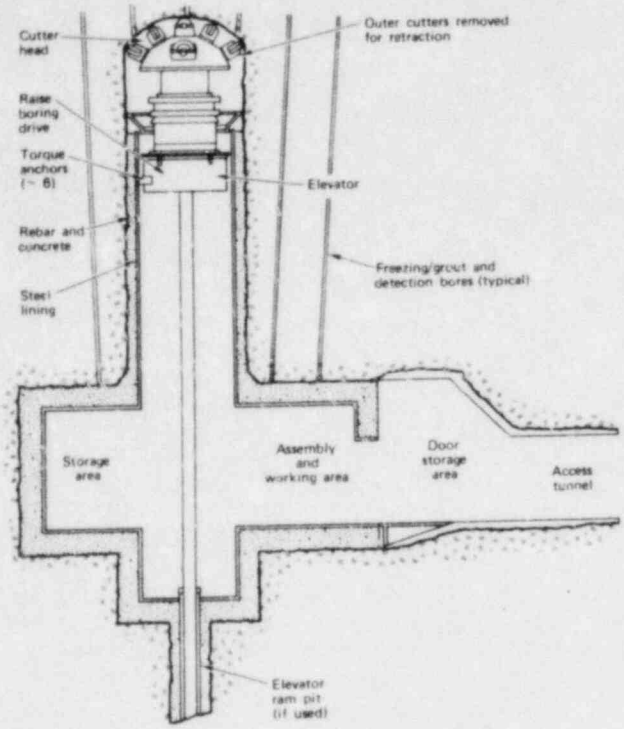

Figure 4.

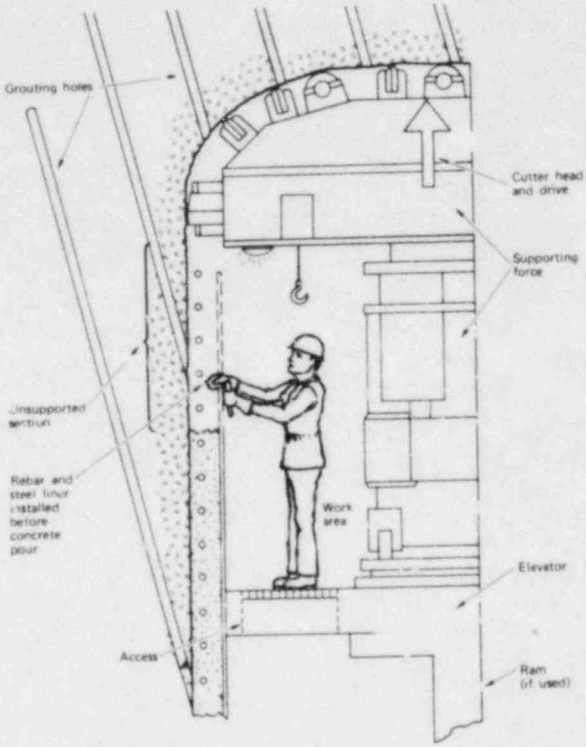

Figure 5.

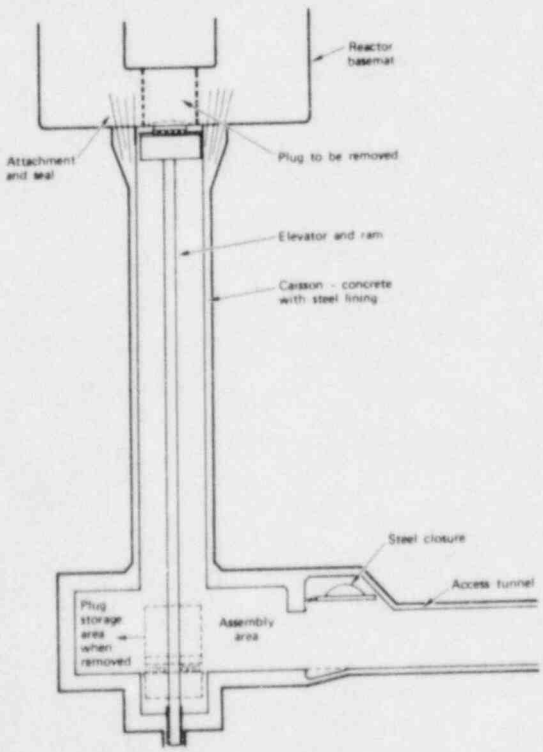

Figure 6.

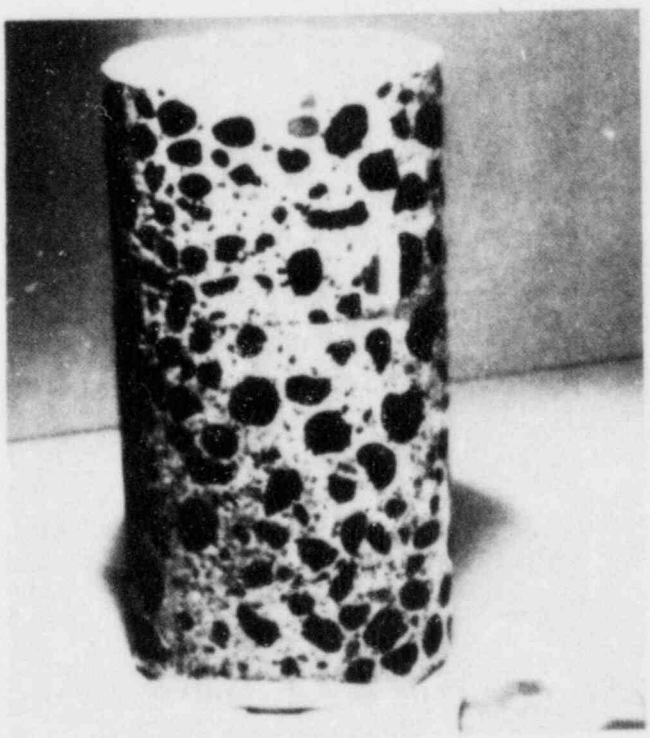

Figure 7.

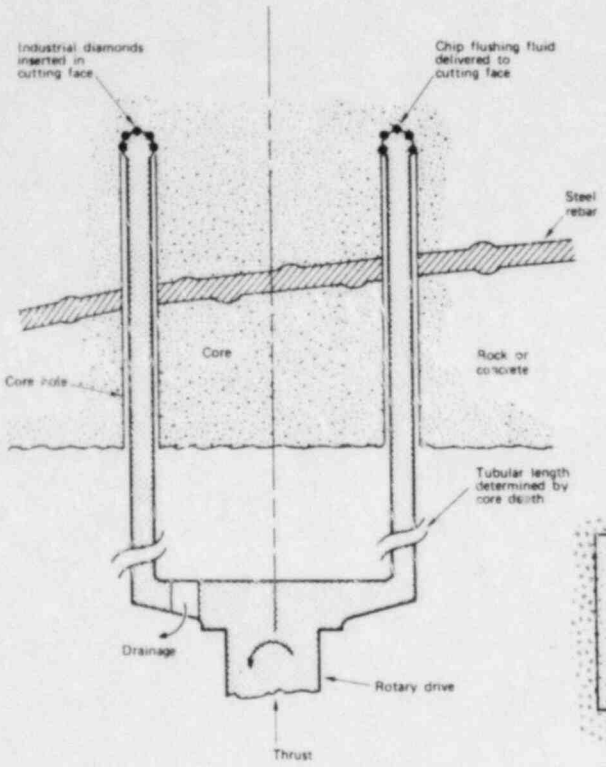

Figure 8.

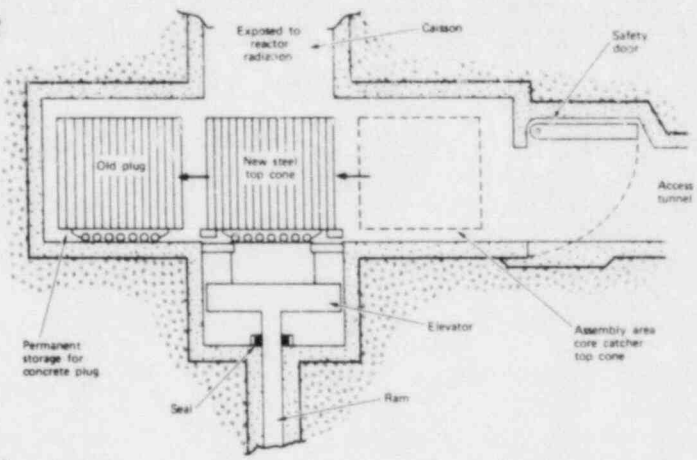

Figure 9.

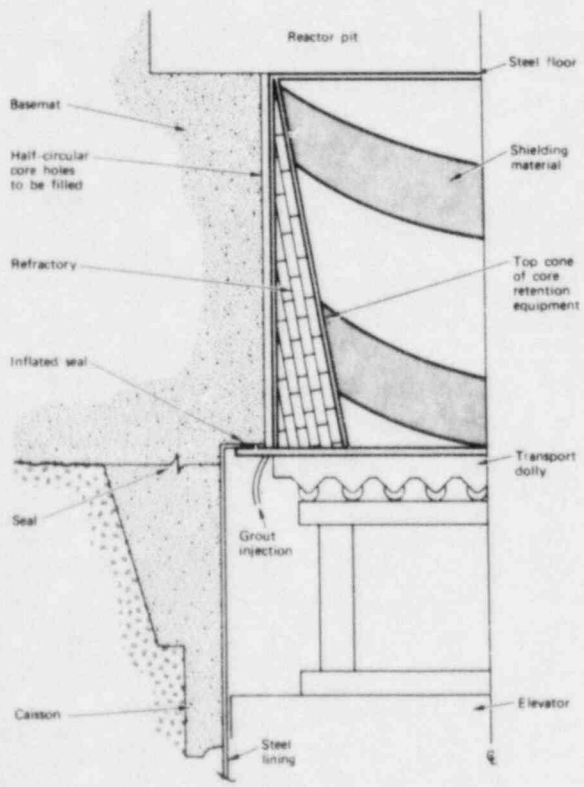

Figure 10.

SCRAM DISCHARGE VOLUME BREAK STUDIES
PART I: ACCIDENT SEQUENCE ANALYSIS

R. M. Harrington
S. A. Hodge

Oak Ridge National Laboratory

This paper is a summary of a report[1] describing the predicted response of Unit 1 at the Tennessee Valley Authority (TVA) Browns Ferry Nuclear Plant to a hypothetical small break loss of coolant accident (SBLOCA) outside of containment. The accident studied would be initiated by a break in the scram discharge volume (SDV) piping when it is pressurized to full reactor vessel pressure as a normal consequence of a reactor scram. If the scram could be reset, the scram outlet valves would close to isolate the SDV and the piping break from the reactor vessel. However, reset is possible only if the conditions that caused the scram have cleared; it has been assumed in this study that the scram signal remains in effect over a long period of time.

The results outlined here are concerned primarily with the worst case severe accident sequence which could result without effective operator action. Consideration is given to operator actions that would prevent the scram discharge break from leading to a severe accident. A companion report[2] presents the estimates of magnitude and timing of the release of noble gas, iodine and cesium fission products which would result from the postulated worst case severe accident sequence.

It has not been necessary for the purpose of this study to specify an exact break location or cause, but it has been assumed that the break is large enough so that the leakage into the Reactor Building is limited only by the flow restriction afforded by the graphitar seals within the control rod drive (CRD) mechanism assemblies. The graphitar seals are subject to degradation at high temperatures and in the calculational model the leakage area is increased after 90 min of seal exposure to the hot coolant leaking from the reactor vessel so that the seals are completely removed at eight hours after the inception of the accident.

The total leakage into the Reactor Building during this accident is the sum of the flow of hot water from the reactor vessel and the room-temperature flow into the CRD mechanism assemblies from the CRD hydraulic system via the open scram inlet valves. These two flows are assumed to mix uniformly within the CRD mechanism assemblies before flowing through the CRD hydraulic system WITHDRAW lines out of the drywell to the SDV piping and from there through the break into the Reactor Building atmosphere.

The scram discharge volume break has not been extensively studied. The Browns Ferry FSAR does not analyze the scram discharge volume break -- possibly because the scram discharge volume is intended to be pressurized with primary coolant only during relatively short periods after reactor trip.

A 1981 report[3] by the USNRC office of Analysis and Evaluation of Operational Data expressed concerns about the scram discharge volume break, including: (1) the possible deleterious effects of the accident environment on safety equipment in the vicinity of the break, and (2) the possibility that the operators might not diagnose the break condition and take corrective action in time to prevent adverse environmental effects (e.g., as a worst case, flooding of the emergency core cooling system pumps located in the basement of the reactor building).

The question of how long it would take for the control room operator to comprehend the scope of this accident is central to the determination of the sequence of events. It must be recognized that an abnormal occurrence, i.e., a scram from full power, would immediately precede the SDV piping break that constitutes the initiating event for the SBLOCA-outside-containment accident sequence considered here. Thus, it would not be difficult for the operator to presume that many of the symptoms of the SDV break were in fact produced by the event causing the scram. For example, if the scram were caused by high main steam line radiation, the operator might incorrectly assume that the high reactor building radiation alarms associated with the SDV piping break were caused by the known high radiation within the main steam lines.

Nevertheless, the probability that the operator would understand that he is confronted with a SBLOCA-outside-containment in addition to the event that initiated the scram would be a strongly increasing function of time. Roving patrols would report the presence of steam in the Reactor Building, the radwaste building control room operator would report a marked increase in flow from the Reactor Building floor drain sump, and there would be both high-temperature and high-radiation alarms in the control room for the monitored locations in the Reactor Building. The indications of an unusual after-scram condition in the scram discharge system would be prominent, including a persistent CRD high-temperature alarm with high temperature readings for all of the mechanisms and an abnormal position indication for all of the control rods caused by the existence of the leakage path from the SDV.

Once the control room operator is aware that there is leakage into the Reactor Building and has correctly diagnosed its cause, there are several corrective actions that he might take. The most effective action would be to reset the scram so that the scram outlet valves would close, isolating the SDV piping and the break from the reactor vessel. However, the scram cannot be reset as long as the scram signal remains in effect* and it has been assumed that the scram was caused by a reactor protection system signal that remains in effect throughout the

---

*During the Browns Ferry partial failure to scram following manual reactor trip event[4] the operators were able to drive the control rods into the core by repeatedly resetting the scram and re-entering the manual reactor trip. This would not have been possible if the initial reactor trip had originated from an accident signal, such as high drywell pressure.

accident. Therefore, in order to reset the scram, the operator would have to override the scram signal by the placement of insulation between the applicable relay contacts in the auxiliary instrument room — certainly not a standard procedure.

If the scram cannot be reset, the next most effective operator action would be to depressurize the reactor vessel as quickly as possible while maintaining vessel level with the High Pressure Coolant Injection (HPCI) system. Depressurization reduces the leakage from the reactor vessel and decreases the potential for seal erosion by reducing the temperature of the leaked coolant. Full depressurization would reduce the flow from the reactor vessel to the point where the leakage from the SDV piping break would consist primarily of the pumped flow from the CRD hydraulic system; the latter flow could then be throttled to reduce the total leakage while keeping the mixture subcooled.

It is a conclusion of this study that core damage can easily be averted if the operator takes the indicated corrective action in a reasonable amount of time. However, it is important to note that much of the safety-related equipment necessary for accident diagnosis and mitigation (such as pump and valve motor control centers located in the vicinity of the SDV piping) has not yet been qualified for exposure to harsh environments. For example, even if the scram signal is cleared and action is taken to reset the scram from the control room, it is possible that the scram pilot valves and hence the scram outlet valves would not close because of the deleterious effects of moisture accumulation in the reactor protection system fuse cabinets located near the SDV break.

Without effective operator action, the situation would develop into a severe accident and subsequent release of fission products to the atmosphere. During the initial phase before core uncovery, the HPCI system would automatically cycle as necessary to maintain reactor vessel water level in a band around the normal operating level. However, the reactor vessel pressure decreases each time the HPCI system is actuated because of the steam flow to the HPCI turbine and the quenching effect produced by the introduction of cold water into the vessel. With the decreasing decay heat and the increasing SDV break size caused by the assumed seal erosion, the average reactor vessel pressure during the level-restoring cycles of the HPCI system would continually decrease.

Without operator action, the turbine-driven feed pumps would cease operation shortly after the scram, but the condensate booster pumps (CBPs) are electric-motor driven and would remain operating with the potential to inject water into the reactor vessel whenever the reactor vessel pressure falls below their shutoff head [2.86 MPa (415 psia)]. The study shows that when this occurs, the reactor vessel rapidly fills with cold water which spills over into the main steam lines, and consequently the steam supply lines to the RCIC and HPCI turbines. This would preclude any further use of these high-pressure injection systems.

With the Main Steam Isolation Valves (MSIVs) shut, main condenser vacuum could not be maintained and makeup flow from the condensate storage tank would be limited to that induced by gravity feed. Since the pumped flow into the reactor vessel would greatly exceed the hotwell makeup rate under these conditions, the hotwell would be pumped dry and the CBPs would trip on low suction pressure. The study shows that there would be no coolant makeup available to the reactor vessel after this point in the no-operator-action sequence, and the core would be uncovered.

The MARCH code was used to study the events after core uncovery. The results indicate that the reactor vessel water level would be below the inlets to CRD mechanism WITHDRAW lines (about 1 ft below the bottom of the core) at about 7.6 h after the inception of the accident, with core melting beginning about 50 min later. The reactor vessel pressure steadily decreases after the fuel bundle flow inlets are uncovered because the leakage medium shifts from water to steam.

When the differential pressure between the reactor vessel and the wetwell has decreased to a value corresponding to the effective shutoff head of the Low-Pressure Emergency Core Cooling Systems (LPECCS), a trickle flow of injection water begins. This study confirms that low-pressure BWR injection systems cannot be effective unless the reactor vessel is depressurized to a pressure much below the LPECCS shutoff head.

About 1 h after melting begins, the core slumps into the lower plenum of the reactor vessel, and about 1.5 h after core slump, the reactor vessel lower head fails, dropping the molten core onto the concrete floor of the drywell. The lower head failure would disrupt the locations of the control rod drive piping, but most of the scram outlet pipes would probably remain open; therefore, the drywell atmosphere would begin to leak through the SDV break. This leakage path is not of sufficient flow area to prevent the gross failure of the drywell, which occurs about 4.5 h after the core is uncovered.

The drywell is assumed to fail by temperature-induced degradation of the electrical penetration assembly (EPA) seals. Temperature of the drywell atmosphere after lower head failure is well above the 138°C (281°F) design temperature of the EPAs. Drywell pressure at the time of EPA failure is about .15 MPa -- well below the 0.91 MPa failure pressure estimated[5] for the Browns Ferry Mark-I containment. The failed containment rapidly releases its internal pressure to the reactor building. As a result there would be a corresponding rapid release of reactor building atmosphere to the surrounding environment through the refueling bay blow-out panels.

After the pressure surge associated with failure of the drywell, the standby gas treatment (SGT) system blowers return the reactor building to below atmospheric pressure until the assumed failure of the SGT system at 860 min into the accident. The influx of hot drywell atmosphere causes the reactor building temperature to increase rapidly to

the setpoint for initiation of the reactor building fire spray systems. The fire sprays cause an abrupt lowering of building temperature and the building temperature ramains low for the remainder of the accident period discussed here.

A worst-case study for the case without operator action has been completed. An estimate of the magnitude and timing of the release of noble gas, cesium, and iodine fission products in this postulated accident sequence is provided in a follow-on report.[2]

References

1. S. A. Hodge et al., "SBLOCA Outside Containment at Browns Ferry Unit One – Accident Sequence Analysis," NUREG/CR-2672, ORNL/NUREG/TM-8119/V1 (Oct. 1982).

2. S. A. Hodge et al., "SBLOCA Outside Containment at Browns Ferry Unit One – Iodine, Cesium, and Noble Gas Distribution and Release," NUREG/CR-2672, ORNL/NUREG/TM-8119/V2 (to be published).

3. S. D. Rubin, "Safety Concerns Associated with Pipe Breaks in the BWR Scram System," USNRC Office for Analysis and Evaluation of Operational Data, NUREG-0785 (Draft, March 1981).

4. "Analysis of Incomplete Control Rod Insertion at Browns Ferry 3," Institute for Nuclear Power Operations and Nuclear Safety Analysis Center, NSAC-20/INPO-3 (Dec. 1980).

5. L. G. Greimann et al., "Reliability Analysis of Steel Containment Strength," NUREG/CR-2442 (June 1982).

UNION CARBIDE ORNL

SCRAM DISCHARGE VOLUME BREAK STUDIES PART I: ACCIDENT SEQUENCE ANALYSIS

R. M. HARRINGTON
INSTRUMENTATION AND CONTROLS DIVISION
OAK RIDGE NATIONAL LABORATORY

PRESENTED AT
TENTH WATER REACTOR SAFETY RESEARCH
INFORMATION MEETING

NATIONAL BUREAU OF STANDARDS
GAITHERSBURG, MARYLAND

OCTOBER 15, 1982

UNION CARBIDE ORNL

THE OBJECTIVE OF THIS ORNL STUDY IS A "BEST ESTIMATE" ANALYSIS OF A HYPOTHETICAL SCRAM DISCHARGE VOLUME (SDV) BREAK ACCIDENT AT A TYPICAL BWR

TIME-DEPENDENT PROGRESSION OF EVENTS CONSIDERING

- PHYSICAL PLANT AT BROWNS FERRY UNIT 1
- NO ADDITIONAL INDEPENDENT EQUIPMENT FAILURES BEYOND THE INITIATING REACTOR TRIP AND SDV BREAK
- BREAK FLOW CONSTRAINED ONLY BY CRD SEALS
- EXISTING INSTRUMENTATION TO DISPLAY PLANT STATUS
- NO OPERATOR ACTION FOR SEVERE ACCIDENT SEQUENCE

ESTIMATE MAGNITUDE AND TIMING OF FISSION PRODUCT RELEASE AND TRANSPORT

UNION CARBIDE ORNL

THE SCRAM DISCHARGE VOLUME BREAK RELEASES COOLANT DIRECTLY INTO THE REACTOR BUILDING

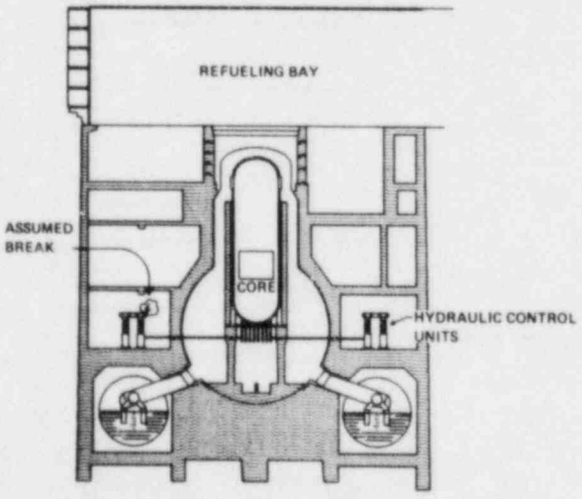

UNION CARBIDE ORNL

SCRAM DISCHARGE BREAK HAS NOT BEEN EXTENSIVELY STUDIED

BROWNS FERRY FSAR DOES NOT CONSIDER SCRAM DISCHARGE VOLUME BREAK

1981 REPORT BY NRC OAEOD IDENTIFIED THE SDV BREAK AS A POTENTIAL SAFETY PROBLEM. PRIME CONCERNS:

- OPERATOR DETECTION OF BREAK CONDITION
- ECCS PUMP FAILURE BY FLOODING
- EFFECT OF ADVERSE BUILDING ENVIRONMENT ON SAFETY EQUIPMENT

UNION CARBIDE ORNL

THE PROBABILITY OF DETECTION OF SDV BREAK WOULD INCREASE STRONGLY AS A FUNCTION OF TIME

CONTROL ROOM ALARMS
- EXHAUST RADIATION
- AREA RADIATION
- BASEMENT FLOODING
- AREA TEMPERATURE

PHYSICAL EVIDENCE
- NOISE, STEAM, HEAT
- RUPTURED BLOWOUT PANELS

UNION CARBIDE ORNL

THE MOST EFFECTIVE OPERATOR ACTION WOULD BE TO ISOLATE THE BREAK BY RESETTING THE SCRAM. ALTERNATIVELY, THE OPERATOR COULD

- DEPRESSURIZE TO REDUCE THE LEAK RATE
- MANUALLY CLOSE THE 185 SCRAM OUTLET ISOLATION VALVES

UNION CARBIDE ORNL

THE SCRAM DISCHARGE VOLUME BREAK ACCIDENT SEQUENCE ANALYSIS EMPLOYED THE "BEST-ESTIMATE" APPROACH FOR

- THE NO OPERATOR ACTION CASE
- THE PERIOD BEFORE CORE UNCOVERY
  - ORNL-DEVELOPED PLANT RESPONSE CODE AND THE TVA SIMULATOR
- THE PERIOD AFTER CORE UNCOVERY
  - THE MARCH CODE

UNION CARBIDE
ORNL

REACTOR VESSEL INJECTION PATHS FOR SCRAM DISCHARGE VOLUME BREAK

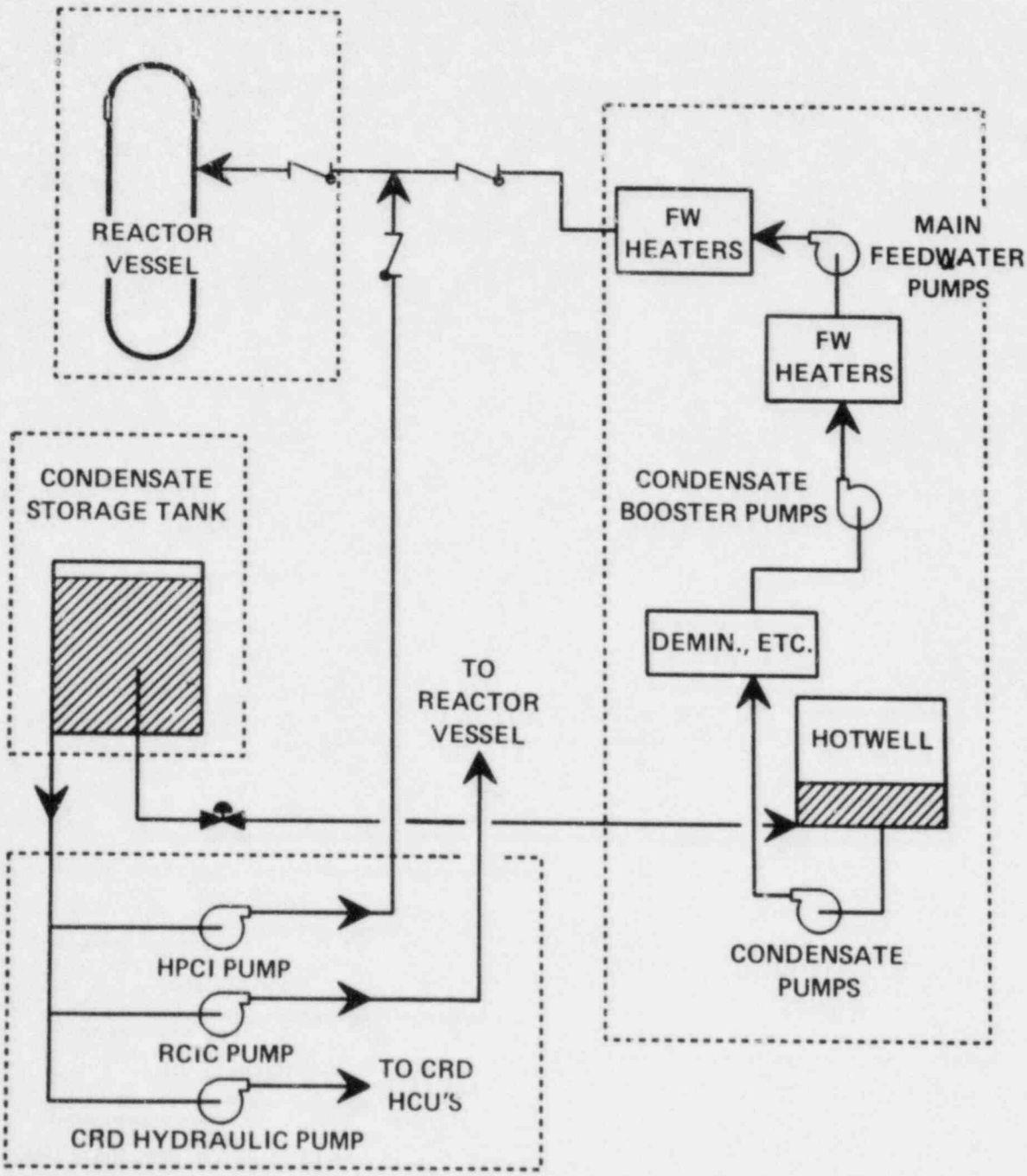

UNION CARBIDE ORNL

DECREASING DECAY HEAT AND ASSUMED CRD SEAL EROSION GRADUALLY DEPRESSURIZE THE REACTOR VESSEL

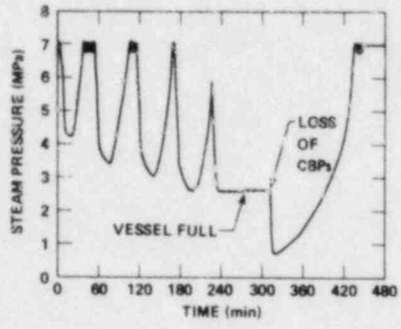

UNION CARBIDE ORNL

LOW REACTOR VESSEL PRESSURE ALLOWS THE MOTOR DRIVEN CONDENSATE PUMPS TO BEGIN INJECTION AND OVERFILL THE REACTOR

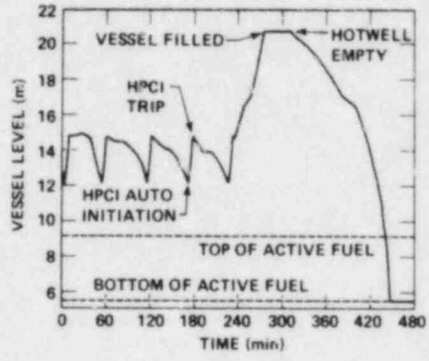

UNION CARBIDE ORNL

THE MARCH CODE WAS USED TO STUDY THE SEQUENCE OF EVENTS FOLLOWING CORE UNCOVERY AND TO PROVIDE NEEDED PARAMETERS FOR THE FISSION PRODUCT TRANSPORT ANALYSIS

EVENT	TIME AFTER TOP OF CORE UNCOVERED
FIRST FUEL RODS FAIL (1300°C)	35 min
FIRST FUEL RODS MELT (2280°C)	1 h 8 min
CENTRAL CORE COLLAPSES INTO LOWER PLENUM	2 h 2 min
VESSEL LOWER HEAD FAILS AND CORE DROPS TO DRYWELL FLOOR	3 h 30 min

UNION CARBIDE ORNL

CONTAINMENT WAS ASSUMED TO FAIL BY TEMPERATURE-INDUCED DEGRADATION OF ELECTRICAL PENETRATION ASSEMBLY (EPA) SEALS

- EPA SEALS HAVE SHORT-TERM RATING OF 163°C (325°F) AND LONG-TERM RATING 138°C (281°F)
- SEALS ASSUMED TO FAIL AT 260°C (500°F)
- FAILURE AREA 1.95 m^2 (21 ft^2)
- FLOW IS THROUGH EPA_s INTO REACTOR BUILDING
- FAILURE OCCURS AT 56 min AFTER CORIUM LEAVES VESSEL

UNION CARBIDE ORNL

HIGH DRYWELL TEMPERATURE IS ASSUMED TO CAUSE FAILURE OF THE DRYWELL ELECTRICAL PENETRATION ASSEMBLIES (EPAs)

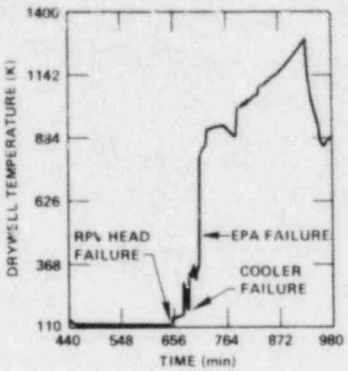

UNION CARBIDE ORNL

STANDBY GAS TREATMENT (SGT) SYSTEM MAINTAINS NEGATIVE BUILDING PRESSURE DURING MUCH OF THE PERIOD AFTER CORE UNCOVERY

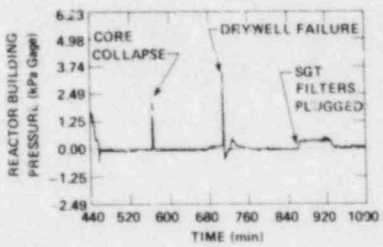

UNION CARBIDE ORNL

BUILDING TEMPERATURE AFTER DRYWELL FAILURE IS REDUCED BY ACTUATION OF THE BUILDING FIRE SPRAYS

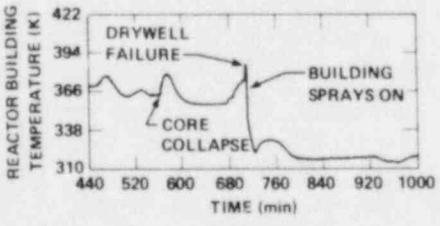

BWR ACCIDENT ANALYSIS SCRAM DISCHARGE VOLUME BREAK STUDIES
PART 2: FISSION PRODUCT TRANSPORT ANALYSES

R. P. Wichner
C. F. Weber
R. A. Lorenz
J. W. Nehls
A. L. Wright

Chemical Technology Division
Oak Ridge National Laboratory
Oak Ridge, Tennessee 37830

INTRODUCTION

This portion of the ORNL-SASA presentation deals with the analysis of the rate of movement of fission products from the overheated core through a series of reactor control volumes, the final one being the exterior of the reactor building. As input for this calculation the following is required:

1. Specification of the accident sequence parameters, i.e., temperatures, gas and water flow rates, and pressures for all control volumes.
2. Identification of failure modes and times of key system items, in this case principally the drywell (DW) pressure boundary and the standby gas treatment system (SGTS).

This input information is developed in separate analyses and has been described in part 1 of this presentation.

STATUS OF WORK

At this time, the analysis of a complete station blackout sequence at Browns Ferry has been completed.[1,2] The fission product transport portion of the study was presented in preliminary form at the 1981 Water Reactor Safety Meeting. Currently, the analysis of the small-break LOCA outside

the containment is in process. The initial study[2] traced noble gases and iodine through the reactor systems during the event sequence; our current work includes an analysis of cesium transport in addition to noble gases and iodine.

OUTLINE OF PRESENTATION

This presentation will cover the following two areas:

1. Description of fission product transport pathways for this accident sequence.
2. An overview of the models required to describe the principal 'transport events." (The term "transport event" is used here to include all important chemical and physical changes as well as inter-control volume mobilities required for the overall analysis.)

TRANSPORT PATHWAYS

Slides 1 through 5 illustrate some of the key features of the small-break LOCA event sequence, abstracted from the work reported in part 1 of this paper. The timing of principal events is shown in slide 1. The three categories of events shown (subdivided by the dashed line) correspond to (1) the initial series of events leading to the core uncovery, (2) events from the time of initial core uncovery up to DW failure, and (3) events following DW failure up to termination of the calculated event sequence at t = 1000 min.

As noted in the first paper, analysis of the behavior of reactor systems in the initial accident phase, where no fuel damage occurs, is

critical for the determination of subsequent events. Here we should note that the SGTS turns on very soon after the introduction of water from the core to the reactor building (RB) following the postulated break in the scram-discharge volume (SDV) piping. Continued water flow through the control rod drive (CRD) "withdraw" lines to the building leads to a water accumulation of $\sim 10^6$ L in the RB by the time of initial core uncovery, which collects in a pool in the basement room of ~0.7-m depth. Note, fuel uncovery is projected to occur at t = 442 min and first cladding failure at 477 min. It was shown in the first presentation that ECCS flow input (initiated at t = 530 min) does not suffice to again cover the CRD inlet ports, located ~0.3 m below the active fuel. Therefore, from the time of cladding failure onward, the main flow from the CRD lines is gaseous (steam/H_2) with water levels in the reactor vessel (RV) maintained below the active core.

Note, the DW is projected to fail at t = 707 min by thermal degradation of the organic seal material used in the electrical penetration assemblies (EPAs). Following this event, hot gases from the DW flow into the RB, setting off the fire spray system. The fire spray system contributes to fission product and aerosol capture in the RB to some degree which is currently being estimated.

In addition to hot gases, aerosols generated by the core debris/concrete interaction also flow into the RB following failure of the EPA seals. Our estimates of the rate of aerosol formation, the degree of aerosol transport through the DW and the RB, and the plugging characteristics of the HEPA filters in the SGTS currently lead us to assume that the SGTS will fail about 2.5 h following DW failure.

The water level in the RV during the period of cladding and fuel damage is illustrated in slide 2, which was also shown by the first speaker. From the point of view of fission product transport, we note that the water level is predicted to be below the bottom of the active fuel (BAF) at all times following cladding failure, which is estimated to occur at t = 477 min. This is a point of departure from the previous analysis (complete station blackout[1,2]), where fuel damage occurred more quickly due to a greater heat source which resulted from the shorter decay time in that event sequence. Note here also that the projected rate of ECCS injection (initiated at t = 530 min) through the feedwater inlets does not elevate the pool level above the 215-in. mark, slightly below the BAF level.

The temperature map of the core at the time of projected core collapse (t = 564 min) is illustrated in slide 3. The significance, as far as fission product transport is concerned, is that presently available core thermal analyses (i.e., the MARCH code) predict the existence of relatively cool zones within the core at the time of projected collapse. Radial zone 10 remains cool due to a low heat source within that zone, whereas axial zone 10 is cooled by radiant heat loss to the steam separator structure located directly above. Whether or not these cool zones realistically exist, or whether more sophisticated core thermal models would predict a more uniform heating, is a point that should be resolved. However, the present method predicts a significant inventory of volatile fission products to be contained within the collapsed core material.

Slide 4 illustrates current estimates of the DW gas temperature from t = 440 min (time of initial core uncovery) to t = 980 min. As shown, DW temperatures are predicted to rise fairly rapidly following failure of the

RV at t = 652 min, particularly following the subsequent failure of the DW coolers. A peak DW temperature of 704°C is projected to occur at the 923 min mark following an approximately linear rise with time of ~1.2°C/min for ~210 min. Since currently available temperature prediction procedures do not include estimates of RV temperature during this time period, we can only assume that the average temperature of the pressure vessel contained within the DW boundary is approximately equal to the estimated DW gas temperature shown in the figure. The significance of this observation is that a small but significant portion of the cesium and iodine deposits on the interior wall of the RV becomes revaporized at these temperatures with the associated potential for direct passage into the DW through the failed RV. The degree of such direct transport through the RV failure zone is extremely difficult to calculate, depending as it does on the distribution of localized heat sources and the resulting natural convection flow communicating between the RV and DW volumes. However, a simplified method for estimating the rate of transport through the RV failure zone has been developed based on a gas expansion model determined from the DW temperature rise rate (illustrated in slide 4).

Slide 5 illustrates current estimates of the pressure in the RB from t = 440 to 1000 min. Of course, such an estimate rests heavily on the time and assumed mode of failure (if any) of the SGTS, whose blowers draw a nominal flow of 25,000 standard ft^3/min from the RB. Current estimates indicate that the HEPA filters within the SGTS will plug at about t = 875 min when a total of 81 kg of aerosols are collected. At this time, as shown in slide 5, the RB pressure goes positive and net exfiltration commences. Prior to this

event, the pressure in the RB is predominantly subatmospheric, except for brief periods following core slump and DW failure. Thus, prior to filter plugging, the predominant building leakage flow is inward from the atmosphere. As noted above, however, this behavior depends strongly on the nature of SGTS operation during the accident sequence, a subject which is currently undergoing reexamination.

The principal fission product leakage pathways from the failed fuel elements are illustrated in slides 6, 7, and 8, each slide referring to a particular interval of time during the accident sequence. Prior to reactor vessel meltthrough at t = 652 min, the main pathway leads through the CRD withdraw lines as shown in slide 6. Flow through these lines is either liquid water or gaseous steam/H_2, depending on the current water level in the reactor vessel relative to the height of the CRD inlet ports.

Aerosols generated in the reactor vessel are carried into the CRD withdraw lines during the times when the CRD guide tube inlet ports are uncovered. Also illustrated on slide 6 are water supply lines leading from the condensate storage tank via the CRD hydraulic system to each of the 185 CRD withdraw lines. For times up to RV failure, water flows continually in these lines (~1 gal/min per line), effectively washing the deposited contents of these lines into the water pool accumulated in the basement of the RB. Therefore, the water pool in the basement will, during this time, increase its fission product inventory.

Convective flow in the reactor vessel during this accident sequence would be principally downward toward the openings in the CRD guide tubes. Upward flow in the reactor vessel following fuel failure occurs only for a few moments following core collapse when the SRVs open to relieve the

pressure generated when the molten core slumps into the water in the reactor vessel bottom head.

As noted in slides 6 and 7, prior to drywell failure, fission products collect in the reactor building principally from flow through the CRD withdraw lines and secondarily via the expected gas leakage of the drywell. No water flow would occur to the liquid radwaste system after fuel failure because of early failure of the reactor building sump pumps by submergence.

Volatile material tends to equilibrate between the water and gas phases in the reactor building. Prior to the assumed failure of the SGTS, the flow patterns within the reactor building are dominated by the suction of the SGTS blowers. After the assumed failure of the SGTS ~2.5 h following drywell failure, the main flow direction would be through the reactor building-to-refueling floor blowout panels and from there through leakage to the atmosphere.

Slide 6 also shows a liquid fission product release pathway via leakage past the motor-operated steam isolation valves (MSIVs). Steam condensation occurs behind closed valves and subsequently flows by gravity into the main condenser. This is the same pathway to the turbine building as was described in the analysis of the complete station blackout accident sequence.

Slide 7 shows the pathway changes caused by the failure of the reactor vessel at t = 652 min. Initially, gaseous fission products and aerosols are transported by the blowdown of the reactor vessel into the drywell. The fission products remaining in the reactor vessel consist of those contained in the fuel elements that are assumed to remain in place, and material plated out on interior RV surfaces.

An additional source of fission product release into the reactor vessel gas space after failure of the bottom head is due to the vaporization of

material deposited on the extensive (separators, dryers) but relatively cool surfaces above the core. Virtually all of this material would be associated with aerosols deposited on these structural surfaces.

The fuel rubble on the drywell floor releases fission products directly into the drywell aided by the sparging action of concrete degradation gas.

Slide 8 illustrates the situation following failure of the DW at t = 707 min. Gaseous flow to the RB is predominantly through the electrical penetration assembly (EPA) seal failure zone, dominating the smaller flow continuing through the CRD lines. Note that the initiation of the fire protection system water sprays occurs soon after, creating an extremely wet situation in the RB. We are currently treating the RB as a series of wet-walled rooms for fission product transport estimation. An assessment of the effectiveness of the water sprays for soluble fission product and aerosol removal by use of the CORRAL-II program is currently in process.

Slides 9 through 12 list many of the principal fission product transport models currently being used to assess the transport rates along the pathways indicated in the earlier slides. The initial slide in this series lists four procedures used for calculating the rates of fission product release from fuel material, the rate of aerosol production by the overheated core in the RV and due to core/concrete interaction in the DW, and the procedures used for assessing aerosol transport rates. The rate of fission product release (currently, noble gases, iodine, and cesium) from damaged fuel elements is being determined by a procedure developed in ref. 7 based on an established value of a release rate coefficient for each fission product assumed to depend solely on the local fuel temperature. Release rate coefficient values for noble gases, iodine, and cesium appear to be fairly well established at

least up to ~1700°C. Release rate values are less certain for higher temperatures and for the less volatile fission products. Currently, we have no well-grounded model for releases from core debris beds, either of the type that would form in the RV or on the concrete basement of the DW. As an interim procedure for these situations, we are calculating release rates based on a temperature-dependent release rate coefficient appropriate for fuel element geometry corrected by a factor equal to the estimated area ratio of the debris bed to the fuel element. This interim procedure will be replaced as soon as a satisfactory replacement becomes available.

As indicated in slide 10, deposition rate expressions are required for a number of cesium and iodine chemical species onto various types of surfaces. These calculational methods are described in Chapter 4 of ref. 2. In general, the lower volatility cesium and iodine species, CsOH and CsI, are assumed to deposit via condensation. These deposition rates are assumed to be mass transport limited and do not depend on the type of surface. The deposition of the more volatile iodine species, HI, I_2, atomic I, and organic-iodide, probably occurs predominantly by chemisorption, hence would be surface material dependent, and, in addition, dependent on the degree of surface coverage. Published values of "deposition velocities" onto various solid surfaces were used for the determination of rate of deposition of these materials.

The rate of organic iodide formation in the DW and RB may be a significant factor in assessing the net leakage of iodine to the atmosphere in this accident sequence. This is due to the lower removal efficiency of organic iodide in the SGTS charcoal beds relative to I_2 and also due to its lower solubility in water pools which collect in the RB. Since the developed

level of organic iodide concentration depends on a dynamic balance between the formation rate and various removal mechanisms, available reviews on this subject are not helpful since results are presented solely in terms of equilibrium levels and not in terms of formation rates. In order to develop a formation rate model, we went back to the original experiments referenced in the reviews. Of all these experiments, the ones reported by Hilliard[3] and Parker[4] best show the time-dependence of the amount of iodine converted to organic iodides. Both of these reports show that the major portion of the ultimate organic iodide level is formed in the first 10 to 20 min of iodine introduction into the test vessel. Supplementing these dynamic tests results are data on equilibrium formation levels over a wide range of conditions presented in a review by Postma and Zavadoski.[5] Organic iodide formation data presented in refs. 3-5 were combined with thermal decomposition rates presented by Lorenz[6] to yield an organic iodide formation rate model.

Slide 11 shows the means used for assessing the principal iodine and cesium chemical forms in the RV and DW. As shown, chemical equilibrium values are assumed for the reducing conditions which exist in the RV prior to meltthrough. For this case, compositions were taken directly from results presented in Chapter 5 of ref. 7. Assessment of chemical forms which exist in the DW is more difficult because (1) the gaseous environment is initially oxidizing, changing to reducing as the original atmosphere is flushed out by concrete degradation gases; (2) the DW contains numerous materials which may react with both CsOH and CsI under some conditions; and (3) temperatures are lower than those in the RV, hence chemical equilibria may not develop and, generally, radiolytic effects become more important.

Until the chemical conditions in the DW can be more carefully and extensively analyzed, our judgement indicates it is best to assume the principal iodine species to be molecular iodine.

The failure mode and failure time of the SGTS is a critical factor in assessing fission product behavior in this accident sequence. As seen in slide 1, the SGTS is activated soon after SDV failure early in the sequence due to high radiation detected in the RV. We currently believe that the set of three SGTS blowers will continue operation throughout the sequence. However, indications are that the HEPA filters associated with the SGTS will plug when loaded with ~3 kg per filter. Since there are 27 parallel filters in the three absorption trains, ~81 kg of aerosol transported to the SGTS suffice to plug the upstream set of filters. According to our current aerosol production rate and transport estimates, this occurs ~1 h after DW failure. Subsequently, our current information indicates that the plugged filter will probably tear causing the HEPA filter set downstream from the charcoal absorbers to begin loading with aerosols. Consequently, the downstream HEPA filters will also ultimately fail by the same sequence of plugging followed by tearing. This marks the point in time that the SGTS ceases to function as designed. Thus, for times following this event, the SGTS may operate without the benefit of HEPA filtration. However, since the SGTS blowers appear to continue to function nominally, the charcoal beds remain relatively cool and hence retain their expected sorbency for I_2 and organic iodide.

REFERENCES

1. D. H. Cook et al., Station Blackout at Browns Ferry – Accident Sequence Analysis, NUREG/CR-2182 (ORNL/TM-455V1).
2. R. P. Wichner et al., Iodine and Noble Gas Distribution and Release Following Station Blackout at Browns Ferry, NUREG/CR-2182 (ORNL/TM-455V2).
3. R. K. Hilliard et al., Comparisons of the Containment Behavior of a Simulant with Fission Products Released from Irradiated UO_2, BNWL-581 (March 1968).
4. G. W. Parker et al., Fission Product Transport and Behavior in the Stainless Steel Lined Containment Research Installation, ORNL-4502 (February 1971).
5. A. K. Postma and R. W. Zavodski, Review of Organic Iodine Formation, WASH-1233 (1972).
6. R. A. Lorenz et al., Behavior of Iodine, Methyl Iodine/Cesium Oxide, and Cesium Iodide in Steam and Argon, ORNL/NUREG/TM-25 (July 1976).
7. Technical Bases for Estimating Fission Product Behavior During LWR Accidents, NUREG-0772 (June 1981).
8. R. A. Lorenz, "The Vaporization of Structural Materials in Severe Accidents," presented at the Thermal Reactor Safety Meeting, Chicago, August 29, 1982.
9. D. A. Powers, "Containment Safety Studies," App. 5A, in Zion/Indian Point Study: Vol. I, prepared by W. B. Murfin, Sandia Laboratories, NUREG/CR-1410 (August 1980).
10. D. M. Rastler, Suppression Pool Scrubbing Factors for BWR Accident Conditions, NEDO-25420 (June 1981).

SLIDE 1

SBLOCA EVENT SEQUENCE

EVENT	TIME (MIN)
TRIP, SDV BREAK, SGTS ON	0-1
RV WATER LEVEL MAINTAINED BY HPCI	3-232
CBP OPERATION	234-311
ALL WATER INFLOW ENDS	318
TOP OF FUEL UNCOVERED	442
BOTTOM OF FUEL UNCOVERED	455
CRD INLET PORTS UNCOVERED	456
FIRST CLADDING FAILURE	477
ECCS TURNS ON	530
CORE SLUMP	564
RV MELTTHROUGH	652
DW EPA SEALS FAIL	707
RB FIRE WATER ON	710
SGTS PLUGS	857
RUN ENDS	1000

SLIDE 2

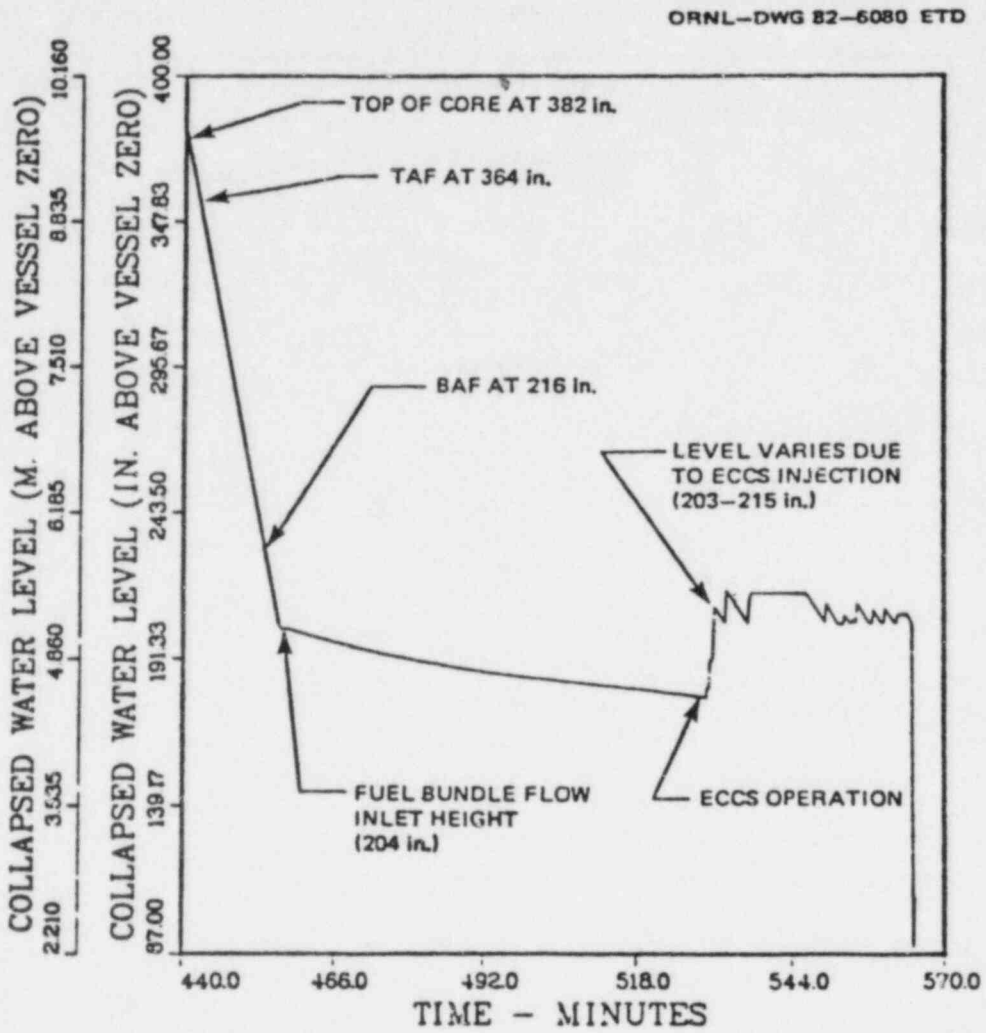

REACTOR VESSEL COLLAPSED WATER LEVEL

SLIDE 3

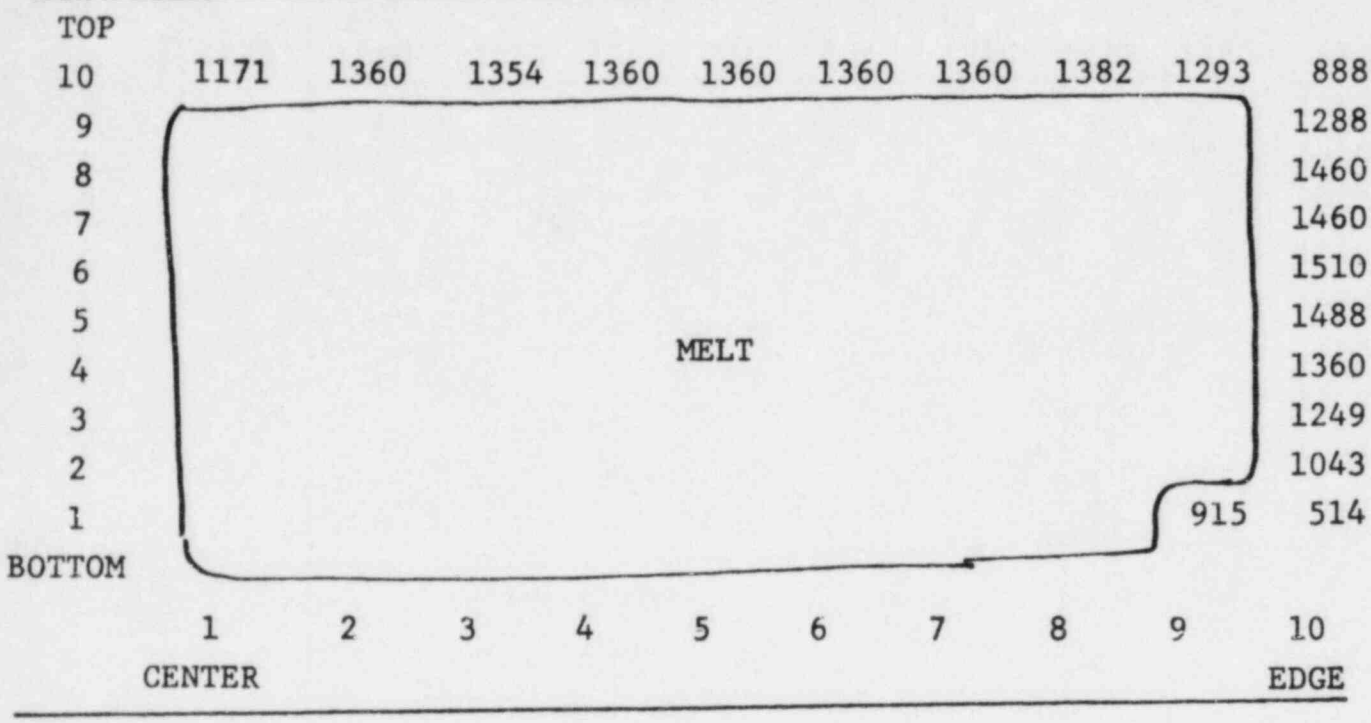

CORE TEMPERATURE MAP (°C) AT TIME OF CORE SLUMP;
TIME = 564 (MIN)
(75% OF CORE MELTED)

SLIDE 4

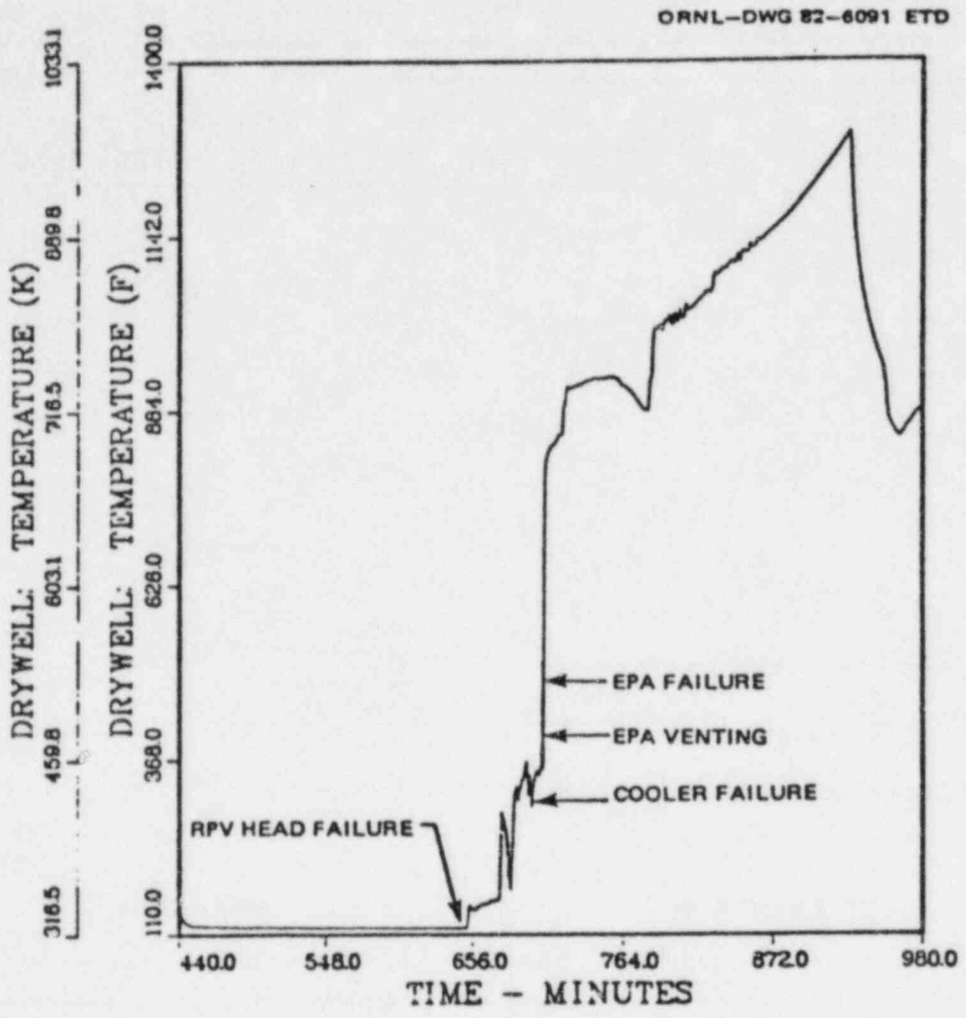

DRYWELL GAS TEMPERATURE

SLIDE 5

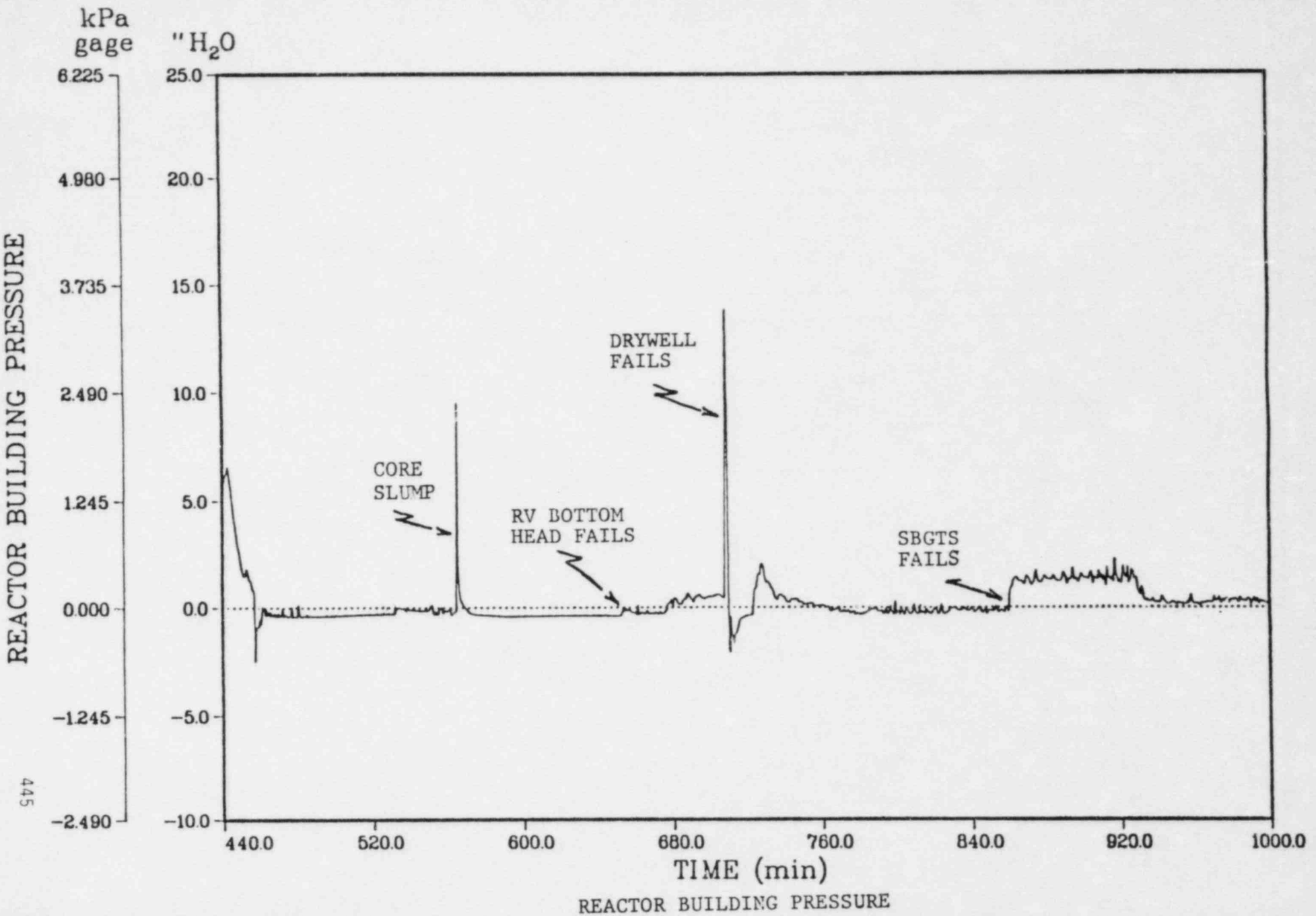

REACTOR BUILDING PRESSURE

SLIDE 6

ORNL-DWG 82-16498R

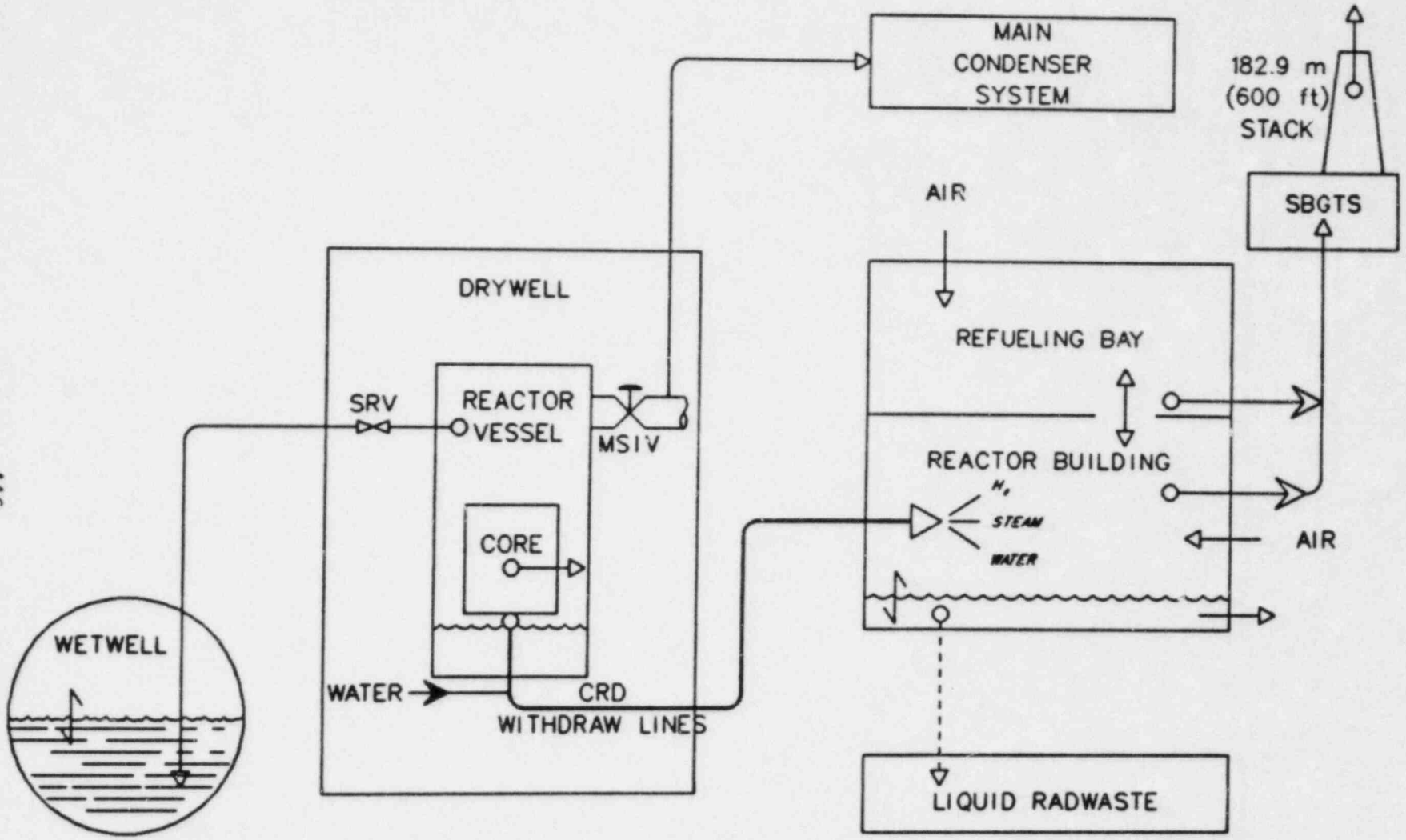

446

PRINCIPAL FISSION PRODUCT PATHWAYS UP TO TIME OF REACTOR VESSEL MELT-THROUGH (t = 652 min)

SLIDE 7

ORNL-DWG 82-16439R

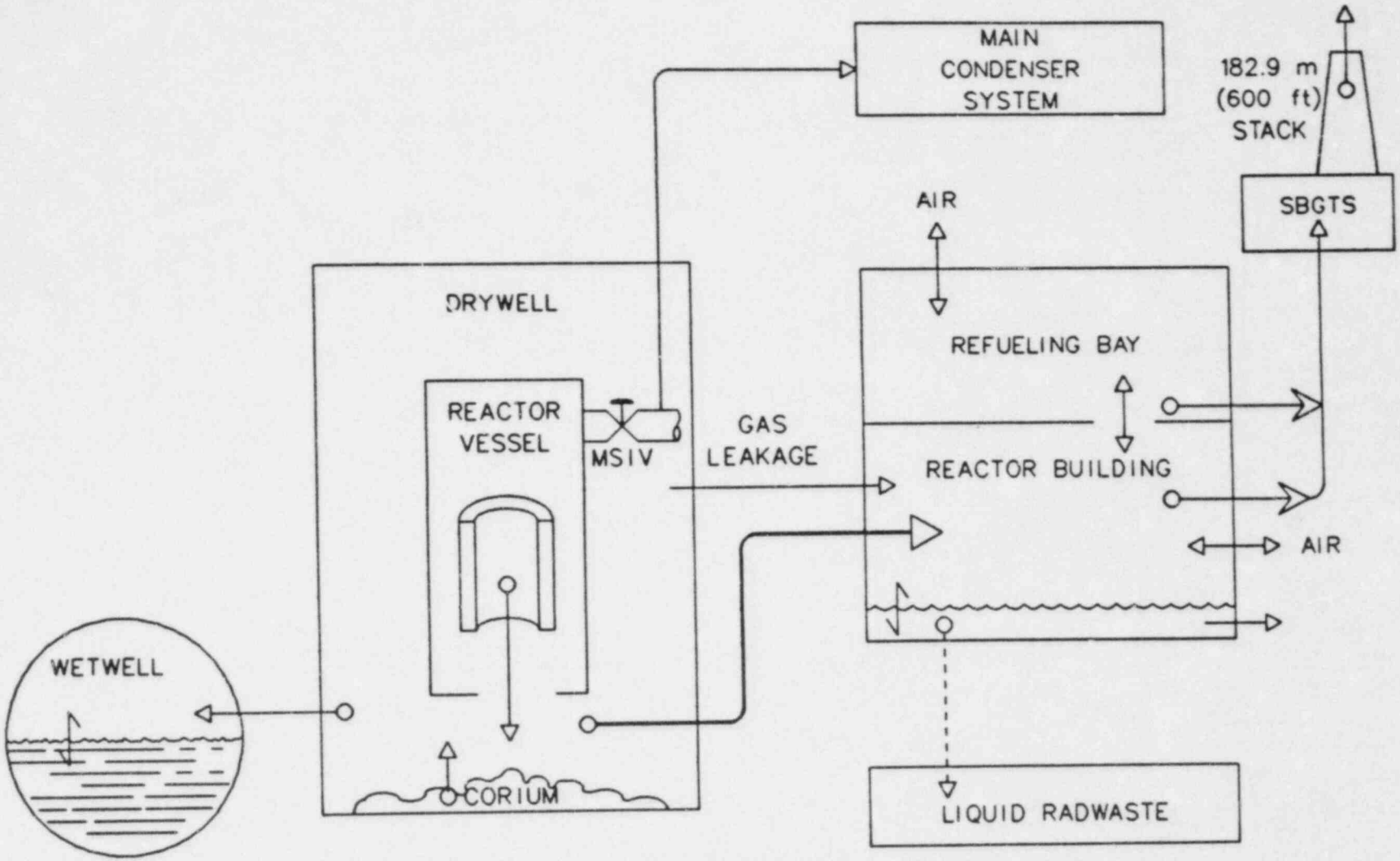

PRINCIPAL FISSION PRODUCT PATHWAYS FROM TIME OF REACTOR VESSEL MELT-THROUGH (t = 652 min) TO DRYWELL FAILURE (t = 707 min)

SLIDE 8

ORNL-DWG 82-16500R

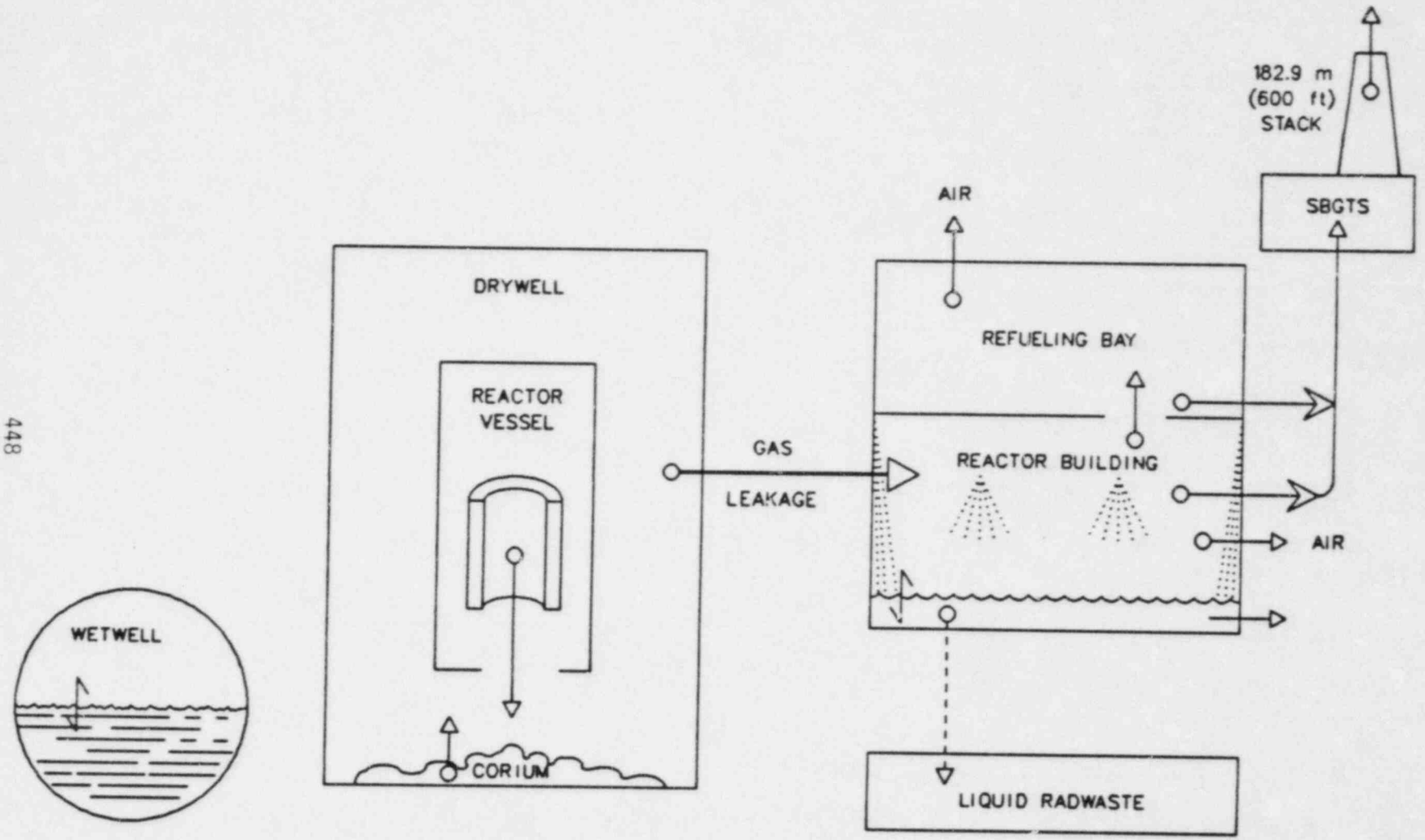

PRINCIPAL FISSION PRODUCT PATHWAYS FOLLOWING DRYWELL FAILURE (at t = 707 min)

SLIDE 9

OVERVIEW OF MAJOR FISSION PRODUCT TRANSPORT EVENTS

- RELEASE RATE FROM FAILED FUEL ELEMENTS

  USED RELEASE RATE COEFFICIENT CONCEPT DEVELOPED FOR NUREG-0772.[7] NEW DATA CORROBORATES FOR Xe, Kr, Cs, AND I UP TO 1700°C.

- RELEASE RATE FROM CORE DEBRIS

  INTERIM METHOD USES AREA RATIO SCALING ON $\kappa(T)$ WHICH GREATLY LOWERS CALCULATED RELEASE.

  WE ARE TRYING TO IMPROVE THIS MODEL BY MASS TRANSPORT ANALYSIS OF RUBBLE BED IN RV AND DW.

- AEROSOL PRODUCTION

  USED MASS TRANSPORT MODEL FOR LOW VOLATILES IN THE RV.[8]

  USED SANDIA CORRELATION FOR CORE/CONCRETE AEROSOLS IN THE DW.[9] STRONG FUNCTION OF DW RUBBLE TEMPERATURE.

- AEROSOL DEPOSITION AND TRANSPORT

  FOR THE RB WE CONSULT BCL PREDICTIONS, BUT NO TRAP-MELT RUNS EXIST FOR PRESENT CASE. WE WILL INVESTIGATE PARAMETRICALLY.

  HAARM-3 IS USED FOR THE DW AND RB. CURRENTLY, LARGE PERCENT-RELEASE (~90%) ARE BEING PREDICTED FOR THE DW DUE TO LARGE FLOW RATES. LOWER AEROSOL RELEASE RATES ARE PREDICTED FOR THE RB (~17%) DUE TO LARGER AVAILABLE DEPOSITION SURFACE AND LONGER HOLDUP TIMES.

  WE WILL CHECK RB RESULTS IN THE WET RB USING CORRAL II.

SLIDE 10

OVERVIEW OF MAJOR FISSION PRODUCT TRANSPORT EVENTS

- FISSION PRODUCT DEPOSITION ON WALLS AND AEROSOLS

  THESE MODELS ARE DESCRIBED IN REF. 2

MATERIALS	SURFACES	MECHANISMS
CsI	STEEL	CONDENSATION
CsOH	OXIDIC	CHEMISORPTION
I_2	WATER	DISSOLUTION
HI	PAINTS	CHEMICAL REACTION
I		
ORG-I		

- ORGANIC IODIDE PRODUCTION

  AVAILABLE REVIEWS ARE NOT HELPFUL SINCE THEY DEAL ONLY WITH EQUILIBRIUM LEVEL AND NOT WITH FORMATION RATE. ALSO, THERE IS NO AGREEMENT ON FORMATION MECHANISM.

  WE HAVE DEVELOPED A FORMATION RATE MODEL BY EXAMINING ORIGINAL TEST DATA OF PARKER, HILLIARD, BENNETT, LORENZ.

- DISSOLUTION IN WATER

  SUPPRESSION POOL DF'S OBTAINED FROM RASTLER.[10]
  I-SOLUBILITIES OBTAINED FROM CURRENT ORNL STUDY.

  DISSOLUTION OF I IN RB POOL ASSUMED TO BE MASS TRANSFER LIMITED. CORRAL-II CHECK.

  NOBLE GASES IN RB POOL ARE ASSUMED TO BE IN EQUILIBRIUM WITH AIR IN RB.

SLIDE 11

OVERVIEW OF MAJOR FISSION PRODUCT TRANSPORT EVENTS

- ASSESSMENT OF CHEMICAL FORMS

IN RV

ASSUME CHEMICAL EQUILIBRIUM ABOVE ~700°C.

IODINE PREDOMINANTLY (>90%) CsI FOR T < 1200°C.
FOR 1200°C < T < 1800°C, HI AND I CONTRIBUTE 10 TO 90%.

MAIN CESIUM FORM IS CsOH UP TO ~1400°C.

RADIOLYSIS PROBABLY CAUSES NO MAJOR IMPACT ABOVE T = 700°C.

IN DW

MORE DIFFICULT TO ASSESS BECAUSE

(1) ENVIRONMENT INITIALLY OXIDIZING, THEN REDUCING.

(2) PRESENCE OF OXIDIC AEROSOLS; REACTIVE WITH CsI AND CsOH IN OXIDIZING ATMOSPHERE TO FORM STABLE Cs COMPOUNDS.

(3) LOWER T'S, SLOWER CHEMICAL REACTION RATES.
THEREFORE, RADIOLYSIS IMPORTANT.

(4) LARGE VOLUME, NON-UNIFORM CONDITIONS.
AT PRESENT WE ASSUME MAIN IODINE SPECIES TO BE I_2.

SLIDE 12

OVERVIEW OF FISSION PRODUCT TRANSPORT EVENTS

- BEHAVIOR OF THE SGTS

  SGTS TURNS ON AT τ = 1 MIN.

  WE ESTIMATE HEPA FILTERS WILL PLUG ~30 MIN AFTER DW FAILURE (τ = 737 MIN) BASED ON AEROSOL GENERATION AND HAARM-3 TRANSPORT MODELS.

  THE PLUGGED FILTERS PROBABLY TEAR, INITIATING LOADING OF DOWNSTREAM FILTER.

  THE DOWNSTREAM FILTER WILL PLUG (AND PROBABLY TEAR) 30 MIN LATER, AT τ = 767 MIN.

Improvement of MARCH for BWR Applications

S. R. Greene

Oak Ridge National Laboratory

The MARCH (Meltdown Accident Response CHaracteristics) code[1] describes the response of light-water reactor and containment systems to core meltdown accidents. The original MARCH 1.0 version was officially released by Battelle Columbus Laboratories near the end of 1980. A second version of the code (MARCH 1.1) was released a few months later. Since MARCH was developed for early LWR probabilistic risk assessment (PRA) evaluations, the code's structure and modeling sophistication reflect the limited goals of such applications. Although MARCH 1.1 is a remarkably versatile and useful tool for many LWR accident analysis applications, its suitability for realistic BWR severe accident analysis is significantly compromised by its failure to consider many of the basic design and operating differences which distinguish BWRs from PWRs. The purpose of this paper is to briefly summarize these MARCH modeling deficiencies and describe efforts currently underway to improve the code's BWR simulation capabilities.

In the interval since its development MARCH has proven to be a useful tool for LWR severe accident evaluation. All or parts of the code have been utilized in studies such as the RSS,[2] Limerick,[3] and GESSAR[4] PRAs, as well as severe accident sequence analyses evaluations for the Zion[5] pressurized water reactor. In addition to these applications, the code has been utilized in several containment integrity and accident mitigation studies.[6-8] During the past two years Oak Ridge National Laboratory has been involved in the application of MARCH to analysis of severe accidents in commercial boiling water reactors as part of the Nuclear Regulatory Commission's Severe Accident Sequence Analysis (SASA) program. Specifically, ORNL has applied MARCH to evaluations of station blackout,[9] scram discharge volume break,[10] and loss of decay heat removal capability[11] accidents at the Browns Ferry nuclear plant.

Rivard et al[12] have identified many general and PWR-related MARCH modeling problems. As a result of the SASA MARCH 1.1 application experience, ORNL has identified several significant problem areas associated with application of MARCH to BWR severe accident assessment (Ref. 10, Ap. B). A total of 36 discrete problems have been identified to date. In general, these problems stem from the code's lack of recognition of unique BWR internal structural and containment designs. A complete description of the identified problems is given in Ref. 10 Only a limited number of examples will be described here.

Many of the more severe MARCH modeling concerns are related to the code's simulation of the core heatup, relocation, and vessel head failure phases of the accident. The most commonly used MARCH 1.1 core melt model employs a coherent core collapse criteria which allows core relocation only after a user specified core melt fraction is exceeded. This appears to be an unrealistic model for BWRs since the weight of each assembly is supported from underneath by its associated control rod drive (CRD) guide tube and drive housing. In addition, BWR channel box and control rod assemblies cannot be modeled within the present MARCH configuration. Localized vessel head failure via CRD stub tube penetrations cannot be modeled, and the code does not have the capability of simulating core spray systems.

MARCH's reactor vessel water level and mass calculations are incorrect since they do not include the impact of the variable flow areas of the shroud head, standpipes, and steam separators. MARCH 1.1 does not allow separate primary system break and SRV flow paths, which is incorrect for BWRs where SRV flow is routed to the pressure suppression pool. BWR high pressure coolant injection (HPCI) and reactor core isolation cooling (RCIC) systems are driven by turbines which draw steam from the primary system and exhaust it to the pressure suppression pool. The impact of this steam flow is not represented in either the primary system or suppression pool models. Finally, MARCH 1.1 does not allow pump-driven emergency core cooling system (ECCS) flows to continue after vessel head failure.

The MARCH 1.1 BWR modeling problems described above can significantly compromise the results of both PRA and SASA analyses due to resulting uncertainties in the timing and mode of vessel and containment failure, as well as reactor primary and containment system fission product transport. Fortunately, two new MARCH versions are under development which will address many of the identified BWR modeling problems. The first of the two new versions, MARCH 2.0, is being developed jointly by Battelle Columbus Laboratories (BCL), Sandia National Laboratory (SNL), Brookhaven National Laboratory (BNL), the Tennessee Valley Authority (TVA), and Oak Ridge National Laboratory (ORNL), and should be released by early November 1982. MARCH 2.1, scheduled for limited release by early March 1983, is being developed by BCL, ORNL, Rensselaer Polytechnic Institute (RPI) and SNL.

MARCH 2.0 will feature significant improvements in the code's decay heat, in-vessel thermodynamics, break flow, RPV head failure, and combustible gas burning models. MARCH 2.1 is being developed primarily to improve the code's BWR simulation capabilities and will feature a new distributed (nine volume) reactor primary system model and a detailed BWR core melt model developed at RPI. Additionally, MARCH 2.1 will feature new MARK-II containment and reactor core spray models, improvements in the existing MARCH melt models A and B, and replacement of the core/concrete subroutine INTER with the CORCON[13] code.

Although the MARCH 2.0 and 2.1 codes will feature significant improvements in many PWR and BWR modeling areas, these versions will not address all of the MARCH BWR modeling problems which have been identified to date. For example, lower plenum melt progression and CRD tube failure phenomena will continue to be modeled in a non-mechanistic fashion. Localized pressure suppression pool heatup and resulting containment over-pressurization will not be modeled. BWR primary/secondary containment interactions will continue to be modeled in a simplistic fashion, and the code will not have the capability to assess the impacts of drywell flooding on accident progression.

As one task in the MARCH 2.1 development program, ORNL is conducting a study to identify computer modeling requirements necessary for realistic simulation of severe accidents in BWRs. The results of this study will be documented in NUREG/CR-2940[14] and will consist of a general description of those phenomenological and system models which are necessary for realistic simulation of a broad range of severe accidents in BWRs. An effort will be made to identify subsystem interactions and non-safety system operations that have the capability to modify the outcome of severe BWR accidents. Where appropriate, an attempt will be made to differentiate between the calculational requirements of PRA and SASA evaluations.

The results of the BWR modeling needs assessment described above will provide the background for an evaluation of the BWR severe accident modeling capabilities of the MARCH 2.1 code. This evaluation will draw heavily on the information developed in the modeling needs assessment and discussions with active BWR MARCH users. The results of this analysis will be documented in NUREG/CR-2979.[15] The fundamental goal of this evaluation is to provide the MARCH user with a concise document containing information necessary for formulation of realistic MARCH models for a wide range of severe BWR accidents.

References

1. R. O. Wooton and H. I. Avci, MARCH Code Description and User's Manual, Battelle Columbus Laboratories, NUREG/CR-1711 (1980).

2. Reactor Safety Study, WASH-1400 (NUREG-75/014), U.S. Nuclear Regulatory Commission (1975).

3. Limerick Generating Station Probabilistic Risk Assessment, Philadelphia Electric Company (June 1982).

4. General Electric Standard Safety Analysis Report, GESSAR II, General Electric Company (Feb. 1982).

5. J. L. Darby, F. E. Haskin, W. B. Murfin, Analysis of Hypothetical Severe Core Damage Accidents for the Zion Pressurized Water Reactor, Sandia National Laboratory, NUREG/CR-1989 (April 1982).

6. Preliminary Assessment of Core Melt Accidents at the Zion and Indian Point Nuclear Power Plants and Strategies for Mitigating Their Effects, U.S. Nuclear Regulatory Commission, NUREG-0850 (Nov. 1981).

7. J. W. Yang, Cooling of Core Debris and the Impact on Containment Pressure, Brookhaven National Laboratory, NUREG/CR-2066 (July 1981).

8. R. O. Wooten, R. S. Denning, P. Cybulskis, Analysis of the Three Mile Island Accident and Alternative Sequences, Battelle Columbus Laboratories, NUREG/CR-1219 (Jan. 1980).

9. D. H. Cook et al., Station Blackout at Browns Ferry Unit One — Accident Sequence Analysis, Oak Ridge National Laboratory, NUREG/CR-2182 (Nov. 1981).

10. S. R. Greene et al., SBLOCA Outside Containment at Browns Ferry Unit One — Accident Sequence Analysis, Oak Ridge National Laboratory, NUREG/CR-2672 (Oct. 1982).

11. D. H. Cook et al., Loss of DHR Sequences at Browns Ferry Unit One — Accident Sequence Analysis, Oak Ridge National Laboratory, NUREG/CR-2973 (to be published).

12. J. B. Rivard et al., Interim Technical Assessment of the MARCH Code, Sandia National Laboratory, NUREG/CR-2285 (Nov. 1981).

13. J. F. Muir et al., CORCON-MOD 1: An Improved Model for Molten-Core/Concrete Interactions, Sandia National Laboratory, NUREG/CR-2142 (July 1981).

14. S. R. Greene et al., Realistic Simulation of Severe Accidents in BWRs: Computer Modeling Requirements, Oak Ridge National Laboratory, NUREG/CR-2940 (to be published).

15. S. R. Greene et al., Application of MARCH 2.1 to BWR Severe Accident Evaluation, Oak Ridge National Laboratory, NUREG/CR-2979 (to be published).

UNION CARBIDE
ORNL

IMPROVEMENT OF MARCH FOR BWR APPLICATIONS

SHERRELL R. GREENE
OAK RIDGE NATIONAL LABORATORY

PRESENTED AT
TENTH WATER REACTOR SAFETY RESEARCH
INFORMATION MEETING

NATIONAL BUREAU OF STANDARDS
GAITHERSBURG, MARYLAND

OCTOBER 15, 1982

UNION CARBIDE
ORNL

MARCH HAS PROVEN TO BE A VERSATILE TOOL FOR LWR SEVERE ACCIDENT EVALUATION

- PROBABILISTIC RISK ASSESSMENT
- SEVERE ACCIDENT SEQUENCE ANALYSIS
- CONTAINMENT INTEGRITY STUDIES
- ACCIDENT MITIGATION STUDIES

UNION CARBIDE
ORNL

ORNL HAS EXTENSIVE MARCH APPLICATION EXPERIENCE VIA NRC SASA PROGRAM

- BWR 4/MK I STATION BLACKOUT
- BWR 4/MK I SCRAM DISCHARGE VOLUME BREAK (SBLOCA/OC)
- BWR 4/MK I LOSS OF DECAY HEAT REMOVAL

UNION CARBIDE ORNL

MOST MARCH BWR MODELING DEFICIENCIES RELATED TO UNIQUE BWR INTERNAL STRUCTURES AND CONTAINMENT DESIGN

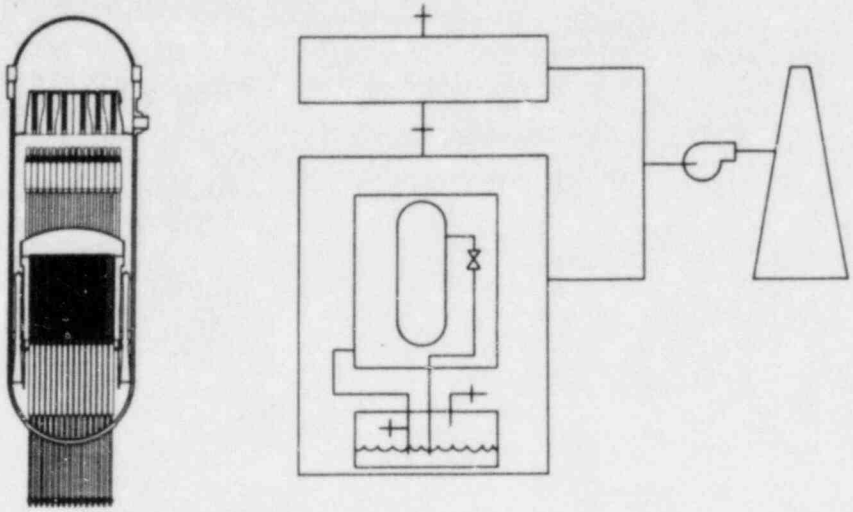

UNION CARBIDE ORNL

THIRTY–SIX PROBLEMS ASSOCIATED WITH MARCH 1.1 APPLICATION TO BWRs HAVE BEEN IDENTIFIED*

- UNREALISTIC BWR CORE COLLAPSE MODEL
- HEAD FAILURE VIA CRD TUBE PENETRATIONS NOT CONSIDERED
- SHROUD AND CONTROL RODS NOT MODELED
- CORE SPRAY SYSTEMS NOT MODELED

*NUREG/CR–2672, APP. B

UNION CARBIDE ORNL

MARCH 1.1 BWR MODELING CONCERNS (CONTINUED)

- PRIMARY WATER MASS AND LEVEL CALCULATIONS INCORRECT
- SEPARATE BREAK AND SRV FLOW PATHS NOT ALLOWED
- ECCS TURBINE EXTRACTION STEAM NOT MODELED
- PUMP DRIVEN ECCS FLOWS TERMINATE ON RPV HEAD FAILURE

UNION CARBIDE ORNL

MARCH 1.1 BWR MODELING PROBLEMS CAN SIGNIFICANTLY INFLUENCE

- TIMING AND MODE OF VESSEL AND CONTAINMENT FAILURE
- FISSION PRODUCT DISTRIBUTION IN REACTOR PRIMARY AND CONTAINMENT
- EFFECTIVENESS OF IN-VESSEL AND EX-VESSEL ESFs
- IMPACT OF 'NON-SAFETY' SYSTEM OPERATION

UNION CARBIDE ORNL

NEW MARCH VERSIONS WILL ADDRESS MANY IDENTIFIED PROBLEMS

- MARCH 2.0 – NOVEMBER 1982 (BCL, SNL, BNL, TVA, ORNL)
- MARCH 2.1 – MARCH 1983 (BCL, ORNL, RPI, SNL)

UNION CARBIDE ORNL

MARCH 2.0 WILL FEATURE SIGNIFICANT IMPROVEMENTS IN THE FOLLOWING AREAS

- DECAY HEAT
- IN-VESSEL THERMODYNAMICS
- BREAK FLOW MODELING
- STEAM GENERATOR HEAT TRANSFER
- LOWER RPV HEAD MELT PHENOMENA
- H_2 AND CO BURNING

UNION CARBIDE ORNL

PURPOSE OF MARCH 2.1 IS ADDITIONAL IMPROVEMENT OF BWR SIMULATION CAPABILITIES

- DISTRIBUTED PRIMARY MODEL
- MARK II CONTAINMENT MODEL
- DETAILED BWR CORE MELT MODEL
- CORE SPRAY MODEL
- IMPROVED MELT MODELS A AND B
- CORCON INTEGRATION

UNION CARBIDE ORNL

REVISIONS CURRENTLY PLANNED WILL NOT ADDRESS THE FOLLOWING MARCH BWR MODELING DEFICIENCIES

- LOWER PLENUM MELT PROGRESSION
- CRD TUBE FAILURE
- LOCALIZED PRESSURE SUPPRESSION POOL HEATUP
- PRIMARY/SECONDARY CONTAINMENT INTERACTIONS
- DRYWELL FLOODING

UNION CARBIDE ORNL

ORNL CONDUCTING STUDY TO IDENTIFY BWR SEVERE ACCIDENT MODELING REQUIREMENTS

- FSAR REVIEWS
- PRA REVIEWS
- USER DISCUSSIONS

UNION CARBIDE ORNL

RESULTS OF ORNL EFFORT WILL BE DOCUMENTED IN NUREG/CR–2940

- IDENTIFICATION OF NECESSARY AND DESIRABLE MODELING NEEDS
- PRA VERSUS SASA
- MARCH 2.1 ASSESSMENT

UNION CARBIDE ORNL

ORNL IS ACTIVELY ENGAGED IN BWR SEVERE ACCIDENT METHODOLOGY APPLICATIONS AND DEVELOPMENT

- SASA
- MARCH 1.1 ASSESSMENT
- MARCH 2.1 DEVELOPMENT
- MODELING NEEDS ASSESSMENT
- MARCH 2.1 CRITIQUE

ANALYSIS IN SUPPORT OF OPERATOR GUIDELINES FOR SEVERE ACCIDENTS[a]

J. A. Hunter
EG&G Idaho, Inc.

Several accident scenarios were identified during a review of operator guidelines for transients and accidents requiring further evaluation. The purpose of the evaluation was to determine the validity of certain operator actions and to determine the capability of the available reactor systems to restore the plant to a controllable, cooled mode following certain multiple failure events. Three specific accident scenario management guideline categories have been analyzed. They were:

1. Depressurization strategies for Combustion Engineering (CE) plants without power operated relief valves (PORV)

2. Cooldown strategies for Babcock and Wilcox (B&W) plants experiencing a loss-of-feedwater (LOFW) transient

3. Guideline adequacy for two loop plants experiencing a steam generator tube rupture.

CE Plant Depressurization No PORVs

The depressurization strategies for CE plants possessing no PORVs focused on the use of the reactor vessel head vents or the auxiliary pressurizer spray to depressurize the plant below the high pressure injection (HPI) shutoff head. The initiating event was a LOFW. A preliminary calculation indicated that a LOFW, due to a feedwater control failure, was found not to require the use of emergency depressurization procedures because of

---

a. Work supported by the U.S. Nuclear Regulatory Commission, Office of Nuclear Regulatory Research under DOE Contract No. DE-AC07-76ID01570.

the increased heat transfer allowed by reactor coolant pump operation. Therefore, the transient was assumed to start with a LOFW with the concurrent failure of all offsite power.

The two strategies investigated were the use of the reactor vessel head vent and the auxiliary pressurizer spray (APS) system to depressurize the plant. The head vents were found to not depressurize the plant since the heat removed by the flow through the valve (approximately 1200 BTU/s) was much less than the estimated reactor decay heat input (2,500 to 3,000 BTU/s). The APS was effective in depressurization when the pressurizer contained a bubble. This effectiveness was lost when the pressurizer filled due to activation of the HPI on low pressurizer pressure. The use of APS and the HPI delayed the time of core uncovery. Without additional operator action such as starting/stopping APS, inhibiting HPI, and recovering the secondary heat sink, the core could uncover with the potential for core damage. The subject analysis is documented in Reference 1.

B&W Loss of Feedwater Transient

If the LOFW transient were complicated by a loss of auxiliary feedwater, the primary system could remain overpressurized. By losing mass through the safety and relief valves, reactor core uncovery potentially will occur.

The two operator actions postulated were the opening of the two atmospheric dump valves and the manual initiation of the high pressure injection system. Both loop atmospheric dump valves that allow steam to flow directly from the steam lines to the atmosphere were opened 1200 s after the loss-of-feedwater event began. Manual initiation of the high pressure injecton was performed when subcooling was lost in the primary system. Injection capacity was limited to a single-pump train for the calculation. The conclusions of these two calculations are:

1. The atmosphere dump valves provide virtually no cooling capacity of a loss-of-feedwater transient without an active feedwater source

2. A single high pressure injection train is effective in core cooling by decreasing void formation, making up coolant lost through the primary relief valves, and extending the time the primary system is in a condition where the primary pumps can effectively operate.

The details of this analysis are documented in Reference 2.

Steam Generator Tube Rupture Behavior

The purpose of this investigation was to study the thermal-hydraulic response of a pressurized water reactor (PWR) to a double-ended guillotine steam generator tube rupture (SGTR) in plants with only two steam generators. The emphasis was placed on determining which steam generator was faulted and on determining whether the existing operator guidelines for managing a SGTR were adequate.

In general, the key to the diagnosis of a SGTR lies with a radiological release from the primary system to the secondary system. Radiation alarms of various locations (steam generator blowdown surge tank, condenser air ejector) as well as primary phenomena such as decreasing pressurizer pressure and level will signal a SGTR to the plant's control room. This has been confirmed through actual SGTR events documented in Reference 3.

Operator guidelines for SGTR events are fairly general. These guidelines require the operator to identify the faulted steam generator, isolate it, and cooldown with the intact steam generator. The guidelines for faulted steam generator identification follow the computer code suggested indication exactly. For example, the Zion Emergency Operating Procedure for Steam Generator Tube Failure (Reference 4) requires operators to (a) compare levels and feedwater flows, (b) compare feed regulatory valve position, and (c) monitor individual steam lines for radiation. Based on the subject analysis, there appears to be no further amplification of these guidelines that can be gained through the use of computer calculations.

REFERENCES

1. B. F. Saffell, Jr., letter to J. E. Solecki, "Severe Accident Sequence Analysis (SASA) Results for Combustion Engineering (CE) Pressurized Water Reactor (PWR)," Saff-144-82, April 9, 1982.

2. J. D. Burtt, RELAP4/MOD7 Calculations for a Loss of Feedwater Transient in a Babcock and Wilcox Pressurized Water Reactor, EGG-CAAD-5832, March, 1982.

3. L. B. Marsh, Evaluation of Steam Generator Tube Rupture Events, NUREG-0651.

4. Zion Station Emergency Operating Procedures EOP-10: Steam Generator Tube Failure, Rev. 0. January, 1977.

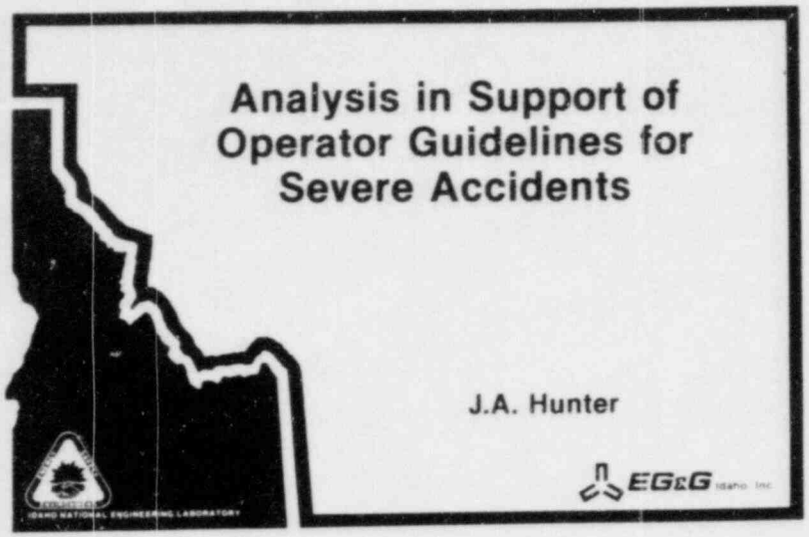

Accident Scenarios

- Depressurization of CE plants without PORVs
- B&W loss of feedwater transient
- Steam generator tube rupture behavior

S2 10 235

Depressurization of CE Units. No PORVs

- Purpose:
  - Study potential emergency depressurization capabilities
- Sequence:
  - Loss of offsite power, loss of feedwater (fail main coolant pumps)
- Depressurization strategies:
  - Reactor vessel head vent
  - Auxiliary pressurizer spray

S2 10 234

Depressurization CE Units. No PORVs System Behavior - Head Vents

Time	Event
46-53 min.	Steam generators dry out
60 min.	Pressurizer filled Decay heat exceeds safety valve capacities
103 min.	Core uncovers

S2 10 236

Depressurization of CE Units.
No PORVs
Head Vent Effectiveness

- Vent: 3/4 inch line. Valve (3/16 inch orifice)
- Heat rejection rate insignificant
- Not effective

52 10 233

Depressurization of CE Units.
No PORVs
System Behavior - Aux Spray

Time	Event
.5 min.	Initiate aux spray
8 min.	HPI initiated
11 min.	Pressurizer filled
33 min.	Pressurizer safety valves ope
70 min.	Primary coolant - net mass loss
150 min.	Core uncovers

52 10 245

Depressurization of CE Units.
No PORVs
Auxiliary Pressurizer Spray Effectiveness

- Aux spray effective with pressurizer bubble present
- Without primary letdown, pressurizer fills
- Aux spray detrimental - fills pressurizer, lose pressure control

52 10 246

Depressurization of CE Units.
No PORVs
Auxiliary Pressurizer Spray Effectiveness
(continued)

- Aux spray benefit - delays core uncovery
- Without operator action, core uncovers

52 10 247

Depressurization of CE Units. No PORVs Recommendations - Aux Spray

- Regain secondary heat sink
- Intermittent aux spray operation (delay uncovery)
- Inhibit HPI (delay uncovery)

S2 10 248

B&W Loss of Feedwater Transient

- Purpose:
  - Assess effects of operator actions
    - Open two ADVs
    - Manually initiate one HPI - loss of subcooling
- Sequences
  - LOFW, no HPI, no Aux feedwater, SORV
    - Open ADVs 1200s
  - LOFW, no aux feedwater, one HPI train
    - Assess HPI cooling capabilities

S2 10 250

B&W LOFW System Assumptions

System	ADV	HPI
PORV	Stuck open P_{sys}>2270 psia	Normal, locked open - loss subcooling
Primary safeties	Hold P_{sys}~2500 psia	Hold P_{sys}~2500 psia
HPI	Failed	Manual initiation, one train, loss subcooling
Aux feed	Failed	Failed
ADVs	Open two at 1200s	Locked shut

S2 10 244

B&W LOFW System Behavior - Identical for Both Cases

Time(s)	Event
0.0	Feedwater lost, turbine tripped
0.3	Reactor tripped
44.0	Steam generators decoupled
100-103	Steam generator dried out
452	Pressurizer filled solid
485	PORV lifted
690	Primary safeties lifted
1200	Subcooling lost ADVs opened or HPI initiated

S2 10 243

B&W LOFW
ADVs - Effectiveness

- Secondary pressure rapidly decreased
- Heat removal degrades
- ADV flow limited
- Limited amount of secondary mass available for release
- ADVs ineffective without adding mass to secondary

S2 10 249

B&W LOFW
HPI - Effectiveness

- HPI decreased bubble generation (extends primary pump operation)
- HPI reduced primary mass loss to zero net
- Single HPI cools core

S2 10 237

Steam Generator Tube Ruptures

- Purpose:
  - — Characterize thermal hydraulic response
    - Two loop PWR
    - Double ended guillotine tube rupture
    - Identify faulted generator
    - Assess operator guidelines

S2 10 240

Steam Generator Tube Ruptures
(continued)

Sequence

- One full tube rupture
- 1/10 tube leak
- No charging flow
- Reactor power 102%
- Scram on low pressurizer pressure

S2 10 239

Steam Generator Tube Rupture System Behavior

- Radiation alarms activate
- Plant scrams
- Steam generator level increases
  - Aux feedwater active
  - Identifies faulted generator

S2 10 241

Steam Generator Tube Rupture Current Guidelines (Zion)

- Compare levels and feedwater flows
- Compare feed regulatory valve position
- Monitor individual steam lines for radiation
- Guidelines adequate

S2 10 239

Summary

- CE depressurization - no PORV
  - Auxiliary spray delays uncovery
- B&W loss of feedwater
  - Single HPI cools core
- Steam generator tube rupture - two loop plant
  - Guidelines adequate

S2 10 242

THE STATION BLACKOUT TRANSIENT AT THE BROWNS FERRY UNIT-1 PLANT A SEVERE ACCIDENT SEQUENCE ANALYSIS (SASA) PROGRAM STUDY[a]

R. R. Schultz
EG&G Idaho, Inc.

Operating plant transients are of great interest for many reasons, not the least of which is the potential for a mild transient to degenerate to a severe transient yielding core damage. Using the Browns Ferry (BF) Unit-1 plant as a basis of study, the station blackout sequence was investigated by the Severe Accident Sequence Analysis (SASA) Program in support of the Nuclear Regulatory Commission's Unresolved Safety Issue A-44: Station Blackout (see Reference 1). A station blackout transient occurs when the plant's AC power from a commercial power grid is lost and cannot be restored by the diesel generators. Under normal operating conditions, if a loss of offsite power (LOSP) occurs [i.e., a complete severance of the BF plants from the Tennessee Valley Authority (TVA) power grid], the eight diesel generators at the three BF units would quickly start and power the emergency AC buses. Of the eight diesel generators, only six are needed to safely shut down all three units.

Examination of BF-specific data show that LOSP frequency is low at Unit 1. The station blackout frequency is even lower (5.7×10^{-4} events per year) and hinges on whether the diesel generators start. The frequency of diesel generator failure is dictated in large measure by the emergency equipment cooling water (EECW) system that cools the diesel generators.

Once a station blackout has occurred, the station operator is most concerned about starting the diesel generators and reconnecting the station to the TVA power grid. However, until AC power is restored, the operator will have (a) the plant station battery (available for 7 h), (b) both the

---

a. Work supported by the U.S. Nuclear Regulatory Commission, Office of Nuclear Regulatory Research under DOE Contract No. DE-AC07-76ID01570.

high pressure coolant injection (HPCI) and the reactor core isolation cooling (RCIC) systems [i.e., the vessel water inventory (VWI) equipment], and (c) 135,000 gallons of water reserved in the condensate storage tank (CST) [a Technical Specification (TS) Limit].

Major objectives of the SASA Program analysis of the BF Unit-1 station blackout sequence were to (a) characterize the transient as the plant operator would see it, (b) determine the time to core uncovery, and (c) calculate the quantity of mass and energy transferred from the reactor pressure vessel to the pressure suppression pool (PSP). The analysis was performed using the RELAP5 Mod-1 Cycle 13 thermal-hydraulic code. However, several updates were used both to improve the cycle and to make the cycle appropriate to a boiling water reactor (BWR). Specifically, updates were added to enhance the behavior of the interphase drag models and the reactivity feedback models. In addition, the jet pump was treated as a special component in the BF model. Finally, the RELAP5 separator model was updated.

In the event a LOSP occurs, the power-load (time zero) unbalance experienced by the plant's main generator will be sufficient to initiate a reactor scram. The reactor vessel will be isolated during the scram phase of the transient. During the much longer period when only core decay heat is present, the VWI will boil and flash. The excess steam will bleed from the vessel through the safety relief valves (SRVs) to the PSP. Initially enough VWI will be lost so that the water level in the vessel downcomer will not be measurable on the level instrumentation available in the control room. The Emergency Operating Procedures (EOPs) dictate that the RCIC and the HPCI systems be manually activated as soon as possible. However, if the operator does not activate these systems, enough VWI will be lost to activate the vessel downcomer low-low trip and, thus, automatically turn on the RCIC and HPCI systems.

If neither the HPCI nor RCIC is available, the VWI will continually decrease as the SRVs open at regular intervals to bleed steam to the PSP. Core heatup would begin at 2300 s under such circumstances (but at 1680 s if a SRV became jammed open at the first cycle).

However, if either or both of the RCIC and HPCI systems are activated, water from the CST will be pumped into the vessel through the feedwater sparger. CST water will be delivered until either the operator manually shuts the systems off or the downcomer fills to the high level trip elevation, which will automatically deactivate the RCIC/HPCI systems.

Throughout the sequence, the SRVs will cycle either automatically as the vessel pressure exceeds plant setpoints, or manually as the operator follows EOPs. Left in the automatic mode, the same SRV will probably open and shut repeatedly to bleed the steam boiled by the core decay heat. Thus, a localized hot spot will be formed in the PSP at the SRV discharge port.

To change the location of steam delivery to the PSP and to reduce the number of SRV cycles, the operator is directed by the EOP to manually cycle alternate SRVs over a larger pressure range, e.g., about 200 psi. Such a procedure could be followed indefinitely if it were not for the heat transfer from the vessel to the drywell environment. Without the drywell coolers (lost during the LOSP), the drywell atmosphere will be heated to temperatures exceeding drywell seal specifications, which will lead to an increased potential for containment failure.

Consequently, the operator will probably depressurize the vessel after an initial waiting period (about an hour) at a rate that would not change the vessel temperature by more than 100°F/h (a TS limit). Thus, the heat load to the drywell would be reduced by the corresponding decrease in saturation temperature and the excess energy would be transferred to the PSP.

Several significant conclusions and observations resulted from the study:

1. A station blackout transient is improbable. Equipment or system unavailabilities yield a station blackout event frequency of 5.7×10^{-4} events/year.

2. The VWI equipment available to the operator during a station blackout is sufficient to maintain the VWI during the time when the station battery is available, even with a stuck-open relief valve.

3. Ultimate shutdown of the plant can only be accomplished if AC power is restored together with the residual heat removal (RHR) system.

4. RELAP5 can be used to model BWR long term sequences. The code has completed 7.8 and 9.7 h transients in 4.9 and 4.4 h calculated times, respectively.

Reference

1. R. R. Schultz and S. R. Wagoner, The Station Blackout Transient at the Browns Ferry Unit-1 Plant: A Severe Accident Sequence Analysis, EGG-NTAP-6002, EG&G Idaho, Inc., August 1982.

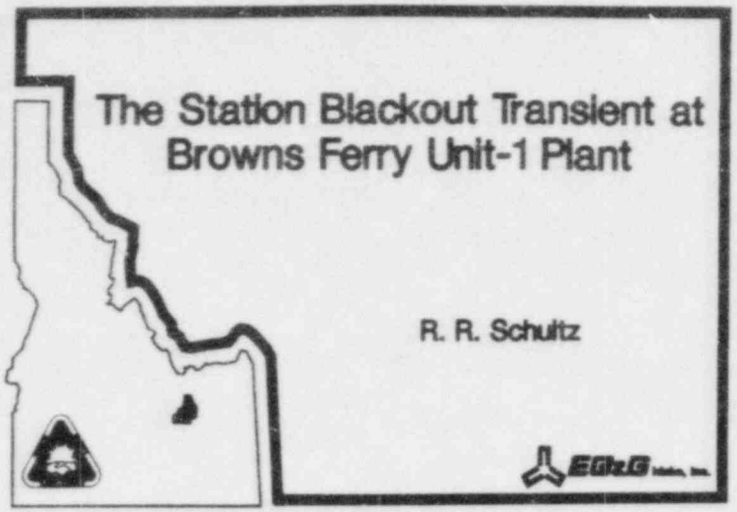

Outline of Presentation

- Analysis objectives
- Assumptions
- Analysis sequences
- Initial chronology
- Station Blackout analyses
- Conclusions

C2 0480

Analysis Objectives

Characterize the transient as the plant operator would see it.

- Determine time to core uncovery
- Calculate amount of mass and energy transferred from vessel to pressure suppression pool (PSP)

C2 0481

Assumptions

- Browns Ferry Unit-1 at 100% power when loss of offsite power (LOSP) occurs
- No AC power available, i. e., no diesel generators
- DC power available for 7 h
- No heat transfer from vessel walls to containment

C2 0482

Analysis Sequences

- Boiloff
- Boiloff with a stuck-open relief valve (SORV)
- Reactor core isolation cooling (RCIC) available
- High pressure coolant injection (HPCI) available
- RCIC available with a SORV
- RCIC available with a controlled depressurization

Initial Chronology

Time (s)	Event
0	LOSP, scram logic initiated, recirculation pumps trip off, feedwater pumps trip off
0.1	Turbine bypass valves open
0.2	Turbine control valves shut
3.0	Four safety relief valves (SRVs) open
3.9	Scram is complete
5.0	Feedwater flow is zero
8.0	Main steam line isolation valves (MSIVs) shut

Station Blackout Analyses

- Boiloff calculation
- Boiloff with SORV
- RCIC system available
- RCIC system available and a SORV
- Mitigating actions

Boiloff Calculation

- Assumptions :
  - No emergency core cooling systems (ECCSs) available
  - RCIC not available
- Core uncovery at 2300 s

Vessel Steam Dome Pressure

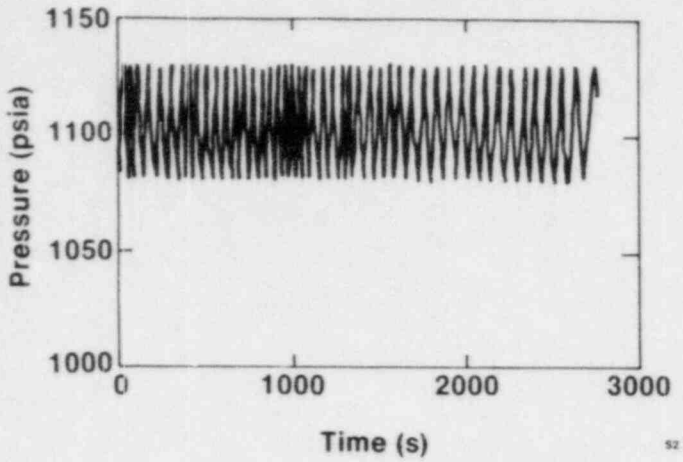

S2 3461

Boiloff with SORV

- Assumptions :
  - No ECCS available
  - No RCIC available
  - An SRV opens 3 s after LOSP occurs and remains stuck open
- Core uncovery at 1680 s

C2 0487

Vessel Steam Dome Pressure

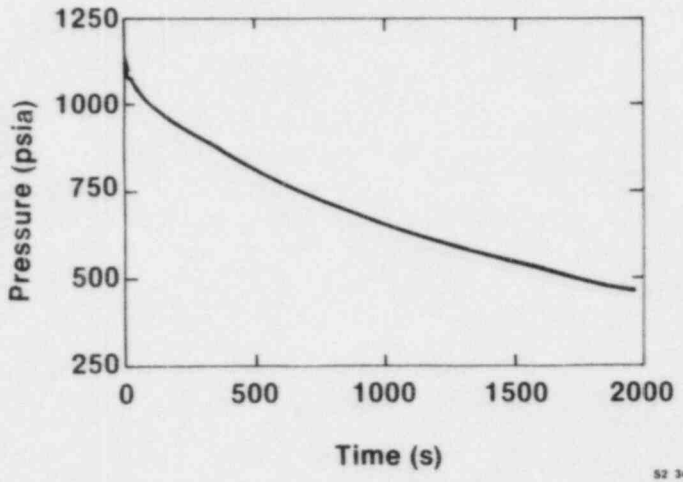

S2 3462

RCIC System Available

- Assumptions (operator actions) :
  - RCIC manually initiated 90 s after LOSP
  - RCIC manually operated to turn on at 44.83 ft and turn off at 48.17 ft
  - SRVs manually opened at 120 s
  - SRVs cycled to maintain vessel pressure between 1115 and 915 psia
- Core uncovery at 34000 s

C2 0488

Downcomer Water Level

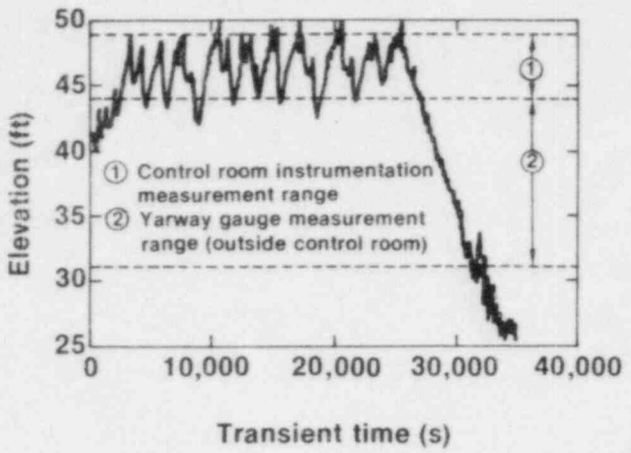

S2 3463

RCIC System Available and a SORV

- Assumptions (operator actions):
  - RCIC manually initiated 90 s after LOSP
  - RCIC manually operated to turn on at 44.83 ft and turn off at 48.17 ft
  - SRV fails to close on first cycle
- Core uncovery at 36400 s

C2 0488

Vessel Steam Dome Pressure

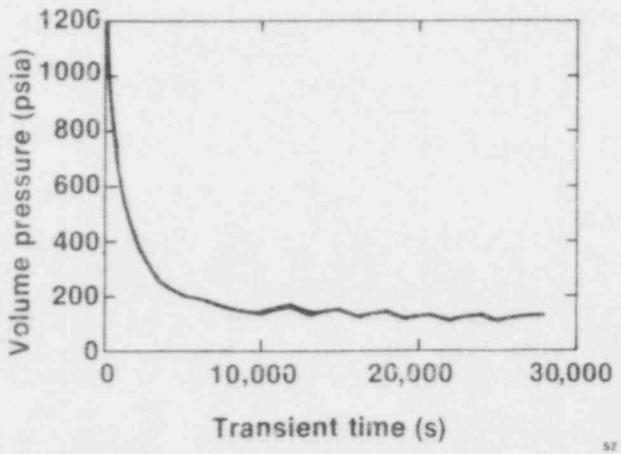

S2 3464

Mitigating Actions

- Short term (prior to 7 h)
  - Ensure availability of RCIC and/or HPCI
  - RCIC can be safely used to maintain vessel water inventory (VWI) even with a SORV
- Long term (after 7 h)
  - Ensure AC power restoration combined with residual heat removal (RHR) system

C2 0800

Conclusions

- A station blackout event is improbable. Equipment unavailabilities give a frequency of 5.7×10^{-4} events/year

- RELAP5 can be used to model boiling water reactor (BWR) long term transients. The code calculated 7.8 and 9.7 h transients in 4.9 and 4.4 h, respectively

C2 0801

SAND82-2120C

Containment Management Study for Severe PWR Accidents

F. E. Haskin
V. L. Behr
J. Jung

Sandia National Laboratories
Albuquerque, New Mexico 87185

Probabilistic risk assessments have determined that risk from nuclear power reactors is dominated by severe, core-damage accidents. Radiological consequences from severe accidents can range from minor to major depending on the degree to which radionuclides released from the core are retained within containment. Since core damage accidents were not considered in establishing design requirements for existing containments, we have undertaken, as part of the Severe Accident Sequence Analysis (SASA) Program, a systematic study of PWR containment loadings and operator actions which could affect PWR containment integrity during such accidents. Our primary objective is to identify strategies which could be used by operators to preclude or delay loss of containment integrity. In addition, we attempt to identify plant states in which a breach of aboveground containment is likely or eminent. Such information is vital to emergency response teams.

Our study involves detailed analyses of containment loadings (pressure-temperature histories) and thresholds for containment failure due to high pressure or temperature for specific PWRs. To date, we have performed analyses of containment loadings for the Zion plant and structural analyses to estimate containment failure thresholds for the Watts Bar plant. We have just initiated a cooperative SASA effort with Tennessee Valley Authority (TVA) for the Bellefonte plant. Zion and Bellefonte have large dry prestressed concrete containments. Watts Bar has a steel-shell, ice-condenser containment. Over the next two years we plan to complete containment management studies for Bellefonte and Watts Bar. Subsequently, we may perform a similar study for a subatmospheric containment.

Results of Analyses for Zion

References 1 and 2 present the detailed results of our SASA Program analyses for Zion. Findings relevant to containment management are summarized below.

Operator actions to assure containment isolation are obviously important. A relatively small opening can lead to large leak rates; for example, an opening approximately 0.1 inches in diameter would result in design leakage of 0.1 volume percent per day for the Zion containment at its design pressure. In accidents involving containment bypass, prompt operator action

to isolate the bypass may be required. For example, in the V-Sequence LOCA, too long a delay could result in failure of the isolation-valve motor operator and emergency core cooling equipment due to steam flooding in the auxiliary building. Diagnosis of the need to isolate should be based in part on auxiliary-building pressure, temperature, and radiation level indications.

Given containment isolation, some containment heat removal is required to prevent containment failure due to the buildup of steam and noncondensable gases. However, at Zion, such overpressure could not occur until at least 6 hours into the accident - this much time would be required if all decay heat were effective in heating and evaporating water. Thus, for Zion, the operators have at least 6 hours (and usually much more time) to establish sufficient containment cooling capacity to prevent containment failure due to steam overpressure. A single fan cooler or a single spray train would suffice to prevent overpressure failure.

Containment failure due to hydrogen burning at Zion can also be prevented, albeit indirectly, by containment heat removal. With sprays or fan coolers operating at capacity, the steam content will be low enough to permit burning; however, for reasonable ignition points (8 to 10 mole percent hydrogen), the preburn pressure would be low enough that the peak pressure due to burning would not exceed the containment failure threshold. If neither the containment sprays nor the fan coolers operate, the containment pressure will rapidly become high enough to suppress hydrogen burning by steam inerting.

Using either the sprays or the fan coolers, containment heat removal is accomplished through condensation of steam and thus can reduce the steam mole fraction to the point (56 mole percent) where hydrogen burning is no longer steam suppressed. If containment heat removal is delayed until well after the onset of melt/concrete interactions, accumulated H_2 and CO could then be sufficient to result in containment failure due to hydrogen burning. In this situation, the prudent course of action would be to maintain steam inerting unless it can be demonstrated that the amounts of H_2 and CO is containment are sufficiently low to preclude containment failure due to burning. Sprays or fan coolers could be used to keep the containment pressure below the failure threshold yet above the point corresponding to a steam inert atmosphere (i.e., 56 psig for Zion). The sprays would be preferable to fan coolers for such control since evaporation of spray droplets would provide some pressure suppression should a burn occur. The strategy just described would extend the time which local authorities have to evacuate the surrounding population. Operator action would be based upon containment pressure and temperature readings and knowledge of hydrogen/steam/oxygen fractions gathered from on-site chemical analysis of containment air samples.

Containment Structural Analyses for Watts Bar

A structural analysis of the Watts Bar steel containment is being conducted with the objective of determining a realistic static failure pressure. The components of the containment which are included in the analysis are: (1) the containment shell, (2) the equipment hatch, (3) the containment anchorage system, (4) the personnel lock, and (5) the electrical penetrations. Analyses of Items (1) through (4) have been completed while that for Item (5) is in progress.

Our containment shell analysis was axisymmetric and accounted for large displacements and finite strains. Actual material properties (i.e., yield stress and ultimate strength values) were used. Based on a maximum von Mises equivalent stress criterion for failure, the analysis predicts that the containment shell would fail in the dome at an internal pressure of approximately 175 psig. This, of course, assumes unrestrained deflection. Thus, in contrast to similar containments having thinner steel shells, penetrations or deflection limits appear to control the failure threshold for Watts Bar. For example, our analysis indicates buckling of the equipment hatch would occur between 112-140 psig. The capacity of the containment anchorage system is between 118-144 psig, but the personnel lock capacity is in excess of 150 psig.

Conclusions

Our studies to date indicate the importance of emphasizing containment isolation, containment and auxiliary-building instrumentation, and containment heat removal in training and procedures for severe accidents. Strategies for preventing or delaying aboveground containment failure exist for some cases but may prove to be plant and accident specific.

The scope of instrumentation set forth in Regulatory Guide 1.97, Revision 2, appears consistent with the operator actions and strategies which we have studied thus far. However, in some cases (e.g., continuous hydrogen monitoring), instruments capable of surviving severe accident are not yet commercially available.

Our structural analyses indicate the importance of containment penetrations in estimating containment failure thresholds. Also, containments which are very similar in type, size and internal-arrangement may have very different failure thresholds.

References

1. F. E. Haskin, W. B. Murfin, J. B. Rivard, and J. L. Darby, Analysis of a Hypothetical Core Meltdown Accident Initiated by Loss of Offsite Power for the Zion 1 Pressurized Water Reactor, NUREG/CR-1988, SAND81-0503, Revised December 1981.

2. F. E. Haskin, J. L. Darby and W. B. Murfin, Analysis of Hypothetical Core Meltdown Accident Initiated by Loss of Offsite Power for the Zion 1 Pressurized Water Reactor, NUREG/CR-1989, SAND81-0504, October 1982.

PWR CONTAINMENT MANAGEMENT STUDY

JUSTIFICATION

- SEVERE ACCIDENTS DOMINANT RISK
- RADIOLOGICAL CONSEQUENCES FROM SEVERE ACCIDENTS DEPEND ON CONTAINMENT INTEGRITY
- CONTAINMENTS WERE NOT SPECIFICALLY DESIGNED FOR SEVERE ACCIDENTS
- CONTAINMENT RESPONSE MODELING FOR SEVERE ACCIDENTS RAPIDLY DEVELOPING
- NEED CURRENT, SYSTEMATIC STUDY OF CONTAINMENT LOADINGS, FAILURE MODES, AND OPERATOR ACTIONS

PWR CONTAINMENT MANAGEMENT STUDY

TASKS

THERMAL-HYDRAULICS

- DEVELOP PLANT MODELS
- SELECT BASE SEQUENCES
- HANDS-OFF ANALYSES
- ANALYZE OPERATOR ACTIONS

STRUCTURAL ANALYSES

- ULTIMATE CAPACITY
- LARGE PENETRATIONS
- TYPICAL PENETRATIONS
- CYLINDER-BASEMAT JUNCTION

MITIGATING FEATURES

UNCERTAINTIES

PWR CONTAINMENT MANAGEMENT STUDY

PLANT SELECTION

- LARGE DRY - ZION, BELLEFONTE
- ICE CONDENSER - WATTS BAR/SEQUOYAH
- SUB-ATMOSPHERIC - SURRY

REASONS

- PROTOTYPES
- INFORMATION AVAILABILITY
- COORDINATION WITH OTHER RESEARCH PROGRAMS

LARGE, DRY PWR CONTAINMENTS

- LARGE FREE VOLUME (2.7×10^6 FT^3 AT ZION)
- FAIRLY "OPEN" -- FEW ISOLATED COMPARTMENTS
- RELATIVELY HIGH ESTIMATED FAILURE PRESSURE (APPROXIMATELY 149 PSIA AT ZION)
- CONTAINMENT SPRAYS
- AT ZION
  - THREE SPRAY TRAINS -- ONE DIESEL DRIVEN
  - FIVE FAN COOLERS
  - WATER OVERFLOW TO REACTOR CAVITY

SANDIA SASA APPROACH

- USE AVAILABLE COMPUTER CODES AND BOUNDING HAND CALCULATIONS TO PERFORM REALISTIC ANALYSES FOR SPECIFIC PLANTS AND ACCIDENT SEQUENCES IDENTIFYING
  - HANDS-OFF MELTDOWN ACCIDENT SIGNATURES
  - EFFECTS OF OPERATOR ACTIONS
  - INFORMATION NEEDED FOR MAKING DECISIONS
  - RADIOLOGICAL CONSEQUENCES
  - UNCERTAINTIES

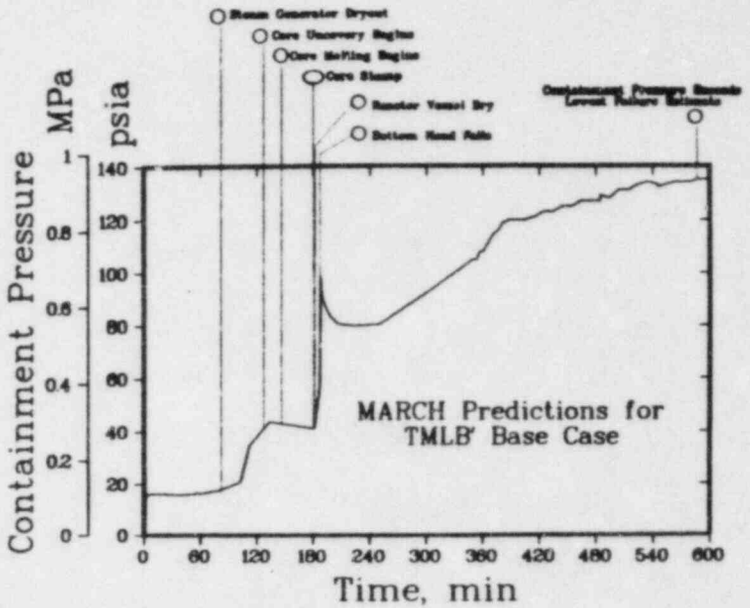

ENERGY BALANCE APPROACH TO OVERPRESSURE FAILURE

1. ENERGY SOURCES: INITIAL INTERNAL ENERGIES
   DECAY HEAT
   CHEMICAL REACTIONS

2. ENERGY SINKS: PASSIVE HEAT SINKS
   CORE-CONCRETE DEBRIS
   WATER IN CONTAINMENT
   CONTAINMENT ATMOSPHERE

3. FASTEST WAY TO OVERPRESSURE FAILURE IS BY STEAM PRODUCTION

4. ASSUME SATURATED CONTAINMENT ATMOSPHERE

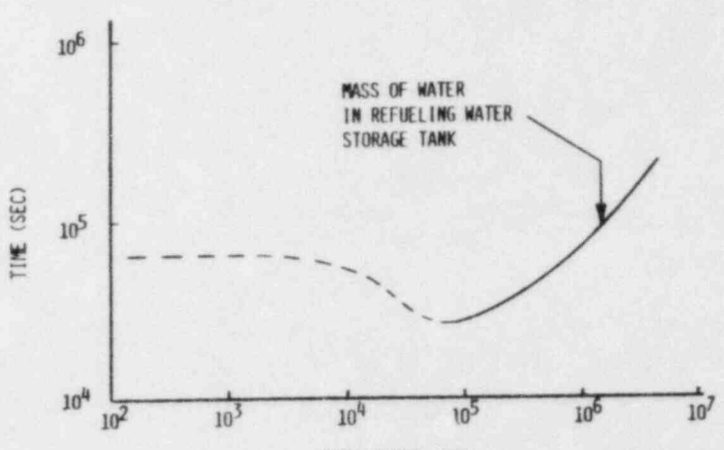

CONCLUSIONS - OVERPRESSURE FAILURE

1. FOR LARGE, DRY PWR CONTAINMENTS SUCH AS ZION, CONTAINMENT HEAT REMOVAL SYSTEMS WOULD HAVE TO FAIL
2. MINIMUM TIME TO CONTAINMENT FAILURE OCCURS WHEN ALL AVAILABLE ENERGY EVAPORATES WATER TO SATURATE CONTAINMENT ATMOSPHERE AT FAILURE PRESSURE
3. IF SOME ENERGY IS USED TO HEAT ADDITIONAL WATER, OVERPRESSURIZATION WILL BE DELAYED
4. IF DEBRIS-WATER CONTACT IS PRECLUDED, OVERPRESSURIZATION WILL BE DELAYED (CORE-CONCRETE INTERACTIONS)

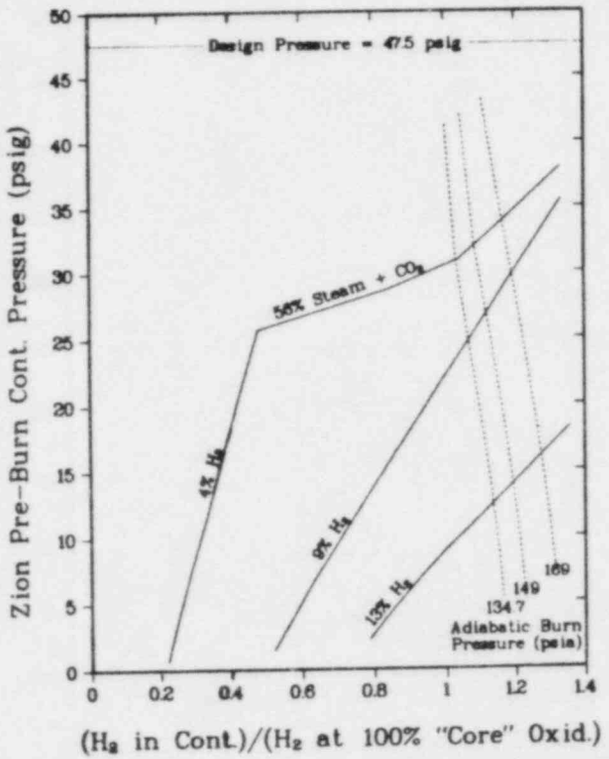

COMBUSTIBLE GAS REGIONS - ASSUMPTIONS

1. CONTAINMENT ATMOSPHERE IS UNIFORMLY MIXED
2. CONTAINMENT ATMOSPHERE IS SATURATED
3. 100% FUEL ASSEMBLY OXIDATION BEFORE CORE-CONCRETE INTERACTIONS
4. H_2 = CO = CO_2 = 1 = 2 = 2.5 FROM CORE-CONCRETE INTERACTIONS
5. IDEAL GAS LAW FOR NONCONDENSIBLES
6. COMPLETE, ISOCHORIC, ADIABATIC BURNS OF H_2 AND CO
7. ZION FREE VOLUME

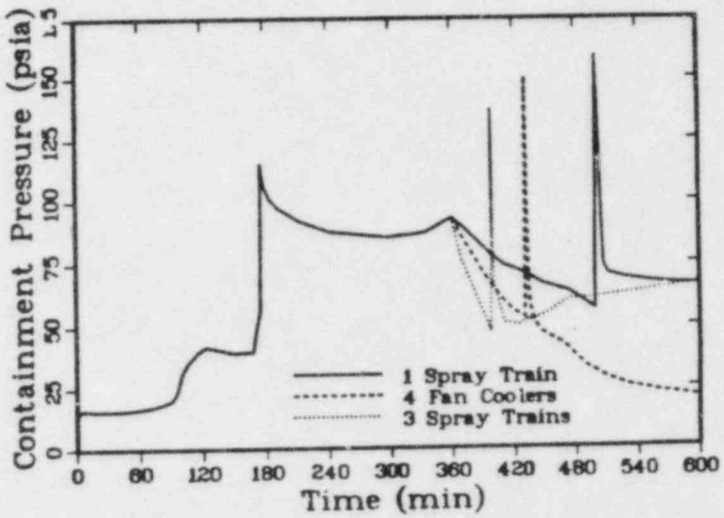

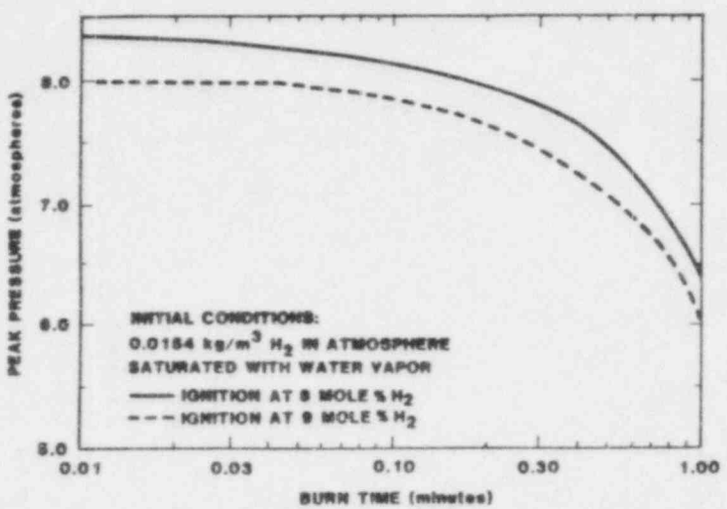

CONCLUSIONS - HYDROGEN BURNING AT ZION

1. WITH CONTAINMENT HEAT REMOVAL, BURN LIKELY BEFORE SUFFICIENT H_2 HAS ACCUMULATED TO RESULT IN CONTAINMENT FAILURE

2. WITHOUT CONTAINMENT HEAT REMOVAL, BURNS WILL BE PRECLUDED BY EXCESS STEAM IN ATMOSPHERE

3. IF CONTAINMENT HEAT REMOVAL RE-ESTABLISHED AFTER H_2, CO BUILDUP CHOICE BETWEEN

   A. MAINTAINING STEAM INERTING BY CONTROLLING CONTAINMENT PRESSURE

   B. BRING PRESSURE DOWN INTO COMBUSTIBLE REGION - PREFERABLY WITH FULL HEAT REMOVAL CAPACITY

   SHOULD KNOW H_2 LEVEL TO OPT FOR 3B

OPERATOR ACTIONS WHEN FAN COOLERS AND CONTAINMENT SPRAYS ARE AVAILABLE

1. OPERATE FAN COOLERS CONTINUOUSLY
2. LIMIT USE OF SPRAY INJECTION IF ECC INJECTION IS OPERATING
3. OPERATE SPRAYS CONTINUOUSLY AFTER CORE UNCOVERING
4. IF POSSIBLE, ESTABLISH BACKUP CSI CAPABILITY IN CASE OF CSR FAILURE
   A. KEEP ONE SPRAY TRAIN IN STANDBY
   B. REPLENISH RWST

OPERATOR ACTIONS WHEN CONTAINMENT SPRAYS ARE AVAILABLE BUT FAN COOLERS ARE NOT

1. OPERATE SPRAYS AS REQUIRED TO CONTROL CONTAINMENT PRESSURE BEFORE CORE UNCOVERING
2. OPERATE SPRAYS CONTINUOUSLY AFTER CORE UNCOVERING
3. IF POSSIBLE, ESTABLISH BACKUP CSI CAPABILITY

OPERATOR ACTIONS WHEN FAN COOLERS ARE AVAILABLE BUT CONTAINMENT SPRAYS ARE NOT

1. OPERATE FAN COOLERS CONTINUOUSLY
2. ATTEMPT TO RE-ESTABLISH CONTAINMENT SPRAY CAPABILITY
3. WHETHER OR NOT TO ADD WATER VIA OTHER SYSTEMS REQUIRES PLANT-SPECIFIC ANALYSIS

OPERATOR ACTIONS WHEN FAN COOLERS AND CONTAINMENT SPRAYS ARE UNAVAILABLE

1. VENTING BEFORE CORE UNCOVERING COULD BE EFFECTIVE BUT WOULD REQUIRE A SYSTEM SPECIFICALLY DESIGNED FOR THIS PURPOSE
2. WATER ADDITION VIA OTHER SYSTEMS WOULD PROBABLY BE APPROPRIATE IF ECC HAS ALSO FAILED
3. UPON REESTABLISHING CONTAINMENT HEAT REMOVAL DECISION TO BRING PRESSURE DOWN DEPENDS ON ESTIMATE OF H_2 AND CO IN CONTAINMENT ATMOSPHERE
4. IF DECISION IS MADE TO BRING PRESSURE DOWN, DO SO AS RAPIDLY AS POSSIBLE USING MAXIMUM HEAT REMOVAL CAPABILITY AVAILABLE.

WATTS BAR CONTAINMENT ANALYSIS

- CONTAINMENT SHELL ANALYSIS
- EQUIPMENT HATCH AMALYSIS
- CONTAINMENT ANCHORAGE ANALYSIS
- PERSONNEL LOCK ANALYSIS
- ELECTRICAL PENETRATIONS ANALYSIS

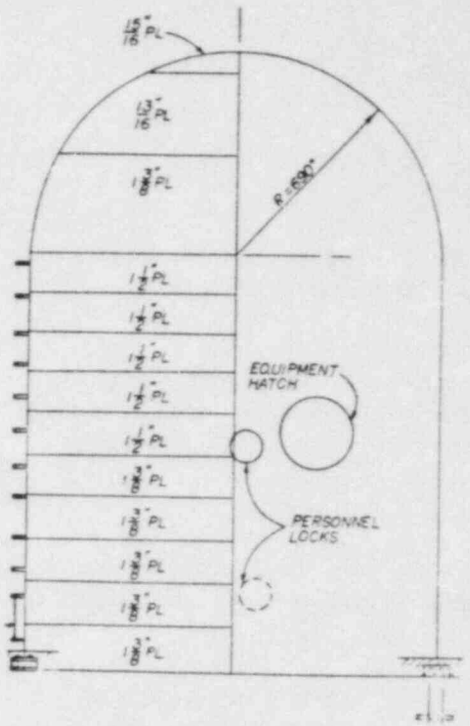

STEEL CONTAINMENT VESSEL

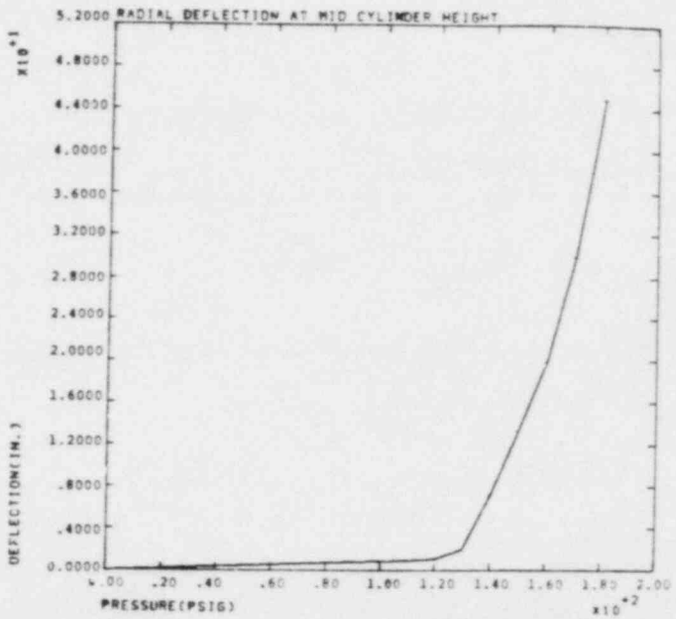

SUMMARY OF RESULTS

- CONTAINMENT SHELL CAPACITY
  APPROXIMATELY 175 PSIG
  (ASSUMING UNRESTRAINED DEFLECTIONS)
- EQUIPMENT HATCH BUCKLING PRESSURE
  APPROXIMATELY 112 - 140 PSIG
- CONTAINMENT ANCHORAGE CAPACITY
  BETWEEN 118 - 144 PSIG
- PERSONNEL LOCK CAPACITY
  GREATER THAN 150 PSIG

ANALYSIS IN SUPPORT OF OPERATOR GUIDELINES FOR SEVERE ACCIDENTS USING TRAC-PWR

by
Nelson S. DeMuth
Dean Dobranich
Rudolph J. Henninger
Energy Division
Los Alamos National Laboratory

INTRODUCTION

In the aftermath of the Three Mile Island accident, investigators pointed out the need for simulating a wide range of postulated transient or accident conditions including equipment failures and operator actions, for adding and upgrading instrumentation to monitor plant conditions during accidents, and for improving emergency procedures and training to assure proper operator response to various accident conditions. The Nuclear Regulatory Commission (NRC), as part of its response to these needs, initiated the Severe Accident Sequence Analysis (SASA) program to further our understanding both of reactor accident phenomena and of the human-machine interface during a spectrum of accidents. Efforts at Los Alamos for the SASA program have focused on (1) identification of potential accidents involving multiple equipment failures, (2) computer simulations of postulated accident sequences including equipment malfunctions and operator actions and (3) evaluation of critical safety equipment and operator responses (References 1-4).

Recent analyses at Los Alamos have used the Transient Reactor Analysis Code (TRAC), version PF1[5], to investigate the movement of hydrogen in pressurized water reactors (PWRs) following a small-break loss-of-coolant accident (SB-LOCA). Also, TRAC is being used to study severe accidents in Babcock and Wilcox (B&W) plants. The results of the hydrogen-movement investigations, along with the ongoing B&W severe accident analyses will be discussed.

MOVEMENT OF HYDROGEN FOLLOWING AN SB-LOCA

Noncondensable gas, such as hydrogen, produced during an accident can collect at system high points, specifically the tops of the primary coolant loops. Natural circulation cooling may be blocked by this hydrogen. As part of the Three Mile Island Action Plan, the NRC has required that each licensee install valves on the reactor coolant system (RCS) loops and on the reactor vessel head. The purpose of these high point vents (HPVs) is to allow noncondensable gases to be vented from the RCS. TRAC-PF1 calculations and analyses were performed to provide guidance to the reactor operator for the use of the HPVs. Also investigated were the consequences of operator error involving use of the HPVs. The framework for our investigations was provided by TRAC-PF1 calculations for two PWR types. One plant [Oconee, designed by B&W] has once-through steam generators (SGs). The other plant [Zion, designed by Westinghouse (W)] has U-tube SGs. These plants were chosen because of possible differences in the initial movement of hydrogen and the differences in venting capability. The B&W plant has HPVs both at the top of the hot-leg candy canes and the top of the vessel head. The W plant has a HPV on the vessel head only.

The initiating event for the transient for both PWRs was a 4-in.-diam cold leg break. It was assumed that emergency core cooling (ECC) was unavailable initially. The core temperature was allowed to increase until 70 kg of hydrogen was generated from zirconium oxidation. ECC was then initiated to prevent further core damage. The questions addressed by the calculations were:

1. where does hydrogen go,

2. how does the operator know if hydrogen is present,

3. how can the operator remove the hydrogen, and

4. how do errors in HPV operation affect the outcome of the transient?

The calculations show that hydrogen moves with the steam to points of low pressure within the primary loops. In the B&W plant, the loop seals did not clear during the transient. In the W plant, a loop seal cleared providing a preferential flow path for the steam-hydrogen mixture. If the break remains open, most of the hydrogen generated in the core region simply flows out the break. Operation of the HPVs (which are small openings compared to the break) does not alter this result. The disposition of hydrogen is thus out of the control of the operator if the break remains open.

If the break is isolated, then the points of low pressure in the primary system are steam condensation sites. Steam condenses at two sites within each loop, in the SG and near the ECC inlets in the cold legs. The hydrogen moves with the steam and collects at the condensation sites. In the B&W plant, hydrogen collected equally in the two loops. In the W plant most of the hydrogen collected in the loop with the cleared loop seal. As the system refilled and repressurized, hydrogen was pushed to the top of the loop in which it had collected (the hot leg candy canes in the B&W plant and the tops of the SG U-tubes in the loop with the initially cleared loop seal in the W plant). The indications that the operator is receiving at this time are that the coolant temperature, level, and pressure are increasing. If, in addition to these indications the operator determines that the primary liquid is subcooled and that cooling the SG secondaries (by dumping steam) does not result in primary cooling, then the presence of a bubble is indicated. Having determined that a bubble is blocking flow, the operator must act to remove it. In a B&W plant it is possible to remove the hydrogen by means of the candy cane HPVs. Venting the hydrogen allows the loops to be filled with liquid. Cooling the SG secondaries will then result in natural circulation flow and primary cooling.

In the W plant the presence of hydrogen in one loop will not prevent cooling by means of natural circulation flow through the other SGs. The hydrogen bubble located in the tops of the SG U-tubes cannot be vented directly. "Bumping" the pumps was found to be effective in moving the hydrogen to the vessel head where it could be vented. Several cycles of pump "bumping" followed by venting will remove enough hydrogen to refill the affected loop with liquid and allow natural circulation to begin.

Optimum HPV operation requires the operator to carefully monitor the primary pressure. While the HPVs are open, the pressure decreases. When all, or most, of the hydrogen has been vented from a given location, the pressure will begin to level or increase. Because of the small size of the HPV lines and valve orifices and the resulting low flows, errors in their operation will not significantly impair plant recovery if other plant equipment, specifically the HPI system, is functioning properly.

SEVERE ACCIDENT STUDIES IN A B&W PLANT

Los Alamos is currently performing accident analyses for the Oconee plant which has a Nuclear Steam Supply System designed by B&W. A representative set of the risk-dominant sequences as identified by the Reactor Safety Study Methodology Applications Program (RSSMAP)[6] will be simulated using TRAC.

First, the sequences will be analyzed assuming no operator actions are taken to terminate the transient and the time of core uncovery will be determined. Next, potential operator actions to halt progression to core uncovery will be examined. The time available to initiate action in a given sequence will determine which specific actions are feasible. For example, in sequences that do not lead to early core uncovery, the operator has time to consider recovering lost systems or to develop fairly sophisticated actions using other plant systems (such as using control rod drive pumps to cool the Browns Ferry core during the fire). In summary, operator actions and the times by which they must be taken will be examined.

REFERENCES

1. N. S. DeMuth, D. Dobranich, R. J. Henninger, "Loss-of-Feedwater Transients for the Zion-1 Pressurized Water Reactor," NUREG/CR-2656, Los Alamos National Laboratory report LA-9296-MS (May 1982).

2. N. S. DeMuth, D. Dobranich, R. J. Henninger, "Loss-of-Feedwater Transients for the Zion-1 Pressurized Water Reactor", (to be published) Nuclear Safety.

3. R. J. Henninger, S. B. Woodruff, "Unmitigated Boron Dilution Events in PWRs", (to be published) Proceedings of Second International Topical Meeting on Nuclear Reactor Thermal Hydraulics, Santa Barbara, Ca (Jan. 11-14, 1983).

4. Dean Dobranich, "Thermal-Hydraulic Analyses of Pressurized-Thermal-Shock-Induced Vessel Ruptures," (to be published) Proceedings of Second International Topical Meeting on Nuclear Reactor Thermal Hydraulics, Santa Barbara, Ca (Jan. 11-14, 1983).

5. Safety Code Development Group, "TRAC-PF1, An Advanced Best-Estimate Program for Pressurized Water Reactor Analysis," Los Alamos National Laboratory report (to be published).

6. G. J. Kolb, S. W. Hatch, P. Cybulskis, and R. O. Wooten, "Reactor Safety Study Methodology Applications Program: Oconee #3 PWR Power Plant," NUREG/CR-1659, Sandia National Laboratories Report SAND-1897 (May 1981).

ANALYSIS IN SUPPORT OF OPERATOR GUIDELINES FOR SEVERE ACCIDENTS USING TRAC-PWR

Nelson S. DeMuth
Dean Dobranich
Rudolph J. Henninger

SAFETY ANALYSIS GROUP
ENERGY DIVISION
LOS ALAMOS NATIONAL LABORATORY

PRESENTED TO

TENTH WATER REACTOR SAFETY RESEARCH INFORMATION MEETING

GAITHERSBURG, MD

OCT 15, 1982

SASA PROGRAM ACTIVITIES AT LOS ALAMOS

- INVESTIGATE THE EFFECTIVENESS OF CRITICAL EQUIPMENT AND OPERATOR ACTIONS IN PREVENTING OR MITIGATING SEVERE ACCIDENTS
- ASSIST NRC IN RESOLVING A VARIETY OF PLANT-SPECIFIC AND GENERIC SAFETY ISSUES
- RESPOND TO NRR REQUESTS FOR ASSISTANCE IN EVALUATING EQUIPMENT PERFORMANCE AND EMERGENCY PROCEDURES

SASA ACTIVITIES AT LOS ALAMOS

1. MOVEMENT OF HYDROGEN FOLLOWING A PWR SB-LOCA
2. SEVERE ACCIDENT STUDIES FOR B&W PLANTS (OCONEE-3)

MOVEMENT OF HYDROGEN FOLLOWING A PWR SB-LOCA

- H_2 GENERATION IN COURSE OF SB-LOCA MAY BLOCK FLOW AND COOLING
- TMI ACTION PLAN REQUIRES HIGH POINT VENTS (HPV)
- PURPOSE OF THIS WORK IS TO PROVIDE GUIDANCE FOR USE OF HPVs
- TRAC-PF1 CALCULATIONS FOR AN SB-LOCA IN OCONEE AND ZION PROVIDE FRAMEWORK FOR INVESTIGATIONS

IMPORTANT ISSUES

- WHERE DOES H_2 GO?
  - EFFECT OF BREAK ISOLATION
- HOW CAN OPERATOR DETERMINE IF H_2 IS PRESENT?
- WHAT IS THE OPTIMAL RECOVERY PROCEDURE?

INITIATING TRANSIENT

- COLD LEG BREAK (0.008107 M^2, 4 IN DIAMETER)
- ECC INITIALLY UNAVAILABLE
- TEMPERATURE INCREASE RESULTS IN 70 KG OF H_2
- ECC INITIATED TO PREVENT FURTHER DAMAGE
- BREAK LEFT OPEN OR ISOLATED

Los Alamos

OCONEE

INITIAL H_2 MOVEMENT WITH BREAK OPEN

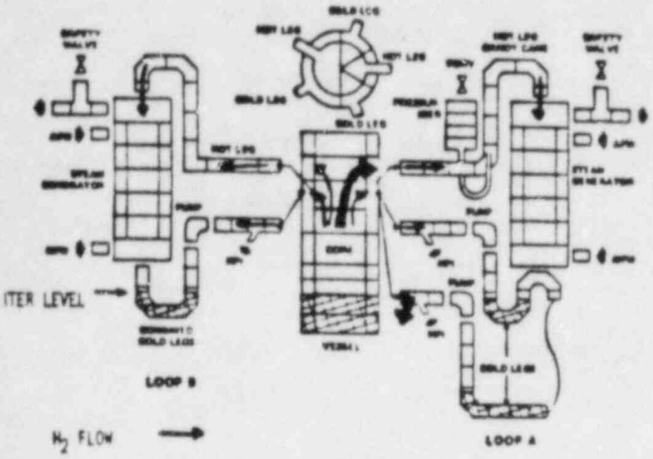

OCONEE

H_2 LOCATION AT 6500 s WITH BREAK ISOLATED

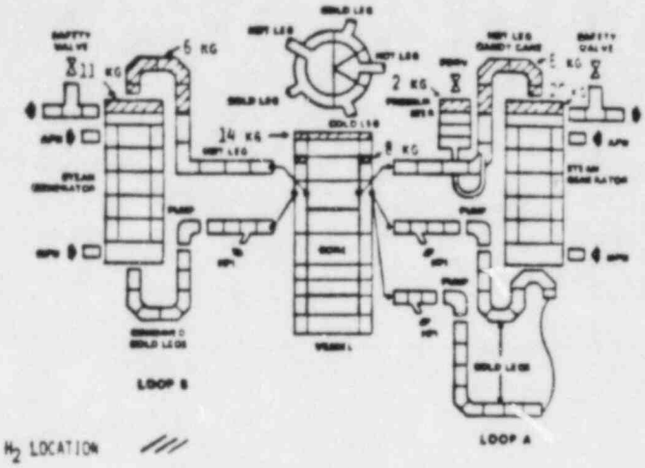

INDICATIONS AVAILABLE TO OPERATOR

- HPI IS FUNCTIONING
- SYSTEM NEAR NORMAL OPERATING CONDITIONS AND INCREASING (14.0 MPa, 570 K, 6 M PRESSURIZER LEVEL)
- SYSTEM IS 30 K SUBCOLLED
- IF ATTEMPTS TO COOL PLANT BY DUMPING SECONDARY STEAM FAIL, THEN A BUBBLE IS INDICATED

- THREE STRATEGIES ATTEMPTED TO VENT H_2 AND ESTABLISH COOLING
  1. OPEN HPV, OPEN STEAM DUMP VALVES (SDVs)
  2. OPEN HPV ONLY
  3. "BUMP" PUMPS IN ONE LOOP

OPENING HPVs REMOVES HYDROGEN AND REDUCES PRESSURE
OPENING SDVs RESULTS IN COOLING

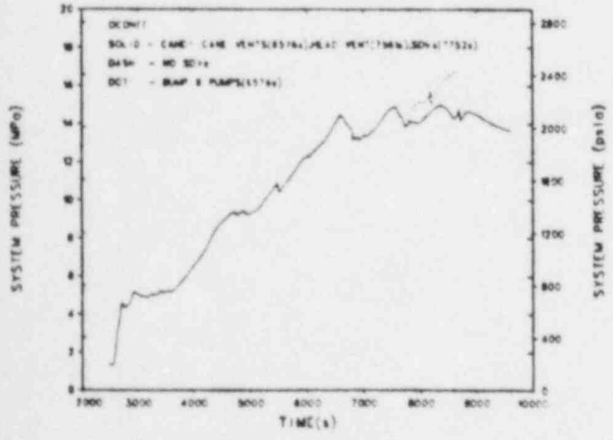

ZION

H_2 LOCATION AT 3900 s WITH BREAK ISOLATED

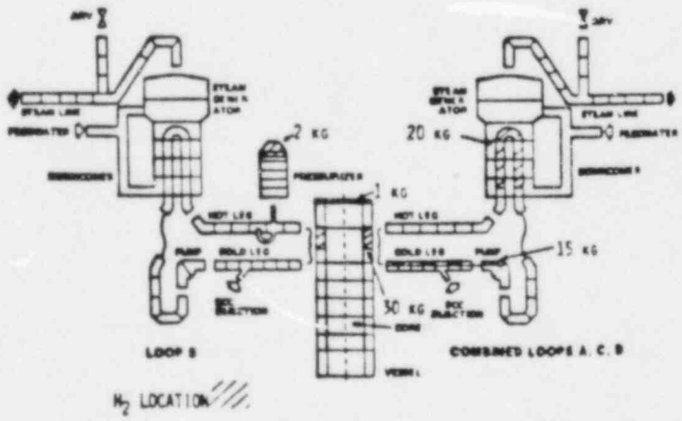

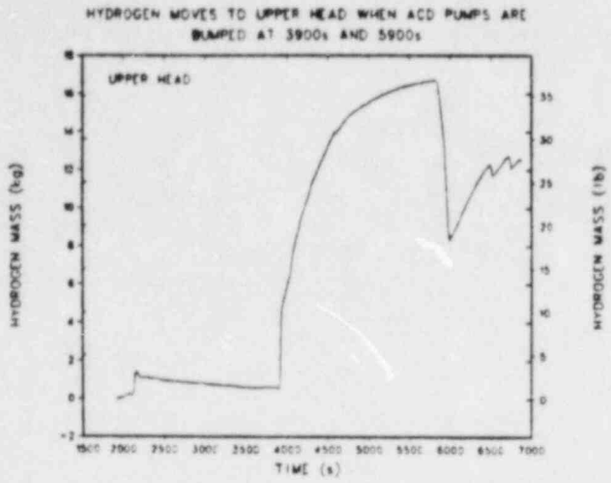

CONCLUSIONS

- WHERE DOES H_2 GO?
  - BREAK OPEN OUT BREAK
  - BREAK ISOLATED INITIALLY TO CONDENSATION SITES, THEN TO HIGH POINTS WHEN REFILLED
- HOW CAN OPERATOR DETERMINE IF H_2 IS PRESENT?
  - NO DIRECT MEANS
  - PRESENCE INFERRED FROM PRIMARY CONDITIONS

CONCLUSIONS (CONT'D)

- WHAT IS THE OPTIMAL RECOVERY PROCEDURE?

OCONEE (B & W)

- BLEED H_2 USING CANDY CANE HPVs

ZION (W)

- BUMP PUMP
- BLEED H_2 USING VESSEL HPV

OPEN HPVs UNTIL PRIMARY PRESSURE BEGINS TO INCREASE

SYSTEM RECOVERY NOT ENDANGERED BY OPEN HPV IF ECC IS FUNCTIONING NORMALLY

SEVERE ACCIDENT STUDIES FOR B&W PLANTS

- USE DOMINANT ACCIDENT SEQUENCES IDENTIFIED IN RSSMAP STUDY OF OCONEE-3
- CONSIDER DELAYED OR DEGRADED PERFORMANCE OF CRITICAL SYSTEMS
- ASSESS OPERATOR RESPONSES IN EMERGENCY PROCEDURES GUIDELINES (ATOGs)
- INVESTIGATE STRATEGIES FOR PREVENTING CORE DAMAGE
- ESTABLISH ACCIDENT SIGNATURES AND CRITICAL EQUIPMENT/OPERATOR ACTIONS

Los Alamos

NRC FORM 335 (7.77)

U.S. NUCLEAR REGULATORY COMMISSION

BIBLIOGRAPHIC DATA SHEET

1. REPORT NUMBER *(Assigned by DDC)*
NUREG/CP-0041, Volume 2

4. TITLE AND SUBTITLE *(Add Volume No., if appropriate)*
Proceedings of the Tenth Water Reactor Safety Research Information Meeting

2. *(Leave blank)*

3. RECIPIENT'S ACCESSION NO.

7. AUTHOR(S)
Compiled by: Stanley A. Szawlewicz, Consultant

5. DATE REPORT COMPLETED
MONTH: December YEAR: 1982

9. PERFORMING ORGANIZATION NAME AND MAILING ADDRESS *(Include Zip Code)*
U.S. Nuclear Regulatory Commission
Office of Nuclear Regulatory Research
Washington, DC 20555

DATE REPORT ISSUED
MONTH: January YEAR: 1983

6. *(Leave blank)*

8. *(Leave blank)*

12. SPONSORING ORGANIZATION NAME AND MAILING ADDRESS *(Include Zip Code)*
Same as Item 9.

10. PROJECT/TASK/WORK UNIT NO.

11. CONTRACT NO.

13. TYPE OF REPORT
Compilation of Conference Papers

PERIOD COVERED *(Inclusive dates)*
October 12-15, 1982

15. SUPPLEMENTARY NOTES

14. *(Leave blank)*

16. ABSTRACT *(200 words or less)*

This report is a compilation of papers which were presented at the Tenth Water Reactor Safety Research Information Meeting held at the National Bureau of Standards, Gaithersburg, Maryland, October 12-15, 1982. It consists of six volumes. The papers describe recent results and planning of safety research work sponsored by the Office of Nuclear Regulatory Research, NRC. It also includes a number of invited papers on water reactor safety research prepared by the Electric Power Research Institute and various government and industry organizations from Europe and Japan.

17. KEY WORDS AND DOCUMENT ANALYSIS

17a. DESCRIPTORS

17b. IDENTIFIERS/OPEN-ENDED TERMS

18. AVAILABILITY STATEMENT
Unlimited

19. SECURITY CLASS *(This report)*
Unclassified

21. NO. OF PAGES

20. SECURITY CLASS *(This page)*
Unclassified

22. PRICE
$

NRC FORM 335 (7.77)

UNITED STATES
NUCLEAR REGULATORY COMMISSION
WASHINGTON, D.C. 20555

120555078877 1 ANR1R3R4
US NRC
ADM DIV OF TIDC
PDR NUREG COPY
POLICY & PUBLICATNS MGT BR
W-501
WASHINGTON DC 20555